NASA Contractor Report 187472

Composite Materials for Space Applications

S.P. Rawal
M.S. Misra
R.G. Wendt

Martin Marietta Astronautics Group
Denver, Colorado

Contract NAS1-18230
August 1990

National Aeronautics and
Space Administration

Langley Research Center
Hampton, Virginia 23665-5225

NASA Contractor Report 187472

Composite Materials for Space Applications

S.P. Rawal
M.S. Misra
R.G. Wendt

Martin Marietta Astronautics Group
Denver, Colorado

Contract NAS1-18230
August 1990

National Aeronautics and
Space Administration

Langley Research Center
Hampton, Virginia 23665-5225

FOREWORD

Work reported in this final report was conducted under NASA Contract NAS1-18230, Task 6 during the period from 31 August 1987 through 15 July 1990. The work was funded by Strategic Defense Initiative Office (SDIO) work package directive PMA 1504, Advanced Materials for Space Structures. Technical effort was directed to generate a viable database of advanced composites and to determine the effect of thermal cycling on material properties. The technical monitor for the program was Mr. Louis A. Teichman of National Aeronautics and Space Administration (NASA), Langley Research Center, Materials Division. Mr. Allan W. Gunderson was the Wright Research and Development Center, Materials Laboratory advisor to the program.

Martin Marietta Astronautics Group was the prime contractor for this program. Major subcontractors included: (1) BEMCO Inc., Pacoima, CA for the design and fabrication of accelerated thermal cycling chamber; (2) Thermophysical Properties Research Laboratory (TPRL), Purdue University, West Lafayette, IN, for thermal-physical property tests; and (3) Harrop Industries, Columbus, OH, for thermal expansion tests.

Team members, their tasks, and organization are listed below:

Name	Task	Organization
Dr. Mohan S. Misra	Program Manager	Martin Marietta
Dr. Suraj P. Rawal	Principal Investigator	Martin Marietta
Mr. Robert G. Wendt	Material Characterization	Martin Marietta
Mr. Brian J. Maclean	Material Characterization	Martin Marietta
Ms. Jean Eha	Material Property Tests	Martin Marietta
Mr. Ed Maslo	Thermal Cycling	Martin Marietta

Subcontractors

Name	Task	Organization
Mr. Dennis Gherardi	Task Leader	BEMCO Inc., CA
Dr. Raymond E. Taylor	Task Leader	TPRL, IN
Mr. Edward Whalen	Task Leader	Harrop Industries, OH

CONTENTS

LIST OF FIGURES *

Figure

* Figures Related to Material Properties Test Data From Chapters 2 to 11 are Presented in Matrix Form

LIST OF FIGURES-MATRIX: P75/1962

TEST DATA	P75/1962							
	$[0]_8$ PANEL		$[0, \pm45, 90]_S$ PANEL		$[\pm30, 0_4]_S$ PANEL		$[\pm30, 0_4]_S$ TUBE	
	Figure #	Page #	Figure #	Page #	Figure #	Page #	Figure #	Page #
• **As Fabricated**								
Microstructure	2.1-1	2-3	2.2-1	2-14	2.2-2	2-15	—	—
Stress-strain Response	—	—	2.2-3	2-21	—	—	—	—
Thermal Expansion	2.1-2	2-8	2.2-4,5	2-24	2.2-6,7	2-24,25	—	—
Specific Heat	2.1-3	2-9	2.2-8	2-26	2.2-8	2-26	—	—
Thermal Diffusivity	2.1-4,5	2-10	2.2-9	2-27	2.2-9	2-27	—	—
Thermal Conductivity	2.1-6,7	2-12	2.2-10	2-27	2.2-10	2-27	—	—
Electrical Resistivity	—	—	—	—	—	—	—	—
Hemispherical Emissivity	—	—	—	—	—	—	—	—
Reflectance vs. Wavelength	—	—	2.2-11,13	2-29,30	2.2-12	2-29	—	—
Fabrication Process	—	—	—	—	—	—	—	—
Dimensions	—	—	—	—	—	—	—	—

LIST OF FIGURES-MATRIX: P75/PEEK

TEST DATA	P75/PEEK			
	$[0, \pm 45, 90]_S$ PANEL		$[\pm 30, 0_4]_S$ PANEL	
	Figure #	Page #	Figure #	Page #
• **As Fabricated**				
Microstructure	3-1	3-4	3-2	3-5
Stress-strain Response	—	—	3-3	3-6
Thermal Expansion	3-4,5	3-15	3-6,7	3-16
Specific Heat	3-8	3-17	3-8	3-17
Thermal Diffusivity	3-9,10	3-20	3-9,10	3-20
Thermal Conducitivity	—	—	3-11	3-22
Electrical Resistivity	—	—	—	—
Hemispherical Emissivity	—	—	—	—
Reflectance vs. Wavelength	—	—	3-12	3-24
Fabrication Process	—	—	—	—

LIST OF FIGURES-MATRIX: AS4/PES

TEST DATA	AS4/PES			
	$[0, \pm 45, 90]_S$ PANEL		$[\pm 30, 0_4]_S$ PANEL	
	Figure #	Page #	Figure #	Page #
• **As Fabricated** Microstructure	4-1	4-3	4-2	4-4
Stress-strain Response	—	—	—	—
Thermal Expansion	4-3,4	4-14	4-5,6	4-15
Specific Heat	4-7	4-16	4-7	4-16
Thermal Diffusivity	4-8	4-17	4-8	4-17
Thermal Conducitivity	4-9	4-20	4-9	4-20
Electrical Resistivity	—	—	—	—
Hemispherical Emissivity	—	—	—	—
Reflectance vs. Wavelength	4-10	4-20	4-11	4-21
Fabrication Process	—	—	—	—

LIST OF FIGURES-MATRIX: 25 V/O DISCONTINUOUS SiC/2124-T6

TEST DATA	25 v/o Discontinuous SiC/2124-T6							
	SiC_p/Al PANEL		SiC_w/Al PANEL		SiC_p/Al TUBE		SiC_w/Al TUBE	
	Figure #	Page #	Figure #	Page #	Figure #	Page #	Figure #	Page #
• **As Fabricated** Fabrication Process	5.1-1	5-2	5.1-1	5-2	5.2-1	5-26	5.2-1	5-26
Microstructure	5.1-2	5-5	5.1-3	5-6	—	—	—	—
Stress-strain Response	5.1-4	5-9	—	—	—	—	—	—
Thermal Expansion	5.1-5,6	5-17	5.1-7,8	5-18	5.2-2	5-31	5.2-3	5-31
Specific Heat	5.1-9	5-19	5.1-8	5-19	—	—	—	—
Thermal Diffusivity	5.1-10	5-20	5.1-10	5-20	—	—	—	—
Thermal Conductivity (x,y)	5.1-11	5-20	5.1-11	5-20	—	—	—	—
Thermal Condcutivity (z)	5.1-12	5-21	5.1-12	5-21	—	—	—	—
Electrical Resistivity	5.1-13	5-23	5.1-13	5-23	—	—	—	—
Hemispherical Emissivity	5.1-14	5-23	5.1-14	5-23	—	—	—	—
Reflectance vs. Wavelength	5.1-15	5-24	5.1-15	5-24	—	—	—	—
Dimensions	—	—	—	—	—	—	—	—

LIST OF FIGURES-MATRIX: 35 V/O DISCONTINUOUS SiC/2124-T6

TEST DATA	35 v/o Discontinuous SiC/2124-T6							
	SiC $_p$/Al PANEL		SiC $_w$/Al PANEL		SiC $_p$/Al TUBE		SiC $_w$/Al TUBE	
	Figure #	Page #	Figure #	Page #	Figure #	Page #	Figure #	Page #
• **As Fabricated** Fabrication Process	6.1-1	6-2	6.1-1	6-2	6.2-1	6-27	6.2-1	6-27
Microstructure	6.1-2	6-5	6.1-3	6-6	—	—	—	—
Stress-strain Response	—	—	—	—	—	—	—	—
Fractograph	—	—	6.1-5	6-10	—	—	—	—
Tension Compress. Compar.	6.1-6	6-18	6.1-9,10	6-19	6.2-2	6-33	6.2-3	6-33
Thermal Expansion	6.1-7,8	6-15	6.1-6	6-15	—	—	—	—
Specific Heat	6.1-11	6-20	6.1-11	6-20	—	—	—	—
Thermal Diffusivity	—	—	—	—	—	—	—	—
Thermal Conductivity	6.1-12	6-23	6.1-12	6-23	—	—	—	—
Electrical Resistivity	6.1-13	6-23	6.1-13	6-23	—	—	—	—
Hemispherical Emissivity	6.1-14	6-25	—	—	—	—	—	—
Reflectance vs. Wavelength	6.1-15	6-25	6.1-16	6-20	—	—	—	—

LIST OF FIGURES-MATRIX: P100/6061 Al

TEST DATA	P100/6061 Al							
	$[0]_2$ PANEL		$[0]_2$ PANEL		$[0]_2$ DIFFUSION BONDED TUBE		$[0]_2$ PULTRUDED TUBE	
	Figure #	Page #	Figure #	Page #	Figure #	Page #	Figure #	Page #
• **As Fabricated** Microstructure	7.1-1,2	7-5	—	—	7.2-1,2	7-23	—	—
Stress-strain Response	—	—	—	—	—	—	—	—
Thermal Expansion	7.1-3,4	7-13	—	—	7.2-4	7-29	7.2-3	7-29
Specific Heat	7.1-5	7-14	7.1-5	7-14	—	—	—	—
Thermal Diffusivity	—	—	—	—	—	—	—	—
Thermal Conductivity	7.1-6	7-17	7.1-6	7-17	—	—	—	—
Electrical Resistivity	7.1-7	7-17	7.1-7	7-17	—	—	—	—
Hemispherical Emissivity	—	—	—	—	—	—	—	—
Reflectance vs. Wavelength	7.1-8	7-19	—	—	—	—	—	—
Fabrication Process	—	—	—	—	—	—	—	—
Dimensions	—	—	—	—	—	—	—	—

LIST OF FIGURES-MATRIX: P100/AZ91C Mg

TEST DATA	P100/AZ91C Mg $[\pm 16]_s$					
	TUBE v/o = 30.1		TUBE v/o = 27.9		TUBE v/o = 23.7	
	Figure #	Page #	Figure #	Page #	Figure #	Page #
• **As Fabricated** Microstructure	8-1	8-5	—	—	—	—
Stress-strain Response	—	—	—	—	—	—
Thermal Expansion	—	—	8-2	8-9	8-3	8-9
Specific Heat	8-4	8-11	8-4	8-11	—	—
Thermal Diffusivity	—	—	8-5	8-12	8-5	8-12
Thermal Conductivity	—	—	8-6	8-13	8-6	8-13
Electrical Resistivity	—	—	8-7	8-13	8-7	8-13
Hemispherical Emissivity	—	—	—	—	—	—
Reflectance vs. Wavelength	—	—	—	—	—	—
Fabrication Process	—	—	—	—	—	—
Dimensions	—	—	—	—	—	—

LIST OF FIGURES-MATRIX: HMU/7070

TEST DATA	HMU/7070			
	$[0]_{12}$ PANEL		$[0/90]_6$ PANEL	
	Figure #	Page #	Figure #	Page #
• **As Fabricated**				
Fabrication Process	9.1-1	9-2	—	—
Microstructure	9.1-2	9-4	9.2-1	9-10
Stress-strain Response	9.1-3	9-6	—	—
Thermal Expansion	9.1-4	9-8	9.2-2	9-13
Specific Heat	—	—	9.2-3	9-13
Thermal Diffusivity	—	—	9.2-4	9-15
Thermal Conducitivity	—	—	9.2-5	9-15
Electrical Resistivity	—	—	—	—
Hemispherical Emissivity	—	—	—	—
Reflectance vs. Wavelength	—	—	9.2-6	9-16

LIST OF FIGURES-MATRIX: P100/CARBON

TEST DATA	P100/Carbon					
	$[0]_3$ PANEL		[0/90/0] PANEL		$[0]_S$ TUBE	
	Figure #	Page #	Figure #	Page #	Figure #	Page #
• **As Fabricated**						
Microstructure	10.1-1	10-6	10.2-1	10-17	—	—
Stress-strain Response	10.1-2	10-7	—	—	—	—
Thermal Expansion	10.1-3,4	10-11	10.2-2,3	10-22	—	—
Specific Heat	—	—	10.2-4	10-24	—	—
Thermal Diffusivity	—	—	10.2-5	10-24	—	—
Thermal Conductivity	10.1-5	10-13	10.2-6	10-26	—	—
Electrical Resistivity	—	—	—	—	—	—
Hemispherical Emissivity	—	—	—	—	—	—
Reflectance vs. Wavelength	—	—	—	—	—	—
Fabrication Process	—	—	—	—	—	—
Dimensions	—	—	—	—	—	—

LIST OF FIGURES-MATRIX: EFFECT OF THERMAL CYCLING ON MATERIALS

EFFECT OF THERMAL CYCLING ON MATERIALS

Material	MICROCRACKING		THERMAL EXPANSION RESPONSE	
	Figure #	Page #	Figure #	Page #
P75/1962				
•62.2v/o, $[0, \pm45, 90]_s$	11-2	11-18	11-13,14	11-63
•62.2v/o, $[\pm30, 0_4]_s$	11-5	11-21	11-15,16	11-64
•62.2v/o, $[0]_8$	11-9	11-26	—	—
P75/PEEK				
•62.2v/o, $[0, \pm45, 90]_s$	11-3	11-19	11-17,18	11-65
•62.2v/o, $[\pm30, 0_4]_s$	11-6	11-22	11-19,20	11-66
AS4/PES				
•62.2v/o, $[0, \pm45, 90]_s$	11-4	11-20	11-21,22	11-67
•62.2v/o, $[\pm30, 0_4]_s$	11-7	11-23	11-23,24	11-68
SIC_p/Al				
•25 v/o, N/A	11-10	11-26	11-25.26	11-69
•35 v/o, N/A	—	—	11-29,30	11-71
SIC_w/Al				
•25 v/o, N/A	—	—	11-27,28	11-70
•35 v/o, N/A	—	—	—	—
P100/Al				
•42.2 v/o, [0, 0]	11-11	11-27	11-31	11-72
HMU/7070				
•44 v/o, $[0]_{12}$	—	—	—	—
•40.5 v/o, $[0/90]_6$	11-8	11-24	11-36,37	11-75
C-C				
•52.48 v/o, [0, 0, 0]	—	—	11-34,35	11-74
•53.0 v/o, [0/90/0]	—	—	11-32,33	11-73
P100/6061				
•DB Tube	—	—	11-38	11-76
•PT Tube	—	—	11-39	11-76

LIST OF TABLES *

Table

APPENDIX

* Tables of Material Property Test Data From Chapters 2 to 11 are Presented in Matrix Form.

LIST OF TABLES-MATRIX: P75/1962 TEST DATA

TEST DATA	P75/1962							
	$[0]_8$ PANEL		$[0, \pm45, 90]_S$ PANEL		$[\pm30, 0_4]_S$ PANEL		$[\pm30, 0_4]_S$ TUBE	
	Table #	Page #	Table #	Page #	Table #	Page #	Table #	Page #
• **As Fabricated**								
Dimensions	—	—	—	—	—	—	2.3-1	2-32
Fiber Volume	—	—	—	—	—	—	2.3-2	2-32
Tension	2.1-1	2-5	2.2-1,2	2-15	2.2-3,4	2-17	2.3-3	2-33
Compression	2.1-2	2-5	2.2-5,6	2-19	2.2-7,8	2-20	2.3-4	2-33
Inplane Shear	2.1-3	2-6	—	—	—	—	—	—
Flexure	2.1-4	2-6	2.2-9	2-22	2.2-9	2-22	—	—
Interlaminar Shear	2.1-5	2-6	2.2-10	2-22	2.2-9	2-22	—	—
Coefficient of Thermal Exp.	2.2-11	2-25	2.2-11	2-26	2.2-11	2-26	—	—
Hoop							2.3-5	2-35
Torsion							2.3-6	2-35
Test Data Summary	2.4-1	2-37	2.4-2	2-38	2.4-3	2-39	2.4-4	

LIST OF TABLES-MATRIX: P75/PEEK Test Data

TEST DATA	P75/PEEK			
	$[0, \pm 45, 90]_S$ PANEL		$[\pm 30, 0_4]_S$ PANEL	
	Table #	Page #	Table #	Page #
• **As Fabricated**				
Dimensions	—	—	—	—
Fiber Volume	—	—	—	—
Tension	3-1,2	3-7	3-3,4	3-8
Compression	3-5,6	3-10	3-7,8	3-11
Inplane Shear	—	—	—	—
Flexure	3-9	3-12	3-9	3-12
Interlaminar Shear	3-10	3-13	3-10	3-13
Coefficient of Thermal Exp.	3-11	3-17	3-11	3-17
Thermal Diffusivity Specimens	3-12	3-19	3-12	3-19
Thermal Diffusivity	3-13	3-19	3-13	3-18
Thermal Conductivity	3-15	3-22	3-14	3-21
Test Data Summary	3-16	3-25	3- 17	3-26

LIST OF TABLES-MATRIX: AS4/PES TEST DATA

TEST DATA	AS4/PES			
	$[0, \pm 45, 90]_S$ PANEL		$[\pm 30, 0_4]_S$ PANEL	
	Table #	Page #	Table #	Page #
• **As Fabricated** Dimensions	—	—	—	—
Fiber Volume	—	—	—	—
Tension	4-1,2	4-6	4-3,4	4-7
Compression	4-5,6	4-8	4-7,8	4-9
Tension-Compress. Comparison	4-9	4-11	4-9	4-11
Inplane Shear	—	—	—	—
Flexure	4-10	4-11	4-10	4-11
Interlaminar Shear	4-11	4-12	4-11	4-12
Coefficient of Thermal Exp.	4-12	4-16	4-12	4-16
Thermal Diffusivity	4-13	4-17	4-13	4-17
Thermal Conductivity	4-14	4-19	4-14	4-19
Test Data Summary	4-15	4-22	4-16	4-23

LIST OF TABLES-MATRIX: 25 V/O DISCONTINUOUS SiC/2124-T6 TEST DATA

25 v/o Discontinuous SiC/2124-T6

TEST DATA	SiC_p/Al PANEL		SiC_w/Al PANEL		SiC_p/Al TUBE		SiC_w/Al TUBE	
	Table #	Page #	Table #	Page #	Table #	Page #	Table #	Page #
• **As Fabricated** Dimensions	—	—	—	—	5.2-1	5-26	5.2-1	5-26
Fiber Volume	—	—	—	—	—	—	—	—
Tension	5.1-1,2	5-8	5.1-3,4	5-10	5.2-2	5-28	5.2-3	5-28
Compression (ACMC)	5.1-5,6	5-11	5.1-9,10	5-14	5.2-4	5-30	5.2-5	5-30
Compression (DWA)	5.1-7,8	5-12	—	—	—	—	—	—
Inplane Shear	—	—	—	—	—	—	—	—
Flexure	5.1-11,12	5-15	5.1-13	5-15	—	—	—	—
Interlaminar Shear	—	—	—	—	—	—	—	—
Coefficient of Thermal Exp.	5.1-14,15	5-19	5.1-14,15	5-19	—	—	—	—
Thermal Conductivity	5.1-16	5-21	5.1-16	5-21	—	—		
Hoop	—	—	—	—	5.2-6	5-30	5.2-6	5-30
Test Data Summary	5.3-1	5-33	5.3-2	5-34	5.3-3	5-35	5.3-4	5-36

LIST OF TABLES-MATRIX: 35 V/O DISCONTINUOUS SiC/2124-T6 TEST DATA

TEST DATA	35 v/o Discontinuous SiC/2124-T6							
	SiC p/Al PANEL		SiC w/Al PANEL		SiC p/Al TUBE		SiC w/Al TUBE	
	Table #	Page #	Table #	Page #	Table #	Page #	Table #	Page #
• As Fabricated Dimensions	—	—	—	—	6.2-1	6-28	6.2-1	6-28
Fiber Volume	—	—	—	—	—	—	—	—
Tension	6.1-1,2	6-7	6.1-3,4	6-9	6.2-2	6-30	6.2-3	6-30
Compression (ACMC)	6.1-5,6	6-11	6.1-9,10	6-14	6.2-4	6-32	6.2-5	6-32
Compression (DWA)	6.1-7,8	6-12	—	—	—	—	—	—
Inplane Shear	6.1-11	6-15	—	—	—	—	—	—
Flexure	6.1-12	6-16	6.1-13	6-16	—	—	—	—
Interlaminar Shear	—	—	—	—	—	—	—	—
Coefficient of Thermal Exp.	6.1-14	6-20	—	—	—	—		
Thermal Conductivity (z)	6.1-15	6-20	6.1-15	6-20	—	—	—	—
Thermal Conductivity (z, y)	6.1-16	6-22	6.1-16	6-22	—	—	—	—
Test Data Summary	6.3-1	6-35	6.3-2	6-36	6.3-3	6-37	6.3-4	6-38

LIST OF TABLES-MATRIX: P100/6061 Al TEST DATA

TEST DATA	P100/6061 Al							
	$[0]_2$ PANEL		$[0]_2$ PANEL		$[0]_2$ DB TUBE		$[0]_2$ PT TUBE	
	Table #	Page #	Table #	Page #	Table #	Page #	Table #	Page #
• **As Fabricated** Dimensions	—	—	—	—	7.2-1,2	7-21	7.2-1,2	7-21
Fiber Volume	—	—	—	—	—	—	—	—
Tension (x)	7.1-1	7-6	7.1-2	7-6	7.2-3	7-25	7.2-3	7-25
Tension (y)	7.1-3	7-7	7.1-4	7-7	7.2-4	7-26	7.2-4	7-26
Compression (x)	7.1-1	7-8	7.1-6	7-8	—	—	—	—
Inplane Shear	7.1-7	7-10	—	—	—	—	—	—
Flexure	7.1-8	7-10	7.1-8	7-10	—	—	—	—
Interlaminar Shear	7.1-9	7-11	—	—	—	—	—	—
Coefficient of Thermal Exp.	—	—	—	—	7.2-6	7-27	7.2-6	7-27
Thermal Conductivity (K_z)	7.1-10	7-14	7.1-10	7-14	7.2-5	7-27	7.2-5	7-27
Inplane Thermal Conductivity	7.1-11	7-16	7.1-11	7-16	—	—	—	—
Solar Asorptance	7.1-12	7-19	—	—	—	—	—	—
Total Hemispherical Emissivity	7.1-13	7-19	—	—	—	—	—	—
Hoop	—	—	—	—	—	—	—	—
Torsion	—	—	—	—	—	—	—	—
Test Data Summary	7.3-1	7-30	7.3-2	7-31	7.3-3	7-32	7.3-4	7-33

LIST OF TABLES-MATRIX: P100/AZ91C Mg TEST DATA

TEST DATA	P100/AZ91C Mg [±16]$_s$					
	TUBE v/o = 30.1		TUBE v/o = 27.9		TUBE v/o = 23.7	
	Table #	Page #	Table #	Page #	Table #	Page #
• As Fabricated Dimensions	—	—	—	—	—	—
Fiber Volume	—	—	—	—	—	—
Tension	8-1	8-5	8-2	8-6	8-3	8-6
Hoop	8-4	8-8	8-4	8-8	8-4	8-8
Coefficient of Thermal Exp.	8-5	8-8	8-5	8-8	8-5	8-8
Specific Heat	—	—	8-6	8-11	—	—
Thermal Conductivity (K_z)	—	—	8-7	8-12	—	—
Test Data Summary	8-8	8-15	8-9	8-16	8-10	8-17

LIST OF TABLES-MATRIX: HMU/7070 TEST DATA

TEST DATA	HMU/7070			
	$[0]_2$ PANEL		$[0/90]_6$ PANEL	
	Table #	Page #	Table #	Page #
• **As Fabricated** Dimensions	—	—	—	—
Fiber Volume	—	—	—	—
Tension	9.1-1	9-6	9.2-1	9-11
Compression	9.1-2	9-6	9.2-2,3	9-11
Inplane Shear	9.1-3	9-7	9.2-4	9-11
Flexure	—	—	—	—
Interlaminar Shear	—	—	—	—
Coefficient of Thermal Exp.	—	—	—	—
Hoop	—	—	—	—
Torsion	—	—	—	—
Test Data Summary	9.3-1	9-17	9.3-2	9-18

LIST OF TABLES-MATRIX: P100/CARBON TEST DATA

TEST DATA	P100/Carbon					
	$[0]_3$ PANEL		[0/90/0] PANEL		$[0]_3$ TUBE	
	Table #	Page #	Table #	Page #	Table #	Page #
• **As Fabricated** Processing Data/Dimensions	10.1-1	10-3	10.2-1	10-15	10.3-1	10-29
Fiber Volume	—	—	—	—	—	—
Tension	10.1-2,3	10-6	10.2-2,3	10-18	10.3-2	10-31
Compression	10.1-4,5	10-8	10.2-4,5	10-20	10.3-3	10-31
Inplane Shear	10.1-6	10-10	—	—	—	—
Flexure	—	—	10.2-6	10-20	—	—
Interlaminar Shear	—	—	10.2-7	10-21	—	—
Coefficient of Thermal Exp.	10.1-7	10-10	10.2-8	10-21	—	—
Thermal Conductivity	10.1-8	10-14	10.2-9,10	10-25,26	—	—
Test Data Summary	10.4-1	10-33	10.4-2	10-34	10.4-3	10-35

LIST OF TABLES-MATRIX: TENSILE TEST DATA OF THERMAL CYCLED COMPOSITE SPECIMEN

LIST OF TABLES-MATRIX: COMPRESSION TEST DATA OF THERMAL CYCLED COMPOSITE SPECIMEN

SPECIMEN INDEXING CODES

Each test specimen of different composite materials was given a Martin Marietta I.D. # using an alpha-numeric code outline below:

- 10 Digit Code --- (12)(34)(56)-789-10

(reinforcement, matrix)(vendor, layup)(condition,form)-test,orientation-test#

Reinforcement Codes:

P-Silicon Carbide Particulate

G-Graphite fibers

C-Carbon (AS4)

W-Silicon Carbide Whisker

Matrix Codes:

A-Aluminum

C-Carbon

E-Epoxy

K-PEEK

M-Magnesium

P-PPS

S-Glass

Z-PES

Form Codes:

P-Panel

T-Tube

Test Codes:

TN-Tension

CM Compression

TO-Torsion

IL-Interlaminar Shear

FX-Flexure

TE-Thermal Expansion

NE-Normal Emissivity

IP-Inplane Shear

TK-Thermal Conductivity

VO-Fiber Volume Analysis

CP-Specific Heat

TD-Thermal Diffusivity

HE-Hemispherical Emissivity

AB-Absorptance

Vendor Codes:

A-Amercom

B-Specmat

C-ACMC

D-DWA

H-Hitco

M-MCI

P-ACPI

S-Martin Marietta

Layup Codes:

Q-Quasi-isotropic

Z-Zero CTE

U-Unidirectional

B-Bidirectional

Q-Particulate

Q-Whisker

Condition Codes:

A-As Fabricated

T-Thermally Cycled

Orientation Codes:

L-Longitudinal (x)

T-Transverse (y)

O-(Out-of-Plane) (z)

Example: (GA)(DU)(AP)-TNL-1 is the Graphite-Aluminum: DWA's Unidirectional As Fabricated Plate: a Tension Longitudinal Specimen #1.

(GK)(PQ)(TP)-FXT-5 is the fifth transverse flexure specimen of thermal cycled quasi-isotropic graphite reinforced PEEK from ACPI.

ACRONYMS

AF	As Fabricated
aF	Acceleration Factor
Al	Aluminum
ATCC	Accelerated Thermal Cycling Chamber
ACMC	Advanced Composite Material Corp., SC
ACPI	Advanced Composite Producted Inc., CT
ASTM	American Society for Testing and Materials
BP-DWA	British Petroleum - Dolowy Webb Associates, CA
C	Carbon
CTE	Coefficient of Thermal Expansion
CV	Coefficient of Variation
D	Thermal Diffusivity
DoD	Department of Defense
E	Epoxy
GEO	Geosynchronous Earth Orbit
Gl	Glass
GN_2	Gas Nitrogen
Gr	Graphite
LEO	Low Earth Orbit
LN_2	Liquid Nitrogen
MCI	Material Concepts Inc., Columbus, OH
Mg	Magnesium
MMC	Metal Matrix Composites
MMES	Martin Marietta Energy systems, Oakridge, TN
MTBF	Mean Time Between Failures

NDE	Non-Destructive Evaluation
OMC	Organic Matrix Composites
P	Particulate
p (subscript)	Pitch
QI	Quasi-isotropic
ROM	Rule of Mixture
RT	Room Temperature
SDS	Strategic Defense System
SiC	Silicon Carbide
SOA	State-of-the-Art
Std. Dev.	Standard Deviation
TP	Thermoplastic
UTRC	United Technology Research Center, CT
w (subscript)	Whisker

SYMBOLS

v/o	Percentage Fiber Volume
V_f	Fiber Volume Fraction
V_v	Void Volume
t	Specimen Thickness
θ	Ply Orientation
ρ	Density
E_x^T	Longitudinal Tensile Modulus
E_x^C	Longitudinal Compressive Modulus
E_y^T	Transverse Tensile Modulus
E_y^C	Transverse Compressive Modulus
σ_x^{TU}	Longitudinal Ultimate Tensile Strength
σ_x^{CU}	Longitudinal Ultimate Compressive Strength
σ_y^{TU}	Transverse Ultimate Tensile Strength
σ_y^{CU}	Transverse Ultimate Compressive Strength
ν_{xy}	Longitudinal Tensile Poisson Ratio
ν_{yx}	Transverse Tensile Poisson Ratio
G_{xy}	Inplane Shear Modulus
IPSS	Inplane Shear Strength
ILSS	Interlaminar Shear Strength
$\alpha_x = CTE_x$	Longitudinal Coefficient of Thermal Expansion
$\alpha_y = CTE_y$	Transverse Coefficient of Thermal Expansion
$\alpha_z = CTE_z$	Through Thickness Coefficient of Thermal Expansion
C_p	Specific Heat
D	Thermal Diffusivity
K_x	Longitudinal Thermal Conductivity

K_y	Transverse Thermal Conductivity
K_z	Through Thickness Thermal Conductivity
ε_H	Total Hemispherical Emissivity
ε_N	Total Normal Emittance
α_s	Solar Absorptance
CV	Coefficient of Variation
μm	Mirocrometer = Micron

CONVERSION FACTORS

1-in. = 2.54 cm

1-lb.= 0.454 kgm

1-lb/in^3 = 27.68 gm/cm^3 = 27.68 x 10^3 kg/m^3

1 ksi = 6.895 Mega Pascals (MPa)

1 Msi = 6.895 Giga Pascals (GPa)

°F = 1.8°C + 32

1 ppm/°F = 1.8 ppm/°C

1 watt-sec (W.s) = 1 Joule

Btu/(lb·°F) = 4184 W.s/(Kg.K) = 4.184 W.s/(gm.K)

1 Btu//(hr·ft·°F) = 12 Btu-in//(hr·ft^2·°F)

Btu/(hr·ft·°F) = 0.0833 Btu//(hr·in·°F)

1 Btu//(hr·ft·°F) = 1.73 W/(m.K) = 0.0173 W/(cm.K)

1 Btu-in/hr·ft^2·°F) = 0.144 W/m.K)

Microhm.cm = 10^{-8} ohm.m

Introduction and Summary

1.0 INTRODUCTION AND SUMMARY

Future NASA and DoD spacecraft missions offer demanding challenges for advanced materials to satisfy mission performance and reliability requirements. For example, the beam expander metering structure for the Space Based Laser (SBL) spacecraft, and parabolic panels for Large Deployable Reflector Telescope will be required to maintain ultra-precision alignment and dimensional stability in the presence of dynamic and thermal disturbances. Conventional materials do not provide adequate stiffness and thermal response to maintain this level of precision. However, composite materials provide the necessary characteristics to produce light-weight and dimensionally stable structures because of their unique combination of high specific stiffness and low coefficient of thermal expansion (Ref 1-10).

Composites include both continuous and discontinuous reinforced organic matrix, metal matrix, ceramic matrix, and carbon/carbon (C/C) composite materials. Of the organic matrix composites, graphite/epoxy (Gr/E) has been used for various structural applications such as antenna support structures, waveguides, multi-horn feed support towers, and parabolic reflectors. Although, Gr/E composites have proven adequate in antenna applications to date, they are prone to microcracking during exposure to thermal cycling and radiation conditions encountered in the space environment (Ref 11-18). As a result of microdamage, the long term dimensional stability of the composites may be significantly reduced. For long-life space missions (10-20 years) and large high frequency antennas, the durability of these materials in the hostile space environment has been identified as a key material technology need. Therefore, damage resistant organic matrix composites and other composite materials are being developed for structures requiring long term dimensional stability.

Composite material development is an ongoing process. In some space applications such as precision pointing and optical bench structures, composites will provide an enabling technology only to satisfy system performance requirements, while in others (e.g., Brilliant Pebbles, Submillimeter Explorer, Large Multiple Aperture Telescope, and Space Surveillance and

Tracking System), they will provide cost savings and weight reduction. However, for composites to be utilized in the design of SDS spacecraft or other near term structural applications, data must be available to aid designers in performing preliminary design trade studies and assist in material selection efforts. In several Department of Defense (DoD) sponsored programs, mechanical and/or thermophysical property data of various composite systems (Ref 19-47) have been obtained at different stages of the material development. As the fabrication technology is nearing maturity, reliable and reproducible test data for all State-of-the-Art (SOA) composites need to be generated using standardized or recommended test procedures (Ref 48-62). This data will facilitate the verification of analytical models that are used to predict properties. The accuracy of property prediction shall enable the assessment of performance of these materials during their operational life. In addition, there is a critical need to assess the reproducibility and reliability of materials using SOA non-destructive evaluation (NDE) techniques. After verifying the material property data and establishing the reliability of the components, the designers will be able to integrate composites into structural applications. The major thrust of this program was to generate a viable database of advanced composite material properties by utilizing a singular contractor and implementing the same test methods and environments for composites considered under this program.

In the current program, extensive mechanical and thermophysical property tests of various SOA composites have been conducted, and a reliable database has been constructed for spacecraft material selection. The composites included Gr/E, graphite/thermoplastic (Gr/TP), carbon/thermoplastics (C/TP), discontinuous silicon carbide/aluminum (SiC/Al), graphite/aluminum (Gr/Al), graphite/magnesium (Gr/Mg), carbon/glass (C/Gl), and C/C materials. Of the test methods, American Society for Testing and Materials (ASTM) standards were used whenever they were applicable. In the absence of an ASTM Standard, DoD/NASA, Thermophysical Property Research Laboratory (TPRL), or Martin Marietta Astronautics Group recommended test methods were used.

Material property results for the majority of the as-fabricated composites were consistent

with the predicted values, providing a measure of consolidation integrity attained during fabrication. To determine the effect of thermal cycling on mechanical properties and dimensional stability, approximately 500 composite specimens were exposed to ~10,000 cycles between -150°F and +150°F. These specimens were placed in a large (18-ft^3 workspace) thermal cycling chamber that was specially designed and fabricated in this program to simulate one year orbital thermal cycling (i.e., about 5840 cycles between -150°F and +150°F in low earth orbit (LEO) in 20 days. With this rate of thermal cycling, this is the largest thermal cycling unit in the country.

Reference specimens of each composite were also cycled in this chamber to examine the extent of microcracking as a result of thermal cycling. After 10,000 thermal cycles, only a few new microcracks and delaminations were observed in the organic matrix composite (OMC) laminates indicating that the thermal stresses were mostly accommodated by the microcracks that were generated during the consolidation process. In unidirectional Gr/E, discontinuous SiC/Al, Gr/Al, C/Gl, and C/C no new cracks were detected. Material property measurements of the Gr/E, Gr/TP, and C/TP laminate specimens exhibited less than 25% decrease in strength, whereas, the remaining materials exhibited less than 8% decrease in strength. The thermal expansion response of each of the thermal cycled specimens revealed significant reduction in hysteresis and residual strain, and the average CTE values were close to the predicted values.

For both the as-fabricated and thermal cycled composite materials, the test results are summarized in Section 1.5 and 1.6, and discussed in detail in the subsequent chapters.

1.1 OBJECTIVE

The objectives of the program were to:

(1) Generate mechanical, thermal, and physical property test data for as-fabricated

advanced composite materials,

(2) Design and fabricate an accelerated thermal cycling chamber, and

(3) Determine the effect of thermal cycling on the thermo-mechanical properties and dimensional stability of composites.

1.2 PROGRAM PLAN

A systematic test plan that was used to accomplish the program objectives is outlined in Figure 1-1. The plan included composite material acquisition, product evaluation, specimen preparation, material property tests, and data analysis. Also, included was the design and fabrication of a large thermal cycling chamber in which composite specimens were exposed to repeated temperature excursions between -150°F and +150°F. The thermal cycling of a select few specimens was interrupted after 100, 300, 500, 1000, 2000, 5000, and 10,000 cycles to examine the microcrack density (i.e., number of cracks/inch). Subsequently, tension compression and CTE tests were performed to determine the effect of thermal cycling on composite strength and dimensional stability.

1.3 TEST MATERIALS

Table 1-1 lists the advanced composite materials that were extensively characterized in the program. These materials were obtained in the flat panel and tubular form from the major composite manufacturers (Table 1-1). In the fabrication of these composites, either pitch (P) graphite (Gr) or pan carbon (C) fibers were used. The typical properties of these fibers are listed in Appendix A.

In the case of Gr/E, Gr/Al, C/C, and C/Gl flat lamina (unidirectional) panels were included to obtain the input material properties required for analytical modeling to predict laminate response. The Gr/E and Gr/TP laminates were obtained with two types of ply orientation: quasi-isotropic $[0, 45, 90, -45]_S$, and near zero-CTE $[30, -30, 0_4]_S$. The C/C and C/Gl

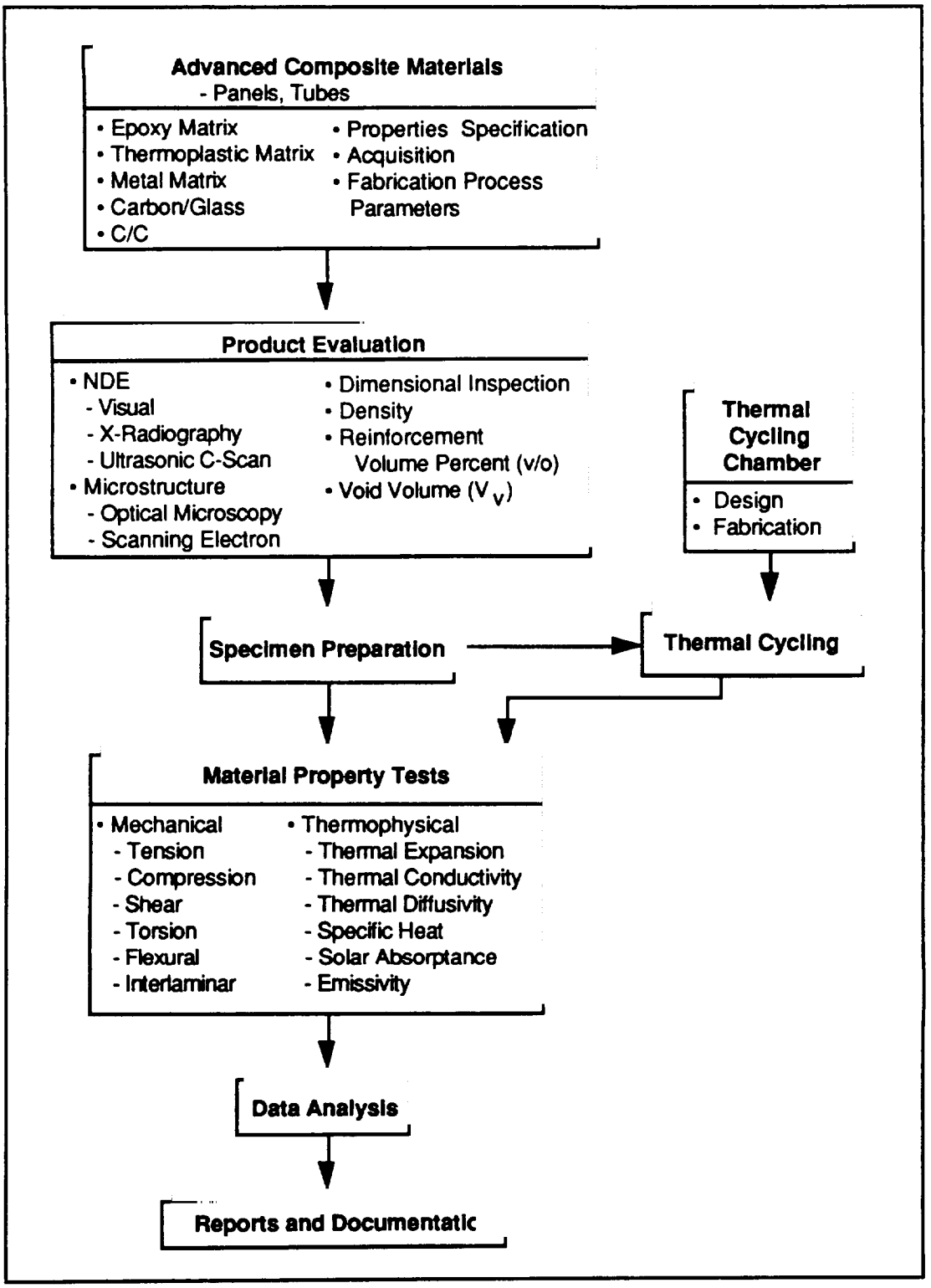

Figure 1-1 Program Test Plan Flowchart

Table 1-1 List of Compostie Materials Tested in This Program

Advanced Composites	Test Material • Ply Orietnation	Form	Manufacturer
Continuously Reinforced Graphite/Thermoset	**P75/ERLX 1962**		ACPI, CT
	• $[0]_8$	Flat Panel	
	• $[0, 45, 90, -45]_s$	Flat Panel	
	• $[\pm 30, 0_4]_s$	Flat Panel/Tube	
Graphite/ Thermoplastics	**P75/PEEK**		ACPI, CT (via MMES Oakridge, TN)
	• $[0, \pm 45, 90]_s$	Flat Panel	
	• $[\pm 30, 0_4]_s$	Flat Panel	
	AS4/PES		SPECMET, UK (via MMES, Oakridge, TN
	• $[0, \pm 45, 90]_s$	Flat Panel	
	• $[\pm 30, 0_4]_s$	Flat Panel	
Discontinuously Reinforced Metal Matrix Composites	25 SiC_p/2124 Al–T6	Flat Panel/Tube	ACMC, SC & BP-DWA, CA
	25 SiC_w/2124 Al–T6	Flat Panel/Tube	ACMC, SC & BP-DWA, CA
	35 SiC_p/2124 Al–T6	Flat Panel/Tube	ACMC, SC
	35 SiC_w/2124 Al–T6	Flat Panel/Tube	ACMC, SC
Continuously Reinforced Gr/Metals	**P100/6061 Al**	Flat Panel/Tube	DWA, CA & Amercom, CA
	• $[0]_2$		DWA, CA & FMI/STD, OH
	P100/AZ91C Mg	Tube	Martin Marietta Astronautics Group, CO
	• $[\pm 16]_s$		
Carbon/Carbon	**P100/C**		BP-HITCO, CA
	• $[0]_3$	Flat Panel/Tube	
	• [0/90/0]	Flat Panel	
Carbon/Glass	**HMU/7070**		UTRC, CT
	• $[0]_{12}$	Flat Panel	
	• $[0/90]_6$	Flat Panel	

composites were obtained in unidirectional and bidirectional [0/90] ply orientation. Of the continuously reinforced metal matrix composites, Gr/Al panels and tubes were unidirectional, while Gr/Mg tubes had $[\pm 16°]_s$ orientation. Silicon carbide particulate reinforced 2124-T6 aluminum (SiC_p/2124-T6) flat panels and tubes were obtained from ACMC and BP-DWA to characterize typical material from the two manufacturers. Silicon carbide whisker reinforced 2124-T6 aluminum (SiC_w/2124-T6) panels and tubes were obtained only from ACMC.

Typical composite panels were 12-in. x 12-in. from which about 50 specimens were carefully cut for microstructural evaluation, reinforcement volume analysis, mechanical and thermophysical property tests. The details of specimen layout on flat panels and tubes with general procedures used for specimen preparation are described in Appendix B.

1.4 EXPERIMENTAL PROCEDURES

Each composite material was extensively characterized by NDE techniques to evaluate the product quality, dimensionally inspected to determine flatness/bow and wall thickness variation, and tested to determine mechanical and thermophysical properties. The test matrix for as-fabricated and thermal cycled composites is listed in Table 1-2. A minimum of 5 specimens were used for each mechanical property test and 3 specimens for each thermophysical property test. While the details of product evaluation and property tests for each composite are discussed in subsequent chapters, the experimental procedures and results are summarized below.

1.4.1 Product Evaluation

Comprehensive evaluation of each flat panel and tube included:

- Fabrication data;
- Non-Destructive Evaluation;
- Dimensional Inspection;
- Microstructural Evaluation;
- Specific Gravity and Density; and
- Reinforcement Content.

Fabrication data was supplied by the manufacturer. The NDE techniques included visual examination to observe surface imperfections; X-radiography to assess fiber collimation, fiber breakage, voids or other defects; ultrasonic C-scanning to find delaminations and voids, and

Table 1-2 Test Matrix for Composite Materials

Material Property Tests	Test Specimens					
	As -Fabricated			Thermally-Cycled		
	[0°]	[0/±θ]	Tubes	[0°]	[0/±θ]	Tubes
Mechanical Properties						
• Tension (x, y)	10	10	3	10	10	3
• Compression (x, y)	10	10	3	10	10	3
• Inplane Shear	4	–	–	–	–	–
• Flexure	5	5	–	–	–	–
• Interlaminar Shear	5	10	–	–	10	–
• Torsion	–	–	3	–	–	3
• Hoop	–	–	3	–	–	3
Thermophysical Properties						
• CTE (x, y)	5	5	3	5	5	3
• Specific Heat (C p)	3	3	–	–	–	–
• Thermal Conductivity, K (x&y)	5	5	–	–	–	–
• Thermal Diffusivity (D)	1	1	–	–	–	–
• Electrical Resistivity (ρ_e	(5)	(5)	–	–	–	–
• Emissivity (ε_H	3	3	–	–	–	–
• Solar Absorptance (α_s	3	3	–	–	–	–
Miscellaneous						
• Density	5	5	5	–	–	–
• Fiber Volume & Porosity	5	5	5	–	–	–
• Microstructure	3	3	3	3	3	3

thermography to find delamination or voids. Microstructural evaluation using optical and scanning electron microscopy was used to reveal the consolidation quality, ply orientation, voids, microcracks and fiber-matrix distribution.

While NDE results and microstructures provided an adequate means to detect internal defects, the specific gravity, reinforcement volume percentage (v/o), and void volume (Vv) measurements) also provided an assessment of the material or processing quality. The specific gravity and density of each composite was determined by the displacement method described in ASTM-D792. To determine the v/o, ASTM-D3171 test method was used for Gr/E and Gr/TP composites, and ASTM-D3553 method was used for metal matrix composites. The Vv in the

Gr/E, Gr/TP, Gr/Al and Gr/Mg was determined by the procedures described in ASTM-D2734. For C/C, the measured value of 8% porosity was determined by the manufacturer (HITCO, CA) using the mercury pore symmetry test method.

The measured values of density, v/o, Vv, and ply thickness for each composite are listed in Table 1-3. These results of low void volume (≤1.0%) and uniform ply thickness indicated that the consolidation quality of the laminates was satisfactory.

Table 1-3 Measured Density and Reinforcement Volume of Composite Materials

Material	Density (lb/in^3) Matrix	Reinforcement	Composite	Reinforcement Volume (v/o)†		Void Volume† V_v	Ply Thickness (-in)
P75/1962							
• $[0]_8$	0.046	0.072	0.0623	62.5	(1.0)*	≤0.5	0.0048
• $[0,\pm45,90]_S$	0.046	0.072	0.0624	62.2	(0.9)	≤0.5	0.0048
• $[\pm30,0_4]$	0.046	0.072	0.0625	62.7	(0.9)	≤0.5	0.0048
P75/PEEK							
• $[0,\pm45,90]_S$	0.046	0.072	0.0628	62.2	(2.86)	≤1.0	0.0056
• $[\pm30,0_4]_S$	0.046	0.072	0.0628	62.2	(3.7)	≤0.6	0.0051
AS4/PES							
• $[0,\pm45,90]_S$	0.0495	0.065	0.058	53.7	(1.52)	≤1.0	0.005
• $[\pm30,0_4]_S$	0.0495	0.065	0.058	54.96	(0.623)	≤1.0	0.005
P100/Al							
• $[0]_2$	0.098	0.078	0.090	42.2	(0.56)	≤0.1	0.0216
SIC_p/Al							
• 25 v/o	0.098	0.134	0.104	25	(1.1)	≤0.1	N/A
• 25 v/o	0.098	0.134	0.106	35	(1.4	≤0.1	N/A
SIC_w/Al							
• 35 v/o	0.098	0.134	0.104	25	(0.8)	≤0.1	N/A
• 35 v/o	0.098	0.134	0.106	35	(1.1)	≤0.1	N/A
P100/Mg							
•$[\pm16]_S$	0.065	0.078	0.069	30.1	(1.66)	<0.5	0.0125
C-C							
• $[0]_3$	—	0.078	0.060	52.48	(0.5)	8	0.017
• [0/90/0]	—	0.078	0.060	53.0	(0.41)	8	0.017
HMU/7070							
• $[0]_{12}$	0.080	0.066	0.072	44.5	(0.3)	≤0.2	0.0052
• $[0/90]_6$	0.080	0.066	0.071	40.5	(0.4)	≤0.2	0.0054

* Standard Deviation; † Percent

1.4.2 Test Methods

After completing the product evaluation of each panel and tube, the specimens were prepared for mechanical and thermophysical property tests. For these tests either an ASTM standard or recommended methods were used as listed in Table 1-4. The details of test method including specimen dimension, specimen configuration, and fixture designs are described in Appendix C.

Table 1-4 Test Methods for Composite Materials

Material Property Tests	Test Methods †
Mechanical	
• Tension (x, y)	ASTM D-3552 (MMC, CMC, C-C) ASTM D-3039 (OMC)
• Hoop	NOL Ring Test
• Compression (x,y)	ASTM D-3410 (Celanese Fixture)
• Inplane Shear	10°off axis (NASA-Lewis)
• Interlaminar Shear (Short Beam - 3 point bend)	ASTM-D-2344
• Flexure Test	ASTM D-790M-84
• Torsion	Designed Fixture
Thermophysical Properties	
• Thermal Expansion (x,y)	ASTM E-80/ASTM E-228 (Push Rod Dilatometer)
• Thermal Conductivity* (x,y)	Kohlrausch Method
• Electrical Resistivity* (x,y)	Kohlrausch Method
• Specific Heat*	ASTM E1269
• Solar Absorptance	ASTM E-903
• Hemispherical Emissivity*	ASTM C-835
• Total Normal Emissivity	ASTM E-408B
• Thermal Diffusivity*	Laser Flash
• Density	ASTM D-792
• Fiber Volume	ASTM D-3171 (OMC), D2734 ASTM D-3553 (MMC)

* Tests were conducted at Thermophysical Properties Research Lab, Purdue Univ., West Lafayette, IN.

† Tension and compression tests of the tube specimens were performed by using a fixture and test method recommended for ASTM standards

1.4.3 Accelerated Thermal Cycling

1.4.3.1 Thermal Cycling Chamber—Based on the operational principle and requirements defined by Martin Marietta Astronautics Group, CO, a thermal cycling chamber (18-ft^3 workspace) was designed and fabricated by BEMCO Inc., CA. The operational principle and requirements were:

Principle:	Forced convection of dry nitrogen gas from hot and cold chambers located on either side of a central specimen workspace.
Workspace:	3-ft x 2-ft x 3-ft
Thermal cycles:	-150°F → 150°F → -150°F in 5 minutes
Peak Temp Variation	±10°F

The specially designed unit was able to simulate one year orbital (LEO) cycling in 20 days (i.e., acceleration factor (aF = 365/20 = 18.25)). Martin Marietta Astronautics Group also installed a 6,000 gallon (gal) liquid nitrogen dewer to provide a continuous gas supply for thermal cycling, as the chamber was fully automated for unattended operation. The thermal cycling chamber is shown in Figure 1-2 and the 6,000 gal dewer is shown in Figure 1-3. While the details of the thermal cycling chamber are described in Chapter 11, the key operational features are outlined below:

- ***Thermal Cycling Operation:***

  Above and below the 3-ft x 2-ft x 2-ft workspace the heating and cooling "servo" systems are located respectively. These systems condition the nitrogen gas through the chamber to create the thermal cycling in the workspace.

  Individually, the servos operate alternately with each other to create the cycling effect in the workspace. The flow dampers, one per servo, close during the inactive phase of a

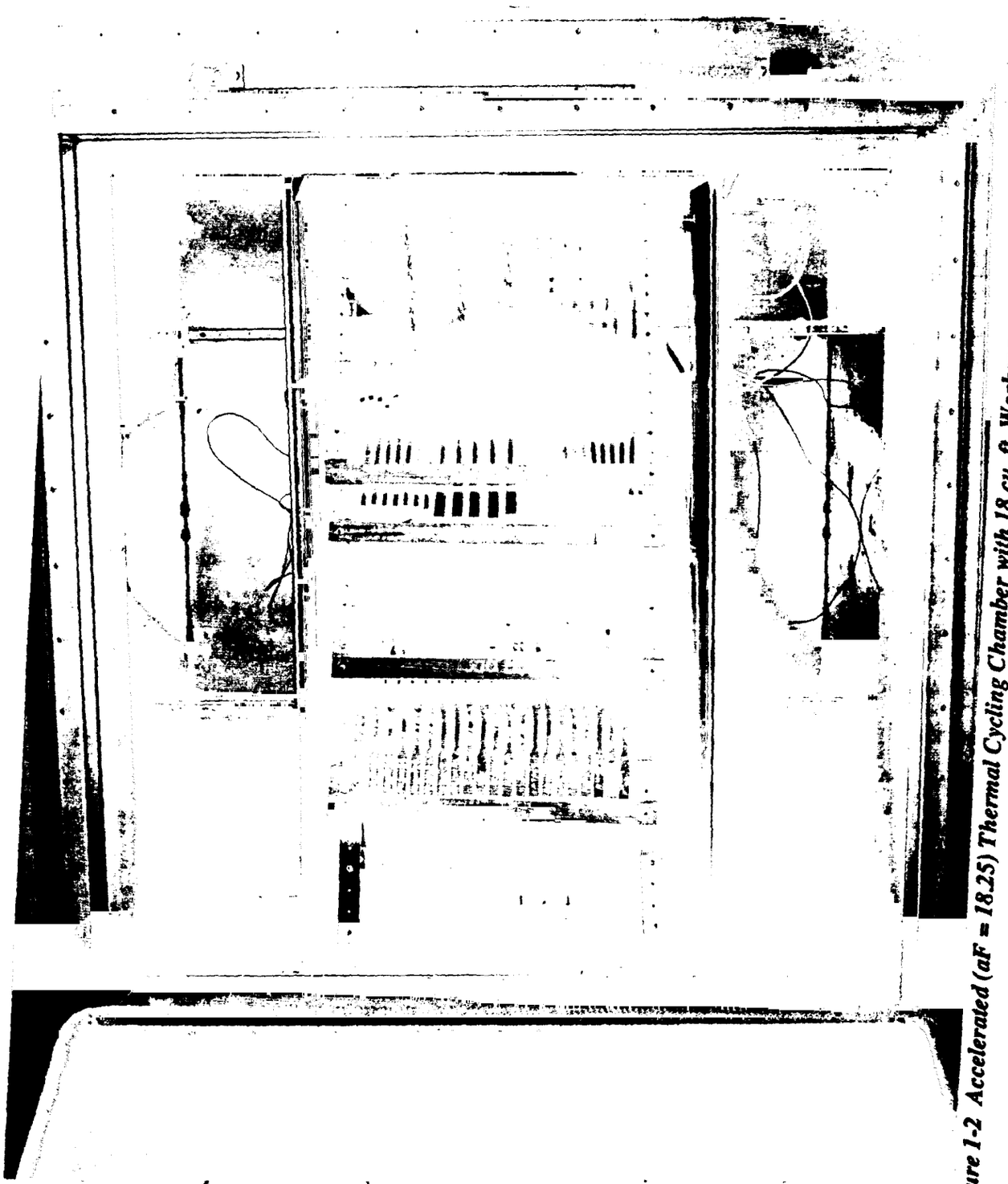

Figure 1-2 Accelerated (aF = 18.25) Thermal Cycling Chamber with 18 cu. ft. Workspace

ORIGINAL PAGE
BLACK AND WHITE PHOTOGRAPH

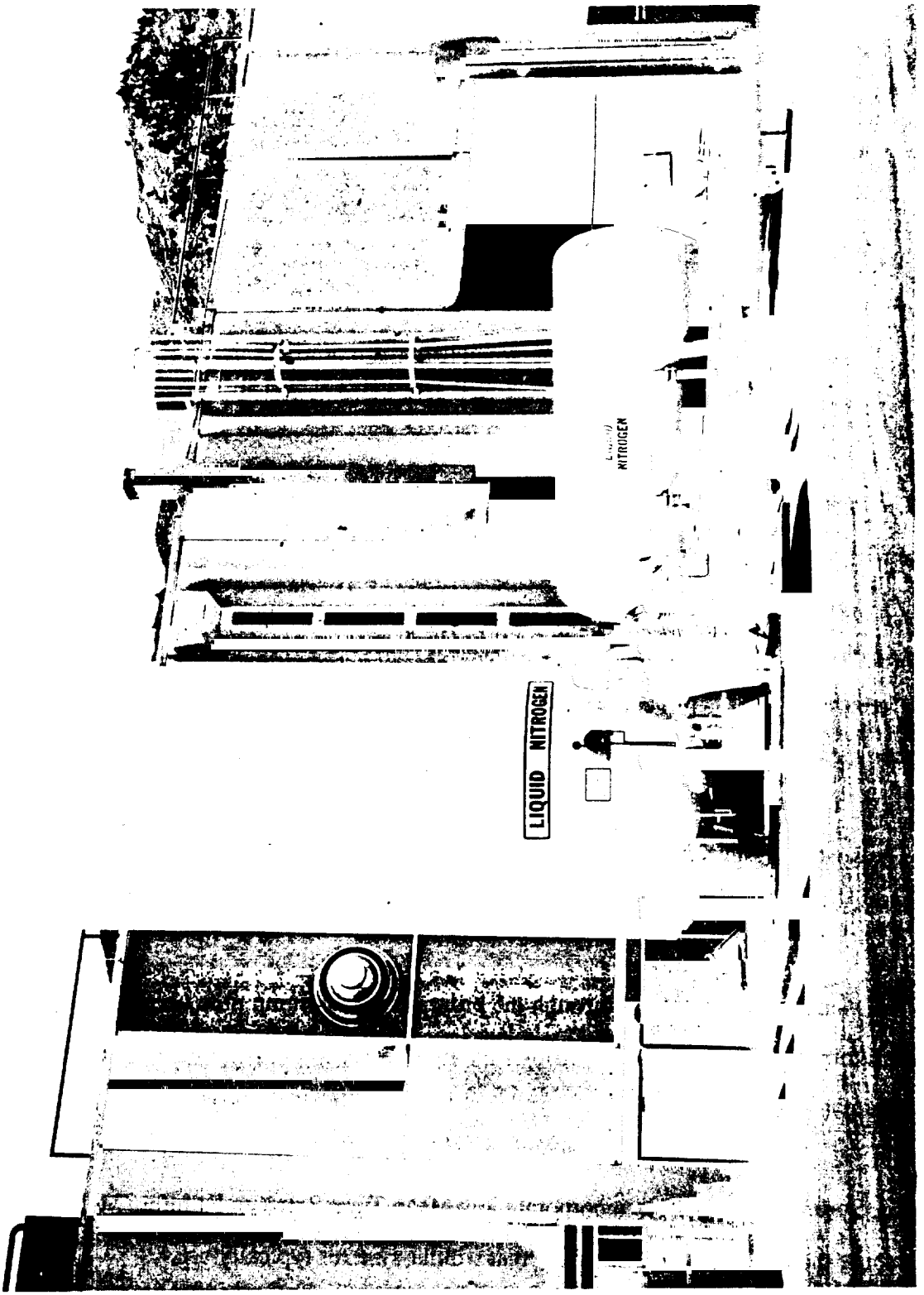

Figure 1-3 6000 Gallon Capacity Dewer for LN_2 Supply to the Accelerated Thermal Cycling Chamber

servo cycle, while the damper of the active servo is open. Each servo has a stainless steel squirrel cage type blower which is cycled on and off with active and inactive phases of the servo. During the inactive phase, cooling servo cold gas tends to stay down in the servo, which would otherwise cause the heater servo to compensate by adding more heat. Similarly, hot, inactive servo gas stays up in the heating servo, where it does not interfere with active cooling.

The thermal cycling operation is schematically shown in Figure 1-4, where during the cool cycle, the heating servo remains inactive and the damper remains closed to prevent gas circulation through the hot components. Similarly in the hot cycle, the cooling servo remains inactive.

- The entire workspace liner and two servo system liners are constructed of type 304 stainless steel.

- The chamber has an automatic nitrogen gas (GN_2) purge system which purges GN_2 into the workspace every time the chamber door is closed. The purge lasts for 90 seconds, and then automatically shuts off.

- The heating system consists of resistive wire elements and a control circuit. The elements are shielded so that no radiant heat, and only forced convective heat reaches the workspace.

- Transient rates are variable through the programming of ramp time versus temperature at the Programmer Controller and can be modified to other test requirements that do not exceed the design capacity of the chamber.

- The system is designed to incorporate low Mean Time Between Failures (MTBF) factors by reducing the number of moving parts that similar systems typically use.

(a) Cool Cycle

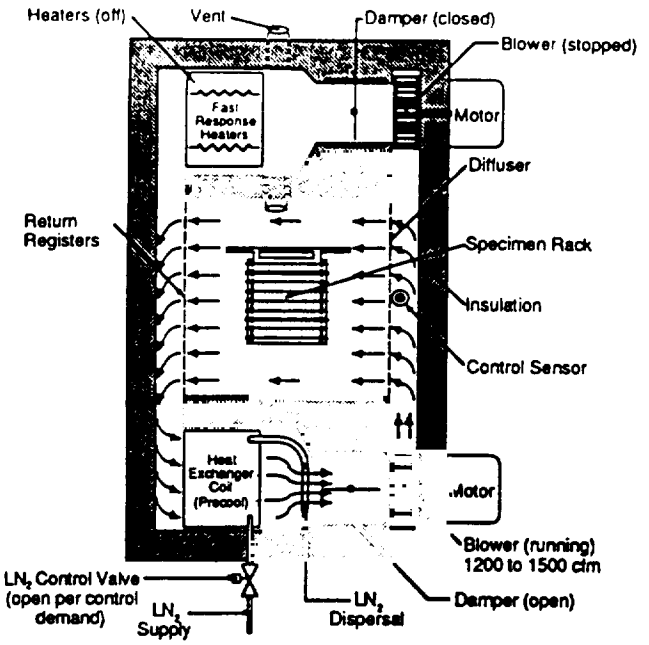

(b) Heat Cycle

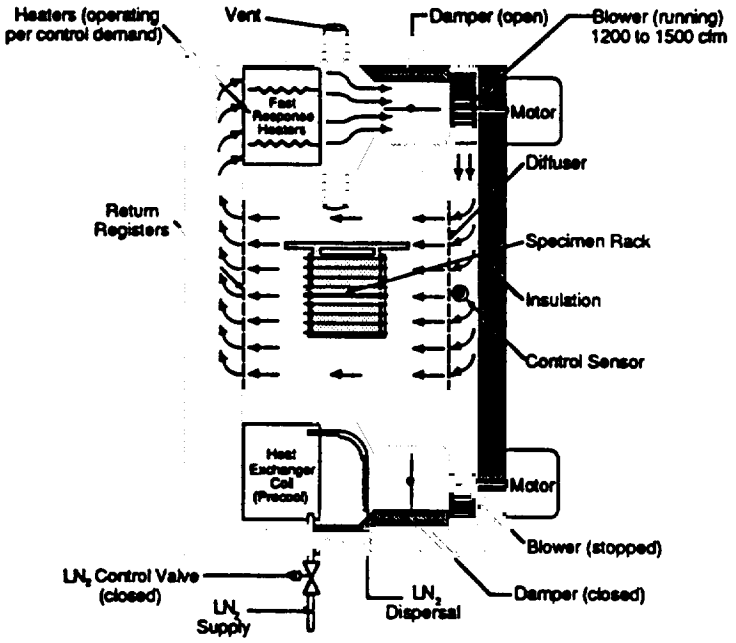

Figure 1-4 The Schematic of Thermal cycling Operation (a) Cool Cycle: Heating Servo Inactive and Damper Closed to Prevent GN_2 Circulation Through Hot Components. (b) Hot cycle: Cooling Servo Inactive and Damper Closed to Prevent GN_2 Circulation Through Cold Components

• Expansion/contraction joints and seams are used at all critical locations, to eliminate fatigue and stress failures of the liner assemblies.

• Penetrations and access ports are equipped with thermal barriers to reduce thermal losses, and prevent frosting or condensation on outside surfaces.

• The chamber is designed with various safety systems to avoid excessive heating or cooling during its operation.

1.4.3.2 Thermal Cycling of Composite Specimens—Nearly 500 specimens from different panels and tubes were simultaneously cycled between -150°F and 150°F. A few coupons (with prepolished edges) were also included to examine the microcracking induced in each composite, after 100, 300, 500, 1000, 3000 and 5000 cycles.

During thermal cycling, the specimen temperature was monitored by attaching thermocouples to different composites. The temperature measurements that at each end of the hot or cold cycle temperature was within ±10°F. The specific details of liquid nitrogen (LN_2) consumption per cycle and average extreme temperature recorded during the thermal cycling are as follows:

Total number of cycles:	10,099
Total LN_2 used:	73,574 gallons
Average LN_2/cycle:	7.28 gallon/cycle
Average hot temperature:	160°F
Average cold temperature:	-144°F

Average LN_2 consumption rate of 7.28 gal/cycle was slightly high because of the numerous interruptions caused by the blockage of cold gas passages and the malfunction of controllers. To eliminate the freezing of cold gas passages, Martin Marietta introduced an intermediate warm-up cycle (while the specimens were held at about 140°F) after every 75 cycles. However, if the

chamber operation remained uninterrupted, then LN_2 consumption should be about 6 gallons per cycle. Near the end of thermal cycling tests, BEMCO had provided another set of controllers which should nearly eliminate the number of interruptions and effectively reduce the LN_2 consumption. After completing 10,099 cycles, each specimen was prepared for tension, compression, and thermal expansion tests.

1.5 MATERIAL PROPERTY TEST DATA SUMMARY

The average mechanical and thermophysical properties obtained from room temperature tests of as-fabricated composites are summarized in Table 1-5 and details of these results are discussed in Chapters 2 to 10. Measured properties of the composites are in agreement with the values predicted from the simple rule of mixture (ROM) equations (Appendix D) and the laminate properties estimated by the computer analysis. Quantitative comparison for each composite system are presented in respective chapters. In the modulus and strength measurements, the coefficient of variation (CV) is less than 6%, whereas in Poisson ratio and strain to failure measurements the CV is about 12%. This level of scatter is reasonable to expect in SOA composites. Of the various tests, in general compressive property measurements indicated more scatter in the data than other mechanical and thermophysical property tests. The extent of scatter in compressive properties can be attributed both to the test method (Celanese compression - using 0.5 in. gauge length) and to inherent material response.

Overall, the reasonable agreement between the measured and predicted properties (Table 1-6) and low CV indicated that SOA composites have adequate consolidation quality. For example, of the organic matrix composites, Gr/E composites exhibited higher tensile strength and modulus than Gr/PEEK, for the same fiber orientation and fiber volume (Figure 1-5). These property differences in terms of processing techniques and microstructural characteristics of Gr/PEEK are discussed in chapter 3.0. The AS4/PES panels exhibited slightly lower strength values than expected due to the presence of disbonded and delaminated regions in the as-consolidated

Table 1-5 As-Fabricated Composite Materials Tested at Room Temperature

MATERIAL PROPERTY			Gr/Ep P75/1962	Gr/Ep P75/1962	Gr/TP P75/PEEK	Gr/TP P75/PEEK	Gr/TP AS4/PES	Gr/TP AS4/PES
Density	ρ	lb/in^3	0.0624	0.0625	0.0628	0.0628	0.0578	0.0578
Fiber Volume Fraction	V_f		0.622	0.627	0.622	0.622	0.537	0.5496
Nominal Ply Thickness	t	in.	0.00463	0.00458	0.0050	0.005	0.005	0.005
Max. Continuous Use Temp.	T	°F	260	260	250	250	250	250
Ply Orientation	θ	deg	$[0/45/90/-45]_s$	$[30/-30/0_4]_s$	$[0/\pm45/90]_s$	$[30/-30/0_4]_s$	$[0/\pm45/90]_s$	$[30/-30/0_4]_s$
Longitudinal Tensile Strength	σ_x^{TU}	ksi	44.6	85.5	34.91	68.77	80.34	101.61
Transverse Tensile Strength	σ_y^{TU}	ksi	50.1	4.4	43.2	5.46	77.69	4.54
Longitudinal Comp. Strength	σ_x^{CU}	ksi	26.5	54.3	21.35	51.38	47.31	90.29
Transverse Comp. Strength	σ_y^{CU}	ksi	27.6	17.7	21.75	17.54	30.36	21.07
Interlaminar Shear Strength	ILSS	ksi	5.03	6.38	4.78	7.41	7.11	9.81
Longitudinal Tensile Strain	ε_x^T	---	0.261	0.243	0.263	0.23	1.35	0.90
Transverse Tensile Strain	ε_y^T	---	0.301	0.23	0.286	0.44	1.18	0.308
Longitudinal Tensile Modulus	E_x^T	Msi	15.2	32.68	13.3	30.06	6.38	14.18
Transverse Tensile Modulus	E_y^T	Msi	15.2	1.79	14.0	1.40	6.51	1.57
Longitudinal Comp Modulus	E_x^C	Msi	13.9	27.64	9.02	28.40	5.82	12.36
Transverse Comp Modulus	E_y^C	Msi	13.6	1.73	9.36	1.14	5.63	1.26
In-Plane Shear Modulus	G	Msi	---	---	---	---	---	---
Longitudinal Flexural Modulus	F_x	Msi	15.17	14.56	16.29	12.05	9.26	7.18
Transverse Flexural Modulus	F_y	Msi	6.35	1.90	2.4	0.943	1.68	1.34
Long. Tensile Poisson's Ratio	ν_{xy}	---	0.3066	1.2122	0.3487	1.3685	0.2918	0.8872
Trans. Tensile Poisson's Ratio	ν_{yx}	---	0.3146	0.0825	0.3378	0.0719	0.3240	0.083
Long. Thermal Conductivity	K_x	(1)	2.1	3.97	2.23	3.74	0.11	0.115
Trans. Thermal Conductivity	K_y	(1)	2.11	0.40	2.34	0.38	0.19	0.043
Specific Heat	Cp	(2)	0.193	0.193	0.203	0.193	0.197	0.196
Longitudinal CTE	α_x	(2)	-0.454	-1.02	-0.28	-0.39	1.08	-0.66
Transverse CTE	α_y	(3)	-0.014	+5.83	0.04	10.17	1.38	12.6

(1) Btu/(hr·in.·°F); (2) Btu/(lb·°F); (3) µin./in/°F

Table 1-5 As-Fabricated Composite Materials Tested at Room Temperature (Cont')

MATERIAL PROPERTY			MMC's SiC_p/2124 Al	MMC's SiC_w/2124 Al	MMC's SiC_p/2124 Al	MMC's SiC_p/2124 Al	Gr/Metals P100/6061 Al	Gr/Metals P100/AZ91CMg
Density	ρ	lb/in^3	0.104	0.104	0.106	0.106	0.090	0.0683
Fiber Volume Fraction	V_f		25	25	35	35	0.422	0.301
Nominal Ply Thickness	t	in.	0.060	0.060	0.060	0.060	0.0216	0.0125
Max. Continuous Use Temp.	T	°F	550	550	550	550	550	550
Ply Orientation	θ	deg	N/A	N/A	N/A	N/A	$[0]_2$	$[16]_6$
Longitudinal Tensile Strength	σ_x^{TU}	ksi	84.5	102.0	96.5	85.7	131.3	61.2
Transverse Tensile Strength	σ_y^{TU}	ksi	77.5	97.4	97.0	57.7	3.62	3.69
Longitudinal Comp. Strength	σ_x^{CU}	ksi	80.8	102.5	103.3	97.0	46.62	29.1
Transverse Comp. Strength	σ_y^{CU}	ksi	75.8	91.0	103.4	82.4	15.21	---
Interlaminar Shear Strength	ILSS	ksi	---	---	---	---	5.487	---
Longitudinal Tensile Strain	ε_x^T	---	1.258	1.62	1.038	1.0	0.262	0.21
Transverse Tensile Strain	ε_y^T	---	1.18	1.83	1.074	0.9	0.0707	---
Longitudinal Tensile Modulus	E_x^T	Msi	16.64	17.6	19.9	18.8	49.71	25.44
Transverse Tensile Modulus	E_y^T	Msi	17.0	16.42	19.4	17.2	5.14	4.1
Longitudinal Comp Modulus	E_x^C	Msi	18.5	18.15	20.4	19.22	48.15	18.9
Transverse Comp Modulus	E_y^C	Msi	17.9	16.5	21.0	17.2	4.82	---
In-Plane Shear Modulus	G	Msi	---	—	---	---	2.62	---
Longitudinal Flexural Modulus	F_x	Msi	13.51	13.1	16.9	13.11	26.25	---
Transverse Flexural Modulus	F_y	Msi	13.02	11.8	17.0	11.8	4.16	---
Long. Tensile Poisson's Ratio	ν_{xy}	---	0.267	0.2934	0.2539	0.2711	0.2949	0.46
Trans. Tensile Poisson's Ratio	ν_{yx}	---	0.279	0.2717	0.2481	0.2363	0.0211	---
Long. Thermal Conductivity	K_x	(1)	5.740	4.87	5.75	4.24	15.278	---
Trans. Thermal Conductivity	K_y	(1)	5.616	4.71	5.42	4.28	3.333	---
Specific Heat	Cp	(2)	0.1984	0.199	0.189	0.189	0.194	0.219
Longitudinal CTE	α_x	(2)	8.16	8.03	5.86	5.91	-0.27	---
Transverse CTE	α_y	(3)	7.86	7.77	6.11	6.29	11.37	---

(1) Btu/(hr·in.·°F); (2) Btu/(lb·°F); (3) µin./in/°F

Table 1-5 As-Fabricated Composite Materials Tested at Room Temperature (Cont')

MATERIAL PROPERTY			C/Glass HMU/7070	C/Glass HMU/7070	C/C P100/C	C/C P100/C		
Density	ρ	lb/in^3	0.072	0.071	0.060	0.060		
Fiber Volume Fraction	V_f		0.44	0.40	0.5248	0.53		
Nominal Ply Thickness	t	in.	0.052	0.052	0.017	0.017		
Max. Continuous Use Temp.	T	°F	1500	1500	3700	3700		
Ply Orientation	θ	deg	$[0]_{12}$	$[0/90]_6$	$[0]_3$	[0/90/0]		
Longitudinal Tensile Strength	σ_x^{TU}	ksi	95.5	>40.9	81.5	44.1		
Transverse Tensile Strength	σ_y^{TU}	ksi	---	---	2.04	29.0		
Longitudinal Comp. Strength	σ_x^{CU}	ksi	126.3	86.7	47.8	6.95		
Transverse Comp. Strength	σ_y^{CU}	ksi	---	78.4	4.6	9.4		
Interlaminar Shear Strength	ILSS	ksi	---	3.35	3.47	1.96		
Longitudinal Tensile Strain	ε_x^T	---	0.353	0.405	0.225	0.17		
Transverse Tensile Strain	ε_y^T	---	---	---	0.208	~0.15		
Longitudinal Tensile Modulus	E_x^T	Msi	26.43	11.7	43.7	32.4		
Transverse Tensile Modulus	E_y^T	Msi	---	---	1.45	20.3		
Longitudinal Comp Modulus	E_x^C	Msi	21.3	12.7	39.4	29.1		
Transverse Comp Modulus	E_y^C	Msi	---	11.9	1.3	15.5		
In-Plane Shear Modulus	G	Msi	2.6	---	1.44	---		
Longitudinal Flexural Modulus	F_x	Msi	---	---	---	---		
Transverse Flexural Modulus	F_y	Msi	---	---	---	---		
Long. Tensile Poisson's Ratio	ν_{xy}	---	0.227	0.033	0.3690	0.145		
Trans. Tensile Poisson's Ratio	ν_{yx}	---	---	---	0.0446	0.1		
Long. Thermal Conductivity	K_x	(1)	---	0.83	9.86	6.83		
Trans. Thermal Conductivity	K_y	(1)	---	0.83	0.38	3.25		
Specific Heat	Cp	(2)	---	0.18	---	0.169		
Longitudinal CTE	α_x	(2)	-0.38	-0.075	-0.98	-0.95		
Transverse CTE	α_y	(3)	---	---	-0.42	---		

(1) Btu/(hr·in.·°F); (2) Btu/(lb·°F); (3) µin./in/°F

Table 1-6 Comparison of Measured and Predicted Properties of Selected Composite Materials

Composite	E_x^T (Msi)		CTE_x (ppm/°F)	
P75/1962, v/o = 62.2	Measured	Predicted	Measured†	Predicted
$[0]_8$	46.3	46.8	-0.69	-0.60
$[0, \pm45, 90]_S$	15.2	15.8	-0.454	-0.34
P75/PEEK v/o = 62.2				
$[0, \pm45, 90]_S$	14.0	16.0	-0.28	-0.30
$[\pm30, 0_4]_S$	30.06	34.5	-0.39*	-1.01
25 v/o SiC/Al	16.64	16.8	8.16	8.56
P100/6061 Al v/0 = 42.2				
$[0]_2$	49.71	50.9	-0.27**	0.73

†Slope of a line joining the extreme points (±150°F) of the first cycle thermal expansion curve
* After thermal cycling CTE_x = -0.81 ppm/°F
** After thermal cycling CTE_x = 0.99 ppm/°F

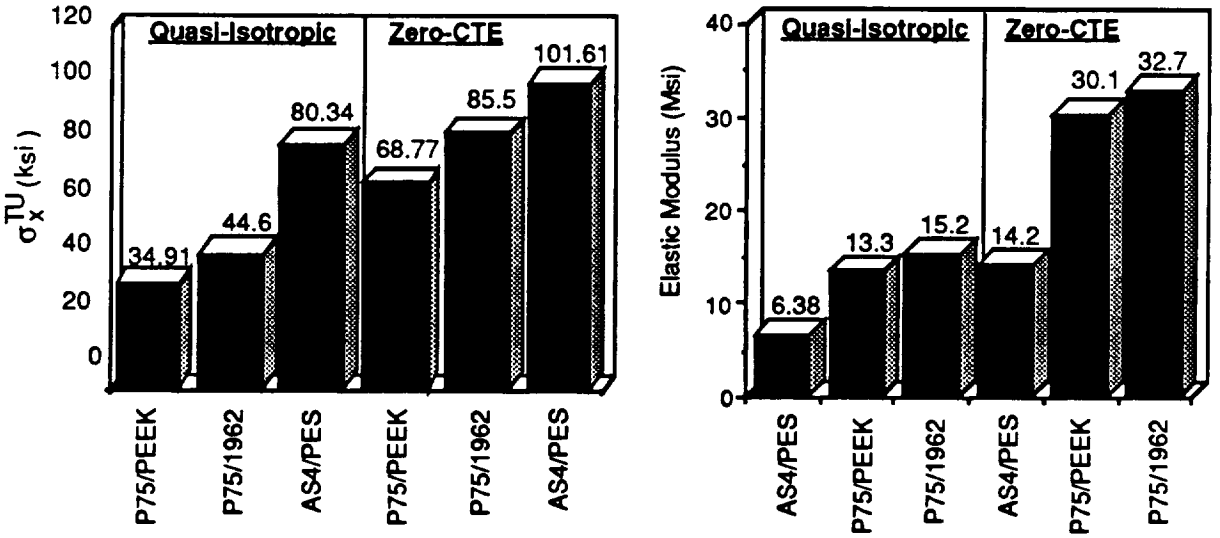

Figure 1-5 Tensile Modulus and Strength Comparison of Gr/E and Gr/TP Composites

laminate. Thus, the presence of any internal defects created during the processing of the composite was verified by the anamolous response in material property tests. Of the discontinuous metal matrix composites (MMC's), 25 v/o SiC_w/2124-T6 exhibited the expected modulus and strength values and nearly isotropic response (Figure 1-6), whereas the 35v/o SiC_w/2124-T6 showed lower than expected modulus in both the longitudinal and transverse direction. Reduced modulus in this composite was attributed to the absence of whisker/matrix

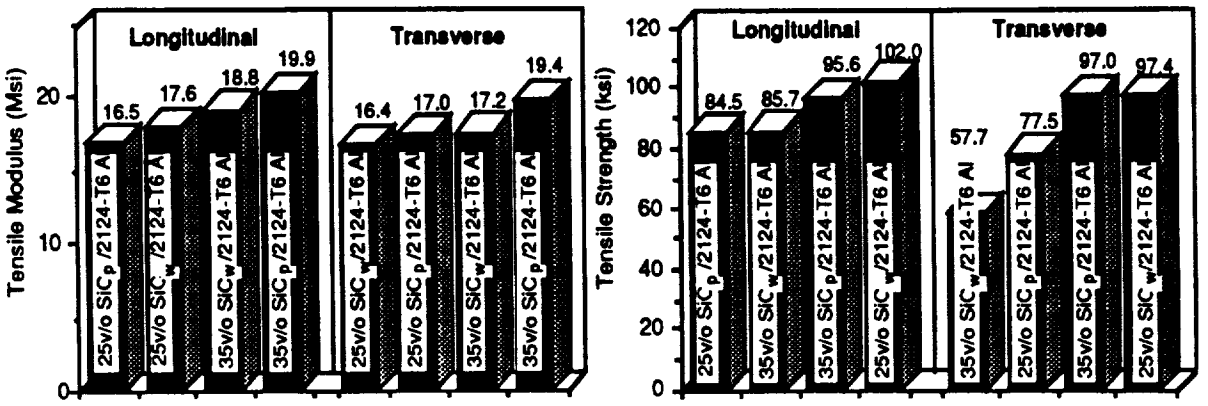

Figure 1-6 Longitudinal and Transverse Modulus Comparison of Discontinuous SiC/Al Composites

bonding in random locations where the whisker clustered and lacked matrix infiltration during consolidation. Measured mechanical properties of continuous fiber reinforced composites such as P100/Al, P100/Mg, and P100/C and C/Gl composites were in good agreement with the predicted values.

During thermophysical property tests, each composite exhibited reproducible thermal conductivity, specific heat and electrical resistivity values which were consistent with the expected values. The average CTE values (in Table 1-6) were obtained by joining the extreme points of thermal expansion response curve in the first cycle (RT → +150°F → -150°F → RT) because it is difficult to assign a single CTE values when it continuously changes with temperature.

For the P75/1962 [0]8, discontinuous SiC/Al, HMU/7070, and C/C composites, the measured CTE values were in close agreement with the predicted values. Whereas, in the remaining organic matrix and metal matrix composites, the difference in average CTE and predicted values were attributed to the following two reasons:

(i) First cycle response was significantly influenced by the residual stress state generated during fabrication, and

(ii) push rod dilatometer has relatively poor strain resolution (≈ 10 ppm) compared to

1ppm for laser interferometric dilatometer (Details in Appendix C).

For example, the P75/PEEK and AS4/PES [0, ±45, 90]s laminates do not exhibit nearly quasi-isotropic thermal expansion response (in the first cycle)because of fiber waviness and differences in residual stress state and defect density between the longitudinal and transverse directions. In general, the thermal expansion response of each composite exhibited maximum hysteresis and residual strain in the first cycle. As discussed in the literature (Ref 12, 31, 32, 40, 42, 54, 63-67), the hysteresis and residual strain are gradually reduced as the residual stresses at the reinforcement/matrix interface are relieved during subsequent thermal cycles.

1.6 EFFECT OF THERMAL CYCLING ON MATERIAL PROPERTIES

Thermal stress generated at the reinforcement/matrix interfaces during LEO cycling between 150°F and -150°F can induce microdamage in composites. This microdamage will change the thermal-mechanical properties of the material, and as a result significantly affect the dimensional stability and performance of the composite structure (Ref 11-18, 63-70). Therefore, to examine the effect of thermal cycling, the technical approach included (1) dimensional change measurements (2) microstructural examination of damage, and (3) material property tests (tension, compression and CTE).

1.6.1 Dimensional Measurements

Length and width of thermal cycled specimens were determined and compared with their initial dimensions. Dial calipers used for measuring length and micrometers used for measuring width were calibrated, both with a sensitivity of 0.001-in. These measurements indicated that after 10,099 cycles, the transverse test specimens from [30, -30, 0_4]$_S$ laminate showed a slightly larger length increase than longitudinal specimens. These differences in transverse and longitudinal specimens were consistent with their differences in CTE. While the dimensional changes

indicated a trend, their absolute values should be taken with caution for the following reasons (1) sensitivity limitation of the calipers and micrometers; and (2) flatness of edge finish.

1.6.2 Microstructural Examination of Damage

Initially the edges of a 1-in. x 1-in. reference specimen (from each composite) were polished, and subsequently examined under the optical microscope to evaluate the damage during cycling. Microstructures of these specimens indicated that there was a high incidence of microcrack initiation (and extension) in quasi-isotropic and zero-CTE P75/1962, P75/PEEK, and AS4/PES panels. In most cases a pre-existing microcrack propagated, though a few new cracks were also observed. In metal matrix, glass matrix and C/C composites, no detectable increase in the baseline microcrack density was observed. It appears that the thermal stresses generated during cycling of MMC are accommodated by microplastic deformation at the reinforcement matrix interface. Whereas in C/glass and C/C composite, thermal stresses at the interface may not be high enough to induce damage.

1.6.3 Material Property Tests

Material properties of thermal-cycled composites are listed in Table 1-7. To determine the effect of the thermal cycling, the longitudinal and transverse mechanical properties have been compared with the properties of the as-fabricated composites in Table 1-8 and 1-9 respectively. These results indicated ≤25% reduction in the tensile strength of the quasi-isotropic Gr/E, and zero-CTE Gr/E and AS4/PES laminates, whereas the Gr/PEEK composites exhibited no degradation of tensile or compressive properties. The mechanical property responses of thermal cycled Gr/Al, SiC_p/Al, C/C and C/Gl composites were nearly similar to the responses obtained in as-fabricated composites. In the case of SiC_w/Al, there was about a 10% decrease in strength without any significant change in the elastic modulus.

Table 1-7 Thermal Cycled Composite Materials Tested at Room Temperature

MATERIAL PROPERTY			Gr/Ep P75/1962	Gr/Ep P75/1962	Gr/TP P75/PEEK	Gr/TP P75/PEEK	Gr/TP AS4/PES	Gr/TP AS4/PES
Density	ρ	lb/in^3	0.0624	0.0625	0.0628	0.0628	0.0578	0.0578
Fiber Volume Fraction	V_f		0.622	0.627	0.622	0.622	0.537	0.5496
Nominal Ply Thickness	t	in.	0.00463	0.00458	0.005	0.005	0.005	0.005
Max. Continuous Use Temp.	T	°F	260	260	250	250	250	250
Ply Orientation	θ	deg	$[0/45/90/-45]_s$	$[30/-30/0_4]_s$	$[0/\pm45/90]_s$	$[30/-30/0_4]_s$	$[0/\pm45/90]_s$	$[30/-30/0_4]_s$
Longitudinal Tensile Strength	σ_x^{TU}	ksi	31.5	64.9	37.2	68.14	77.1	78.4
Transverse Tensile Strength	σ_y^{TU}	ksi	42.2	4.06	39.7	5.61	71.4	5.21
Longitudinal Comp. Strength	σ_x^{CU}	ksi	26.5	49.71	24.21	40.2	45.45	76.38
Transverse Comp. Strength	σ_y^{CU}	ksi	25.08	17.58\	25.46	17.96	26.67	17.65
Interlaminar Shear Strength	ILSS	ksi	---	---	---	---	---	---
Longitudinal Tensile Strain	ε_x^T	---	---	---	---	---	---	---
Transverse Tensile Strain	ε_y^T	---	---	---	---	---	---	---
Longitudinal Tensile Modulus	E_x^T	Msi	14.35	28.2	13.3	31.6	6.41	14.5
Transverse Tensile Modulus	E_y^T	Msi	15.5	1.70	13.6	1.21	6.7	1.46
Longitudinal Comp Modulus	E_x^C	Msi	13.9	23.09	10.3	21.43	5.42	10.86
Transverse Comp Modulus	E_y^C	Msi	11.58	1.44	9.43	1.17	5.95	1.25
In-Plane Shear Modulus	G	Msi	---	---	---	---	---	---
Longitudinal Flexural Modulus	F_x	Msi	---	---	---	---	---	---
Transverse Flexural Modulus	F_y	Msi	---	---	---	---	---	---
Long. Tensile Poisson's Ratio	ν_{xy}	---	---	---	---	---	---	---
Trans. Tensile Poisson's Ratio	ν_{yx}	---	---	---	---	---	---	---
Long. Thermal Conductivity	K_x	(1)	---	---	---	---	---	---
Trans. Thermal Conductivity	K_y	(1)	---	---	---	---	---	---
Specific Heat	Cp	(2)	---	---	---	---	---	---
Longitudinal CTE	α_x	(2)	-0.585	-1.02	-0.248	-0.81	0.65	-0.37
Transverse CTE	α_y	(3)	-0.395	2.92	-0.201	7.60	0.285	10.68

(1) Btu/(hr·in.·°F); (2) Btu/(lb·°F); (3) µin./in/°F

Table 1-7 Thermal Cycled Composite Materials Tested at Room Temperature (Cont')

MATERIAL PROPERTY			MMC's SiC_p/2124 Al	MMC's SiC_w/2124 Al	MMC's SiC_p/2124 Al	MMC's SiC_p/2124 Al		
Density	ρ	lb/in^3	0.101	0.101	0.104	0.104		
Fiber Volume Fraction	V_f		25	25	35	35		
Nominal Ply Thickness	t	in.	0.060	0.060	0.060	0.060		
Max. Continuous Use Temp.	T	°F	550	550	550	550		
Ply Orientation	θ	deg	N/A	N/A	N/A	N/A		
Longitudinal Tensile Strength	σ_x^{TU}	ksi	86.2	96.7	92.8	75.3		
Transverse Tensile Strength	σ_y^{TU}	ksi	90.6	93.0	91.92	56.7		
Longitudinal Comp. Strength	σ_x^{CU}	ksi	76.85	94.26	92.98	97.64		
Transverse Comp. Strength	σ_y^{CU}	ksi	86.33	75.76	97.7	95.33		
Interlaminar Shear Strength	ILSS	ksi	---	---	---	---		
Longitudinal Tensile Strain	ε_x^T	---	---	---	---	---		
Transverse Tensile Strain	ε_y^T	---	---	---	---	---		
Longitudinal Tensile Modulus	E_x^T	Msi	16.64	17.1	19.9	18.9		
Transverse Tensile Modulus	E_y^T	Msi	16.8	16.3	19.1	16.6		
Longitudinal Comp Modulus	E_x^C	Msi	16.5	16.13	18.18	19.28		
Transverse Comp Modulus	E_y^C	Msi	17.73	15.98	18.98	17.8		
In-Plane Shear Modulus	G	Msi	---	---	---	---		
Longitudinal Flexural Modulus	F_x	Msi	---	---	---	---		
Transverse Flexural Modulus	F_y	Msi	---	---	---	---		
Long. Tensile Poisson's Ratio	ν_{xy}	---	---	---	---	---		
Trans. Tensile Poisson's Ratio	ν_{yx}	---	---	---	---	---		
Long. Thermal Conductivity	K_x	(1)	---	---	---	---		
Trans. Thermal Conductivity	K_y	(1)	---	---	---	---		
Specific Heat	Cp	(2)	---	---	---	---		
Longitudinal CTE	α_x	(2)	8.69	8.56	6.78	---		
Transverse CTE	α_y	(3)	7.78	8.65	7.55	---		

(1) Btu/(hr·in.·°F); (2) Btu/(lb·°F); (3) µin./in/°F

Table 1-7 Thermal Cycled Composite Materials Tested at Room Temperature (Cont')

MATERIAL PROPERTY			Gr/Metals P100/6061 Al	C/Gl HMU/7070	C/C P100/C			
Density	ρ	lb/in^3	0.090	0.071	0.0605			
Fiber Volume Fraction	V_f		0.422	0.40	0.53			
Nominal Ply Thickness	t	in.	0.0216	0.0052	0.017			
Max. Continuous Use Temp.	T	°F	550	1500	3700			
Ply Orientation	θ	deg	$[0]_2$	[0/90]6	[0/90/0]			
Longitudinal Tensile Strength	σ_x^{TU}	ksi	127.0	—	36.78			
Transverse Tensile Strength	σ_y^{TU}	ksi	---	—	28.7			
Longitudinal Comp. Strength	σ_x^{CU}	ksi	43.70	84.68	15.63			
Transverse Comp. Strength	σ_y^{CU}	ksi	20.30	74.57	8.63			
Interlaminar Shear Strength	ILSS	ksi	---		---			
Longitudinal Tensile Strain	ε_x^T	---	---		---			
Transverse Tensile Strain	ε_y^T	---	---		---			
Longitudinal Tensile Modulus	E_x^T	Msi	52.48		26.79			
Transverse Tensile Modulus	E_y^T	Msi	---		13.7			
Longitudinal Comp Modulus	E_x^C	Msi	45.33	12.44	28.58			
Transverse Comp Modulus	E_y^C	Msi	4.40	13.14	9.26			
In-Plane Shear Modulus	G	Msi	---		---			
Longitudinal Flexural Modulus	F_x	Msi	---		---			
Transverse Flexural Modulus	F_y	Msi	---		---			
Long. Tensile Poisson's Ratio	ν_{xy}	---	---		---			
Trans. Tensile Poisson's Ratio	ν_{yx}	---	---		---			
Long. Thermal Conductivity	K_x	(1)	---		---			
Trans. Thermal Conductivity	K_y	(1)	---		---			
Specific Heat	Cp	(2)	---		---			
Longitudinal CTE	α_x	(2)	0.99	0.28	-0.737			
Transverse CTE	α_y	(3)	---	0.40	-0.87			

(1) Btu/(hr·in.·°F); (2) Btu/(lb·°F); (3) µin./in/°F

Table 1-8 Effect of Thermal Cycling on the Longitudinal Tensile and Compressive Properties of Composite Materials

Material	Density (lb/in^3)	Tension				Compression			
		E_X^T (Msi)		σ_X^{TU} (ksi)		E_X^C (Msi)		σ_X^{CU} (ksi)	
		AF	TC	AF	TC	AF	TC	AF	TC
P75/1962									
•62.2v/o, $[0, \pm45, 90]_s$	0.0623	15.2	14.35	44.6	31.5	13.9	9.88	26.5	25.66
•62.2v/o, $[\pm30, 0_4]_s$	0.0623	32.68	28.2	85.5	64.9	27.6	23.09	54.3	49.71
P75/PEEK									
•62.2v/o, $[0, \pm45, 90]_s$	0.063	13.3	13.3	34.91	37.2	9.02	10.30	21.35	24.21
•62.2v/o, $[\pm30, 0_4]_s$	0.063	30.06	31.6	68.77	68.14	28.40	21.43	51.38	40.2
AS4/PES									
•62.2v/o, $[0, \pm45, 90]_s$	0.058	6.38	6.41	80.34	77.1	5.82	5.42	47.31	45.45
•62.2v/o, $[\pm30, 0_4]_s$	0.058	14.18	14.5	101.61	78.4	12.36	10.86	90.29	76.88
SIC_p/Al									
•25 v/o, N/A	0.104	16.64	16.8	84.5	86.2	18.5	16.50	73.5	76.85
•35 v/o, N/A	0.106	19.9	19.9	95.6	92.8	20.4	18.18	103.3	92.98
SIC_w/Al									
•25 v/o, N/A	0.104	17.6	17.1	102.0	96.7	18.15	16.13	102.5	94.26
•35 v/o, N/A	0.106	18.8	18.9	85.7	75.3	19.22	19.28	97.02	97.64
P100/Al									
•42.2 v/o, [0, 0]	0.090	49.71	52.48	131.3	127.0	48.15	45.33	46.62	43.70
HMU/7070									
•44 v/o, $[0]_{12}$	0.072	26.43	—	95.5	—	21.3	21.66	126.3	115.34
•40.5 v/o, $[0/90]_6$	0.071	11.7	—	40.9	—	12.5	12.44	86.7	84.68
C-C									
•52.48 v/o, [0, 0, 0]	0.060	43.7	—	81.5	—	39.4	—	47.8	—
•53.0 v/o, [0/90/0]	0.060	32.4	—	44.1	36.78	29.1	28.58	6.95	15.63
SIC_p/Al Tubes									
•25 v/o, N/A	0.104	15.8	16.34	>63.4	85.5	17.3	16.33	90.1	84.6
•35 v/o, N/A	0.106	18.9	17.36	90.6	87.65	19.3	18.05	113.1	89.75
SIC_w/Al Tubes									
•25 v/o, N/A	0.104	19.8	17.73	>86.9	99.2	19.6	20.16	130.3	112.7
•35 v/o, N/A	0.106	22.3	19.93	>85.6	74.0	22.4	20.72	133.3	115.55

Table 1-9 Effect of Thermal Cycling on the Transverse Tensile and Compressive Properties of Composite Materials

Material	Density (lb/in^3)	Tension				Compression			
		E_x^T (Msi)		σ_x^{TU} (ksi)		E_x^C (Msi)		σ_x^{CU} (ksi)	
		AF	TC	AF	TC	AF	TC	AF	TC
P75/1962									
•62.2v/o, $[0, \pm 45, 90]_s$	0.0623	15.2	15.5	50.1	42.2	14.54	11.58	27.6	25.08
•62.2v/o, $[\pm 30, 0_4]_s$	0.0623	1.79	1.70	4.4	4.06	1.73	1.44	17.7	17.58
P75/PEEK									
•62.2v/o, $[0, \pm 45, 90]_s$	0.063	14.45	13.6	46.12	39.7	9.36	9.43	21.75	25.46
•62.2v/o, $[\pm 30, 0_4]_s$	0.063	1.40	1.21	5.46	5.61	1.14	1.17	17.54	17.96
AS4/PES									
•62.2v/o, $[0, \pm 45, 90]_s$	0.058	6.51	6.7	77.69	71.4	5.63	5.95	30.36	26.67
•62.2v/o, $[\pm 30, 0_4]_s$	0.058	1.57	1.46	4.54	5.21	1.26	1.25	21.07	17.65
SIC_p/Al									
•25 v/o, N/A	0.104	17.0	16.8	77.5	90.6	17.9	17.73	75.8	86.33
•35 v/o, N/A	0.106	19.4	19.1	97.0	91.92	21.0	18.98	103.4	97.7
SIC_w/Al									
•25 v/o, N/A	0.104	16.42	16.3	97.4	93.0	16.5	15.98	91.0	75.76
•35 v/o, N/A	0.106	17.2	16.6	57.7	56.7	17.2	17.8	66.02	96.53
P100/Al									
•42.2 v/o, [0, 0]	0.090	5.14	—	3.62	—	4.82	4.40	15.21	20.30
HMU/7070									
•44 v/o, $[0]_{12}$	0.072	—	—	—	—	—	—	—	—
•40.5 v/o, $[0/90]_6$	0.071	11.9	—	78.4	—	—	13.14	—	74.57
C-C									
•52.48 v/o, [0, 0, 0]	0.060	1.45	—	2.04	—	1.3	—	4.6	—
•53.0 v/o, [0/90/0]	0.060	20.3	—	29.0	28.7	15.5	—	9.4	8.36
SIC_p/Al									
•25 v/o, N/A	0.104	—	—	—	—	—	—	—	—
•35 v/o, N/A	0.106	—	—	—	—	—	—	—	—
SIC_w/Al									
•25 v/o, N/A	0.104	—	—	—	—	—	—	—	—
•35 v/o, N/A	0.106	—	—	—	—	—	—	—	—

The CTE values of thermal cycled and as-fabricated composites are listed in Table 1-10. As expected, the thermal expansion of cycled specimens exhibited reduced residual strain and RT hysteresis. The average CTE values were more consistent with the predicted values, as the residual stresses were relieved during cycling. For example the $[0, 45, 90, -45]_s$ Gr/E, Gr/TP laminates exhibited the quasi-isotropic CTE values. For Gr/Al panel, the measured CTE of 0.99 ppm/°F was close to the predicted value of 0.73 ppm/°F. The CTE values of all composites were indicative of a stabilized thermal expansion response after cycling.

1.7 CONCLUDING REMARKS

Although extensive material property data of several composites exist, use of this data in structural design efforts is severely limited due to lack of standardized test methods and procedures, and the large number of organizations reporting the limited data. In response to these needs, the current program was designed to generate a viable database of advanced composite material properties by utilizing a singular contractor and implementing the same test methods and environments for the composites considered. This database, although limited, should prove extremely valuable to spacecraft designers for preliminary material trade-off studies. The test data listed in Table 1-5 (and discussed in Chapters 2 to 10) provides the typical material properties of SOA composites. Also, the test data presented in Table 1-7 to 1-10 (and discussed in Chapter 11) provides an assessment of the effect of thermal cycling on the mechanical properties and dimensional stability of these composites. The results of both the as-fabricated and thermal cycled composites have been included in the "Strategic Defense System (SDS) Spacecraft Structural Composite Materials Selection Guide" prepared by Ketema, Inc., Composite Materials Division, CA (Ref 21). While extensive data has been generated in this technical effort, a large number of specimens from different production batches should be tested before and after thermal cycling to build confidence in the reproducibility and reliability of composite material properties.

Table 1-10 Summary of Thermal Expansion Response of Composite Specimens After 10, 099 Thermal Cycles Between -150°F and +150°F

					Thermal Expansion Response After 10,099 Cycles			0 Cycles
Material		Layup	v/o	Test Dir.	RT Hysteresis ppm	Residual Strain, ppm	CTE* ppm/°F	CTE* ppm/°F
PANELS								
1	P75/1962	$[0, \pm45, 90]_S$	62.2	x	-30.15	-4.02	-0.585	-0.454
2	P75/1962	$[0, \pm45, 90]_S$	62.2	y	-30.15	-35.17	-0.395	-0.14
3	P75/1962	$[\pm30, 0_4]_S$	62.7	x	-27.64	6.53	-1.00	-1.02
4	P75/1962	$[\pm30, 0_4]_S$	62.7	y	-45.22	-12.56	2.92	5.83
5	P75/PEEK	$[0, \pm45, 90]_S$	62.2	x	-57.79	26.13	-0.248	-0.28
6	P75/PEEK	$[0, \pm45, 90]_S$	62.2	y	-55.78	-9.045	-0.201	+0.04
7	P75/PEEK	$[\pm30, 0_4]_S$	62.2	x	-80.40	-188.44	-0.81	-0.39
8	P75/PEEK	$[\pm30, 0_4]_S$	62.2	y	5.78	-90.45	7.60	10.17
9	AS4/PES	$[0, \pm45, 90]_S$	53.7	x	-16.08	-50.25	0.65	1.08
10	AS4/PES	$[0, \pm45, 90]_S$	53.7	y	-12.90	15.58	0.285	1.38
11	AS4/PES	$[\pm30, 0_4]_S$	54.96	x	-42.72	-22.11	-0.37	-0.66
12	AS4/PES	$[\pm30, 0_4]_S$	54.96	y	-165.82	-201.00	10.68	12.60
13	P100/6061 Al	$[0]_2$	42.2	x	-10.05	4.02	0.99	-0.27**
14	SiC_p/2124-T6	N/A	25	x	55.28	-97.99	8.69	8.16
15	SiC_p/2124-T6	N/A	25	y	-100.50	-90.45	7.78	7.86
16	SiC_w/2124-T6	N/A	25	x	11.56	-100.50	8.56	8.03
17	SiC_w/2124-T6	N/A	25	y	50.25	-80.40	8.65	7.77
18	SiC_p/2124-T6	N/A	35	x	0.00	-75.38	6.78	5.91
19	SiC_p/2124-T6	N/A	35	y	50.25	-45.23	7.55	6.11
—	SiC_w/2124-T6	N/A	35	x	—	—	—	5.91
—	SiCw/2124-T6	N/A	35	y	—	—	—	6.29
20	Carbon-Carbon	[0/90/0]	53.0	x	-50.25	-12.56	-0.737	-0.95
21	Carbon-Carbon	[0/90/0]	53.0	y	-40.95	-13.57	-0.87	-0.87
22	Carbon-Carbon	$[0]_3$	52.48	x	-29.65	-21.10	-0.94	-0.98
23	Carbon-Carbon	$[0]_3$	52.48	y	-65.32	-47.70	0.29	-0.42
24	HMU/7070	$[0/90]_6$	40.5	x	8.75	-2.00	0.28	-0.075
25	HMU/7070	$[0/90]_6$	40.5	y	-13.00	-2.50	0.40	—
TUBES								
26	P100/Al, DB	$[0]_2$	43.63	x	10.01	-10.01	0.50	0.33
27	P100/Al, PT	$[0]_2$	44.35	x	-4.00	6.00	0.38	0.37
—	P100/AZ91C Mg	$[\pm16°]_S$	23.7	x	—	—	—	1.52
—	P100/AZ91C Mg	$[\pm16°]_S$	27.9	x	—	—	—	0.80
—	P100/AZ91C Mg	$[\pm16°]_S$	30.1	x	—	—	—	—

*Slope of a line joining extreme points at +150° and -150°F
**Calculated CTE: 0.70 ppm/°F

Graphite/Epoxy
P75/1962

Graphite/Epoxy
P75/1962

2.0 GRAPHITE/EPOXY: P75/ERLX 1962 (P75/1962)

Of the Gr/E composites, a high performance P75/1962 has been identified as a candidate material for space applications. Therefore, flat panels and tubes with the fiber orientation:

(1) $[0]_8$: Unidirectional Panel,

(2) $[0, 45, 90, -45]_S$: Quasi-isotropic (QI) Panel

(3)$[30, -30, 0_4]_S$: Zero-CTE Laminate Panel, and

(4) $[30, -30, 0_4]_S$: Zero-CTE Tube

were procured for material property characterization. The fabrication data, and the results of product evaluation, mechanical, and thermophysical property tests of these materials are discussed in this chapter.

2.1 P75/1962 $[0]_8$ FLAT PANELS

2.1.1 Fabrication Data:

Material System:	P75/1962
Fiber Layup:	$[0]_8$
Manufacturer:	ACPI, CT
Prepreg Source:	AMOCO
ACPI: Processing Date:	5/10/88
Martin Marietta ID#:	(GE)(PU)(AP)
Fabrication Process:	Vacuum bagged, and cured for 2 hrs at 350°F and 80 psi
Condition:	as fabricated
Dimensions	12-in. x 12-in. x 0.038-in.
Ply Thickness	0.0048-in.

2.1.2 Product Evaluation

(a) Density:

P75 Fiber:	0.072 lb/in^3 (2.09 gm/cm^3)
ERLX 1962:	0.046 lb/in^3 (1.28 gm/cm^3)
P75/1962:	0.0623 lb/in^3 (1.79 gm/cm^3)

(b) Fiber Volume:

Fiber Volume (v/o):	62.5
Std. Dev:	1.0
Void Volume (%Vv):	≤0.5

(c) Non-Destructive Evaluation

Visual, X-radiographic and ultrasonic techniques were used to inspect all P75/1962 $[0]_8$ flat panels. Each panel appeared to be of good quality without any surface imperfections. X-radiographic examination revealed that fiber collimation in each panel was excellent and ultrasonic C-scans showed no major defects such as voids or delaminations.

(d) Microstructure

Longitudinal and transverse microstructures of P75/1962 $[0]_8$ lamina are shown in Figure 2.1-1 (a) and (b). Each photomicrograph shows that the overall fiber matrix distribution is uniform, and fibers are aligned along the longitudinal direction.

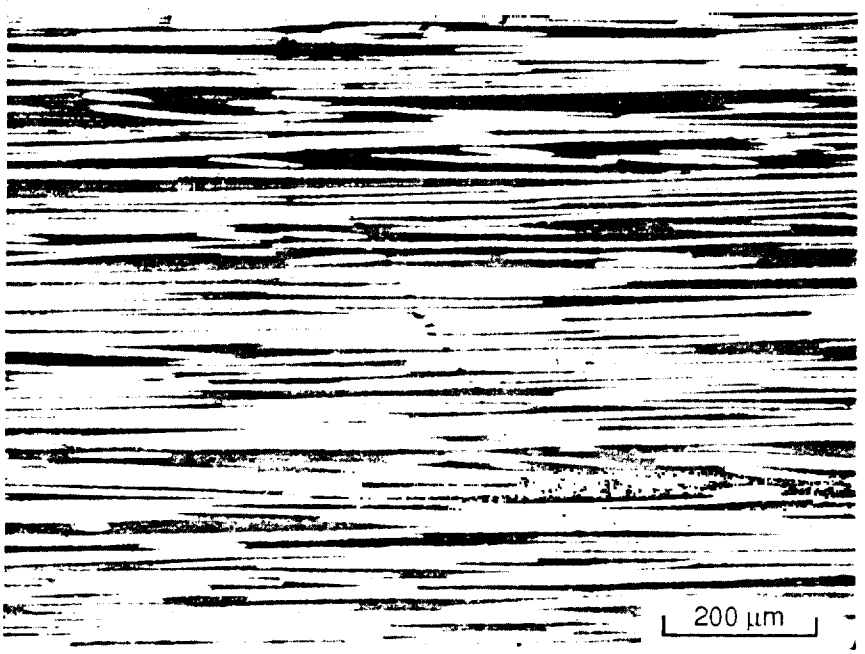

(a) Longitudinal

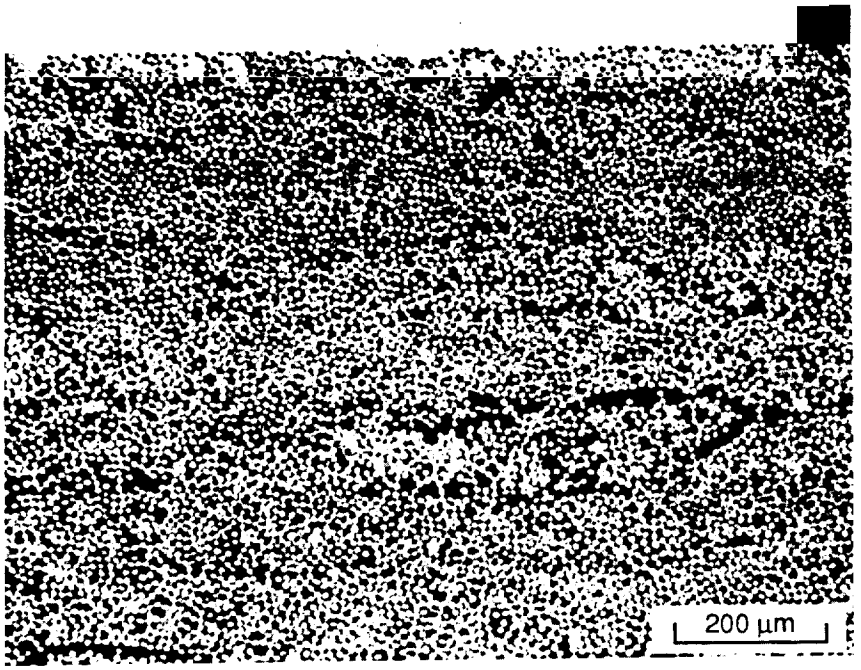

(b) Transverse

Figure 2.1-1 Photomicrographs of P75/1962 $[0]_8$ Lamina Showing Uniform Fiber/Matrix Distribution

2.1.3 Mechanical Properties

(a) Tension and Compression

In tension and compression tests, each specimen exhibited linear elastic response until failure. Longitudinal tensile and compressive properties of unidirectional P75/1962 $[0]_8$ are listed in Tables 2.1-1 and 2.1-2. Measured tensile modulus of 46.3 Msi was in excellent agreement with the rule of mixture (ROM) prediction of 46.8 Msi. These test results were consistent with the typical values established in the literature for P75/934 [0°] composites (Ref 49). Transverse test specimens were extremely fragile and a few got damaged during handling. From the undamaged specimens an average transverse modulus of 0.7 Msi and a strength of 2 ksi were obtained. In the compression tests, the measured modulus was about 20% lower than the tensile modulus, and the ultimate compressive strength was nearly half of the tensile strength.

(b) In-plane Shear

Shear modulus and in-plane shear strength values of unidirectional P75/1962 are listed in Table 2.1-3. Measured shear modulus of 1.67 Msi was consistent with the predicted value of 1.2 Msi.

(c) Flexure

Longitudinal and transverse flexure modulus and strength values of unidirectional P75/1962 determined by three point bend tests are listed in Table 2.1-4. As expected, these results showed that the transverse flexural modulus and strength values were significantly lower than the corresponding value in the longitudinal direction.

(d) Interlaminar Shear Strength (ILSS)

The apparent interlaminar shear strength values of unidirectional P75/1962 specimens determined by short beam shear-three point bend tests are listed in Table 2.1-5. The ILSS value of 7.31 ksi was consistent with the values available in the literature. Optical microscopic examination of the 0.5-in. specimens confirmed that failure was primarily interlaminar shear.

Table 2.1-1 Longitudinal Tensile Properties of Unidirectional P75/1962, Fiber Volume = 62.5%

Specimen # (GE)(PU)(AP)	Elastic Modulus E_x^T (Msi)	Ultimate Tensile Strength (ksi)	Poisson Ratio ν_{xy}	Strain To Failure (%)
TNL-1	44.8	119.3	0.370	0.266
TNL-2	43.8	115.4	0.303	0.264
TNL-3	46.3	118.1	0.287	0.253
TNL-4	48.6	129.8	0.268	0.267
TNL-5	48.1	135.0	0.263	0.280
Mean Value	46.3	123.5	0.298	0.266
Std. Dev.	2.063	8.43	0.0431	0.0096
CV (%)	4.5	6.8	14.5	3.6

Table 2.1-2 Longitudinal Compressive Properties of Unidirectional P75/1962, Fiber Volume = 62.5%

Specimen # (GE)(PU)(AP)	Elastic Modulus E_x^C (Msi)	Ultimate Comp. Strength (ksi)	Poisson Ratio ν_{xy}	Strain To Failure (%)
CML-1	35.7	59.9	0.304	—
CML-2	37.5	62.2	0.275	0.202
CML-3	34.4	67.2	0.274	0.242
CML-4	35.6	43.3†	0.213	0.146
CML-5	38.2	64.4	0.271	0.202
Mean Value	36.3	63.43	0.267	0.198
Std. Dev.	1.542	3.12	0.0332	0.0395
CV (%)	4.2	4.9	12.4	19.9

Table 2.1-3 Inplane Shear Strength Properties of Unidirectional P75/1962, Fiber Volume = 62.5%

Specimen # (GE)(PU)(AP)	G_{xy} (Msi)	IPSS (ksi)
IP-1	1.54	6.584
IP-2	1.84	6.527
IP-3	1.77	7.010
IP-4	1.53	6.585
Mean	1.67	6.677
Std. Dev.	0.159	0.224
CV (%)	9.5	3.35

Table 2.1-4 Longitudinal and Transverse Flexural Properties of Unidirectional P75/1962, Fiber Volume = 62.5%

	Longitudinal Flexural			Transverse Flexural	
Specimen # (GE)(PU)(AP)	Modulus (Msi)	Strength (ksi)	Specimen # (GE)(PU)(AP)	Modulus (Msi)	Strength (ksi)
FXL-1	24.9	122.2	FXT-1	1.00	7.31
FXL-2	27.4	128.0	FXT-2	0.92	8.81
Mean	26.2	125.1	Mean	0.96	8.06
Standard Deviation	1.767	4.101	Standard Deviation	0.0566	1.061
CV(%)	6.7	3.3	CV(%)	5.9	13.2

Table 2.1-5 Apparent Interlaminar Shear Strength Properties of Unidirectional P75/1962, Fiber Volume = 62.5%

P75/1962:Unidirectional $[0°]_8$	
Specimen # (GE)(PU)(AP)	ILSS (ksi)
IL-1	7.63
IL-2	7.31
IL-3	7.41
IL-4	7.71
IL-5	6.82
IL-6	6.78
IL-7	7.48
Mean Value	7.31
Std. Dev.	0.370
CV %	5.1

2.1.4 Thermophysical Properties

(a) Coefficient of Thermal Expansion (CTE)

Figures 2.1-2a shows the thermal expansion response of a longitudinal P75/1962 $[0]_8$, 62.5 v/o specimen in the first cycle from RT → 150°F → -150°F → RT obtained by push rod dilatometry. This curve shows CTE_x = -0.69 ppm/°F (from the slope of a line joining extreme points of thermal expansion curve), compared to the predicted value of -0.6 ppm/°F. Also, this specimen exhibited room temperature (RT) hysteresis of 98.8 ppm and residual strain of 154.26 ppm.

For comparison, Figure 2.1-2 b and c show a typical thermal expansion response of P75/1962 $[0]_8$, 52.03 v/o composite in the longitudinal and transverse directions respectively, obtained by laser interferometric dilatometer (S.S. Tompkins, NASA LaRC, private communication, Appendix C). In contrast to the thermal strain response from push rod dilatometry, these curves show nearly zero residual strain and hysteresis [CTE_x = -0.53 ppm/°F (predicted CTE_x = -0.51 ppm/°F) and CTE_y = 20.5 ppm/°F] indicative of the difference in strain sensitivity between the two dilatometers.

(b) Specific Heat (Cp)

Specific heat results are shown in Figure 2.1-3. The average Cp increased with increasing temperature, yielding a value of 0.203 Btu/lb°F at RT.

(c) Thermal Diffusivity

Thermal diffusivity results are plotted in Figures 2.1-4 (thickness and transverse directions) and 2.1-5 (longitudinal direction). Thermal diffusivity in the longitudinal direction at RT was 0.66 cm^2/sec compared to the transverse direction value of 0.008 cm^2/sec. The values in the thickness and transverse directions were similar above 200°F, but the values in the transverse direction increased faster at lower temperatures.

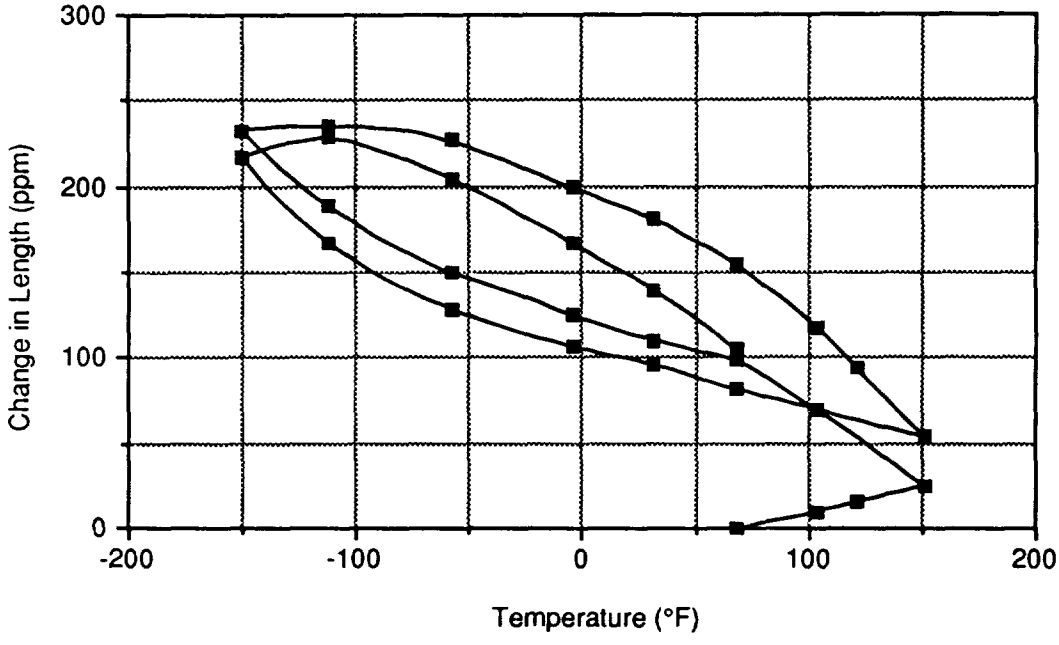

Figure 2.1-2a Longitudinal Thermal Expansion Response of P75/1962 $[0]_8$, v/o = 62.5 Obtained With a Push Rod Dilatometer.

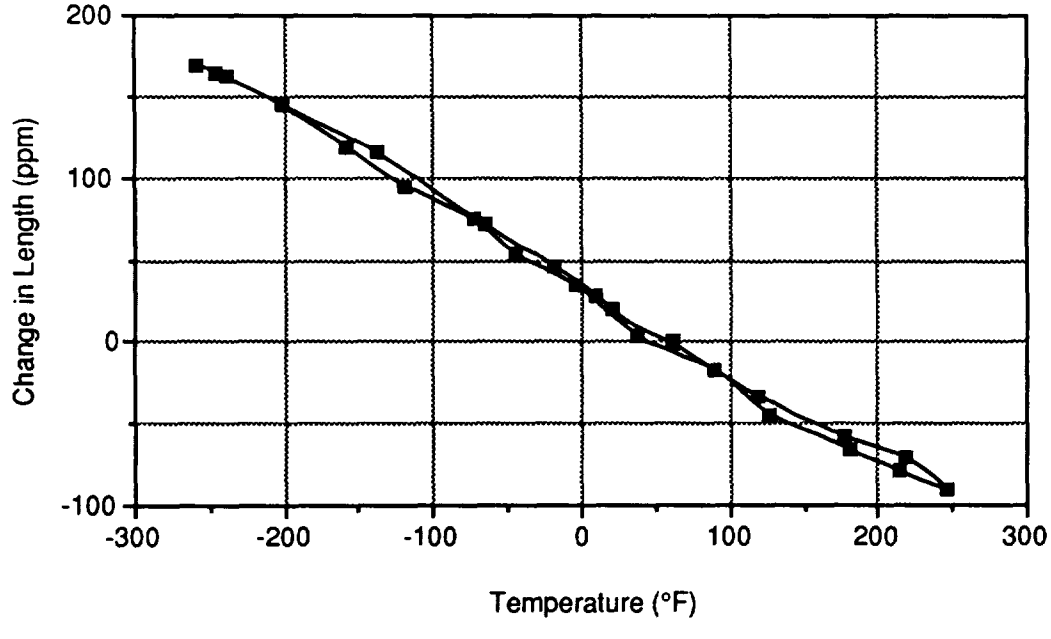

Figure 2.1-2b Longitudinal Thermal Expansion Response of P75/1962 $[0]_8$, v/o = 52.03 Obtained With a Laser Interferometric Dilatometer

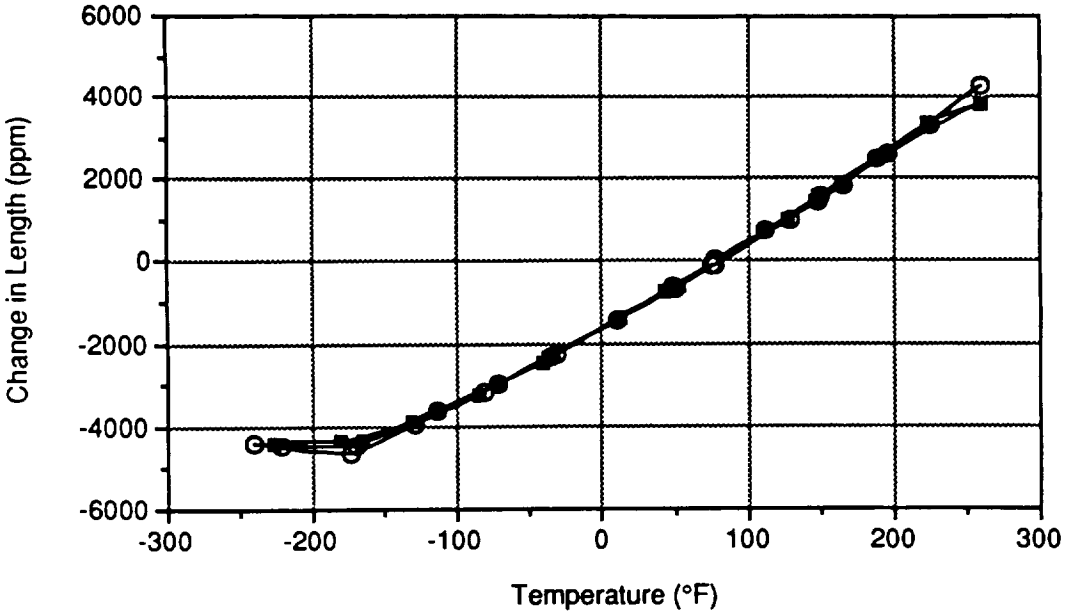

Figure 2.1-2c Transverse Thermal Expansion Response of P75/1962 $[0]_8$, v/o = 52.03 Obtained With a Laser Interferometric Dilatometer

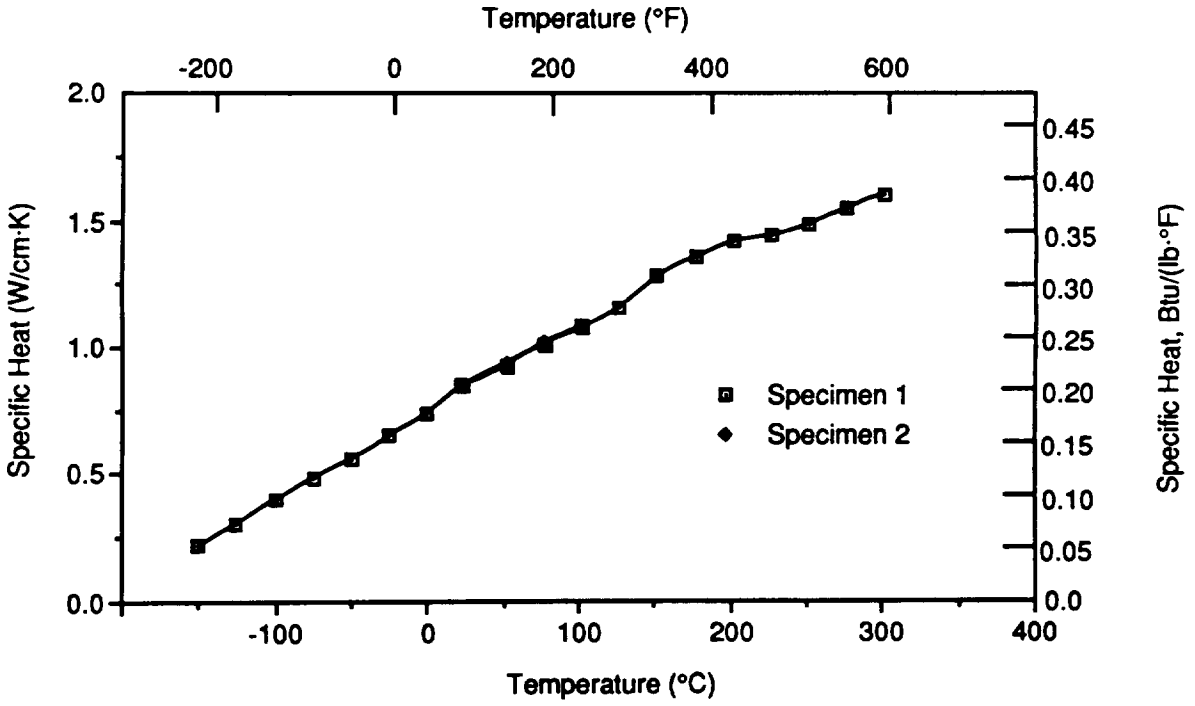

Figure 2.1-3 Specific Heat of P75/1962, $[0]_8$, v/o = 62.5

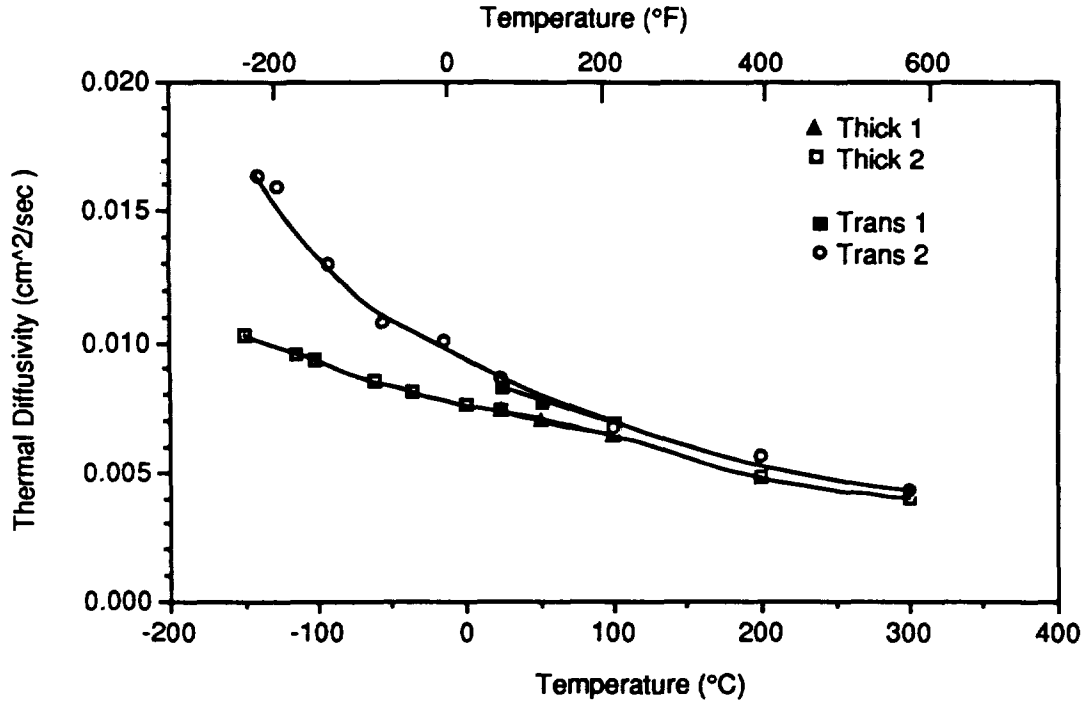

Figure 2.1-4 Thermal Diffusivity (Through Thickness and Transverse) of P75/1962, $[0]_8$, v/o = 62.5

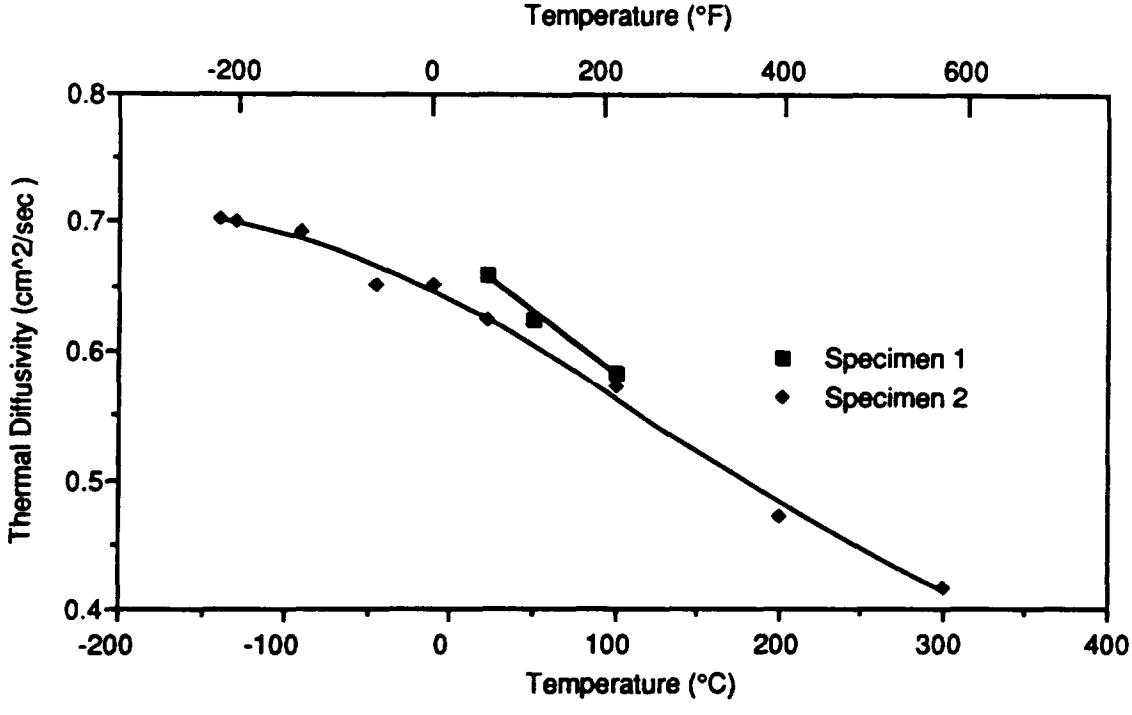

Figure 2.1-5 Thermal Diffusivity (Longitudinal) of P75/1962, $[0]_8$, v/o = 62.5

(d) Thermal Conductivity

Because Gr/E composites do not conduct electricity, thermal conductivity could not be obtained using the Kohlrausch method. Consequently, 0.5-in. x 0.5-in size specimens were stacked together to form a 0.2-in thick specimen to determine in-plane and through-thickness conductivity by laser flash technique.

From these measurements, the calculated thermal conductivity values are plotted in Figures 2.1-6 (thickness and transverse directions) and 2.1-7 (longitudinal direction). Like thermal diffusivity, longitudinal thermal conductivity (K_x) at RT 628.85 Btu·in/hr·ft^2·°F was significantly larger than K_y and K_z values of 8.5 Btu·in/hr·ft^2·°F.

2.2 QUASI-ISOTROPIC $[0, 45, 90, -45]_S$ AND ZERO-CTE $[30, -30, 0_4]_S$ FLAT PANELS

2.2.1 Fabrication Data

Material system:	P75/1962	P75/1962
Fiber Layup:	$[0, 45, 90, -45]_s$	$[30, -30, 0_4]_s$
ACPI: Processing Date:	4/29/88	5/4/88
Fabrication Process:	Vacuum bagged, and cured for 2 hrs at 350°F and 80 psi.	
Condition:	As-fabricated	As-fabricated
Dimensions:	12-in. x 12-in. x 0.037-in.	12-in. x 12-in. x 0.055-in.
Ply Thickness:	0.0046-in.	0.0046-in.

2.2.2 Product Evaluation

(a) Density

P75/1962,

$[0, 45, 90, -45]_s$	$[30, -30, 0_4]_s$
0.0624 lb/in^3	0.065 in/lb^3

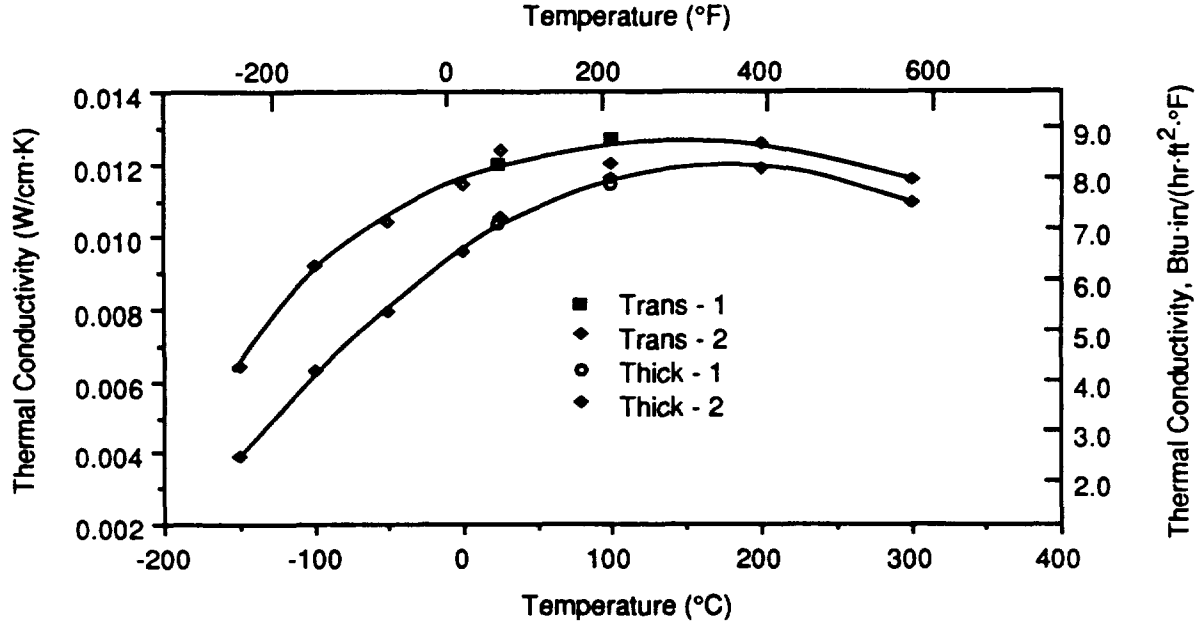

Figure 2.1-6 Thermal Conductivity (Through Thickness and Transverse) of P75/1962, $[0]_8$, v/o = 62.5

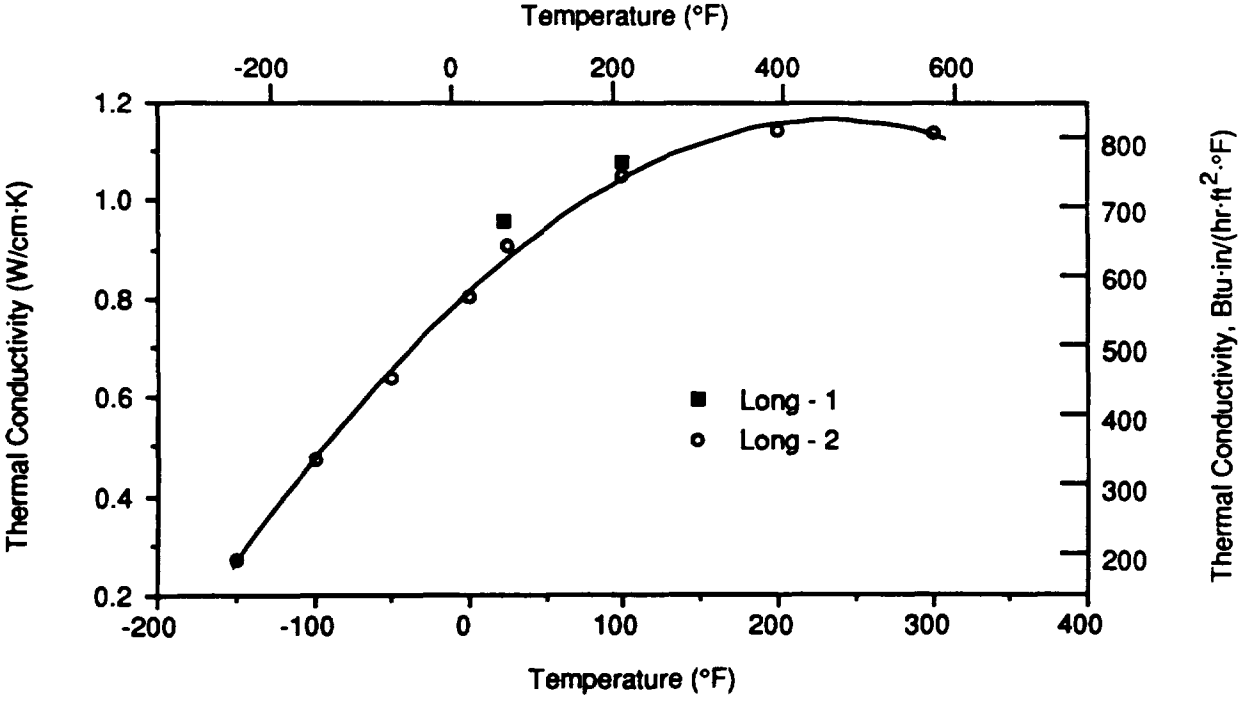

Figure 2.1-7 Thermal Conductivity (Longitudinal) of P75/1962, $[0]_8$, v/o = 62.5

(b) Fiber Volume

- P75/1962 $[0, 45, 90, -45]_S$: 62.2%

  Std. Dev.: 0.9

  Void Volume: ≤0.5%

- P75/1962 $[30, -30, 0_4]_S$: 63.7%

  Std. Dev.: 0.9

  Void Volume: ≤0.5%

(c) Non-Destructive Evaluation

Visual, X-radiographic and ultrasonic techniques were used to inspect P75/1962 laminate panels. Each panel appeared to be of good quality without any surface imperfections. X-radiographic examination revealed that fiber collimation in each panel was excellent and ultrasonic C-scans showed no major defects such as voids or delaminations.

(d) Microstructure

Typical microstructures of quasi-isotropic and zero-CTE laminates are shown in Figures 2.2-1 and 2.2-2 respectively. Each photomicrograph shows that the overall fiber-matrix distribution is quite uniform. Microstructural examination of quasi-isotropic laminate confirmed that the fiber layup was $[0, 45, 90, -45]_S$. Longitudinal and transverse micrographs revealed a few voids, particularly at the interply interfaces, and some microcracks in off-axis plies.

2.2.3 Mechanical Properties

(a) Tension

The tension test properties of quasi-isotropic and zero-CTE laminates are listed in Table 2.2-1 to 2.2-4. During these tests, each specimen exhibited linear elastic response until just before failure. As expected, measured modulus and strength values of $[30, -30, 0_4)_S$ laminate were

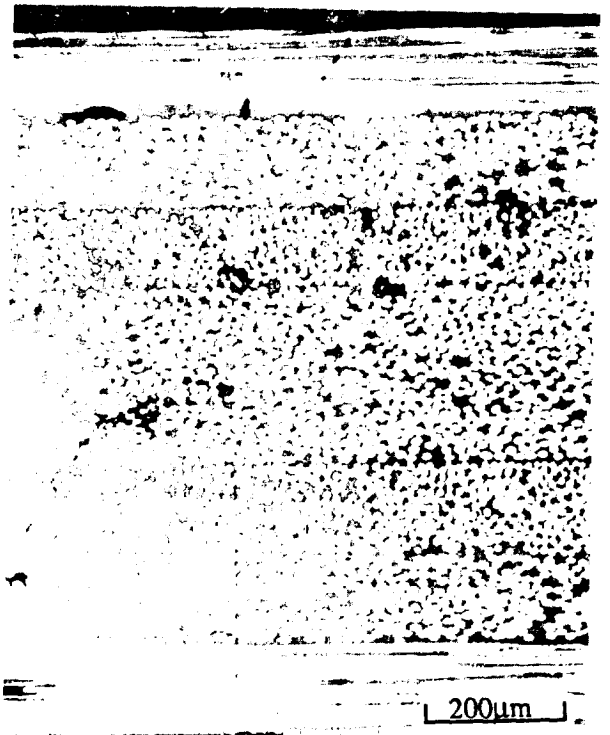

(a) Longitudinal

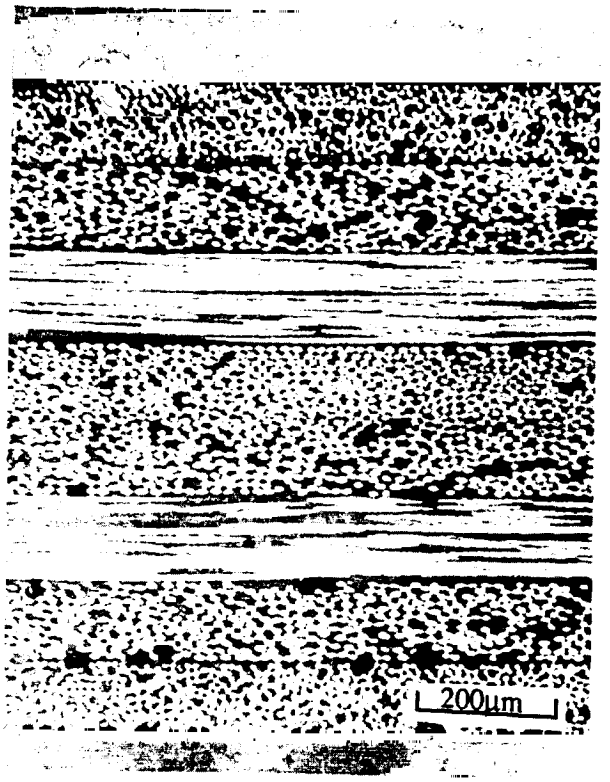

(b) Transverse

Figure 2.2-1 Longitudinal and Transverse Micrographs of Quasi-Isotropic P75/1962 Laminate Confirming the $[0, 45, 90, -45]_s$ Layup and Revealing a Few Voids at Interply Regions (100X)

(a) Longitudinal

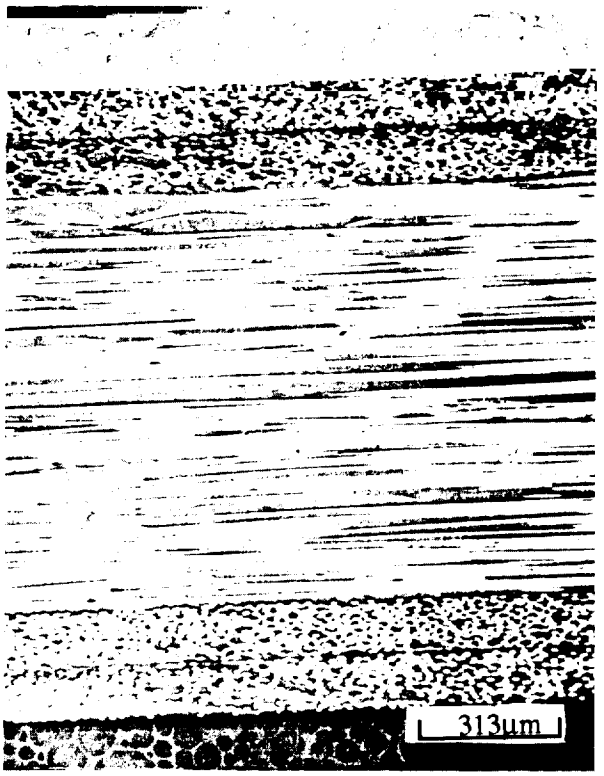

(b) Transverse

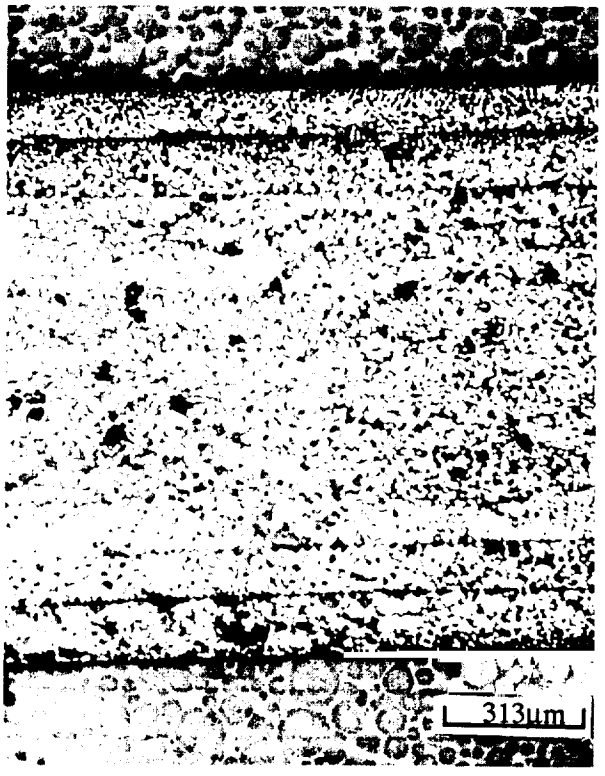

Figure 2.2-2 Longitudinal and Transverse Micrographs of Zero-CTE P75/1962 Laminate $[30, -30, 0_4]_s$ Revealing a Few Voids and Disbonds (64X)

Table 2.2-1 Longitudinal Tensile Properties of Quasi-isotropic P75/1962, $[0, +45, 90, -45]_S$, Fiber Volume = 62.4%.

Specimen # (GE)(PQ)(AP)	Elastic Modulus E_x^T (Msi)	Ultimate Tensile Strength (ksi)	Poisson Ratio ν_{xy}	Strain To Failure (%)
TNL-1	15.0	45.2	0.2982	0.277
TNL-2	15.6	46.9	0.3123	0.278
TNL-3	15.0	45.0	0.2871	0.226
TNL-4	14.9	45.2	0.3274	0.279
TNL-5	15.5	40.8	0.3078	0.244
Mean Value	15.2	44.6	0.3066	0.261
Std. Dev.	0.324	2.3	0.0151	0.024
CV (%)	2.1	5.1	4.9	9.4

Table 2.2-2 Transverse Tensile Properties of Quasi-isotropic P75/1962, $[0, +45, 90, -45]_S$, Fiber Volume = 62.4%.

Specimen # (GE)(PQ)(AP)	Elastic Modulus E_y^T (Msi)	Ultimate Tensile Strength (ksi)	Poisson Ratio ν_{yx}	Strain To Failure (%)
TNT-1	14.2	52.2	0.2902	0.317
TNT-2	16.0	55.4	0.3139	0.314
TNT-3	15.6	50.4	0.3505	0.297
TNT-4	15.3	49.8	0.3078	0.303
TNT-5	15.1	42.9	0.3106	0.273
Mean Value	15.2	50.1	0.3146	0.301
Std. Dev.	0.673	4.6	0.022	0.018
CV (%)	4.4	9.2	7.0	5.8

Table 2.2-3 Longitudinal Tensile Properties of Zero-CTE P75/1962, $[\pm 30, 0_4]_S$, Fiber Volume = 62.4%.

Specimen # (GE)(PZ)(AP)	Elastic Modulus E_x^T (Msi)	Ultimate Tensile Strength (ksi)	Poisson Ratio ν_{xy}	Strain To Failure (%)
TNL-1	32.6	91.11	1.2233	0.26
TNL-2	33.6	85.8	1.20	0.24
TNL-3	33.6	91.2	1.2253	0.255
TNL-4	30.9	73.8	1.200	0.2195
Mean Value	32.68	85.5	1.2122	0.243
Std. Dev.	1.27	8.2	0.014	0.018
CV (%)	3.9	9.6	1.2	7.4

Table 2.2-4 Transverse Tensile Properties of Zero-CTE P75/1962, $[\pm 30, 0_4]_S$, Fiber Volume = 62.4%.

Specimen # (GE)(PZ)(AP)	Elastic Modulus E_y^T (Msi)	Ultimate Tensile Strength (ksi)	Poisson Ratio ν_{yx}	Strain To Failure (%)
TNT-1	1.85	4.3	0.0839	0.228
TNT-2	1.79	4.6	0.0794	0.254
TNT-3	1.81	4.4	0.0860	0.24
TNT-4	1.80	4.2	0.0830	0.225
TNT-5	1.70	4.3	0.0802	0.247
Mean Value	1.79	4.4	0.0825	0.239
Std. Dev.	0.0552	0.152	0.0027	0.012
CV (%)	3.1	3.4	3.3	5.2

higher than the modulus and strength values of $[0, 45, 90, -45]_s$ laminate. Also, the longitudinal and transverse modulus and strength values in $[0, 45, 90, -45]_s$ were nearly similar, indicating the quasi-isotropic response. The fracture surface examination of each test specimen revealed overall adequate interfacial bond between the plies and no delaminations.

(b) Compression

The compression test results for $[0, 45, 90, -45]_s$ and $[30, -30, 0_4]_s$ layups are listed in Tables 2.2-5 to 2.2-8. These results indicate similar longitudinal and transverse moduli and strength values in the quasi-isotropic laminate. The typical compressive stress-strain response of longitudinal quasi-isotropic specimen (Figure 2.2-3) showed a deviation from linear response at about 30% of the compressive strength value. In the zero-CTE laminate, E_x^C was significantly larger than the transverse modulus, consistent with the predicted behavior.

(c) Flexure

Flexural modulus and strength values for the P75/1962 specimens using three point bend tests are listed in Table 2.2-9. The flexural modulus of highly anisotropic laminates is a critical function of ply stacking sequence and does not necessarily correlate with the tensile modulus. During flexure testing, the load-deflection response is primarily influenced by the outermost lamina subjected to a tensile stress state. Therefore, the longitudinal flexural modulus of $[0, 45, 90, -45]_s$ quasi-isotropic laminate with the outermost [0°] ply was higher than the transverse flexural modulus with a [90°] outer ply.

(d) Interlaminar Shear Strength (ILSS)

The apparent interlaminar shear strength values of both quasi-isotropic and zero-CTE laminates as determined by short beam shear-three point bend tests are listed in Table 2.2-10.

ILSS = 5.03 ksi for quasi-isotropic, and

ILSS = 6.38 ksi for zero-CTE laminate.

Table 2.2-5 Longitudinal Compressive Properties of Quasi-isotropic P75/1962, [0, +45, 90 -45]$_S$, Fiber Volume = 62.4%.

Specimen # (GE)(PQ)(AP)	Elastic Modulus E_x^C (Msi)	Ultimate Comp. Strength (ksi)	Poisson Ratio ν_{xy}	Strain To Failure (%)
CML-1	14.1	28.8	0.2730	*
CML-2	14.2	26.8	0.3625	0.315
CML-3	13.5	28.2	0.3041	*
CML-4	14.1	24.0	0.3326	0.479
CML-5	13.6	24.8	0.3675	*
Mean Value	13.9	26.5	0.3279	
Std. Dev.	0.3240	2.09	0.0399	
CV (%)	2.3	7.9	12.2	

Table 2.2-6 Transverse Compressive Properties of Quasi-isotropic P75/1962, [0, +45, 90 -45]$_S$, Fiber Volume = 62.4%.

Specimen # (GE)(PZ)(AP)	Elastic Modulus E_y^C (Msi)	Ultimate Comp. Strength (ksi)	Poisson Ratio ν_{yx}	Strain To Failure (%)
CMT-1	16.5	27.5	0.2952	*
CMT-2	13.5	29.3	0.3030	*
CMT-3	13.5	27.9	0.3289	*
CMT-4	13.9	26.9	0.3083	*
CMT-5	15.3	26.5	0.4047	*
Mean Value	14.54	27.6	0.3280	
Std. Dev.	1.32	1.07	0.0446	
CV (%)	9.08	3.9	13.6	

Table 2.2-7 Longitudinal Compressive Properties of Zero-CTE P75/1962, $[\pm 30, 0_4]_S$, Fiber Volume = 62.4%.

Specimen # (GE)(PZ)(AP)	Elastic Modulus E_x^C (Msi)	Ultimate Tensile Strength (ksi)	Poisson Ratio ν_{xy}	Strain To Failure (%)
CML-1	26.6	49.1	1.0545	0.2965
CML-2	28.2	52.4	1.2325	0.239
CML-3	26.9	55.3	1.2519	0.309
CML-4	29.5	55.82	1.2395	0.275
CML-5	27.0	58.93	1.1600	0.379
Mean Value	27.6	54.3	1.1877	0.2996
Std. Dev.	1.205	3.71	0.0826	0.052
CV (%)	4.4	6.8	6.95	17.2

Table 2.2-8 Transverse Compressive Properties of Zero-CTE P75/1962, $[\pm 30, 0_4]_S$, Fiber Volume = 62.4%.

Specimen # (GE)(PZ)(AP)	Elastic Modulus E_y^C (Msi)	Ultimate Tensile Strength (ksi)	Poisson Ratio ν_{yx}	Strain To Failure (%)
CMT-1	2.09	16.21	0.1012	†
CMT-2	1.87	18.5	0.1429	†
CMT-3	1.61	17.05	0.1239	1.085
CMT-4	1.60	17.35	0.1188	*
CMT-5	1.50	19.36	0.1171	*
Mean Value	1.73	17.7	0.1208	
Std. Dev.	0.2415	1.24	0.015	
CV (%)	14.	7.0	12.4	

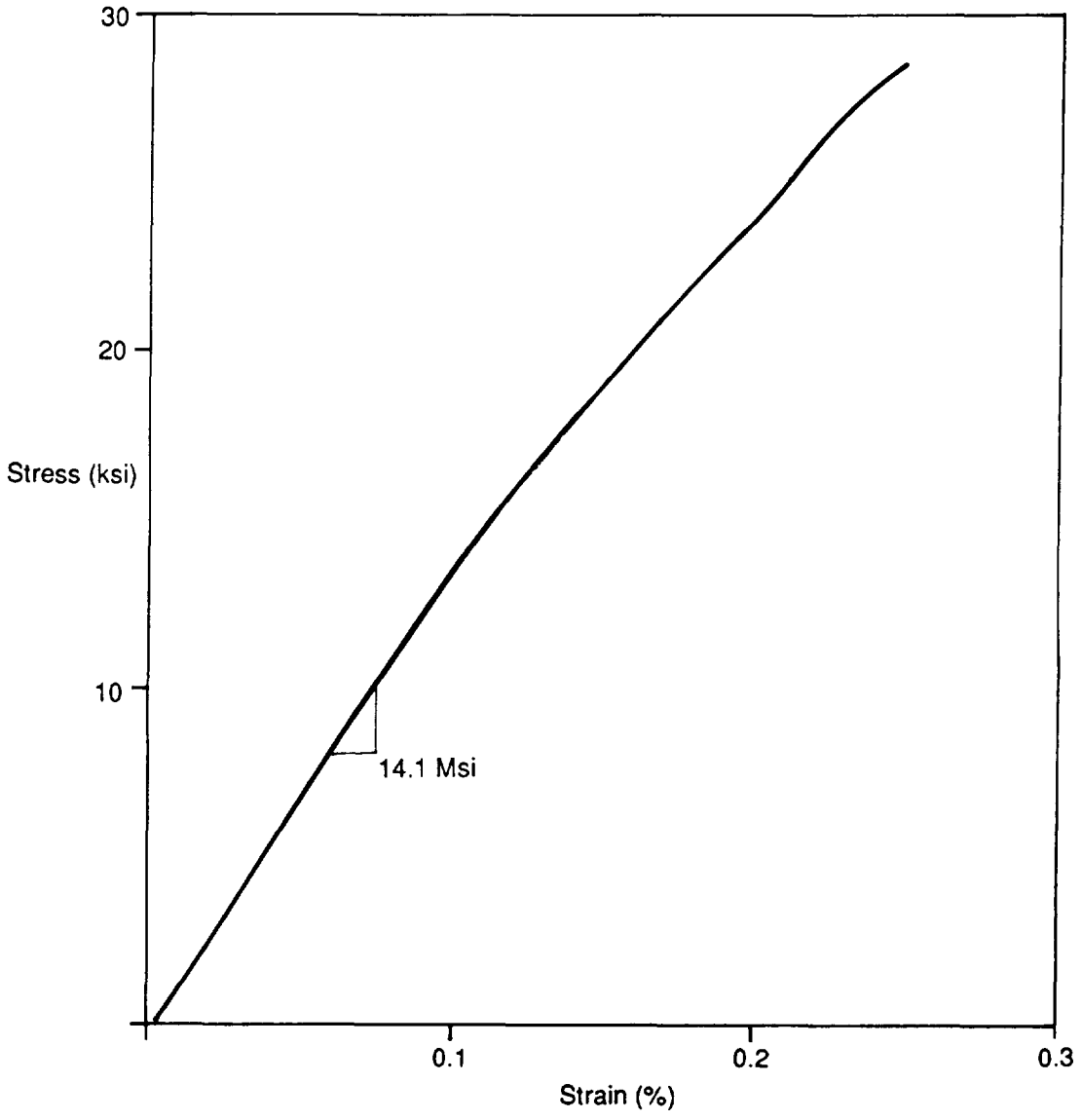

Figure 2.2-3 Typical Compressive Stress-Strain Response of P75/1962, [0, 45, 90, -45]$_S$, v/o = 62.2

Table 2.2-9 Longitudinal and Transverse Flexural Properties of Quasi-isotropic [0, +45, 90, -45]$_s$ and Zero-CTE [±30, 0$_4$]$_s$ P75/1962

Flat Panel[0,45,90,-45]$_s$, --SN 001Q: v/o=62.2			Flat Panel [30,-30,0$_4$]$_s$, --SN004 v/o=62.7		
Specimen # (GE)(PQ)(AP)	Longitudinal Flexural		Specimen # (GE)(PZ)(AP)	Longitudinal Flexural	
	Modulus (Msi)	Strength (ksi)		Modulus (Msi)	Strength (ksi)
FXL-51	15.83	74.10	FXL-51	14.98	94.88
FXL-52	14.20	61.84	FXL-52	14.36	93.84
FXL-53	15.49	66.57	FXL-53	14.35	92.20
Mean	15.17	67.5	Mean	14.56	93.64
Standard Deviation	0.859	6.18	Standard Deviation	0.3609	1.351
CV(%)	5.7	9.2	CV(%)	2.5	1.4
Specimen # (GE)(PQ)(AP)	Transverse Flexural		Specimen # (GE)(PZ)(AP)	Transverse Flexural	
	Modulus (Msi)	Strength (ksi)		Modulus (Msi)	Strength (ksi)
FXT-71	6.52	49.25	FXT-71	1.99	18.24
FXT-72	6.00	54.72	FXT-72	1.92	20.14
FXT-73	6.54	52.11	FXT-73	1.80	20.29
Mean	6.35	52.03	Mean	1.90	19.56
Standard Deviation	0.306	2.736	Standard Deviation	0.096	1.143
CV(%)	4.8	5.3	CV(%)	5.1	5.8

Table 2.2-10 Longitudinal and Transverse Apparent Interlaminar Shear Strength Properties of Quasi-isotropic [0, +45, 90, -45]$_s$ and Zero-CTE [±30, 0$_4$]$_s$ P75/1962

P75/1962 [0,45,90,-45]$_s$		P75/1962 [30,-30,0$_4$]$_s$	
Specimen # (GE)(PQ)(AP)	ILSS (ksi)	Specimen # (GE)(PQ)(AP)	ILSS (ksi)
IL-1Q1	5.01	IL-1	6.56
IL-1Q3	5.08	IL-3	6.54
IL-1Q5	4.76	IL-5	6.35
IL-1Q7	5.25	IL-7	6.64
IL-1Q9	5.35	IL-9	6.10
IL-1Q11	4.56	IL-11	6.20
IL-1Q13	5.36	IL-13	6.56
IL-1Q15	5.17	IL-15	6.32
IL-1Q17	4.99	IL-17	6.20
IL-1Q19	4.81	IL-19	6.33
Mean Value	5.03	Mean Value	6.38
Std. Dev.	0.264	Std. Dev.	0.185
CV %	5.25	CV %	2.9

2.2.4 Thermophysical Properties

(a) Thermal Expansion

For the quasi-isotropic and zero-CTE laminates the thermal expansion response curves over the first cycle (RT → 150° → -150° → RT) are shown in Figure 2.2-4 to 2.2-7. These results indicating CTE, strain hysteresis, and residual strain are summarized in Table 2.2-11. For the quasi-isotropic laminate, the longitudinal and transverse CTE should be nearly the same, whereas the measured values were -0.454 ppm/°F (CTE_x) and -0.014 ppm/°F (CTE_y) respectively. These differences in CTE are attributed to the first cycle response which is significantly influenced by the residual stress state in the composites. A quasi-isotropic CTE should be expected when the residual stresses are relieved in the subsequent thermal cycles.

(b) Specific Heat

Specific heat results are plotted in Figure 2.2-8. For both the quasi-isotropic and zero-CTE laminates, the specific heat values (0.193 Btu/lb·°F at RT) were nearly identical.

(c) Thermal Diffusivity

In-plane and through-the-thickness thermal diffusivity results are plotted in Figure 2.2-9. The diffusivity values in the through-the-thickness direction were about 10% different between quasi-isotropic and zero-CTE laminates. As expected, the diffusivity values for the quasi-isotropic material in the longitudinal and transverse directions were about the same. The diffusivity values for zero-CTE material in the transverse direction were between those for the through-the-thickness and longitudinal directions, but closer to the through-the-thickness values. In each case, the thermal response was consistent with the expected response for the specific fiber orientation.

(d) Thermal Conductivity

The calculated thermal conductivity results at temperatures between -200°F and 750°F are plotted in Figure 2.2-10. For the zero-CTE laminate $K_x > K_y \approx K_z$, and for the quasi-isotropic

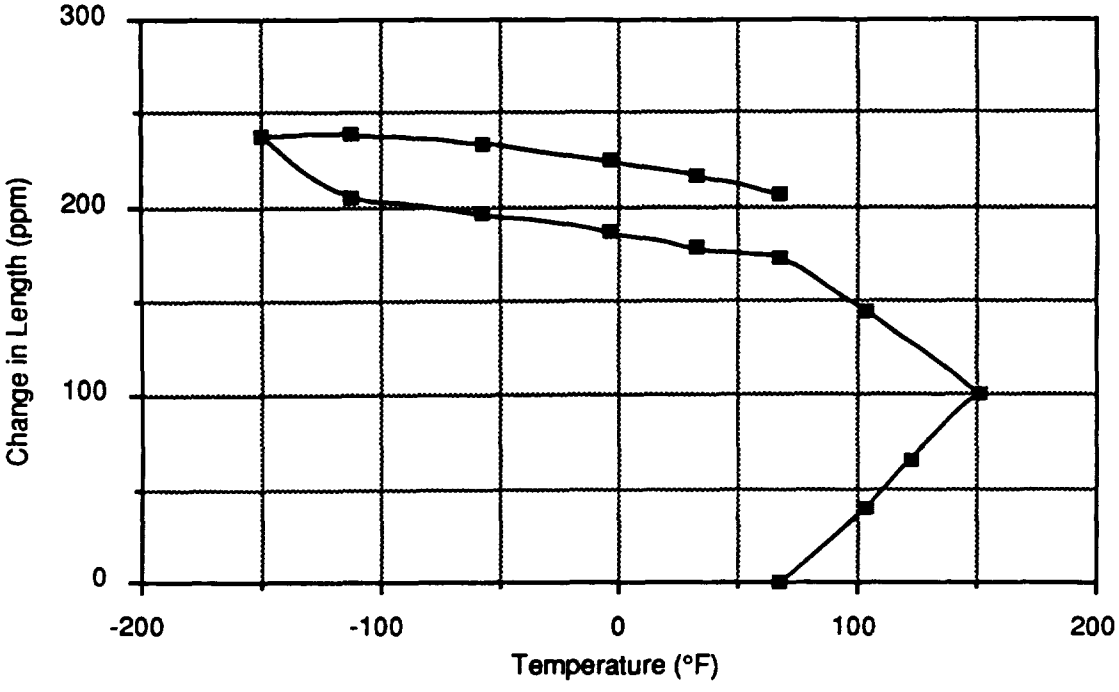

Figure 2.2-4 Longitudinal Thermal Expansion Behavior of Quasi-isotropic, $[0, 45, 90, -45]_S$, P75/1962 in a Heat/Cool/Heat Cycle using Push Rod Dilatometer

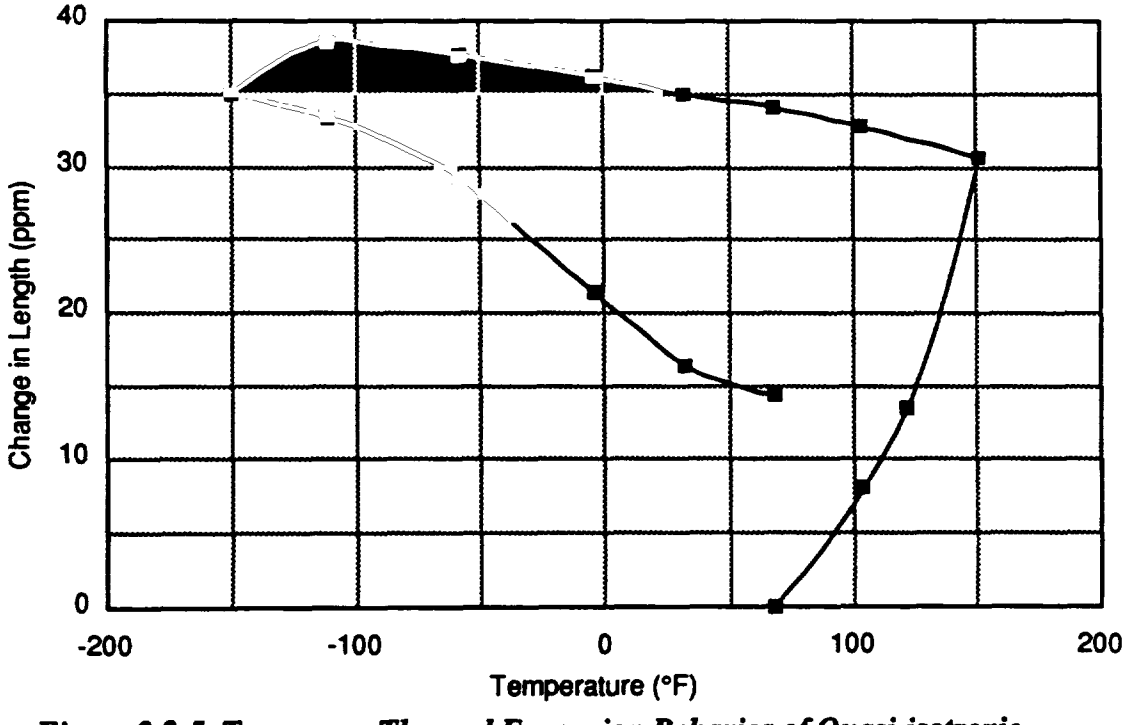

Figure 2.2-5 Transverse Thermal Expansion Behavior of Quasi-isotropic, $[0, 45, 90, -45]_S$, P75/1962 in a Heat/Cool/Heat Cycle using Push Rod Dilatometer

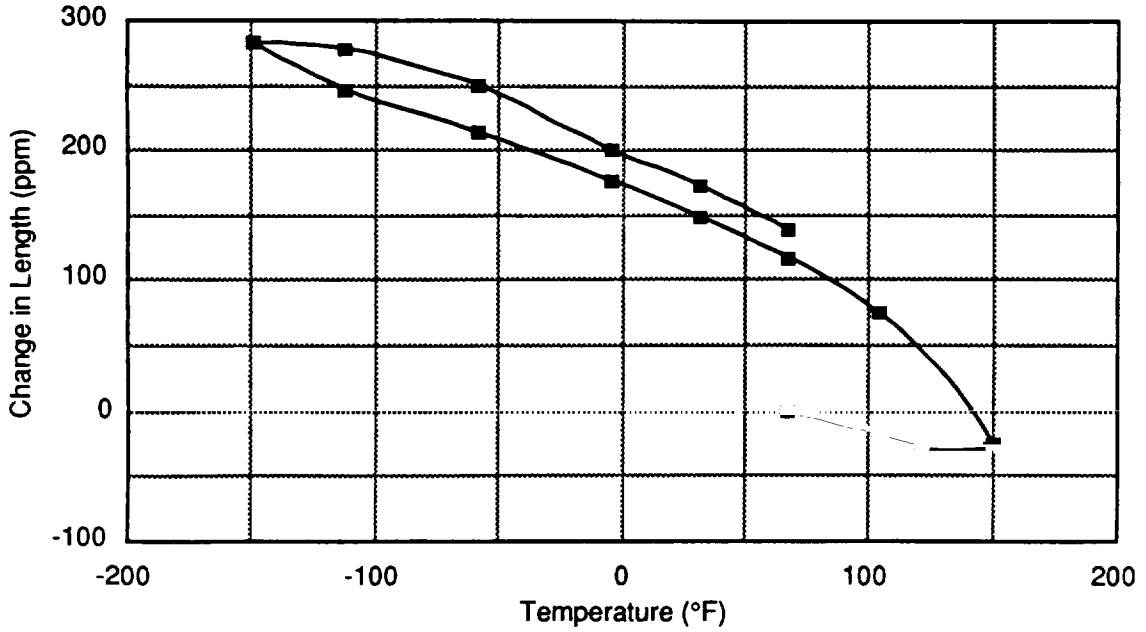

Figure 2.2-6 Longitudinal Thermal Expansion Behavior of $[\pm 30, 0_4]_S$, P75/1962 in a Heat/Cool/Heat Cycle using Push Rod Dilatometer

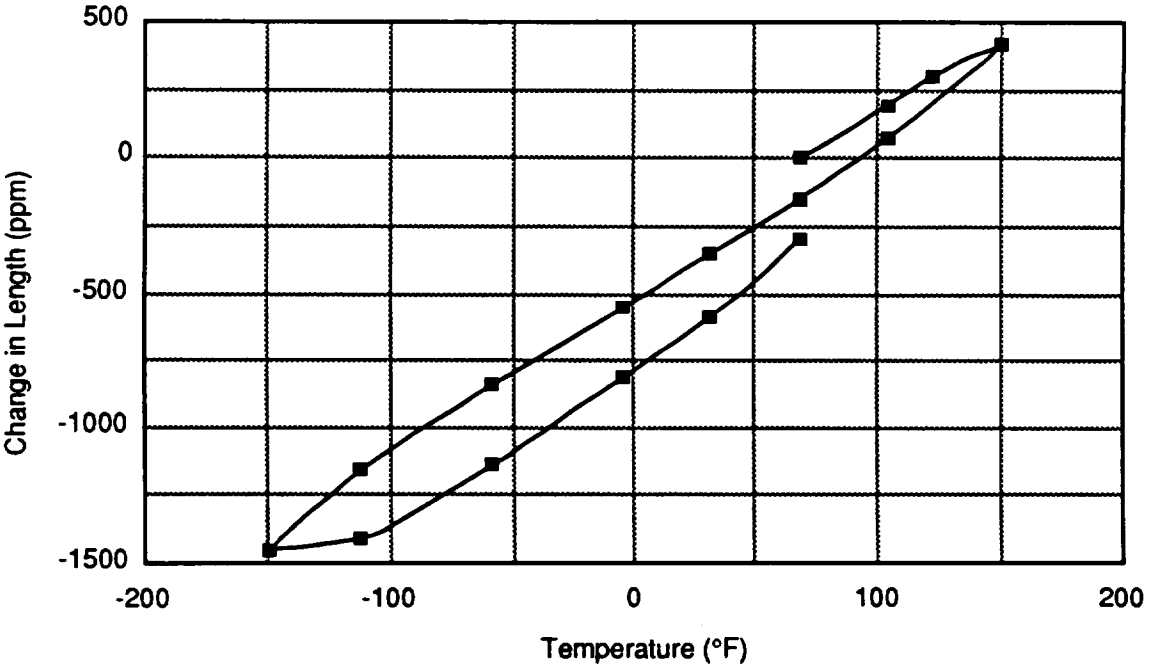

Figure 2.2-7 Transverse Thermal Expansion Behavior of $[\pm 30, 0_4]_S$, P75/1962 in a Heat/Cool/Heat Cycle using Push Rod Dilatometer

Table 2.2-11 Thermal Expansion Response of P75/1962 Composites

Thermal Expansion Measurements	P75/1962 $[0, \pm 45, 90]_s$ $V_f = 0.622$		P75/1962 $[30, -30, 0_4]_s$ $V_f = 0.622$		P75/1962 $[0_8]$ $V_f = 0.625$
	Longitudinal	Transverse	Longitudinal	Transverse	Longitudinal
CTE (ppm/°F)*	-0.454	-0.014	-1.02	5.83	-0.689
Residual strain (ppm)	206.3	14.38	138.0	-297.5	154.26
Strain Hysteresis (ppm)†	172.6	34.1	116.7	-150.5	98.81

*(end to end point average), † at RT(i.e., RT→150°F→RT)

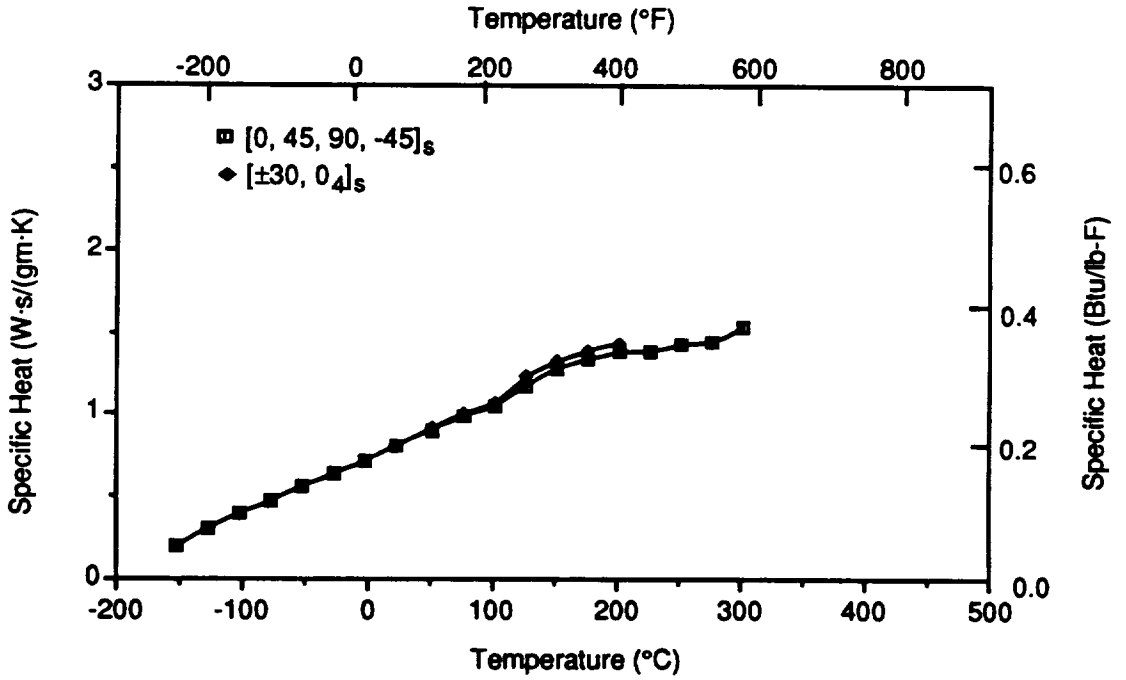

Figure 2.2-8 Specific Heat as a Function of Temperature for Quasi-isotropic and Zero-CTE P75/1962

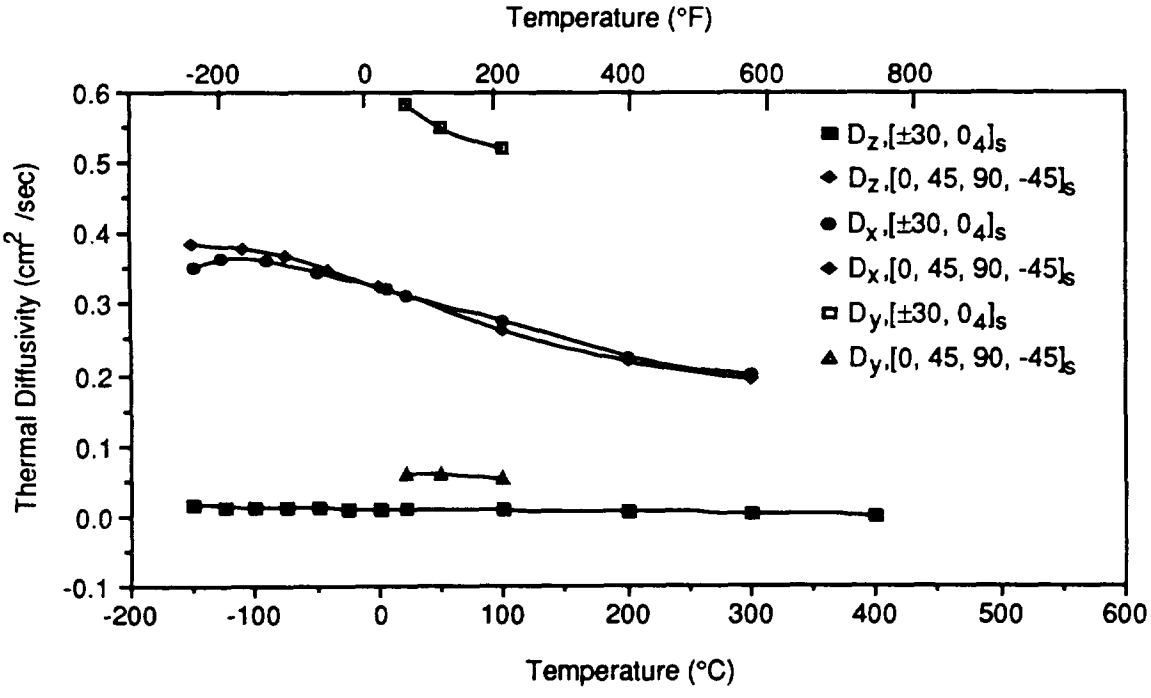

Figure 2.2-9 Thermal Diffusivity as a Function of Temperature for Quasi-isotropic and Zero-CTE P75/1962

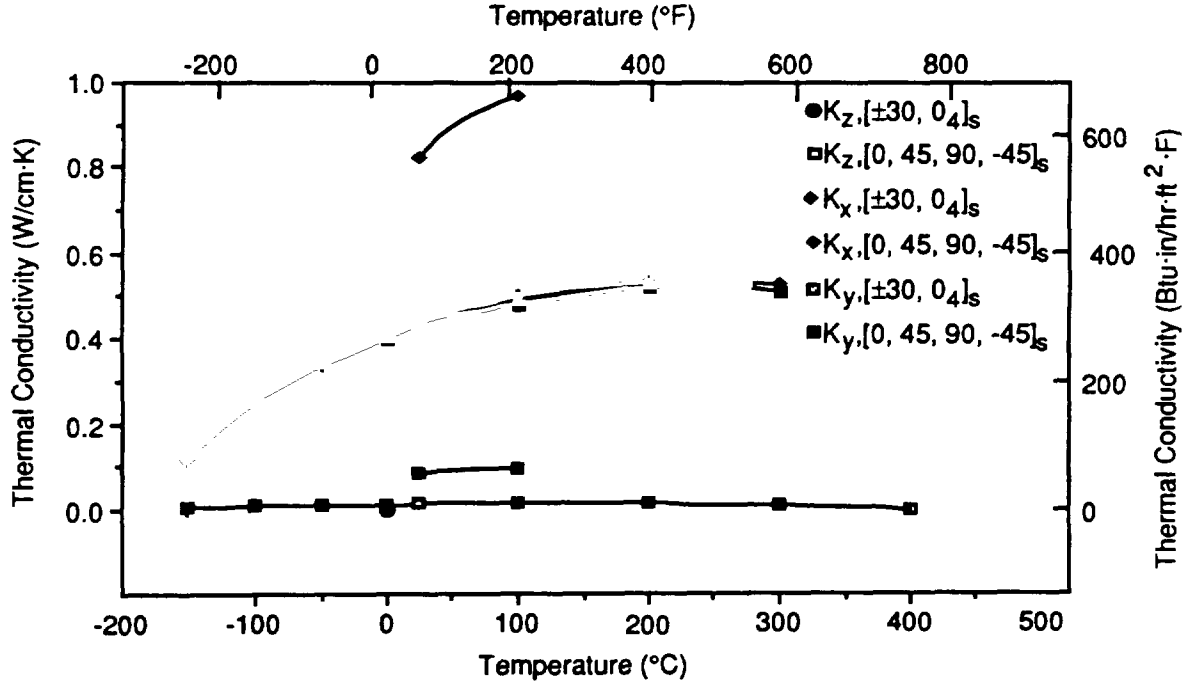

Figure 2.2-10 Thermal Conductivity of Quasi-isotropic and Zero-CTE P75/1962 as a Function of Temperature

C-2

laminate the in-plane conductivities (K_x and K_y) were nearly similar. These measurements were consistent with the expected response for each laminate.

(e) Optical Properties

•The solar absorptance (α_s) and normal emissivity (ε_N) values of the as fabricated quasi-isotropic and zero-CTE laminates are quite similar:

(1) quasi-isotropic: α_s - 0.905

ε_N - 0.78

(2) Zero-CTE laminate: α_s - 0.895

ε_N - 0.79

•Reflectance vs. Wavelength - Typical Fourier Transform-Infrared (FTIR) diffuse reflectance spectra of as-received quasi-isotropic and zero-CTE layup flats are shown in Figure 2.2-11 and 2.2-12 respectively. These measurements in the 2.0 to 14.0 μm wavelength region were taken for specimens oriented longitudinally and transversely. In the case of quasi-isotropic layup, a slight increase in reflectance was observed in a specimen oriented longitudinally (Figure 2.2-13). Also, the average reflectance of quasi-isotropic specimens was consistently higher than the zero-CTE specimens. These measurements indicated that at 10.6 μm, average emissivity of quasi-isotropic flats was 0.6 and of zero-CTE layup was 0.8.

2.3 P75/ERLX 1962 TUBES

2.3.1 Fabrication Data

P75/ERLX 1962 tubes with $[30, -30, 0_4]_s$ fiber layup, were cured in an air circulating oven at 355°F for 2 hours. Cure processing was applied via a controlled tension tape wrap system. These 12 ply Gr/Epoxy tubes were fabricated at Advanced Composite Products, Inc, CT, (on 5/20/88).

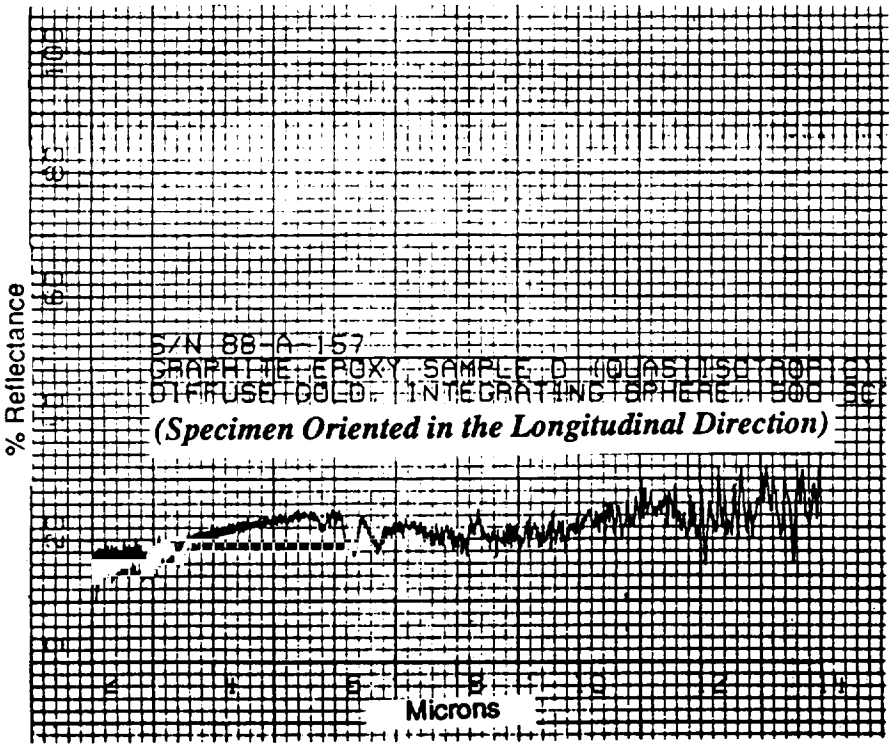

Figure 2.2-11 FTIR Diffuse Reflectance Spectra for Quasi-isotropic P75/1962

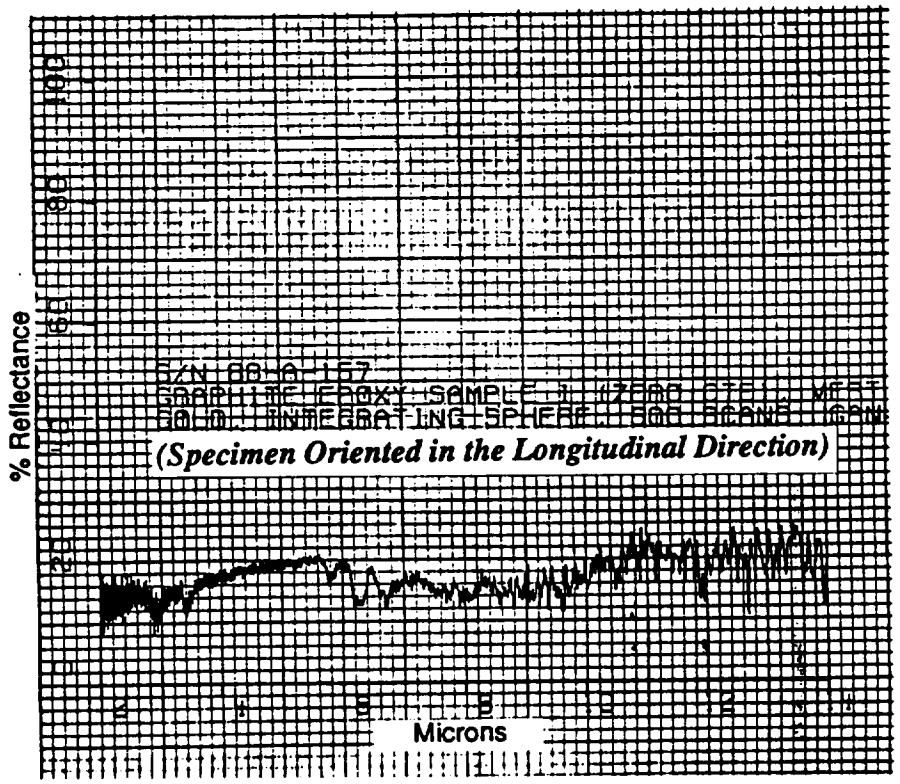

Figure 2.2-12 FTIR Diffuse Reflectance Spectra for Zero-CTE P75/1962

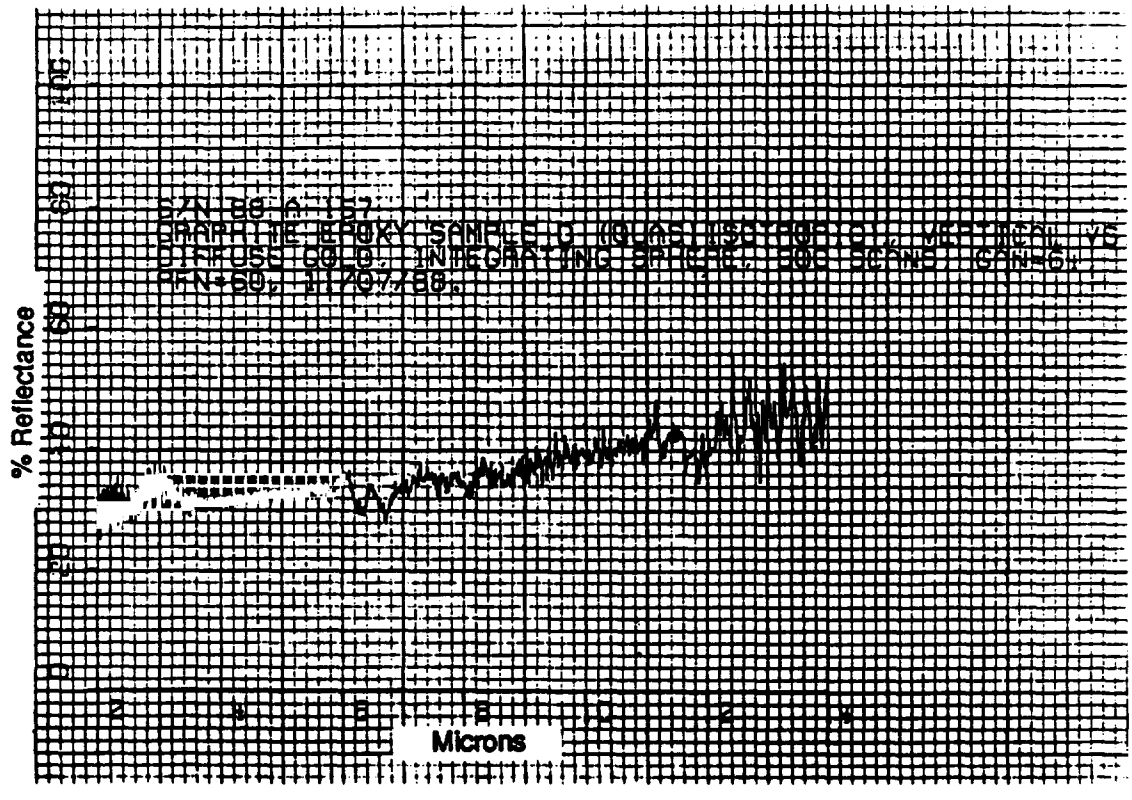

Figure 2.2-13 FTIR Diffuse Reflectance Spectra for Quasi-isotropic P75/1962 (Specimen Oriented in the Longitudinal Direction)

2.3.2 Product Evaluation

(a) Dimensional Inspection:

The tube dimensions including length, wall thickness, outer diameter (OD) and bow are listed in Table 2.3-1.

(b) Density:

P75/1962 tube density: 0.0611 lb/in^3

Std. Dev.: 0.007

(c) Fiber Volume Analysis

Table 2.3-2 lists the fiber volume and specific gravity values that were obtained by analyzing random specimens cut from each tube.

(d) Non-Destructive Examination

Visual examination of I.D and O.D. surfaces revealed that each tube had good overall quality. X-radiographic examination indicated good fiber collimation with a few voids, disbonds, and microcracks.

2.3.3 Mechanical Properties

(a) Tension and Compression

Tensile and compressive properties of these P75/1962 $[30, -30, 0_4]_S$, v/o 59.9 are listed in Table 2.3-3 and 2.3-4 respectively.

Table 2.3-1 Dimensions of Zero-CTE P75/1962 Tubes

	Tube Number		
	SN-1	SN-2	SN-3
Length	48-in.	48-in.	48-in.
Wall Thickness	0.058-in./0.062-in.	0.061-in./0.064-in.	0.061-in./0.065-in.
Inside Diameter	1.00-in./0.0998-in.	1.00-in./0.0998-in.	1.00-in./0.0998-in.
Outside Diameter	1.132-in./1.122-in.	1.128-in./1.122-in.	1.128-in./1.122-in.
Weight	287 gm (0.633 lb)	293 gm	284 gm
Bow	0.03-in.	0.05-in.	0.06-in.

Table 2.3-2 Fiber Volume, Void Volume, and Specific Gravity of Zero-CTE P75/1962 Tubes

Specimen #	Fiber Volume (%)	Void Volume (%)	Specific Gravity
1	61.3	0	1.70
2	61.6	0	1.70
3	60.3	0	1.69
4	58.7	0	1.69
5	57.7	0	1.69
6	59.7	0	1.68
Average	59.9	0	1.69

Table 2.3-3 Tension Test Results of P75/ERLX 1962 [30, -30, 0_4]$_s$, v/o 59.9 Tube

Speciment # (GE)(PZ)(AT)	Elastic Modulus† (Msi)				Ultimate Tensile Strength (ksi)	Strain To Failure (%)	Poisson Ratio
	E_{X1}	E_{X2}	E_{X3}	E_X			
TNL-1	32.3	31.3	32.6	32.1	> 59.9*	> 0.19	1.2581
TNL-2	33.0	32.3	32.9	32.7	> 64.6*	> 0.2	1.3038
TNL-3	33.4	32.2	32.2	32.8	> 52.4*	> 0.18	1.2448
Mean				32.5	> 59.0		1.2689
Std. Dev.				0.378	6.15		0.0309
CV (%)				1.2	10.4		2.4

† One biaxial (#1) and two uniaxial (#243) strain gages were placed 120° apart.
* Each specimen exhibited a bond line failure.

Table 2.3-4 Compression Test Results of P75/ERLX 1962 [30, -30, 0_4]$_2$, v/o 59.9 Tube

Speciment # (GE)(PZ)(AT)	Elastic Modulus† (Msi)				Ultimate Comp. Strength (ksi)	Strain To Failure (%)	Poisson Ratio
	E_{X1}	E_{X2}	E_{X3}	E_X			
CML-1	31.3	24.1	24.1	26.5	49.8	0.274	1.283
CML-2	31.1	31.1	25.1	29.1	47.0	0.229	1.293
CML-3	19.6	31.8	31.8	27.7	45.3	0.233	1.044
Mean				27.8	47.4	0.245	1.206
Std. Dev.				1.301	2.27	0.0249	0.141
CV (%)				4.7	4.8	10.2%	11.7

During tension test, each specimen showed a bond line failure suggesting that actual tensile strength and strain to failure values were greater than the measure values. Still, the elastic modulus and poisson ratios were consistent with the corresponding values obtained for zero-CTE flat laminates.

During compression test, each specimen showed failure initiating along ±30° fibers, leading to final bucking failure of [0°] fibers. While the measured elastic modulus from the stress-strain from one biaxial (#1) and two uniaxial strain gages showed significant variation, still the average modulus, strength, strain to failure, and poisson ratio values were similar to the values obtained for zero-CTE flat laminates.

(b) Hoop Properties

The NOL bursting ring test was used to measure the hoop modulus, strength and strain to failure. During the test, an internal pressure (P) was gradually applied to each ring (with radius, r and thickness, t) specimen and hoop strength (F_{TH}) and hoop modulus (E_{TH}) were determined by:

$$F_{TH} = P_u r/t \quad \text{and} \quad E_{TH} = P_\varepsilon r/\varepsilon_t \text{ respectively,}$$

where ε = strain, P_ε is the internal pressure corresponding to ε, and P_u is the internal pressure at failure,

The results for P75/1962 Epoxy composites are listed in Table 2.3-5 indicating an average hoop strength of 4.1 ksi.

(c) Torsion

The shear modulus and ultimate shear stress values obtained from the torsion test of tubes are listed in Table 2.3-6. Near the average 12.0 ksi failure shear stress level, these tubes exhibited a few longitudinal and axial cracks that were visible with the unaided eye.

Table 2.3-5 NOL Burst Ring Test Data for P75/1962 Composite Tube

Material	Area (in^2)	Ultimate (psi) Pressure	Hoop Stress F_{TH} = Pr/t (ksi)	Modulus E_H (Msi)	Strain to Failure
P75 Gr/Epoxy 1962 ERLX	0.2278 (6.3%)†	584.5 (20.7%)	4.1 (16.3%)	1.53 (10%)	0.00286 (15.1%)

† Precentage coefficientof variation

Table 2.3-6 Shear Properties of Zero-CTE P75/1962 Tubes By Torsion Test

Tube I.D. No.	Area (in^2)	Shear Stress (ksi)	Shear Modulus (Msi)
TO1-3	0.2139	11.9	2.5
TO2-3	0.2143	12.6	2.2
TO3-2	0.2151	11.7	2.3
Average	0.2144	12.1	2.33
Standard Deviation	0.0006	0.473	0.153
CV (%)	0.3	3.9	6.6

2.4 SUMMARY OF P75/1962 TEST DATA

All the mechanical and thermophysical property test data of unidirectional and quasi-isotropic panels, and zero-CTE laminate panels and tubes are summarized in Table 2.4-1 to 2.4-4.

Table 2.4-1 P75/1962 Graphite/Epoxy (Unidirectional Panel)

NOT DESIGN ALLOWABLE DATA

PROPERTIES												TEMPERATURE (°F)			Std. Dev. / No. of Specimens at RT	Test Method
PHYSICAL			MECHANICAL & THERMAL									Low	Room	High		
Density (lb / in^3)		0.0623	Longitudinal Tensile Strength	σ_x^{TU}	ksi								123.5		±8.43 / 5	ASTM D-3039
Fiber volume fraction		0.625	Transverse Tensile Strength	σ_y^{TU}	ksi								2.0			ASTM D-3039
Void volume fraction		≤0.5	Longitudinal Comp. Strength	σ_x^{CU}	ksi								63.43		±3.12 / 5	ASTM D-3410
Nominal ply thickness	in	0.0046	Transverse comp. strength	σ_y^{CU}	ksi								—			ASTM D-3410
Max. cont. use temp.	°F	260	In-plane shear strength	IPSS	ksi								6.677		±0.224 / 4	10° Off Axis
Ply Orientation	θ	$[0]_8$	Interlaminar shear strength	ILSS	ksi								7.31		±0.370 / 7	ASTM D-2344
OPTICAL & ELECTRICAL (at room temperature)			Longitudinal tensile strain **	ε_x^T	%								0.266		±0.0096 / 5	ASTM D-3039
Solar Absorptance	α_s		Transverse tensile strain **	ε_y^T	%											ASTM D-3039
Normal Emissivity	ε_N		Longitudinal comp. strain **	ε_x^C	%								0.198		±0.0395 / 5	ASTM D-3410
			Transverse comp. strain **	ε_y^C	%											ASTM D-3410
			Longitudinal tensile modulus	E_x	Msi								46.3		±2.063 / 5	ASTM D-3039
			Transverse tensile modulus	E_y	Msi								0.7			ASTM D-3039
			Longitudinal comp. modulus	E_x	Msi								36.3		±1.542 / 5	ASTM D-3410
			Transverse comp. modulus	E_y	Msi								—			ASTM D-3410
			In-plane shear modulus	G	Msi								1.67		±0.159 / 4	10° Off-Axis
			Longitudinal flexural modulus	F_x	Msi								26.2		±1.767 / 2	ASTM D-790M
			Transverse flexural modulus	F_y	Msi								0.96		±0.566 / 2	ASTM D-790M
			Long. tensile Poisson's ratio	ν_{xy}									0.298			ASTM D-3039
			Trans. tensile Poisson's ratio	ν_{yx}												ASTM D-3039
			Long. thermal conductivity	K_x	(1)								4.37			Kohlrausch
			Trans. thermal conductivity	K_y	(1)								0.058			Kohlrausch
			Thru thickness thermal cond.	K_z	(1)								0.049			
			Specific heat	C_p	(2)								0.203			ASTM E-1269
			Longitudinal CTE	α_x	(3)								-0.69			ASTM E-228
			Transverse CTE	α_y	(3)								—			ASTM E-228
			Thru thickness CTE	α_z	(3)											

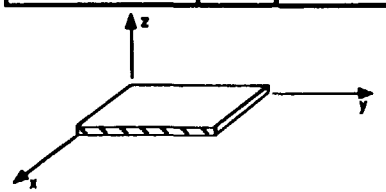

Notes:
(**) - Strain to failure; (1) Btu/(hr·in·°F); (2) Btu/(lb·°F); (3) μin./in./°F

Table 2.4-2 P75/1962 Graphite/Epoxy [0, 45, 90, -45]$_s$

NOT DESIGN ALLOWABLE DATA

PROPERTIES					TEMPERATURE (°F)			Std. Dev. / No. of Specimens at RT	Test Method
PHYSICAL			MECHANICAL & THERMAL			Low	Room	High		
Density (lb / in^3)		0.0624	Longitudinal Tensile Strength	σ_x^{TU}	ksi		44.6		± 2.3 / 5	ASTM D-3039
Fiber volume fraction		0.622	Transverse Tensile Strength	σ_y^{TU}	ksi		50.1		± 4.6 / 5	ASTM D-3039
Void volume fraction		—	Longitudinal Comp. Strength	σ_x^{CU}	ksi		26.5		2.09 / 5	ASTM D-3410
Nominal ply thickness	in	0.00463	Transverse comp. strength	σ_y^{CU}	ksi		27.6		1.07 / 5	ASTM D-3410
Max. cont. use temp.	°F	260	In-plane shear strength	IPSS	ksi					
Ply Orientation	θ	[0/±45/90]s	Interlaminar shear strength	ILSS	ksi		5.03		± 0.264 / 10	ASTM D-2344
OPTICAL & ELECTRICAL (at room temperature)			Longitudinal tensile strain **	ε_x^T	%		0.261		± 0.024 / 5	ASTM D-3039
Solar Absorptance	α_s	0.905	Transverse tensile strain **	ε_y^T	%		0.301		± 0.018 / 5	ASTM D-3039
Normal Emissivity	ε_N	0.78	Longitudinal comp. strain **	ε_x^C	%		-0.345		—	ASTM D-3410
			Transverse comp. strain **	ε_y^C	%		-0.30		—	ASTM D-3410
			Longitudinal tensile modulus	E_x	Msi		15.2		± 0.324 / 5	ASTM D-3039
			Transverse tensile modulus	E_y	Msi		15.2		± 0.673 / 5	ASTM D-3039
			Longitudinal comp. modulus	E_x	Msi		13.9		0.3240 / 5	ASTM D-3410
			Transverse comp. modulus	E_y	Msi		14.54		1.32 / 5	ASTM D-3410
			In-plane shear modulus	G	Msi					
			Longitudinal flexural modulus	F_x	Msi		15.17		± 0.859 / 3	ASTM D-790M
			Transverse flexural modulus	F_y	Msi		6.35		± 0.306 / 3	ASTM D-790M
			Long. tensile Poisson's ratio	ν_{xy}			0.3066		± 0.0151 / 5	ASTM D-3039
			Trans. tensile Poisson's ratio	ν_{yx}			0.3146		± 0.022 / 5	ASTM D-3039
			Long. thermal conductivity	K_x	(1)		2.1			Kohlrausch
			Trans. thermal conductivity	K_y	(1)		2.11			Kohlrausch
			Thru thickness thermal cond.	K_z	(1)		0.065			
			Specific heat	C_p	(2)		0.193			ASTM E-1269
			Longitudinal CTE	α_x	(3)		-0.454			ASTM E-228
			Transverse CTE	α_y	(3)		-0.014			ASTM E-228
			Thru thickness CTE	α_z	(3)		—			

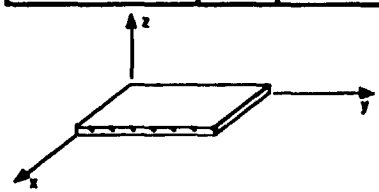

Notes:
(**) - Strain to failure; (1) Btu/(hr·in·°F); (2) Btu/(lb·°F); (3) μin./in./°F

Table 2.4-3 P75/1962 Graphite/Epoxy [±30, 0_4]$_s$

NOT DESIGN ALLOWABLE DATA

PROPERTIES						TEMPERATURE (°F)				
PHYSICAL			MECHANICAL & THERMAL			Low	Room	High	Std. Dev. / No. of Specimens at RT	Test Method
Density (lb / in^3)		0.0625	Longitudinal Tensile Strength	σ_x^{TU}	ksi		85.5		± 8.2 / 4	ASTM D-3039
Fiber volume fraction		0.627	Transverse Tensile Strength	σ_y^{TU}	ksi		4.4		±0.152 / 5	ASTM D-3039
Void volume fraction		—	Longitudinal Comp. Strength	σ_x^{CU}	ksi		54.3		±3.71 / 5	ASTM D-3410
Nominal ply thickness	in	0.00458	Transverse comp. strength	σ_y^{CU}	ksi		17.7		±1.24 / 5	ASTM D-3410
Max. cont. use temp.	°F	260	In-plane shear strength	IPSS	ksi					
Ply Orientation	θ	[30/-30/04]s	Interlaminar shear strength	ILSS	ksi		6.38		±0.185 / 10	ASTM D-2344
			Longitudinal tensile strain **	ε_x^T	%		0.243		±0.018 / 4	ASTM D-3039
OPTICAL & ELECTRICAL (at room temperature)			Transverse tensile strain **	ε_y^T	%		0.239		±0.012 / 5	ASTM D-3039
Solar Absorptance	α_s	0.895	Longitudinal comp. strain **	ε_x^C	%		0.30		±0.052 / 5	ASTM D-3410
Normal Emissivity	ε_N	0.79	Transverse comp. strain **	ε_y^C	%		—			ASTM D-3410
			Longitudinal tensile modulus	E_x	Msi		32.68		±1.27 / 4	ASTM D-3039
			Transverse tensile modulus	E_y	Msi		1.79		±0.0552 / 5	ASTM D-3039
			Longitudinal comp. modulus	E_x	Msi		27.64		±1.205 / 5	ASTM D-3410
			Transverse comp. modulus	E_y	Msi		1.73		±0.2415 / 5	ASTM D-3410
			In-plane shear modulus	G	Msi		—			
			Longitudinal flexural modulus	F_x	Msi		14.56		±0.3609 / 3	ASTM D-790M
			Transverse flexural modulus	F_y	Msi		1.90		±0.096 / 3	ASTM D-790M
			Long. tensile Poisson's ratio	ν_{xy}			1.2122		±0.014 / 4	ASTM D-3039
			Trans. tensile Poisson's ratio	ν_{yx}			0.0825		±0.0027 / 5	ASTM D-3039
			Long. thermal conductivity	K_x	(1)		3.97			Kohlrausch
			Trans. thermal conductivity	K_y	(1)		0.40			Kohlrausch
			Thru thickness thermal cond.	K_z	(1)		0.0725			
			Specific heat	C_p	(2)		0.193			ASTM E-1269
			Longitudinal CTE	α_x	(3)		-1.02			ASTM E-228
			Transverse CTE	α_y	(3)		5.83			ASTM E-228
			Thru thickness CTE	α_z	(3)		—			

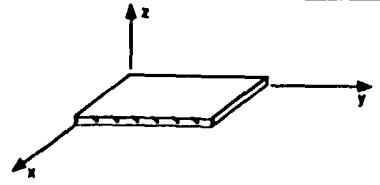

Notes:
(**) - Strain to failure; (1) Btu/(hr·in·°F); (2) Btu/(lb·°F); (3) µin./in./°F

Table 2.4-4 P75/1962 Graphite/Epoxy Tubes $[\pm 30, 0_4]_s$

NOT DESIGN ALLOWABLE DATA

PROPERTIES					TEMPERATURE (°F)			Std. Dev. / No. of Specimens at RT	Test Method
PHYSICAL			MECHANICAL & THERMAL			Low	Room	High		
Density (lb / in^3)		0.101	Longitudinal Tensile Strength	σ_x^{TU}	ksi		59.0		6.1 / 3	ASTM D-3552
Fiber volume fraction		0.25	Transverse Tensile Strength	σ_y^{TU}	ksi		4.1			NOL
Void volume fraction		<0.001	Longitudinal Comp. Strength	σ_x^{CU}	ksi		47.4		± 2.27 / 3	ASTM D-3410
Nominal ply thickness	In	0.065	Transverse comp. strength	σ_y^{CU}	ksi					
Max. cont. use temp.	°F	~550	In-plane shear strength	IPSS	ksi		12.1		± 0.47 / 3	
			Interlaminar shear strength	ILSS	ksi					
			Longitudinal tensile strain **	ε_x^T	%					ASTM D-3552
			Transverse tensile strain **	ε_y^T	%					NOL
OPTICAL & ELECTRICAL (at room temperature)			Longitudinal comp. strain **	ε_x^C	%		0.245		± 0.02 / 3	ASTM D-3410
			Transverse comp. strain **	ε_y^C	%					
Solar Absorptance	α		Longitudinal tensile modulus	E_x	Msi		32.5		± 0.38 / 3	ASTM D-3552
			Transverse tensile modulus	E_y	Msi		1.53			NOL
Normal Emissivity	ε		Longitudinal comp. modulus	E_x	Msi		27.8		± 1.3 / 3	ASTM D-3410
			Transverse comp. modulus	E_y	Msi					
Electrical Resistivity	R		In-plane shear modulus	G	Msi		2.33		± 0.153 / 3	Torsion Test
			Longitudinal flexural modulus	F_x	Msi					
			Transverse flexural modulus	F_y	Msi					
			Long. tensile Poisson's ratio	ν_{xy}			1.2689		± 0.03 / 3	ASTM D-3552
			Trans. tensile Poisson's ratio	ν_{yx}						NOL
			Long. thermal conductivity	K_x	(1)					
			Trans. thermal conductivity	K_y	(1)					
			Thru thickness thermal cond.	K_z	(1)					
			Specific heat	C_p	(2)					
			Longitudinal CTE	α_x	(3)					ASTM E-80
			Transverse CTE	α_y	(3)					
			Thru thickness CTE	α_z	(3)					

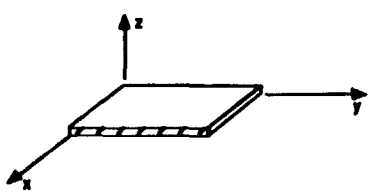

Notes:
(**) - Strain to failure; (1) Btu/(hr·in·°F); (2) Btu/(lb·°F); (3) μin./in./°F

Graphite/Thermoplastic
P75/PEEK

3.0 GRAPHITE/THERMOPLASTICS: P75/PEEK

Of the graphite/thermoplastic composites, P75/PEEK is being developed for potential spacecraft structural applications. Therefore, P75/PEEK flat panels with the $[0, \pm 45, 90]_S$ (quasi-isotropic) and $[30, -30, 0_4]_S$ (zero-CTE) layups were procured to generate material property test data. The fabrication data and the results of product evaluation and material property tests of both the laminates are discussed in this chapter:

3.1 P75/PEEK FLAT PANELS

- Quasi-isotropic $[0, \pm 45, 90]_S$
- Zero-CTE $[30, -30, 0_4]_S$

3.1.1 Fabrication Data

Material System:	P75/PEEK	P75/PEEK
Fiber Lay-up:	$[0, \pm 45, 90]_S$	$[30, -30, 0_4]_S$
	Quasi-isotropic	Zero-CTE
Fabricator:	ACPI	ACPI
Fabrication Process:	All panels were consolidated in a platen press at 750°F under an applied pressure of 250 psi for 2 hours. Co-woven fabric for panels was prepared by Textile Technologies, Inc., PA.	
Martin Marietta ID No.:	(GK)(PQ)(AP)	(GK)(PZ)(AP)
ACPI ID No.:	SN001Q	SN001A, SN004
Condition:	As fabricated	As fabricated
Dimension:	12-in. x 12-in. x .040-in.	12-in. x 12-in. x 0.60-in.
Ply Thickness:	0.005-in.	0.005-in.

3.1.2 Product Evaluation

(a) Density

P75 Fiber:	0.072 lb/in^3
	(2.09 gm/cm^3)
PEEK:	0.046 lb/in^3
	(1.27 gm/cm^3)
P75/PEEK:	0.0628 lb/in^3 (Average) for $[0, \pm 45, 90]_S$ and $[30, -30, 0_4]_S$
	(1.74 gm/cm^3)

(b) Fiber Volume

P75/PEEK $[0, \pm 45, 90]_S$:	62.2%
Std. Dev:	2.86
Void Volume:	1.0%

P75/PEEK $[30, -30, 0_4]_S$:	62.2%
Std. Dev:	3.7
Void Volume:	0.6%

(c) Non-Destructive Evaluation

Visual, X-radiographic and ultrasonic techniques were used to inspect P75/PEEK flat panels. Each appeared to be of good quality without surface imperfections. X-radiographic examinations revealed that many fiber tows in the [0°] lay-up were not straight, and to a certain extent, fiber tows in the 30° and 45° plies also had a slight curvature. It is likely that the curvature was caused by unequal tension applied to the co-woven fabric during consolidation

process. Ultrasonic C-scan of $[30, -30, 0_4]_s$ panels showed very few voids near the edge, whereas C-scan of $[0, \pm 45, 90]_s$ showed microvoids dispersed throughout the entire panel.

(d) Microstructure

Longitudinal and transverse microstructure of $[0, \pm 45, 90]_s$ and $[30, -30, 0_4]_s$ Gr/PEEK panels are shown in Figures 3-1 and 3-2 respectively. Each photomicrograph revealed a few uninfiltrated regions and microcracks that were usually contained within the 45°, 90°, or 30° ply. Most likely, these microcracks were caused by thermal-mechanical conditions experienced by the co-woven fabric during consolidation processes. Microstructural examination at different locations of the panel also indicated that matrix distribution was generally not as uniform as observed in the P75/1962 Gr/Ep panels. In recent R&D programs related to Gr/thermoplastic composites, Advanced Composite Products, Inc., CT, has demonstrated that uniform matrix distribution can be obtained by using a co-mingled fabric instead of a co-woven fabric.

3.1.3 Mechanical Properties

(a) Tension

During the tension tests, each specimen exhibited a linear elastic stress strain response until failure. A typical stress strain response of a $[30, -30, 0_4]_s$ laminate is shown in Figure 3-3. Longitudinal and transverse tensile properties of $[0, \pm 45, 90]_s$ and $[30, -30, 0_4]_s$ laminates are listed in Tables 3-1 to 3-4.

For $[0, \pm 45, 90]_s$ laminate, the longitudinal and transverse modulus values were nearly the same indicating the expected quasi-isotropic response. The measured modulus of 14.0 Msi was slightly lower than the predicted value of 16.0 Msi obtained from first ply failure analysis. Also, for $[30, -30, 0_4]_s$ laminate the measured modulus of 30.06 Msi was lower than predicted value of 34.5 Msi. These differences can be attributed to the lack of fiber collimation in the cowoven laminate.

(a) Longitudinal

(b) Transverse

Figure 3-1 Longitudinal and Transverse Micrographs of Quasi-isotropic [0, ±45, 90]$_s$ P75/PEEK Laminate Revealing a Few Voids, Microcracks, and Uninfiltrated Regions (80X)

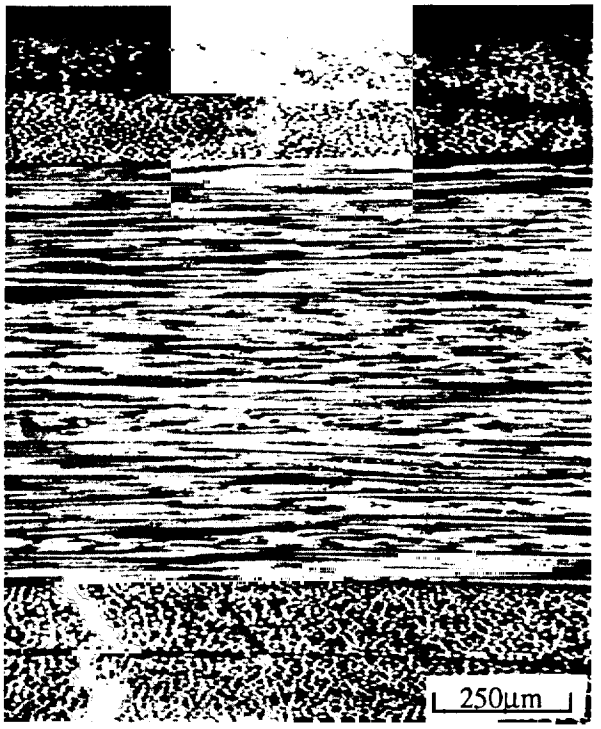

(a) Longitudinal

(b) Transverse

Figure 3-2 Longitudinal and Transverse Micrographs of Zero-CTE $[\pm 30, 0_4]_s$ P75/PEEK Laminate Revealing a Few Voids and Microcracks, (80X)

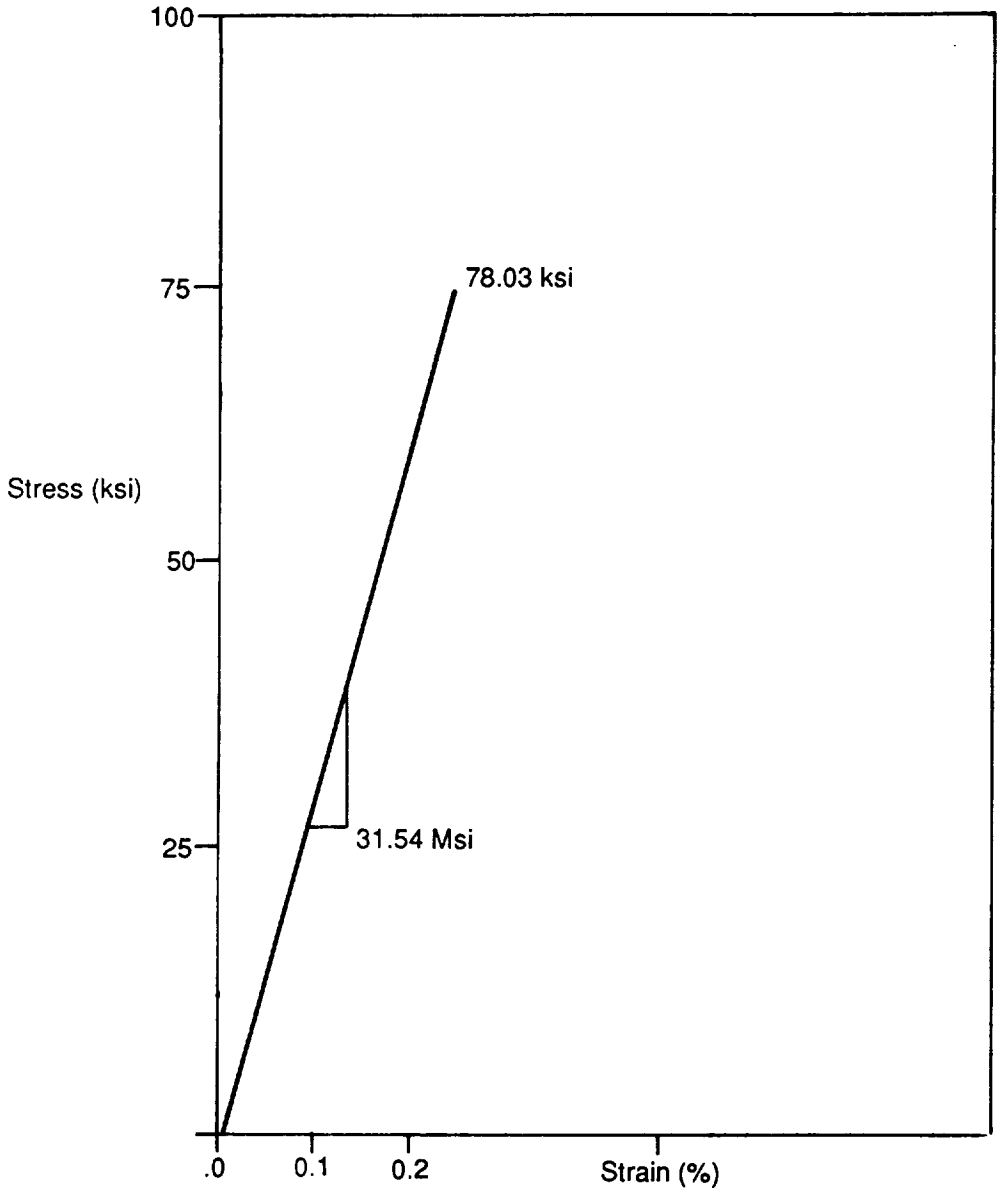

Figure 3-3 Typical Tensile Stress-Strain Response of a Zero-CTE, [30, -30, 0_4]$_S$ P75/PEEK Laminate

Table 3-1 Longitudinal Tensile Properties of P75/PEEK, $[0, \pm 45, 90]_s$, Fiber Volume = 62.2%

Specimen # (GK)(PQ)(AP)	Elastic Modulus E_x^T (Msi)	Ultimate Tensile Strength (ksi)	Poisson Ratio ν_{xy}	Strain To Failure (%)
TNL-1	14.19	35.77	0.3608	0.25
TNL-2	13.37	35.31	0.3439	0.265
TNL-3	12.81	33.66	0.3154	0.265
TNL-4	12.57	37.05	0.2860	0.295
TNL-5	13.54	32.77	0.4375	0.24
Mean Value	13.30	34.91	0.3487	0.263
Std. Dev.	0.64	1.704	0.0572	0.02
CV (%)	4.8	4.9	16.4	7.6

Table 3-2 Transverse Tensile Properties of P75/PEEK, $[0, \pm 45, 90]_s$, Fiber Volume = 62.2%

Specimen # (GK)(PQ)(AP)	Elastic Modulus E_y^T (Msi)	Ultimate Tensile Strength (ksi)	Poisson Ratio ν_{yx}	Strain To Failure (%)
TNT-1	12.20	31.49	0.2941	0.17
TNT-2	14.29	48.32	0.3263	0.34
TNT-3	14.55	48.53	0.3312	0.32
TNT-4	15.17	43.10	0.3724	0.28
TNT-5	13.80	44.53	0.3649	0.32
Mean Value	14.0	43.2	0.3378	0.286
Std. Dev.	1.122	6.96	0.0317	0.07
CV (%)	8.0	10.1	9.4	24.5

Table 3-3 Longitudinal Tensile Properties of P75/PEEK, $[\pm 30, 0_4]_s$, Fiber Volume = 62.2%

Specimen # (GK)(PZ)(AP)	Elastic Modulus E_x^T (Msi)	Ultimate Tensile Strength (ksi)	Poisson Ratio ν_{xy}	Strain To Failure (%)
TNL-1	28.02	56.66	1.5112	0.21
TNL-2	29.62	73.38	1.4016	0.20
TNL-3	29.51	58.97	1.2232	0.21
TNL-4	31.54	78.03	1.4852	0.255
TNL-5	31.60	76.79	1.3685	0.27
Mean Value	30.06	68.77	1.3685	0.23
Std. Dev.	1.52	10.2	.1395	0.03
CV (%)	5.1	4.8	10.2	13.0

Table 3-4 Transverse Tensile Properties of P75/PEEK, $[\pm 30, 0_4]_s$, Fiber Volume = 62.2%

Specimen # (GK)(PZ)(AP)	Elastic Modulus E_y^T (Msi)	Ultimate Tensile Strength (ksi)	Poisson Ratio ν_{yx}	Strain To Failure (%)
TNT-1	1.38	5.15	0.0842	0.44
TNT-2	-	-	-	-
TNT-3	1.43	5.63	0.0814	0.5
TNT-4	1.43	5.43	0.0608	0.4
TNT-5	1.34	5.61	0.0611	0.43
Mean Value	1.40	5.46	0.0719	0.44
Std. Dev.	0.0436	0.22	0.0127	0.04
CV (%)	3.1	4.1	17.6	9.1

(b) Compression

Longitudinal and transverse compressive properties of quasi-isotropic and zero-CTE laminates are listed in Table 3-5 to 3-8. During the test, each specimen exhibited the deviation from linear elastic response at ≥ 35% of the ultimate strength level. In each case the compressive modulus values were lower than the tensile modulus values consistent with the predicted response. For the $[0, \pm 45, 90]_s$ laminate, the nearly same E_x^C (9.02 Msi) and E_y^C (9.36 Msi) values confirmed the quasi-isotropic character of the composite.

(c) Flexure Tests

Flexural modulus and strength values for the P75/PEEK specimens, using three point bend tests are listed in Table 3-9. The flexural modulus of highly anisotropic laminates is a critical function of ply stacking sequence and does not necessarily correlate with tensile modulus which is independent of stacking sequence. For example, during longitudinal flexure test of quasi-isotropic $[0, \pm 45, 90]_s$ P75/PEEK outer [0°] ply and during transverse flexure test outer [90°] ply significantly influenced the load deflection response. Therefore, longitudinal flexural modulus values of quasi-isotropic P75/PEEK were higher than the transverse flexural modulus values.

(d) Interlaminar Shear Stress (ILSS)

Short beam shear-three point bend tests were conducted to determine the apparent interlaminar shear strength values listed in Table 3-10. After the test, each specimen (0.5-in. long) was examined under an optical microscope, and observations confirmed that failure was primarily interlaminar shear.

Table 3-5 Longitudinal Compressive Properties of P75/PEEK, $[0, \pm 45, 90]_s$, Fiber Volume = 62.2%

Specimen # (GK)(PQ)(AP)	Elastic Modulus E_x^C (Msi)	Ultimate Comp. Strength (ksi)	Poisson Ratio ν_{xy}	Strain To Failure (%)
CML-1	8.56	20.97	0.2012	0.30
CML-2	9.84	21.16	0.2439	0.32
CML-3	8.46	20.12	0.2468	0.34
CML-4	9.23	23.13	0.2053	0.30
Mean Value	9.02	21.35	0.2243	0.315
Std. Dev.	0.643	1.27	0.024	0.019
CV (%)	7.1	5.9	10.9	6.0

Table 3-6 Transverse Compressive Properties of P75/PEEK, $[0, \pm 45, 90]_s$, Fiber Volume = 62.2%

Specimen # (GK)(PQ)(AP)	Elastic Modulus E_y^C (Msi)	Ultimate Comp. Strength (ksi)	Poisson Ratio ν_{yx}	Strain To Failure (%)
CMT-1	9.53	21.51	0.161	0.34
CMT-2	8.98	21.82	0.146	0.40
CMT-3	9.51	22.76	0.158	0.36
CMT-4	9.43	20.91	0.166	0.32
Mean Value	9.36	21.75	0.158	0.355
Std. Dev.	0.259	0.772	0.008	0.034
CV (%)	2.8	3.6	5.4	9.5

Table 3-7 Longitudinal Compressive Properties of P75/PEEK, $[\pm 30, 0_4]_S$, Fiber Volume = 62.2%

Specimen # (GK)(PZ)(AP)	Elastic Modulus E_x^C (Msi)	Ultimate Comp. Strength (ksi)	Poisson Ratio ν_{xy}	Strain To Failure (%)
CML-1	26.70	52.58	0.646	—
CML-2	28.67	48.76	0.492	0.22
CML-3	30.16	50.84	0.5143	0.22
CML-4	28.06	53.34	0.735	0.26
Mean Value	28.40	51.38	0.597	0.23
Std. Dev.	1.435	2.036	0.114	0.023
CV (%)	5.1	4.0	19.2	10.0

Table 3-8 Transverse Compressive Properties of P75/PEEK, $[\pm 30, 0_4]_S$, Fiber Volume = 62.2%

Specimen # (GK)(PZ)(AP)	Elastic Modulus E_y^C (Msi)	Ultimate Comp. Strength (ksi)	Poisson Ratio ν_{yx}	Strain To Failure (%)
CMT-1	0.98	16.72	0.0674	0.34
CMT-2	1.12	18.82	0.095	0.35
CMT-3	1.23	17.15	0.101	0.30
CMT-4	1.24	17.45	0.065	0.32
Mean Value	1.14	17.54	0.084	0.328
Std. Dev.	0.1212	0.912	0.0219	0.022
CV (%)	10.6	5.2	26.1	6.7

Table 3-9 Longitudinal and Transverse Flexural Properties (3 point bend) of P75/PEEK Composites

Flat Panel $[0, \pm 45, 90]_S$, — SN 001Q: V = 62.2			Flat Panel $[30, -30, 0_4]_S$, — SN004: V = 62.16		
	Longitudinal Flexural			Longitudinal Flexural	
Specimen # (GK)(PQ)(AP)	Modulus (Msi)	Strength (ksi)	Specimen # (GK)(PZ)(AP)	Modulus (Msi)	Strength (ksi)
FXL-51	15.80	63.16	FXL-51	12.32	95.33
FXL-52	16.64	66.92	FXL-52	11.72	90.52
FXL-53	16.42	63.22	FXL-53	12.10	87.43
Mean	16.29	64.43	Mean	12.05	91.09
Std. Dev.	0.436	2.154	Std. Dev.	0.304	3.98
CV (%)	2.7	3.3	CV (%)	2.5	4.4
	Transverse Flexural			Transverse Flexural	
Specimen # (GK)(PQ)(AP)	Modulus (Msi)	Strength (ksi)	Specimen # (GK)(PZ)(AP)	Modulus (Msi)	Strength (ksi)
FXT-71	2.12	39.88	FXT-71	0.875	16.56
FXT-72	2.06	35.08	FXT-72	0.954	18.52
FXT-73	2.14	42.98	FXT-73	1.00	18.43
Mean	2.11	39.31	Mean	0.943	17.84
Std. Dev.	0.042	3.98	Std. Dev.	0.0632	1.11
CV (%)	2.0	10.1	CV (%)	6.7	6.2

Table 3-10 (Apparent) Interlaminar Shear Strength of P75/PEEK Composites

P75/PEEK $[0, \pm 45, 90]_s$		P75/PEEK $[30, -30, 0_4]_s$	
Specimen # (GK)(PQ)(AP)	ILSS (ksi)	Specimen # (GK)(PZ)(AP)	ILSS (ksi)
IL-1Q1	5.25	IL-41	7.31
IL-1 Q2	5.32	IL-42	6.76
IL-1Q3	4.28	IL-43	7.22
IL-IQ4	4.39	IL-44	7.75
IL-1Q5	4.78	IL-45	7.85
IL-1Q6	--	IL-46	6.98
IL-1Q7	4.32	IL-47	7.84
IL-1Q8	5.02	IL-48	7.66
IL-1Q9	4.81	IL-49	6.58
IL-1Q10	4.80	IL-410	7.02
IL-1Q11	4.82	IL-411	8.49
Mean	4.78		7.41
Std. Dev.	0.363		0.567
CV %	7.6		7.7

3.1.4 Thermophysical Properties

(a) CTE

Thermal expansion response of the quasi-isotropic and zero-CTE laminates is presented in Figures 3-4 to 3-7. The average CTE (obtained from the slope of a line joining the end points of the response) residual strain and RT hysteresis are listed in Table 3-11.

(b) Specific Heat

Specific heat test data of P75/PEEK specimens with quasi-isotropic $[0, \pm 45, 90]_s$ and near zero-CTE layups $[30, -30, 0_4]_s$ over the -241°F to 750°F temperature range is plotted in Figure 3-8. The specific heat values for both laminates were similar, with the values of the zero-CTE laminate (0.193 Btu/(lb·°F)) being slightly below those of the quasi-isotropic laminate (0.203 Btu/(lb·°F)). Both materials exhibited a peak near 330°C (630°F) that could be attributed to the melting of a constituent polymer in the PEEK matrix.

(c) Thermal Diffusivity, Bulk Density, and Thermal Conductivity

In preliminary thermal conductivity tests it was found that the Kohlrausch technique could not be used because of the high and variable electrical resistivity of P75/PEEK specimens in the in-plane directions. Therefore, diffusivity (D) and bulk density (ρ) measurements were made to calculate thermal conductivity (K) using the following relationship:

$$K = D \cdot Cp \cdot \rho,$$

where Cp is the specific heat. Test specimens were prepared for transverse, longitudinal, and through-the-thickness diffusivity measurements. Sample geometries and bulk density values are given in Table 3-12. The density values for the zero-CTE laminate (PZ) ranged from 0.061 to 0.0626 lb/in^3 while the density of the quasi-isotropic (PQ) specimens fall in the 0.0603 to 0.0608 lb/in^3 range.

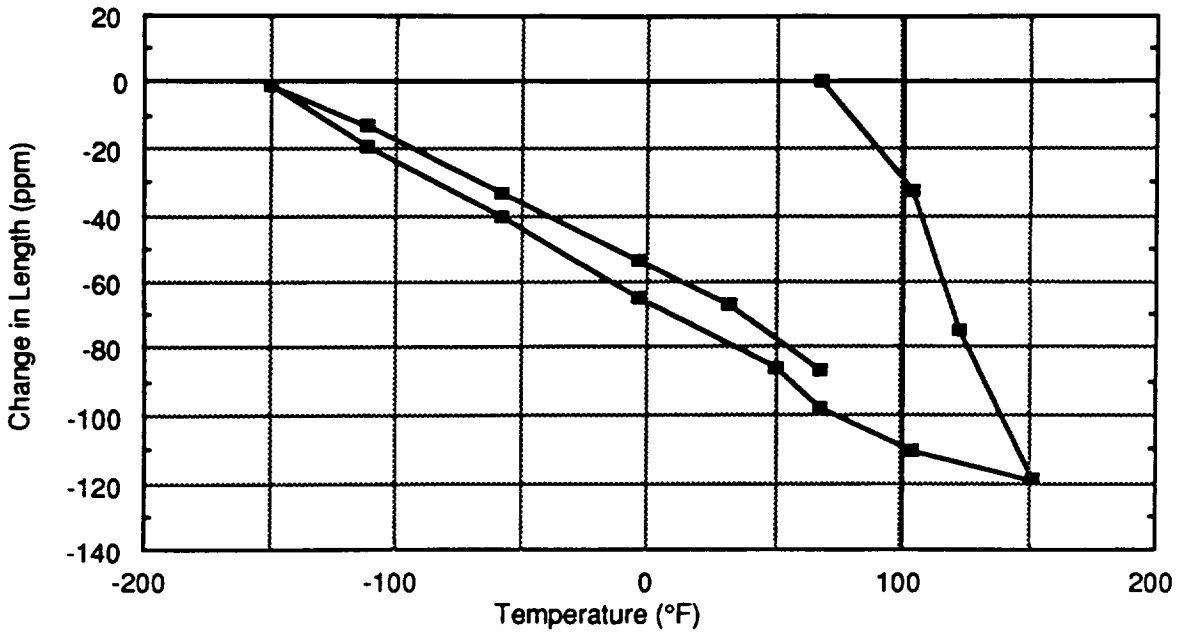

Figure 3-4 Thermal Expansion Behavior of Longitudinal P75/PEEK [0, ±45, 90]$_s$ Specimen in a Heat/Cool/Heat Cycle Using Push Rod Dilatometer

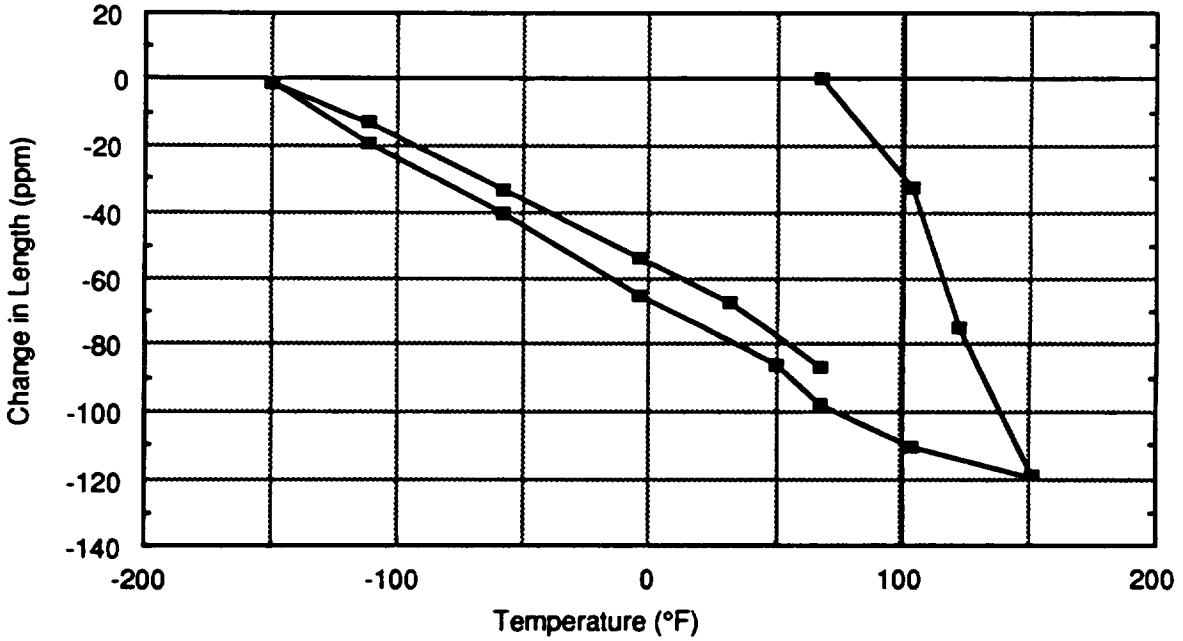

Figure 3-5 Thermal Expansion Behavior of Transverse P75/PEEK [0, ±45, 90]$_s$ Specimen in a Heat/Cool/Heat Cycle Using Push Rod Dilatometer

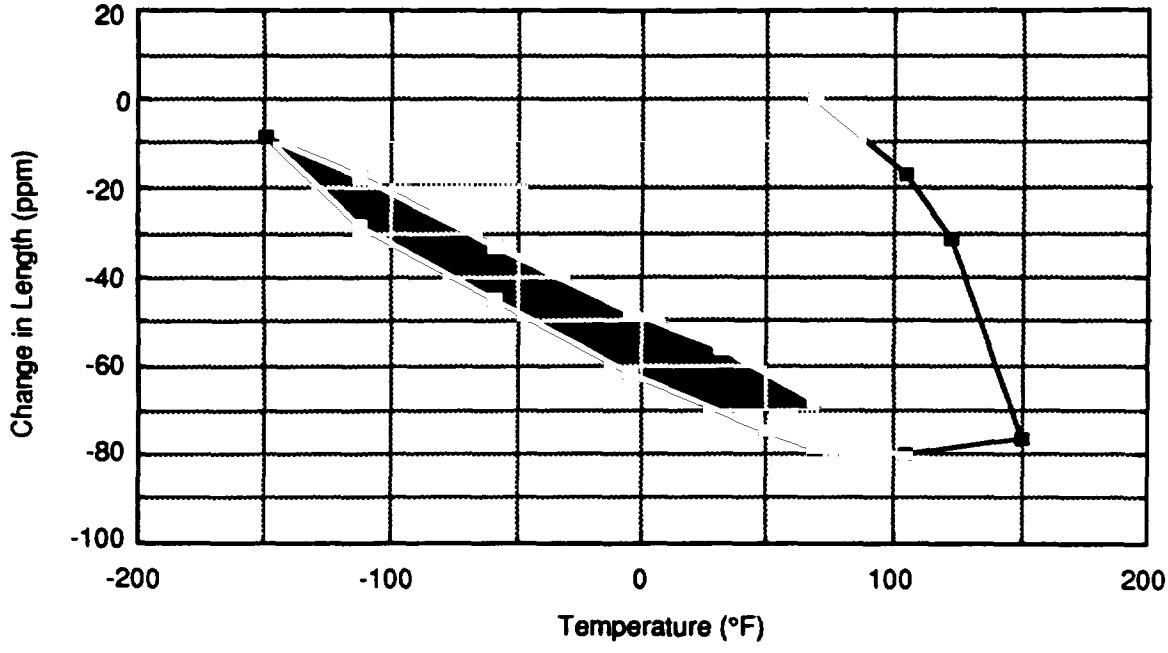

Figure 3-6 Thermal Expansion Behavior of Longitudinal P75/PEEK $[\pm 30, 0_4]_s$ Specimen in a Heat/Cool/Heat Cycle Using Push Rod Dilatometer

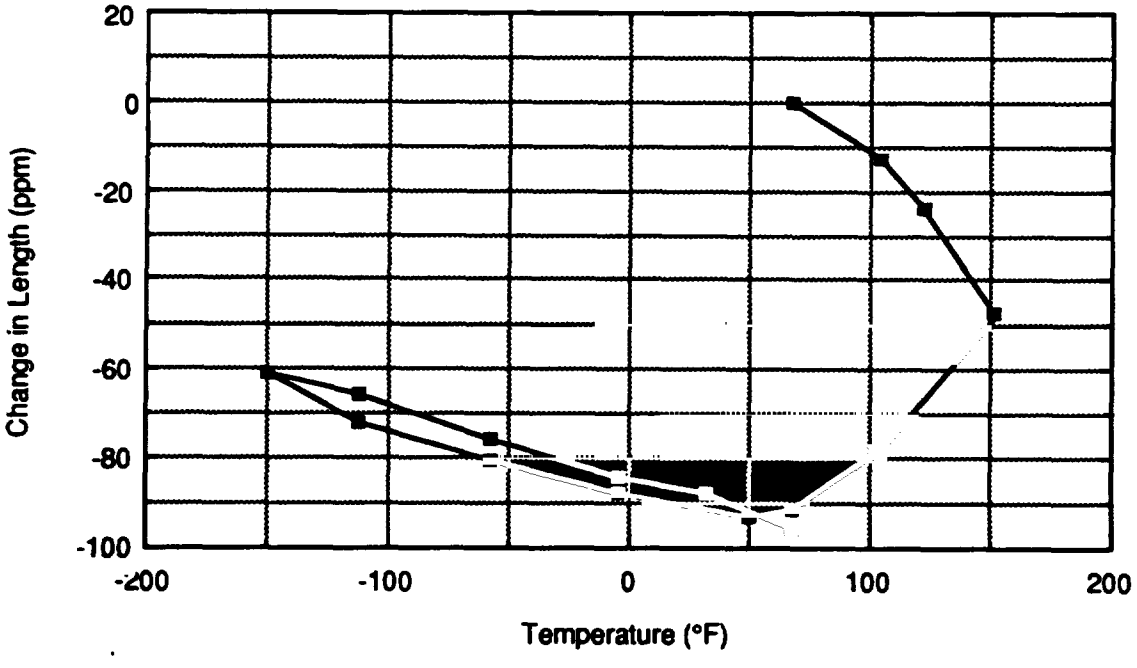

Figure 3-7 Thermal Expansion Behavior of Transverse P75/PEEK $[\pm 30, 0_4]_s$ Specimen in a Heat/Cool/Heat Cycle Using Push Rod Dilatometer

Table 3-11 Summary of Thermal Expansion Test Data of P75/PEEK Composites

Thermal Expansion Measurements	P75/PEEK $[0, \pm 45, 90]_S$ $V_f = 0.622$		P75/PEEK $[30, -30, 0_4]_S$ $V_f = 0.622$	
	Longitudinal	Transverse	Longitudinal	Transverse
CTE (ppm/°F)*	-0.28	+0.04	-0.39	+10.17
Residual strain (ppm)	-67.80	-95.77	-86.34	-3.20
Strain Hysteresis (ppm)†	-78.60	-91.30	-98.10	-109.60

*(end to end point average); †at RT (i.e., RT → 150°F → RT)

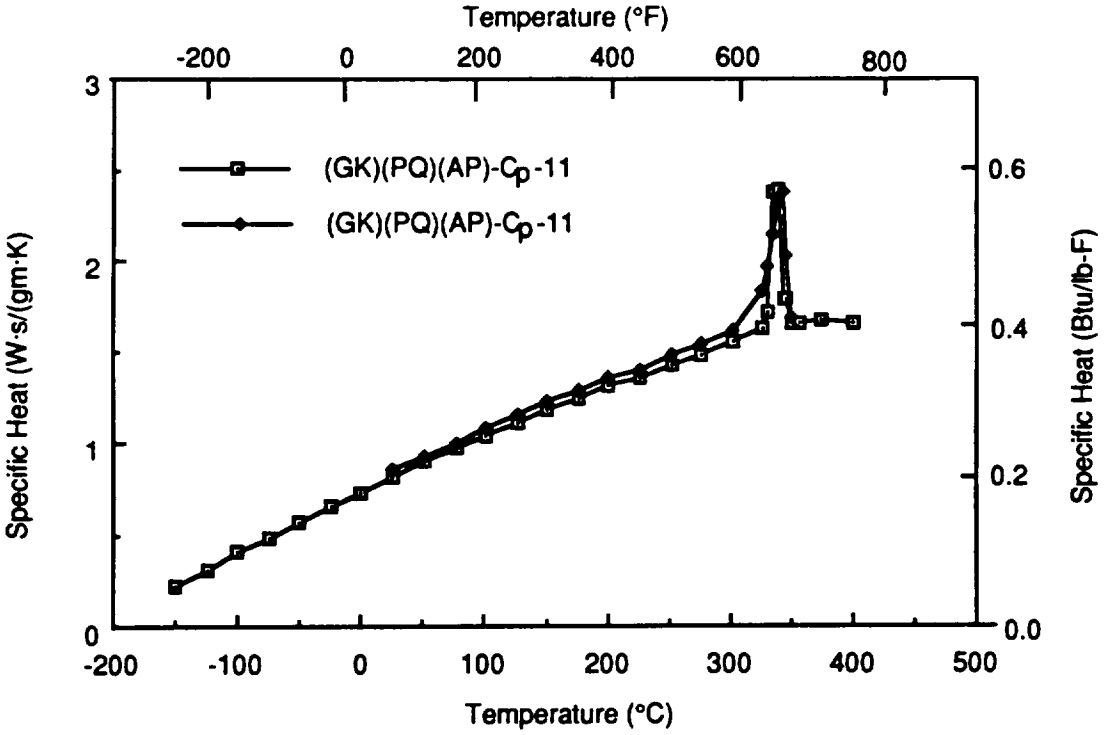

Figure 3-8 Specific Heat Response of P75/PEEK Showing a Peak at 630°F Related to a Phase Transformation in the PEEK Matrix

Thermal diffusivity results are listed in Table 3-13 and plotted in Figures 3-9 and 3-10 for the following specimens.

Laminate	Specimen #	Direction
Quasi-isotropic	PQ-TKT	Transverse
	PQ-TKL	Longitudinal
	PQ-TD-11	Through-the-thickness
Zero-CTE	PZ-TKT	Transverse
	PZ-TKL	Longitudinal
	PZ-TD-12	Through-the-thickness

The longitudinal and transverse thermal diffusivity values of the quasi-isotropic laminate were near 0.29 cm^2/sec at RT and 0.00945 cm^2/sec for the through-the-thickness value. In similar measurements of the zero-CTE laminate at RT, the longitudinal thermal diffusivity value of 0.590 cm^2/sec was about ten times larger than in the transverse direction, and the through-the-thickness value was 0.0114 cm^2/sec.

Based on the specific heat, thermal diffusivity and bulk density measurements at different temperatures, the calculated thermal conductivity values for zero-CTE laminates are listed in Table 3-14 and plotted in Figure 3-11. The conductivity in the longitudinal direction was considerably larger than those for the other directions, and the conductivity in the though-plane direction was the lowest, as expected. For comparison, calculated thermal conductivity values at 212°F for quasi-isotropic laminate are given in Table 3-15.

(d) Optical Properties

The solar absorptance (α_S) and normal emissivity (ε_N) values of as fabricated panels of both quasi-isotropic and zero-CTE laminates were nearly identical:

Table 3-12 Sample Geometries, Masses, and Bulk Density Values of P75/PEEK Composites

P75/PEEK					
Sample Designation	Thick (in)	Width (in)	Width (in)	Mass (gm)	Density (gms cm^{-3})
GK-PZ-AP-TKT	0.2426	0.5025	0.5014	1.7040	1.701
GK-PZ-AP-TKL	0.2428	0.5023	0.5033	1.7039	1.695
GK-PZ-AP-TD-12	0.0550	0.5027	0.4996	0.3921	1.732
GK-PQ-AP-TKT	0.2428	0.4735	0.5053	1.6000	1.681
GK-PQ-AP-TKL	0.2418	0.4925	0.5073	1.6508	1.668
GK-PQ-AP-TD-11	0.0425	0.5003	0.5035	0.2953	1.683

Table 3-13 Thermal Diffusivity of P75/PEEK Composites

Temp. (°C)	(PQ)TD-11	(PZ)TD-12	(PQ)TKL	(PZ)TKL	(PQ)TKT	(PZ)TKT
-143		0.0164		0.673		0.0715
-122		0.0153		0.647		0.0710
-70		0.0136		0.642		0.0681
-5		0.0120		0.613		0.0600
23	0.00945	0.0114	0.282	0.590	0.299	0.0575
100	0.00823	0.0100	0.257	0.481	0.268	0.0520
200		0.00815		0.395		0.0435
300		0.00663		0.338		0.0364
400		0.00470		0.300		0.0285
*cm^2 sec^1	Through-Thickness		Longitudinal		Transverse	

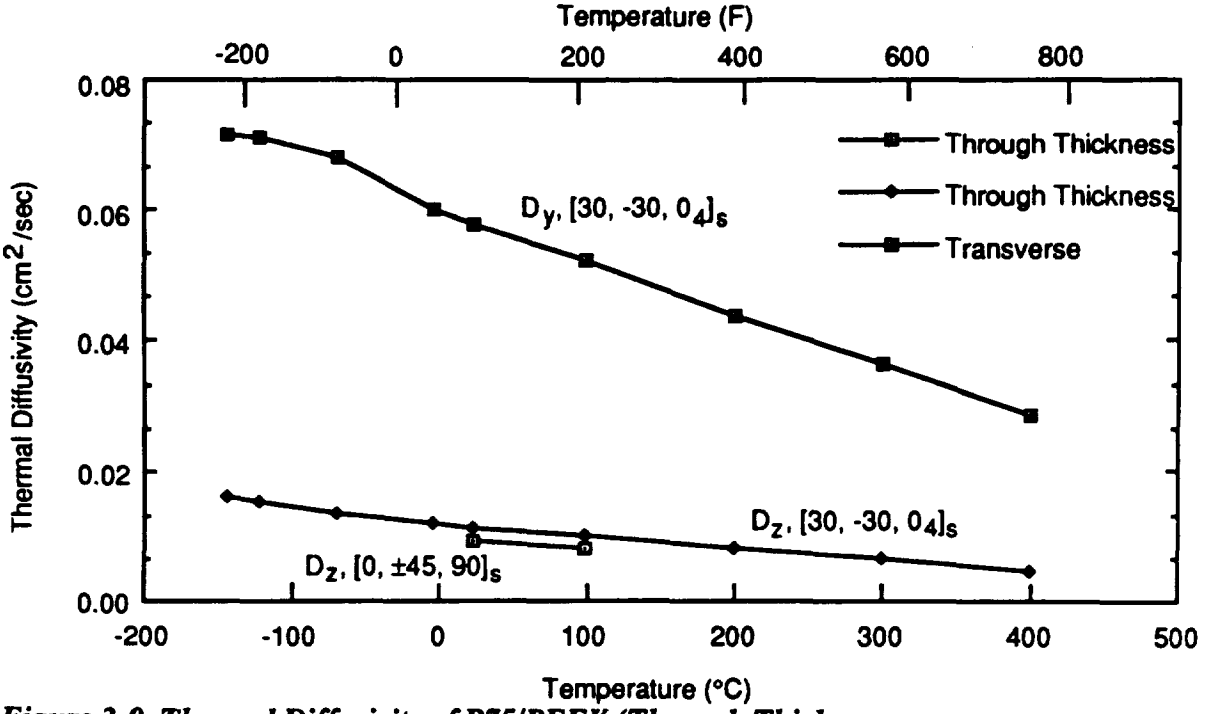

Figure 3-9 Thermal Diffusivity of P75/PEEK (Through Thickness $[0, \pm 45, 90]_S$, and Transverse and Through Thickness $[30, -30, 0_4]_S$

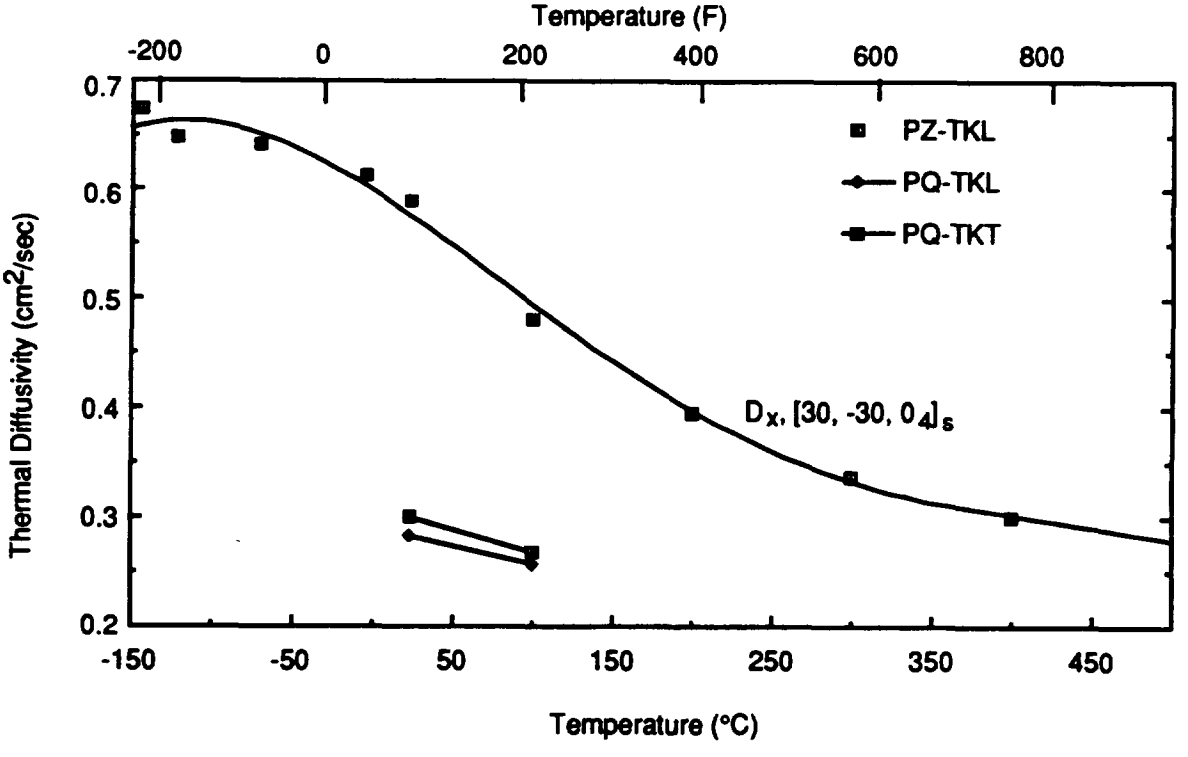

Figure 3-10 Thermal Diffusivity of P75/PEEK (Samples PQ-TKL, PZ-TKL, and PQ-TKT)

Table 3-14 Thermal Conductivity Calculations (P75/PEEK: Zero CTE Laminate)

Sample (No.)	Temp. (°C)	Density ($gm \cdot cm^{-3}$)	Specific Heat ($W \cdot s/gm \cdot K$)	Diffusivity (cm^2 /sec)	Conductivity (W/cm·K)	Conductivity (Btu Units*)	Temp. (°F)
†PZ-TD-12	-150	1.732	0.2200	0.01670	0.00636	4.41	-238
PZ-TD-12	-100	1.732	0.4010	0.01460	0.01014	7.03	-148
PZ-TD-12	-50	1.732	0.5710	0.01320	0.01305	9.05	-58
PZ-TD-12	0	1.732	0.7290	0.01190	0.01503	10.42	32
PZ-TD-12	25	1.732	0.8090	0.01140	0.01597	11.08	77
PZ-TD-12	100	1.732	1.0450	0.01000	0.01810	12.55	212
PZ-TD-12	200	1.732	1.3120	0.00826	0.01877	13.01	392
PZ-TD-12	300	1.732	1.5610	0.00650	0.01757	12.18	572
PZ-TD-12	400	1.732	1.6730	0.00471	0.01365	9.46	752
††PZ-TKL	-150	1.695	0.2200	0.65600	0.24462	169.61	-238
PZ-TKL	-100	1.695	0.4010	0.64400	0.43772	303.49	-148
PZ-TKL	-50	1.695	0.5710	0.63800	0.61749	428.13	-58
PZ-TKL	0	1.695	0.7290	0.60800	0.75128	520.90	32
PZ-TKL	25	1.695	0.8090	0.56700	0.77750	539.08	77
PZ-TKL	100	1.695	1.0450	0.48000	0.85021	589.49	212
PZ-TKL	200	1.695	1.3120	0.39600	0.88064	610.59	392
PZ-TKL	300	1.695	1.5610	0.33800	0.89431	620.07	572
PZ-TKL	400	1.695	1.6730	0.30000	0.85072	589.84	752
†††PZ-TKT	-150	1.701	0.2200	0.07110	0.02661	18.45	-238
PZ-TKT	-100	1.701	0.4010	0.07040	0.04802	33.29	-148
PZ-TKT	-50	1.701	0.5710	0.06530	0.06342	43.97	-58
PZ-TKT	0	1.701	0.7290	0.05970	0.07403	51.33	32
PZ-TKT	25	1.701	0.8090	0.05780	0.07954	55.15	77
PZ-TKT	100	1.701	1.0450	0.05180	0.09208	63.84	212
PZ-TKT	200	1.701	1.3120	0.04420	0.09864	68.39	392
PZ-TKT	300	1.701	1.5610	0.03650	0.09692	67.20	572
PZ-TKT	400	1.701	1.6730	0.02860	0.08139	56.43	752

* - ($Btu \cdot in/hr \cdot ft^2 \cdot F$); † - Through-plane; †† - Longitudinal Direction; ††† - Transverse Direction

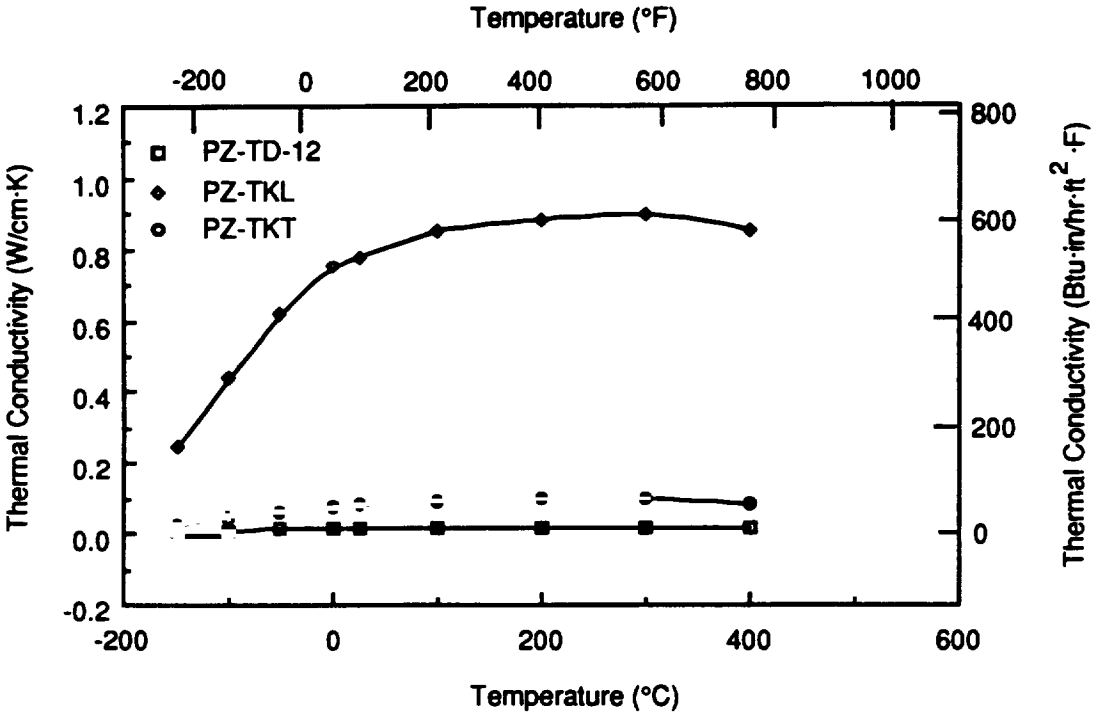

Figure 3-11 Thermal Conductivity Versus Temperature of P75/PEEK: Zero-CTE Laminate

Table 3-15 Thermal Conductivity Calculations of Quasi-isotropic P75/PEEK

Sample (No.)	T emp. (°C)	Density (gm cm^{-3})	Specific Heat (W • s gm^{-1} K^{-1})	Diffusivity (cm^2 sec^{-1})	Conductivity (W • cm^{-1} K^{-1})	Conductivity (Btu Units*)	Temp. (°F)
PQ-TD**	100	1.683	1.0800	0.00823	0.01496	10.37	212
PQ-TKL†	100	1.683	1.0800	0.25700	0.46297	321.00	212
PQ-TKT§	100	1.683	1.0800	0.26800	0.48655	337.35	212
* - (Btu·in/hr·ft^{2}F), **Through Thickness, †Longitudinal, §Transverse							

$\alpha_s/\varepsilon_N = 0.895/0.815 = 1.098$ for quasi-isotropic laminate

$\alpha_s/\varepsilon_N = 0.905/0.825 = 1.097$ for zero-CTE laminate

Reflectance vs. wavelength plot - For the as consolidated laminate surface, the reflectance vs. wavelength (2.0 - 14.0 μm) is shown in Figure 3-12. For example at 10.6 μm the reflectance value of 0.1 (10%) suggested the emittance value of 0.9.

3.2 SUMMARY OF P75/PEEK TEST DATA

Material properties of $[0, \pm 45, 90]_S$ and $[30, -30, 04]_S$ laminates are summarized in Tables 3-16 and 3-17 respectively.

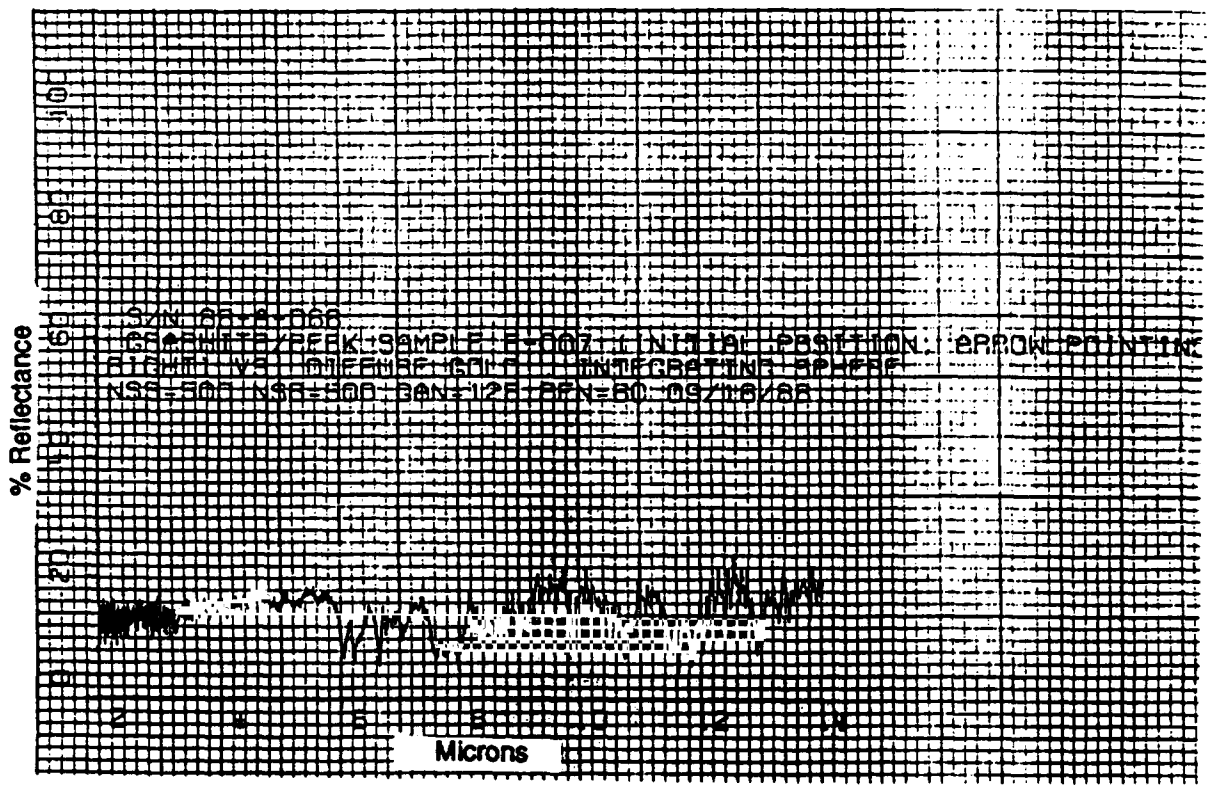

Figure 3-12 FTIR Reflectance Spectra of P75/PEEK

Table 3-16 P75/PEEK Graphite/Thermoplastic $[0, \pm 45, 90]_s$

NOT DESIGN ALLOWABLE DATA

PROPERTIES							TEMPERATURE (°F)			Std. Dev. / No. of Specimens at RT	Test Method
PHYSICAL			MECHANICAL & THERMAL				Low	Room	High		
Density (lb / in^3)		0.0628	Longitudinal Tensile Strength	σ_x^{TU}	ksi			34.91		± 1.704 / 5	ASTM D-3039
Fiber volume fraction		0.622	Transverse Tensile Strength	σ_y^{TU}	ksi			43.2		±6.96 / 5	ASTM D-3039
Void volume fraction		0.6	Longitudinal Comp. Strength	σ_x^{CU}	ksi			21.35		±1.27 / 5	ASTM D-3410
Nominal ply thickness	in	0.005	Transverse comp. strength	σ_y^{CU}	ksi			21.75		±0.772 / 4	ASTM D-3410
Max. cont. use temp.	°F	250	In-plane shear strength	IPSS	ksi						
Ply Orientation	θ	[0/±45/90]s	Interlaminar shear strength	ILSS	ksi			4.78		±0.363 / 10	ASTM D-2344
OPTICAL & ELECTRICAL (at room temperature)			Longitudinal tensile strain **	ε_x^T	%			0.263		±0.002 / 5	ASTM D-3039
Solar Absorptance	α	0.895	Transverse tensile strain **	ε_y^T	%			0.286		±0.07 / 5	ASTM D-3039
Normal Emissivity	ε	0.815	Longitudinal comp. strain **	ε_x^C	%			0.315		±0.019 / 4	ASTM D-3410
			Transverse comp. strain **	ε_y^C	%			0.355		±0.034 / 4	ASTM D-3410
			Longitudinal tensile modulus	E_x	Msi			13.3		±0.64 / 5	ASTM D-3039
			Transverse tensile modulus	E_y	Msi			14.0		±1.122 / 5	ASTM D-3039
			Longitudinal comp. modulus	E_x	Msi			9.02		0.643 / 4	ASTM D-3410
			Transverse comp. modulus	E_y	Msi			9.36		±0.259 / 4	ASTM D-3410
			In-plane shear modulus	G	Msi						
			Longitudinal flexural modulus	F_x	Msi			16.29		±0.436 / 3	ASTM D-790M
			Transverse flexural modulus	F_y	Msi			2.11		±0.042 / 3	ASTM D-790M
			Long. tensile Poisson's ratio	ν_{xy}				0.3487		±0.0572 / 5	ASTM D-3039
			Trans. tensile Poisson's ratio	ν_{yx}				0.3378		±0.0317 / 5	ASTM D-3039
			Long. thermal conductivity	K_x	(1)			2.23			Kohlrausch
			Trans. thermal conductivity	K_y	(1)			2.34			Kohlrausch
			Thru thickness thermal cond.	K_z	(1)			0.072			Laser Flash
			Specific heat	C_p	(2)			0.203			ASTM E-1269
			Longitudinal CTE	α_x	(3)			-0.28			ASTM E-228
			Transverse CTE	α_y	(3)			+0.04			ASTM E-228
			Thru thickness CTE	α_z	(3)			—			

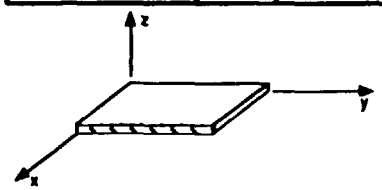

Notes:
(**) - Strain to failure; (1) Btu/(hr·in·°F); (2) Btu/(lb·°F); (3) μin./in./°F

Table 3-17 P75/PEEK Graphite/Thermoplastic [±30, 0_4]$_s$

NOT DESIGN ALLOWABLE DATA

PHYSICAL		
Density (lb / in^3)		0.0628
Fiber volume fraction		0.627
Void volume fraction		1.0
Nominal ply thickness	in	0.005
Max. cont. use temp.	°F	250
Ply Orientation	θ	[30/-30/04]s

OPTICAL & ELECTRICAL (at room temperature)		
Solar Absorptance	α	0.895
Normal Emissivity	ε	0.79

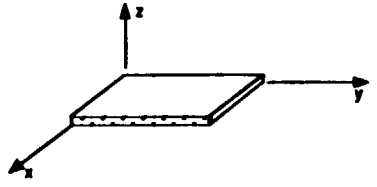

PROPERTIES			TEMPERATURE (°F)			Std. Dev. / No. of Specimens at RT	Test Method
MECHANICAL & THERMAL			Low	Room	High		
Longitudinal Tensile Strength	σ_x^{TU}	ksi		68.77		± 10.2 / 5	ASTM D-3039
Transverse Tensile Strength	σ_y^{TU}	ksi		5.46		±0.22 / 4	ASTM D-3039
Longitudinal Comp. Strength	σ_x^{CU}	ksi		51.38		±2.036 / 4	ASTM D-3410
Transverse comp. strength	σ_y^{CU}	ksi		17.54		±0.912 / 4	ASTM D-3410
In-plane shear strength	IPSS	ksi					
Interlaminar shear strength	ILSS	ksi		7.41		±0.567 / 11	ASTM D-2344
Longitudinal tensile strain **	ε_x^T	%		0.23		±0.03 / 5	ASTM D-3039
Transverse tensile strain **	ε_y^T	%		0.44		±0.04 / 4	ASTM D-3039
Longitudinal comp. strain **	ε_x^C	%		0.23		±0.023 / 4	ASTM D-3410
Transverse comp. strain **	ε_y^C	%		0.328		±0.022 / 4	ASTM D-3410
Longitudinal tensile modulus	E_x	Msi		30.06		±1.52 / 5	ASTM D-3039
Transverse tensile modulus	E_y	Msi		1.40		±0.0436 / 4	ASTM D-3039
Longitudinal comp. modulus	E_x	Msi		28.40		±1.435 / 4	ASTM D-3410
Transverse comp. modulus	E_y	Msi		1.14		±0.1212 / 4	ASTM D-3410
In-plane shear modulus	G	Msi					
Longitudinal flexural modulus	F_x	Msi		12.05		±0.304 / 3	ASTM D-790M
Transverse flexural modulus	F_y	Msi		0.943		±0.0632 / 3	ASTM D-790M
Long. tensile Poisson's ratio	ν_{xy}			1.3685		±0.1395 / 5	ASTM D-3039
Trans. tensile Poisson's ratio	ν_{yx}			0.0719		±0.0127 / 5	ASTM D-3039
Long. thermal conductivity	K_x	(1)		3.74			Kohlrausch
Trans. thermal conductivity	K_y	(1)		0.38			Kohlrausch
Thru thickness thermal cond.	K_z	(1)		0.078			Laser Flash
Specific heat	C_p	(2)		0.193			ASTM E-1269
Longitudinal CTE	α_x	(3)		-0.39			ASTM E-228
Transverse CTE	α_y	(3)		+10.17			ASTM E-228
Thru thickness CTE	α_z	(3)		—			

Notes:
(**) - Strain to failure; (1) Btu/(hr·in·°F); (2) Btu/(lb·°F); (3) μin./in./°F

Carbon/Thermoplastic
AS4/PES

Carbon/Thermoplastic
AS4/PES

4.0 CARBON/THERMOPLASTIC: AS4/PES

Of the carbon/thermoplastic composites, AS4/PES is a potential material for strength critical structural applications. Therefore, AS4/PES flat panels with the $[0, \pm 45, 90]_S$ (quasi-isotropic), and $[30, -30, 0_4]_S$ (zero-CTE) layups were procured to generate mechanical and thermophysical property data. The fabrication data, and the results of product evaluation and material property tests of both the laminates are discussed in this chapter.

4.1 AS4/PES FLAT PANELS

- Quasi Isotropic $[0, \pm 45, 90]_S$
- Zero-CTE $[30, -30, 0_4]_S$

4.1.1 Fabrication Data

Material System:	AS4/PES
	- Quasi-isotropic $[0, 45, 90, -45]_S$
	- Zero-CTE $[30, -30, 0_4]_S$
Condition:	As fabricated
Fabrication Process:	Consolidated in a platen press
	(Pressure, temperature, and time details: not available)
Fabricator:	Specmet, UK (received from Martin Marietta Energy Systems, Inc., TN)
Dimensions:	0.040-in. x 12-in. x 12-in. $[0, \pm 45, 90]_S$
	0.060-in. x 12-in. x 12-in. $[30, -30, 0_4]_S$
Ply Thickness:	0.005-in. for both laminates
Specmat Job Number:	SN1018 for $[30, -30, 04]_S$, panel #SN002, SN004
	SN1019 for $[0, \pm 45, 90]$, panel #SN007, SN008

Martin Marietta ID: (CZ)(BQ)(AP) $[0, \pm 45, 90]_s$

(CZ)(BZ)(AP) $[30, -30, 04]_s$

4.1.2 Product Evaluation

(a) Density

Fiber: AS4: 0.065 lb/in^3 (1.80 gm/cm^3)

Matrix: PES: 0.0495 lb/in^3 (1.37 gm/cm^3)

Laminate: AS4/PES: 0.058 lb/in^3 (1.6 gm/cm^3)

($[0, \pm 45, 90]_s$ and Zero-CTE $[30, -30, 0_4]_s$)

(b) Fiber Volume

- AS4/PES $[0, \pm 45, 90]_s$

v/o: 53.7%

Std. Dev.: 1.52

Void Volume: ≤1.0%

- AS4/PES $[30, -30, 0_4]_s$

v/o: 54.96%

Std. Dev.: 0.623

Void Volume: ≤1.0%

(c) Non-Destructive Evaluation

On visual examination, each panel appeared to be of good quality with a good surface finish and uniform thickness. In each panel, fibers in the outer plies seemed to have curved from the desired 0° or 30° direction. X-radiography of each panel also confirmed the fiber curvature along with waviness in localized regions of different plies which must have been caused due to

slight pressure differences during the consolidation process. Ultrasonic C-scan of zero-CTE laminates revealed only a few voids and delamination, whereas C-scans of quasi-isotropic laminates revealed a few large areas (1-in. x 1-in.) indicating delamination.

(d) Microstructure

Typical microstructures of quasi-isotropic and zero-CTE laminates are shown in Figure 4-1 and 4-2 respectively. Overall examination of each panel showed quite uniform fiber distribution in the matrix with a few microcracks and voids in off-axis plies.

4.1.3 Mechanical Properties

(a) Tension

For both the $[0, \pm 45, 90]_s$ and $[30, -30, 0_4]_s$ laminates, the longitudinal and transverse tension test results are listed in Tables 4-1 to 4-4. The longitudinal and transverse tensile modulus values of 6.38 Msi and 6.51 Msi for the $[0, \pm 45, 90]_s$ laminate were about 85% of the 7.5 Msi modulus value predicted by composite laminate analyses model (CLAM). For the zero-CTE $[30, -30, 0_4]_s$ laminate, the longitudinal tensile modulus of 14.18 Msi was 90% of the predicted modulus, 15.71 Msi; and the transverse tensile modulus of 1.57 Msi was nearly equivalent to the predicted 1.62 Msi.

(b) Compression

Longitudinal and transverse compressive properties of the $[0, \pm 45, 90]_s$ and $[30, -30, 0_4]_s$ laminates are listed in Tables 4-5 to 4-8. In both laminates, the compressive modulus values were slightly lower than the corresponding tensile modulus values, consistent with the predicted response. But, in the quasi-isotropic laminate, the transverse compressive strength (30.36 ksi) was significantly lower than the longitudinal compressive strength (47.31 ksi). The reduced transverse strength was due to the presence of delaminated region (in the specimens) along with

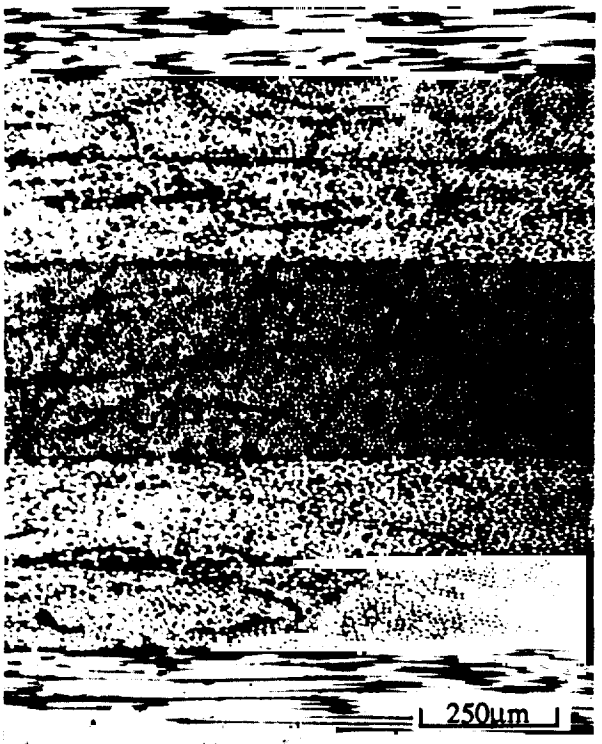

(a) Longitudinal

(b) Transverse

Figure 4-1 Longitudinal and Transverse Photomicrographs of Quasi-isotropic AS4/PES Laminate Showing Uniform Fiber Distribution and a Few Microcracks

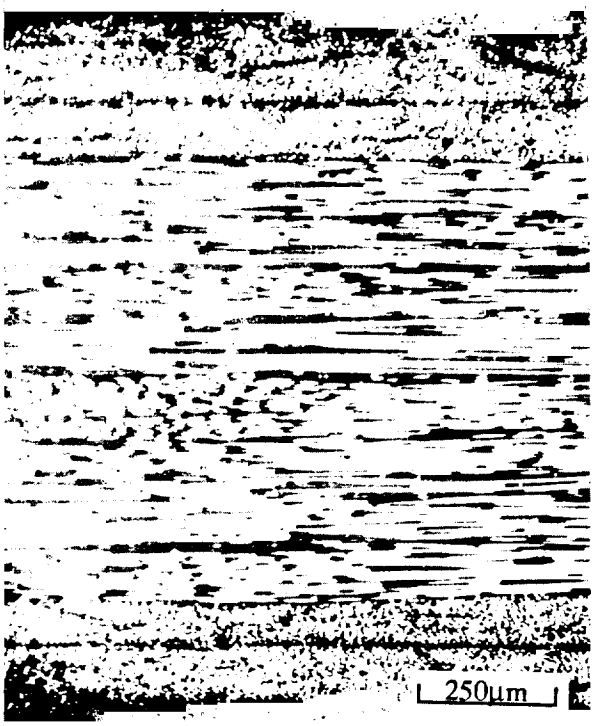

(a) Longitudinal

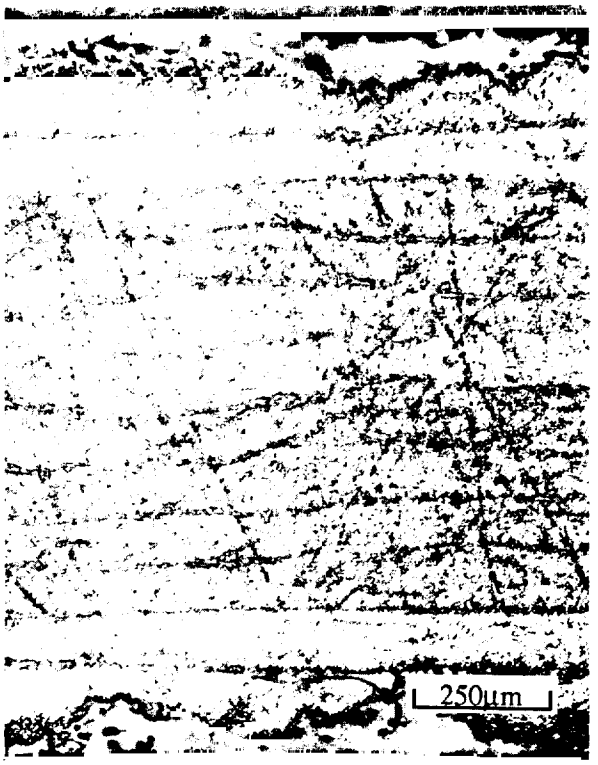

(b) Transverse

Figure 4-2 Longitudinal and Transverse Photomicrographs of Zero-CTE AS4/PES Laminate Showing Uniform Fiber Distribution and a Few Microcracks

Table 4-1 Longitudinal Tensile Properties of AS4/PES, $[0, \pm 45, 90]_s$, Fiber Volume = 53.7%

Specimen # (CZ)(BQ)(AP)	Elastic Modulus E_x^T (Msi)	Ultimate Tensile Strength (ksi)	Poisson Ratio ν_{xy}	Strain To Failure (%)
TNL-1	6.56	86.13	0.2741	1.39
TNL-2	6.31	72.06	0.2787	1.2
TNL-3	6.42	81.12	0.3070	1.33
TNL-4	6.35	86.01	0.3256	1.5
TNL-5	6.28	76.39	0.2735	1.33
Mean Value	6.38	80.34	0.2918	1.35
Std. Dev.	0.111	6.13	0.0234	0.108
CV (%)	1.74	7.6	8.0	8.0

Table 4-2 Transverse Tensile Properties of AS4/PES, $[0, \pm 45, 90]_s$, Fiber Volume = 53.7%

Specimen # (CZ)(BQ)(AP)	Elastic Modulus E_Y^T (Msi)	Ultimate Tensile Strength (ksi)	Poisson Ratio ν_{yx}	Strain To Failure (%)
TNT-1	6.87	72.55	0.3577	1.09
TNT-2	6.75	79.27	0.3284	1.21
TNT-3	6.76	83.94	0.3097	1.22
TNT-4	5.99	78.85	0.3104	1.2
TNT-5	6.19	73.85	0.3140	1.2
Mean Value	6.51	77.69	0.3240	1.18
Std. Dev.	0.394	4.58	0.3240	0.053
CV (%)	6.1	5.9	6.3	4.49

Table 4-3 Longitudinal Tensile Properties of AS4/PES, $[\pm 30, 0_4]_s$, Fiber Volume = 54.96%

Specimen # (CZ)(BZ)(AP)	Elastic Modulus E_x^T (Msi)	Ultimate Tensile Strength (ksi)	Poisson Ratio ν_{xy}	Strain To Failure (%)
TNL-1	13.99	83.79	0.8755	0.68
TNL-2	13.90	93.17	0.8306	0.672
TNL-3	13.69	99.23	0.8667	1.16
TNL-4	14.89	114.23	0.9442	1.17
TNL-5	14.45	117.63	0.9191	0.816
Mean Value	14.18	101.61	0.8872	0.90
Std. Dev.	0.483	14.23	0.0448	0.249
CV (%)	3.4	14.0	5.0	27.6

Table 4-4 Transverse Tensile Properties of AS4/PES, $[\pm 30, 0_4]_s$, Fiber Volume = 54.96%

Specimen # (CZ)(BZ)(AP)	Elastic Modulus E_y^T (Msi)	Ultimate Tensile Strength (ksi)	Poisson Ratio ν_{yx}	Strain To Failure (%)
TNT-1	1.37	4.03	0.0610	0.336
TNT-2	1.57	5.57	0.0737	0.363
TNT-3	1.71	5.12	0.0991	0.305
TNT-4	1.68	2.09*	0.0897	0.214
TNT-5	1.53	5.09	0.0899	0.323
Mean Value	1.57	4.54	0.0827	0.308
Std. Dev.	0.135	1.08	0.0152	0.050
CV (%)	8.6	23.7	1838	16.23

*Failure at doubler end

Table 4-5 Longitudinal Compressive Properties of AS4/PES, $[0, \pm 45, 90]_s$, Fiber Volume = 53.7%

Specimen # (CZ)(BQ)(AP)	Elastic Modulus E_x^C (Msi)	Ultimate Comp. Strength (ksi)	Poisson Ratio ν_{xy}	Strain To Failure (%)
CML-1	6.56	59.49	0.3692	0.924
CML-2	5.47	41.44	0.3245	0.876
CML-3	5.69	47.53	0.328	1.4
CML-4	6.19	47.68	0.3	†
CML-5	5.20	40.42	0.31	†
Mean Value	5.82	47.31	0.326	1.06
Std. Dev.	0.49	7.59	0.026	0.29
CV (%)	8.4	16.0	7.9	27.3

†Change in strain gage polarity, difficult to determine strain failure

Table 4-6 Transverse Compressive Properties of AS4/PES, $[0, \pm 45, 90]_s$, Fiber Volume = 53.7%

Specimen # (CZ)(BQ)(AP)	Elastic Modulus E_Y^C (Msi)	Ultimate Comp. Strength (ksi)	Poisson Ratio ν_{yx}	Strain To Failure (%)
CMT-1	4.71	28.80	0.2832	2.1
CMT-2	7.31	39.92	0.3202	--
CMT-3	4.02	26.93	0.2516	1.85
CMT-4	5.12	31.83	0.2388	1.33
CMT-5	7.0	31.31	0.2977	1.25
Mean Value	5.63	30.36	0.2783	1.63
Std. Dev.	1.45	2.18	0.033	0.41
CV (%)	25.7	7.18	11.85	25.1

Table 4-7 Longitudinal Compressive Properties of AS4/PES, $[\pm 30, 0_4]_S$, Fiber Volume = 54.96%

Specimen # (CZ)(BZ)(AP)	Elastic Modulus E_x^C (Msi)	Ultimate Comp. Strength (ksi)	Poisson Ratio ν_{xy}	Strain To Failure (%)
CML-1	12.95	93.54	0.9673	*
CML-2	12.52	89.73	1.0123	*
CML-3	12.40	95.51	1.00	*
CML-4	11.64	84.05	0.9138	1.88
CML-5	12.30	88.60	0.9291	1.53
Mean Value	12.36	90.29	0.964	> 1.88
Std. Dev.	0.47	4.47	0.043	—
CV (%)	3.8	4.95	4.46	—

* Strain to failure ~2.1%; (specimen failed just beyond strain gage saturation limit of 2%

Table 4-8 Transverse Compressive Properties of AS4/PES, $[\pm 30, 0_4]_S$, Fiber Volume = 54.96%

Specimen # (CZ)(BZ)(AP)	Elastic Modulus E_y^C (Msi)	Ultimate Comp. Strength (ksi)	Poisson Ratio ν_{yx}	Strain To Failure (%)
CMT-1	1.14	17.08	0.2557	*
CMT-2	1.40	24.10	0.1409	*
CMT-3	1.24	22.05	0.1429	*
CMT-4	--	--	--	--
CMT-5	--	--	--	--
Mean Value	1.26	21.07	0.1798	~ 2.0
Std. Dev.	0.13	3.6	0.066	
CV (%)	10.3	17.0	36	

* Strain to failure ~2.1%; (specimen failed just beyond strain gage saturation limit of 2%

the fiber misalignment in the laminate.

In general, longitudinal and transverse compressive behavior of the $[30, -30, 0_4]_s$ laminate was similar to the P75/PEEK composite, though the strain to failure of approximately 2% was significantly higher than 0.35% ε_f for the P75/PEEK laminates. For both of the laminates, the tension and compression test data is summarized in Table 4-9. The high coefficient of variation (>10%) in the data of these laminates can be attributed to fiber misalignment and localized delamination in test specimens.

(c) Flexure Tests

Flexure modulus and strength values of longitudinal and transverse AS4/PES specimens obtained from three point bend tests are listed in Table 4-10. These test results indicate that the flexural modulus of highly anisotropic laminates is a critical function of ply stacking sequence, and does not correlate with t he tensile modulus which is independent of stacking sequence. For example, in the longitudinal $[0, \pm 45, 90]_s$ specimens, outer [0°] ply significantly influenced the load-deflection response, as compared to the 90° outer ply in the transverse flexure test. Therefore, the longitudinal flexural modulus of 9.26 Msi was considerably higher than the transverse modulus of 1.68 Msi.

(d) Interlaminar Shear Strength (ILSS)

Short beam shear three-point bend tests were conducted to determine the apparent interlaminar shear strength values as listed in Table 4-11 for the quasi-isotropic and zero-CTE laminates. The ILSS values of 7.11 ksi and 9.81 ksi respectively, were consistent with the expected response of organic matrix composites. After testing, each specimen was examined under an optical microscope which confirmed that the failure was primarily interlaminar shear.

Table 4-9 Summary of Tensile and Compressive Properties of AS4/PES Composites

Material AS4/PES		Tension				Compression			
Flat Panels	Test Direction	E (Msi)	F^{TU} (ksi)	e_f (%)	ν_{xy}	E (Msi)	F^{CU} (ksi)	e_f (%)	ν_{xy}
(CZ)(BQ)(AP) -Quasi-Isotropic $[0,\pm45,90]_s$ V_f=0.537	X	6.38	80.34	1.35	0.2918	5.82	47.31	1.06	0.326
	Y	6.51	77.69	1.18	0.324	5.63	30.36	1.63	0.2783
(CZ)(BZ)(AP) -Zero CTE Layup $[30,-30,0_4]_s$ V_f=0.549	X	14.18	101.61	0.90	0.8872	12.36	90.29	>1.8	0.964
	Y	1.57	4.54	0.308	0.0827	1.26	21.07	~2.0	0.1798

Table 4-10 Longitudinal and Transverse Flexural Properties (3 point bend) of AS4/PES Composites

Flat Panel $[0,\pm45,90]_s$, --SN 008Q: v/o=53.7			Flat Panel $[30,-30,0_4]_s$, --SN002Z v/o=54.96		
Specimen # (GE)(PQ)(AP)	Longitudinal Flexural Modulus (Msi)	Strength (ksi)	Specimen # (CZ)(BZ)(AP)	Longitudinal Flexural Modulus (Msi)	Strength (ksi)
FXL-51	9.36	157.10	FXL-51	7.06	149.88
FXL-52	9.43	160.95	FXL-52	7.09	151.64
FXL-53	9.00	153.44	FXL-53	7.41	154.13
Mean	9.26	157.16	Mean	7.18	151.88
Standard Deviation	0.23	3.75	Standard Deviation	0.19	2.13
CV(%)	2.48	2.39	CV(%)	2.64	1.4
Specimen # (CZ)(BQ)(AP)	Transverse Flexural Modulus (Msi)	Strength (ksi)	Specimen # (CZ)(BZ)(AP)	Transverse Flexural Modulus (Msi)	Strength (ksi)
FXT-71	1.60	64.91	FXT-71	1.38	27.73
FXT-72	1.65	69.70	FXT-72	1.33	27.75
FXT-73	1.79	79.20	FXT-73	1.31	28.00
Mean	1.68	71.27	Mean	1.34	27.83
Standard Deviation	0.09	7.27	Standard Deviation	0.036	0.15
CV(%)	5.35	10.2	CV(%)	2.68	0.54

Table 4-11 (Apparent) Interlaminar Shear Strength of AS4/PES Composites

AS4/PES $[0, \pm 45, 90°]_S$		AS4/PES $[30, -30, 0_4]_S$	
Specimen # (CZ)(BQ)(AP)	ILSS (ksi)	Specimen # (CZ)(BZ)(AP)	ILSS (ksi)
IL-8Q1	7.64	IL-2Z1	10.97
IL-8 Q2	8.44	IL-2Z3	10.74
IL-8Q3	6.43	IL-2Z4	10.24
IL-8Q4	6.71	IL-2Z5	9.85
IL-8Q6	6.89	IL-2Z6	9.54
IL-8Q7	6.86	IL-2Z7	10.13
IL-8Q8	7.44	IL-2Z8	9.60
IL-8Q10	6.79	IL-2Z10	8.07
IL-8Q11	6.74	IL-2Z11	9.75
IL-8Q12	7.15	IL-2Z12	9.18
Mean	7.11	Mean	9.81
Std. Dev.	0.59	Std. Dev.	0.82
CV %	8.30	CV %	8.36

4.1.4 Thermophysical Properties

(a) Coefficient of Thermal Expansion

Thermal expansion response of quasi-isotropic and zero-CTE laminates is presented in Figures 4-3 to 4-6. These results, including average CTE, residual strain and RT hysteresis are summarized in Table 4-12. For the $[0, \pm 45, 90]_S$ laminate, the nearly equivalent longitudinal CTE (1.08 ppm/°F) and transverse CTE (1.38 ppm/°F) values confirmed the quasi-isotropic behavior of composite. Yet, the differences in residual strain and hysteresis between the longitudinal and transverse directions were indicative of the differences in the residual stress state particularly in the first cycle. In contrast, the thermal expansion response of $[30, -30, 0_4]_S$ laminate showed low residual strain and hysteresis, suggesting reduced residual stress levels in the as-consolidated of zero-CTE panels.

(b) Specific Heat

Figure 4-7 shows the specific heat versus temperature response for the AS4/PES laminates. The specific heat values for the quasi-isotropic and zero-CTE laminates were nearly identical between -150°F and 775°F.

(c) Thermal Diffusivity

Thermal diffusivity results are presented in Table 4-13 and plotted in Figure 4-8. These results indicate:

- Through-the-thickness diffusivity values in both the quasi-isotropic and zero-CTE laminates are identical.
- Longitudinal diffusivity values in both the laminates are about the same.
- Transverse diffusivity values in zero-CTE laminate are intermediate between the diffusivity values in through-the-thickness and longitudinal direction.
- In the quasi-isotropic laminate, transverse direction values are about 50% larger than

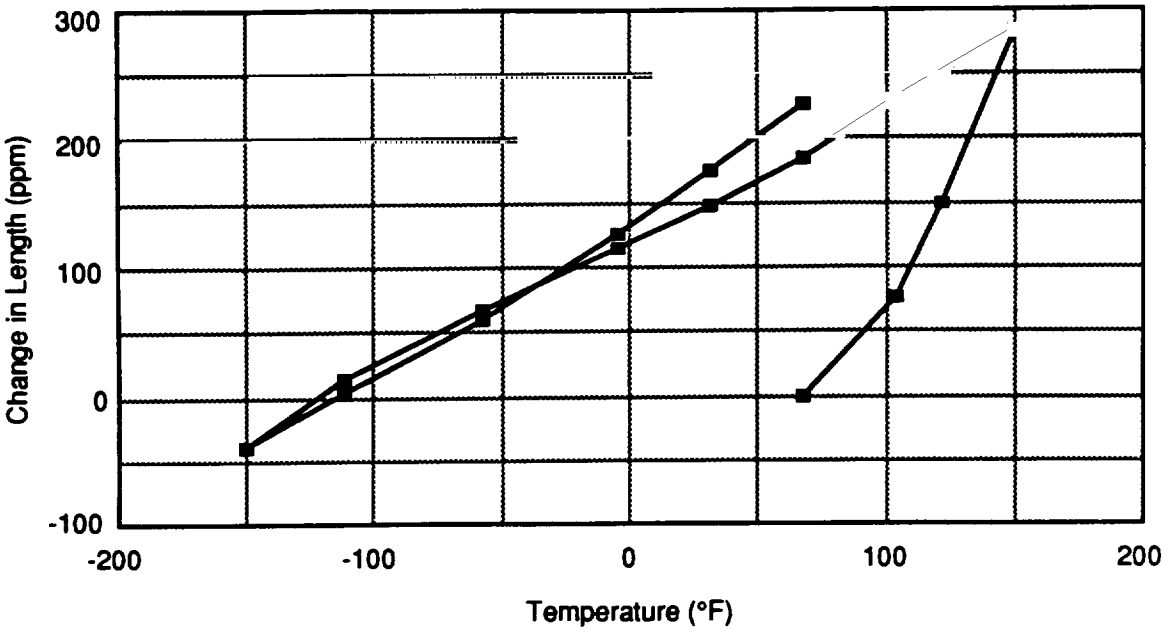

Figure 4-3 Thermal Expansion Behavior of Longitudinal AS4/PES [0, ±45, 90]$_s$ Specimen in a Heat/Cool/Heat Cycle Using Push Rod Dilatometer

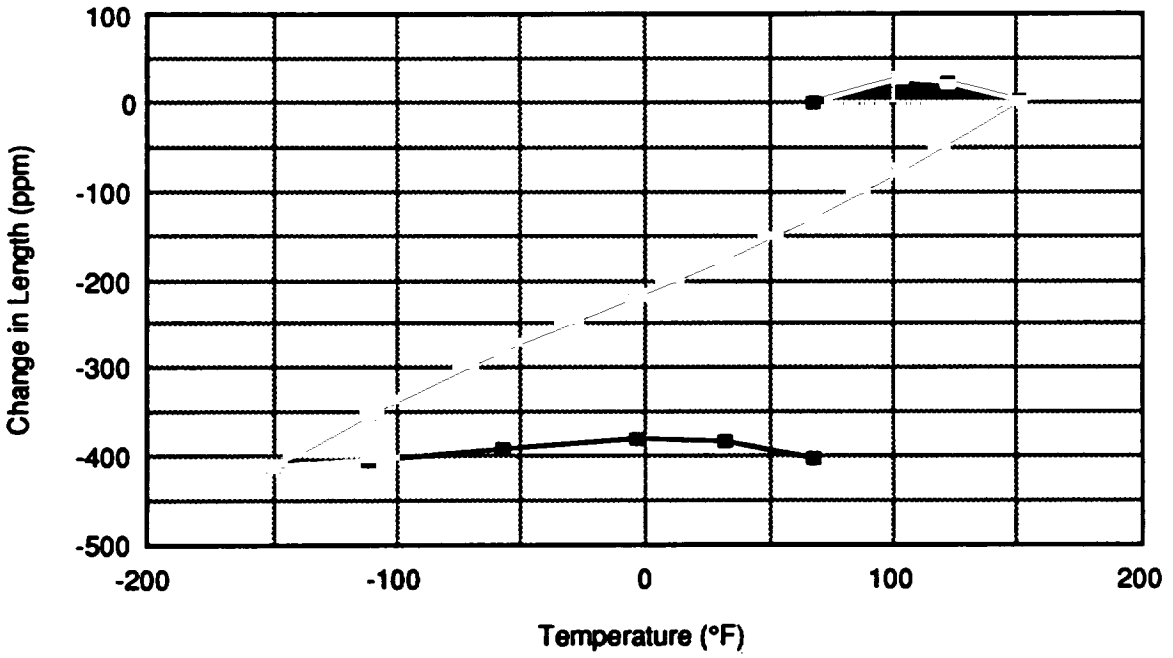

Figure 4-4 Thermal Expansion Behavior of Transverse AS4/PES [0, ±45, 90]$_s$ Specimen in a Heat/Cool/Heat Cycle Using Push Rod Dilatometer

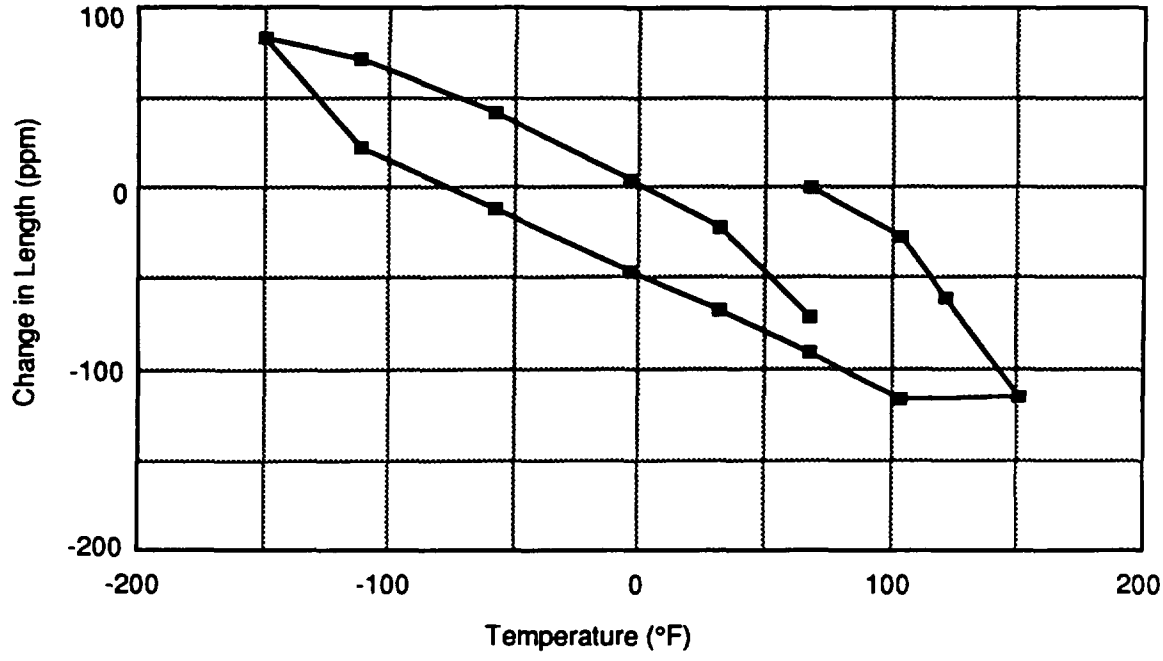

Figure 4-5 Thermal Expansion Behavior of Longitudinal AS4/PES [±30, 0_4]$_s$ Specimen in a Heat/Cool/Heat Cycle Using Push Rod Dilatometer

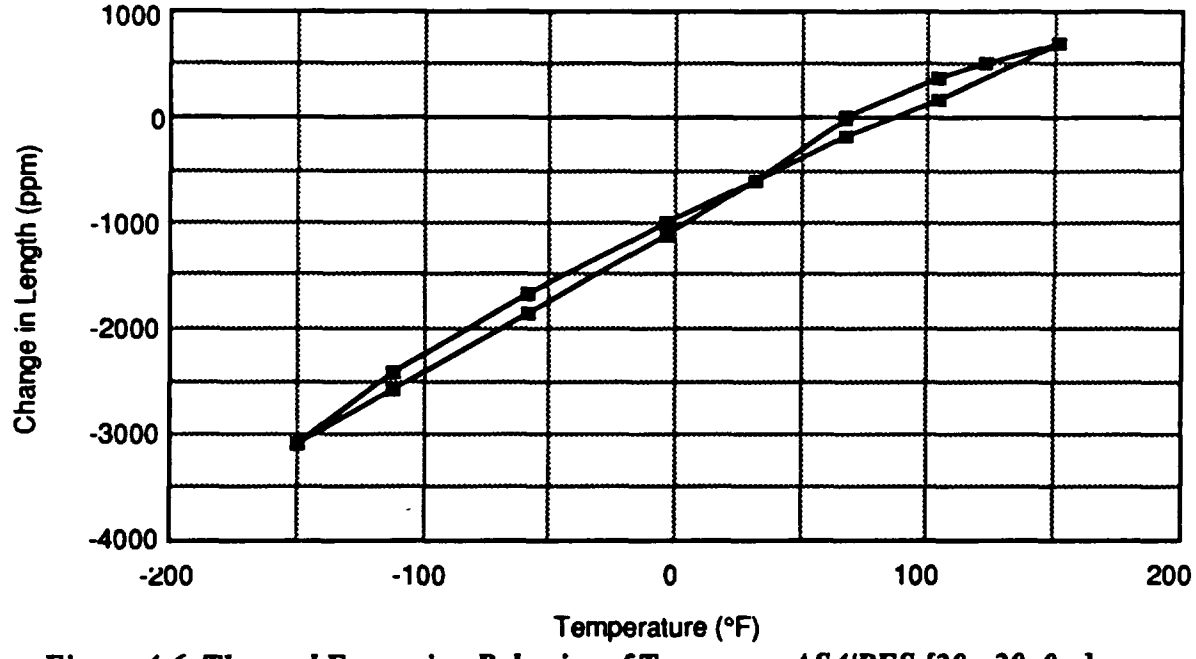

Figure 4-6 Thermal Expansion Behavior of Transverse AS4/PES [30, -30, 0_4]$_s$ Specimen in a Heat/Cool/Heat Cycle Using Push Rod Dilatometer

Table 4-12 Summary of Thermal Expansion Test Data of AS4/PES Composites

Thermal Expansion Measurements	AS4/PES $[0, \pm 45, 90]_s$ $V_f = 0.537$		AS4/PES $[30, -30, 0_4]_s$ $V_f = 0.5496$	
	Longitudinal	Transverse	Longitudinal	Transverse
CTE (ppm/°F)*	1.08	1.38	-0.66	12.6
Residual strain (ppm)	226	-403.6	-71.55	-14.4
Strain Hysteresis (ppm)†	184.2	-128.6	-91.5	-195.2

*(end to end point average); †at RT (i.e., RT → 150°F → RT)

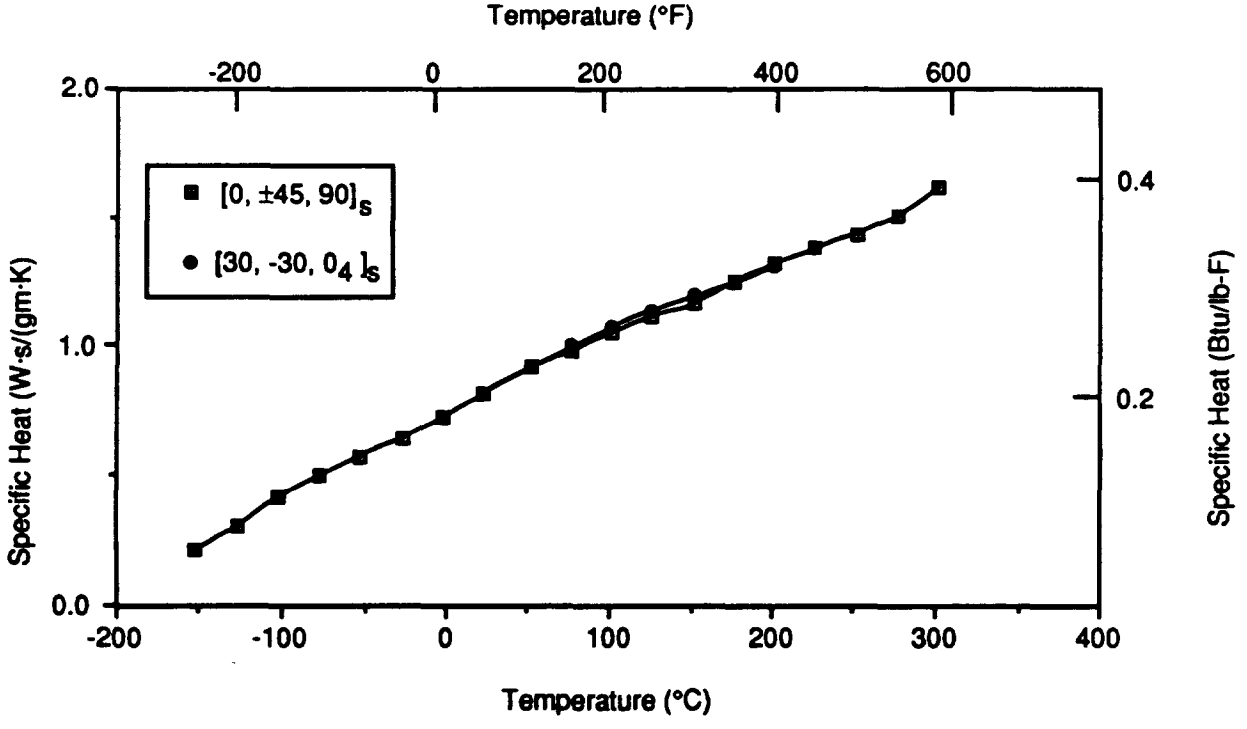

Figure 4-7 Specific Heat Versus Temperature for AS4/PES

Table 4-13 Thermal Diffusivity of AS4/PES Composites

Thermal Diffusivity cm^2/sec								
Temp (°C)	BZ-TT	BQ-TT	Temp (°C)	BZ-L	BQ-L	Temp (°C)	BZ-T	BQ-T
-150.0	0.00511		-150.0	0.0196		-150.0	0.0097	
-125.0	0.00490		-121.0	0.0193		-110.0	0.0088	
-100.0	0.00472		-92.0	0.0192		-100.0	0.0088	
-75.0	0.00456		-53.0	0.0189		-49.0	0.0081	
-50.0	0.00437		-3.0	0.0186		-3.0	0.0071	
-25.0	0.00421		23.0	0.0183	0.0179	23.0	0.0069	0.0305
0.0	0.00406		50.0	—	0.0176	50.0	—	0.0300
23.0	0.00393	0.00395	100.0	0.0175	0.0171	100.0	0.0062	0.0030
100.0	0.00363		200.0	0.0164		200.0	0.0053	
200.0	0.00310		300.0	0.0146		300.0	0.0044	
300.0	0.00065		400.0	0.0137				
Through Thickness			Longitudinal			Transverse		

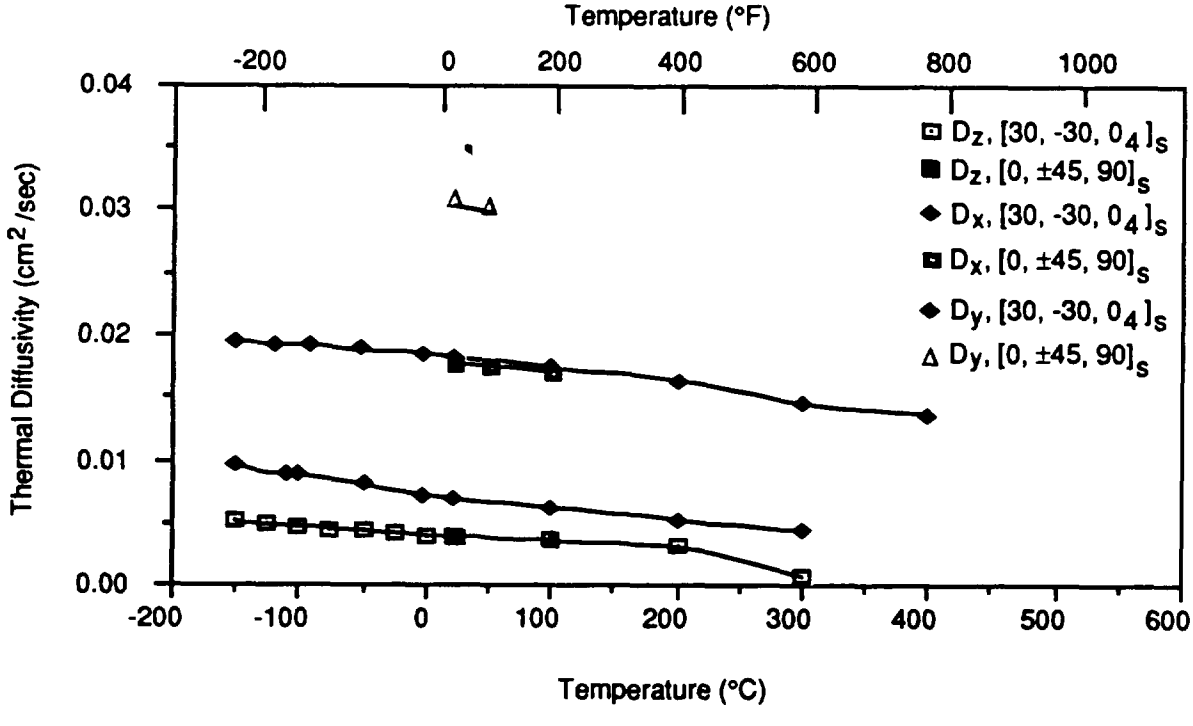

Figure 4-8 Thermal Diffusivity Versus Temperature of AS4/PES Composites

the diffusivity values in longitudinal direction.

Both the lack of quasi-isotropic response in $[0, \pm 45, 90]_s$, and low longitudinal diffusivity in $[30, -30, 0_4]_s$ suggest the presence of disbonds or microcracks in the longitudinal specimens compared to the transverse specimens, because these internal defects significantly influence the thermal diffusivity and conductivity values.

(d) Thermal Conductivity

Thermal conductivity results of both the laminates are presented in Table 4-14 and plotted in Figure 4-9. These values are calculated from the product of the measure thermal diffusivity (D), specific heat (Cp), and density (ρ). Therefore, the remarks related to thermal diffusivity of each laminate are also applicable to the conductivity results.

(e) Optical Properties

For both the quasi-isotropic and zero-CTE laminates:

- Solar absorptance (α_s) = 0.92 (measured over 0.3-0.4 μm wavelength)
- Normal emissivity (ε_N) = 0.89
- Fourier transform infra-red (FTIR) reflectance spectra: Figure 4-10 and 4-11 show the FTIR reflectance spectra between 2 μm and 14 μm wavelength for the $[0, \pm 45, 90]_s$ and $[30, -30, 0_4]_s$ laminate respectively. Both the laminates show similar optical response. Based on these reflectance measurements, the emissivity varied between 0.85 and 0.96.

4.2 SUMMARY OF AS4/PES TEST DATA

Material properties of $[0, \pm 45, 90]_s$ and $[30, -30, 0_4]_s$ laminates are summarized in Table 4-15 and 4-16 respectively.

Table 4-14 Thermal Conductivity Calculations of AS4/PES Composites

Sample (No.)	Temp. (°C)	Density ($gm \cdot cm^{-3}$)	Specific Heat ($W \cdot s \cdot gm^{1} \cdot K^{1}$)	Diffusivity ($cm^2\ sec^{1}$)	Conductivity ($W \cdot cm^{-1}\ K^{-1}$)	Conductivity (Btu Units*)	Temp. (°F)
(CZ)(BZ)-TT	-150	1.594	0.2150	0.00511	0.00175	1.21	-238
(CZ)(BZ)-TT	-100	1.594	0.4200	0.00472	0.00316	2.19	-148
(CZ)(BZ)-TT	-50	1.594	0.5790	0.00437	0.00403	2.80	-58
(CZ)(BZ)-TT	0	1.594	0.7290	0.00406	0.00472	3.27	32
(CZ)(BZ)-TT	25	1.594	0.8200	0.00393	0.00514	3.56	77
(CZ)(BZ)-TT	100	1.594	1.0570	0.00363	0.00612	4.24	212
(CZ)(BZ)-TT	200	1.594	1.3230	0.00310	0.00654	4.53	392
(CZ)(BZ)-TT	300	1.594	1.6200**	0.00065	0.00168	1.16	572
(CZ)(BZ)-TKL	-150	1.573	0.2150	0.01950	0.00659	4.57	-238
(CZ)(BZ)-TKL	-100	1.573	0.4200	0.00192	0.00127	0.88	-148
(CZ)(BZ)-TKL	-50	1.573	0.5790	0.01900	0.01730	12.00	-58
(CZ)(BZ)-TKL	0	1.573	0.7290	0.01870	0.02144	14.87	32
(CZ)(BZ)-TKL	25	1.573	0.8200	0.01860	0.02399	16.63	77
(CZ)(BZ)-TKL	100	1.573	1.0570	0.01760	0.02926	20.29	212
(CZ)(BZ)-TKL	200	1.573	1.3230	0.01630	0.03392	23.52	392
(CZ)(BZ)-TKL	300	1.573	1.6200**	0.01500	0.03822	26.50	572
(CZ)(BZ)-TKL	400	1.573	1.7600**	0.01370	0.03793	26.30	752
(CZ)(BZ)-TKT	-150	1.587	0.2150	0.00980	0.00334	2.32	-238
(CZ)(BZ)-TKT	-100	1.587	0.4200	0.00870	0.00580	4.02	-148
(CZ)(BZ)-TKT	-50	1.587	0.5790	0.00780	0.00717	4.97	-58
(CZ)(BZ)-TKT	25	1.587	0.8200	0.00680	0.00885	6.14	77
(CZ)(BZ)-TKT	100	1.587	0.7920	0.00620	0.00717	4.97	212
(CZ)(BZ)-TKT	200	1.587	0.8700	0.00530	0.00732	5.07	392
(CZ)(BZ)-TKT	300	1.587	1.0570	0.00440	0.00738	5.12	572
(CZ)(BQ)-TT	25.0	1.594	0.8250	0.00395	0.00519	3.60	77.0
(CZ)(BQ)-TKL	25.0	1.563	0.8250	0.01790	0.02308	16.00	77.0
(CZ)(BQ)-TKL	100.0	1.563	1.0810	0.01710	0.02889	20.03	212.0
(CZ)(BQ)-TKT	25.0	1.570	0.8250	0.03050	0.03951	27.39	77.0
(CZ)(BQ)-TKT	100.0	1.570	1.0810	0.02950	0.05007	34.71	212.0

* - ($Btu \cdot in \cdot hr^{1}\ ft^{2}\ F^{1}$); TT - Through-plane; TKL - Longitudinal Direction; TKT - Transverse Direction

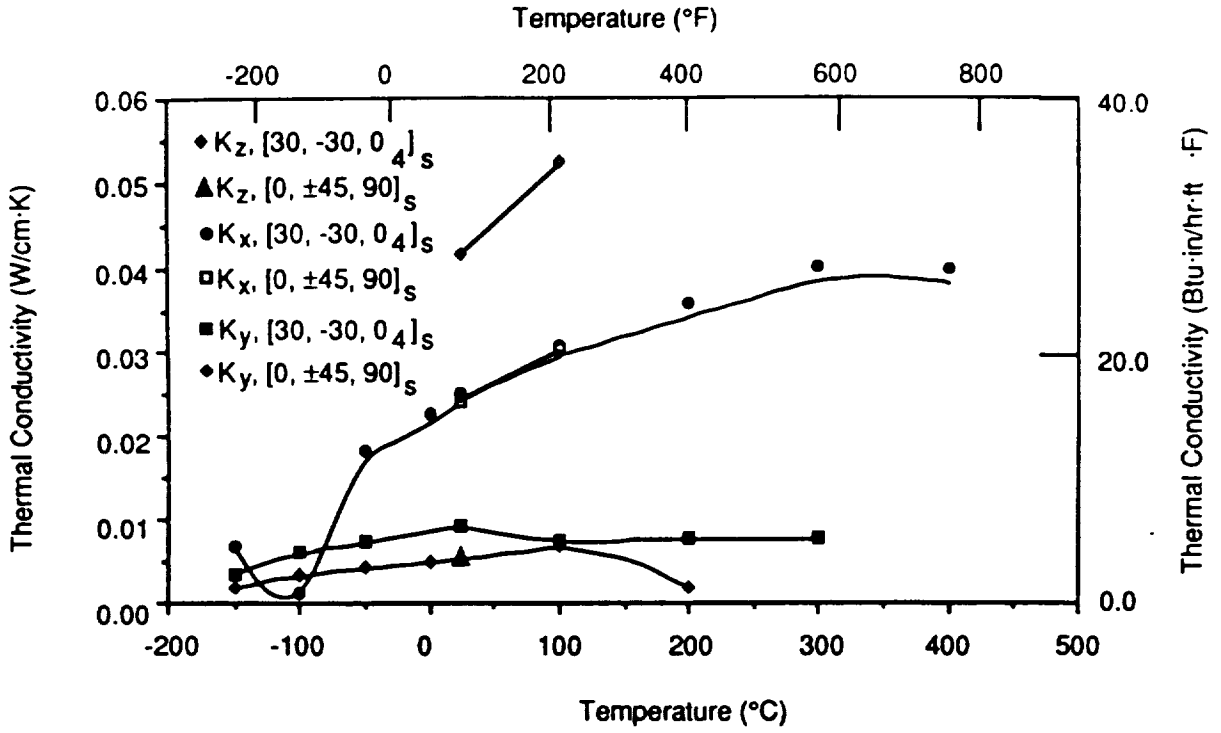

Figure 4-9 Thermal Conductivity Versus Temperature of AS4/PES Composites

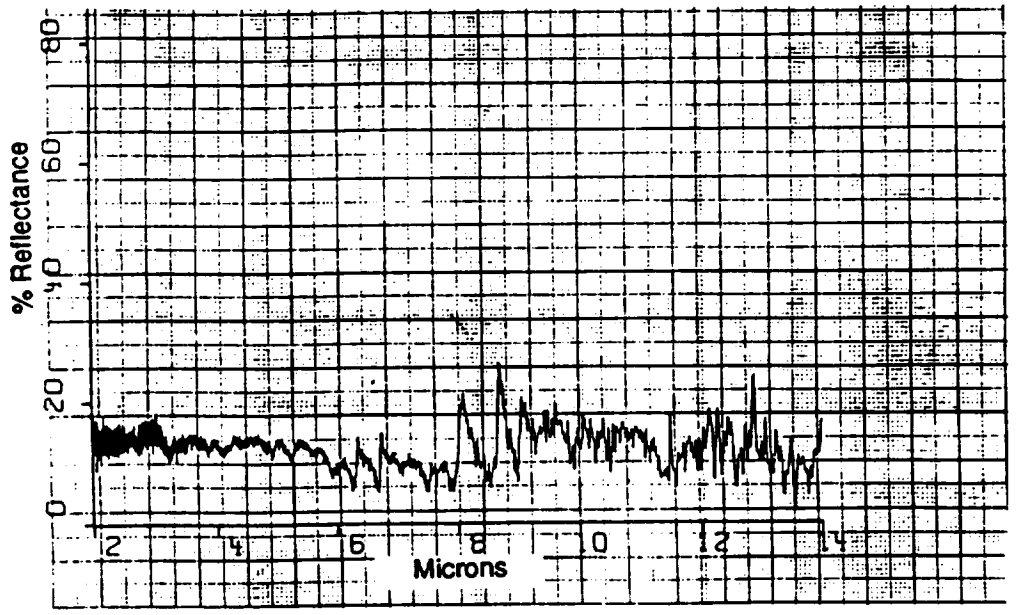

Figure 4-10 Reflectance as a Function of Wavelength of the Quasi-isotropic AS4/PES [0, ±45, 90]$_s$ Laminate, v/o = 53.7

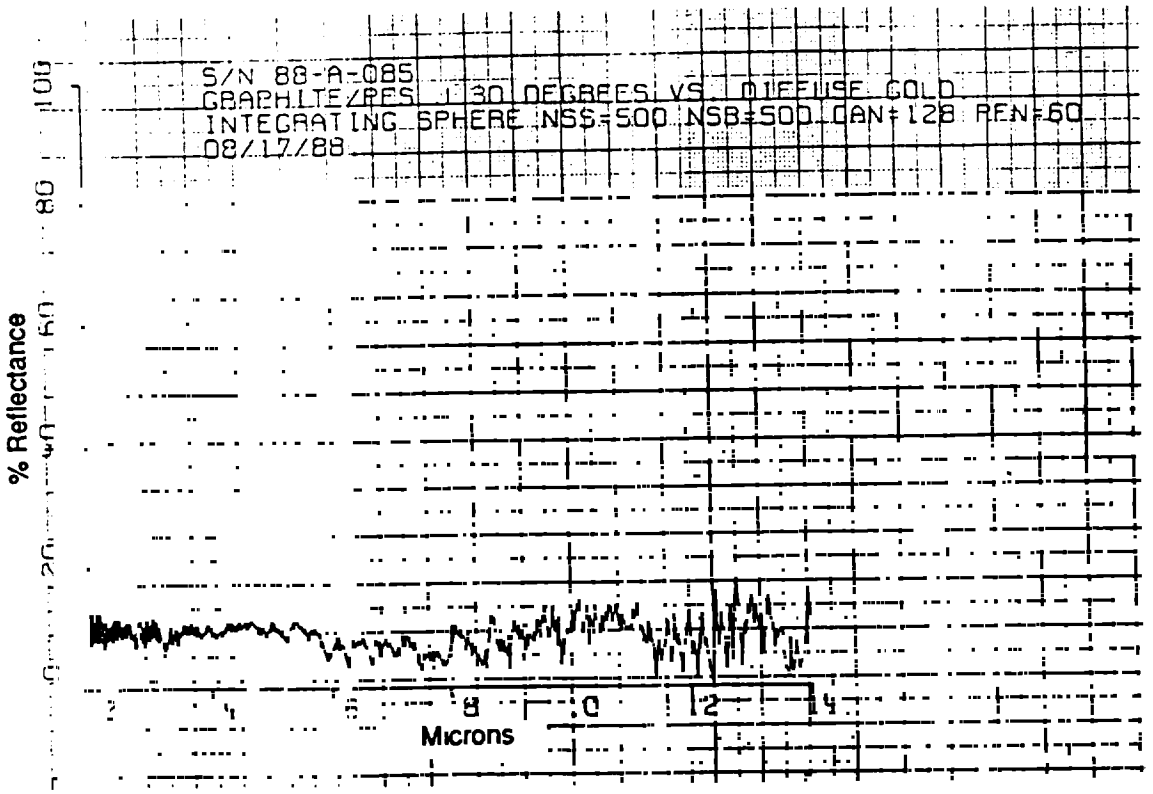

Figure 4-11 Reflectance as a Function of Wavelength of the Zero-CTE AS4/PES $[\pm 30, -30, 0_4]_s$ Laminate, v/o = 54.96

Table 4-15 AS4/PES Carbon/Thermoplastic [0, ±45, 90]$_s$

NOT DESIGN ALLOWABLE DATA

PROPERTIES							TEMPERATURE (°F)			Std. Dev. / No. of Specimens at RT	Test Method
PHYSICAL			MECHANICAL & THERMAL				Low	Room	High		
Density (lb / in^3)		0.0578	Longitudinal Tensile Strength	σ_x^{TU}	ksi			80.34		± 6.13 / 5	ASTM D-3039
Fiber volume fraction		0.537	Transverse Tensile Strength	σ_y^{TU}	ksi			77.69		±4.58 / 5	ASTM D-3039
Void volume fraction		0.01	Longitudinal Comp. Strength	σ_x^{CU}	ksi			47.31		±7.59 / 5	ASTM D-3410
Nominal ply thickness	in	0.005	Transverse comp. strength	σ_y^{CU}	ksi			30.36		±2.18 / 4	ASTM D-3410
Max. cont. use temp.	°F	250	In-plane shear strength	IPSS	ksi						
Ply Orientation	θ	[0/±45/90]s	Interlaminar shear strength	ILSS	ksi			7.11		±0.59 / 10	ASTM D-2344
			Longitudinal tensile strain **	ε_x^T	%			1.35		±0.108 / 5	ASTM D-3039
			Transverse tensile strain **	ε_y^T	%			1.18		±0.053 / 5	ASTM D-3039
			Longitudinal comp. strain **	ε_x^C	%			1.06		±0.29 / 2	ASTM D-3410
			Transverse comp. strain **	ε_y^C	%			1.63		±0.41 / 5	ASTM D-3410
OPTICAL & ELECTRICAL (at room temperature)			Longitudinal tensile modulus	E_x	Msi			6.38		±0.111 / 5	ASTM D-3039
Solar Absorptance	α	0.92	Transverse tensile modulus	E_y	Msi			6.51		±0.394 / 5	ASTM D-3039
Normal Emissivity	ε	0.89	Longitudinal comp. modulus	E_x	Msi			5.82		0.49 / 5	ASTM D-3410
			Transverse comp. modulus	E_y	Msi			5.63		±1.45 / 5	ASTM D-3410
			In-plane shear modulus	G	Msi						
			Longitudinal flexural modulus	F_x	Msi			9.26		±0.23 / 3	ASTM D-790M
			Transverse flexural modulus	F_y	Msi			1.68		±0.09 / 3	ASTM D-790M
			Long. tensile Poisson's ratio	ν_{xy}				0.2918		±0.0234 / 5	ASTM D-3039
			Trans. tensile Poisson's ratio	ν_{yx}				0.3240		±0.32 / 5	ASTM D-3039
			Long. thermal conductivity	K_x	(1)			0.11			Kohlrausch
			Trans. thermal conductivity	K_y	(1)			0.19			Kohlrausch
			Thru thickness thermal cond.	K_z	(1)			0.025			Laser Flash
			Specific heat	C_p	(2)			0.197			ASTM E-1269
			Longitudinal CTE	α_x	(3)			1.08			ASTM E-228
			Transverse CTE	α_y	(3)			1.38			ASTM E-228
			Thru thickness CTE	α_z	(3)			—			

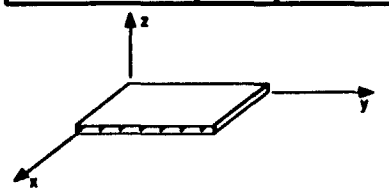

Notes:
(**) - Strain to failure; (1) Btu/(hr·in·°F); (2) Btu/(lb·°F); (3) μin./in./°F

Table 4-16 AS4/PES Carbon/Thermoplastic [±30, 0_4]$_s$

NOT DESIGN ALLOWABLE DATA

PROPERTIES						TEMPERATURE (°F)			Std. Dev. / No. of Specimens at RT	Test Method
PHYSICAL			MECHANICAL & THERMAL			Low	Room	High		
Density (lb / in^3)	X	0.0578	Longitudinal Tensile Strength	σ_x^{TU}	ksi		101.61		± 14.23 / 5	ASTM D-3039
Fiber volume *fraction*	X	0.5496	Transverse Tensile Strength	σ_y^{TU}	ksi		4.54		±1.08 / 5	ASTM D-3039
Void volume fraction	X	0.01	Longitudinal Comp. Strength	σ_x^{CU}	ksi		90.29		±4.47 / 5	ASTM D-3410
Nominal ply thickness	In	0.005	Transverse comp. strength	σ_y^{CU}	ksi		21.07		±3.6 / 5	ASTM D-3410
Max. cont. use temp.	°F	250	In-plane shear strength	IPSS	ksi					
Ply Orientation	θ	[30/-30/04]s	Interlaminar shear strength	ILSS	ksi		9.81		±0.82 / 10	ASTM D-2344
OPTICAL & ELECTRICAL (at room temperature)			Longitudinal tensile strain **	ε_x^T	%		0.90		±0.249 / 5	ASTM D-3039
Solar Absorptance	α	0.92	Transverse tensile strain **	ε_y^T	%		0.308		±0.05 / 5	ASTM D-3039
Normal Emissivity	ε	0.89	Longitudinal comp. strain **	ε_x^C	%		1.88			ASTM D-3410
			Transverse comp. strain **	ε_y^C	%		2.0			ASTM D-3410
			Longitudinal tensile modulus	E_x	Msi		14.18		±0.483 / 5	ASTM D-3039
			Transverse tensile modulus	E_y	Msi		1.57		±0.135 / 5	ASTM D-3039
			Longitudinal comp. modulus	E_x	Msi		12.36		±0.47 / 5	ASTM D-3410
			Transverse comp. modulus	E_y	Msi		1.26		±0.13 / 5	ASTM D-3410
			In-plane shear modulus	G	Msi					
			Longitudinal flexural modulus	F_x	Msi		7.18		±0.19 / 3	ASTM D-790M
			Transverse flexural modulus	F_y	Msi		1.34		±0.036 / 3	ASTM D-790M
			Long. tensile Poisson's ratio	ν_{xy}	X		0.8872		±0.0448 / 5	ASTM D-3039
			Trans. tensile Poisson's ratio	ν_{yx}	X		0.0827		±0.0152 / 5	ASTM D-3039
			Long. thermal conductivity	K_x	(1)		0.115			Kohlrausch
			Trans. thermal conductivity	K_y	(1)		0.043			Kohlrausch
			Thru thickness thermal cond.	K_z	(1)		0.025			Laser Flash
			Specific heat	C_p	(2)		0.196			ASTM E-1269
			Longitudinal CTE	α_x	(3)		-0.66			ASTM E-228
			Transverse CTE	α_y	(3)		+12.6			ASTM E-228
			Thru thickness CTE	α_z	(3)		—			

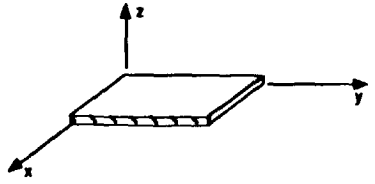

Notes:
(**) - Strain to failure; (1) Btu/(hr·in·°F); (2) Btu/(lb·°F); (3) µin./in./°F

25 V/O Discontinuous
SiC/AL

25 V/O Discontinuous
SiC/AL

5.0 25 V/O DISCONTINUOUS SiC/Al

Discontinuous SiC/Al composites offer higher specific stiffness, a lower CTE, and an improved temperature capability compared to conventional metals used for spacecraft structural applications. In addition these composites have isotropic properties and can be readily fabricated into complex shaped structural components and attachment fittings. Therefore, 25 and 35 v/o SiC_p/2124-T6 flat panels and tubes were procured to generate material property test data. The fabrication data and the results of product evaluation, mechanical and thermophysical property tests for 25 v/o SiC_w/2124-T6 are discussed in this chapter.

5.1 FLAT PANELS

- 25 v/o SiC_p/2124-T6 and
- 25 v/o SiC_w/2124-T6

5.1.1 Fabrication Data

The particulate reinforcement composite panels were procured from two sources: ACMC and BP-DWA to generate representative data of SOA materials, whereas whisker reinforced panels were procured only from ACMC. All the panels were fabricated by conventional powder metallurgy technique which included consolidation of billets followed by hot extrusion and hot rolling steps (Figure 5.1-1). After final hot rolling step, each panel was heat treated to -T6 condition.

Material:	25 v/o SiC_p/2124-T6	25 v/o SiC_w/2124-T6
Fabrication Process:	Powder metallurgy/hot extrusion and rolling	Powder metallurgy/hot extrusion and rolling
Manufacturer:	(i) ACMC, SC (2) BP-DWA, CA	ACMC, SC

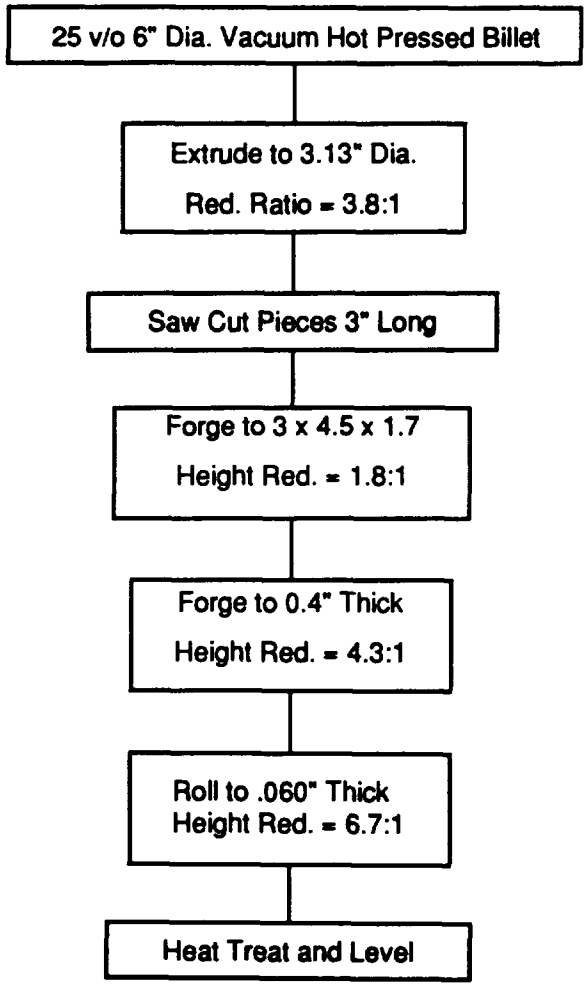

Figure 5.1-1 Fabrication Process to Produce Discontinuous 25 v/o SiC/Al Flat Plates (at ACMC, SC)

Dimension:	12-in. x 12-in. x 0.040-in. (from ACMC, SC) 12-in. x 12-in. x 0.040-in. (from BP-DWA, CA)	12-in. x 12-in. x 0.060-in.
Warpage:	0.375-in./12-in. maximum	0.375-in./12-in. maximum
Lot No.:	ACMC: A6660X3 DWA: P3094	ACMC: A6679Z and A6657Z
Martin Marietta ID:	(25PA)(CQ)(AP) for ACMC panels; and (25PA)(DQ)(AP) for DWA panels	(25WA)(CQ)(AP)

5.1.2 Product Evaluation

(a) Density

- 25 v/o SiC_p/2124-T6: 0.101 lb/in^3

  Std. Dev.: 0.0005

- 25v/o SiC_w/2124-T6: 0.101 lb/in^3

  Std. Dev.: 0.0003

(b) Reinforcement Volume

- ACMC: SiC_p/2124-T6: v/o: 25.3

  Std. Dev.: 1.1

- DWA: SiC_p/2124-T6: v/o: 25.2

  Std. Dev.: 0.8

- ACMC: SiC_w/2124-T6: v/o: 25.3

  Std. Dev.: 0.8

In each case, void volume ≤0.1%

(c) Non-Destructive Evaluation

Based on visual examination, surface quality of each panel was good without voids and scratches. Also, in X-radiographs and ultrasonic C-scans of the panels, no voids, cracks, stringer, or related defects were detected. During in-house quality control evaluation of SiC_w/Al panels at the intermediate production stages, ACMC detected a few fine cracks at the surface along the rolling direction, and therefore marginally approved the material. The X-radiographs and ultrasonic C-scans of these panels did not reveal any microcracks.

(d) Microstructure

Typical microstructures of both particulate and whisker reinforced composites are shown in Figure 5.1-2 and 5.1-3 respectively. These microstructures indicate that the overall reinforcement distribution is nearly uniform in both composites. In the particulate reinforced panels from ACMC the average particle size was 3 μm compared to 12 μm in the panels from DWA. In SiC_w/Al panels, the average aspect ratio of whiskers was 12.6 (10 - 12 μm length and 0.6 - 1 μm diameter).

5.1.3 Mechanical Properties

Tension, compression, flexure test results of 25 v/o SiC_p and SiC_w/1214-T6 panels from ACMC; and compression and flexure test results of 25 v/o SiC_p/2124-T6 panels from DWA are discussed below.

(a) Tension

25 v/o SiC_p/2124-T6 (ACMC) - Longitudinal and transverse tensile properties of these

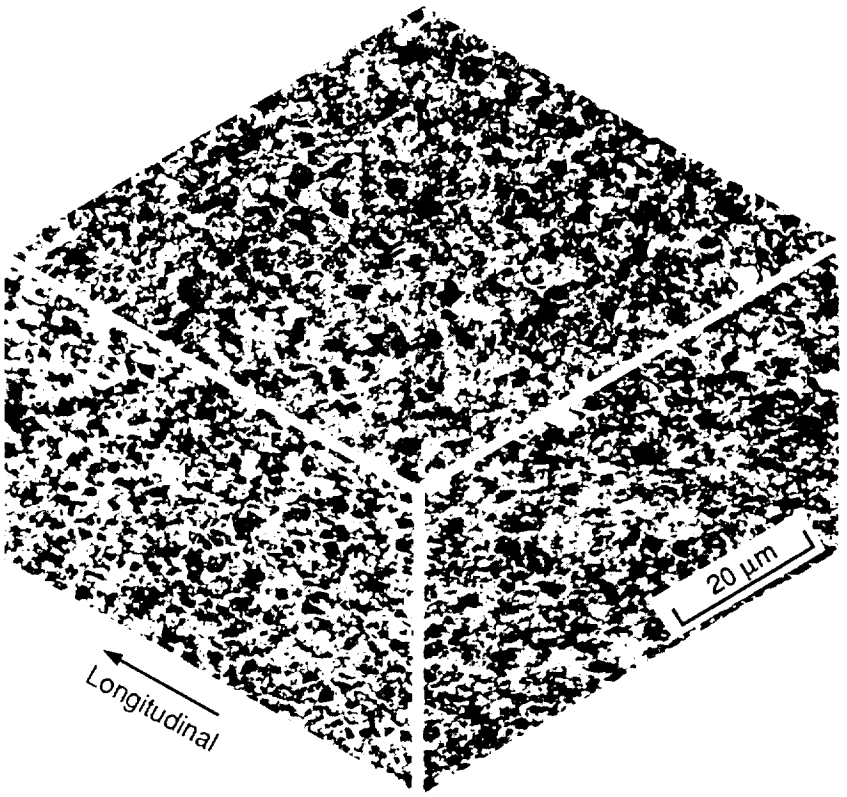

Figure 5.1-2 Three Dimensional Microstructure of 25 v/o SiC_p /2124-T6 Al

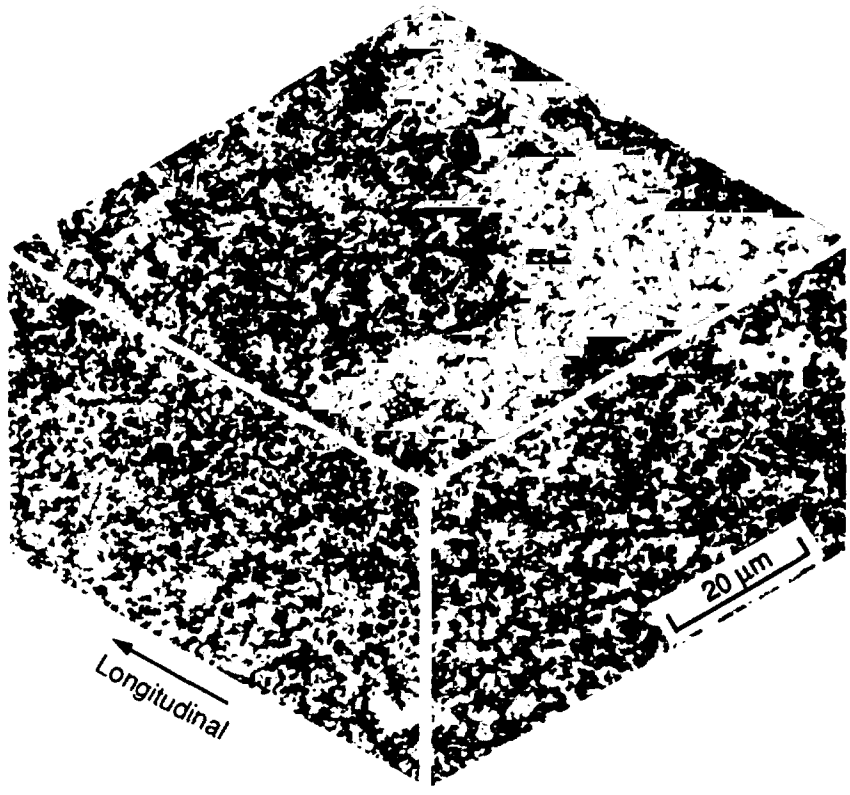

Figure 5.1-3 Three Dimensional Microstructure of 25 v/o SiC_w /2124-T6 Al

composites are listed in Tables 5.1-1 and 5.1-2 respectively. In these tests, the stress strain response of each specimen exhibited the elastic-plastic behavior as shown in Figure 5.1-4.

Mean longitudinal elastic modulus (16.64 Msi) was nearly identical to the transverse modulus (17.0 Msi), suggesting random distribution of the particles in the panels. Yet, the longitudinal strength (84.5 ksi) was about 8% higher than the transverse strength (77.5 ksi). These differences in in-plane strength provide an indication of the anisotropy of residual stresses generated in each direction during cross rolling steps.

25 v/o SiC_w/2124-T6 (ACMC) - Longitudinal and transverse tensile properties of 25 v/o SiC_w/2124-T6 are listed in Table 5.1-3 and 5.1-4 respectively. These results indicate a slightly anisotropic response with a longitudinal elastic modulus of 17.6 Msi and transverse elastic modulus of 16.42 Msi. The high longitudinal modulus was attributed to the alignment of whiskers in the extrusion (longitudinal) direction, as was also evident in the microstructural examination. In addition, the whisker reinforced composite panels yielded a longitudinal modulus value 6% higher and a tensile strength 20% higher than the corresponding particulate reinforced composites.

(b) Compression

25 v/o SiC_p/2124-T6 - Compression test data for ACMC panels are listed in Table 5.1-5 and 5.1-6, and the data for DWA panels are listed in 5.1-7 and 5.1-8. These results indicated that:

(1) ACMC panels exhibited elastic modulus nearly identical in the longitudinal (i.e., 18.5 Msi) and transverse direction (17.9 Msi), indicating an isotropic material response.

(2) DWA panels also exhibited nearly isotropic behavior: E_x^C = 15.9 Msi and E_y^C = 15.35 Msi.

(3) In both the panels, longitudinal strength was higher than the transverse strength, and ACMC panels exhibited higher strength levels than DWA panels.

Table 5.1-1 Longitudinal Tensile Properties of 25v/o SiC_p/2124-T6

Specimen # (25PA)(CQ)(AP)	Elastic Modulus E_x^T (Msi)	Yield Strength (ksi)	Ultimate Tensile Strength (ksi)	Poisson Ratio ν_{xy}	Strain To Failure (%)
TNL-1	17.0	72.7	87.9	0.267	1.26
TNL-2	17.1	72.3	87.3	0.269	1.26
TNL-3	16.1	68.7	81.2	0.268	1.26
TNL-4	16.5	69.1	79.6	0.263	1.26
TNL-5	16.5	69.4	86.3	0.267	1.25
Mean Value	16.64	70.44	84.5	0.267	1.258
Std. Dev.	0.410	1.90	3.79	0.0023	0.0045
CV (%)	2.46	2.69	4.6	0.85	0.36

Table 5.1-2 Transverse Tensile Properties of 25v/o SiC_p/2124-T6

Specimen # (25PA)(CQ)(AP)	Elastic Modulus E_Y^T (Msi)	Yield Strength (ksi)	Ultimate Tensile Strength (ksi)	Poisson Ratio ν_{YX}	Strain To Failure (%)
TNT-1	17.3	68.1	82.3	0.271	1.28
TNT-2	16.8	67.5	78.9	—	1.26
TNT-3	16.7	67.5	79.6	0.298	1.28
TNT-4	16.8	66.9	77.7	—	1.28
TNT-5	17.4	65.9	69.4	0.267	0.80
Mean Value	17.0	67.18	77.5	0.279	1.18
Std. Dev.	0.324	0.83	4.87	0.017	0.212
CV (%)	1.91	1.2	6.3	6.09	17.9

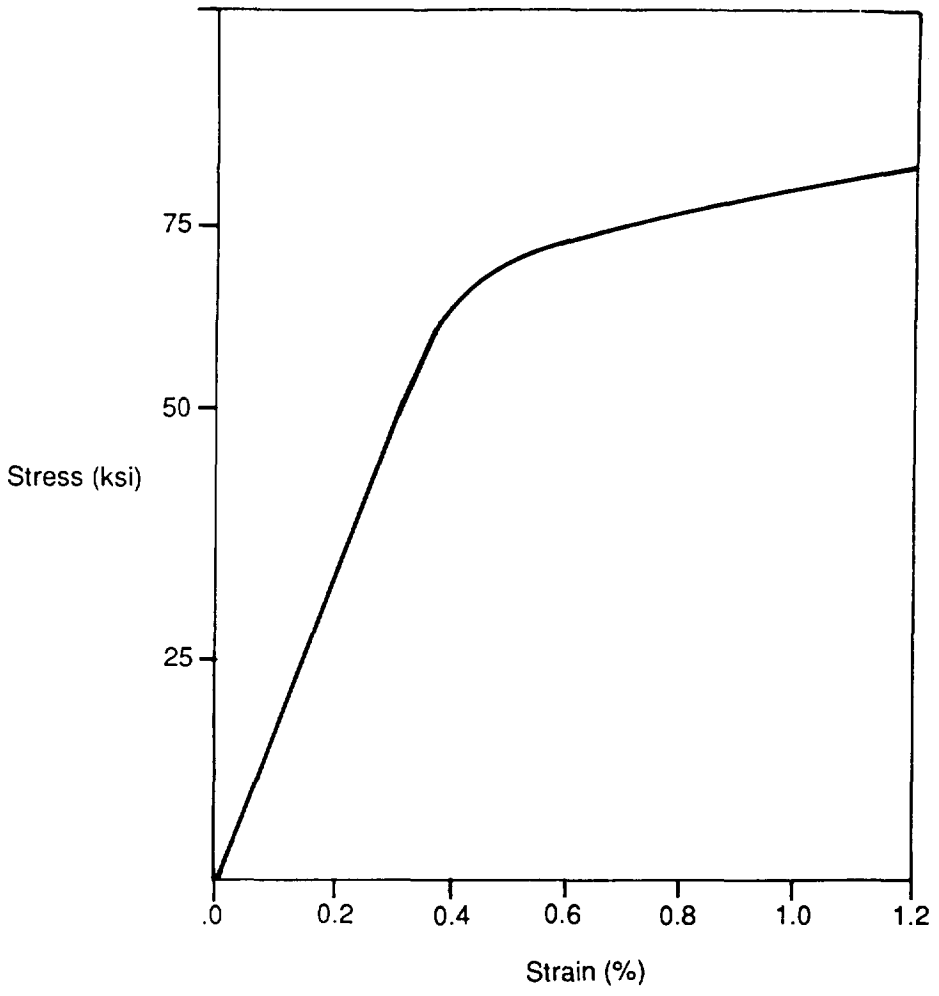

Figure 5.1-4 Typical Stress-Strain Response of 25v/o Discontinuous SiC/2124-T6 Al Composites

Table 5.1-3 Longitudinal Tensile Properties of 25v/o SiCw/2124-T6

Specimen # (25WA)(CQ)(AP)	Elastic Modulus E_x^T (Msi)	Yield Strength (ksi)	Ultimate Tensile Strength (ksi)	Poisson Ratio ν_{xy}	Strain To Failure (%)
TNL-1	17.5	76.4	98.8	0.2793	1.6
TNL-2	17.3	77.0	96.2	0.2883	1.52
TNL-3	17.3	74.8	104.0	0.2933	1.8
TNL-4	17.5	76.1	103.2	0.2904	1.74
TNL-5	18.3	76.9	108.0	0.3159	1.45
Mean Value	17.6	76.2	102.0	0.2934	1.62
Std. Dev.	0.415	0.885	4.62	0.0136	0.15
CV (%)	2.4	1.2	4.5	4.6	9.2

Table 5.1-4 Transverse Tensile Properties of 25v/o SiCw/2124-T6

Specimen # (25WA)(CQ)(AP)	Elastic Modulus E_y^T (Msi)	Yield Strength (ksi)	Ultimate Tensile Strength (ksi)	Poisson Ratio ν_{yx}	Strain To Failure (%)
TNT-1	16.5	71.6	99.2	0.2775	1.78
TNT-2	16.5	72.2	96.3	0.2662	1.8
TNT-3	16.3	71.4	96.1	0.2701	1.9
TNT-4	16.0	69.8	99.0	0.2651	1.8
TNT-5	16.8	70.9	96.5	0.2791	1.85
Mean Value	16.42	71.2	97.4	0.2717	1.83
Std. Dev.	0.295	0.901	1.54	0.00651	0.048
CV (%)	1.8	1.3	1.6	2.4	2.6

Table 5.1-5 Longitudinal Compressive Properties of 25v/o SiC_p/2124-T6 (Vendor: ACMC, SC)

Specimen # (25WA)(CQ)(AP)	Elastic Modulus E_x^C (Msi)	Yield Strength (ksi)	Ultimate Compressive Strength (ksi)	Strain To Failure (%)	Poisson Ratio ν_{xy}
CML-1	18.7	75.2	83.0	0.62	0.261
CML-2	18.3	72.2	77.4	0.62	0.272
CML-3	18.5	73.3	81.3	0.62	0.268
CML-4	18.4	73.3	80.7	0.615	0.267
CML-5	18.8	73.4	81.5	0.615	0.262
Mean Value	18.5	73.5	80.8	0.618	0.266
Std. Dev.	0.207	1.08	2.071	0.0024	0.00453
CV (%)	1.1	1.5	2.6	0.38	1.7

Table 5.1-6 Transverse Compressive Properties of 25v/o SiC_p/2124-T6 (Vendor: ACMC, SC)

Specimen # (25WA)(CQ)(AP)	Elastic Modulus E_y^C (Msi)	Yield Strength (ksi)	Ultimate Compressive Strength (ksi)	Strain To Failure (%)	Poisson Ratio ν_{yx}
CMT-1	18.0	68.0	73.9	0.625	0.271
CMT-2	19.3	72.4	76.6	0.625	0.296
CMT-3	18.0	72.2	74.4	0.62	0.264
CMT-4	17.6	67.0	76.2	0.61	0.275
CMT-5	16.8	68.4	77.8	0.62	0.266
Mean Value	17.9	69.6	75.8	0.62	0.274
Std. Dev.	0.904	2.58	1.610	0.006	.0.0128
CV (%)	5.1	3.6	2.1	0.97	4.7

Table 5.1-7 Longitudinal Compressive Properties of 25v/o SiCp/2124-T6 (Vendor: DWA, CA)

Specimen # (25PA)(DQ)(AP)	Elastic Modulus E_x^C (Msi)	Yield Strength (ksi)	Ultimate Compressive Strength (ksi)	Poisson Ratio ν_{xy}	Strain To Failure (%)
CML-1	15.76	51.84	62.49	0.3755	—
CML-2	15.84	49.69	60.21	0.3140	—
CML-3	16.43	49.43	60.21	0.3240	—
CML-4	15.44	50.31	59.86	0.2942	—
CML-5	—	—	58.90	—	—
Mean Value	15.9	50.32	60.33	0.3269	
Std. Dev.	0.41	1.080	1.32	0.0347	
CV (%)	2.6%	2.15	2.2%	10.6%	

Table 5.1-8 Transverse Compressive Properties of 25v/o SiCp/2124-T6 (Vendor: DWA, CA)

Specimen # (25PA)(DQ)(AP)	Elastic Modulus E_y^C (Msi)	Yield Strength (ksi)	Ultimate Compressive Strength (ksi)	Poisson Ratio ν_{yx}	Strain To Failure (%)
CMT-1	13.7*	46.14	58.74	0.342	—
CMT-2	15.6	48.4	56.8	0.3333	—
CMT-3	15.77	49.28	58.94	0.3050	—
CMT-4	15.04	46.84	54.17	0.3174	—
CMT-5	15.03	50.56	59.02	0.2670	—
Mean Value	15.35	48.77	57.53	0.3057	
Std. Dev.	0.374	1.56	2.091	0.0283	
CV (%)	2.4%	3.2%	3.6%	9.2%	

These differences in modulus and strength values between the ACMC and DWA panels could be primarily attributed to two reasons: (1) particle size effect and (2) differences in heat treatment. The finer particles (3 μm) used in ACMC consolidation process than the 12 μm particles used in DWA panels yield increased contribution to mechanical properties. Also, during heat treatment, matrix in DWA panels may not have fully attained -T6 condition.

25 v/o SiC_w/2124-T6 - Compressive property data of these composites are listed in Table 5.1-9 and 5.1-10. Like tensile test measurements, these results also indicated a slightly anisotropic response with the higher longitudinal elastic modulus (18.15 Msi) than the transverse modulus of 16.5 Msi. The longitudinal compressive strength of 102.5 ksi was nearly identical to the longitudinal tensile strength of 102.0 ksi, but the transverse tensile strength of 97.4 ksi was slightly higher than the transverse compressive strength of 91.0 ksi.

(b) Flexure

25 v/o SiC_p/2124-T6 - Flexure test results of ACMC and DWA panels are listed in Table 5.1-11 and 5.1-12 respectively. Like the compressive property response, average flexural modulus and strength values for ACMC panels were slightly higher than DWA panels.

25 v/o SiC_w/2124-T6 - Flexure test results of 25 v/o SiC_w/2124-T6 are listed in Table 5.1-13. The longitudinal flexural modulus and strength values of 13.1 Msi and 173.1 ksi respectively are slightly higher than the transverse flexural modulus and strength values of 11.8 Msi and 157.4 ksi respectively. Again, the anisotropic behavior was expected due to whisker alignment along the extrusion direction tests, consistent with tension and compression tests.

Table 5.1-9 Longitudinal Compressive Properties of 25v/o SiCw/2124-T6

Specimen # (25WA)(CQ)(AP)	Elastic Modulus E_x^C (Msi)	Yield Strength (ksi)	Ultimate Compressive Strength (ksi)	Poisson Ratio ν_{xy}	Strain To Failure (%)
CML-1	18.1	87.4	101.2	0.2904	1.1
CML-2	17.8	89.4	104.8	0.2748	1.15
CML-3	18.4	—	102.2	0.2819	1.1
CML-4	18.3	88.0	101.9	0.2922	1.1
CML-5	—	—	—	—	—
Mean Value	18.15	88.3	102.5	0.2848	1.11
Std. Dev.	0.265	1.03	1.57	0.0081	0.025
CV (%)	1.46	1.2	1.5	2.8	2.25

Table 5.1-10 Transverse Compressive Properties of 25v/o SiCw/2124-T6

Specimen # (25WA)(CQ)(AP)	Elastic Modulus E_y^C (Msi)	Yield Strength (ksi)	Ultimate Compressive Strength (ksi)	Poisson Ratio ν_{yx}	Strain To Failure (%)
CMT-1	16.4	73.4	90.7	0.2593	1.15
CMT-2	16.6	75.6	91.1	0.2649	1.3
CMT-3	16.4	73.5	88.4	0.2632	1.25
CMT-4	'16.0	75.6	94.3	0.2585	1.4
CMT-5	16.9	75.5	90.3	0.2609	1.2
Mean Value	16.5	74.7	91.0	0.2614	1.26
Std. Dev.	0.33	1.16	2.13	0.0027	0.096
CV (%)	2.0	1.6	2.3	1.0	7.6

Table 5.1-11 Longitudinal and Transverse Flexural Properties (3 Point Bend) of 25 v/o SiC_p/Al (Vendor: ACMC, SC)

Specimen # (25PA)(CQ)(AP)	Longitudinal Flexural		Specimen # (25PA)(CQ)(AP)	Transverse Flexural	
	Modulus (Msi)	Strength (ksi)		Modulus (Msi)	Strength (ksi)
FXL-1	13.43	158.9	FXT-1	13.81	147.3
FXL-2	13.69	140.1	FXT-2	13.33	146.5
FXL-3	13.41	161.0	FXT-3	12.54	152.2
Mean	13.51	153.3	Mean	13.02	148.7
Standard Deviation	0.156	11.51	Standard Deviation	0.4195	3.086
CV(%)	1.1	7.5	CV(%)	3.2	2.1

Table 5.1-12 Longitudinal and Transverse Flexural Properties (3 Point Bend) of 25 v/o SiC_p/Al (Vendor: BP-DWA, CA)

Specimen # (25PA)(DQ)(AP)	Longitudinal Flexural		Specimen # (25PA)(DQ)(AP)	Transverse Flexural	
	Modulus (Msi)	Strength (ksi)		Modulus (Msi)	Strength (ksi)
FXL-1			FXT-1	12.87	138.2
FXL-2			FXT-2	12.81	137.9
FXL-3			FXT-3	12.37	126.2
Mean			Mean	12.68	134.1
Standard Deviation			Standard Deviation	0.27	6.84
CV(%)			CV(%)	2.1	5.1

Table 5.1-13 Longitudinal and Transverse Flexural Properties (3 Point Bend) of 25 v/o SiC_w/Al (Vendor: ACMC, SC)

Specimen # (25WA)(CQ)(AP)	Longitudinal Flexural		Specimen # (25WA)(CQ)(AP)	Transverse Flexural	
	Modulus (Msi)	Strength (ksi)		Modulus (Msi)	Strength (ksi)
FXL-1	12.9	180.4	FXT-1	11.8	159.8
FXL-2	13.2	162.9	FXT-2	11.9	152.3
FXL-3	13.3	172.9	FXT-3	11.8	160.0
Mean	13.1	172.1	Mean	11.8	157.4
Standard Deviation	0.208	8.8	Standard Deviation	0.0577	4.39
CV(%)	1.6	5.1	CV(%)	0.5	2.8

5.1.4 Thermophysical Properties

(a) Coefficient of Thermal Expansion

Thermal expansion test results of 25 v/o particulate and whisker reinforced panels are presented in Figure 5.1-5 to 5.1-8. These results including CTE, RT strain hysteresis, and residual strain are summarized in Table 5.1-14.

Measured CTE values of these composites were compared with the values predicted by Kerner equations for random particulate distribution and aligned distribution (Appendix D) Table 5.1-15 shows that measured CTE values are in agreement with the predicted values. These results also suggest that whiskers are aligned during rolling or extrusion steps of the fabrication process.

(b) Specific Heat

Specific heat results of 25 v/o particulate and whisker reinforced composites are presented in Figure 5.1-9. The measured Cp of 0.198 Btu/lb·°F (0.830 $W \cdot s \cdot gm^{-1} \cdot K^{-1}$) at RT is in excellent agreement with predicted value of 0.197 Btu/lb·°F. Also, each specimen exhibited a relatively stable peak in Cp values at 435°F, corresponding to the phase transformation in Al matrix.

(c) Thermal Diffusivity

For the 25 v/o discontinuous SiC/Al composites, the diffusivity values are presented in Figure 5.1-10. In the diffusivity values for duplicate sample, the scatter in measurements was within 7%. At temperatures below RT, the average diffusivity of the SiC_p/Al was higher than the SiC_w/Al.

(d) Thermal Conductivity

In-plane thermal conductivity values are plotted in Figure 5.1-11 and through thickness conductivity results are presented in Figure 5.1-12. These results show:

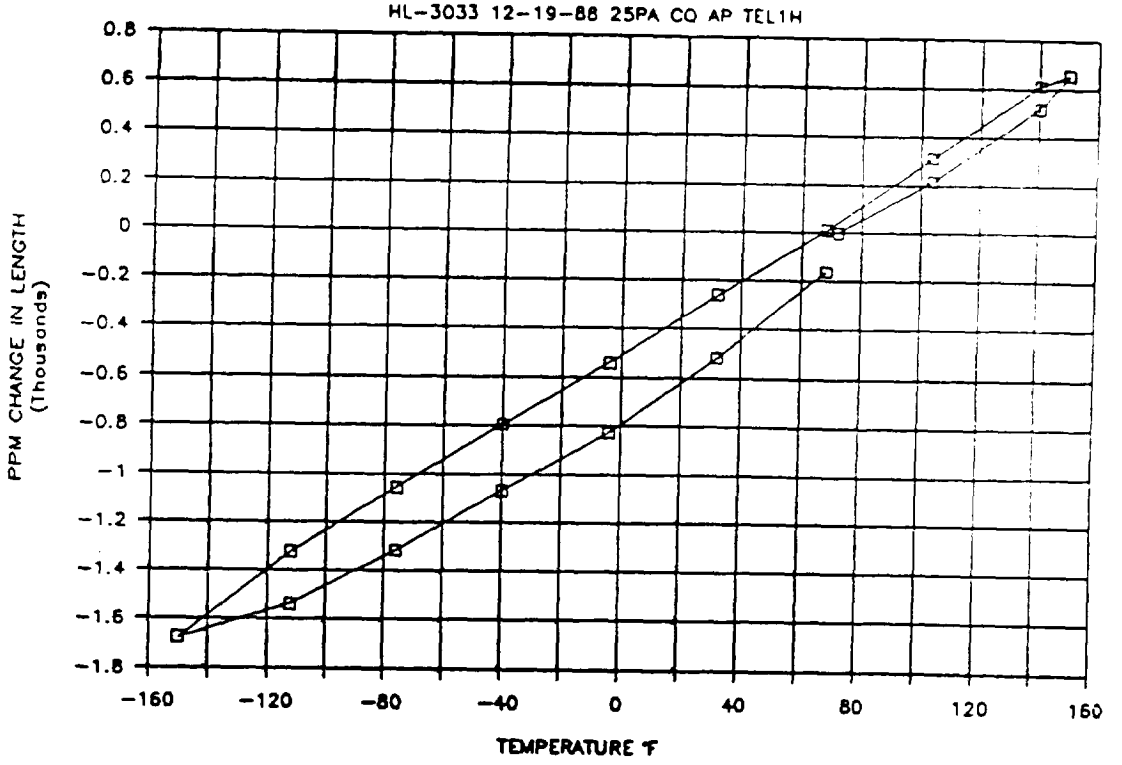

Figure 5.1-5 Thermal Expansion Behavior of 25v/o SiC_p/2124-T6 Specimen Parallel to the Extrusion Direction in a Heat/Cool/Heat Cycle Using Push Rod Dilatometer

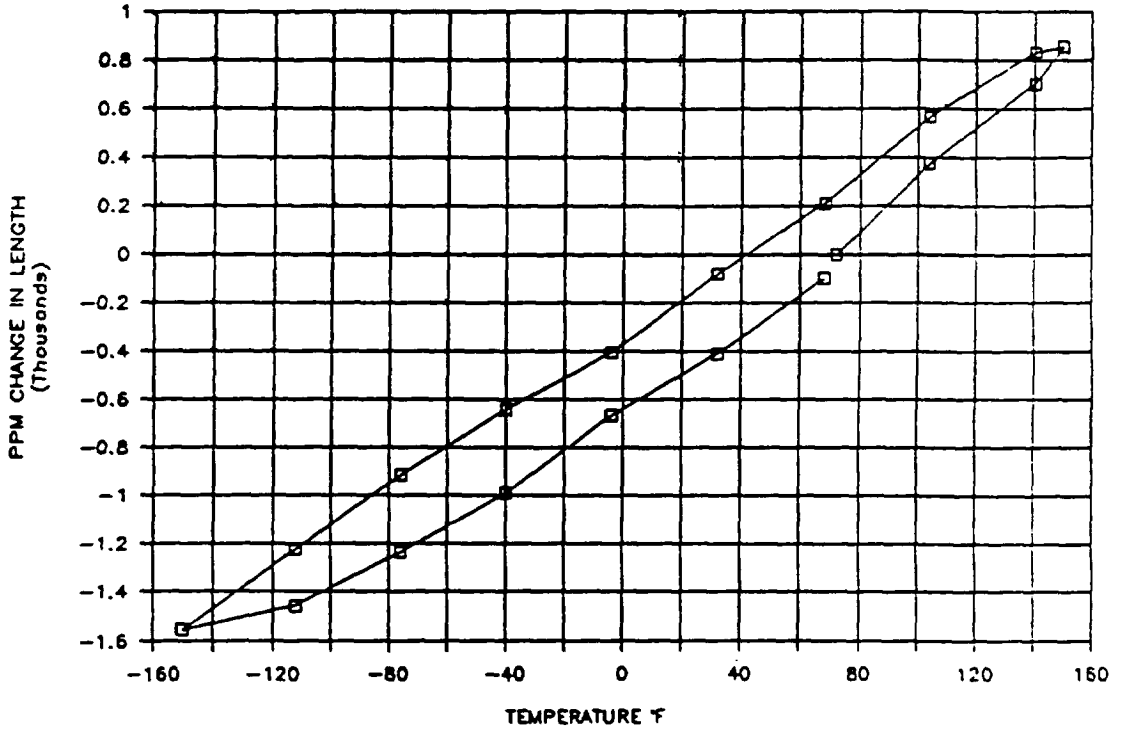

Figure 5.1-6 Thermal Expansion Behavior of 25v/o SiC_p/2124-T6 Specimen Transverse to the Extrusion Direction in a Heat/Cool/Heat Cycle Using Push Rod Dilatometer

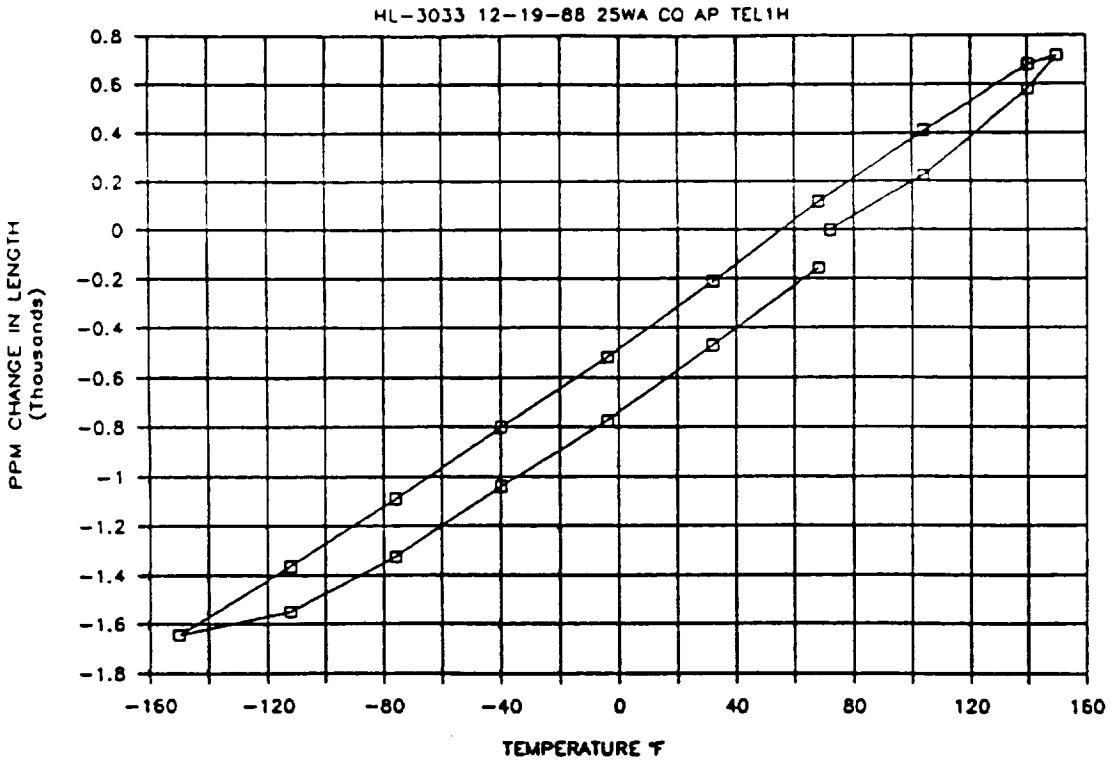

Figure 5.1-7 Thermal Expansion Behavior of 25v/o SiCw/2124-T6 Specimen Parallel to the Extrusion Direction in a Heat/Cool/Heat Cycle Using Push Rod Dilatometer

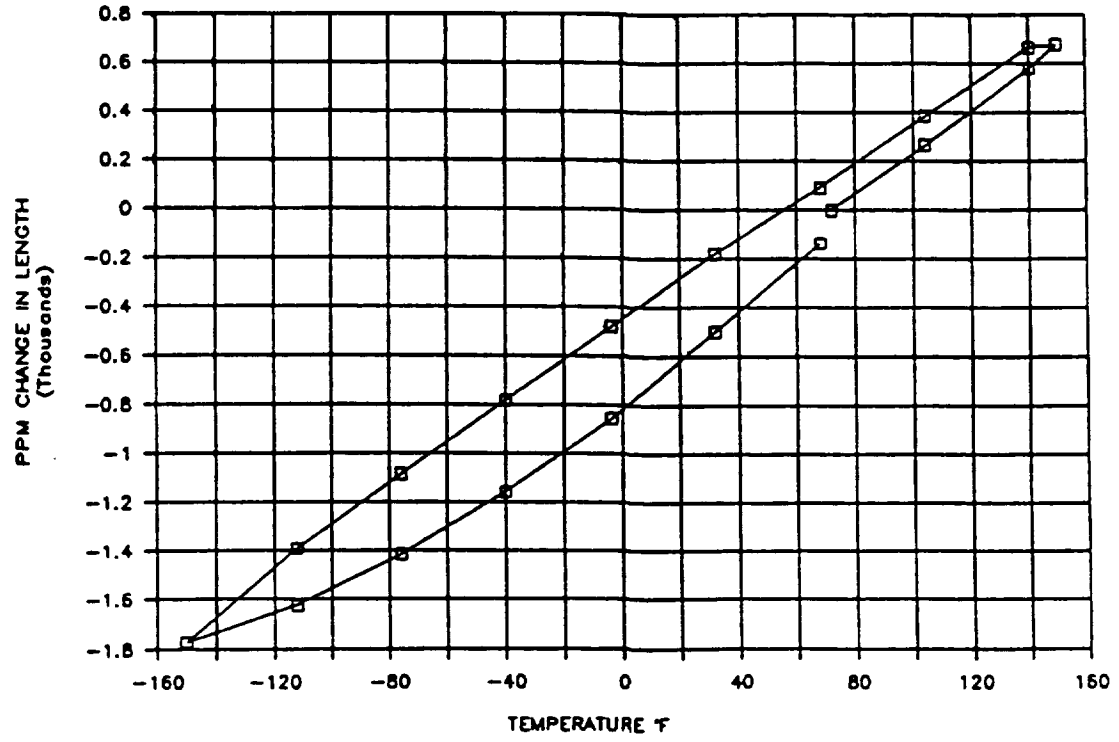

Figure 5.1-8 Thermal Expansion Behavior of 25v/o SiC_w/2124-T6 Specimen Transverse to the Extrusion Direction in a Heat/Cool/Heat Cycle Using Push Rod Dilatometer

Figure 5.1-14 Summary of Thermal Expansion Test Results of Discontinuous SiC/Al Composites

Material SiC/2124-T6 Al	Measured † CTE ppm/°F	Strain Hysteresis @ RT (ppm)	Residual Strain (ppm)	Figure
• Flat Plates				
25 v/o Particulate				
- L (x)	8.16	91.2	-136.8	5.1-5
- T (y)	7.86	115.2	-156.8	5.1-6
25 v/o Whiskers				
- L (x)	8.03	213.2	-96.8	5.1-7
- T (y)	7.77	11.2	-160.8	5.1-8

Table 5.1-15 Comparison of Measured and Predicted CTE Values of Discontinuous SiC/2124-T6 Al

v/o	Direction	CTE (ppm/°F)			
		SiCp/2124-T6 Measured	SiCw/2124-T6 Measured	(Random) Predicted	(Aligned) Predicted
• Plate 25	-L (x)	8.03	8.16	[9.47 (hi)]	6.28
	-T (y)	7.77	7.86	[7.66 (lo)]	

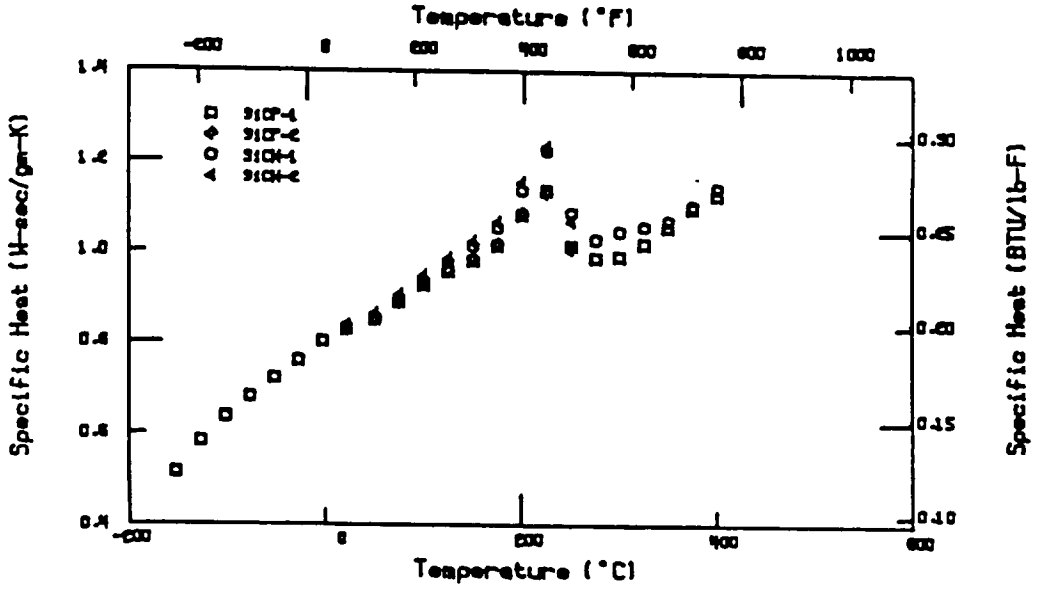

Figure 5.1-9 Specific Heat versus Temperature of 25v/o Discontinuous SiC/Al

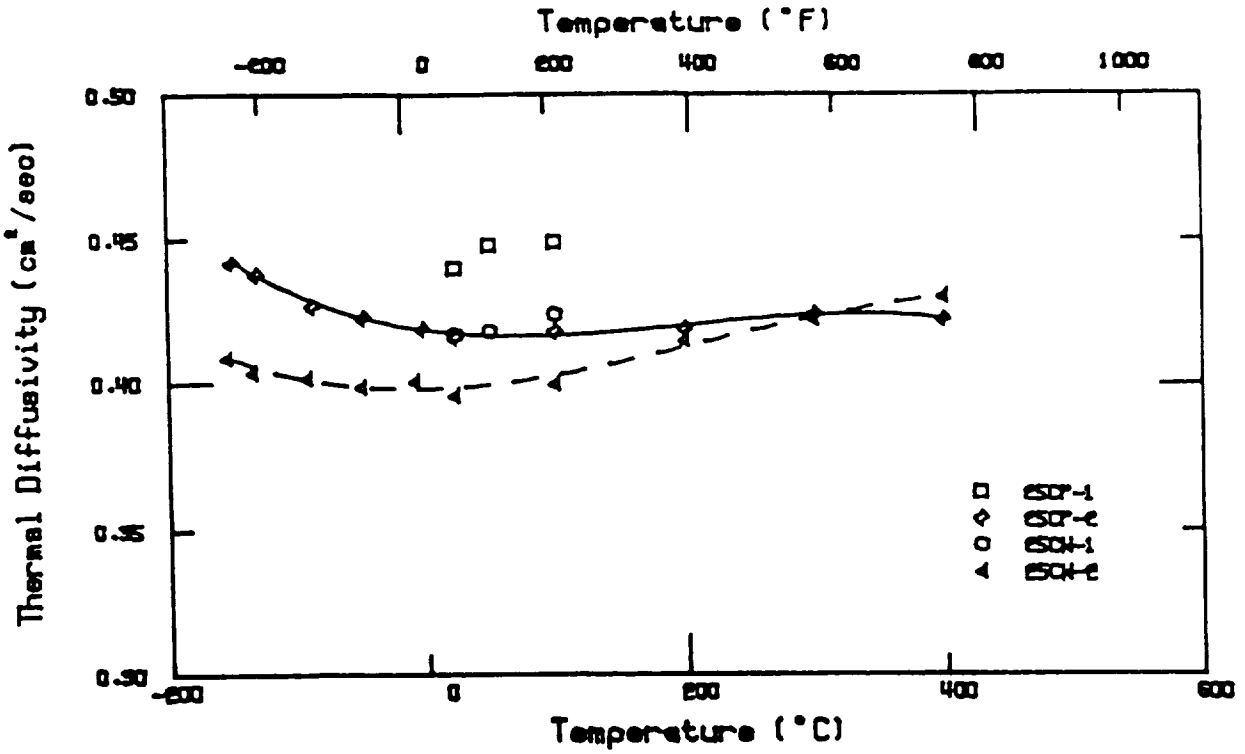

Figure 5.1-10 Thermal Diffusivity of 25v/o Discontinuous SiC/Al

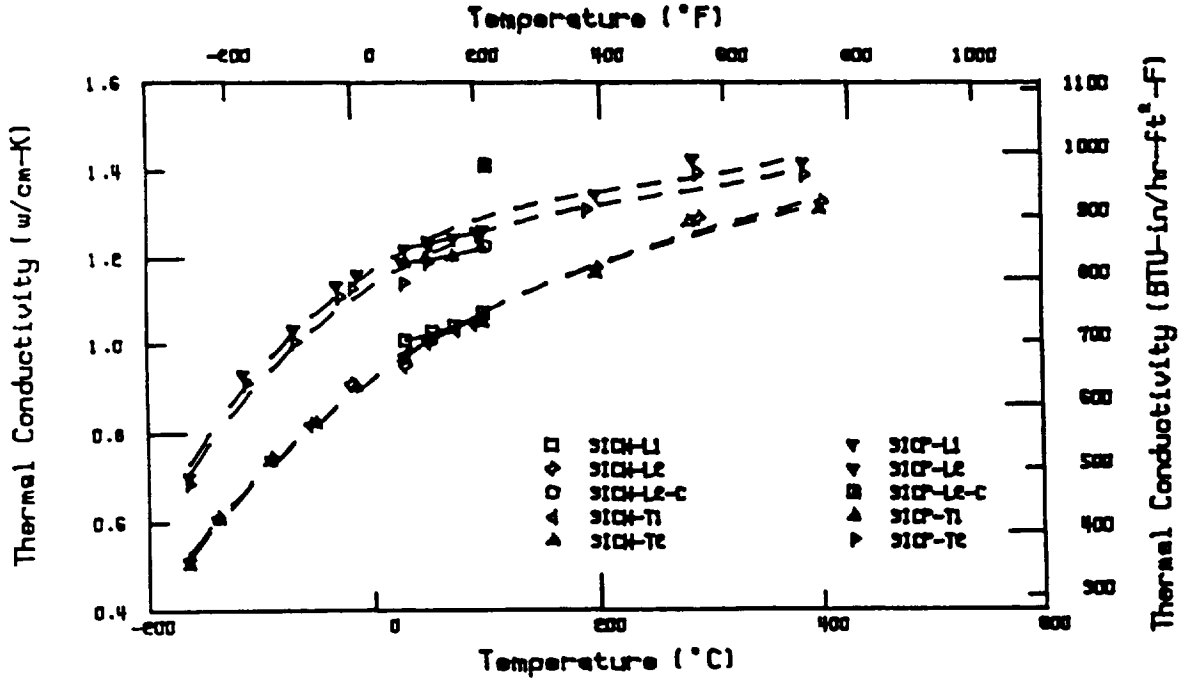

Figure 5.1-11 Thermal Conductivity (Longitudinal and Transverse) Versus Temperature of 25v/o Discontinuous SiC/Al

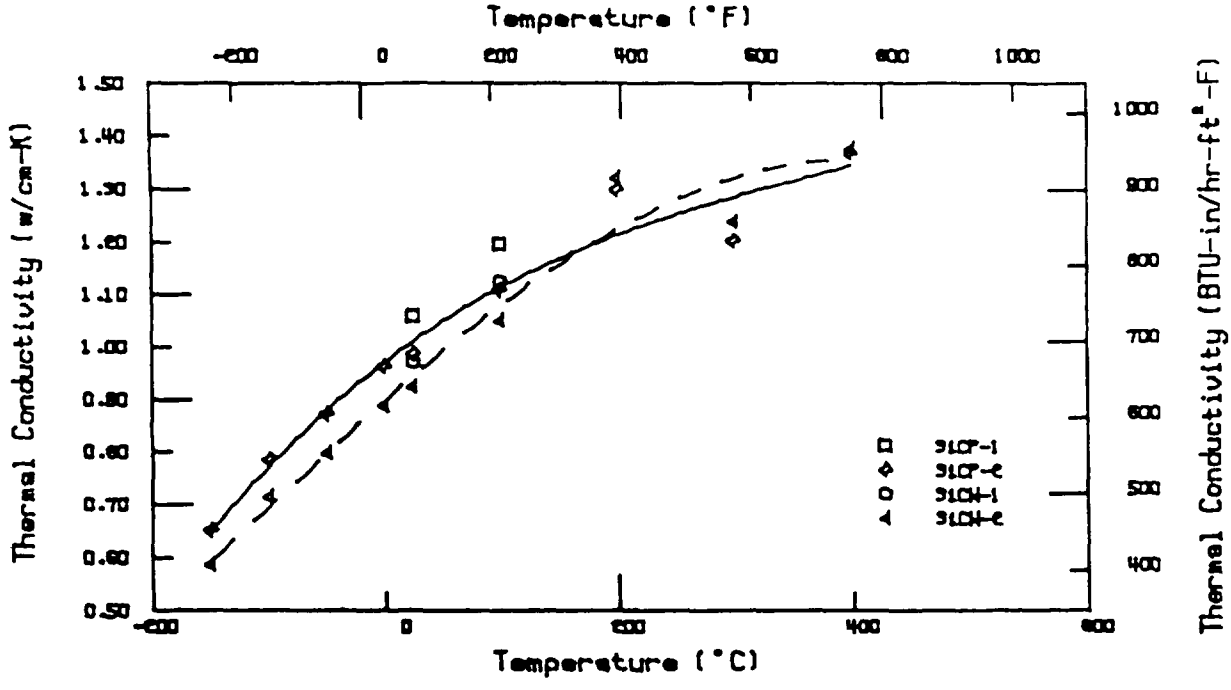

Figure 5.1-12 Thermal Conductivity (Through Thickness) Versus Temperature of 25v/o Discontinuous SiC/Al

Table 5.1-16 Measured and Predicted Thermal Conductivity of 25v/o Discontinuous SiC/Al

Material	Thermal Conductivity, Btu/(lb·ft·°F)		
		M	P†
SiC $_p$/2124-T6	K_y	69.6	73.99
	K_x	67.17	73.99
	K_z	59.24	—
SiC$_w$/2124-T6	K_x	56.65	66.4
	K_y	56.1	66.4
	K_z	53.53	—

† Using Halpin-Tsai Equation and Behrens Equation; M - Measured; P - Predicted

(1) Both materials are nearly isotropic (in-plane)

(2) Based on in-plane and through-the-thickness K values of SiC_w/Al may be considered as isotropic. Whereas SiC_p/Al is slightly anisotropic because K_x, $K_y > K_z$;

(3) SiC_w/Al exhibited higher conductivity than SiC_p/Al; and

(4) Thermal conductivity values are slightly increased upon heating to 750°F.

Also the measured conductivity values showed an agreement with the predicted values (Table 5.1-16).

(e) Electrical Resistivity

For 25 v/o discontinuous SiC/Al, the electrical resistivity values are presented in Figure 5.1-13. At RT, the average resistivity value was 8.5 μohms·cm. Also, each specimen exhibited an increase in resistivity with the increase in temperature.

(f) Optical Properties

- Solar absorptance (α_s) = 0.57
- Normal emittance (ε_N) = 0.15
- Total hemispherical emissivity (ε_H) as measured over the 200°F to 800°F temperature range was about 0.52 (Figure 5.1-14).

• Reflectance vs. Wavelength: Reflectance spectra in Figure 5.1-15 show that both particulate and whisker reinforced panels exhibited 7.80% reflectance (i.e., emittance ≤ 0.2) at 10.6 μm wavelength.

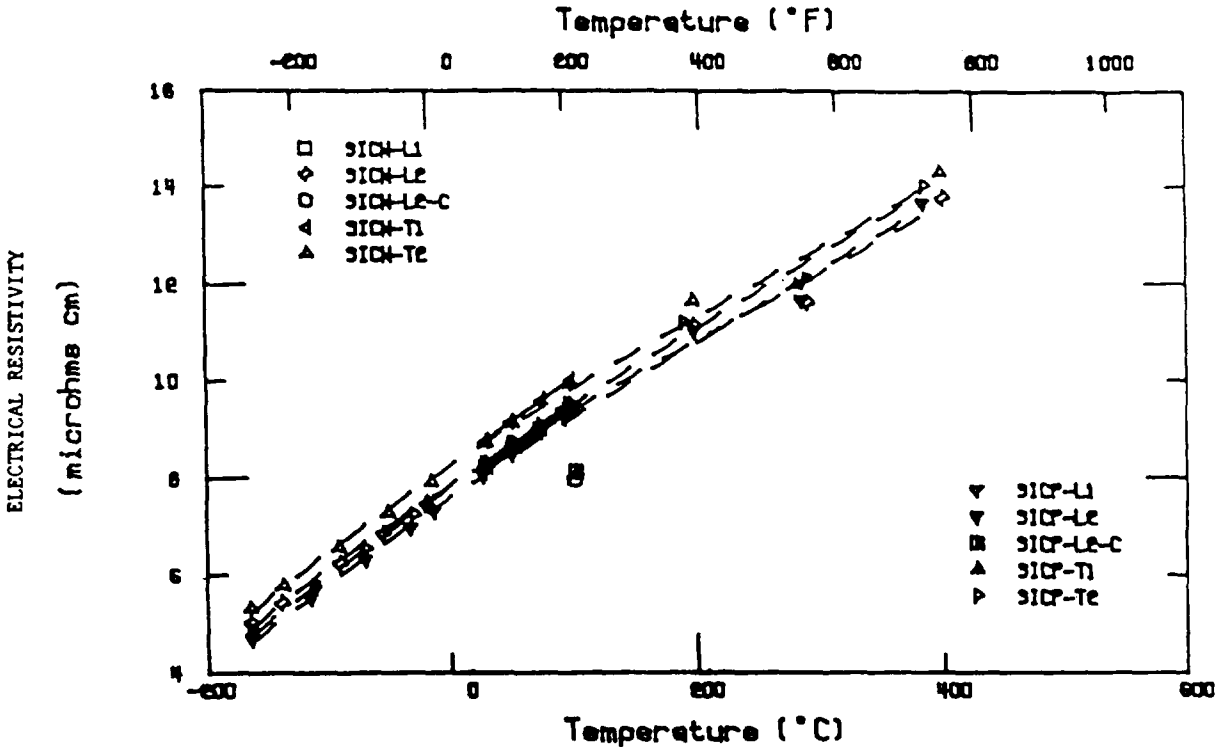

Figure 5.1-13 Electrical Resistivity Versus Temperature of 25v/o Discontinuous SiC/Al

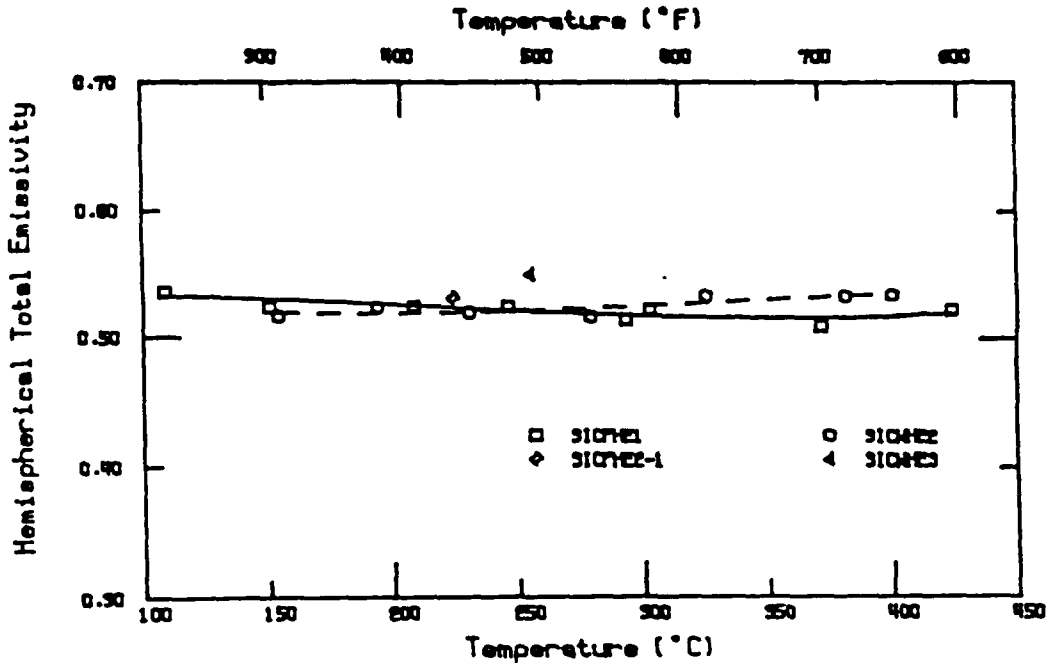

Figure 5.1-14 Hemispherical Emissivity Versus Temperature of 25v/o Discontinuous SiC/Al

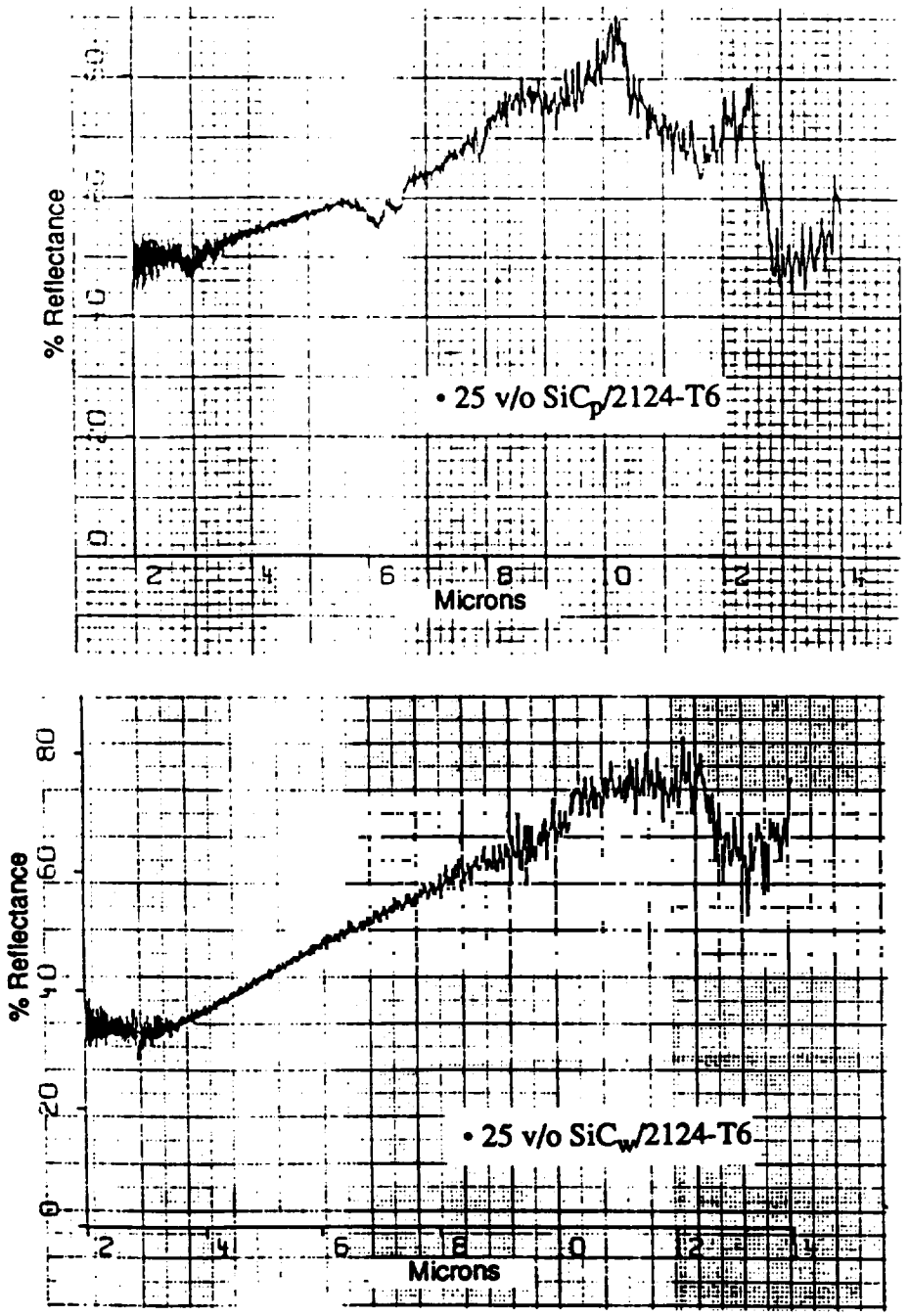

Figure 5.1-15 FTIR Reflectance Spectra of 25v/o Discontinuous SiC/Al

5.2 TUBES

- 25 v/o SiC_p/2124-T6; and
- 25 v/o SiC_w/2124-T6

5.2.1 Fabrication Data

•Fabrication Process—Figure 5.2-1 shows different steps (including billet consolidation and extrusion) involved in the fabrication of tubes.

Material:	25 v/o SiC_p/2124-T6	25 v/o SiC_w/2124-
System Manufacturer:	ACMC, SC	ACMC, SC
Martin Marietta ID:	(25PA)(CQ)(AT)	(25WA)(CQ)(AT)
Prescribed Dimensions:	1.5-in. ± 0.01-in. dia	1.5-in. ± 0.01-in. dia
	0.065-in. ± 0.002-in. thick	0.065 in. ± 0.002-in. thick

•Dimensional Measurements—The diameter and wall thickness measurements of SiC_p and SiC_w/2124-T6 tubes are listed in Table 5.2-1, where the O.D. value is an average of eight measurements made at each end. The average wall thickness of the 25 v/o composites is close to the nominal value 0.065 in.

5.2.2 Product Evaluation

(a) Density

- 25 v/o SiC_p/2124-T6 Tube

  Density = 0.101 lb/in^3

  Std. Dev.: 0.001

- 25 v/o SiC_w/2124-T6 Tube

  Density = 0.101 lb/in^3

  Std. Dev.: 0.005

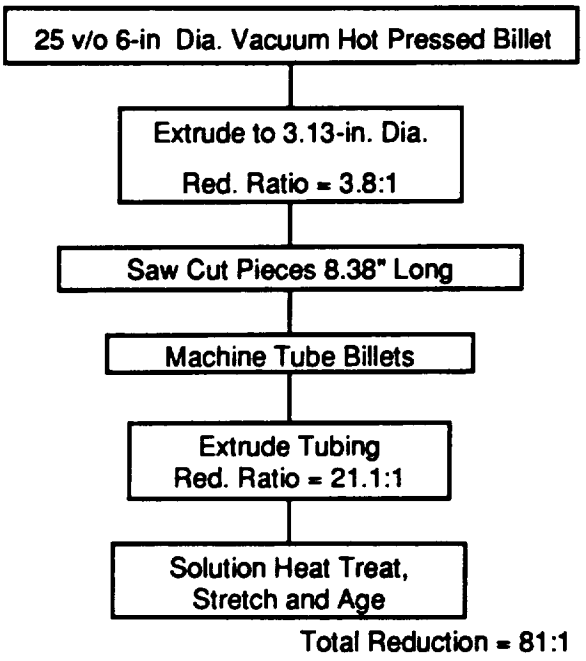

Figure 5.2-1 Fabrication Process to Produce SiC/Al Tubes at ACMC, SC.

Table 5.2-1 Diameter and Wall Thickness Variation of SiC/Al Tubes

	SiC_p /2124-T6		SiC_w/2124-T6	
	25 v/o		25 v/o	
	OD (in)	ID (in)	OD (in)	ID (in)
	1.505 1.504 1.507 1.514 1.502 1.503	1.375 1.374 1.377 1.374 1.362 1.363	1.497 1.494 1.494 1.508 1.50 1.501	1.367 1.364 1.364 1.378 1.370 1.371
Average Std. Dev.	1.506 0.004	1.371 0.006	1.499 0.005	1.369 0.005
Wall Thickness	0.0675		0.065	

(b) Reinforcement Volume

	SiC_p/2124-T6	SiC_w/2124-T6
v/o	25.3	25.35
Std. Dev.	1.1	0.8
Void Volume	<<0.1	<<0.1

(c) Non-Destructive Evaluation

Based on visual examination, ID and OD surfaces of each tube was free or scratches of extrusion marks. Also in X-radiographs and ultrasonic C-scans no void, cracks, or extrusion defects were detected.

5.2.3 Mechanical Properties

(a) Tension

Tensile properties of 25 v/o, SiC_p and SiC_w/2124-T6 composites are listed in Table 5.2-2 and 5.2-3 respectively. During tension tests, a few of the specimens failed within the gage length and the remaining specimens showed a bond-line failure. The incidence of failure at grip ends was attributed to inadequate surface preparation during bonding operation. Therefore, the measured yield and ultimate tensile strength values should be considered the (apparent) lower bound.

Tensile test results show that the average longitudinal elastic modulus and yield strength values obtained for the SiC_w/Al tube specimens were higher than the corresponding values for the flat specimens. The improved mechanical properties in the tubes could be attributed to alignment of the reinforcements in the extrusion direction. For example, in the 25 v/o SiC_w/2124-T6, the elastic modulus of tube specimens was 19.8 Msi as compared to 17.6 Msi for flat specimens.

Table 5.2-2 Longitudinal Tensile Properties of 25 v/o SiC_p/2124-T6 Tubes

Speciment # (25PA)(CQ)(AT)	Elastic Modulus† (Msi)				Yield Strength (ksi)	Ultimate Tensile Strength (ksi)	Strain To Failure (%)	Poisson Ratio
	E_{X1}	E_{X2}	E_{X3}	E_X				
TNL-1	17.4	17.3	15.4	16.7	—	49.4	0.33	0.2677
TNL-2	15.1	16.2	15.2	15.5	—	44.1	0.31	0.2754
TNL-3	15.1	14.2	15.9	15.1	58.4	≥63.4	1.0	0.2701
Mean				15.8	≥58.4	≥63.4	~1.0	0.2711
Std. Dev.				0.84				0.004
CV (%)				5.3				1.4
(25PA)(CQ)(AP) Plate				16.64	68.8	84.5	1.25	0.267

Table 5.2-3 Longitudinal Tensile Properties of 25 v/o SiC_w/2124-T6 Tubes

Speciment # (25WA)(CQ)(AT)	Elastic Modulus† (Msi)				Yield Strength (ksi)	Ultimate Tensile Strength (ksi)	Strain To Failure (%)	Poisson Ratio
	E_{X1}	E_{X2}	E_{X3}	E_X				
TNL-1	18.5	19.0	18.7	18.7	—	>71.8*	>0.48	—
TNL-2	26.2	18.7	20.1	21.7	84.8	>92.0*	>0.79	0.3831
TNL-3	18.2	20.2	19.0	19.1	86.5	>96.9*	>0.95	0.2827
Mean				19.8	85.65	>86.9	>0.95	0.3329
Std. Dev.				1.63	1.2			0.07
CV (%)				8.2	1.4			21.0
(25WA)(CQ)(AP) Plate				17.6	76.2	102.0	1.62	0.2934

(b) Compression

Compression properties of both 25 SiC_p and SiC_w/2124-T6 Al tube specimens are listed in Table 5.2-4 and 5.2-5 respectively. Each specimen exhibited compressive failure within the gage length, without bending or buckling effects. Average compressive modulus values were comparable with the tensile moduli, whereas compressive strengths were slightly higher than in tension. High compressive strength values have been generally attributed to increased stress levels required to offset the residual tensile stresses in the matrix for discontinuous silicon carbide aluminum composites (Ref 71).

(c) Hoop Tensile Properties

For both 25 v/o SiC_p and SiC_w/2124-T6 tube specimens, the measured hoop modulus and strength values are listed in Table 5.2-6. based on these results, the particulate reinforced tubes exhibited nearly isotropic response as E_H = 15.5 Msi value was nearly identical to E_x^T 15.8 Msi. The whisker reinforced tube specimens exhibited a lower hoop modulus (14.14 Msi) than the 19.8 Msi axial modulus, thus indicating the anisotropic response due to alignment of whisker along the axial direction.

5.2.4 Thermophysical Properties

(a) Coefficient of Thermal Expansion

Thermal expansion response of 25 v/o SiC_p and SiC_w/2124-T6 tube specimen is shown in Figure 5.2-2 and 5.2-3 respectively.

	25 v/o SiC_p/2124-T6	25 v/o SiC_w/2124-T6
CTE_x (ppm/°F)	7.81	6.613
Residual Strain (ppm)	59.2	83.2
RT Hysteresis (ppm)	-56.8	-4.8

These results show a slightly lower CTE (residual strain and RT hysteresis) compared to the 25 v/o panels, indicating the effect of reinforcement alignment during extrusion of tubes.

Table 5.2-4 Longitudinal Compressive Properties of SiC_p/2124-T6 Tubes

Speciment # (25PA)(CQ)(AT)	Elastic Modulus† (Msi)				Yield Strength (ksi)	Ultimate Comp. Strength (ksi)	Strain To Failure (%)	Poisson Ratio
	E_{X1}	E_{X2}	E_{X3}	E_X				
CML-1	17.4	18.9	16.3	17.5	60.7	93.9	2.32	0.2872
CML-2	—	—	—	—	—	87.5	2.17	—
CML-3	15.9	18.1	17.4	17.1	60.4	88.0	2.21	0.2747
Mean				17.3	60.6	90.1	2.23	0.2810
Std. Dev.				0.283	0.21	3.4	0.077	0.0088
CV (%)				1.6	0.4	3.8	3.45	3.1

Table 5.2-5 Longitudinal Compressive Properties of SiC_w /2124-T6 Tubes

Speciment # (25WA)(CQ)(AT)	Elastic Modulus† (Msi)				Yield Strength (ksi)	Ultimate Comp. Strength (ksi)	Strain To Failure (%)	Poisson Ratio
	E_{X1}	E_{X2}	E_{X3}	E_X				
CML-1	20.0	19.4	17.5	19.0	94.4	125.0	1.69	0.2833
CML-2	18.4	20.7	20.1	19.7	91.1	131.3	1.64	0.2807
CML-3	20.2	19.5	20.7	20.1	94.4	134.7	1.70	0.2886
Mean				19.6	93.3	130.3	1.68	0.2842
Std. Dev.				0.557	1.91	4.92	0.032	0.004
CV (%)				2.8	2.0	3.8	1.9	1.4

Table 5.2-6 NOL Burst Ring Test Data for SiC/Al Composite Tubes

Material	Area (in^2)	Ultimate (psi) Pressure	Hoop Stress F_{TH} = P r/t (ksi)	Modulus E_H (Msi)	Strain to Failure
25 v/o SiC_p/Al	0.3167 (6.7%)	6546 (12%)	64.0 (7.7%)	15.5 (8.8%)	*
25 v/o SiC_w/Al	0.2938 (1.9%)	5794 (6%)	60.5 (6.2%)	14.14 6%	*

† Precentage coefficientof variation

* Strain exceed beyond the conditioner output @ 13.5 vol (i.e., ≥ 0.007 in/in)

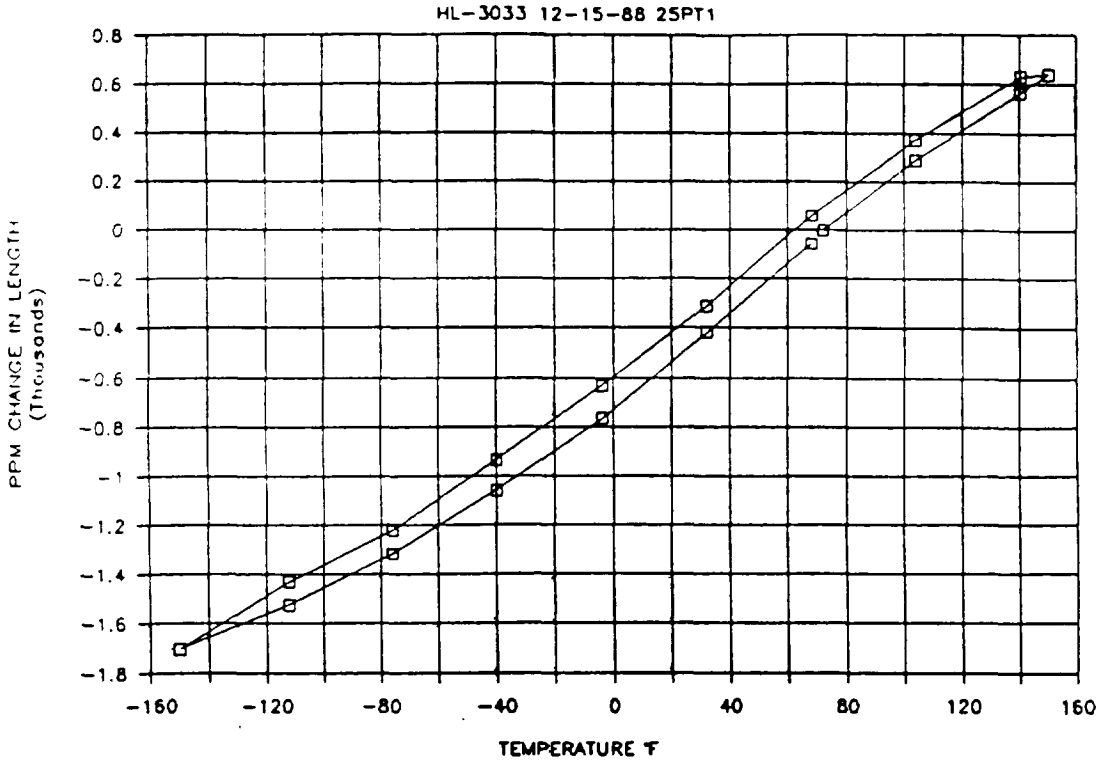

Figure 5.2-2 Thermal Expansion Behavior of 25v/o SiCp/2124-T6 Specimen Parallel to the Extrusion Direction in a Heat/Cool/Heat Cycle Using Push Rod Dilatometer

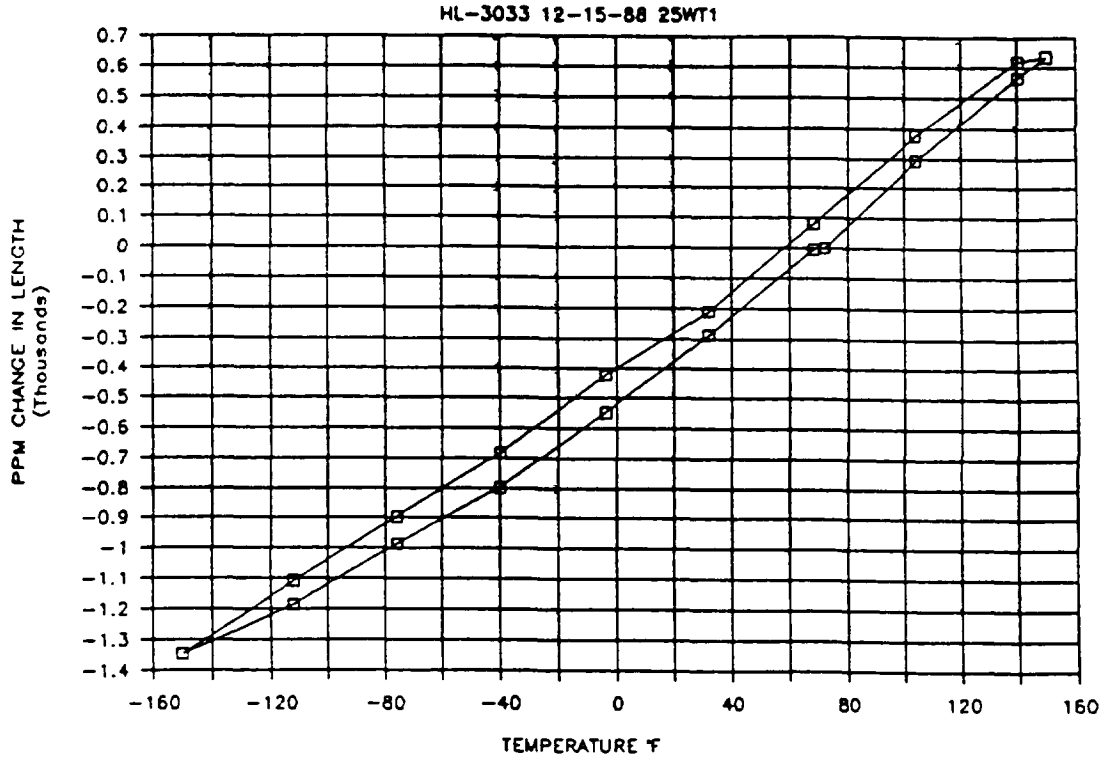

Figure 5.2-3 Thermal Expansion Behavior of 25v/o SiCw/2124-T6 Specimen Parallel to the Extrusion Direction in a Heat/Cool/Heat Cycle Using Push Rod Dilatometer

5.3 SUMMARY OF 25 V/O DISCONTINUOUS SiC/Al TEST DATA

Mechanical and thermophysical property test data of 25 v/o discontinuous SiC/2124-T6 are summarized in the following tables:

25 v/o SiC_p/2124-T6 Al Panel	Table 5.3-1
25 v/o SiC_w/2124-T6 Al Panel	Table 5.3-2
25 v/o SiC_p/2124-T6 Al Tube	Table 5.3-3
25 v/o SiC_w/2124-T6 Al Tube	Table 5.3-4

Table 5.3-1 25v/o SiCp/Al 2124 - T6 Panels

NOT DESIGN ALLOWABLE DATA

PROPERTIES							TEMPERATURE (°F)			Std. Dev. / No. of Specimens at RT	Test Method
PHYSICAL			MECHANICAL & THERMAL				Low	Room	High		
Density (lb / in^3)		0.101	Longitudinal Tensile Strength	σ_x^{TU}	ksi			84.5		± 3.79 / 5	ASTM D-3552
Fiber volume fraction		0.25	Transverse Tensile Strength	σ_y^{TU}	ksi			77.5		±4.87 / 5	ASTM D-3552
Void volume fraction		<0.001	Longitudinal Comp. Strength	σ_x^{CU}	ksi			80.8		±2.071 / 5	ASTM D-3410
Nominal ply thickness	In	0.060	Transverse comp. strength	σ_y^{CU}	ksi			75.8		±1.610 / 5	ASTM D-3410
Max. cont. use temp.	°F	~550	In-plane shear strength	IPSS	ksi						
OPTICAL & ELECTRICAL (at room temperature)			Interlaminar shear strength	ILSS	ksi						
Solar Absorptance	α	0.57	Longitudinal tensile strain **	ε_x^T	%			1.258		±0.0045 / 5	ASTM D-3552
Normal Emissivity	ε	0.150	Transverse tensile strain **	ε_y^T	%			1.18		±0.212 / 5	ASTM D-3552
Electrical Resistivity	R	8.5 μΩ·cm	Longitudinal comp. strain **	ε_x^C	%			0.618		±0.0024 / 5	ASTM D-3410
			Transverse comp. strain **	ε_y^C	%			0.620		±0.006 / 5	ASTM D-3410
			Longitudinal tensile modulus	E_x	Msi			16.64		±0.410 / 5	ASTM D-3552
			Transverse tensile modulus	E_y	Msi			17.0		±0.324 / 5	ASTM D-3552
			Longitudinal comp. modulus	E_x	Msi			18.5		±0.207 / 5	ASTM D-3410
			Transverse comp. modulus	E_y	Msi			17.9		±0.904 / 5	ASTM D-3410
			In-plane shear modulus	G	Msi						
			Longitudinal flexural modulus	F_x	Msi			13.51		±0.156 / 3	ASTM D-790M
			Transverse flexural modulus	F_y	Msi			13.02		±0.4195 / 3	ASTM D-790M
			Long. tensile Poisson's ratio	ν_{xy}				0.267		±0.0023 / 5	ASTM D-3552
			Trans. tensile Poisson's ratio	ν_{yx}				0.279		±0.017 / 5	ASTM D-3552
			Long. thermal conductivity	K_x	(1)	3.373		5.740	6.486		Kohlrausch
			Trans. thermal conductivity	K_y	(1)	3.3026		5.6116	6.111		Kohlrausch
			Thru thickness thermal cond.	K_z	(1)						
			Specific heat	C_p	(2)	0.123		0.1984	0.243		ASTM E1269
			Longitudinal CTE	α_x	(3)			8.16			ASTM E-80
			Transverse CTE	α_y	(3)			7.86			ASTM E-80
			Thru thickness CTE	α_z	(3)			—			

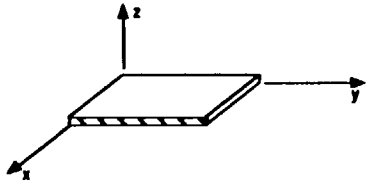

Notes:
(**) - Strain to failure; (1) Btu/(hr·in·°F); (2) Btu/(lb·°F); (3) μin./in./°F

Table 5.3-2 25v/o SiCw/Al 2124 - T6 Panels

NOT DESIGN ALLOWABLE DATA

PROPERTIES					TEMPERATURE (°F)			Std. Dev. / No. of Specimens at RT	Test Method
PHYSICAL			MECHANICAL & THERMAL			Low	Room	High		
Density (lb / in^3)		0.101	Longitudinal Tensile Strength	σ_x^{TU}	ksi		102.0		± 4.62 / 5	ASTM D-3552
Fiber volume fraction		0.25	Transverse Tensile Strength	σ_y^{TU}	ksi		97.4		±1.54 / 5	ASTM D-3552
Void volume fraction		<0.001	Longitudinal Comp. Strength	σ_x^{CU}	ksi		102.5		±1.57 / 4	ASTM D-3410
Nominal ply thickness	In	0.060	Transverse comp. strength	σ_y^{CU}	ksi		91.0		±2.13 / 5	ASTM D-3410
Max. cont. use temp.	°F	~550	In-plane shear strength	IPSS	ksi		—			
			Interlaminar shear strength	ILSS	ksi					
OPTICAL & ELECTRICAL (at room temperature)			Longitudinal tensile strain **	ε_x^T	%		1.62		±0.15 / 5	ASTM D-3552
			Transverse tensile strain **	ε_y^T	%		1.83		±0.048 / 5	ASTM D-3552
Solar Absorptance	α	0.57	Longitudinal comp. strain **	ε_x^C	%		1.11		±0.025 / 4	ASTM D-3410
Normal Emissivity	ε	0.150	Transverse comp. strain **	ε_y^C	%		1.26		±0.096 / 5	ASTM D-3410
Electrical Resistivity	R	8.5 μΩ·cm	Longitudinal tensile modulus	E_x	Msi		17.6		±0.415 / 5	ASTM D-3552
			Transverse tensile modulus	E_y	Msi		16.42		±0.295 / 5	ASTM D-3552
			Longitudinal comp. modulus	E_x	Msi		18.15		±0.265 / 4	ASTM D-3410
			Transverse comp. modulus	E_y	Msi		16.5		±0.33 / 5	ASTM D-3410
			In-plane shear modulus	G	Msi		—			
			Longitudinal flexural modulus	F_x	Msi		13.1		±0.208 / 3	ASTM D-790M
			Transverse flexural modulus	F_y	Msi		11.8		±0.0577 / 3	ASTM D-790M
			Long. tensile Poisson's ratio	ν_{xy}			0.2934		±0.0136 / 5	ASTM D-3552
			Trans. tensile Poisson's ratio	ν_{yx}			0.2717		±0.00651 / 5	ASTM D-3552
			Long. thermal conductivity	K_x	(1)		4.87			Kohlrausch
			Trans. thermal conductivity	K_y	(1)		4.71			Kohlrausch
			Thru thickness thermal cond.	K_z	(1)		4.57			
			Specific heat	C_p	(2)		0.199			ASTM E1269
			Longitudinal CTE	α_x	(3)		8.03			ASTM E-80
			Transverse CTE	α_y	(3)		7.77			ASTM E-80
			Thru thickness CTE	α_z	(3)		—			

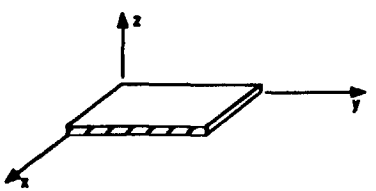

Notes:
(**) - Strain to failure; (1) Btu/(hr·in·°F); (2) Btu/(lb·°F); (3) μin./in./°F

Table 5.3-3 25v/o SiCp/Al 2124 - T6 Tubes

NOT DESIGN ALLOWABLE DATA

PROPERTIES				TEMPERATURE (°F)			Std. Dev. / No. of Specimens at RT	Test Method
PHYSICAL				Low	Room	High		
Density (lb / in^3)		0.101						
Fiber volume fraction		0.25						
Void volume fraction		<0.001						
Nominal ply thickness	in	0.065						
Max. cont. use temp.	°F	~550						
OPTICAL & ELECTRICAL (at room temperature)								
Solar Absorptance	α							
Normal Emissivity	ε							
Electrical Resistivity	R							
MECHANICAL & THERMAL								
Longitudinal Tensile Strength	σ_x^{TU}	ksi			>63.4			ASTM D-3552
Transverse Tensile Strength	σ_y^{TU}	ksi			64.0			NOL
Longitudinal Comp. Strength	σ_x^{CU}	ksi			90.1		± 3.4 / 3	ASTM D-3410
Transverse comp. strength	σ_y^{CU}	ksi			—			
In-plane shear strength	IPSS	ksi						
Interlaminar shear strength	ILSS	ksi						
Longitudinal tensile strain **	ε_x^T	%			~1.0			ASTM D-3552
Transverse tensile strain **	ε_y^T	%			—			NOL
Longitudinal comp. strain **	ε_x^C	%			2.23		± 0.077 / 3	ASTM D-3410
Transverse comp. strain **	ε_y^C	%			—			
Longitudinal tensile modulus	E_x	Msi			15.8			ASTM D-3552
Transverse tensile modulus	E_y	Msi			15.5			NOL
Longitudinal comp. modulus	E_x	Msi			17.3		± 0.283 / 3	ASTM D-3410
Transverse comp. modulus	E_y	Msi						
In-plane shear modulus	G	Msi						Torsion Test
Longitudinal flexural modulus	F_x	Msi						
Transverse flexural modulus	F_y	Msi						
Long. tensile Poisson's ratio	ν_{xy}				0.2711		± 0.004 / 3	ASTM D-3552
Trans. tensile Poisson's ratio	ν_{yx}							NOL
Long. thermal conductivity	K_x	(1)						
Trans. thermal conductivity	K_y	(1)						
Thru thickness thermal cond.	K_z	(1)						
Specific heat	C_p	(2)			7.81			
Longitudinal CTE	α_x	(3)						ASTM E-80
Transverse CTE	α_y	(3)						
Thru thickness CTE	α_z	(3)						

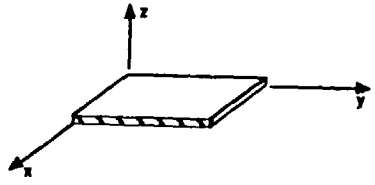

Notes:
(**) - Strain to failure; (1) Btu/(hr·in·°F); (2) Btu/(lb·°F); (3) µin./in./°F

Table 5.3-4 25v/o SiCw/Al 2124 - T6 Tubes

NOT DESIGN ALLOWABLE DATA

PROPERTIES							TEMPERATURE (°F)			Std. Dev. / No. of Specimens at RT	Test Method
PHYSICAL			MECHANICAL & THERMAL				Low	Room	High		
Density (lb / in^3)		0.101	Longitudinal Tensile Strength	σ_x^{TU}	ksi			>86.9			ASTM D-3552
Fiber volume fraction		0.25	Transverse Tensile Strength	σ_y^{TU}	ksi			60.5			NOL
Void volume fraction		<0.001	Longitudinal Comp. Strength	σ_x^{CU}	ksi			130.3		± 4.92 / 3	ASTM D-3410
Nominal ply thickness	in	0.065	Transverse comp. strength	σ_y^{CU}	ksi						
Max. cont. use temp.	°F	~550	In-plane shear strength	IPSS	ksi						
OPTICAL & ELECTRICAL (at room temperature)			Interlaminar shear strength	ILSS	ksi						
			Longitudinal tensile strain **	ε_x^T	%			>0.95			ASTM D-3552
			Transverse tensile strain **	ε_y^T	%			—			NOL
			Longitudinal comp. strain **	ε_x^C	%			1.68		± 0.032 / 3	ASTM D-3410
			Transverse comp. strain **	ε_y^C	%			—			
Solar Absorptance	α		Longitudinal tensile modulus	E_x	Msi			19.8			ASTM D-3552
			Transverse tensile modulus	E_y	Msi			14.14			NOL
Normal Emissivity	ε		Longitudinal comp. modulus	E_x	Msi			19.6		± 0.557 / 3	ASTM D-3410
			Transverse comp. modulus	E_y	Msi						
Electrical Resistivity	R	μΩ-cm	In-plane shear modulus	G	Msi						Torsion Test
			Longitudinal flexural modulus	F_x	Msi						
			Transverse flexural modulus	F_y	Msi						
			Long. tensile Poisson's ratio	ν_{xy}				0.3329			ASTM D-3552
			Trans. tensile Poisson's ratio	ν_{yx}							NOL
			Long. thermal conductivity	K_x	(1)						
			Trans. thermal conductivity	K_y	(1)						
			Thru thickness thermal cond.	K_z	(1)						
			Specific heat	C_p	(2)						
			Longitudinal CTE	α_x	(3)			6.613			ASTM E-80
			Transverse CTE	α_y	(3)						
			Thru thickness CTE	α_z	(3)						

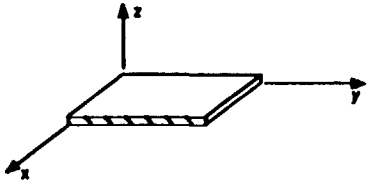

Notes:
(**) - Strain to failure; (1) Btu/(hr·in·°F); (2) Btu/(lb·°F); (3) μin./in./°F

35 V/O Discontinuous SiC/AL

6.0 35 V/O DISCONTINUOUS SiC/Al

Discontinuous SiC/Al composites offer higher specific stiffness, a lower CTE, and an improved temperature capability compared to conventional metals used for spacecraft structural applications. In addition these composites have isotropic properties and can be readily fabricated into complex shaped structural components and attachment fittings. Therefore, 25 and 35 v/o SiC_p/2124-T6 flat panels and tubes were procured to generate material property test data. The fabrication data and the results of product evaluation, mechanical and thermophysical property tests for 35 v/o SiC_w/2124-T6 are discussed in this chapter.

6.1 FLAT PANELS

- 35 v/o SiC_p/2124-T6 and
- 35 v/o SiC_w/2124-T6

6.1.1 Fabrication Data

The particulate reinforcement composite panels were procured from two sources: ACMC and BP-DWA to generate representative data of SOA materials, whereas whisker reinforced panels were procured only from ACMC. All the panels were fabricated by conventional powder metallurgy technique which included consolidation of billets followed by hot extrusion and hot rolling steps (Figure 6.1-1). After final hot rolling step, each panel was heat treated to -T6 condition.

Material:	35 v/o SiC_p/2124-T6	35 v/o SiC_w/2124-T6
Fabrication Process:	Powder metallurgy/hot extrusion and rolling	Powder metallurgy/hot extrusion and rolling
Manufacturer:	(1) ACMC, SC	ACMC, SC
	(2) BP-DWA, CA	—

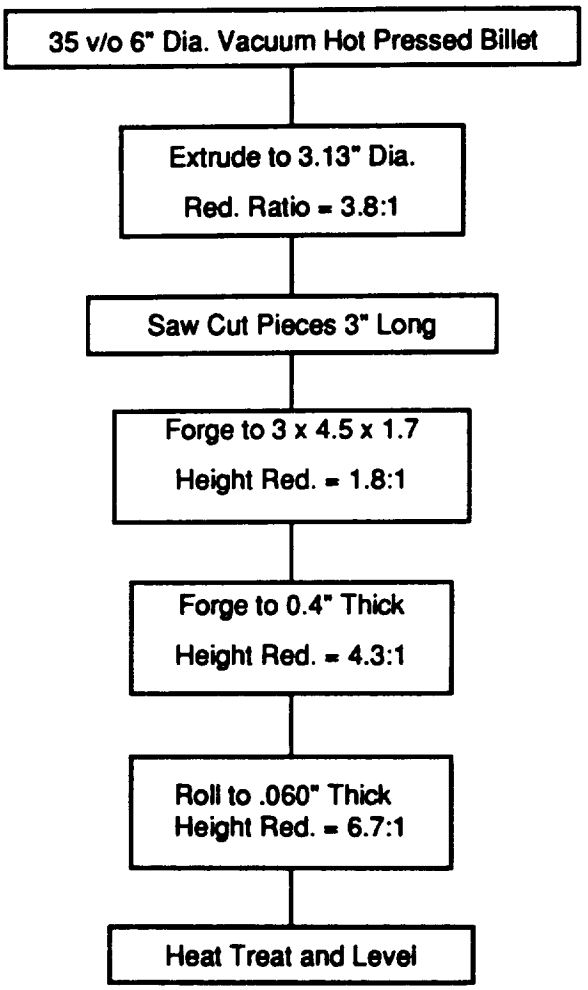

Figure 6.1-1 Fabrication Process to Produce Discontinuous 25 v/o SiC/Al Flat Plates (at ACMC, SC)

Dimension:	12-in. x 12-in. x 0.060-in. (from ACMC, SC) 12-in. x 12-in. x 0.040-in. (from BP-DWA, CA)	12-in. x 12-in. x 0.060-in.
Warpage:	0.375-in./12-in. maximum	0.375-in./12-in. maximum
Lot No.:	ACMC: A6660X3 DWA: P3094	ACMC: A6679Z and A6657Z
Martin Marietta ID No.:	(35PA)(CQ)(AP) for ACMC panels; and (35PA)(DQ)(AP) for DWA panels	(35WA)(CQ)(AP)

6.1.2 Product Evaluation

(a) Density

- 35 v/o SiC_p/2124-T6

  Density: 0.104 lb/in^3

  Std. Dev.: 0.0005

- 35v/o SiC_w/2124-T6

  Density: 0.104 lb/in^3

  Std. Dev.: 0.0008

(b) Reinforcement Content

ACMC	SiC_p/2124-T6	v/o:	35.3
		Std. Dev.:	1.4
DWA	SiC_p/2124-T6	v/o:	35.2
		Std. Dev.:	1.1
ACMC	SiC_w/2124-T6	v/o:	35.4
		Std. Dev. =	1.4

In each case void volume ≤0.1%.

(c) Non-Destructive Evaluation

Based on visual examination, each panel had smooth scratch-free surfaces. Large panels (i.e., 12-in. x 18-in.) had maximum warpage of 0.3-in./ft. Both x-radiographic and ultrasonic inspections confirmed that the fabrication quality of SiC_p and SiC_w reinforced aluminum composites was excellent as none of the panels revealed any voids, stringers, or related defects.

(d) Microstructures

Typical microstructures of both 35 v/o SiC_p/2124-T6 Al and 35 v/o SiC_w/2124-T6 Al are shown in Figure 6.1-2 and 6.1-3 respectively. These microstructures indicated that the overall reinforcement distribution was quite uniform, however in the whisker reinforced composite, there appeared to be small clusters of whiskers randomly dispersed in the matrix. The average particulate size in 35 v/o SiC_p/2124-T6 was 3 μm, and the average aspect ratio of SiC whiskers was 12.6 with a 0.6 - 1 μm diameter and 10 - 12 μm length.

6.1.3 Mechanical Properties

Tension, compression, and flexure test results of 35 v/o SiC_p and SiC_w/2124-T6 panels from ACMC; compression and flexure test results of 35 v/o SiC_p/2124-T6 panels from DWA are discussed below.

(a) Tension

• ***35 v/o SiC_p/2124-T6***—Tensile test data of both longitudinal and transverse 35 v/o SiC_p/2124-T6 specimens are listed in 6.1-1 and 6.1-2 respectively. In these tests, the stress-strain response of each specimen exhibited elastic-plastic behavior similar to the 25 v/o SiC_p/Al. The longitudinal modulus and strength values of 19.9 Msi and 95.6 ksi respectively were similar to the transverse modulus 19.4 Msi and strength 97 ksi, indicating that the fabrication process yielded nearly isotropic material.

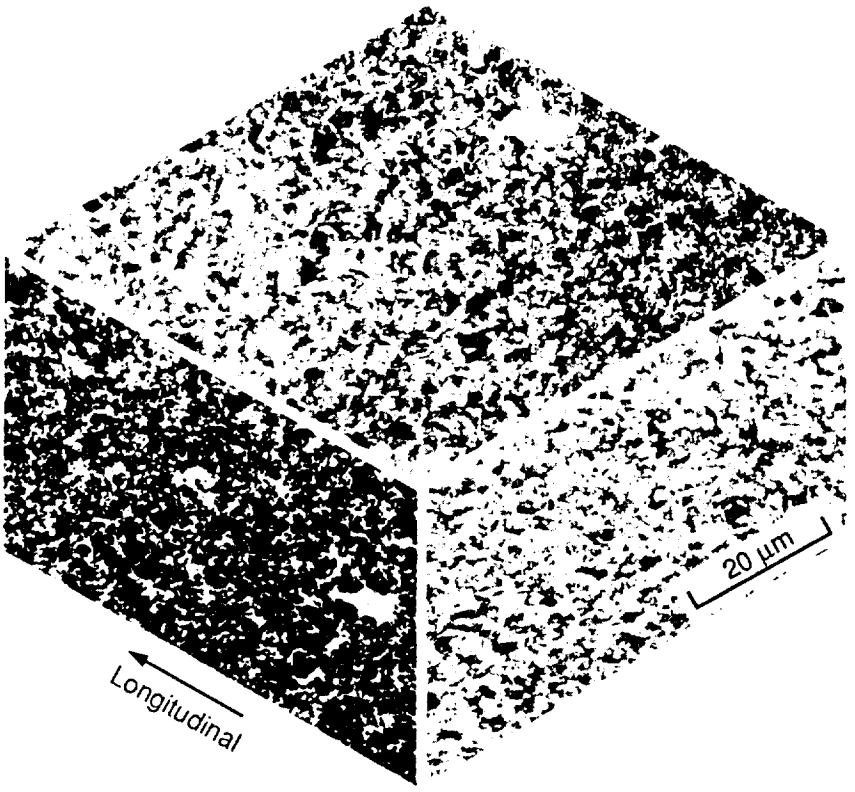

Figure 6.1-2 Three Dimensional Microstructure of 35v/o SiC_p /2124-T6 Al Panels (1000X)

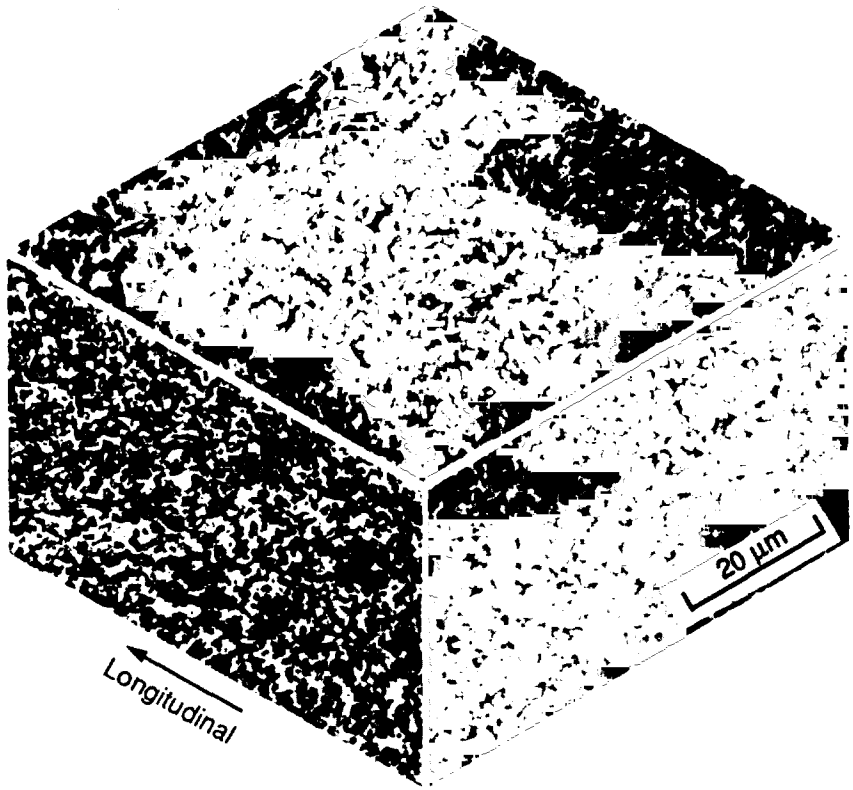

Figure 6.1-3 Three Dimensional Microstructure of 35v/o SiC_w /2124-T6 Al Panels (1000X)

Table 6.1-1 Longitudinal Tensile Properties of 35v/o SiCp/2124-T6

Specimen # (35PA)(CQ)(AP)	Elastic Modulus E_x^T (Msi)	Yield Strength (ksi)	Ultimate Tensile Strength (ksi)	Poisson Ratio ν_{xy}	Strain To Failure (%)
TNL-1	20.6	89.9	100.0	0.2579	1.1
TNL-2	19.6	83.7	95.7	0.2469	1.16
TNL-3	19.5	87.4	92.8	0.2548	0.88
TNL-4	20.0	84.5	88.9	0.2528	0.78
TNL-5	19.6	87.0	100.5	0.2573	1.27
Mean Value	19.9	86.5	95.6	0.2539	1.038
Std. Dev.	0.46	2.47	4.90	0.00443	0.2
CV (%)	2.29	2.85	5.12	1.74	19.2

Table 6.1-2 Transverse Tensile Properties of 35v/o SiCp/2124-T6

Specimen # (35PA)(CQ)(AP)	Elastic Modulus E_x^T (Msi)	Yield Strength (ksi)	Ultimate Tensile Strength (ksi)	Poisson Ratio ν_{yx}	Strain To Failure (%)
TNT-1	19.6	89.5	90.9	0.2482	0.73
TNT-2	19.1	87.8	94.2	0.2445	0.97
TNT-3	19.3	86.6	97.3	0.2456	1.17
TNT-4	19.7	89.6	105.3	0.2524	1.35
TNT-5	19.1	87.6	97.2	0.2500	1.15
Mean Value	19.4	88.2	97.0	0.2481	1.074
Std. Dev.	0.28	1.30	5.34	0.00321	0.23
CV (%)	1.44	1.47	5.51	1.29	21.4

• *35 v/o SiC_w/2124-T6*—Tensile properties of both longitudinal and transverse specimens are listed in Table 6.1-3 and 6.1-4 respectively. In each test, the 0.2% yield strength was determined from the stress-strain curve except for the transverse tensile test specimens which exhibited failure at about 0.39% strain levels (Figure 6.1-4) as compared to 1.0% failure strain values for longitudinal test specimens. Also, the transverse modulus values of 17.2 Msi was 8.5% lower than in the longitudinal direction (18.8 Msi), suggesting the anisotropic response of whisker reinforced composite. For the same 35 v/o reinforcement, the lower transverse modulus (17.2 Msi) in SiC_w/2124-T6 Al as compared to 19.4 Msi in SiC_p/2124-T6 Al composite, along with the low strain to failure value suggested that the whisker-matrix bond was not adequate enough to reinforce the matrix. The fracture surface examination of transverse tensile specimens, using scanning electron microscopy, indicated that there were random clusters of whiskers which lacked matrix infiltration (Figure 6.1-5). In the absence of an adequate whisker-matrix bond, these whiskers do not effectively reinforce the matrix and consequently the materials exhibited reduced modulus and strength levels.

(b) Compression

•*35 v/o SiC_p/2124-T6*—Compression test data for ACMC panels are listed in Table 6.1-5 and 6.1-6, and the data for DWA panels are listed in Table 6.1-7 and 6.1-8. These results indicate:

(1) Both ACMC and DWA panels exhibited nearly identical elastic modulus in longitudinal and transverse directions. e.g., E_x^C = 20.4 Msi and E_y^C = 21.0 Msi in ACMC panels; and E_x^C = 19.0 Msi and E_y^C = 21.6 Msi in DWA panels.

(2) Yield and tensile strength of ACMC panels were significantly higher than the DWA panels.

These differences could be explained primarily due to the differences in the matrix heat treatment. The tensile strength values in DWA panels were somewhat consistent with -T4 temper rather than -T6.

Table 6.1-3 Longitudinal Tensile Properties of 35v/o SiCw/2124-T6

Specimen # (35WA)(CQ)(AP)	Elastic Modulus E_x^T (Msi)	Yield Strength (ksi)	Ultimate Tensile Strength (ksi)	Poisson Ratio ν_{xy}	Strain To Failure (%)
TNL-1	18.7	73.7	85.2	0.2660	0.91
TNL-2	19.6	70.2	87.6	0.2759	1.097
TNL-3	18.9	74.5	86.5	0.2760	1.02
TNL-4	18.8	73.4	85.6	0.2729	1.04
TNL-5	18.1	74.0	83.6	0.2647	0.95
Mean Value	18.8	73.2	85.7	0.2711	1.00
Std. Dev.	0.54	1.70	1.49	0.00541	0.07
CV (%)	2.85%	2.33%	1.74%	2.00%	7.0%

Table 6.1-4 Transverse Tensile Properties of 35v/o SiCw/2124-T6

Specimen # (35WA)(CQ)(AP)	Elastic Modulus E_y^T (Msi)	Yield Strength (ksi)	Ultimate Tensile Strength (ksi)	Poisson Ratio ν_{yx}	Strain To Failure (%)
TNT-1	17.2	N/A	60.1	0.2412	0.4
TNT-2	17.5	N/A	56.9	0.2362	0.35
TNT-3	17.3	N/A	60.3	0.2327	0.385
TNT-4	17.4	N/A	62.8	0.2433	0.48
TNT-5	16.5	N/A	48.4	0.2281	0.32
Mean Value	17.2		57.7	0.2363	0.39
Std. Dev.	0.40		5.60	0.00619	0.06
CV (%)	2.30%		9.71%	2.62%	15.3%

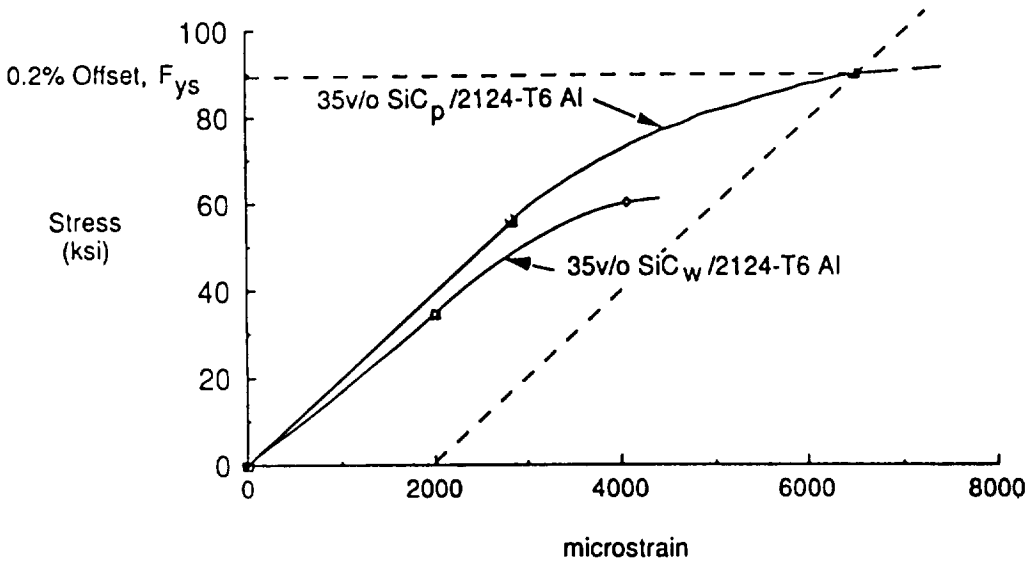

Figure 6.1-4 Transverse Tensile Behavior of 35v/o SiC_w /2124-T6 Al

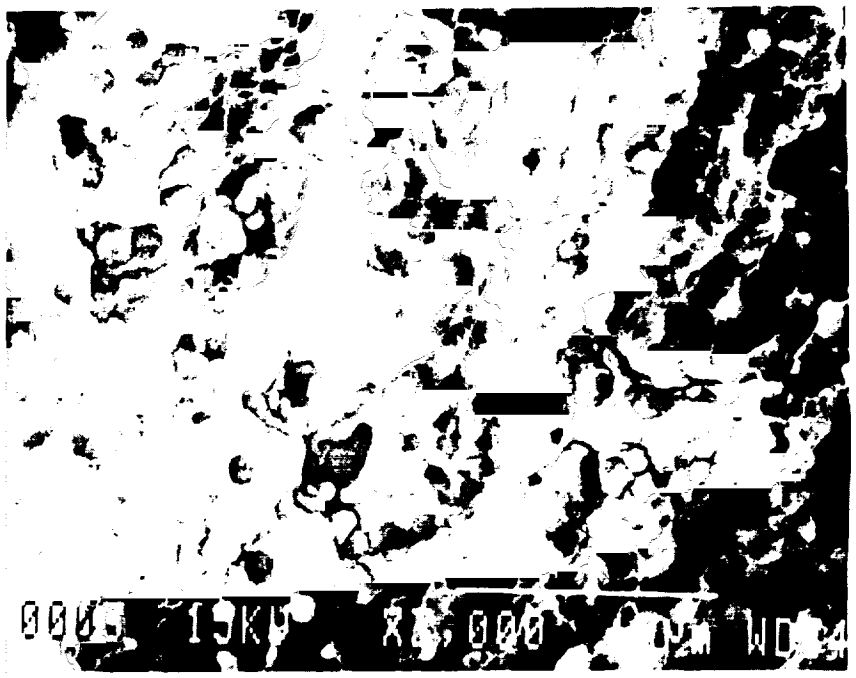

Figure 6.1-5 Fractrograph Showing Random Clusters of Whiskers Devoid of Matrix in 35 v/o SiC_w /2124-T6 Al

Table 6.1-5 Longitudinal Compressive Properties of 35v/o SiC_p/2124-T6 (ACMC, SC)

Specimen # (35PA)(CQ)(AP)	Elastic Modulus E_x^C (Msi)	Yield† Strength (ksi)	Ultimate† Compressive Strength (ksi)	Poisson Ratio ν_{xy}	Strain To Failure (%)
CML-1	18.1	76.7	94.5	0.2500	--
CML-2	20.0	89.5	106.7	0.2570	--
CML-3	21.0	--	103.6	0.2604	--
CML-4	22.1	--	104.7	0.2624	--
CML-5	21.0	92.3	106.9	0.2407	--
Mean Value	20.4	86.2	103.3	0.2541	
Std. Dev.	1.504	8.32	5.10	0.008851	
CV (%)	7.4%	9.6%	4.9%	3.5%	

†Apparent strength values because specimen buckled soon after yielding

Table 6.1-6 Transverse Compressive Properties of 35v/o SiC_p/2124-T6 (ACMC, SC)

Specimen # (35PA)(CQ)(AP)	Elastic Modulus E_y^C (Msi)	Yield† Strength (ksi)	Ultimate† Compressive Strength (ksi)	Poisson Ratio ν_{yx}	Strain To Failure (%)
CMT-1	21.8	88.7	107.9	0.2562	--
CMT-2	20.3	88.3	105.7	0.2538	--
CMT-3	20.7	--	100.3	0.2431	--
CMT-4	21.8	--	99.5	0.2618	--
CMT-5	20.3	83.3	101.8	0.2567	--
Mean Value	21.0	85.1	103.4	0.2543	
Std. Dev.	0.766	3.12	3.61	0.0069	
CV (%)	3.6%	3.7%	3.5%	2.7%	

†Apparent strength values because specimen buckled soon after yielding

Table 6.1-7 Longitudinal Compressive Properties of 35v/o SiC_p/2124-T6 (DWA, CA)

Specimen # (35PA)(dQ)(AP)	Elastic Modulus E_x^C (Msi)	Yield† Strength (ksi)	Ultimate† Compressive Strength (ksi)	Poisson Ratio ν_{xy}
CML-1	17.9	55.7	63.7	0.2326
CML-2	19.2	56.5	65.6	0.2427
CML-3	—	—	65.58	—
CML-4	20.4	57.8	65.9	0.2442
CML-5	18.4	56.8	63.8	0.2554
Mean Value	19.0	56.7	64.92	0.2437
Std. Dev.	1.09	0.8679	1.073	0.0093
CV (%)	5.7%	1.5%	1.7%	3.8%

Table 6.1-8 Transverse Compressive Properties of 35v/o SiC_p/2124-T6 (DWA, CA)

Specimen # (35PA)(CQ)(AP)	Elastic Modulus E_y^C (Msi)	Ultimate† Compressive Strength (ksi)	Poisson Ratio ν_{yx}
CMT-1	19.8	69.93	0.2879
CMT-2	20.56	69.25	0.2488
CMT-3	21.16	67.87	0.2722
CMT-4	21.8	64.79	0.3115
CMT-5	24.66	65.03	0.2917
Mean Value	21.60	67.4	0.2824
Std. Dev.	1.858	2.37	0.0234
CV (%)	8.6%	3.5%	8.3%

• ***35 v/o SiC_w/2124-T6***—Compressive test data of these composite are listed in Table 6.1-9 and 6.1-10. Like tensile test measurements, these results also indicated a slightly anisotropic response with the higher longitudinal compressive modulus (19.22 Msi) compared to the transverse modulus (17.2 Msi).

The tension and compression test results of 35 v/o particulate and whisker reinforced are also compared in the histogram shown in Figure 6.1-6.

(c) Flexure

• ***35 v/o SiC_p/2124-T6***—Flexure test results of ACMC and DWA panels are listed in Table 6.1-11 and 6.1-12 respectively. Based on these results the average flexural modulus and strength of DWA panels was slightly lower than ACMC panels. These differences also suggested that matrix in DWA panels had yet to attain the -T6 temper during heat treatment.

• ***35 v/o SiC_w/2124-T6***—Flexure test results of longitudinal and transverse specimens are listed in Table 6.1-13. Similar to tension and compression test results, these whisker reinforced specimens exhibited significantly lower flexural modulus and strength values compared to particulate reinforced specimens.

Table 6.1-9 Longitudinal Compressive Properties of 35v/o SiCw/2124-T6

Specimen # (35WA)(CQ)(AP)	Elastic Modulus E_x^C (Msi)	Yield Strength (ksi)	Ultimate Compressive Strength (ksi)	Poisson Ratio ν_{xy}	Strain To Failure (%)
CML-1	19.9	--	93.7	0.2778	--
CML-2	19.4	77.4	98.2	0.2846	--
CML-3	18.8	81.0	95.4	0.2672	--
CML-4	20.1	79.0	101.2	0.2859	--
CML-5	17.9	76.0	96.6	0.2568	--
Mean Value	19.22	78.4	97.02	0.2745	
Std. Dev.	0.893	2.15	2.86	0.0123	
CV (%)	4.64%	2.7%	2.9%	4.5%	

Table 6.1-10 Transverse Compressive Properties of 35v/o SiCw/2124-T6

Specimen # (35WA)(CQ)(AP)	Elastic Modulus E_y^C (Msi)	Yield Strength (ksi)	Ultimate Compressive Strength (ksi)	Poisson Ratio ν_{yx}	Strain To Failure (%)
CMT-1	17.8	62.5	83.3	0.2630	--
CMT-2	17.0	68.4	84.2	0.2449	--
CMT-3	17.9	67.8	84.8	0.2460	--
CMT-4	17.6	68.1	82.4	0.2546	--
CMT-5	15.6	63.3	77.4	0.2490	--
Mean Value	17.2	66.02	82.4	0.2515	
Std. Dev.	0.9497	2.87	2.95	0.00745	
CV (%)	5.5%	4.3%	3.6%	3.0%	

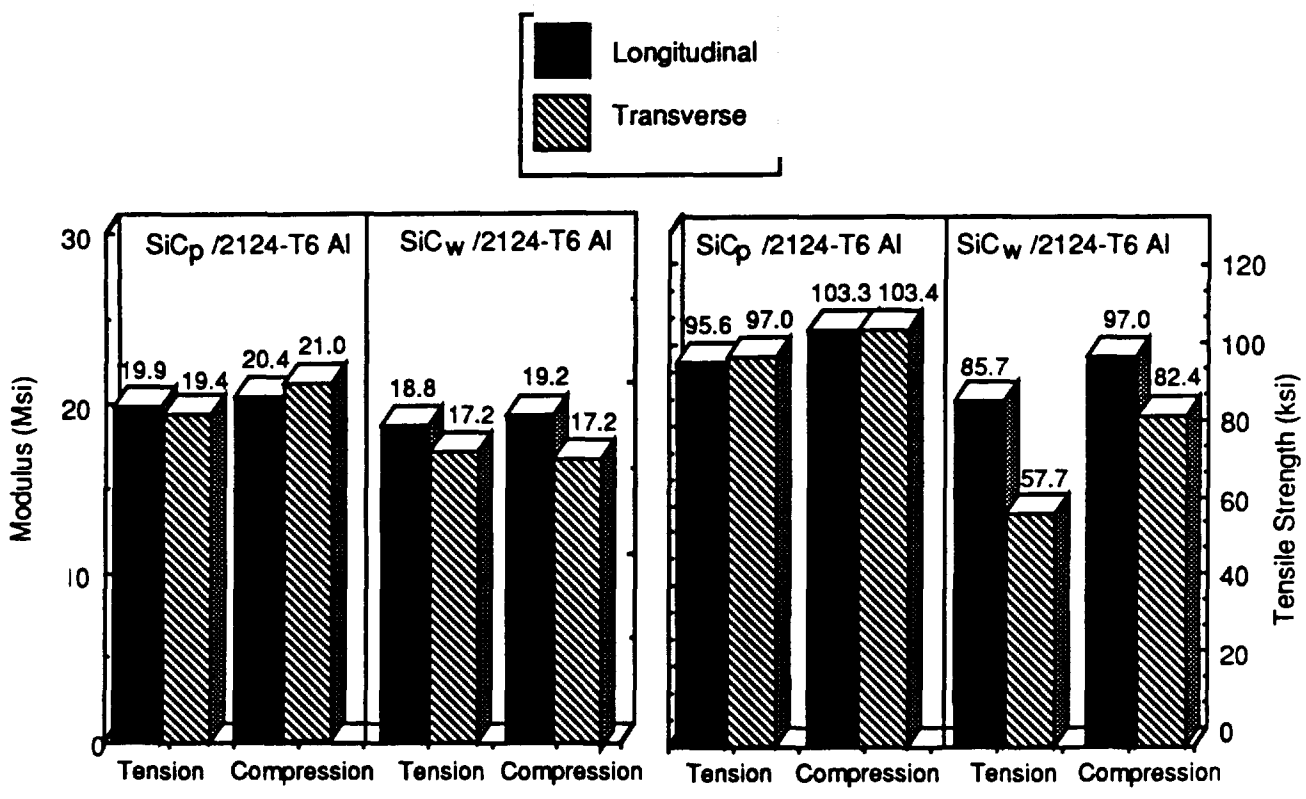

Figure 6.1-9 Histogram Comparing the Tension and Compression Test Results of SiC/Al Composite Panels

Table 6.1-11 Flexural Modulus and Strength of 35v/o SiC p /2124-T6 Al (Vendor: ACMC, SC)

Specimen # (25PA)(CQ)(AP)	Longitudinal Flexural		Specimen # (25PA)(CQ)(AP)	Transverse Flexural	
	Modulus (Msi)	Strength (ksi)		Modulus (Msi)	Strength (ksi)
FXL-1	16.0	187.9	FXT-1	17.1	181.2
FXL-2	17.5	186.6	FXT-2	—	—
FXL-3	17.3	181.5	FXT-3	16.9	176.2
					178.7
Mean	16.9	185.3	Mean	17.0	3.54
Standard Deviation	0.814	3.38	Standard Deviation	0.1414	2.0
CV(%)	4.8	1.8	CV(%)	0.8	

Table 6.1-12 Flexural Modulus and Strength of 35v/o SiC_p /2124-T6 Al (Vendor: DWA, CA)

Specimen # (35PA)(DQ)(AP)	Longitudinal Flexural		Specimen # (25WA)(CQ)(AP)	Transverse Flexural	
	Modulus (Msi)	Strength (ksi)		Modulus (Msi)	Strength (ksi)
FXL-1			FXT-1	16.09	135.3
FXL-2			FXT-2	14.74	134.8
FXL-3			FXT-3	15.14	133.5
Mean			Mean	15.32	134.5
Standard Deviation			Standard Deviation	0.69	0.93
CV(%)			CV(%)	4.5	0.69

Table 6.1-13 Flexural Modulus and Strength of 35v/o SiC_w /2124-T6 Al (Vendor: ACMC, SC)

Specimen # (35PA)(DQ)(AP)	Longitudinal Flexural		Specimen # (25WA)(CQ)(AP)	Transverse Flexural	
	Modulus (Msi)	Strength (ksi)		Modulus (Msi)	Strength (ksi)
FXL-1	112.9	180.4	FXT-1	11.8	159.8
FXL-2	13.2	162.9	FXT-2	11.9	152.3
FXL-3	13.3	172.9	FXT-3	11.8	160.0
Mean	13.1	172.1	Mean	11.8	157.4
Standard Deviation	0.208	8.8	Standard Deviation	0.0577	4.39
CV(%)	1.6	5.1	CV(%)	0.5	2.8

6.1.4 Thermophysical Properties

(a) Coefficient of Thermal Expansion

Both 35 v/o particulate and whisker reinforced aluminum matrix composites have similar thermal expansion behavior response as shown in Figure 6.1-7 to 6.1-10. These results are summarized in Table 6.1-14.

The measured CTE_x = 5.91 ppm/°F and CTE_y = 6.11 ppm/°F are close to the lower bound of the predicted value of 6.41 ppm/°F using Kerner equations based on random reinforcement distribution (Appendix D).

(b) Specific Heat

Specific heat test data for 35 v/o SiC_p/2124-T6 and 35 v/o SiC_w/2124-T6 over the -240°F to 755°F temperature range are plotted in Figure 6.1-11. These results show that the specific heat values (0.189 Btu/lb·°F at RT) for silicon carbide whisker and particulate reinforced aluminum are nearly identical, and the temperature dependence is similar to the response observed for 2124 aluminum.

(c) Thermal Diffusivity and Through-The-Thickness Thermal Conductivity

Through-the-thickness thermal diffusivity (D_z) of particulate and whisker reinforced flat specimens was measured to calculate the through panel thermal conductivity (K_z) values from the following expression:

$$K_z = D_z \cdot C_p \cdot \rho$$

The measured values of specific heat (C_p), density, (ρ) and D_z and the corresponding K_z values at different temperatures are listed in Table 6.1-15. Like the aluminum matrix, the thermal conductivity of composite increases with increase in temperature. These results also indicate

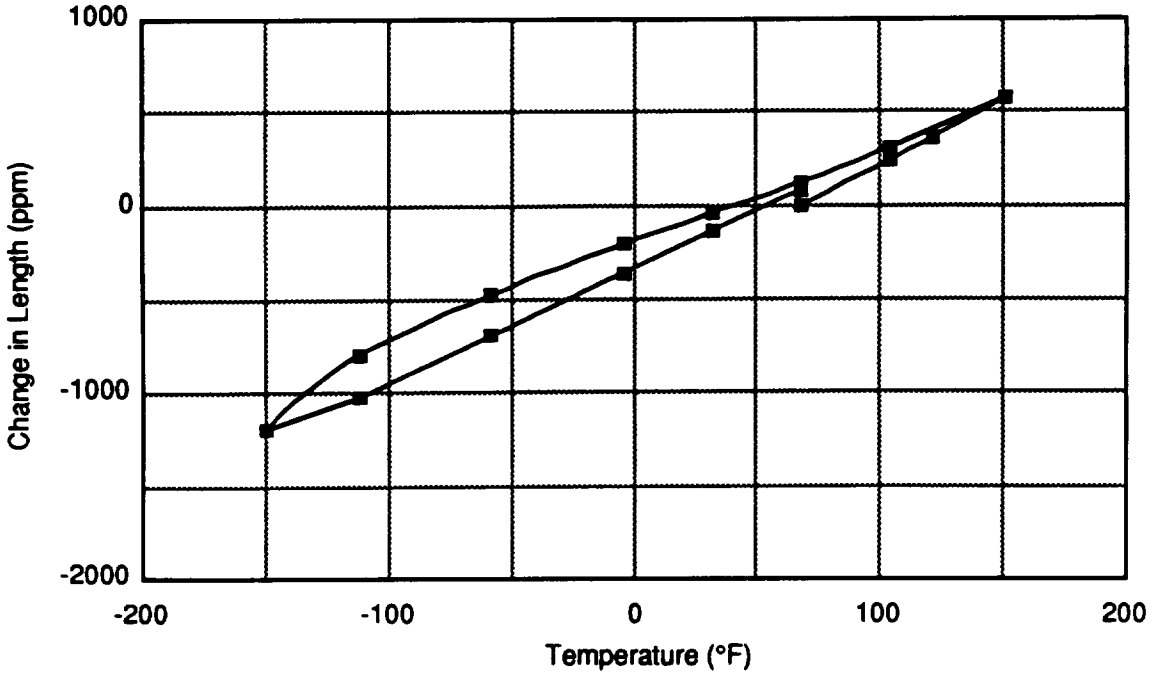

Figure 6.1-7 Thermal Expansion Behavior of 35v/o SiCp/2124-T6 Specimen Parallel to the Extrusion Direction in a Heat/Cool/Heat Cycle Using Push Rod Dilatometer

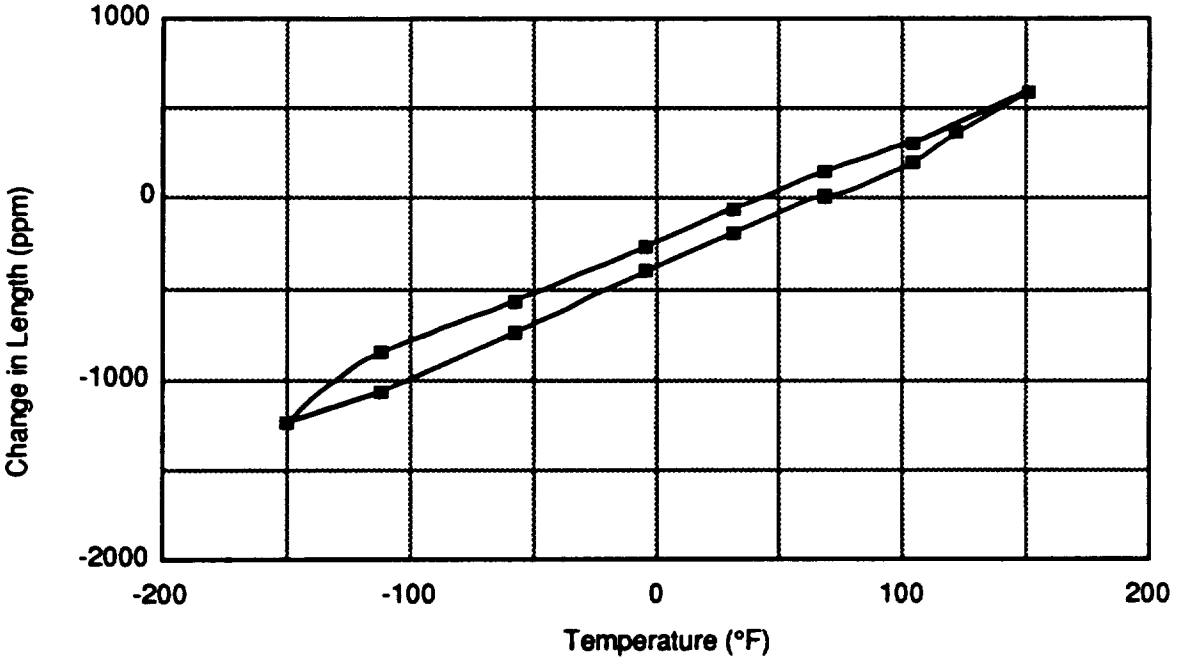

Figure 6.1-8 Thermal Expansion Behavior of 35v/o SiCp/2124-T6 Specimen Transverse to the Extrusion Direction in a Heat/Cool/Heat Cycle Using Push Rod Dilatometer

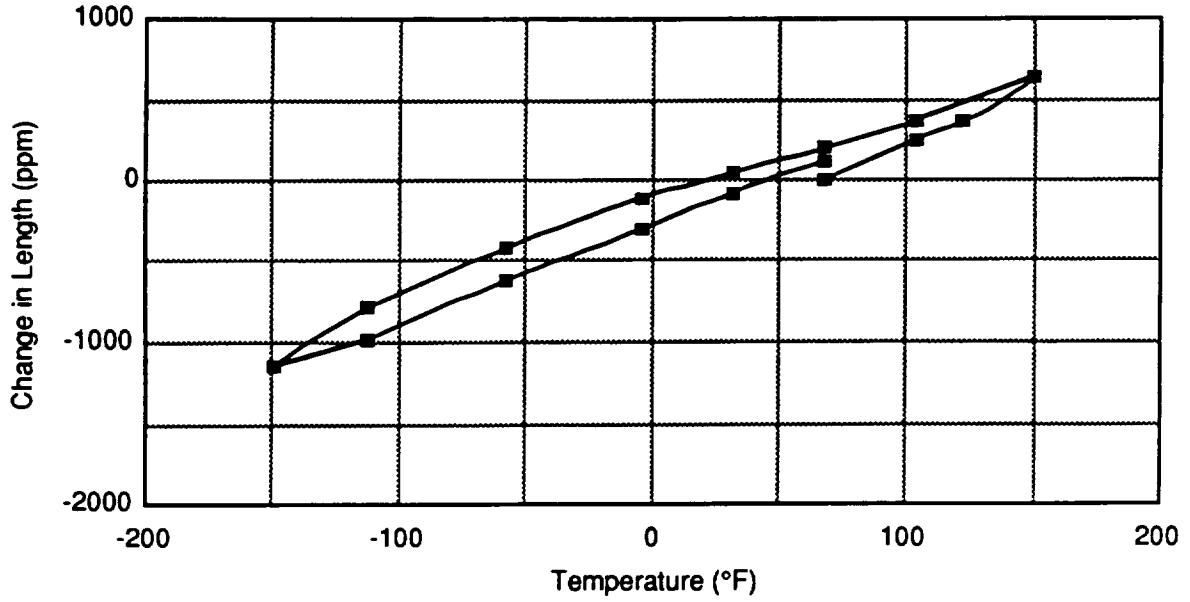

Figure 6.1-9 Thermal Expansion Behavior of 35v/o SiCw/2124-T6 Specimen Parallel to the Extrusion Direction in a Heat/Cool/Heat Cycle Using Push Rod Dilatometer

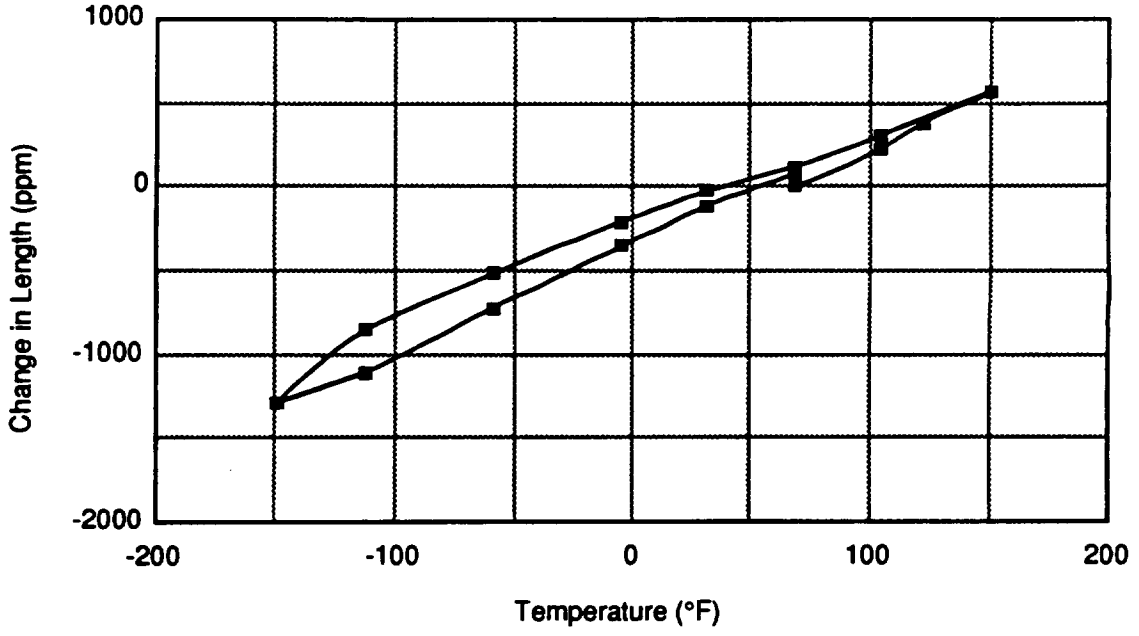

Figure 6.1-10 Thermal Expansion Behavior of 35v/o SiCw/2124-T6 Specimen Transverse to the Extrusion Direction in a Heat/Cool/Heat Cycle Using Push Rod Dilatometer

Table 6-14 Summary of Thermal Expansion Test Data of 35 v/o SiC/Al Composites

Thermal Expansion Measurements	35 v/o SiC_p /2124-T6 Al		35 v/o SiC_w /2124-T6 Al	
	Longitudinal	Transverse	Longitudinal	Transverse
CTE (ppm/°F)*	5.86	6.11	5.91	6.29
Residual strain (ppm)	77.6	20.0	117.6	70.4
Strain Hysteresis (ppm)†	116.8	114.8	198.4	119.2

*(end to end point average); †at RT (i.e., RT → 150°F → RT)

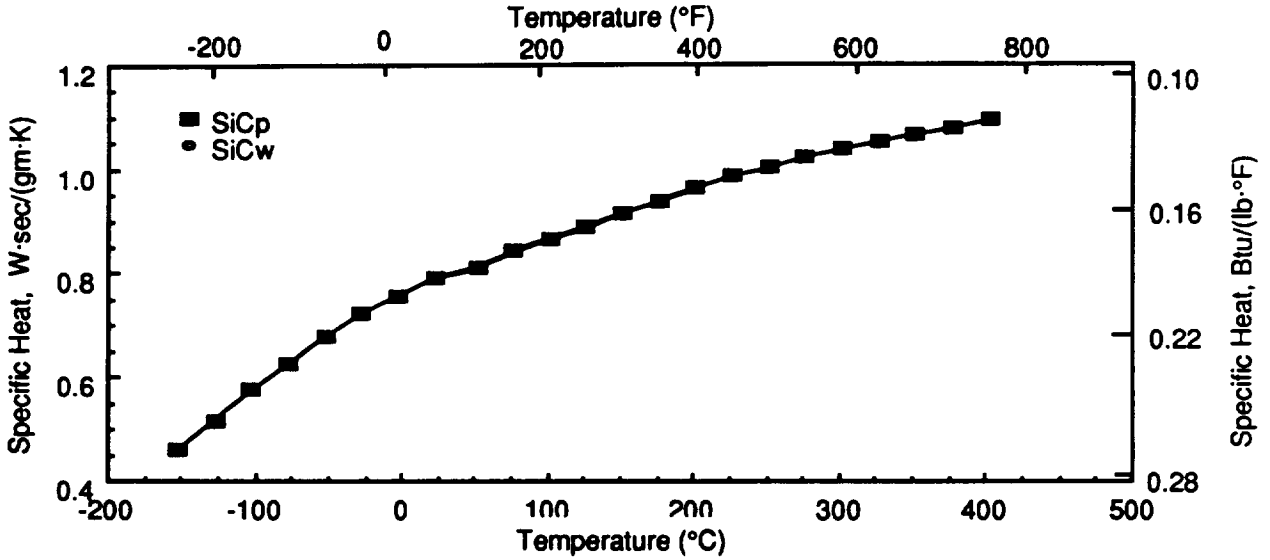

Figure 6.1-11 Specific Heat Versus Temperature of 35v/o Dincontinuous SiC/Al

Table 6.1-15 Calculated Thermal Conductivity Values For 35 v/o Discontinuous SiC/2124-T6 Al

Sample (No.)	T emp. (°C)	Density (gm cm-3)	Specific Heat (W · s gm-1 K-1)	Diffusivity (cm 2sec-1)	Conductivity (W • cm-1 K-1)	Conductivity (Btu Units*)	Temp. (°F)
†35(PA)-TD	-150	2.808	0.4630	0.343	0.44594	309.19	-238
35(PA)-TD	-100	2.808	0.5770	0.330	0.53467	370.71	-148
35(PA)-TD	-50	2.808	0.6770	0.320	0.60833	421.78	-58
35(PA)-TD	0	2.808	0.7560	0.315	0.66870	463.64	33.8
35 (PA)-TD	25	2.808	0.7930	0.313	0.69697	483.24	77
35(PA)-TD	100	2.808	0.8670	0.310	0.75471	523.27	212
35(PA)-TD	200	2.808	0.9620	0.305	0.82390	571.25	392
35(PA)-TD	300	2.808	1.0370	0.300	0.87357	605.69	572
35(PA)-TD	400	2.808	1.0930	0.295	0.90540	627.75	752
35(WA)-TD	25	2.834	0.7920	0.382	0.85741	594.48	77

* - (Btu in hr^{-1} ft^{-2} F^{-1}); † - Through-thickness

that K_z (49.6 Btu/hr·ft·°F at room temperature) for whisker reinforced composite is higher than K_z (40 Btu/hr·ft·°F) for the particulate reinforced composite. The higher K_z value in whisker reinforced materials could be attributed to preferential alignment of whiskers along the through-the-thickness direction.

(d) Thermal Conductivity

Longitudinal and transverse thermal conductivity (and electrical resistivity) values obtained by the Kohlrausch method are listed in Table 6.1-16. The test specimen, if clamped at the ends, had a tendency to distort due to thermal stresses and end constraints. The thermal conductivity and electrical resistivity values obtained upon cooling from 750°F were different from those measured during the heating cycle. For these specimens the thermal conductivity values measured during the cooling cycle were greater than those obtained during the heating cycle. Figure 6.1-12 shows the longitudinal, transverse, and through-the-thickness thermal conductivity values of both the particulate and whisker reinforced composite. These results indicate that whisker reinforced composites were nearly isotropic, whereas in particulate reinforced composites, $K_y > K_x > K_z$, with K_z being about one-half of the K_y values.

(e) Electrical Resistivity

Both for particulate and whisker reinforced Al matrix composite, Figure 6.1-13 shows a plot of electrical resistivity as a function of temperature. The electrical resistivity values at different temperatures in whisker reinforced materials were comparable to those for the particulate material even though the thermal conductivity values were considerably lower. For both the composites, measured electrical resistivity values in the cooling cycle were lower than the corresponding values in the heating cycle providing an indication of a phase transformation such as coarsening of precipitates.

Table 6.1-16 Inplane Thermal Conductivity and Electrical Resistivity Values of 35v/0 SiC/2124-T6 Al Composites

Sample Designation	Temp. (°C)	Conductivity ($W \cdot cm^{-1} K^{-1}$)	Resistivity (microhms·cm)	Conductivity ($BTU \cdot in \cdot hr^{-1} ft^{-2} F^{-1}$)	Temp. (°F)
35(WA)(CQ)-TKL —Longitudinal	32	0.881	10.432	611	90
	52	0.884	10.889	613	126
	75	0.897	11.406	622	177
	102	0.920	11.990	638	215
35(WA)(CQ)-TKT —Transverse	32	0.890	11.140	617	90
	50	0.901	11.557	625	121
	75	0.917	12.144	636	166
	100	0.936	12.731	649	217
35(PA)(CQ)-TKL —Longitudinal	-147	0.863	6.381	598	-232
	-128	0.931	6.782	646	-198
	-96	1.015	7.500	704	-140
	-55	1.092	8.371	757	-67
	-16	1.195	9.250	829	3
	33	1.202	10.233	834	91
	50	1.210	10.615	839	123
	102	1.225	11.737	849	216
	169	1.276	13.191	884	335
	243	1.300	14.139	902	469
	302	1.340	14.647	929	575
	385	1.309	16.942	907	725
	405	1.293	17.573	897	761
35(PA)(CQ)-TKL Cool	206	1.366	12.481	947	404
	93	1.338	9.832	928	200
35(PA)(CQ)-TKT —Transverse	30	1.125	10.481	780	81
	49	1.122	10.914	778	120
	99	1.132	12.038	785	210
	-149	0.774	6.492	536	-236
	-123	0.877	7.047	608	-190
	-101	0.938	7.552	650	-149
	-80	0.972	8.003	674	-112
	-60	1.006	8.457	698	-76
	-40	1.050	8.901	728	-40
	-24	1.084	9.263	751	-11
	98	1.154	11.694	800	208
	169	1.205	13.367	835	336
	237	1.215	14.515	842	458
	307	1.255	15.444	870	585
	384	1.237	17.626	858	723
	409	1.238	18.273	859	768
35(PA)(CQ)-TKT Cool	99	1.269	10.447	880	210
	194	1.296	12.702	898	381

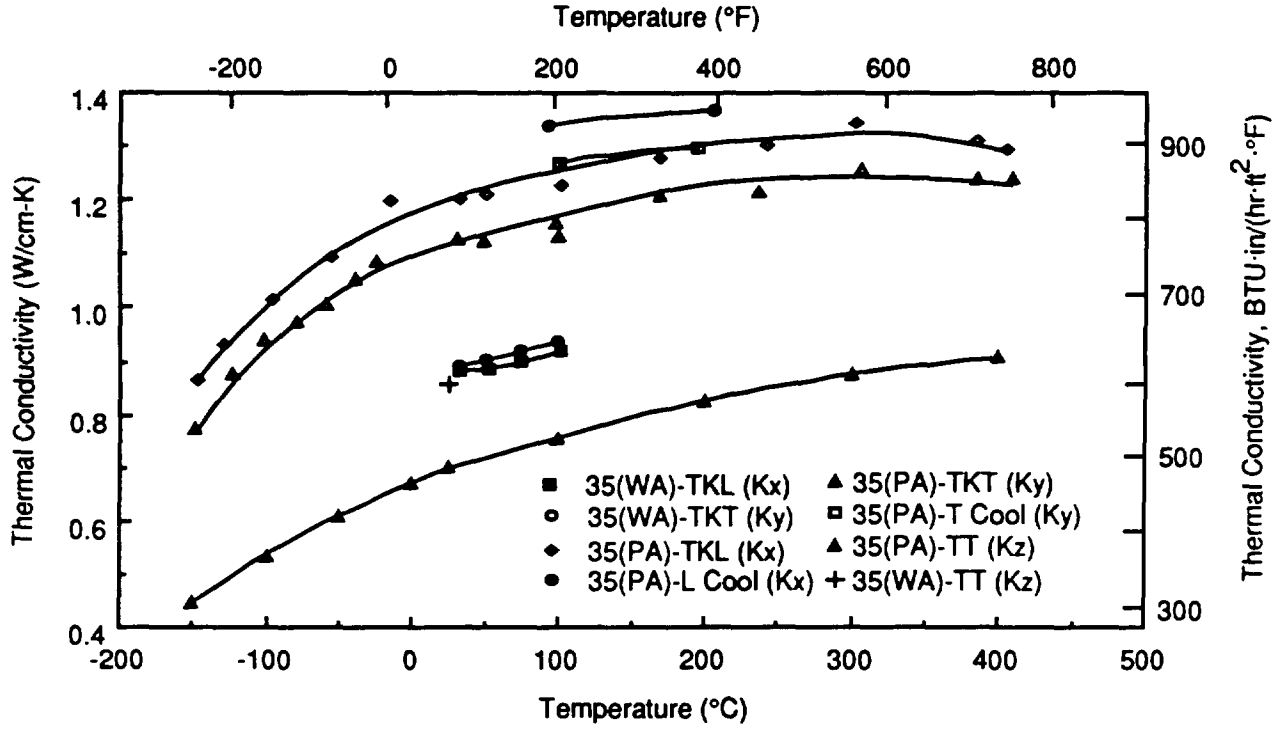

Figure 6.1-12 Inplane Thermal Conductivity Versus Temperature For 35v/o SiC/2124-T6 Al Composites

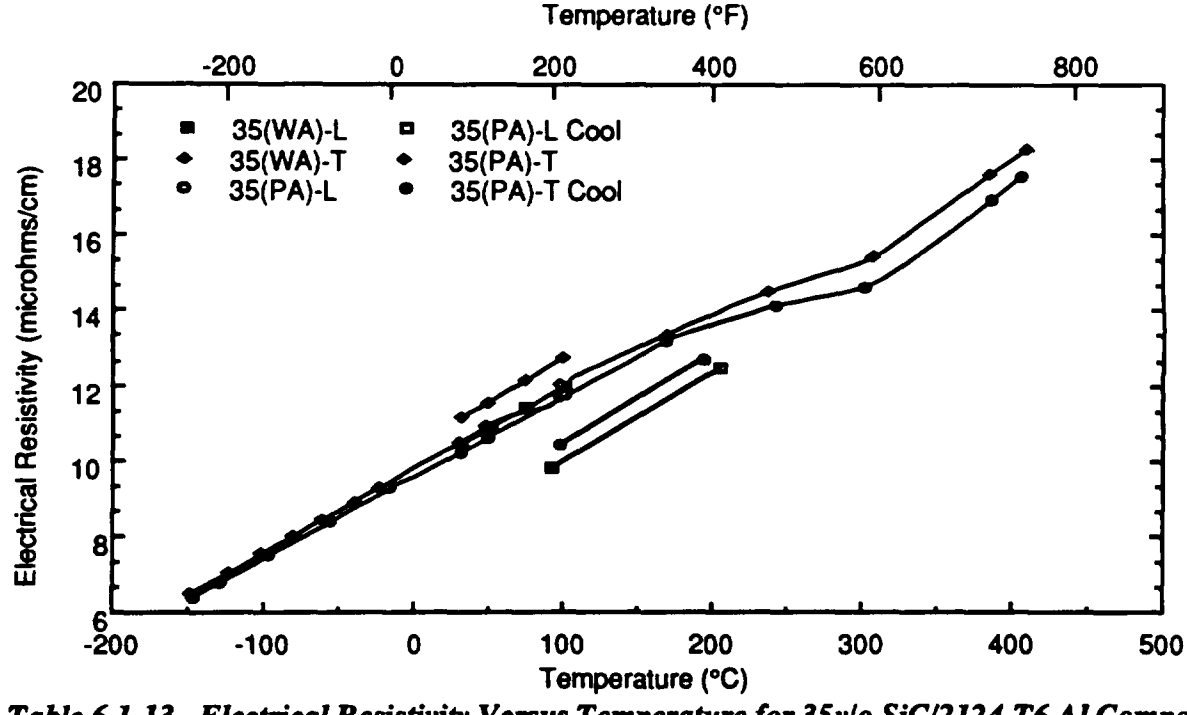

Table 6.1-13 Electrical Resistivity Versus Temperature for 35v/o SiC/2124-T6 Al Composites

(f) Optical Properties

• The total hemispherical emissivity (ε_H) values of 35 v/o SiC_p/2124-T6 measured using the multiproperty test method are plotted in Figure 6.1-14. These ε_H values of 0.529 at 256°F are significantly higher than the normal emissivity (ε_N) values of 0.148 at 70°F. In the normal emissivity measurements both particulate and whisker reinforced composites had nearly similar values:

•35 v/o SiC_p/2124-T6 Al: $\alpha_s = 0.57$

$\varepsilon_N = 0.148$

•35 v/o SiC_w/2124-T6 Al: $\alpha_s = 0.577$

$\varepsilon_N = 0.177$

• Reflectance versus Wavelength—For 35 v/o SiC_p/2123-T6 and SiC_w/2124-T6, the reflectance spectra between 2 and 14 μm wavelength is presented in Figure 6.1-15 and 6.1-16 respectively. Like 25 v/o discontinuous SiC/Al, these 35 v/o panels also showed about 80% reflectance at 10.6 μm wavelength.

6.2 TUBES

• 35 v/o SiC_p/2124-T6

• 35 v/o SiC_w/2124-T6

In addition to the flat plates of 35 v/o SiC particulate and whisker reinforced aluminum composite, 1.5-in. diameter 0.065-in. thickness tubes (fabricator: ACMC) were also tested to determine their mechanical properties. The fabrication details and the results of dimensional measurements and tension compression tests are discussed below.

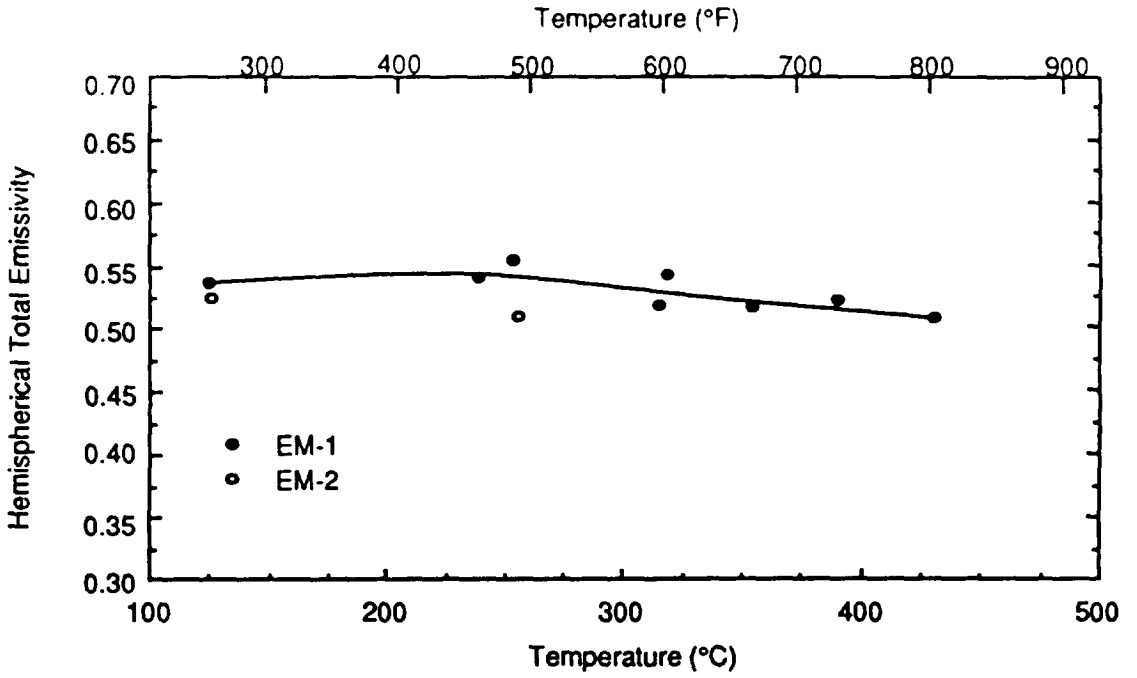

Figure 6.1-14 Total Hemispherical Emissivity Versus Temperature 35v/o SiC/2124-T6 Al

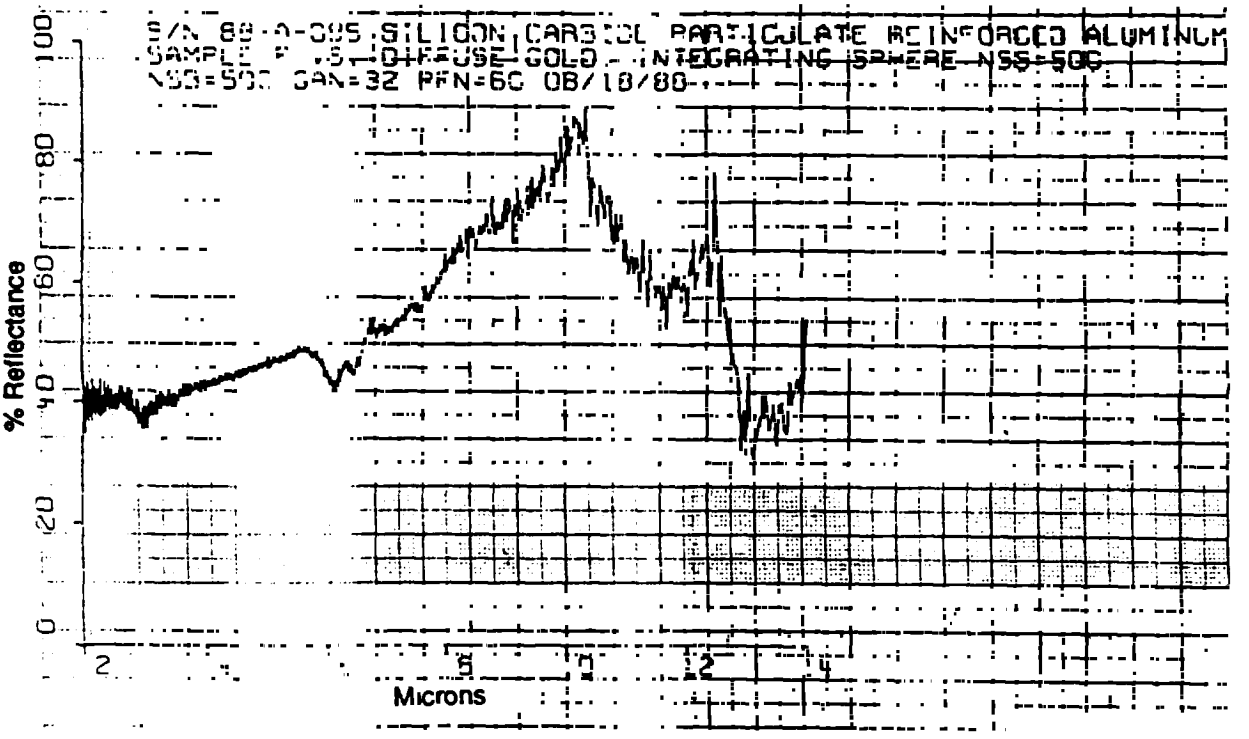

Figure 6.1-15 Reflectance as a Function of Wavelength of 35v/o SiC_p/2124-T6

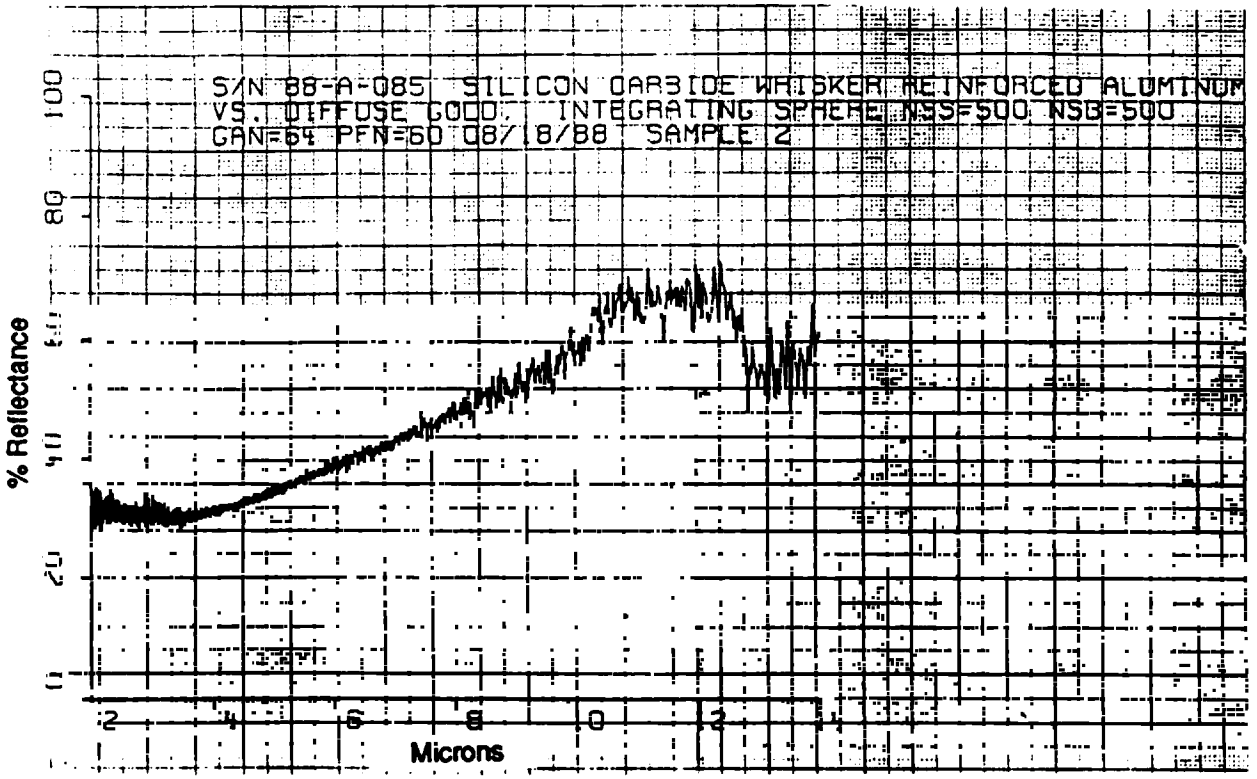

Figure 6.1-16 Reflectance as a Function of Wavelength of 35v/o SiC_w /2124-T6

6.2.1 Fabrication Data

Fabrication Process:	Both 25 and 35 v/o discontinuous SiC/Al tubes were produced by extrusion of billets as shown in Figure 6.2-1.	
Material System:	35 v/o SiC_p/2124-T6	35 v/o SiC_w/2124-T6
Manufacturer:	ACMC, SC	ACMC, SC
Martin Marietta ID No.:	(35PA)(CQ)(AT)	(35WA)(CQ)(AT)
Prescribed Dimensions:	1.5-in. ± 0.01-in. dia	1.5-in. ± 0.01-in. diameter
	0.065-in. ± .003-in. Thick	0.065-in. ± 0.003-in. Thick

• Dimensional Measurement— The diameter and wall thickness measurements of SiC_p and SiC_w/2124-T6 tubes are listed in Table 6.2-1, where the O.D. value is an average of eight measurements made at each end. The average wall thickness of the 25 v/o composites was close to the nominal value 0.065 in. while the 35 v/o composites were less than 0.065 in. thick (e.g., 35 v/o SiC_w ~ 0.0575 in. thick).

6.2.2 Product Evaluation

(a) Density

• 35 v/o SiC_p/2124-T6 Tube

Density: 0.104 lb/in^3

Std. Dev.: 0.001

• 35 v/o SiC_w/2124-T6 Tube

Density : 0.104 lb/in^3

Std. Dev.: 0.005

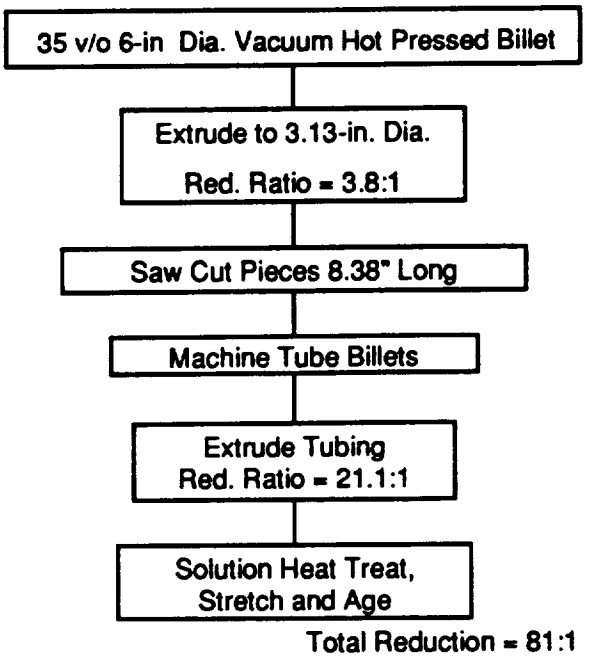

Figure 6.2-1 Fabrication Process to Produce Discontinuous 35 v/o SiC/Al Tubes (at ACMC, SC)

Figure 6.2-1 Diameter and Wall Thickness Variation of 35v/o SiC/Al Compoiste Tubes

	SiC_p /2124-T6		SiC_w /2124-T6	
	35 v/o		35 v/o	
	OD (in)	ID (in)	OD (in)	ID (in)
	1.498	1.374	1.492	1.376
	1.501	1.377	1.497	1.381
	1.505	1.381	1.486	1.370
	1.497	1.373	1.500	1.384
	1.501	1.377	1.496	1.380
	1.496	1.372	1.498	1.382
Average	1.500	1.376	1.495	1.380
Std. Dev.	0.003	0.003	0.005	0.005
Wall Thickness	0.062		0.0575	

(b) Reinforcement Content

	SiC_p/2124-T6	SiC_w/2124-T6
v/o:	35.3	35.4
Std. Dev.:	1.4	1.4
Void Volume:	≤0.1	≤0.1

(c) Non-Destructive Evaluation

Based on visual examination, ID and OD surface of each tube was good without any voids, or scratches. Also, the x-radiographs and ultrasonic C-scans did not reveal any internal voids or defects.

6.2.3 Mechanical Properties

(a) Tension

Tensile properties of 35 v/o SiC_p and SiC_w/2124-T6 tubes are listed in Table 6.2-2 and 6.2-3. During tension tests, a few of the specimen failed within the gage length and remaining specimens showed a bond-line failure. The incidence of failure at grip ends was attributed to inadequate surface preparation during bonding operation. Therefore, the measured yield and ultimate tensile strength values should be considered (apparent) lower bound.

Tensile test results show that the average longitudinal elastic modulus and yield strength values obtained for SiC_w/Al tube specimens were higher than the corresponding values for the flat specimens. The improved mechanical properties in the tubes could be attributed to alignment of the reinforcements in the extrusion direction. For the 35 v/o whisker reinforced tubes had an average elastic modulus value ~ 22.3 Msi, as compared to 18.8 Msi for panels. Also the 35 v/o SiC_w/Al tube specimens showed more improved apparent strength properties than the flat specimens which had localized clusters of whiskers during consolidation.

Table 6.2-2 Longitudinal Tensile Properties of 35v/o SiCp/2124-T6 Al Tubes

Speciment # (35PA)(CQ)(AT)	Elastic Modulus† (Msi)				Yield Strength (ksi)	Ultimate Tensile Strength (ksi)	Strain To Failure (%)	Poisson Ratio
	E_{X1}	E_{X2}	E_{X3}	E_X				
TNL-1	18.6	17.9	20.5	19.0	—	66.9*	>0.36*	0.2716
TNL-2	18.8	18.0	18.3	18.4	—	66.0*	>0.39*	0.2602
TNL-3	18.6	19.3	20.3	19.4	84.6	90.6	0.90	0.2617
Mean				18.9	84.6	90.6	0.90	0.2645
Std. Dev.				0.50				0.00619
CV (%)				2.7				2.3
(35PA)(CQ)(AP) Plate				19.9	86.5	95.6	1.03	0.2539

† One Biaxial (#1) and two (#2 & #3) Strain Gages Placed 120° Apart
*Specimen Exhibited a Bond Line Failure

Table 6.2-3 Longitudinal Tensile Properties of 35v/o SiCw/2124-T6 Al Tubes

Speciment # (35WA)(CQ)(AT)	Elastic Modulus† (Msi)				Yield Strength (ksi)	Ultimate Tensile Strength (ksi)	Strain To Failure (%)	Poisson Ratio
	E_{X1}	E_{X2}	E_{X3}	E_X				
TNL-1	20.6	23.8	21.8	22.1	—	>80.4*	>0.56*	0.2774
TNL-2	23.2	21.5	21.3	22.0	79.3	>84.9*	>0.65*	0.2371
TNL-3	22.2	25.1	21.5	22.9	88.0	>92.4*	>0.68*	0.2199
Mean				22.3	83.6	>85.6*85.7	≥0.68*	0.2448
Std. Dev.				0.493				0.0295
CV (%)				2.2				12.1
(35WA)(CQ)(AP) Plate				18.8	73.2		1.00	0.2711

† One Biaxial (#1) and two (#2 & #3) Strain Gages Placed 120° Apart
*Specimen Exhibited a Bond Line Failure

(b) Compression

Compression properties of 35 v/o SiC_p and SiC_w/2124-T6 Al tube specimens are listed in Table 6.2-4 and 6.2-5. Each specimen exhibited compressive failure within the gage length, without bending or buckling effects. Average compressive modulus values were comparable with the tensile moduli, whereas compressive strengths were slightly higher than in tension. High compressive strength values have been attributed to increased stress levels required to offset the residual tensile stresses in the matrix of discontinuous silicon carbide aluminum composites (Ref 71).

(c) Hoop Tensile Properties

For 35 v/o SiC_p and SiC_w/2124-T6 tube specimens, the measured hoop modulus, strength, and strain to failure values are listed in Table 6.2-6. Based on these results, both particulate and whisker reinforced tubes exhibited the anisotropic response:

in 35 v/o SiC_p/2124-T6 $E_H > E_x^T$; and

in 35 v/o SiC_w/2124-T6 $E_H > E_x^T$

6.2.4 Thermophysical Properties

(a) Coefficient of thermal expansion

Thermal expansion response of 35 v/o SiC_p and SiC_w/2124-T6 tube specimen is shown in Figure 6.2-2 and 6.2-3 respectively. Measured values:

	35 v/o SiC_p/2124-T6	35 v/o SiC_w/2124-T6
CTEx (ppm/°F)	6.96	5.99
Residual Strain (ppm):	51.2	91.2
RT hysteresis (ppm)	-76.8	-46.8

indicate a thermal expansion response similar to the panel specimens.

Table 6.2-4 Longitudinal Compressive Properties of 35v/o SiC_p/2124-T6 Al Tubes

Speciment # (35PA)(CQ)(AT)	Elastic Modulus† (Msi)				Yield Strength (ksi)	Ultimate Comp. Strength (ksi)	Strain To Failure (%)	Poisson Ratio
	E_{X1}	E_{X2}	E_{X3}	E_X				
CML-1	16.9	19.8	19.7	18.8	75.5	111.4	2.18	0.2861
CML-2	19.7	18.1	20.5	19.4	81.1	112.9	2.01	0.2276
CML-3	18.7	20.9	19.5	19.4	81.9	114.9	2.05	0.2886
Mean				19.3	79.5	113.1	2.08	0.2674
Std. Dev.				0.458	3.48	1.76	0.088	0.0345
CV (%)				2.4	4.4	1.6	4.2	12.9

† One Biaxial (#1) and two (#2 & #3) Strain Gages Placed 120° Apart

Table 6.2-5 Longitudinal Compressive Properties of 35v/o SiC_w/2124-T6 Al Tubes

Speciment # (35WA)(CQ)(AT)	Elastic Modulus† (Msi)				Yield Strength (ksi)	Ultimate Comp. Strength (ksi)	Strain To Failure (%)	Poisson Ratio
	E_{X1}	E_{X2}	E_{X3}	E_X				
CML-1	22.7	20.6	21.0	21.4	87.6	124.4	1.63	0.2310
CML-2	25.6	21.3	21.9	22.9	96.8	136.8	1.69	0.2480
CML-3	24.2	21.1	23.2	22.8	97.5	138.7	1.71	0.2317
Mean				22.4	94.0	133.3	1.68	0.2369
Std. Dev.				0.84	5.5	7.77	0.04	0.0096
CV (%)				3.7	5.9	5.8	2.38	4.1

† One Biaxial (#1) and two (#2 & #3) Strain Gages Placed 120° Apart

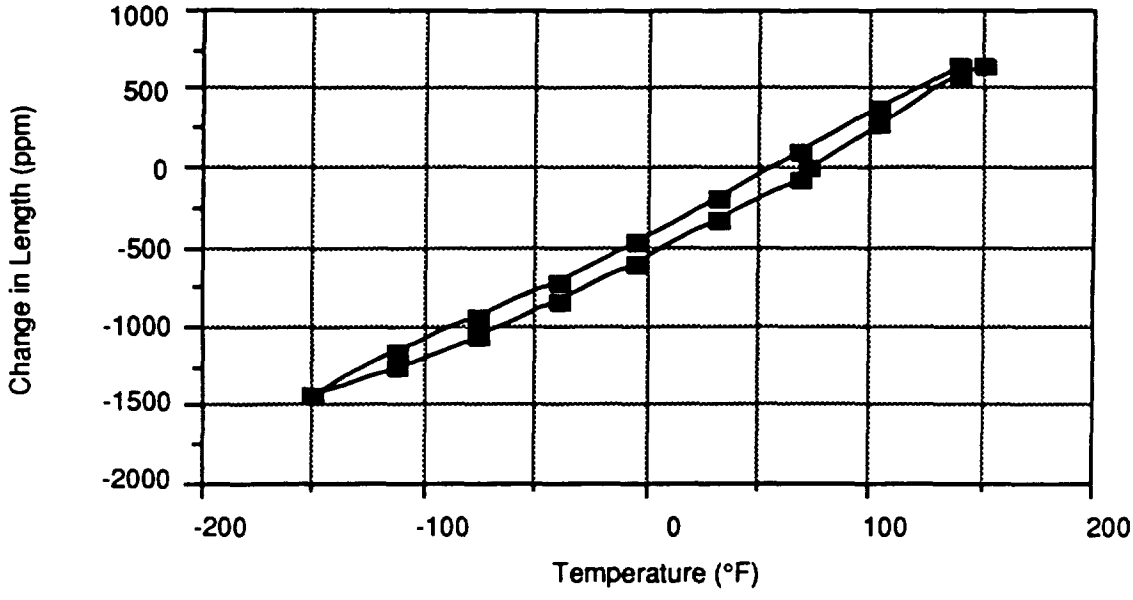

Figure 6.2-2 Thermal Expansion Behavior of 35v/o SiC_p/2124-T6 Tube Specimen Parallel to the Extrusion Direction in a Heat/Cool/Heat Cycle Using Push Rod Dilatometer

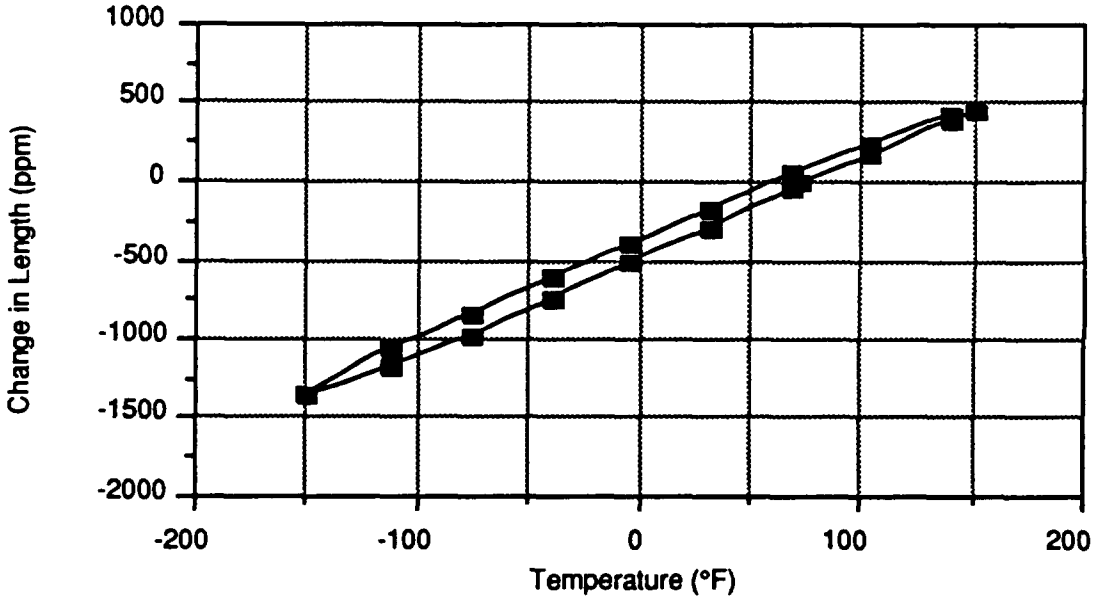

Figure 6.2-3 Thermal Expansion Behavior of 35v/o SiC_w/2124-T6 Tube Specimen Parallel to the Extrusion Direction in a Heat/Cool/Heat Cycle Using Push Rod Dilatometer

6.3 SUMMARY OF 35 v/o DISCONTINUOUS SiC/Al TEST DATA

Mechanical and thermophysical property test data of 35 v/o discontinuous SiC/2124-T6 are summarized in the following tables:

35 v/o SiC_p/2124-T6 Al	Table 6.3-1
35 v/o SiC_w/2124-T6 Al	Table 6.3-2
35 v/o SiC_p/2124-T6 Al Tubes	Table 6.3-3
35 v/o SiC_w/2124-T6 Al Tubes	Table 6.3-4

Table 6.3-1 35v/o SiC_p/Al 2124 - T6 Panels

NOT DESIGN ALLOWABLE DATA

PROPERTIES							TEMPERATURE (°F)			Std. Dev. / No. of Specimens at RT	Test Method
PHYSICAL			MECHANICAL & THERMAL				Low	Room	High		
Density (lb / in^3)		0.104	Longitudinal Tensile Strength	σ_x^{TU}	ksi			95.6		± 4.90 / 5	ASTM D-3552
Fiber volume fraction		0.35	Transverse Tensile Strength	σ_y^{TU}	ksi			97.0		±5.34 / 5	ASTM D-3552
Void volume fraction		<0.001	Longitudinal Comp. Strength	σ_x^{CU}	ksi			103.3		±5.10 / 5	ASTM D-3410
Nominal ply thickness	in	0.060	Transverse comp. strength	σ_y^{CU}	ksi			103.4		±3.61 / 5	ASTM D-3410
Max. cont. use temp.	°F	~550	In-plane shear strength	IPSS	ksi						
OPTICAL & ELECTRICAL (at room temperature)			Interlaminar shear strength	ILSS	ksi						
Solar Absorptance	α	0.57	Longitudinal tensile strain **	ε_x^T	%			1.038		±0.20 / 5	ASTM D-3552
Normal Emissivity	ε	0.150	Transverse tensile strain **	ε_y^T	%			1.074		±0.23 / 5	ASTM D-3552
Electrical Resistivity	R	8.5 μΩ·cm	Longitudinal comp. strain **	ε_x^C	%			—			ASTM D-3410
			Transverse comp. strain **	ε_y^C	%			—			ASTM D-3410
			Longitudinal tensile modulus	E_x	Msi			19.9		±0.46 / 5	ASTM D-3552
			Transverse tensile modulus	E_y	Msi			19.4		±0.28 / 5	ASTM D-3552
			Longitudinal comp. modulus	E_x	Msi			20.4		±1.504 / 5	ASTM D-3410
			Transverse comp. modulus	E_y	Msi			21.0		±0.766 / 5	ASTM D-3410
			In-plane shear modulus	G	Msi			—			
			Longitudinal flexural modulus	F_x	Msi			16.9		±0.814 / 3	ASTM D-790M
			Transverse flexural modulus	F_y	Msi			17.0		±0.1414 / 3	ASTM D-790M
			Long. tensile Poisson's ratio	ν_{xy}				0.2539		±0.00443 / 5	ASTM D-3552
			Trans. tensile Poisson's ratio	ν_{yx}				0.2481		±0.00321 / 5	ASTM D-3552
			Long. thermal conductivity	K_x	(1)	4.153	5.75	6.18			Kohlrausch
			Trans. thermal conductivity	K_y	(1)	3.72	5.42	5.82			Kohlrausch
			Thru thickness thermal cond.	K_z	(1)	2.147	3.356	3.967			Laser Flash
			Specific heat	C_p	(2)	0.110	0.189	0.230			ASTM E-1269
			Longitudinal CTE	α_x	(3)	2.147	5.86	3.967			ASTM E-80
			Transverse CTE	α_y	(3)		6.11				ASTM E-80
			Thru thickness CTE	α_z	(3)		—				

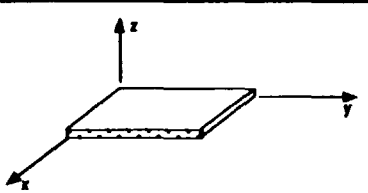

Notes:
(**) - Strain to failure; (1) Btu/(hr·in·°F); (2) Btu/(lb·°F); (3) μin./in./°F

Table 6.3-2 35v/o SiC_w/Al 2124 - T6 Panels

NOT DESIGN ALLOWABLE DATA

PROPERTIES							TEMPERATURE (°F)			Std. Dev. / No. of Specimens at RT	Test Method
PHYSICAL			MECHANICAL & THERMAL				Low	Room	High		
Density (lb / in^3)	X	0.104	Longitudinal Tensile Strength	σ_x^{TU}	ksi			85.7		± 1.49 / 5	ASTM D-3552
Fiber volume fraction	X	0.35	Transverse Tensile Strength	σ_y^{TU}	ksi			57.7		±5.60 / 5	ASTM D-3552
Void volume fraction	X	<0.001	Longitudinal Comp. Strength	σ_x^{CU}	ksi			97.02		±2.86 / 4	ASTM D-3410
Nominal ply thickness	In	0.060	Transverse comp. strength	σ_y^{CU}	ksi			82.4		±2.95 / 5	ASTM D-3410
Max. cont. use temp.	°F	~550	In-plane shear strength	IPSS	ksi						
OPTICAL & ELECTRICAL (at room temperature)			Interlaminar shear strength	ILSS	ksi	X	X	X			
Solar Absorptance	α	0.577	Longitudinal tensile strain **	ε_x^T	%			1.00		±0.07 / 5	ASTM D-3552
Normal Emissivity	ε	0.177	Transverse tensile strain **	ε_y^T	%			0.39		±0.06 / 5	ASTM D-3552
Electrical Resistivity	R	10.432 μΩ·cm	Longitudinal comp. strain **	ε_x^C	%						ASTM D-3410
			Transverse comp. strain **	ε_y^C	%						ASTM D-3410
			Longitudinal tensile modulus	E_x	Msi			18.8		±0.54 / 5	ASTM D-3552
			Transverse tensile modulus	E_y	Msi			17.2		±0.40 / 5	ASTM D-3552
			Longitudinal comp. modulus	E_x	Msi			19.22		±0.893 / 4	ASTM D-3410
			Transverse comp. modulus	E_y	Msi			17.2		±0.9497 / 5	ASTM D-3410
			In-plane shear modulus	G	Msi						
			Longitudinal flexural modulus	F_x	Msi			13.1		±0.208 / 3	ASTM D-790M
			Transverse flexural modulus	F_y	Msi			11.8		±0.0577 / 3	ASTM D-790M
			Long. tensile Poisson's ratio	ν_{xy}		X		0.2711		±0.00541 / 5	ASTM D-3552
			Trans. tensile Poisson's ratio	ν_{yx}		X		0.2363		±0.00619 / 5	ASTM D-3552
			Long. thermal conductivity	K_x	(1)			4.24			Kohlrausch
			Trans. thermal conductivity	K_y	(1)			4.28			Kohlrausch
			Thru thickness thermal cond.	K_z	(1)			4.128			Laser Flash
			Specific heat	C_p	(2)		0.110	0.189	0.230		ASTM E-1269
			Longitudinal CTE	α_x	(3)			5.91			ASTM E-80
			Transverse CTE	α_y	(3)			6.29			ASTM E-80
			Thru thickness CTE	α_z	(3)			—			

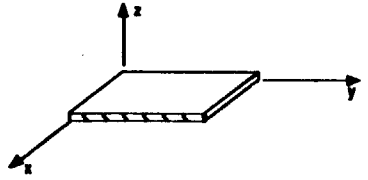

Notes:
(**) - Strain to failure; (1) Btu/(hr·in·°F); (2) Btu/(lb·°F); (3) μin./in./°F

Table 6.3-3 35v/o SiC_p/Al 2124 - T6 Tubes

NOT DESIGN ALLOWABLE DATA

PHYSICAL		
Density (lb / in^3)		0.104
Fiber volume fraction		0.35
Void volume fraction		<0.001
Nominal ply thickness	in	0.065
Max. cont. use temp.	°F	~550

OPTICAL & ELECTRICAL (at room temperature)		
Solar Absorptance	α	
Normal Emissivity	ε	
Electrical Resistivity	R	

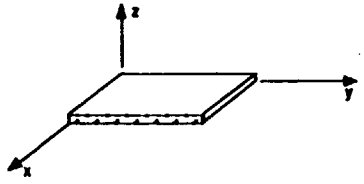

PROPERTIES			TEMPERATURE (°F)			Std. Dev. / No. of Specimens at RT	Test Method
MECHANICAL & THERMAL			Low	Room	High		
Longitudinal Tensile Strength	σ_x^{TU}	ksi		90.6			ASTM D-3552
Transverse Tensile Strength	σ_y^{TU}	ksi		73.6			NOL
Longitudinal Comp. Strength	σ_x^{CU}	ksi		113.1		±1.76 / 3	ASTM D-3410
Transverse comp. strength	σ_y^{CU}	ksi					
In-plane shear strength	IPSS	ksi					
Interlaminar shear strength	ILSS	ksi					
Longitudinal tensile strain **	ε_x^T	%		0.90			ASTM D-3552
Transverse tensile strain **	ε_y^T	%		0.54			NOL
Longitudinal comp. strain **	ε_x^C	%					ASTM D-3410
Transverse comp. strain **	ε_y^C	%					
Longitudinal tensile modulus	E_x	Msi		18.9		±0.5 / 3	ASTM D-3552
Transverse tensile modulus	E_y	Msi		20.3			NOL
Longitudinal comp. modulus	E_x	Msi		19.3		± 0.458 / 3	ASTM D-3410
Transverse comp. modulus	E_y	Msi					
In-plane shear modulus	G	Msi					Torsion Test
Longitudinal flexural modulus	F_x	Msi					
Transverse flexural modulus	F_y	Msi					
Long. tensile Poisson's ratio	ν_{xy}					± 0.00619 / 3	ASTM D-3552
Trans. tensile Poisson's ratio	ν_{yx}						NOL
Long. thermal conductivity	K_x	(1)					
Trans. thermal conductivity	K_y	(1)					
Thru thickness thermal cond.	K_z	(1)					
Specific heat	C_p	(2)					
Longitudinal CTE	α_x	(3)		6.96			ASTM E-80
Transverse CTE	α_y	(3)					
Thru thickness CTE	α_z	(3)					

Notes:
(**) - Strain to failure; (1) Btu/(hr·in·°F); (2) Btu/(lb·°F); (3) µin./in./°F

Table 6.3-4 35v/o SiC_w/Al 2124 - T6 Tubes

NOT DESIGN ALLOWABLE DATA

PROPERTIES						TEMPERATURE (°F)			Std. Dev. / No. of Specimens at RT	Test Method
PHYSICAL			MECHANICAL & THERMAL			Low	Room	High		
Density (lb / in^3)	X	0.104	Longitudinal Tensile Strength	σ_x^{TU}	ksi		>85.6			ASTM D-3552
Fiber volume fraction	X	0.35	Transverse Tensile Strength	σ_y^{TU}	ksi		60.1			NOL
Void volume fraction	X	<0.001	Longitudinal Comp. Strength	σ_x^{CU}	ksi		133.3		± 7.77 / 3	ASTM D-3410
Nominal ply thickness	In	0.060	Transverse comp. strength	σ_y^{CU}	ksi					
Max. cont. use temp.	°F	~550	In-plane shear strength	IPSS	ksi					
OPTICAL & ELECTRICAL (at room temperature)			Interlaminar shear strength	ILSS	ksi	X	X	X		
Solar Absorptance	α		Longitudinal tensile strain **	ε_x^T	%		>0.68			ASTM D-3552
Normal Emissivity	ε		Transverse tensile strain **	ε_y^T	%		0.458			NOL
Electrical Resistivity	R	μΩ·cm	Longitudinal comp. strain **	ε_x^C	%					ASTM D-3410
			Transverse comp. strain **	ε_y^C	%					
			Longitudinal tensile modulus	E_x	Msi		22.3		±0.493 / 3	ASTM D-3552
			Transverse tensile modulus	E_y	Msi		18.3			NOL
			Longitudinal comp. modulus	E_x	Msi		22.4		± 0.84 / 3	ASTM D-3410
			Transverse comp. modulus	E_y	Msi					
			In-plane shear modulus	G	Msi					Torsion Test
			Longitudinal flexural modulus	F_x	Msi					
			Transverse flexural modulus	F_y	Msi					
			Long. tensile Poisson's ratio	ν_{xy}	X					ASTM D-3552
			Trans. tensile Poisson's ratio	ν_{yx}	X					NOL
			Long. thermal conductivity	K_x	(1)					
			Trans. thermal conductivity	K_y	(1)					
			Thru thickness thermal cond.	K_z	(1)					
			Specific heat	C_p	(2)					
			Longitudinal CTE	α_x	(3)		5.99			ASTM E-80
			Transverse CTE	α_y	(3)					
			Thru thickness CTE	α_z	(3)					

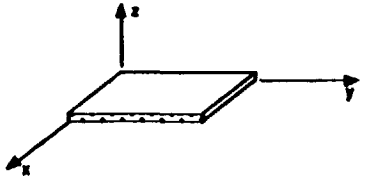

Notes:
(**) - Strain to failure; (1) Btu/(hr·in·°F); (2) Btu/(lb·°F); (3) μin./in./°F

Graphite/Aluminum
P100/6061

7.0 GRAPHITE/ALUMINUM: P100/6061 Al

Continuous fiber reinforced metal matrix composites (MMC) offer high specific stiffness and near zero-CTE in conjunction with high thermal and electrical conductivities, and no outgassing. Because of these attractive properties, MMC are candidate material for dimensionally stable space structures. In particular, P100/6061 Al tubes have been used in the structural antenna support boom for the Hubble Space Telescope. Therefore the SOA P100/6061 flat panels and tubes were obtained to determine their mechanical and thermophysical properties. The fabrication data and the results of product evaluation and material property tests are discussed in this chapter.

7.1 P100/6061 Al FLAT PANELS

Unidirectional P100/6061 Al panels fabricated by two manufacturers: (1) BP-DWA and (2) Amercom, Inc, CA, were tested in this program. These panels were produced under a "Big Buy" program (Ref 22). The results of material evaluation and tests are given below.

7.1.1 Fabrication Data

• DWA (Big Buy) Panel

Material System:	P100 Gr/6061 Al, $[0^\circ]_2$, (0.0035-in big buy wire)
Condition:	As fabricated
Fabrication Process:	Diffusion bonding using MCI Precursor wires
Fabricator:	DWA Specialties, CA
Dimensions:	12-in. x 12-in. x 0.0433-in. thick, 2 ply panel
Ply Thickness:	0.0216-in.
DWA Part ID:	G-5975
Martin Marietta ID:	(GA)(DU)(AP)
DWA Job #:	415 (Dated 6/17 - 6/22/87)

• Precursor wire data: (FMI/STD (formerly MCI) Columbus, OH generated)

Item/I.D. No.	Fiber Volume	UTS (ksi)	Wire Dia.	Roll No.	Grams Used (lb)
02-E-03-040787					
N00L1	51.12	201.4	0.24	G-0968	66.0 (0.1455)
N00L2	51.61	200.5	0.24	G1000	62.0 (0.1367)
N00L3	51.88	204.9	0.24	G-0996	62.0 (0.1367)
N00L4	47.89	194.4	0.25	G-0998	66.5 (0.1466)

•Amercom "Big Buy" Panel

Material System:	P100 Gr/6061 Al, $[0°]_2$, (0.0035-in. big buy wire)
Condition:	As fabricated
Fabrication Process:	Diffusion Bonding
Fabricator:	Amercom Inc., CA
Dimensions:	5-in. x 10.25-in. x 0.0415-in. thick, from a 13in. x 26-in. 2-ply panel
Ply Thickness:	0.020-in.
Amercom Lab No:	6041-1 (P.O. #F33615-85-C-0332)
Martin Marietta ID:	(GA)(AU)(AP)
Amercom Job #:	8460P(5/9/86)

7.1.2 Product Evaluation

(a) Density

• DWA Panel G5975

Density:	0.090 lb/in^3
Std. Dev.:	0.002

• Amercom Panel 8430P

Density:	0.090 lb/in^3
Std Dev.:	0.002

(b) Fiber Volume

• DWA Panel G5975

v/o:	42.2%
Std. Dev.:	0.56
Void Volume:	≤0.1%

• Amercom Panel 8430P

v/o:	46.46%
Std. Dev.:	0.36
Void Volume:	≤0.1%

(c) Non-Destructive Evaluation

Visual, X-radiographic, ultrasonic, and thermographic inspection techniques were used to assess material quality. In general each panel and tube had adequate surface finish with minor face sheet imperfections such as voids and fiber-print through effect. An ultrasonic C-scan of DWA Gr/Al ((GA)(DU)(AP)) panels indicated a few regions of internal voids or delaminations. Also, thermographic inspection of Gr/Al did not reveal internal anomalies because of the high reflectivity of the aluminum face sheets. Even when painted black, the infra-red imaging could not establish any contrast.

(d) Microstructures

Using optical microscopy, various longitudinal and transverse sections of $[0^{\circ}]_2$ Gr/Al panels were examined to reveal the quality of consolidation and fiber distribution. A typical transverse micrograph of a (GA)(DU)(AP) panel is shown in Figure 7.1-1.

Microstructures revealed that the consolidation between precursor wires and face sheets was generally of high quality, with very few voids between the precursor wires. Fiber distribution was nearly uniform with only occasional uninfiltrated regions. In the interfiber matrix region each panel exhibited a few transverse microcracks (Figure 7.1-2.) caused by differential thermal expansion between the fiber and matrix during cooling from consolidation temperatures.

7.1.3 Mechanical Properties

(a) Tension

Longitudinal and transverse tension test results of DWA and Amercom panels are presented in Table 7.1-1 to 7.1-4. These results showed that measured elastic modulus values were in agreement with the values predicted by ROM. For the DWA panel, the measured $E_x^T = 49.71$ Msi was 97.6% of the ROM and for the Amercom panel, the measured $E_x^T = 52.86$ Msi was 99.2% of the ROM.

(b) Compression

Longitudinal compression test results of DWA and Amercom panels are presented in Tables 7.1-5 and 7.1-6 respectively. In both cases, the compression modulus were lower than the corresponding longitudinal elastic modulus values. Also the measured compressive strength values were about 35% of the corresponding tensile strength values.

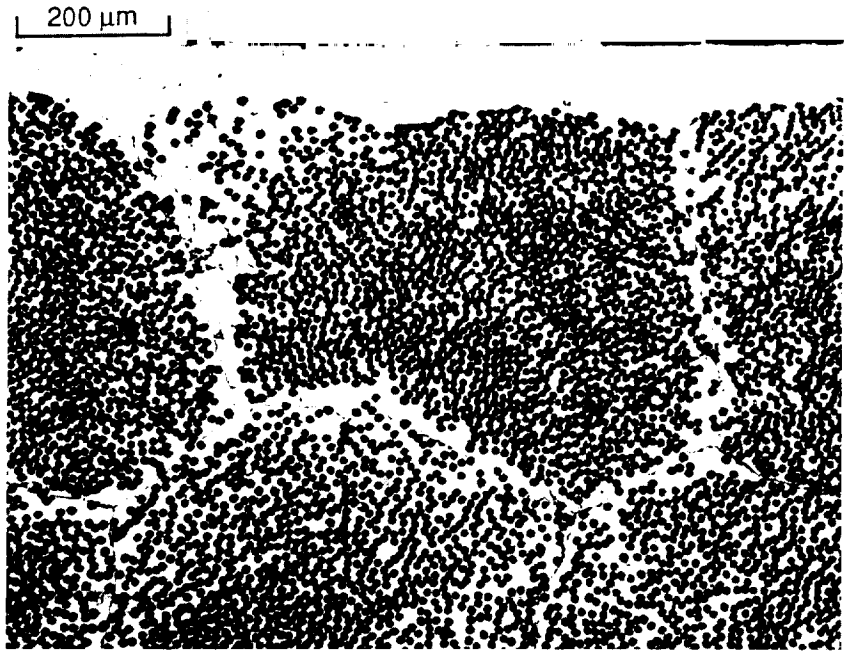

Figure 7.1-1 Transverse Micrograph of Diffusion Bonded 2-ply P100/6061 Al Panel Showing Good Consolidation and Fiber Distribution

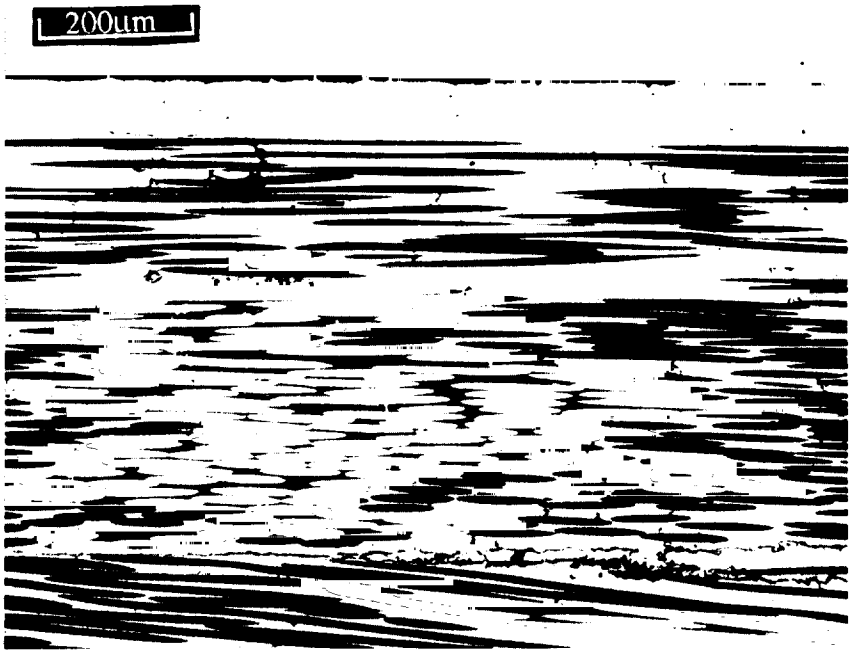

Figure 7.1-2 Longitudinal Micrograph of Diffusion Bonded 2-ply P100/6061 Al Panel Showing A Few Microcracks in the Interfiber Matrix Region

Table 7.1-1 Longitudinal Tensile Properties Of DWA P100/6061 Al, $[0^\circ]_2$, Fiber Volume = 42.2%

Specimen # (GA)(DU)(AP)	Elastic Modulus E_x^T (Msi)	Ultimate Tensile Strength (ksi)	Poisson Ratio ν_{xy}	Strain To Failure (%)
TNL-1	49.84	130.24	0.3125	0.276
TNL-2	—	138.3	—	—
TNL-3	49.80	131.5	0.2797	0.265
TNL-4	50.44	129.0	0.3079	0.258
TNL-5	48.74	127.7	0.2750	0.263
Mean Value	49.71	131.3	0.2949	0.265
Std. Dev.	0.701	4.14	0.0178	0.0076
CV (%)	1.4	3.2	6.0	2.86

Table 7.1-2 Longitudinal Tensile Properties Of Amercom P100/6061 Al, $[0^\circ]_2$, Fiber Volume = 46.46%

Specimen # (GA)(AU)(AP)	Elastic Modulus E_x^T (Msi)	Ultimate Tensile Strength (ksi)	Poisson Ratio ν_{xy}	Strain To Failure (%)
TNL-1	51.84	131.8	0.3736	0.26
TNL-2	53.54	130.0	0.3006	0.244
TNL-3	52.00	132.7	0.3291	0.26
TNL-4	55.08	117.8	0.3072	0.216
TNL-5	51.86	115.6	0.3176	0.22
Mean Value	52.86	125.6	0.3256	0.24
Std. Dev.	1.43	8.21	0.0289	0.021
CV (%)	2.7	6.5	8.9	8.75

Table 7.1-3 Transverse Tensile Properties Of DWA P100/6061 Al, $[0^\circ]_2$, Fiber Volume = 42.2%

Specimen # (GA)(DU)(AP)	Elastic Modulus E_y^T (Msi)	Ultimate Tensile Strength (ksi)	Poisson Ratio ν_{yx}	Strain To Failure (%)
TNT-1	—	—	—	—
TNT-2	5.56	3.44	0.0222	0.067
TNT-3	5.42	3.93	0.0207	0.078
TNT-4	4.39	3.92	0.02	0.070
TNT-5	5.19	3.19	0.0216	0.068
Mean Value	5.14	3.62	0.0211	0.0707
Std. Dev.	0.523	0.366	0.00101	0.0049
CV (%)	10.2	10.1	4.8	6.9

Table 7.1-4 Transverse Tensile Properties Of Amercom P100/6061 Al, $[0^\circ]_2$, Fiber Volume = 46.46%

Specimen # (GA)(AU)(AP)	Elastic Modulus E_y^T (Msi)	Ultimate Tensile Strength (ksi)	Poisson Ratio ν_{yx}	Strain To Failure (%)
TNT-1	—	—	—	—
TNT-2	6.18	2.91	0.018	0.044
TNT-3	5.91	3.23	0.0304	0.05
TNT-4	6.24	3.40	0.016	0.055
TNT-5	5.92	3.62	0.0252	0.065
Mean Value	6.06	3.29	0.0224	0.0535
Std. Dev.	0.1721	0.299	0.0066	0.0089
CV (%)	2.8	9.1	29.46	16.6

Table 7.1-5 Longitudinal Compressive Properties Of DWA P100/6061 Al, $[0^\circ]_2$, Fiber Volume = 42.2%

Specimen # (GA)(DU)(AP)	Elastic Modulus E_x^C (Msi)	Ultimate Comp. Strength (ksi)	Poisson Ratio ν_{xy}	Strain To Failure (%)
CML-1	52.45	47.43	—	0.122
CML-2	46.86	46.48	0.3333	0.14
CML-3	47.17	45.85	0.2731	0.12
CML-4	46.90	—	0.2291	0.10
CML-5	47.37	47.48	0.2918	0.12
Mean Value	48.15	46.62	0.2818	0.1204
Std. Dev.	2.41	0.806	0.043	0.014
CV (%)	5.0	1.7	15.3	11.6

Table 7.1-6 Longitudinal Compressive Properties Of Amercom P100/6061 Al, $[0^\circ]_2$, Fiber Volume = 46.46%

Specimen # (GA)(AU)(AP)	Elastic Modulus E_x^C (Msi)	Ultimate Comp. Strength (ksi)	Poisson Ratio ν_{xy}	Strain To Failure (%)
CML-1	46.75	45.94	0.346	0.14
CML-2	44.83	34.5	0.253	0.09
CML-3	49.16	40.78	0.273	0.07
CML-4	47.65	40.10	0.277	0.12
CML-5	48.08	43.08	0.233	0.12
Mean Value	47.29	40.88	0.2764	0.108
Std. Dev.	1.63	4.24	0.043	0.027
CV (%)	3.4	10.4	15.5	25.6

(c) In-plane Shear

In-plane shear modulus and strength values were obtained by using 10°-off axis tensile tests. Delta Rosette strain gages (EA-13-030YB-120) were used at the middle of gage length to measure the strain variation; and test data obtained were reduced to generate the shear stress-strain curves to failure. The measured in-plane shear modulus and shear strength values are listed in Table 7.1-7. During these tests, each specimen exhibited distinct shear failure along the 10°-off axis. The measured shear modulus value of 2.62 Msi was lower than the predicted value of 3.5 Msi.

(d) Flexure

Flexure modulus and strength values of both DWA and Amercom Gr/Al specimens are listed in 7.1-8. The longitudinal flexural modulus values was about 53% of the tensile modulus. These results are in agreement with the results available in the literature (Ref 20, 22, 39, and 40) for the two ply composite. Theoretical analysis indicates that, as number of plies in the unidirectional composites increase to ≥10, then the flexural modulus tends to approach the tensile modulus (Ref 72).

(e) Interlaminar Shear Strength (Short-Beam Shear)

Apparent interlaminar shear strength values listed in Table 7.1-9 were determined by conducting short beam shear-three point bend tests. After the tests, each specimen was examined under an optical microscope, and observations confirmed that the failure was primarily interlaminar shear.

Table 7.1-7 Inplane Shear Modulus and Strength Values of P100/6061 Al, v/o = 42.2

Specimen # (GA)(DU)(AP)	Shear Modulus (Msi)	Shear Strength (psi)
IP-1A	-	5004.2
IP-2A	2.35	5443.4
IP-3A	2.55	5574.6
IP-4A	2.95	5368.6
Mean Value	2.62	5347.7
Std. Dev.	0.306	244.3
CV (%)	11.7	4.6

Table 7.1-8 Longitudinal and Transverse Flexural Properties (3 Point Bend) of P100/6061 Al Composites

	Specimen #	Longitudinal Flexural		Specimen #	Transverse Flexural	
		Modulus (Msi)	Strength (ksi)		Modulus (Msi)	Strength (ksi)
Flat Panel	FXL-1A	26.25	96.45	FXT-1A	4.18	12.49
--DWA	FXL-2A	27.01	98.07	FXT-2A	4.45	12.55
(GA)(DU)(AP)	FXL-3A	25.05	103.95	FXT-3A	3.85	10.83
v/o = 42.2						
Mean Value		26.25	99.49		4.16	11.96
Std. Dev.		0.755	3.94		0.30	0.9762
CV (%)		2.9	3.97		7.2	8.2
Flat Panel	FXL-1B	28.03	89.27	FXT-1B	3.8	10.54
--Amercom	FXL-2B	27.39	83.65	FXT-2B	4.35	12.03
(GA)(AU)(AP)	FXL-3B	26.53	89.33	FXT-3B	4.43	12.63
v/o = 46.46						
Mean Value		27.32	87.42		4.19	11.73
Std. Dev.		0.753	3.26		0.34	1.076
CV (%)		2.8	3.7		8.2	9.2

Table 7.1-9 Apparent Interlaminar Shear Strength of P100/6061 Al, [0]2, Fiber Volume = 42.2%

*Specimen # (GA)(DU)(AP)	Interlaminar Shear Strength (ksi)
IL-1A	5.21
IL-2A	5.27
IL-3A	5.03
IL-4A	5.33
IL-5A	5.75
IL-6A	5.48
IL-7A	5.77
IL-9A	5.80
IL-10A	5.76
IL-11A	5.47
Mean Value	5.487
Std. Dev.	0.27
CV (%)	4.9

* Specimen length 0.4"

7.1.4 Thermophysical Properties

(a) Coefficient of Thermal Expansion

Thermal expansion response of P100/6061 Al specimens between -150°F to +150°F in a heat/cool/heat cycle is shown in Figures 7.1-3 and 7.1-4. Based on these measurements, the composite exhibited:

Average CTE_x (endpoint to endpoint): -0.27 μin/in/°F

Average CTE_y (endpoint to endpoint): 11.37 μin/in/°F

Residual strain: 122 μin/in

Room temperature hysteresis: -41.5 μin/in.

The average CTE_x value of -0.27 ppm/°F should be taken with caution, as it was obtained from the slope of a line joining the extreme points of the first cycle thermal expansion curve. Also, Figure 7.1-3 shows that the specimen exhibited near zero-CTE_x at RT, compared to the predicted value of 0.73 ppm/°F. This anomaly is primarily attributed to the first cycle thermal response, which is significantly influenced by the residual stress level in the composite. As the residual stresses are relieved in the subsequent cycles, the composite would attain the stable CTE consistent with the expected response (Ref 14, 64, 66 and 73).

(b) Specific Heat

Specific heat test data of P100/6061 Al specimens over the temperature range -220 to 750°F is presented in Figure 7.1-5. The measured specific heat value of 0.194 Btu/lb°F was in agreement with the predicted value of 0.20 Btu/lb°F.

(c) Thermal Diffusivity and Through-The-Thickness Thermal Conductivity

Measured thermal diffusivity values at temperatures between -238°F and 752°F are listed in Table 7.1-10. These results indicate a steady drop in diffusivity with increase in temperature.

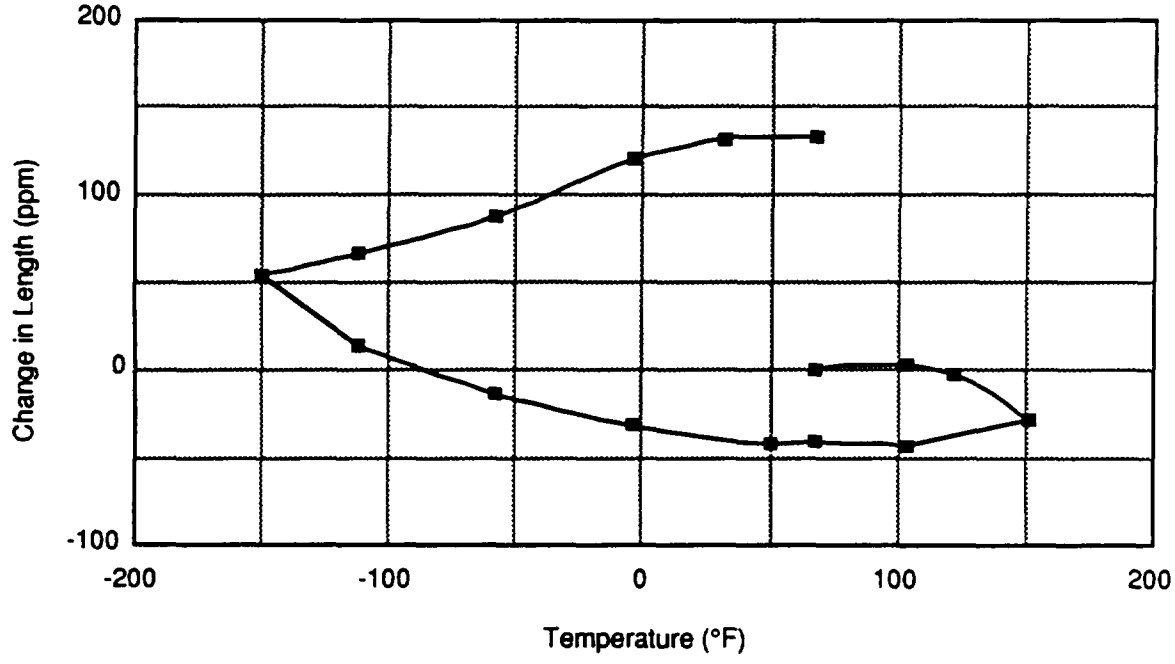

Figure 7.1-3 Thermal Expansion Behavior of Longitudinal P100/Al, [0]2 Specimen in a Heat/Cool/Heat Cycle Using Push Rod Dilatometer

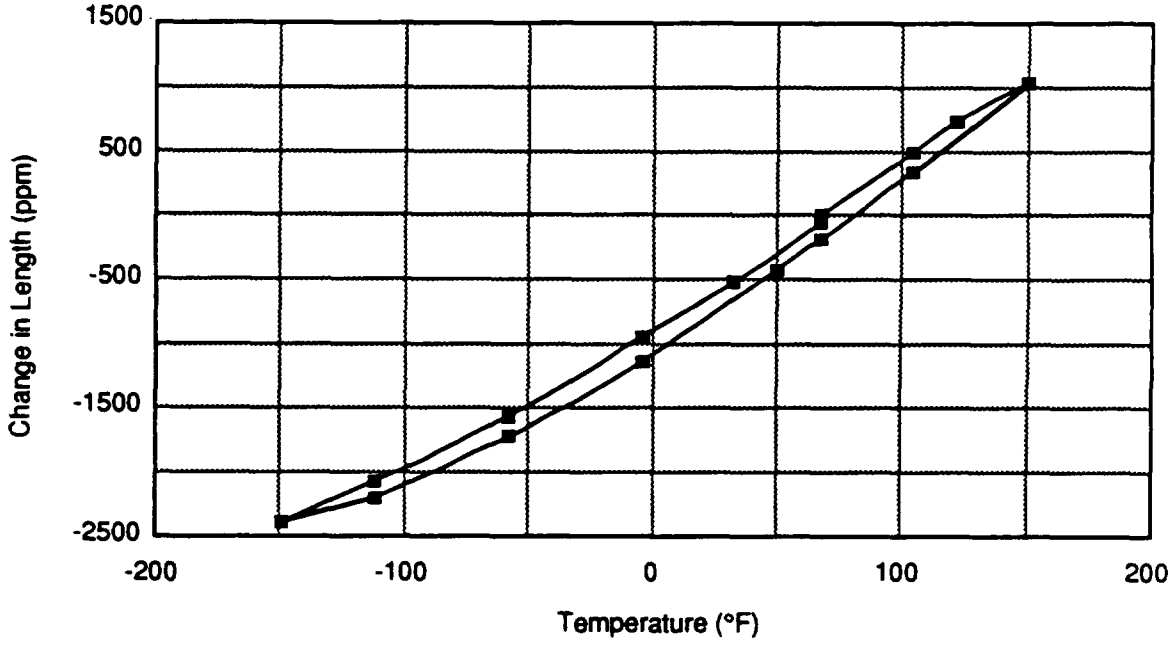

Figure 7.1-4 Thermal Expansion Behavior of Transverse P100/Al, [0]2 Specimen in a Heat/Cool/Heat Cycle Using Push Rod Dilatometer

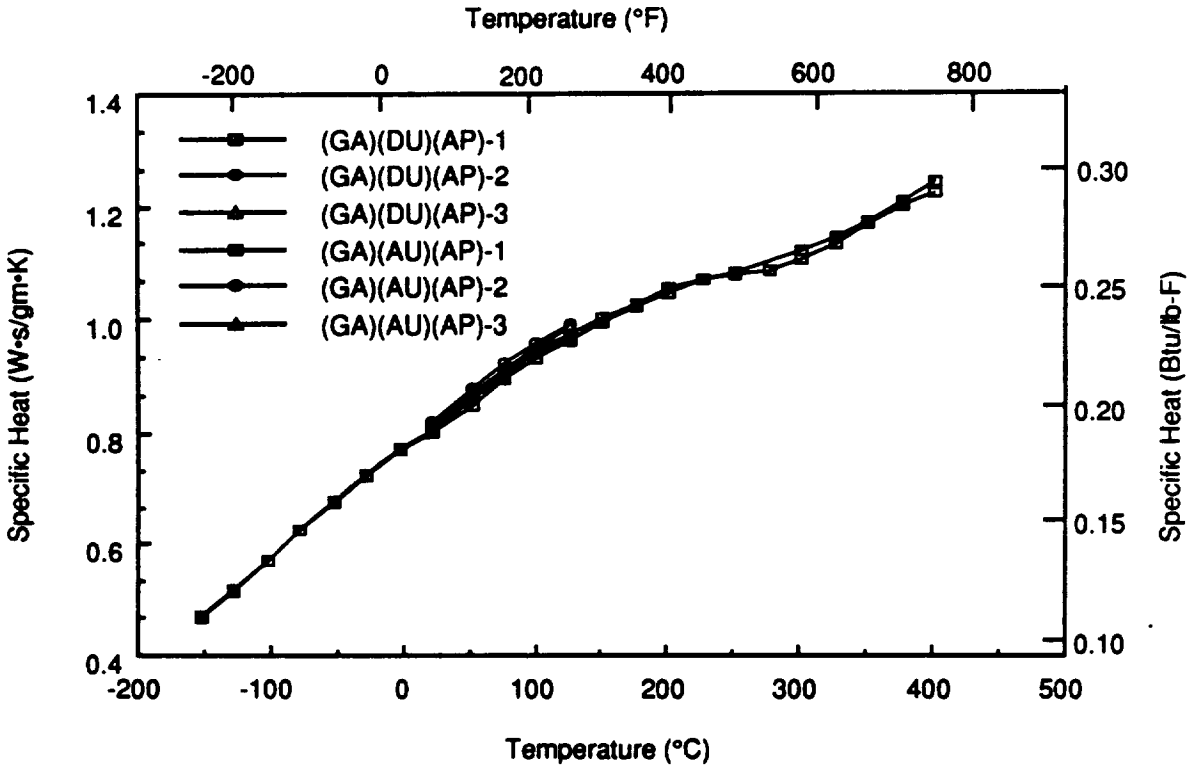

Figure 7.1-5 Specific Heat as a Function of Temperature for P100/6061

Table 7.1-10 Thermal Conductivity Calculations (Through Thickness) of Unidirectional P100/6061 Al

Temp. (°C)	Density ($gm \cdot cm^{-3}$)	Specific Heat ($W \cdot s \cdot gm^{-1} \cdot K^{1}$)	Diffusivity ($cm^{2}\ sec^{-1}$)	Conductivity ($W \cdot cm^{-1}\ K^{1}$)	Conductivity (Btu Units*)	Temp. (°F)
-150	2.415	0.4700	0.28180	0.31986	221.77	-238
-100	2.415	0.5700	0.27350	0.37649	261.04	-148
-50	2.415	0.6740	0.26400	0.42972	297.94	-58
0	2.415	0.7680	0.25450	0.47203	327.28	32
25	2.415	0.8100	0.24900	0.48708	337.72	77
100	2.415	0.9430	0.23550	0.53631	371.85	212
200	2.415	1.0490	0.21650	0.54847	380.28	392
300	2.415	1.1120	0.20500	0.55052	381.70	572
400	2.415	1.2310	0.20600	0.61241	424.61	752

* - ($Btu \cdot in \cdot hr^{-1} \cdot ft^{-2} \cdot °F^{-1}$)

These diffusivity values (along with the known density and specific heat) were used to calculate through thickness conductivity K_z. Based on these measurements the composite exhibited room temperature K_z - 28.14 Btu/(hr·ft·°F).

(d) Thermal Conductivity

Kohlrausch method was used to obtain in-plane thermal conductivity values of DWA and Amercom Gr/Al flat panels. The results of transverse and longitudinal thermal conductivity are given in Table 7.1-11 and plotted in Figure 7.1-6.

A transverse specimen ((GA)(DU) TKT-2A) that was tested between RT and 750°F and then at 207°F, buckled and cracked during heating, therefore, the cool point did not agree with the heating curve. Consequently, another specimen ((GA)(DU)(AP)TKT2-1A) was used to obtain the low temperature data, suggesting that the transverse specimen could not be heated to 750°F with its ends constrained. The conductivity measurements for longitudinal Gr/Al specimen ((GA)(DU)(AP)TKL-1A) were obtained form cryogenic temperatures to 750°F during the heat cycle and rechecked at 206°F during the cool cycle. The specimen did not bend and crack and the datum point obtained during cooling was in good agreement with the heating curve. Measured conductivity values for the Amercom panel were about 10% below those for the DWA panel.

Based on these measurements, the longitudinal thermal conductivity 184.9 Btu/(hr·ft·°F) was in complete agreement with the predicted value of 184.5 Btu/(hr·ft·°F). Also the transverse thermal conductivity (K_y) 44.3 Btu/(hr·ft·°F) was close to the predicted value of 46.5 Btu/(hr·ft·°F). Whereas the through thickness conductivity (K_z) value 28.14 Btu/(hr·ft·°F) was significantly lower than the K_y value indicating the presence of voids (between face sheets and precursor wire) which would reduce the composite conductivity.

Table 7.1-11 Inplane Thermal Conductivity and Electrical Resistivity Values of P100/6061 Al Composites

Kohlrausch Results					
Sample Designation	Temp. (°C)	Conductivity ($W \cdot cm^{-1} \cdot K^{-1}$)	Resistivity (microhms·cm)	Conductivity ($Btu \cdot in \cdot hr^{-1} ft^{-2} \cdot F^{-1}$)	Temp. (°F)
(GA)(DU)TKT-2A	31	0.814	14.84	495	88
-Transverse	51	0.727	15.73	501	123
(DWA)	73	0.728	16.71	505	162
	99	0.739	17.86	512	210
	195	0.769	22.24	533	383
	296	0.760	26.78	527	565
	375	0.704	32.20	488	707
Cool	97	0.677	18.23	469	207
(GA)(DU)TKT-1A	31	0.720	14.88	499	88
-Transverse	48	0.721	15.61	500	118
(DWA)	100	0.733	17.90	508	211
	-166	0.442	6.26	307	-266
	-138	0.505	7.40	350	-216
	-114	0.549	8.46	381	-172
	-70	0.597	10.38	414	-94
	-33	0.648	12.00	449	-28
	-17	0.665	12.74	461	2
(GA)(AU)TKL-1B	31	3.045	7.02	2111	87
-Longitudinal	49	3.060	7.42	2122	120
(Amercom)	72	3.045	7.91	2111	162
	98	3.046	8.46	2112	208
(GA)(DU)TKL-1A	-169	1.496	2.90	1037	-271
-Longitudinal	-138	1.999	3.48	1386	-217
(DWA)	-91	2.592	4.45	1797	-131
	-50	2.918	5.27	2023	-58
	-15	3.155	5.98	2187	5
	30	3.202	6.88	2220	86
	49	3.298	7.26	2287	120
	98	3.283	8.25	2276	209
	193	3.256	10.13	2258	379
	290	3.052	11.92	2116	554
	343	2.959	12.93	2052	649
	399	2.861	14.13	1983	751
Cool	97	3.320	8.08	2302	206

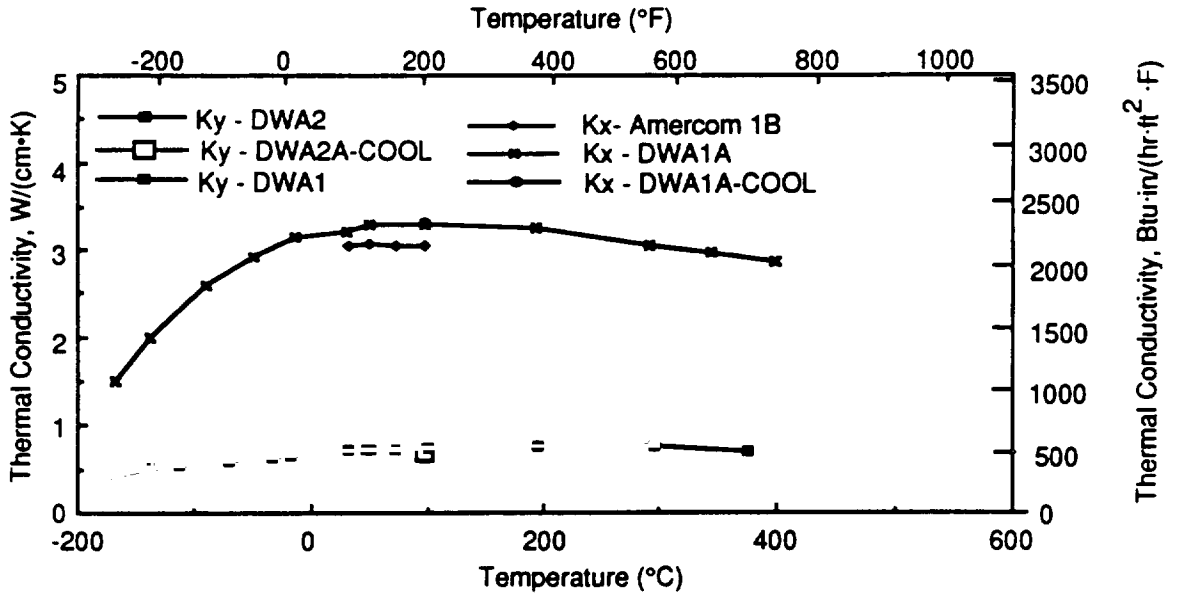

Figure 7.1-6 Inplane Thermal Conductivity Versus Temperature for P100/6061 Al; Longitudinal Thermal Conductivity is Higher Than the Transverse Conductivity. The Amercom Gr/Al Panel Exhibited 10% Lower Longitudinal Thermal Conductivity

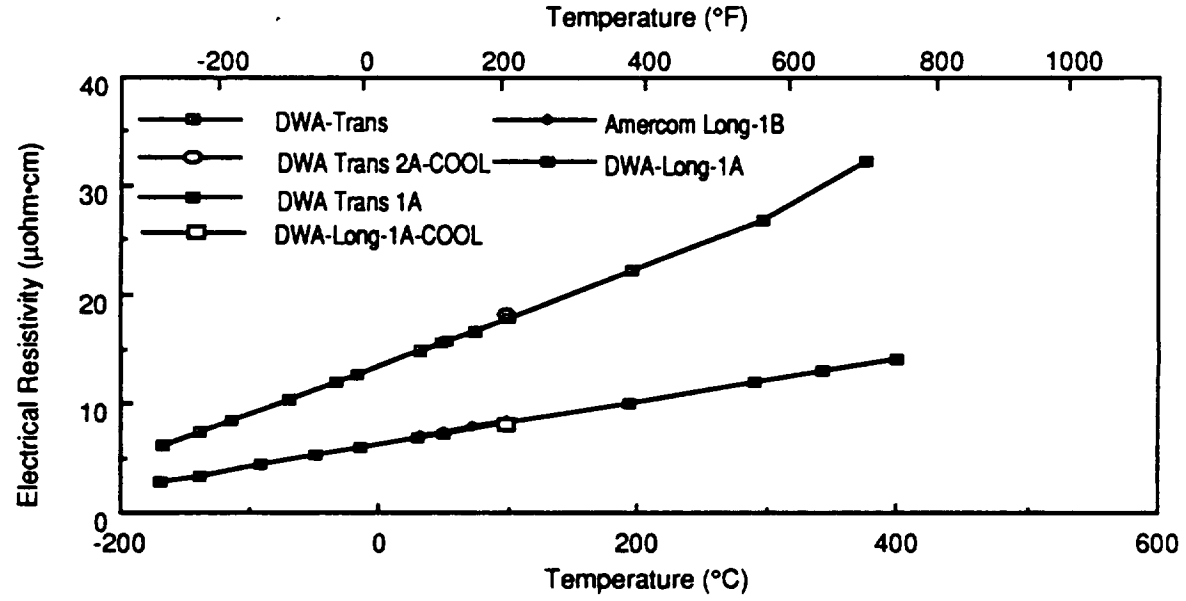

Figure 7.1-7 Electrical Resistivity Versus Temperature for P1000/6061 Al Indicating The Electrical Resistivity in the Transverse Direction is Higher then in the Longitudinal Direction

(e) Electrical Resistivity

Electrical resistivity versus temperature response obtained by Kohlrausch test is presented in Figure 7.1-7. These results showed that the resistivity in both longitudinal and transverse direction increased with the temperature; and the resistivity in the transverse direction was higher than in the longitudinal direction.

(f) Optical Properties

The measured values of normal emissivity and solar absorptance are listed in Table 7.1-12. Also, the results of total hemispherical emissivity at temperatures between 200° and 420°F are listed in Table 7.1-13. These results show that:

$\alpha_s = 0.41$ at RT

$\varepsilon_N \simeq 0.087$ at RT

$\varepsilon_H = 0.121$ at 200°F

For both DWA and Amercom panels, nearly identical reflectance spectra was obtained between 2 and 14 μm wavelength (Figure 7.1-8). Based on this spectra, the DWA panel surface exhibited 88% reflectance at 10.6 μm wavelength.

Figure 7.1-12 Total Normal Emissivity and Solar Absorptance of P100/6061 Al, [0]2, Fiber Volume = 42.2%

Specimen # (GA)(DU)(AP)	Normal Emissivity (NE)	Solar Absorptance (AB)
1A	0.08	0.43
2A	0.09	0.39
3A	0.09	0.42
Mean Value	0.087	0.41
Std. Dev.	0.0058	0.02
CV (%)	6.6	4.87

Figure 7.1-13 Total Hemispherical Emissivity of P100/6061 Al, [0]2, Fiber Volume = 42.2%

Specimen # (GA)(DU)(AP)	Temp. °F	Emissivity (HE)
HE-1A	217	0.121
	344	0.125
	421	0.127
HE-3A	209	0.125
	307	0.128
	398	0.130

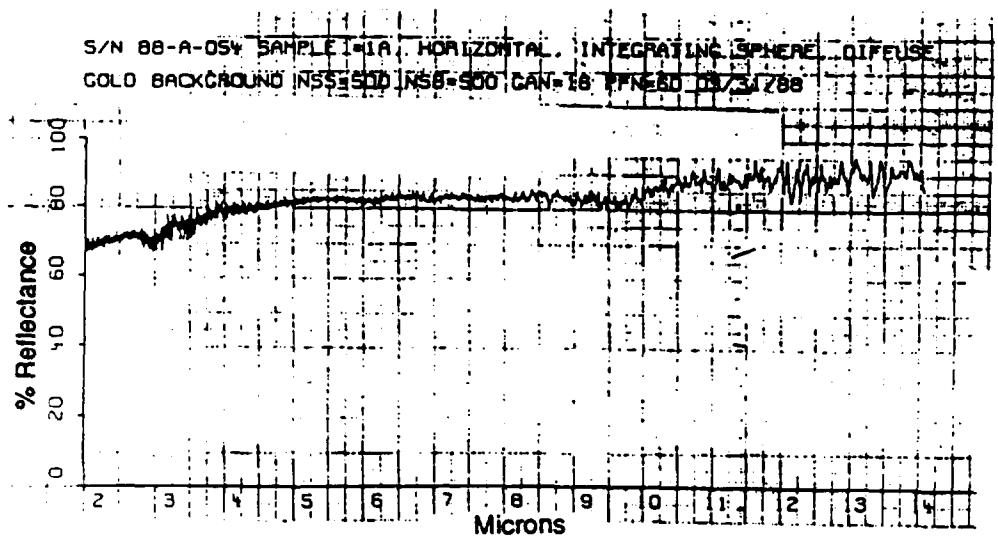

Figure 7.1-8 Reflectance as a Function of Wavelength of P100/6061 Al, v/o = 42.2% (Vendor: DWA, CA)

7.2 P100/6061 TUBES

In this program, P100/6061 Al tubes fabricated by two different processing techniques: (1) Pultrusion and (2) Diffusion bonding were evaluated.

7.2.1 Fabrication Data

•Pultruded Tubes

Type of Tube:	P100/6061 Al/6061Al Clad 2-ply
Fabrication Process:	Pultrusion
Fabricator:	MCI, Columbus, OH
Quantity:	Three
Clad Thickness	0.002-in.

MCI ID#:	Dimensions (in..)			Fiber Volume
	L	D	T	
1220-071087-1	72.3	1.074	.040	47%
1220-071087-2	77.5	1.073	.041	48%
1220-071087-8	74.9"	1.078	.042	48%

L = Length; D = Diameter; T = Wall thickness

DWA ID#	Dimensions (in.)			Ovality(in.)	Bow(in./ft)	Fiber Volume
	L	D	T			
GT-5985-1	65	1.055	.038	0.005-0.008	<0.0025	43%
GT-5986-2	70.5	1.055	.039	0.005	<0.0025	44.1%
FT-5987-3	72.5	1.056	.039	0.003	<0.001	42.5%

• Dimensional Inspection—Typical variation in wall thickness and diameters for both the type of tubes are presented in Table 7.2-1 and 7.2-2.

7.2.2 Product Evaluation

(a) Density

	Pultruded Tube	Diffusion Bonded Tube
Density	0.090 lb/in^3	0.090 lb/in^3
Std. Dev.	0.0015	0.001

(b) Fiber Volume

	Pultruded Tube (MCI)	Diffusion Bonded Tube (BP-DWA)
Mean v/o	44.35	43.63
Std. Dev.	0.52	1.28

(c) Non-Destructive Examination

Visual and X-radiographic techniques were used to assess the quality of diffusion bonded and pultruded tubes. Visual examination revealed good overall quality of both types of tubes with only minor face sheet imperfections. At a few sites, the outer face sheet on the pultruded tubes had thinned down exposing the underlying precursor wires. X-radiographic examination indicated good fiber collimation with only a few voids and disbonds between precursor wires.

(d) Microstructure

Microstructural examination of both diffusion bonded and pultruded tubes revealed that the fiber distribution was normal with only occasional uninfiltrated areas (Figure 7.2-1). Transverse micrographs showed a major groove along the length of the inner facesheet of the pultruded tube. This anomaly corresponded with the X-radiographic observation of a narrow gap between

Table 7.2-1 Wall Thickness Variation in Pultruded and Diffusion Bonded P100/6061 Al Tubes

Fabrication Process	Specimen #	Number of Measurements	Mean Value	Std. Dev.	CV (%)
Diffusion Bonded (GA)(DU)(AT)	1	8	0.0391	0.0020	5.1
	2	8	0.0391	0.0016	4.1
	3	8	0.038	0.0019	5.0
	5	8	0.0391	0.0018	4.6
	6	8	0.0391	0.0019	4.8
	12	8	0.0375	0.0023	6.1
	13	8	0.0390	0.0013	3.3
Pultruded (GA)(MU)(AT)	1	8	0.0426	0.0015	3.52
	2	8	0.0423	0.0007	1.65
	3	8	0.0424	0.001	2.36
	5	8	0.0425	0.0016	3.76
	6	8	0.0421	0.0015	3.56
	12	8	0.0423	0.0008	1.89
	13	8	0.0427	0.002	4.68

Table 7.2-2 Diameter Variations at Each End of Pultruded and Diffusion Bonded P100/6061 Al Tubes

Specimen #	Diameter (in.) at each end							
	Diffusion Bonded (GA)(DU)(AT)-2				Pultruded (GA)(MU)(AT)-8			
	Min.	Max.	Min.	Max.	Min.	Max.	Min.	Max.
TO-1	1.052	1.057	1.057	1.062	1.077	1.078	1.077	1.080
TO-2	1.053	1.055	1.052	1.061	1.076	1.079	1.077	1.080
TO-3	1.053	1.056	1.053	1.057	1.077	1.079	1.075	1.079
CM-4	1.050	1.054	1.053	1.055	1.077	1.079	1.074	1.079
CM-5	1.052	1.055	1.051	1.055	1.075	1.079	1.074	1.079
CM-6	1.053	1.056	1.052	1.055	1.076	1.080	1.076	1.079
TE-7	1.052	1.056	1.054	1.056	1.077	1.080	1.076	1.078
TN-11	1.053	1.054	1.053	1.056	1.076	1.079	1.076	1.080
TN-12	1.055	1.057	1.052	1.055	1.076	1.079	1.078	1.080
TN-13	1.052	1.055	1.054	1.057	1.075	1.079	1.078	1.080

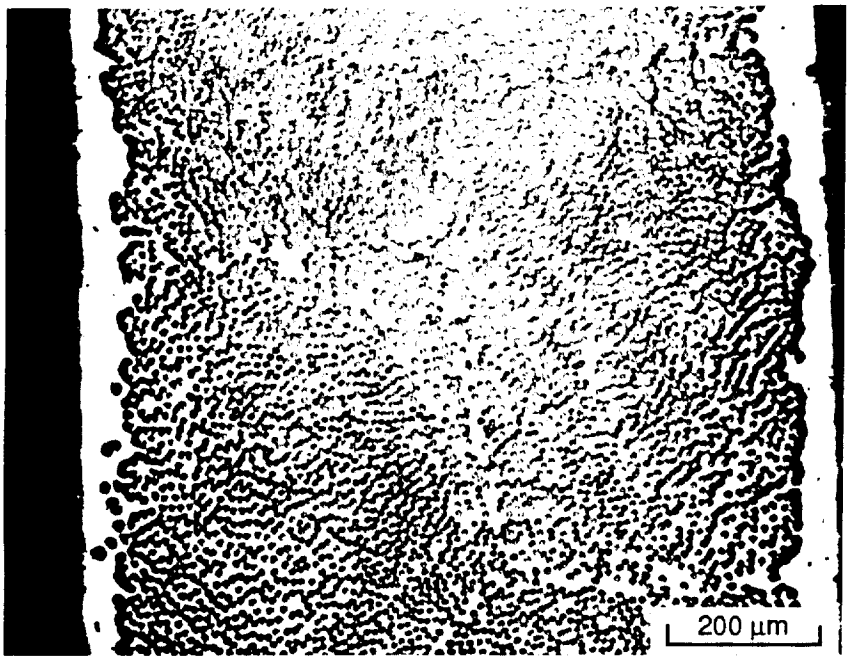

Figure 7.2-1 Transverse Photomicrograph of a Diffusion Bonded P100/6061 Al Tube Showing Good Matrix Infiltration and Fiber Distribution Along the Length of the Tube. A Few Voids Were Observed Between the Precursor Wires with Occasional Uninfiltrated Areas. (100X)

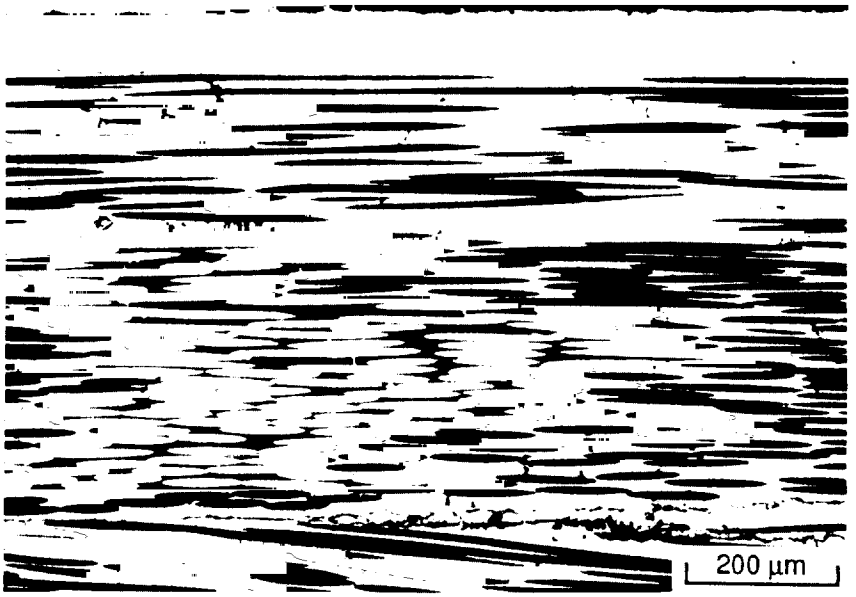

Figure 7.2-2 Longitudinal Photomicrograph of a Diffusion Bonded P100/6061 Al Tube Showing Transverse Microcracks in the Interfiber Matrix Region Observed in Both Diffusion Bonded and Pultruded Tubes (100X)

two adjacent precursor wires. Similar to the Gr/Al flat panel, transverse microcracks in the interfiber matrix region were also observed in both types of Gr/Al tubes, as shown in Figure 7.2-2.

7.2.3 Mechanical Properties

(a) Tension

Tensile test data of both the diffusion bonded and pultruded P100/6061 Al tubes are presented in Table 7.2-3. These results showed that for both the tubes, measured tensile modulus was in excellent agreement with the predicted values. During these tests, the linear elastic stress-strain response was observed up to about 90% of the failure strain.

(b) Compression

Compressive property data of both the diffusion bonded and pultruded tube specimens are listed in Table 7.2-4. These measurements indicated that measured compressive modulus values were 98% of the average tensile modulus.

(c) Hoop Tensile Properties

For both the pultruded and diffusion bonded tubes, the hoop modulus and strength values are listed in Table 7.2-5. Based on these measurements, the pultruded tube specimens exhibited lower hoop properties than the diffusion bonded tube specimens.

Table 7.2-3 Longitudinal Tensile Properties of P100/6061 Al Tubes

		TENSION					
	Specimen #	Elastic Modulus (Msi)				UTS (ksi)	ν_{xy}
		E_{x1}	E_{x2}	E_{x3}	E_x		
Pultruded	TNL-11PT	51.78			51.78	78.33	0.2743
v/o = 44.35%	TNL-12PT	52.56	52.08	51.72	52.12	77.39	-
(GA)(MU)(AT)	TNL-3PT	55.40	53.29	49.75	52.81	74.57	0.3370
	TNL-2PT	44.48	58.76	49.38	50.87*	65.48*	0.3347*
	TNL-1PT	54.37	53.47	53.61	53.83	89.79	0.3352
	TNL-13PT	56.95	53.49	54.65	55.03	82.06	0.2736
(ROM)					(52.14)		
Mean Value					53.11	80.43	0.305
Std. Dev.					1.32	5.86	0.035
CV (%)					2.48	7.28	11.4
Diffusion	TNL-11DB				48.27	70.75*	0.2974
Bonded	TNL-12DB	50.62	53.56	51.88	52.02	121.56	
v/o = 43.63%	TNL-DB2	51.18	55.06	52.57	52.94	126.35	0.2537
(GA)(DU)(AT)	TNL-DB3	53.10	49.39	51.29	51.26	112.55	0.2619
	TNL-13DB	52.71	47.37	50.01	50.03	115.68	0.2905
(ROM)					(51.45)		
Mean Value					51.56	119.03	0.2687
Std. Dev.					1.23	6.14	0.019
CV (%)					2.4	5.15	7.0

* Discarded due to surface defect

Table 7.2-4 Longitudinal Compressive Properties of P100/6061 Al Tubes

COMPRESSION							
	Specimen #	Elastic Modulus (Msi)				UCS (ksi)	ν_{xy}
		E_{x1}	E_{x2}	E_{x3}	E_x		
Pultruded	CML-4PT	49.51			49.51	41.50	0.2127
v/o = 44.35%	CML-5PT	49.36	53.42	54.31	52.36	43.16	
(GA)(MU)(AT)	CML-6PT	58.9	53.66	52.97	55.18	41.51	0.3617
(ROM)					(52.14)		
Mean Value					52.35	42.06	0.287
Std. Dev.					2.83	0.96	0.106
CV (%)					5.4	2.2	36.9
Diff. Bonded	CML-4DB	49.3			49.3	43.75	0.2702
v/o = 43.63%	CML-5DB	53.82	51.95	46.87	50.88	37.82	
(GA)(DU)(AT)	CML-6DB	52.57	51.87	46.37	50.27	38.63	0.3216
(ROM)					(51.45)		
Mean Value					50.15	40.06	0.2959
Std. Dev.					0.80	3.2	0.036
CV (%)					1.6	7.98	12.1

Table 7.2-5 NOL Burst Ring Data for P100/6061 Al Tubes

Material	Area (in^2)	Ultimate (psi) Pressure	Hoop Stress F_{TH} = P r/t (ksi)	Modulus E_H (Msi)	Strain to Failure
P100 Gr/Al Pultruded	0.1483 (0.50%)	102.7 (14.2%)	1.1 (14.2%)	3.53 (23.1%)	0.00035 (21.6%)
P100 Gr/Al Diffusion Bond	0.1357 (1.5%)	167.7 (23 %)	1.9 (24.6%)	5.93 (12.7%)	0.0005 (29.5%)

† Precentage coefficientof variation

Table 7.2-6 CTE of Pultruded and Diffusion Bonded P100/6061 Al Tubes

Thermal Expansion Response	Pultruded v/o = 44.4	Diffusion Bonded v/o = 43.6
CTE_X (ppm/°F)	+0.34	+0.27
Residual Strain (ppm)	-61.5	-65.6
Strain Hysteresis (ppm)	-98.0	-131.6

7.2.4 Thermophysical Properties

a) Coefficient of Thermal Expansion

Typical thermal expansion response of the pultruded and diffusion bonded P100/6061 Al tubes is shown in Figures 7.2-3 and 7.2-4 respectively. These results, including CTE, residual strain, and RT hysteresis are summarized in Table 7.2-6. Both the pultruded and diffusion bonded tubes exhibited almost identical response with the measured CTE values 0.34 ppm/°F and 0.27 ppm/°F respectively, which were in agreement with the predicted value of 0.3 ppm/°F at RT.

7.3 SUMMARY OF P100/6061 Al TEST DATA

Mechanical and thermophysical property test data of P100/6061 Al flat panels and tubes are summarized in Table 7.3-1 to 7.3-4.

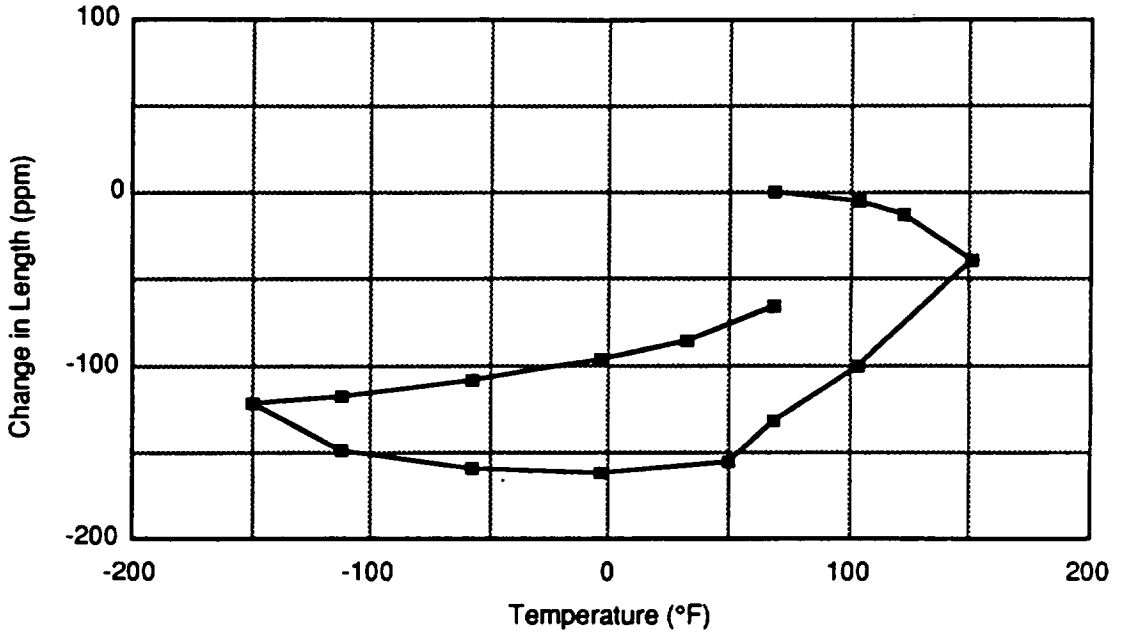

Figure 7.2-3 Thermal Expansion Behavior of Longitudinal DWA P100/Al, [0]2 Tube Specimen in a Heat/Cool/Heat Cycle Using Push Rod Dilatometer

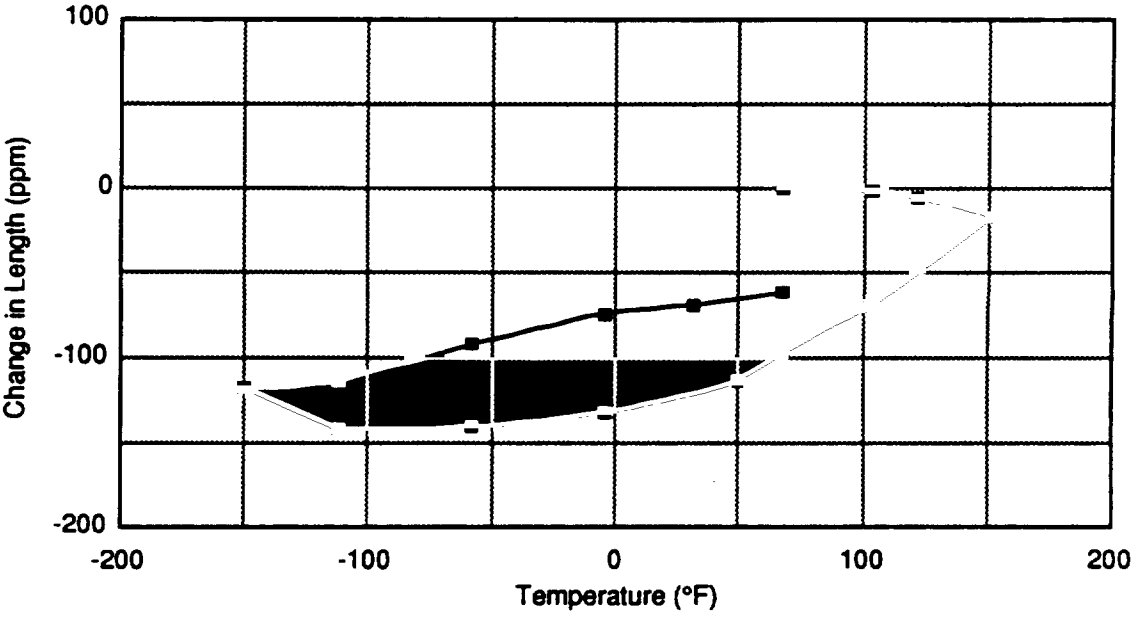

Figure 7.2-4 Thermal Expansion Behavior of Longitudinal MCI P100/Al, [0]2 Tube Specimen in a Heat/Cool/Heat Cycle Using Push Rod Dilatometer

Table 7.3-1 P100/6061 Al Graphite/Aluminum (Unidirectional)

NOT DESIGN ALLOWABLE DATA

PROPERTIES					TEMPERATURE (°F)			Std. Dev. / No. of Specimens at RT	Test Method
PHYSICAL			MECHANICAL & THERMAL			Low	Room	High		
Density (lb / in^3)		0.090	Longitudinal Tensile Strength	σ_x^{TU}	ksi		131.3		± 4.14 / 5	ASTM D-3552
Fiber volume fraction		0.422	Transverse Tensile Strength	σ_y^{TU}	ksi		3.62		±0.366 / 5	ASTM D-3552
Void volume fraction		<0.001	Longitudinal Comp. Strength	σ_x^{CU}	ksi		46.62		±0.806 / 5	ASTM D-3410
Nominal ply thickness	in	0.0216	Transverse comp. strength	σ_y^{CU}	ksi		15.21			ASTM D-3410
Max. cont. use temp.	°F	~550	In-plane shear strength	IPSS	ksi		5.3477		±0.2443 / 5	10° Off-Axis
Ply Orientation	θ	$[0]_2$	Interlaminar shear strength	ILSS	ksi		5.487		±0.27 / 10	ASTM D2344
Foil Material		6061-F	Longitudinal tensile strain **	ε_x^T	%		0.265		±0.0076 / 5	ASTM D-3552
Foil Thickness	in	0.001	Transverse tensile strain **	ε_y^T	%		0.0707		±0.0049 / 5	ASTM D-3552
OPTICAL & ELECTRICAL (at room temperature)			Longitudinal comp. strain **	ε_x^C	%		0.1204		±0.014 / 5	ASTM D-3410
Solar Absorptance	α	0.41 ±0.002	Transverse comp. strain **	ε_y^C	%		0.11		±0.010 / 5	ASTM D-3410
Normal Emissivity	ε	0.087 ±0.006	Longitudinal tensile modulus	E_x	Msi		49.71		±0.701 / 5	ASTM D-3552
Electrical Resistivity	R	6.88 (x) 14.88 (y) μΩ·cm	Transverse tensile modulus	E_y	Msi		5.14		±0.523 / 5	ASTM D-3552
			Longitudinal comp. modulus	E_x	Msi		48.15		±2.41 / 5	ASTM D-3410
			Transverse comp. modulus	E_y	Msi		4.82			ASTM D-3410
			In-plane shear modulus	G	Msi		2.62		±0.306 / 4	
			Longitudinal flexural modulus	F_x	Msi		26.25		±0.755 / 3	ASTM D-790M
			Transverse flexural modulus	F_y	Msi		4.16		±0.30 / 3	ASTM D-790M
			Long. tensile Poisson's ratio	ν_{xy}			0.2949		±0.0178 / 5	ASTM D-3552
			Trans. tensile Poisson's ratio	ν_{yx}			0.0211		±0.00101 / 5	ASTM D-3552
			Long. thermal conductivity	K_x	(1)	7.896	15.278	15.403		Kohlrausch
			Trans. thermal conductivity	K_y	(1)	2.222	3.333	3.611		Kohlrausch
			Thru thickness thermal cond.	K_z	(1)					
			Specific heat	C_p	(2)		0.194			ASTM E-1269
			Longitudinal CTE	α_x	(3)		-0.27			ASTM E-80
			Transverse CTE	α_y	(3)	11.15	11.37	12.4		ASTM E-80
			Thru thickness CTE	α_z	(3)		14.6*			

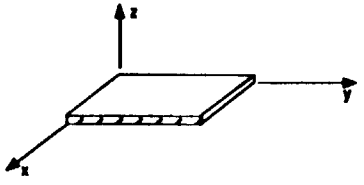

Notes:
(**) - Strain to failure; (1) Btu/(hr·in·°F); (2) Btu/(lb·°F); (3) μin./in./°F

Table 7.3-2 P100/6061 Al Graphite/Aluminum (Unidirectional)

NOT DESIGN ALLOWABLE DATA

PROPERTIES							TEMPERATURE (°F)			Std. Dev. / No. of Specimens at RT	Test Method
PHYSICAL			MECHANICAL & THERMAL				Low	Room	High		
Density (lb / in^3)		0.090	Longitudinal Tensile Strength	σ_x^{TU}	ksi			125.6		± 8.21 / 5	ASTM D-3552
Fiber volume fraction		0.465	Transverse Tensile Strength	σ_y^{TU}	ksi			3.3		±0.299 / 4	ASTM D-3552
Void volume fraction		<0.001	Longitudinal Comp. Strength	σ_x^{CU}	ksi			40.9		±4.24 / 5	ASTM D-3410
Nominal ply thickness	in	0.024	Transverse comp. strength	σ_y^{CU}	ksi			13.3			ASTM D-3410
Max. cont. use temp.	°F	~550	In-plane shear strength	IPSS	ksi			5.3		±0.24 / 4	10° Off-Axis
Ply Orientation	θ	$[0]_2$	Interlaminar shear strength	ILSS	ksi						ASTM D2344
Foil Material		6061-F	Longitudinal tensile strain **	ε_x^T	%			0.24		±0.021 / 5	ASTM D-3552
Foil Thickness	in	0.001	Transverse tensile strain **	ε_y^T	%			0.0535		±0.0089 / 4	ASTM D-3552
OPTICAL & ELECTRICAL (at room temperature)			Longitudinal comp. strain **	ε_x^C	%			0.11		±0.027 / 5	ASTM D-3410
			Transverse comp. strain **	ε_y^C	%						ASTM D-3410
Solar Absorptance	α		Longitudinal tensile modulus	E_x	Msi			52.9		±1.43 / 5	ASTM D-3552
Normal Emissivity	ε		Transverse tensile modulus	E_y	Msi			6.1		±0.172 / 5	ASTM D-3552
Electrical Resistivity	R	μΩ·cm	Longitudinal comp. modulus	E_x	Msi			47.3		±1.63 / 5	ASTM D-3410
			Transverse comp. modulus	E_y	Msi			4.2			ASTM D-3410
			In-plane shear modulus	G	Msi			2.6		±0.306 / 4	
			Longitudinal flexural modulus	F_x	Msi			27.3		±0.753 / 3	ASTM D-790M
			Transverse flexural modulus	F_y	Msi			4.2		±0.34 / 3	ASTM D-790M
			Long. tensile Poisson's ratio	ν_{xy}				0.326		±0.0289 / 5	ASTM D-3552
			Trans. tensile Poisson's ratio	ν_{yx}				0.022		±0.0066 / 4	ASTM D-3552
			Long. thermal conductivity	K_x	(1)			14.660			Kohlrausch
			Trans. thermal conductivity	K_y	(1)						Kohlrausch
			Thru thickness thermal cond.	K_z	(1)						
			Specific heat	C_p	(2)			0.193			ASTM E-1269
			Longitudinal CTE	α_x	(3)			0.193			ASTM E-80
			Transverse CTE	α_y	(3)						ASTM E-80
			Thru thickness CTE	α_z	(3)						

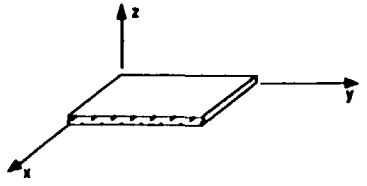

Notes:
(**) - Strain to failure; (1) Btu/(hr·in·°F); (2) Btu/(lb·°F); (3) μin./in./°F

Table 7.3-3 P100/6061 Al Graphite/Aluminum (Unidirectional) Pultruded Tubes

NOT DESIGN ALLOWABLE DATA

PROPERTIES						TEMPERATURE (°F)			Std. Dev. / No. of Specimens at RT	Test Method
PHYSICAL			MECHANICAL & THERMAL			Low	Room	High		
Density (lb / in^3)		0.090	Longitudinal Tensile Strength	σ_x^{TU}	ksi		80.43		± 5.86 / 3	ASTM D-3552
Fiber volume fraction		0.44435	Transverse Tensile Strength	σ_y^{TU}	ksi		1.1			NOL
Void volume fraction		<0.001	Longitudinal Comp. Strength	σ_x^{CU}	ksi		42.06		±0.96 / 3	ASTM D-3410
Nominal ply thickness	In	0.024	Transverse comp. strength	σ_y^{CU}	ksi					
Max. cont. use temp.	°F	~550	In-plane shear strength	IPSS	ksi					
Ply Orientation	θ	$[0]_2$	Interlaminar shear strength	ILSS	ksi					
Foil Material		6061-F	Longitudinal tensile strain **	ε_x^T	%					ASTM D-3552
Foil Thickness	In	0.001	Transverse tensile strain **	ε_y^T	%					NOL
OPTICAL & ELECTRICAL (at room temperature)			Longitudinal comp. strain **	ε_x^C	%					ASTM D-3410
			Transverse comp. strain **	ε_y^C	%					
			Longitudinal tensile modulus	E_x	Msi		53.11		±1.32 / 3	ASTM D-3552
			Transverse tensile modulus	E_y	Msi		3.53			NOL
			Longitudinal comp. modulus	E_x	Msi		52.35		±.2.83 / 3	ASTM D-3410
			Transverse comp. modulus	E_y	Msi					
			In-plane shear modulus	G	Msi					
			Longitudinal flexural modulus	F_x	Msi		27.3			
			Transverse flexural modulus	F_y	Msi		4.2			
			Long. tensile Poisson's ratio	ν_{xy}			0.305		±0.035 / 3	ASTM D-3552
			Trans. tensile Poisson's ratio	ν_{yx}						NOL
			Long. thermal conductivity	K_x	(1)		14.660			
			Trans. thermal conductivity	K_y	(1)					
			Thru thickness thermal cond.	K_z	(1)					
			Specific heat	C_p	(2)					
			Longitudinal CTE	α_x	(3)		0.34			ASTM E-228
			Transverse CTE	α_y	(3)					
			Thru thickness CTE	α_z	(3)					
Solar Absorptance	α									
Normal Emissivity	ε									
Electrical Resistivity	R	μΩ·cm								

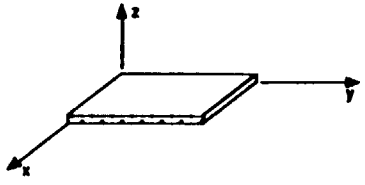

Notes:
(**) - Strain to failure; (1) Btu/(hr·in·°F); (2) Btu/(lb·°F); (3) μin./in./°F

Table 7.3-4 P100/6061 Al Graphite/Aluminum (Unidirectional) Diffusion Bonded Tubes

NOT DESIGN ALLOWABLE DATA

PROPERTIES						TEMPERATURE (°F)			Std. Dev. / No. of Specimens at RT	Test Method
PHYSICAL			MECHANICAL & THERMAL			Low	Room	High		
Density (lb / in^3)		0.090	Longitudinal Tensile Strength	σ_x^{TU}	ksi		119.03		± 6.14 / 3	ASTM D-3552
Fiber volume fraction		0.4363	Transverse Tensile Strength	σ_y^{TU}	ksi		1.9			NOL
Void volume fraction		<0.001	Longitudinal Comp. Strength	σ_x^{CU}	ksi		40.06		±3.2 / 3	ASTM D-3410
Nominal ply thickness	In	0.024	Transverse comp. strength	σ_y^{CU}	ksi					
Max. cont. use temp.	°F	~550	In-plane shear strength	IPSS	ksi					
Ply Orientation	θ	$[0]_2$	Interlaminar shear strength	ILSS	ksi					
Foil Material		6061-F	Longitudinal tensile strain **	ε_x^T	%					ASTM D-3552
Foil Thickness	In	0.001	Transverse tensile strain **	ε_y^T	%					NOL
OPTICAL & ELECTRICAL (at room temperature)			Longitudinal comp. strain **	ε_x^C	%					ASTM D-3410
			Transverse comp. strain **	ε_y^C	%					
Solar Absorptance	α		Longitudinal tensile modulus	E_x	Msi		51.56		±1.23 / 3	ASTM D-3552
Normal Emissivity	ε		Transverse tensile modulus	E_y	Msi		5.93			NOL
Electrical Resistivity	R	μΩ·cm	Longitudinal comp. modulus	E_x	Msi		50.15		±.0.80 / 3	ASTM D-3410
			Transverse comp. modulus	E_y	Msi					
			In-plane shear modulus	G	Msi					
			Longitudinal flexural modulus	F_x	Msi					
			Transverse flexural modulus	F_y	Msi					
			Long. tensile Poisson's ratio	ν_{xy}			0.2287		±0.019 / 3	ASTM D-3552
			Trans. tensile Poisson's ratio	ν_{yx}						NOL
			Long. thermal conductivity	K_x	(1)					
			Trans. thermal conductivity	K_y	(1)					
			Thru thickness thermal cond.	K_z	(1)					
			Specific heat	C_p	(2)					
			Longitudinal CTE	α_x	(3)		0.27			ASTM E-228
			Transverse CTE	α_y	(3)					
			Thru thickness CTE	α_z	(3)					

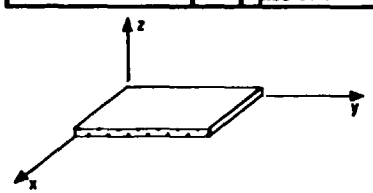

Notes:
(**) - Strain to failure; (1) Btu/(hr·in·°F); (2) Btu/(lb·°F); (3) μin./in./°F

Graphite/Magnesium
P100/AZ91C

Graphite/Magnesium
P100/AZ91C

8.0 GRAPHITE/MAGNESIUM: P100/Mg

Of the continuous fiber reinforced metal matrix composites, Gr/Mg offers the highest specific stiffness with near zero-CTE. Because of these characteristics, Gr/Mg are the key candidate material for the dimensionally stable truss structures. The Gr/Mg tubes can be fabricated by three different processing techniques: (1) diffusion bonding; (2) pultrusion; and (3) casting. In this program the P100/AZ91C Mg tubes produced by a near net shape casting process "filament winding-vacuum casting" (Ref 42, 43) were tested to generate mechanical and thermophysical properties. These tubes were produced under a SDIO/DARPA/NAVSEA sponsored program entitled "Reproducibility of Filament Wound Vacuum Cast Gr/Mg Tubes" (Ref 43). The fabrication data and the results of product evaluation and material tests are discussed in this chapter.

8.1 P100 Gr/AZ91C Mg TUBES

8.1.1 Fabrication Data

Material System:	P100/AZ91C Mg
Fiber Orientation:	$[\pm 16]_s$
Fabrication Process:	Filament winding - Vacuum Casting (FW-VC)
Fabricator:	Martin Marietta Astronautics Group, CO and FMI/STD (formerly MCI) Columbus, OH
Dimensions:	2-in. diameter x 0.048-in. thickness x 48-in. long
Ply thickness:	0.0125-in.
Martin Marietta Part ID:	6, 8+ and 25
Martin Marietta ID:	(GM)(SZ)(AT)

• Dimensional Inspection —Overall average dimensions of P100/AZ91C Mg $[\pm 16]_s$ tubes were:

		Average	Std. Dev.
Outside Diameter (in.)		2.114	0.0056
Inside Diameter (in.)		2.0163	0.0031
Wall Thickness (in.)		0.0489	0.00236
Straightness (in. x 0.001/ft)		4.57	3.76
Eccentricity (in.)	Positive	0.0106	0.0129
	Negative	0.0048	0.0065

8.1.2 Product Evaluation

(a) Density

	Tube #6	Tube #25	Tube 8+
Average Density (lb/in^3)	0.0683	0.0685	0.069
Std. Dev.	0.0005	0.003	0.0

(b) Fiber Volume

Each tube exhibited different fiber volume percentages, which were:

	Tube #6	Tube #25	Tube 8+
Fiber Volume (v/o)	30.1	27.9	23.7
Std. Dev.	1.66	1.21	1.31

(c) Non-Destructive Evaluation

On visual examination, each tube exhibited generally smooth surface showing the dark highlights of the $[\pm 16]_s$ fiber layup. Also, both the outer and inner surfaces revealed a few

localized regions (≤0.12-in. diameter) where magnesium sheet had dislodged during the machining of cast tubes. X-radiographic inspection revealed an overall excellent fiber collimation with no broken fibers and microcracks. At a few of the fiber crossover sites, x0radiographs revealed a darker region compared to the adjacent region indicating lack of Mg matrix at these sites. their size).

(d) Microstructure

Microstructural examination of longitudinal and transverse sections of the cast tubes revealed good infiltration of Mg matrix into the graphite fiber bundles. A typical microstructure shown in Figure 8-1 indicates a nearly uniform fiber distribution and presence of only a few microvoids adjacent to the fibers.

8.1.3 Mechanical Properties

Because each 48-in. long tube exhibited significantly different fiber volumes (30.1, 27.9, and 23.7 v/o), each tube was characterized separately. From these tubes, test specimens were prepared for mechanical property, thermophysical property, and thermal cycling tests. To generate tensile and compressive property data, three types of specimen were prepared. These specimens were:

(1) Tube specimens for tension tests;

(2) 0.5 in. wide strip specimen from tube for tension test; and

(3) Tube specimen for compression tests.

Although tensile strips could not exactly duplicate the tube response, they provided more specimens to generate tensile data. For these strips, 0.5-in. width was chosen to obtain a reasonable cross-section area for stress measurements and to minimize edge and circumferential bending effects. These tension and compression test results are given below.

(a) Tension

• ***P100/AZ91C Mg [±16]$_s$ v/o = 30.1***—Longitudinal tensile test data of tube and strip specimen are presented in Table 8-1. During these tests, each specimen exhibited linear elastic stress strain response until about 50% of the failure stress. In the case of tube specimen, the average modulus was determined from the stress-strain responses of three strain gages that were bonded to the specimen at 120° apart. Measured modulus of 22.2 Msi (Std. Dev. 4.3) was about 80% of the predicted value of 27.8 Msi. In contrast, the strip specimens exhibited a higher modulus (25.44 Msi) providing a measure of the improved casting quality within a region of the tube.,

• ***P100/AZ91C Mg [±16]$_s$ v/o = 27.9***—Longitudinal tensile properties of 27.9 v/o tube and strip specimens are listed in Table 8-2. The measured modulus of 24.3 Msi (tube specimen) was close to the predicted value of 26.5 Msi. But both the tube and strip specimens exhibited significantly lower strength (<20 ksi) values than the expected 60.5 ksi values. These low strength values were primarily due to the presence of localized chipped regions on the specimen surface.

• ***P100/AZ91C Mg [±16]$_s$ v/o = 23.7***—Axial tensile test data of 23.7 v/o tube and strip specimens are listed in Table 8-3. Measured elastic modulus value of 23.4 Msi (from specimen) agreed with the predicted value of 23.4 Msi. Compared to tube specimen, the strip specimen exhibited significantly lower modulus suggesting the presence of interfacial debonds or microvoids which may reduce the load transfer characteristics of the composite. Still the measured strength values of 49.4 Msi was about 91% of the predicted value.

(b) Compression

Compression test data of tube specimens were also obtained from the stress-strain responses of three strain gages that were bonded to the surface at 120° apart. These compressive properties of

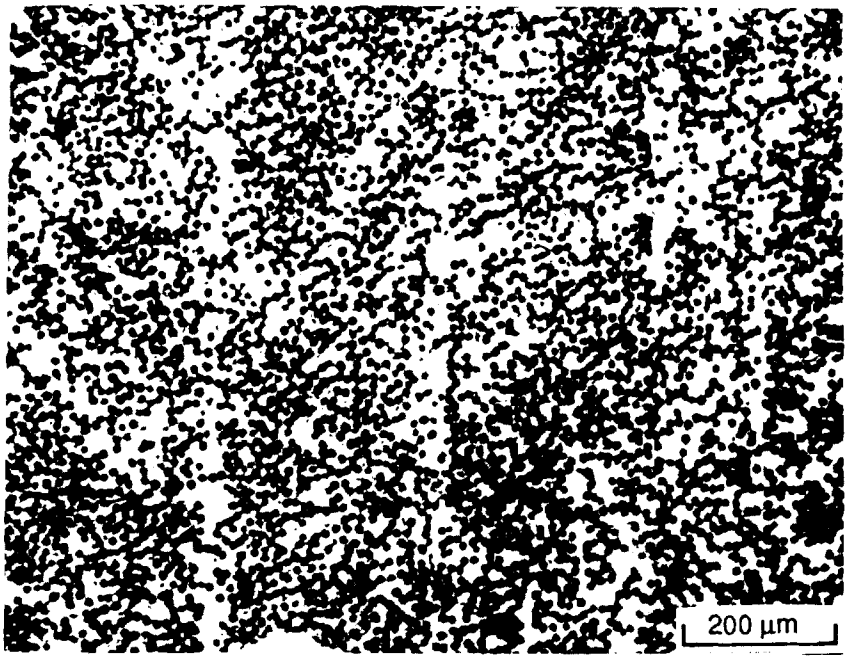

Figure 8-1 Photomicrograph of Filament Wound-Vacuum Cast Gr/Mg Tube Showing Good Matrix Infiltration

Table 8-1 Longitudinal Tensile Properties of P100/AZ91C Mg, [±16°]s, Fiber Volume = 30.1%

Tube # 6 (v/o = 30.1)	Longitudinal Elastic Modulus, E_{TL} (Msi)		Longitudinal Tensile Strength, F_{TL} (ksi)		Strain to Failure (in./in.)	Poisson Ratio
	M	P	M	P		
Strips						
6-1	29.8		66.5		0.00250	0.6644
6-2	25.1		66.4		0.00294	0.2116
6-3	21.7		56.1		0.00293	0.2366
6-4	26.7		—		0.00125	0.7329
65	—		55.8		0.00105	0.4462
Ave.	25.44	27.8	61.2	63.0	0.002134	0.4588
SDev.	3.04		6.06		0.00092	0.2392
%CV	11.96		9.9		43.0	52.1
Tube 6-1	22.2	27.8	57.0	63.0	0.00278	—

Table 8-2 Longitudinal Tensile Properties of P100/AZ91C Mg, [±16°]s, Fiber Volume = 27.9%

Tube # 25 (v/o = 27.9)	Longitudinal Elastic Modulus, E_{TL} (Msi)		Longitudinal Tensile Strength, F_{TL} (ksi)		Strain to Failure (in./in.)	Poisson Ratio
	M	P	M	P		
Strips						
25-1	14.5		10.4		0.00138	0.5626
25-2	17.9		12.3		0.00173	0.6075
25-3	19.7		17.0		0.00215	0.8206
25-4	18.7		19.3		0.00254	0.5301
25-5	17.6		14.8		0.00180	0.7248
Ave.	17.7	26.5	14.8	60.5	0.00192	0.6491
SDev.	1.95		3.56		0.00044	0.121
%CV	11.0		24.1		23.0	18.6
Tube 25-1	24.3	26.5	27.0	60.5	0.001157	0.5514

Table 8-3 Longitudinal Tensile Properties of P100/AZ91C Mg, [±16°]s, Fiber Volume = 23.7%

Tube # 8+ (v/o = 23.7)	Longitudinal Elastic Modulus, E_{TL} (Msi)		Longitudinal Tensile Strength, F_{TL} (ksi)		Strain to Failure (in./in.)	Poisson Ratio
	M	P	M	P		
Strips					—	
8+-1	17.8		47.4		—	—
8+-2	18.6		45.5		—	0.5333
8+-3	16.6		45.9		—	—
8+-4	17.6		49.9		—	0.6545
8+-5	16.8		57.8		—	0.7603
Ave.	17.5	23.4	49.4	54.5	—	0.6493
SDev.	0.81		5.03		—	0.1135
%CV	4.6		10.1		—	17.4
Tube 8+-1	23.4	23.4	39.7	54.5	0.00233	0.4491

	v/o 30.1	v/o 27.9	v/o 23.7
Compressive Modulus	18.9	19.2	17.7
Compressive Strength	29.1	17.0	22.8
Poisson ratio	0.5911	0.75	0.84
Strain to Failure %	0.27	0.27	--

In each case, the measured compressive modulus values were lower than the corresponding tensile modulus values. During these tests, the failure in each tube initiated along 16° fiber direction. Also, each tube exhibited significantly lower strength indicative of the presence of microvoids (or uninfiltrated region) near the fiber cross over sites.

(c) Hoop Tensile Properties

Table 8-4 lists the hoop tensile modulus and strength data for tubes with different fiber volume. Based on these results, the transverse hoop modulus and hoop tensile strength were in adequate agreement with the predicted values.

8.1.4 Thermophysical Properties

(a) Coefficient of Thermal Expansion

Longitudinal thermal expansion response of 27.9 and 23.7 v/o tube specimens are shown in Figures 8-2 and 8-3 respectively. These CTE test results are summarized in Table 8-5. Measured CTE value of 0.8 ppm/°F for 27.9 v/o tube was close to the predicted value of 0.68 ppm/°F.

Table 8-4 Hoop Tensile Properties of [±16°]$_s$ P100/AZ91C Mg Tubes

Tension Tube #	Fiber Volume (%)	Hoop Elastic Modulus, E_H (Msi) M	P	Ultimate Tensile Strength, F_H (ksi) M	P
6I	30.06	3.7	4.63	5.04	5.24
6F		3.7	(88.6%)*	3.62	(70.4%)*
6G		5.0		2.42	
Ave.		4.1		3.69	
SDev.		.751		1.31	
%CV		18.3%		35.6%	
25A	27.9	2.83	4.65	5.23	5.41
25B		—	(98.3%)*	4.96	(88.5%)*
25H		6.3		4.19	
Ave.		4.57		4.79	
SDev.		2.45		0.54	
%CV		53.7%		11.3%	
8A	23.7	4.1	5.09	4.34	5.77
8H		5.89	(98.8%)*	5.13	(78.4%)*
8I		5.09		4.09	
Ave.		5.03		4.52	
SDev.		0.90		0.54	
%CV		17.8%		12.0%	

*Percent of the Predicted Values

Table 8-5 CTE Test Results of P100/AZ91C/Mg Tubes

Material	Fiber Orientation	Fiber Volume (%)	CTE ppm/°F	Strain Hystersiss at RT ppm)	Residual Strain (ppm)
P100/AZ91C Mg	$[\pm 16°]_s$	27.9	0.8	11.6	165.6
P100/AZ91C Mg	$[\pm 16°]_s$	23.7	1.52	29.6	68.9

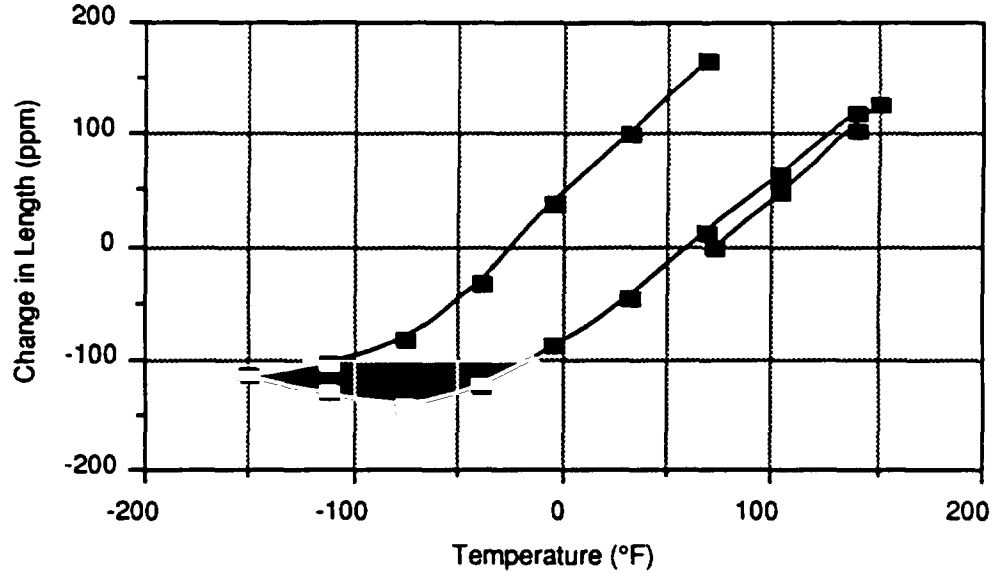

Figure 8-2 Longitudinal Thermal Expansion Behavior of 27.9 v/o P100/AZ91C Mg, [±16°]s

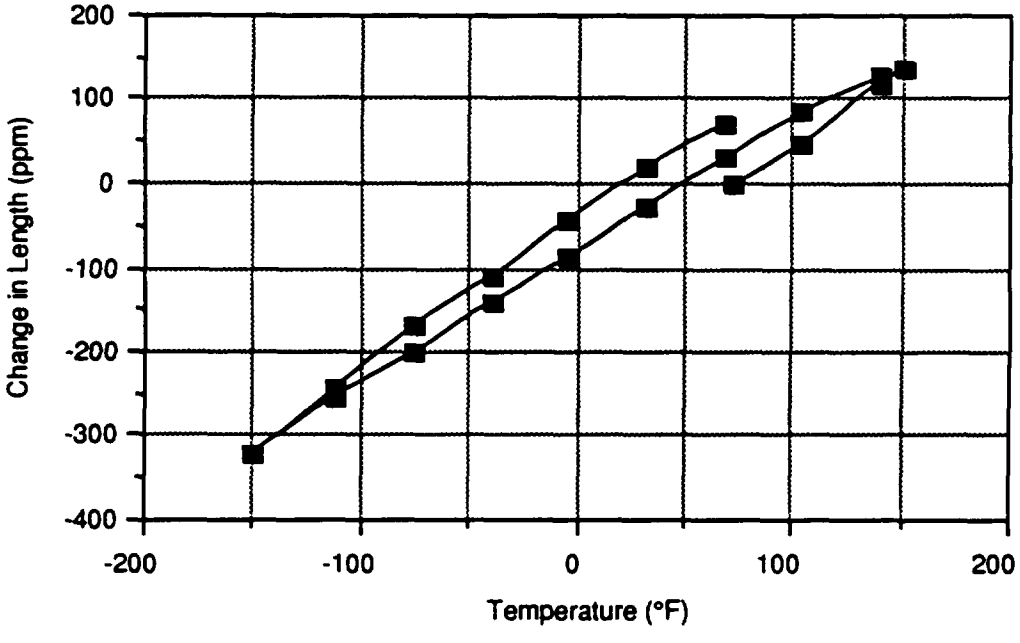

Figure 8-3 Longitudinal Thermal Expansion Behavior of 23.7 v/o P100/AZ91C Mg, [±16°]s

(b) Specific Heat

Results of specific heat measurements between -200°F and 750°F are listed in Table 8-6 and plotted in Figure 8-4. These measurements exhibited a gradual increase in specific heat with increasing temperature. At room temperature the Gr/Mg specimen exhibited Cp = 0.219 Btu/lb°F as compared to 0.245 Btu/lb°F for AZ91C Mg alloy.

(c) Thermal Diffusivity and Through-The-Thickness Thermal Conductivity

Thermal diffusivity test results are plotted in Figure 8-5. Like specific heat, the diffusivity gradually increased with increasing temperature for 27.9 v/o tube specimen. The room temperature diffusivity value was 0.187 cm^2/sec. The diffusivity values were used to calculate the through-the-thickness conductivity (K_z), values which are listed in Table 8-7. At room temperature, the average K_z value was 18.3 Btu/(hr·ft·°F), close to the matrix (cast condition) thermal conductivity value of 21 Btu/(hr·ft·°F).

(d) Thermal Conductivity

Figure 8-6 shows the longitudinal thermal conductivity (K_x) behavior of 27 v/o tube specimens. The P100/Mg [±16°]s tube exhibited the K_x value of 90.3 Btu/(hr·ft·°F) at RT, which agreed with the predicted value value of 89 Btu/(hr·ft·°F). Also, these measurements indicate that the casting did not contain any defects that could have reduced the thermal conductivity.

(e) Electrical Resistivity

Longitudinal electrical resistivity results for 27.9 v/o tube specimen are plotted in Figure 8-7. Based on these measurements, the composite exhibited average resistivity value of 24.598 μohm·cm, compared to the P100 and matrix resistivity values of 11 and 700 microhm-cm respectively.

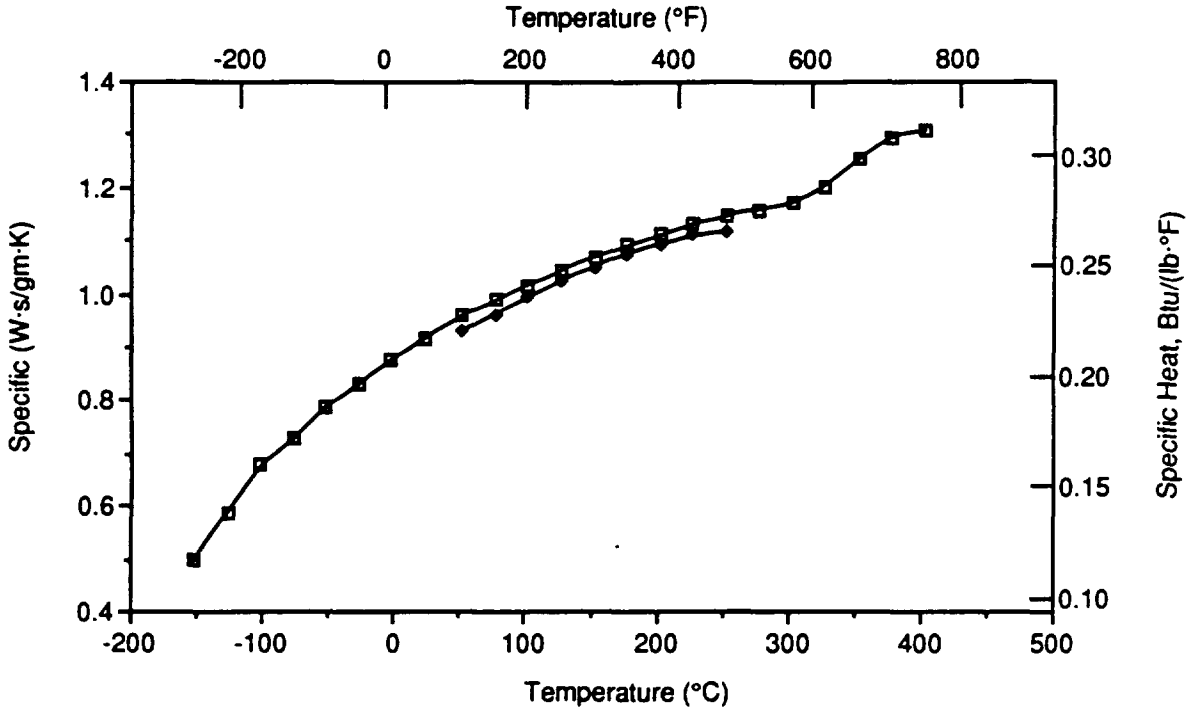

Figure 8-4 Specific Heat as a Function of Temperature for P100/AZ91C Mg Composites

Table 8-6 Specific Heat of P100/AZ91C Mg Composites

Temp. (°C)	(W·s/gm·K)*	Btu/(lb·°F)
-152.0	0.500	0.120
-127.0	0.587	0.140
-102.0	0.667	0.159
-77.0	0.727	0.174
-52.0	0.789	0.189
-27.0	0.831	0.199
-2.0	0.875	0.209
23.0	0.916	0.219
52.0	0.957	0.229
77.0	0.987	0.236
102.0	1.014	0.242
127.0	1.042	0.249
152.0	1.069	0.256
177.0	1.090	0.261
202.0	1.110	0.265
227.0	1.129	0.270
252.0	1.144	0.274

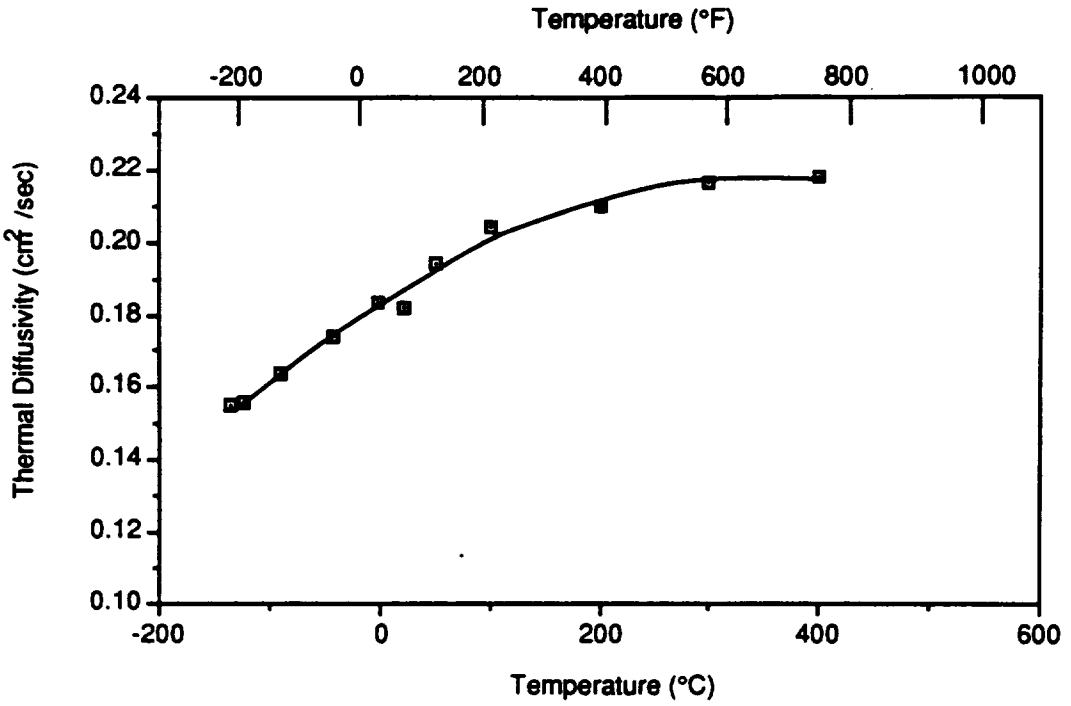

Figure 8-5 Thermal Diffusivity Versus Temperature for P100/AZ91C Mg Composites

Table 8-7 Calculated Through Thickness Thermal Conductivity of P100/AZ91C Mg, $[\pm 16^{\circ}]_s$ Tubes

Temp. (°C)	Density ($gm \cdot cm^{-3}$)	Specific Heat ($W \cdot s \cdot gm^{-1} \cdot K^{1}$)	Diffusivity ($cm^2 sec^{-1}$)	Conductivity ($W \cdot cm^{-1} K^{1}$)	Conductivity (Btu Units*)	Temp. (°F)
-135	1.849	0.5500	0.15500	0.15763	109.29	-211
-100	1.849	0.6650	0.16200	0.19919	138.11	-148
-50	1.849	0.7870	0.17300	0.25174	174.55	-58
0	1.849	0.8730	0.18300	0.29539	204.81	32
23	1.849	0.9160	0.18700	0.31672	219.60	73.4
100	1.849	1.0140	0.20300	0.38060	263.89	212
200	1.849	1.1100	0.21000	0.43100	298.83	392
300	1.849	1.1710	0.21600	0.46768	324.26	572
400	1.849	1.3090	0.21800	0.52763	365.83	752

* - $(Btu \cdot in \cdot hr^{-1} \cdot ft^{-2} \cdot {}^{\circ}F^{-1})$; † - Through-plane;
†† - Longitudinal Direction; ††† - Transverse Direction

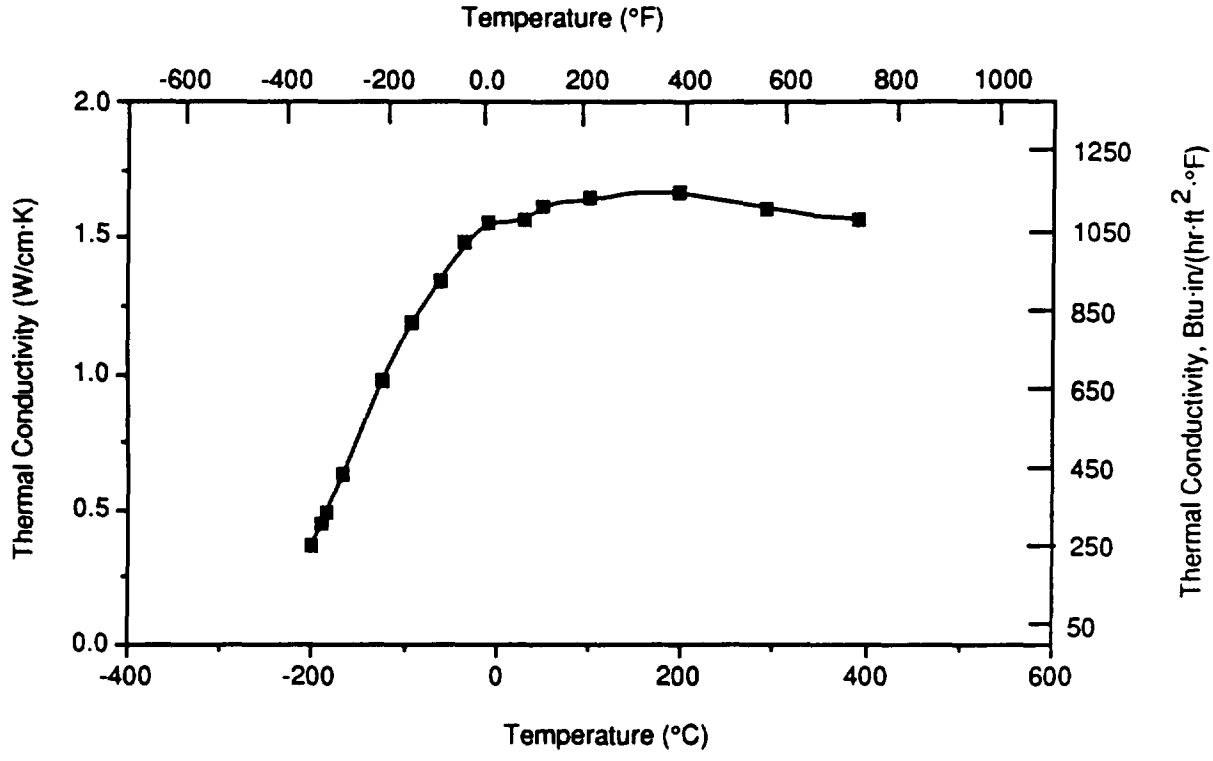

Figure 8-6 Inplane Thermal Conductivity Versus Temperature For P100/AZ91C Mg Composites

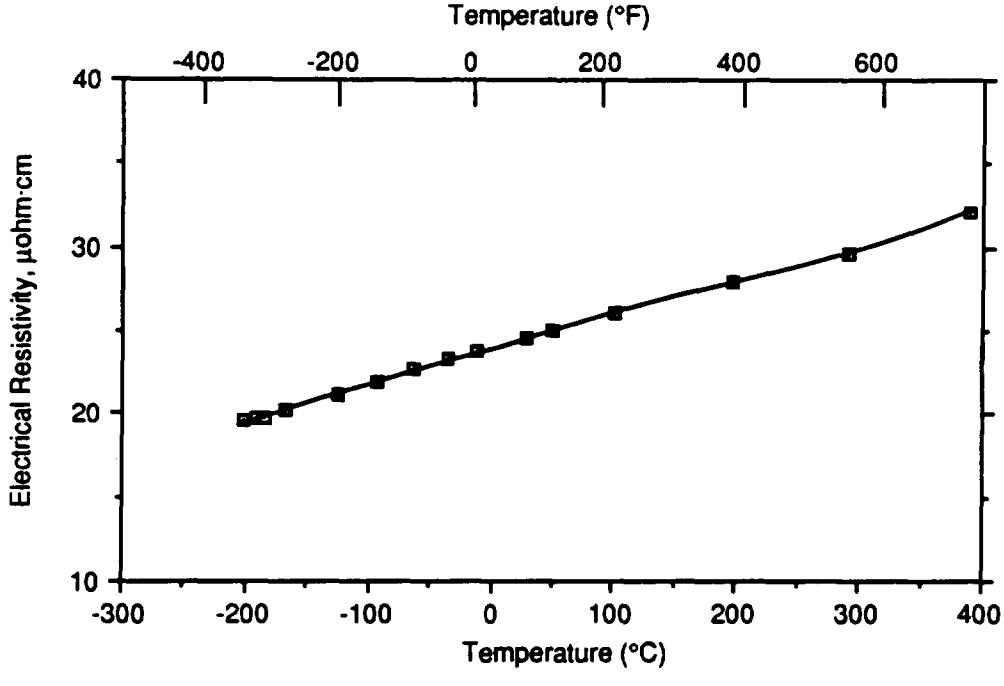

Figure 8-7 Electrical Resistivity of P100/AZ91C Mg

(f) Hemispherical Emissivity

Total hemispherical emissivity of the machined Gr/Mg tube, at temperatures between 400 and 750°F was nearly constant at 0.90. The hemispherical emissivity values in this temperature range were as follows:

Temperature (°F)	Total Hemispherical Emissivity (ε_H)
412	0.891
491	0.904
570	0.893
588	0.900
757	0.908

8.2 SUMMARY OF P100/Mg TEST DATA

Mechanical and thermophysical property test data of P100/AZ91C Mg $[\pm 16]_s$ tubes with 30.1, 27.9, and 23.7 v/o are summarized in Tables 8-8 to 8-10.

Table 8-8 P100/AZ91C Mg [±16]$_s$ Graphite/Magnesium Cast Tube

NOT DESIGN ALLOWABLE DATA

PROPERTIES							TEMPERATURE (°F)			Std. Dev. / No. of Specimens at RT	Test Method
PHYSICAL			MECHANICAL & THERMAL				Low	Room	High		
Density (lb / in^3)	X	0.0683	Longitudinal Tensile Strength	σ_x^{TU}	ksi			61.2		±6.06 / 5	ASTM D-3552
Fiber volume fraction	X	0.301	Transverse Tensile Strength	σ_y^{TU}	ksi			3.69		±1.31 / 3	NOL
Void volume fraction	X	<0.003	Longitudinal Comp. Strength	σ_x^{CU}	ksi			29.1			ASTM D-3410
Nominal ply thickness	in	0.0125	Transverse comp. strength	σ_y^{CU}	ksi						
Max. cont. use temp.	°F	550	In-plane shear strength	IPSS	ksi						
Ply Orientation	θ	$[\pm 16]_s$	Interlaminar shear strength	ILSS	ksi						
			Longitudinal tensile strain **	ε_x^T	%			0.21		±0.0915 / 5	ASTM D-3552
OPTICAL & ELECTRICAL (at room temperature)			Transverse tensile strain **	ε_y^T	%						NOL
			Longitudinal comp. strain **	ε_x^C	%			0.27			ASTM D-3410
Solar Absorptance	α		Transverse comp. strain **	ε_y^C	%						
Normal Emissivity	ε		Longitudinal tensile modulus	E_x	Msi			25.44		±3.04 / 5	ASTM D-3552
			Transverse tensile modulus	E_y	Msi			4.1		±0.75 / 3	NOL
			Longitudinal comp. modulus	E_x	Msi			18.9			ASTM D-3410
			Transverse comp. modulus	E_y	Msi						
			In-plane shear modulus	G	Msi						Torsion Test
			Longitudinal flexural modulus	F_x	Msi						
			Transverse flexural modulus	F_y	Msi						
			Long. tensile Poisson's ratio	ν_{xy}	X			0.46		±0.23 / 5	ASTM D-3552
			Trans. tensile Poisson's ratio	ν_{yx}	X						NOL
			Long. thermal conductivity	K_x	(1)						
			Trans. thermal conductivity	K_y	(1)						
			Thru thickness thermal cond.	K_z	(1)						
			Specific heat	C_p	(2)						
			Longitudinal CTE	α_x	(3)			0.219			ASTM E-80
			Transverse CTE	α_y	(3)						
			Thru thickness CTE	α_z	(3)						

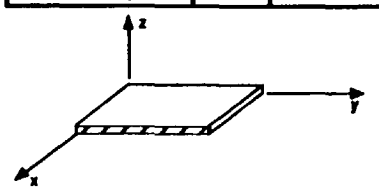

Notes:
(**) - Strain to failure; (1) Btu/(hr·in·°F); (2) Btu/(lb·°F); (3) μin./in./°F

Table 8-9 P100/AZ91C Mg [±16]$_s$ Graphite/Magnesium Cast Tube

NOT DESIGN ALLOWABLE DATA

PHYSICAL		
Density (lb / in^3)		0.0685
Fiber volume fraction		0.279
Void volume fraction		<0.003
Nominal ply thickness	in	0.0125
Max. cont. use temp.	°F	550
Ply Orientation	θ	[±16]$_s$

OPTICAL & ELECTRICAL (at room temperature)

Solar Absorptance	α	
Normal Emissivity	ε	

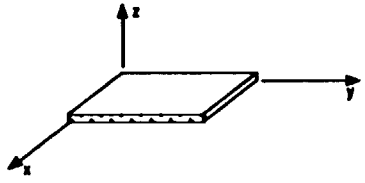

PROPERTIES			TEMPERATURE (°F)			Std. Dev. / No. of Specimens at RT	Test Method
MECHANICAL & THERMAL			Low	Room	High		
Longitudinal Tensile Strength	σ_x^{TU}	ksi		27.0			ASTM D-3552
Transverse Tensile Strength	σ_y^{TU}	ksi		4.79		±0.54 / 3	NOL
Longitudinal Comp. Strength	σ_x^{CU}	ksi		17.0			ASTM D-3410
Transverse comp. strength	σ_y^{CU}	ksi					
In-plane shear strength	IPSS	ksi					
Interlaminar shear strength	ILSS	ksi					
Longitudinal tensile strain **	ε_x^T	%		0.19		±0.04 / 5	ASTM D-3552
Transverse tensile strain **	ε_y^T	%					NOL
Longitudinal comp. strain **	ε_x^C	%		0.27			ASTM D-3410
Transverse comp. strain **	ε_y^C	%					
Longitudinal tensile modulus	E_x	Msi		24.3			ASTM D-3552
Transverse tensile modulus	E_y	Msi		4.57		±2.45 / 3	NOL
Longitudinal comp. modulus	E_x	Msi		19.2			ASTM D-3410
Transverse comp. modulus	E_y	Msi					
In-plane shear modulus	G	Msi					Torsion Test
Longitudinal flexural modulus	F_x	Msi					
Transverse flexural modulus	F_y	Msi					
Long. tensile Poisson's ratio	ν_{xy}			0.649		±0.12 / 5	ASTM D-3552
Trans. tensile Poisson's ratio	ν_{yx}						NOL
Long. thermal conductivity	K_x	(1)		7.52			Kohlrausch
Trans. thermal conductivity	K_y	(1)					
Thru thickness thermal cond.	K_z	(1)					
Specific heat	C_p	(2)		0.219			ASTM E-1269
Longitudinal CTE	α_x	(3)		0.8			ASTM E-80
Transverse CTE	α_y	(3)					
Thru thickness CTE	α_z	(3)					

Notes:
(**) - Strain to failure; (1) Btu/(hr·in·°F); (2) Btu/(lb·°F); (3) μin./in./°F

Table 8-10 P100/AZ91C Mg [±16]$_s$ Graphite/Magnesium Cast Tube

NOT DESIGN ALLOWABLE DATA

PROPERTIES			TEMPERATURE (°F)			Std. Dev. / No. of Specimens at RT	Test Method
MECHANICAL & THERMAL			Low	Room	High		
Longitudinal Tensile Strength	σ_x^{TU}	ksi		49.4		±5.03 / 5	ASTM D-3552
Transverse Tensile Strength	σ_y^{TU}	ksi		4.52		±0.54 / 3	NOL
Longitudinal Comp. Strength	σ_x^{CU}	ksi		22.8			ASTM D-3410
Transverse comp. strength	σ_y^{CU}	ksi					
In-plane shear strength	IPSS	ksi					
Interlaminar shear strength	ILSS	ksi					
Longitudinal tensile strain **	ε_x^T	%		0.23			ASTM D-3552
Transverse tensile strain **	ε_y^T	%					NOL
Longitudinal comp. strain **	ε_x^C	%					ASTM D-3410
Transverse comp. strain **	ε_y^C	%					
Longitudinal tensile modulus	E_x	Msi		23.4			ASTM D-3552
Transverse tensile modulus	E_y	Msi		5.03		±0.913 / 3	NOL
Longitudinal comp. modulus	E_x	Msi		17.7			ASTM D-3410
Transverse comp. modulus	E_y	Msi					
In-plane shear modulus	G	Msi					Torsion Test
Longitudinal flexural modulus	F_x	Msi					
Transverse flexural modulus	F_y	Msi					
Long. tensile Poisson's ratio	ν_{xy}			0.649		±0.11 / 5	ASTM D-3552
Trans. tensile Poisson's ratio	ν_{yx}						NOL
Long. thermal conductivity	K_x	(1)					
Trans. thermal conductivity	K_y	(1)					
Thru thickness thermal cond.	K_z	(1)					
Specific heat	C_p	(2)		0.219			
Longitudinal CTE	α_x	(3)		1.52			ASTM E-80
Transverse CTE	α_y	(3)					
Thru thickness CTE	α_z	(3)					

PHYSICAL		
Density (lb / in^3)		0.069
Fiber volume fraction		0.237
Void volume fraction		<0.003
Nominal ply thickness	in	0.0125
Max. cont. use temp.	°F	550
Ply Orientation	θ	$[\pm 16]_s$

OPTICAL & ELECTRICAL (at room temperature)		
Solar Absorptance	α	
Normal Emissivity	ε	

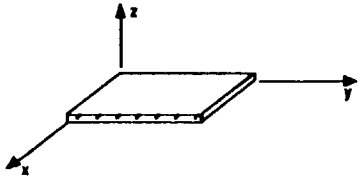

Notes:
(**) - Strain to failure; (1) Btu/(hr·in·°F); (2) Btu/(lb·°F); (3) µin./in./°F

Carbon/Glass
HMU/7070

Carbon/Glass
HMU/7070

9.0 CARBON/GLASS: HMU/7070

Similar to organic and metal matrix composites, carbon fiber reinforced glass (C/Gl) matrix composites offer low density, high stiffness and strength, and near zero CTE. But in C/Gl these material properties can be maintained up to temperatures as high as 2200°F. In addition, these composites can be easily fabricated into complex shapes. With these attributes, C/Gl are candidate material for light weight, dimensionally stable mirrors and support structures for space applications. Therefore, unidirectional and bidirectional HMU/7070 glass flat panels were tested to generate mechanical and thermophysical property tests data. The fabrication data, and the results of product evaluation and material property tests are discussed in this chapter.

9.1 HMU/7070 $[0]_{12}$ FLAT PANELS

9.1.1 Fabrication Data

Material System:	HMU/7070 $[0]_{12}$
Condition:	As fabricated
Manufacturer:	United Technology Research Center, CT
Dimensions:	0.062-in. x 12-in. x 12-in.
Ply thickness:	0.0052-in.
UTRC Panel No.:	679 and 750
Martin Marietta ID:	(CS)(UU)(AP)
Fabrication Process:	Flat panels were fabricated utilizing the tape winding and hot pressing procedure described schematically in Figure 9.1-1. The process involved impregnating the fiber by passing the fiber through a glass powder slurry containing an organic binder while wrapping the fiber on a rotating

drum. The impregnated fiber tape was in turn cut, stacked in the appropriate configuration, binder removed and consolidated by (vacuum) hot press densification under pressure of 1.0 ksi at 2012°F.

9.1.2 Product Evaluation

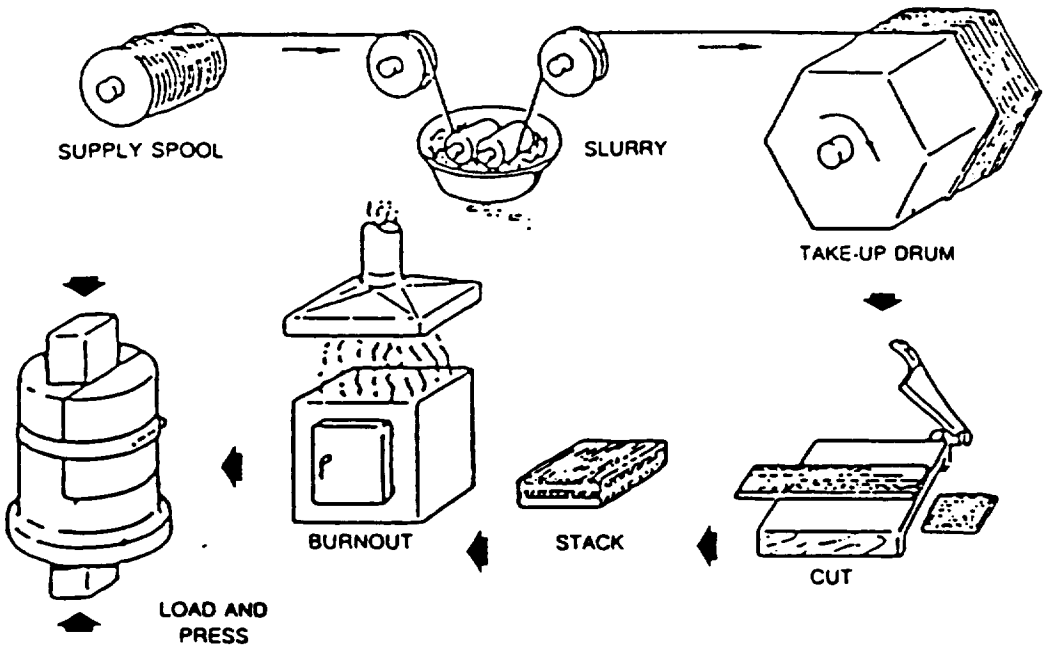

Figure 9.1-1 Carbon/Glass Composite Fabrication Procedure

From the as fabricated $[0]_{12}$ panels, different test specimens were prepared by UTRC, CT, because of their experience in fabrication, handling and cutting various glass matrix composites. Subsequent NDE, microstructural examination and material property tests were performed at Martin Marietta Astronautics Group, CO.

(a) Density

Fiber (HMU):	0.066 lb/in^3
Matrix (7070):	0.0805 lb/in^3
Lamina (HMU/7070):	0.072 lb/in^3
Std. Dev.:	0.0015

(b) Fiber Volume

	Panel #679	Panel #750
v/o	44.0	45.0
Std. Dev.	0.3	0.4
Void Volume	≤0.2	≤0.2

(c) Non-Destructive Evaluation

Visual and X-radiographic inspection techniques were used to evaluate C/Gl specimens. On visual examination, each specimen appeared to be of good quality with smooth surface finish and uniform thickness. X-radiographs of the specimens revealed good fiber collimation with no defects such as voids or cracks.

(d) Microstructure

Transverse photomicrographs of HMU/7070 $[0]_{12}$ are shown in Figure 9.1-2. These microstructures show fibers uniformly distributed in the matrix and no internal defects such as voids and disbonds.

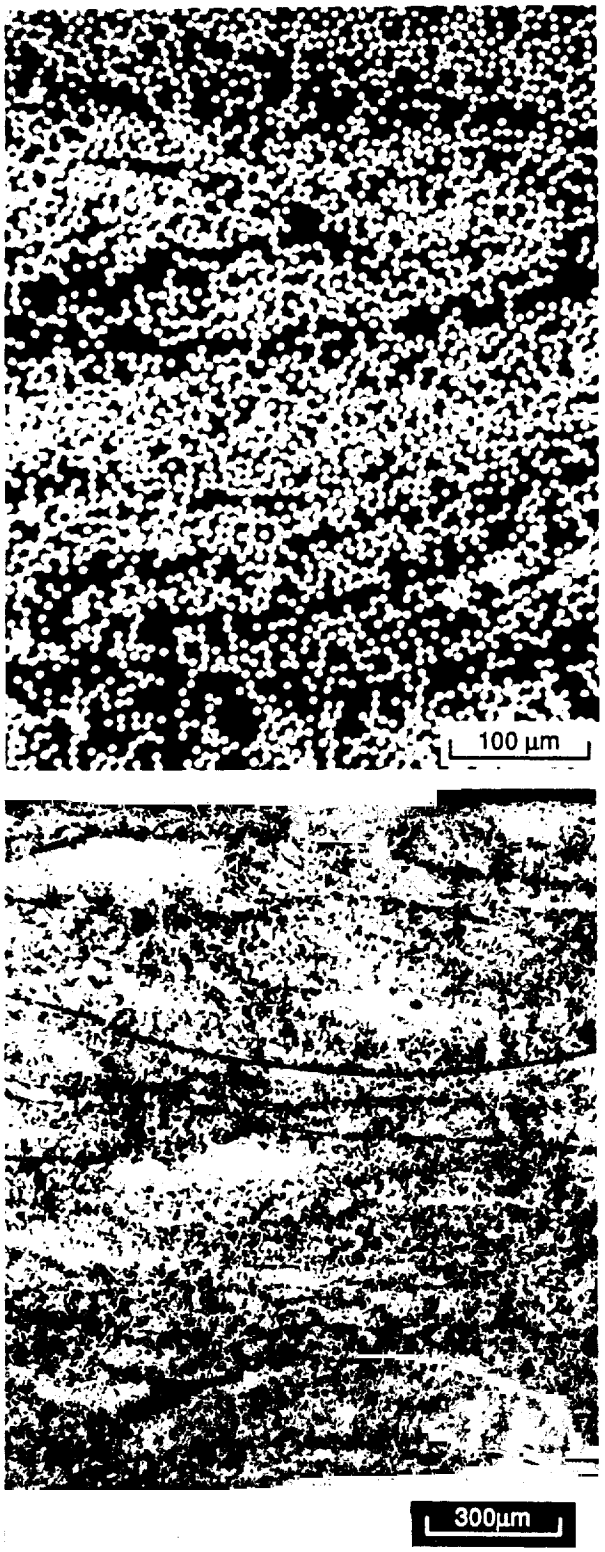

Figure 9.1-2 Transverse Photomicrograph of $[0]_{12}$HMU/7070 Showing Nearly Uniform Fiber Distribution and No Voids and Microcracks

9.1.3 Mechanical Properties

(a) Tension

Longitudinal tension test results of the unidirectional composite as obtained from one 44 v/o specimen and three 45 v/o specimens are listed in Table 9.1.1. The 45 v/o composite exhibited the average elastic modulus value of 26.43 Msi, which was close to the ROM value 29.8 Msi. A typical tensile stress strain curve was linear up to a strain of approximately 0.15% and the (associated proportional limit) stress of 40 ksi. The measured tensile strength of 129.3 ksi obtained from the 44 v/o specimen was in better agreement with the predicted value of 131 ksi, than the tensile strength of 95.5 ksi for 45 v/o specimen. This low tensile strength was primarily attributed to the slight damage that could have been introduced due to a slightly higher applied pressure. Each specimen exhibited a predominantly fiber pull out mode of failure indicating the low interfacial strength in the glass matrix composites.

Table 9.1-1 Longitudinal Tensile Properties of HMU/7070 Glass $[0]_{12}$ Panel 679, v/o = 44v/o and Panel 750, v/o = 45

Specimen # (CS) (UU) (AP)	Elastic Modulus E_X^T(Msi)	Ultimate Tensile Strength (ksi)	Strain to Failure (%)	Poisson's Ratio ν_{xy}
†TNL-679-2	23.5	129.3	—	0.209
†TNL-750-2	26.4	95.9	0.39	0.247
*TNL-750-4	26.2	93.1	0.361	0.214
*TNL-750-6	26.7	97.5	0.37	0.219
Mean	26.43	95.5	0.353	0.2266
Std. Deviation	0.25	2.23	0.011	0.0177
CV (%)	0.95	2.33	3.2	7.8

† Failure Inside Or Near The Doublers
* Failure Inside Gage Length

(b) Compression

Longitudinal compression tests results of 44 v/o unidirectional HMU/7070 BSG are listed in Table 9.1-2, and a typical strain-strain response is shown in Figure 9.1-3. Each test specimen

exhibited a linear elastic response until 0.12% strain and a compressive stress (proportional limit) value of 37 ksi, at which the matrix microcracking begins. The compressive modulus value of 21.3 Msi was slightly lower than the tensile modulus, but compressive and tensile strength values were nearly identical, suggesting that fiber maintained their uniaxial alignment until failure, without microbuckling.

Table 9.1-2 Longitudinal Compressive Properties of HMU/7070 Glass $[0]_{12}$ Panel 679, v/o = 44%

Specimen # (CS) (UU) (AP)	Elastic Modulus E_X^T (Msi)	Ultimate Compressive Strength (ksi)	Strain to Failure (%)	Poisson's Ratio ν_{xy}
†CML-679-2	20.9	125.3	0.6	0.2223
†CML-679-5	21.0	127.0	0.64	0.1899
*CML-679-7	21.9	123.3	0.7	0.1945
*CML-679-9	21.4	129.4	0.68	0.2147
Mean	21.3	126.3	0.655	0.2054
Std. Deviation	0.455	2.59	0.44	0.01561
CV (%)	2.1	2.0	6.7	7.6

† Failure Inside Gage Length; * Failure Adjacent To Doublers

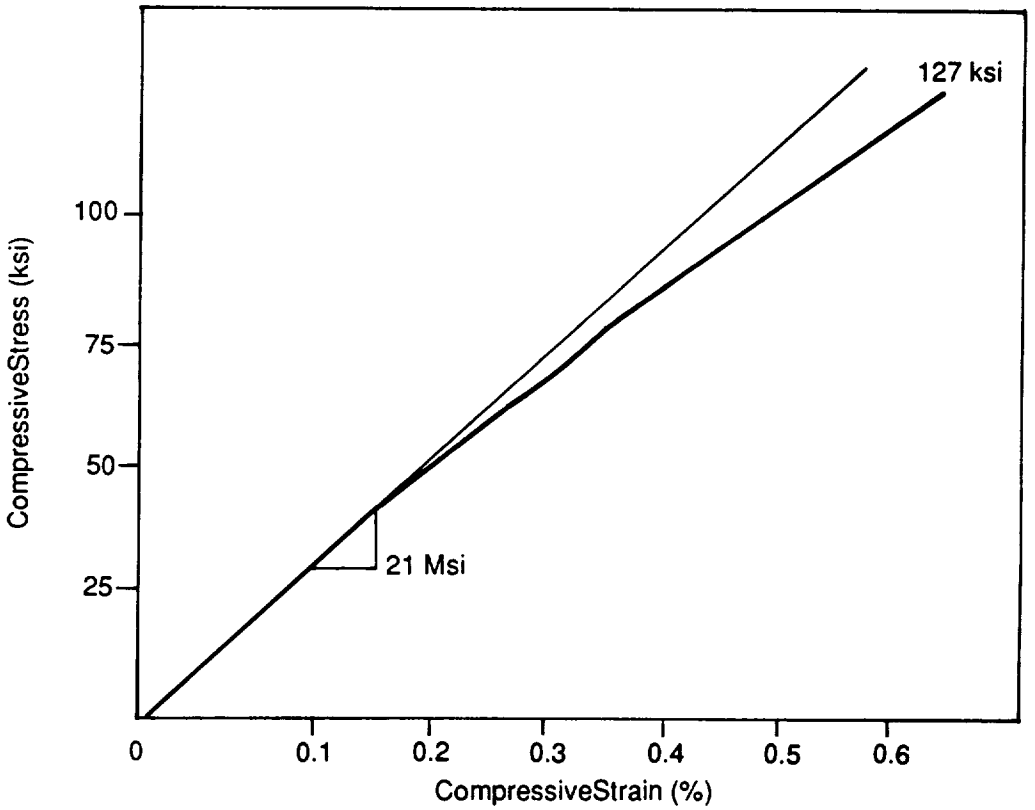

9.1-3 Typical Compressive Stress-Strain Response of HMU/7070 $[0]_{12}$

9.1.3 In-plane Shear

Measured in-plane shear properties of the composite, as obtained from (subscale) 10° off-axis test specimens are listed in Table 9.1-3. Based on these tests, the unidirectional HMU/7070 exhibited 2.6 Msi in-plane shear modulus, and 15.6 ksi shear strength.

Table 9.1-3 Inplane Shear Modulus and Strength Values of HMU/7070, $[0]_{12}$, v/o = 44%

Specimen # (CS) (UU) (AP)	Shear Modulus (Msi)	Shear Strength (ksi)
679-15	2.8	16.3
679-17	2.3	14.8
Mean Value	2.6	15.6
Standard Deviation	0.354	1.061
CV (%)	13.9	6.8

9.1.4 Thermophysical Properties

Of the thermophysical property tests, only CTE and optical property tests were conducted from the available test specimens.

(a) Coefficient of Thermal Expansion

Thermal expansion response of carbon/glass $[0]_{12}$ v/o = 45% is shown in Figure 9.1-4. This change in length versus. temperature plot for the first thermal cycle between -150°F and 150°F indicated average CTE = -0.38 ppm/°F with low residual strain (-7.65 ppm) and RT hysteresis - 28.3 ppm.

(b) Optical Properties

- Solar Absorptance (α_s) = 0.92, Std. Dev. 0.005
- Normal Emittance (ε_N) = 0.805, Std. Dev. 0.005

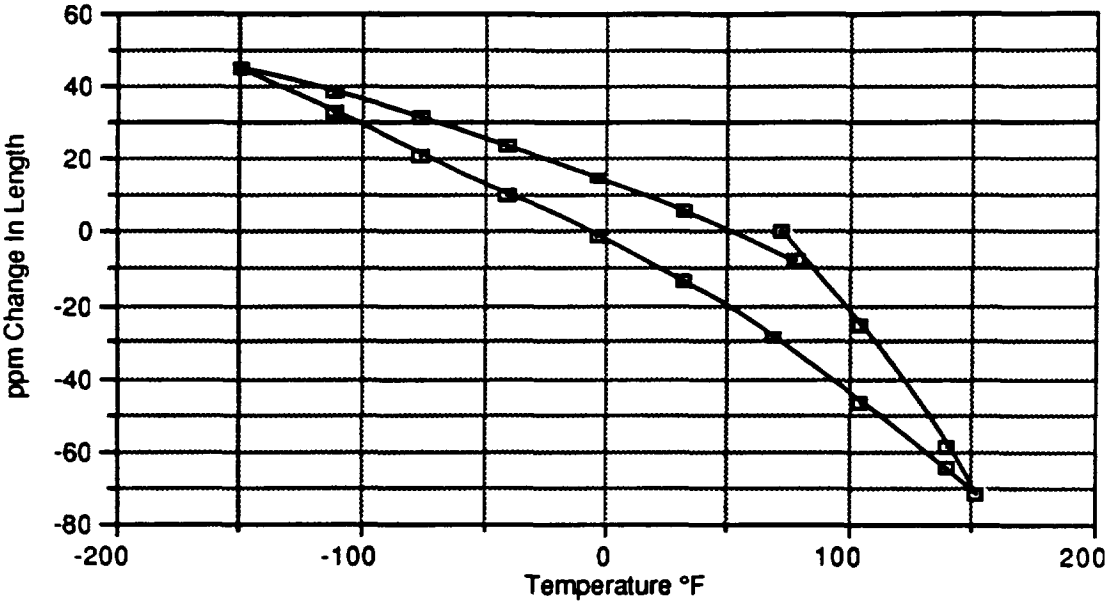

Figure 9.1-4 Thermal Expansion Behavior of HMU/7070, $[0]_{12}$, v/o = 45%

9.2 HMU/7740 BSG $[0/90]_6$ FLAT PANELS

9.2.1 Fabrication Data

Material System:	HMU/7070 $[0/90]_6$
Condition:	As fabricated
Manufacturer:	United Technology Research Center, CT
Dimensions:	0.065-in. x 12-in. x 12-in.
Ply thickness:	0.0054-in.
UTRC Panel No.:	356 and 403
Martin Marietta ID:	(CS)(UB)(AP)
Fabrication Process:	Typical tape winding and hot pressing procedure used in fabricating unidirectional composites (para. 9.1.1).

9.2.2 Product Evaluation

Similar to unidirectional panels, different test specimens for bidirectional panels were also prepared by UTRC, CT because of their experience in fabrication, handling, and cutting glass matrix composites. Subsequent NDE, microstructural examination, and material property tests were performed at Martin Marietta Astronautics Group, CO.

(a) Density

Fiber (HMU):	0.066 lb/in^3
Matrix (7070):	0.0805 lb/in^3
Laminate (HMU/7070):	0.071 lb/in^3
Std. Dev.:	0.001

(b) Fiber Volume

	Panel #356	Panel #403
v/o	41.0	40.0
Std. Dev.	0.4 0.5	
Void Volume (%)	≤0.2	≤0.2

(c) Non-Destructive Evaluation

Visual and X-radiographic inspections were performed to evaluate the bidirectional laminate specimens. On visual examination, each specimen revealed smooth surface finish, with no scratches, voids, or edge defects. X-radiographs of the specimens indicated good fiber collimation with no detectable voids, microcracks or disbonds.

(d) Microstructure

A typical microstructure of HMU/7070 $[0/90]_6$ is shown in Figure 9.2-1. The photomicrograph shows each ply of nearly equal thickness, uniform fiber distribution, and no defects such as voids and disbonds.

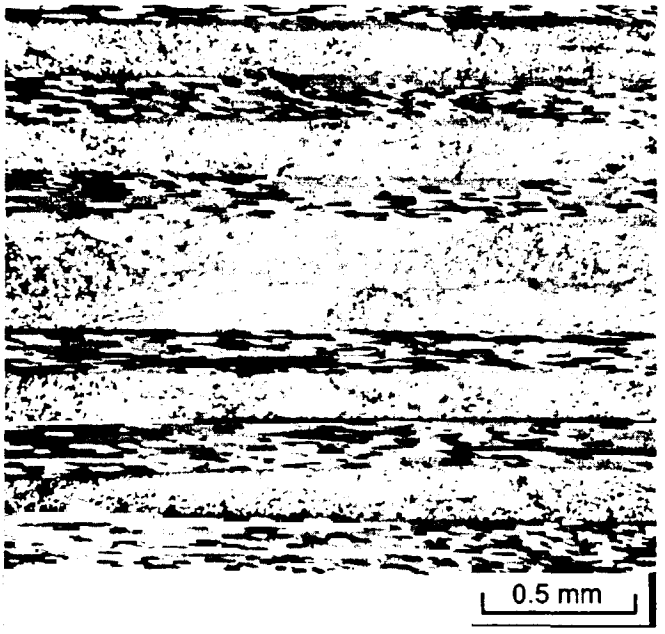

Figure 9.2-1 Typical Microstructure of HMU/7070, $[0/90]_6$

9.2.3 Mechanical Properties

(a) Tension

Longitudinal tension tests results of $[0/90]_6$ specimens are listed in Table 9.2-1. The average elastic modulus value of 11.7 Msi was lower than the predicted value of 16 Msi, but typical of ceramic matrix composites where the load transfer characteristics are influenced by the weak interfacial bond. Similar to unidirectional specimens, the bidirectional panels also exhibited a linear stress strain response until 0.17% strain and 20 ksi stress level. The measured tensile strength of 40.9 ksi was significantly lower than the predicted 80 ksi strength level because each specimen got damaged (within the doubler) due to the high pressure applied during gripping.

Table 9.2-1 Longitudinal Tensile Properties of HMU/7070, $[0/90]_6$, v/o = 40%

Specimen # (CS)(UB)(AP)	Elastic Modulus E_x^T (Msi)	Proportional Limit Stress (ksi)	Ultimate Tensile Strength (ksi)	Strain To Failure (%)	Poisson Ratio ν_{xy}
TNL-1	11.3	14.17	38.8	0.41	0.0347
TNL-2	12.7	23.88	41.2	0.33	0.0313
TNL-3	11.2	22.38	42.7	0.475	0.0342
Mean Value	11.7	20.14	40.9†	0.405	0.0334
Std. Dev.	0.839	5.22	1.97	0.072	0.00184
CV (%)	7.2	25.9	4.8	17.7%	5.5

† Low Strength Due to High Grip Pressure

(b) Compression

Longitudinal and transverse compression test results of $[0/90]_6$ specimens are listed in Table 9.2-2 and 9.2-3 respectively. In both the cases, measured modulus values are nearly identical, and consistent with the tensile modulus. Also, the measured strength values are in agreement with the predicted value of 80 ksi, indicating that 0° fibers effectively contribute to the compressive strength.

Table 9.2-2 Longitudinal Compressive Properties of HMU/7070, $[0/90]_6$, v/o = 40%

Specimen # (CS)(UB)(AP)	Elastic Modulus E_x^C(Msi)	Ultimate Tensile Strength (ksi)
CML-1	12.5	87.2
CML-2	11.4	81.9
CML-3	13.6	91.0
Mean Value	12.5	86.7
Std. Dev.	1.1	4.6
CV (%)	8.8	5.3

Table 9.2-3 Transverse Compressive Properties of HMU/7070, $[0/90]_6$, v/o = 40%

Specimen # (CS)(UQ)(AP)	Elastic Modulus E_y^C(Msi)	Ultimate Tensile Strength (ksi)
CMT-1	11.8	88.4
CMT-2	12.0	68.3†
Mean Value	11.9	78.4
Std. Dev.	0.141	14.2
CV (%)	1.2	18.1

† Doubler failure which caused composite delamination and premature failure

(c) Interlaminar Shear

Measured interlaminar shear strength values of the bidirectional specimens are listed in Table 9.2-4. The average ILSS value of 3.35 ksi provided an indication of adequate interply bonding in the as consolidated composite.

Table 9.2-4 Apparent Interlaminar Shear Strength of HMU/7070, $[0/90]_6$, v/o = 40

HMU/7070 $[0, 90]_6$	
Specimen # (CS)(UB)(AP)	ILSS (ksi)
IL-1	2.801
IL-2	3.818
IL-3	3.430
Mean	3.35
Std. Dev.	0.513
CV %	15.0

9.2.4 Thermophysical Properties

(a) Coefficient of Thermal Expansion

Typical thermal expansion response of 40 v/o HMU/7070 $[0/90]_6$ in a heat/cool/heat cycle between -150°F and 150°F is shown in Figure 9.2-2. Even in the first cycle, the composite exhibited a near zero CTE (-0.075 ppm/°F) with extremely low residual strain (-8.0 ppm).

(b) Specific Heat

The results of specific heat measurements between -200 and 750°F are plotted in Figure 9.2-3, where the RT specific heat value is 0.18 Btu/lb·°F. During these Cp tests, each specimen exhibited identical response, showing an increase in Cp with the increase in temperature.

(c) Thermal Diffusivity

Both the in-plane and through-the-thickness thermal diffusivity results are presented in Figure 9.2-4. Each specimen exhibited a completely reproducible thermal diffusivity response between -200°F and 750°F with a RT diffusivity (in-plane) value of 0.116 cm^2/sec. At each temperature, the in-plane diffusivity value was about 10 times higher than the through-the-thickness diffusivity value.

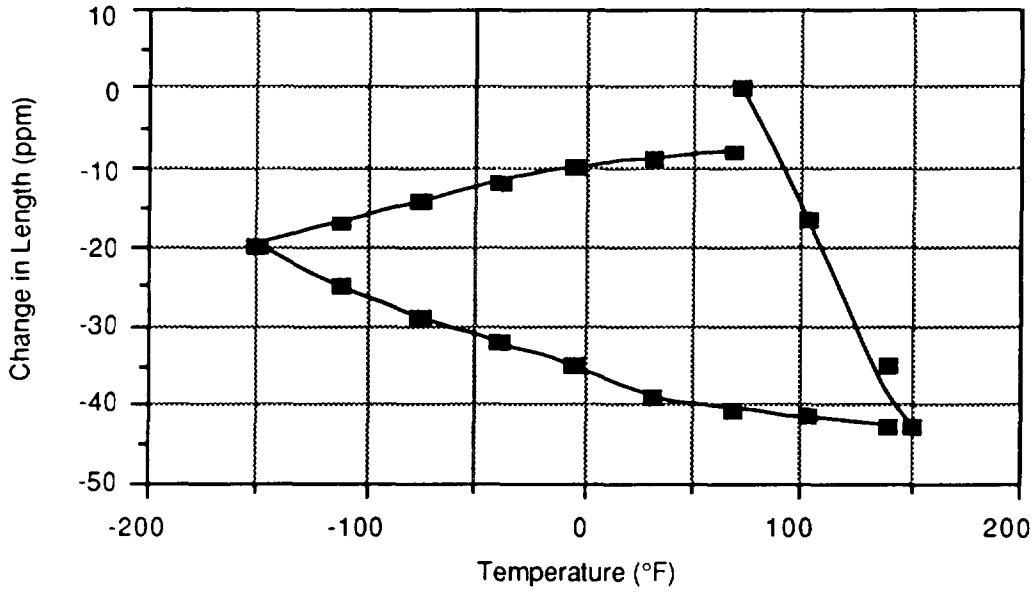

Figure 9.2-2 Thermal Expansion Behavior of HMU/7070, $[0/90]_6$ Laminate

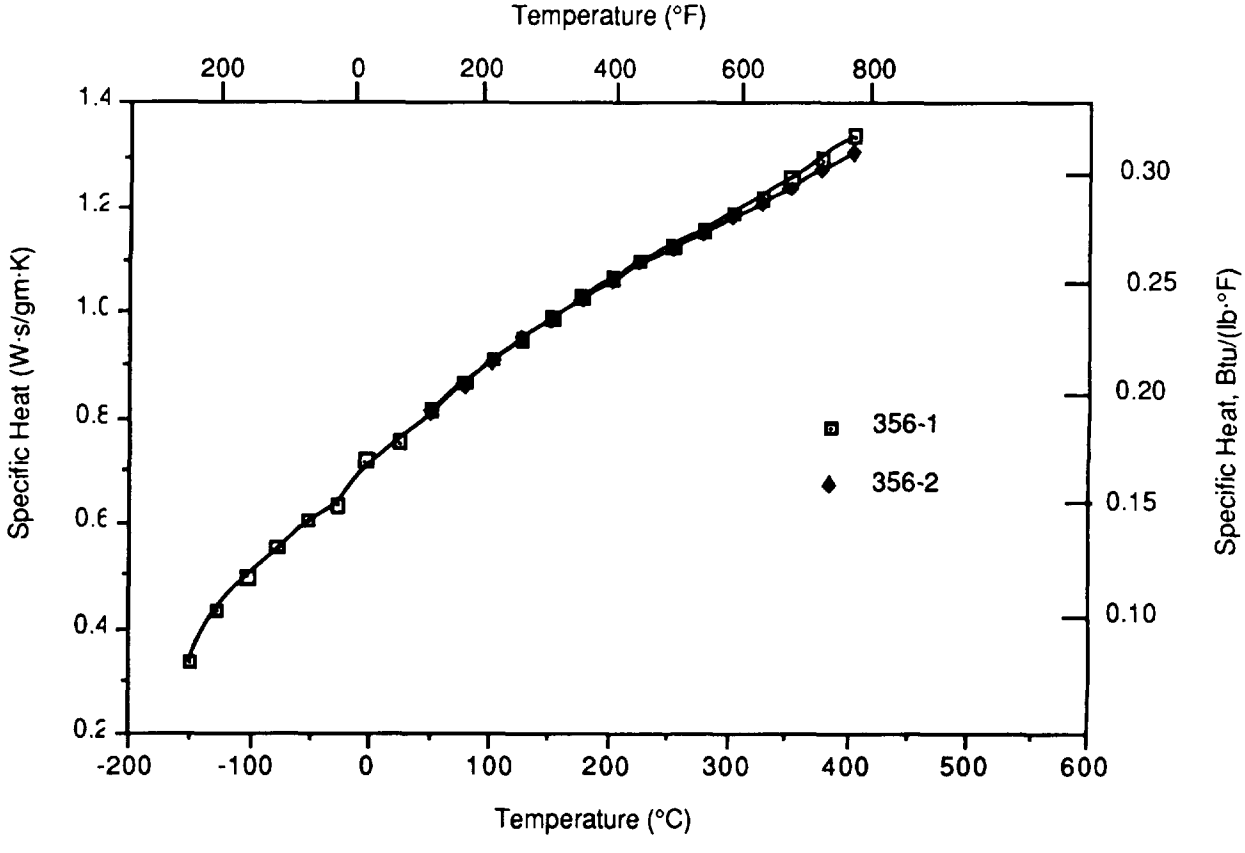

Figure 9.2-3 Specific Heat of HMU/7070, $[0/90]_6$ Laminate

(d) Thermal Conductivity

Kohlrausch method could not be used to determine the in-plane conductivity of the HMU/7070 composites because of the low inherent conductivity of the glass matrix. Therefore, in-plane through thickness conductivity values were calculated from the thermal diffusivity, specific heat, and density measurements. These calculated K_x, K_y and K_z are plotted in Figure 9.2-5. At the test temperatures between -200°F and 750°F, the in-plane conductivity values were higher than the through thickness conductivity. Typical conductivity values at RT were:

$K_x = K_y = 9.91$ Btu/(hr·ft·°F)

$K_z = 0.98$ Btu/(hr·ft·°F)

(e) Optical Properties

- Solar Absorptance (α_s) = 0.92,
- Normal Emittance (ε_N) = 0.805,

- Reflections versus Wavelength—The FTIR diffuse reflectance spectra of HMU/7070 $[0/90]_6$ laminate specimen is shown in Figure 9.2-6. The spectra indicates a highly emissive surface with emissivity (1-reflectance) values of 0.9 at 10.6μm wavelength.

9.3 SUMMARY OF HMU/7070 TEST DATA

Mechanical and thermophysical property test data of HMU/7070 with $[0]_{12}$ and $[0/90]_6$ layup are summarized in Table 9.3-1 and 9.3-2 respectively.

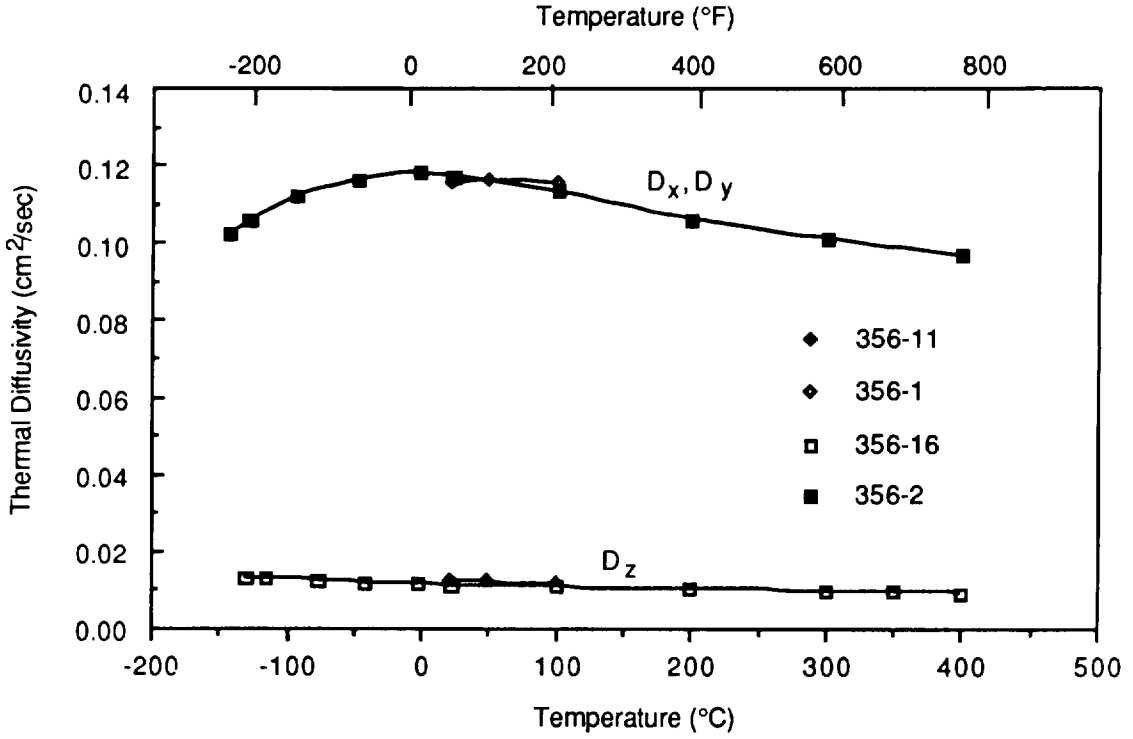

Figure 9.2-4 Inplane and Through-The-Thickness Thermal Diffusivity of HMU/7070, $[0/90]_6$ Laminate

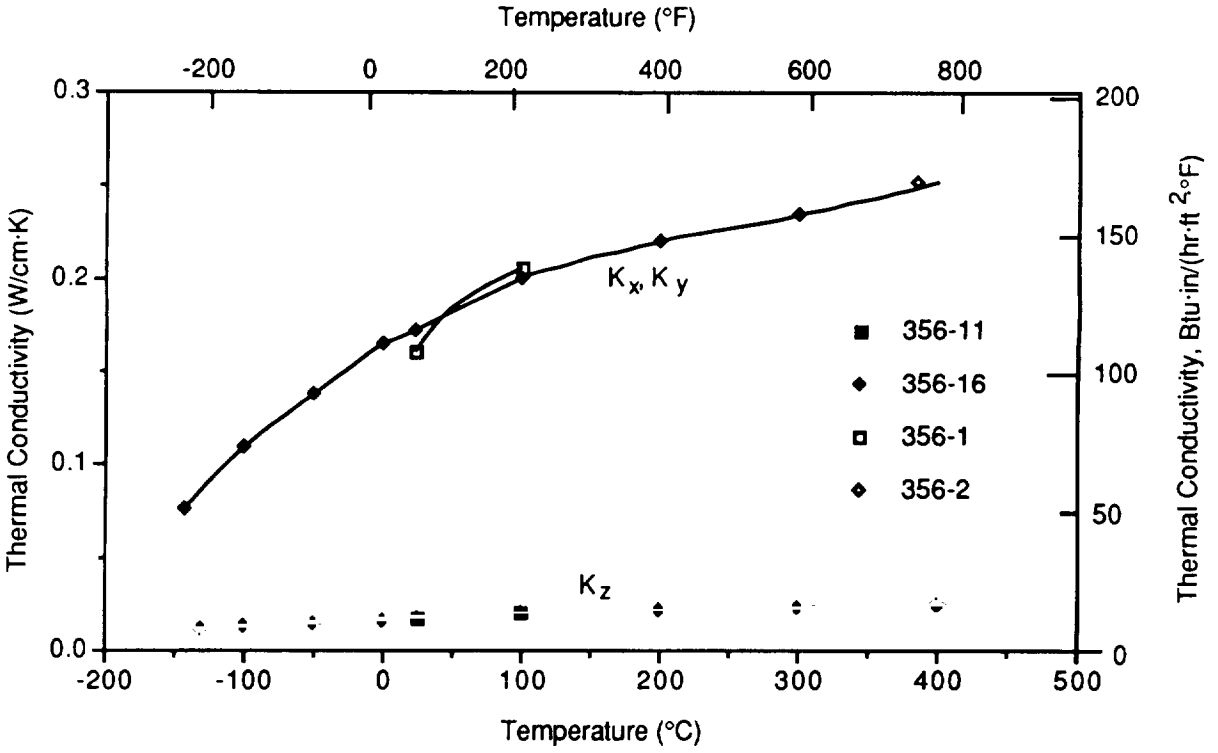

Figure 9.2-5 Inplane and Through-TheThickness Thermal Conductivity of HMU/7070 $[0/90]_6$ Laminate

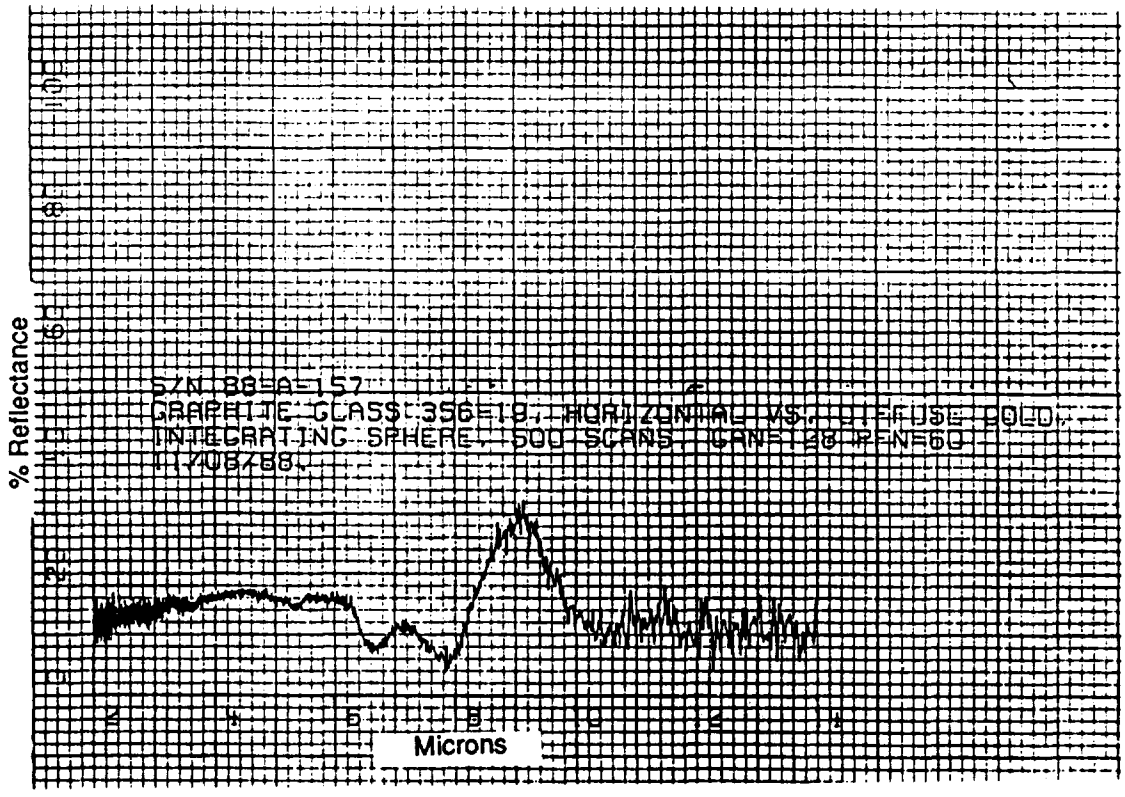

Figure 9.2-6 FTIR Diffuse Reflectance Spectra of HMU/7070, $[0/90]_6$ Laminate

ORIGINAL PAGE IS
OF POOR QUALITY

Table 9.3-1 HMU/7070 Carbon/Glass $[0]_{12}$

NOT DESIGN ALLOWABLE DATA

PHYSICAL		
Density (lb / in^3)	X	0.072
Fiber volume fraction	X	0.44
Void volume fraction	X	≤0.002
Nominal ply thickness	in	0.0052
Max. cont. use temp.	°F	1500
Ply Orientation	θ	$[0]_{12}$
OPTICAL & ELECTRICAL (at room temperature)		
Solar Absorptance	α	0.92
Normal Emissivity	ε	0.805

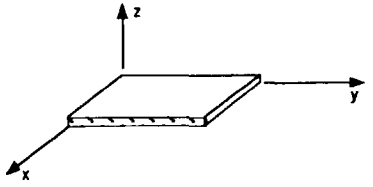

MECHANICAL & THERMAL			TEMPERATURE (°F) Low	Room	High	Std. Dev. / No. of Specimens at RT	Test Method
Longitudinal Tensile Strength	σ_x^{TU}	ksi		≥95.5		± 2.23 / 3	ASTM D-3039
Transverse Tensile Strength	σ_y^{TU}	ksi					ASTM D-3039
Longitudinal Comp. Strength	σ_x^{CU}	ksi		126.3		± 2.59 / 4	ASTM D-3410
Transverse comp. strength	σ_y^{CU}	ksi					ASTM D-3410
In-plane shear strength	IPSS	ksi		15.6		± 1.06 / 2	
Interlaminar shear strength	ILSS	ksi					ASTM D-2344
Longitudinal tensile strain **	ε_x^T	%		0.353			ASTM D-3039
Transverse tensile strain **	ε_y^T	%					ASTM D-3039
Longitudinal comp. strain **	ε_x^C	%		0.655		± 0.44 / 4	ASTM D-3410
Transverse comp. strain **	ε_y^C	%					ASTM D-3410
Longitudinal tensile modulus	E_x	Msi		26.43		±0.25 / 3	ASTM D-3039
Transverse tensile modulus	E_y	Msi					ASTM D-3039
Longitudinal comp. modulus	E_x	Msi		21.3		± 0.45 / 4	ASTM D-3410
Transverse comp. modulus	E_y	Msi					ASTM D-3410
In-plane shear modulus	G	Msi		2.6		± 0.354 / 2	
Longitudinal flexural modulus	F_x	Msi					ASTM D-790M
Transverse flexural modulus	F_y	Msi					ASTM D-790M
Long. tensile Poisson's ratio	ν_{xy}	X		0.227			ASTM D-3039
Trans. tensile Poisson's ratio	ν_{yx}	X					ASTM D-3039
Long. thermal conductivity	K_x	(1)					Kohlrausch
Trans. thermal conductivity	K_y	(1)					Kohlrausch
Thru thickness thermal cond.	K_z	(1)					Laser Flash
Specific heat	C_p	(2)					ASTM E-1269
Longitudinal CTE	α_x	(3)		-0.38			ASTM C-372
Transverse CTE	α_y	(3)					ASTM C-372
Thru thickness CTE	α_z	(3)					

Notes:
(**) - Strain to failure; (1) Btu/(hr·in·°F); (2) Btu/(lb·°F); (3) μin./in./°F

Table 9.3-2 HMU/7070 Carbon/Glass $[0/90]_6$

NOT DESIGN ALLOWABLE DATA

PROPERTIES							TEMPERATURE (°F)			Std. Dev. / No. of Specimens at RT	Test Method
PHYSICAL			MECHANICAL & THERMAL				Low	Room	High		
Density (lb / in^3)		0.071	Longitudinal Tensile Strength	σ_x^{TU}	ksi			≥40.9		±1.971 / 3	ASTM D-3039
Fiber volume fraction		0.40	Transverse Tensile Strength	σ_y^{TU}	ksi						ASTM D-3039
Void volume fraction		≤0.002	Longitudinal Comp. Strength	σ_x^{CU}	ksi			86.7		±4.6 / 3	ASTM D-3410
Nominal ply thickness	in	0.0054	Transverse comp. strength	σ_y^{CU}	ksi			78.4		±14.2 / 2	ASTM D-3410
Max. cont. use temp.	°F	1500	In-plane shear strength	IPSS	ksi						
Ply Orientation	θ	$[0/90]_6$	Interlaminar shear strength	ILSS	ksi			3.35		±0.5 / 3	ASTM D-2344
OPTICAL & ELECTRICAL (at room temperature)			Longitudinal tensile strain **	ε_x^T	%			0.405		±0.07 / 3	ASTM D-3039
Solar Absorptance	α	0.92	Transverse tensile strain **	ε_y^T	%						ASTM D-3039
Normal Emissivity	ε	0.805	Longitudinal comp. strain **	ε_x^C	%						ASTM D-3410
			Transverse comp. strain **	ε_y^C	%						ASTM D-3410
			Longitudinal tensile modulus	E_x	Msi			11.7		±0.839 / 3	ASTM D-3039
			Transverse tensile modulus	E_y	Msi						ASTM D-3039
			Longitudinal comp. modulus	E_x	Msi			12.5		±1.1 / 3	ASTM D-3410
			Transverse comp. modulus	E_y	Msi			11.9		±0.14 / 2	ASTM D-3410
			In-plane shear modulus	G	Msi						
			Longitudinal flexural modulus	F_x	Msi						ASTM D-790M
			Transverse flexural modulus	F_y	Msi						ASTM D-790M
			Long. tensile Poisson's ratio	ν_{xy}				0.033			ASTM D-3039
			Trans. tensile Poisson's ratio	ν_{yx}							ASTM D-3039
			Long. thermal conductivity	K_x	(1)			0.83		±0.002 / 3	Kohlrausch
			Trans. thermal conductivity	K_y	(1)			0.83			Kohlrausch
			Thru thickness thermal cond.	K_z	(1)			0.08			Laser Flash
			Specific heat	C_p	(2)			0.18			ASTM E-1269
			Longitudinal CTE	α_x	(3)			-0.075			ASTM C-372
			Transverse CTE	α_y	(3)						ASTM C-372
			Thru thickness CTE	α_z	(3)						

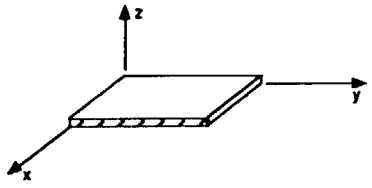

Notes:
(**) - Strain to failure; (1) Btu/(hr·in·°F); (2) Btu/(lb·°F); (3) μin./in./°F

Carbon/Carbon
P100/C

Carbon/Carbon
P100/C

10.0 CARBON/CARBON: P100/C

Future spacecraft and satellites will require lightweight structural materials with high temperature capability, enhanced survivability, and increased thermal and mechanical properties. C/C composites, because of their low density and excellent retention of thermal and mechanical properties at high temperature (≥2000°C), are prime candidate materials for several structural applications in different space systems. The C/C tubes, joints, and stiffened panels are being considered for structural elements of truss and solar array support structures, Mars/Lunar aerobrakes, and avionics/propulsion modules. Also, C/C plates are being developed for survivable thermal radiator and antenna applications. In most of these applications, C/C composites offer an enabling technology, significant mass savings, and improved performance compared to the baseline materials. Therefore, flat panel and tubes with the following fiber orientation:

(1) $[0]_3$ - Unidirectional panel;

(2) [0/90/0] - Bidirectional panel; and

(3) $[0]_3$ - Involute tube

were procured for material property characterization. The fabrication data and the results of product evaluation, mechanical and thermophysical property tests are discussed in this chapter.

10.1 P100/C $[0]_3$ FLAT PANELS

10.1.1 Fabrication Data

Material System:	P100/C
Condition:	As fabricated

Manufacturer:	BP - HITCO, Gardena, CA
Dimensions:	10-in. x 10-in. x 0.052-in
Ply thickness:	0.017-in
Martin Marietta ID:	(CC)(HU)(AP)

Processing Data:

Fabric:

P100/T300 hybrid

P100 warp, 2k fiber, 26 counts/inch

T300 fill, 1k fiber, 10 counts/inch unitized to 93 % by volume P100 in the 0° or warp direction

Resin:

HITCO 134K a Phenolic

Prepregging:

In the impregnator bath, triple roll prepregs were prepared and batch staged in an air circulating oven. These prepregs had about 35% matrix by weight on a solid basis.

Molding:

Autoclave molding of the panels was performed over steel caul plates at 300 psi and 300°F. Specific molding data and processing details are listed in Table 10.1-1.

Carbonization:

To 1000°F in a gas fired oven, taking 96 hours to temperature (linear rise). During the carbonization process, positive pressure was maintained because of the presence of N_2 gas.

Table 10.1-1 Processing Data for P100/Carbon Panels

	[0/0/0]	
Molding Data:	Panel #1	Panel #2
Dry Weight (g.)	83.349	83.349
Post-Mold Weight (g.)	141.011	140.066
Post-Mold P/U (%)	40.892	40.493
Fiber Volume (%)	46.638	47.050
Wall Thick. (in.)	0.050	0.051
Length (in.)	10.500	10.500
Width (in.)	10.500	10.500
Post-Carb Data:		
Pre-Carb Wt. (g.)	141.011	140.066
Post-Carb Wt. (g.)	110.903	109.785
Weight Loss (%)	21.352	21.619
Wall Thick. (in.)	0.049	0.050
Length (in.)	10.500	10.500
Width (in.)	10.500	10.500
Post-CVD Data:		
Pre-CVD Wt. (g.)	110.903	109.785
Post-CVD Wt. (g.)	157.069	156.297
Weight Gain (%)	41.627	42.366
Fiber Volume (%)	52.479	52.741
Wall Thick. (in.)	0.052	0.052
Length (in.)	10.500	10.500
Width (in.)	10.500	10.500

Pyrolysis:

To 2000°F, in an induction heated furnace under N_2.

Chemical Vapor Infiltration (CVI):

HITCO's proprietary conditions for 125 hours using methane gas deposition. Each component was held in fixturing to prevent warpage inside the induction furnace.

10.1.2 Product Evaluation

(a) Density

• P100/C $[0]_3$

Density: 0.060 lb/in^3

Std. Dev.: 0.0001

(b) Fiber Volume

v/o: 52.48

Std. Dev.: 0.5

Void Volume: 8.0% (data provided by the manufacturer)

(c) Non-Destructive Evaluation

On visual examination, the panel revealed the fabric pattern, indicating that P100-2k tows were woven along the warp direction. Also, the carbon matrix had well infiltrated into the edges and the spaces between each fiber tows. X-radiographs of the panels also revealed the woven pattern with microvoids dispersed at almost each warp/fill intersection. The X-radiographic inspection indicated an overall good consolidation quality with no major voids or cracks in the panels.

(d) Microstructure

Typical microstructure of the $[0]_3$ C/C is shown in Figure 10.1-1, which reveals randomly distributed microvoids (i.e., ≈ 10μm dia) within the fiber bundles, and large voids (~400 μm dia) at the warp/fill intersecting regions. The photomicrograph also shows that each fiber bundle is bonded to the adjacent bundle through a thin amorphous carbon film. Microstructural examination of various regions of the panel revealed only a few broken fibers, thus indicating the good quality of weaving and subsequent material handling.

10.1.3 Mechanical Properties

(a) Tension

Longitudinal and transverse tensile test results of the unidirectional P100/C are listed in Table 10.1-2 and 10.1-3 respectively. The longitudinal (warp) tensile modulus of 43.7 Msi was in agreement with the predicted value of 48 Msi; and the average tensile strength value of 81.5 indicated that the adequate fiber-matrix bond integrity was obtained by the CVI process. The tensile stress strain response (Figure 10.1-2) exhibited a deviation from linear elastic response at about 0.1% strain and 45 ksi stress. Often this deviation from linearity at this proportional limit stress is associated with the initiation of matrix cracking.

In the transverse (fill) direction, both the modulus (1.45 Msi) and strength (2.04 ksi) were significantly lower than the values in the longitudinal direction, thus indicating the anisotropic behavior of the unidirectional specimens. Basically, the transverse tensile strength was influenced by the fiber/matrix bond strength in the fill directions.

(b) Compression

Longitudinal and transverse compression tests results of P100/C $[0]_3$ specimens are presented in Table 10.1-4 and 10.1-5 respectively. The longitudinal compressive modulus (39.4 Msi) was

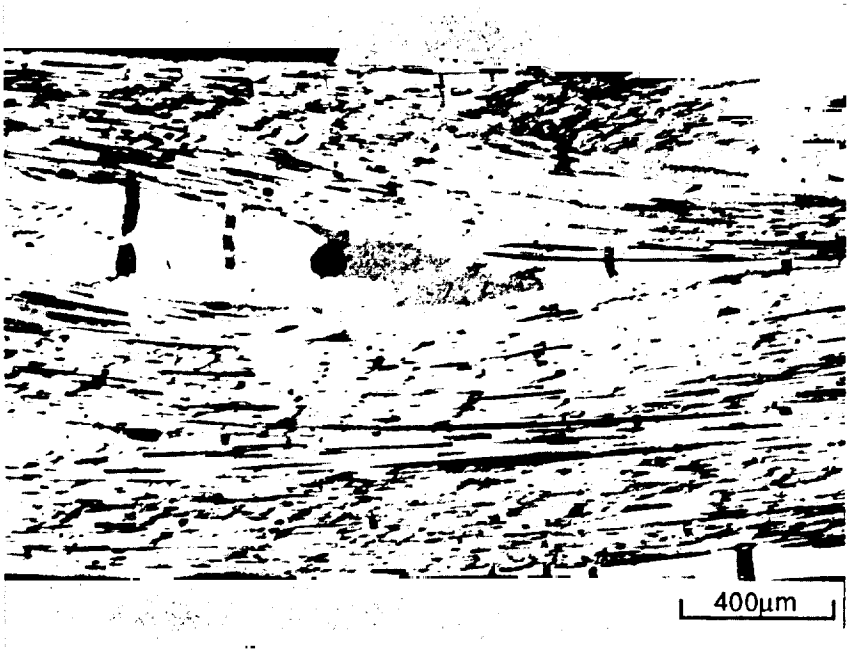

Figure 10.1-1 Longitudinal Photomicrograph of P100/C $[0]_3$ Showing Randomly Dispersed Microvoids Within the Fiber Bundles and Large Voids at the Warp/Fill Intersections

Table 10.1-2 Longitudinal Tensile Properties of Unidirectional P100/C, v/o = 52.48

Specimen # (CC)(HU)(AP)	Elastic Modulus E_x^T (Msi)	Ultimate Tensile Strength (ksi)	Poisson Ratio ν_{xy}	Strain To Failure (%)
TNL-1	40.5	77.0	0.4127	0.244
TNL-2	43.8	82.3	0.2657	0.214
TNL-3	47.0	84.4	0.32	0.215
TNL-4	43.6	82.4	0.4776	0.22
Mean Value	43.7	81.5	0.3690	0.225
Std. Dev.	2.66	3.17	0.0945	0.0165
CV (%)	6.1	3.9	25.6	7.4

Table 10.1-3 Transverse Tensile Properties of Unidirectional P100/C, v/o = 52.48

Specimen # (CC)(HU)(AP)	Elastic Modulus E_y^T (Msi)	Ultimate Tensile Strength (ksi)	Poisson Ratio ν_{yx}	Strain To Failure (%)
TNT-1	1.0	2.04	0.0347	0.278
TNT-2	1.9	2.04	0.0544	0.137
Mean Value	1.45	2.04	0.0446	0.208
Std. Dev.	0.636	0.0	0.0139	0.099
CV (%)	44.0	0.0	31.2	47.9

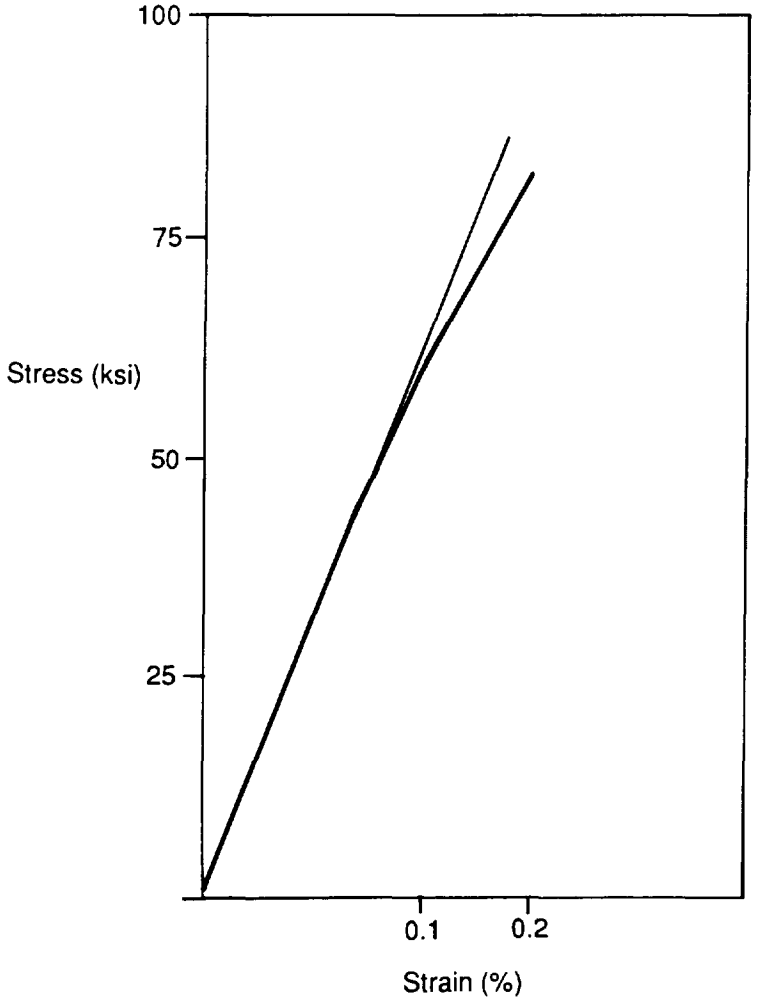

Figure 10.1-2 Typical Tensile Stress-Strain Response for P100/Carbon $[0]_2$

Table 10.1-4 Longitudinal Compressive Properties of Unidirectional P100/C, v/o = 52.48

Specimen # (CC)(HU)(AP)	Elastic Modulus E_x^C (Msi)	Ultimate Comp. Strength (ksi)	Poisson Ratio ν_{xy}	Strain To Failure (%)
CML-1	40.8	—	—	—
CML-2	32.9	43.7	0.5994	—
CML-3	43.9	53.7	0.6818	0.138
CML-4	39.7	59.3	0.5748	0.097
CML-5	39.5	34.5	—	0.157
Mean Value	39.4	47.8	0.6186	0.131
Std. Dev.	4.02	10.97	0.056	0.031
CV (%)	10.2	22.9	9.0	23.4

Table 10.1-5 Transverse Compressive Properties of Unidirectional P100/C, v/o = 52.48

Specimen # (CC)(HU)(AP)	Elastic Modulus E_y^C (Msi)	Ultimate Comp. Strength (ksi)	Poisson Ratio ν_{yx}	Strain To Failure (%)
CMT-1	—	—	—	—
CMT-2	1.6	5.0	0.1143	0.31
CMT-3	1.6	4.6	0.0814	0.20
CMT-4	1.2	4.2	0.0706	0.34
CMT-5	1.6	4.7	—	0.24
Mean Value	1.3	4.6	0.0888	0.27
Std. Dev.	0.473	0.33	0.0228	0.064
CV (%)	36.4	7.2	25.6	23.7

slightly lower than tensile modulus (43.7 Msi), and the compressive strength was about 58% of the tensile strength. The compressive strength was governed by the combined effect of fiber-microbuckling, and matrix shearing at the interfaces. Compared to the longitudinal compressive properties, the transverse compressive modulus and strength values were nearly identical to the corresponding tensile test values.

(c) In-plane Shear

Of the three specimens that were prepared to determine the in-plane shear properties by 10° off-axis test method, two were damaged during handling. Based on the measurements of only one specimen, the composite exhibited in-plane shear modulus value of 1.44 Msi and shear strength value of 4.93 ksi, which were consistent with the predicted values.

(d) Interlaminar Shear

The results of interlaminar shear strength measurements for P100/C $[0]_3$ are listed in Table 10.1-6. These results showed a significant variation in the short beam shear strength values between the warp and fill directions. In the warp (longitudinal) direction, the average interlaminar shear strength value was 3.47 ksi as compared to the 0.419 ksi in the fill direction. The post failure examination of the fill direction specimen indicated a distinctively interlaminar failure, whereas the failure mode in the warp direction specimens exhibited primarily a compressive failure mode. It is likely that if the specimens were thicker than 0.052-in. then the failure mode would shift to interlaminar type.

10.1.4 Thermophysical Properties

(a) Coefficient of Thermal Expansion

The warp and fill direction thermal expansion response of P100/C $[0]_3$ is shown in Figure 10.1-3 and 10.1-4 respectively. Based on these measurements, the CTE, RT hysteresis, and residual

Table 10.1-6 Apparent Interlaminar (Short Beam Shear) Shear Strength of P100/Carbon [0,0,0]

Specimen #	P100/C [0, 0, 0]
CC-HU-AP	Short Beam Shear Strength psi
• Warp	
— SBL1	3,621
— SBL2	3,557
— SBL3	3,433
— SBL4	3,327
— SBL5	3,398
• Warp Mean Value	3,467.2
• Fill	
— SBT6	421
— SBT7	510
— SBT8	401
— SBT9	366
— SBT10	396
• Fill Mean Value	418.8

Table 10.1-7 Thermal Expansion Properties of P100/Carbon

Thermal Expansion Properties*	P100/C [0, 0, 0]	
	Warp	Fill
Average CTE (ppm/°F) (end point to end point)	-0.98	-0.42†
RT Hysteresis (ppm)	-19.25	-21.4
Residual Thermal Strain After First Cycle (ppm)	0	0

* between -150° and 150°F

† between -112° and 150°F; from -112°F to 150°F the specimen showed a slight expansion yielding average CTE - 0.28 ppm/°F

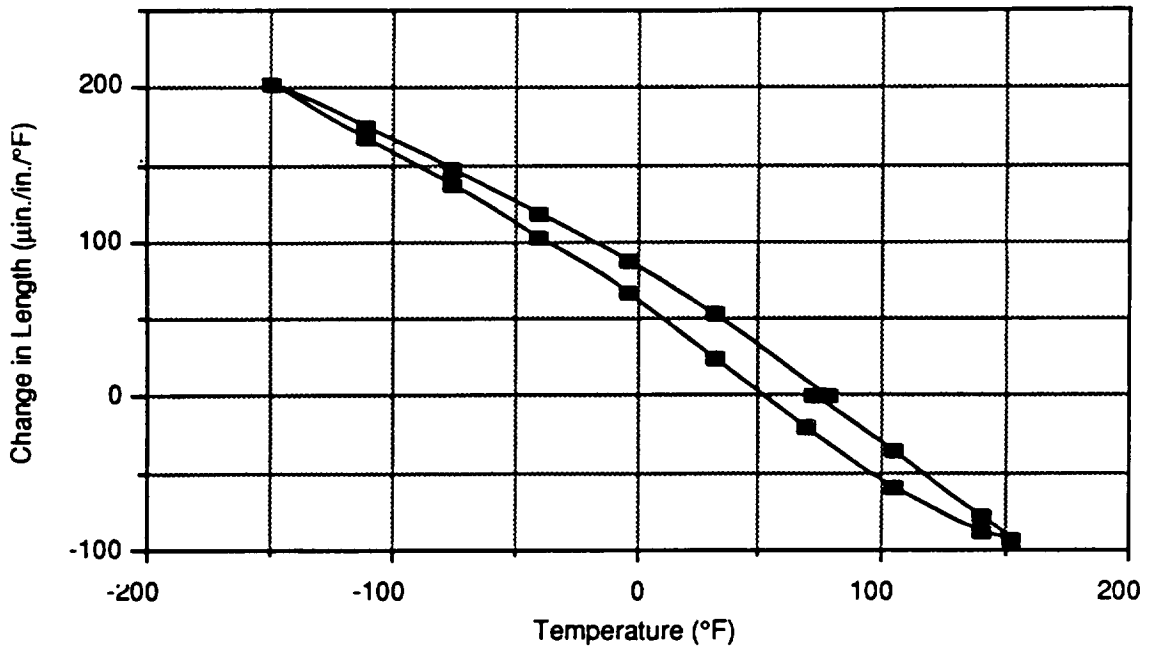

Figure 10.1-3 Thermal Expansion Response of Unidirectional P100/Carbon (Total Fiber Volume = 52.48% with 93% by Volume P100 Along Warp) in the Warp Direction

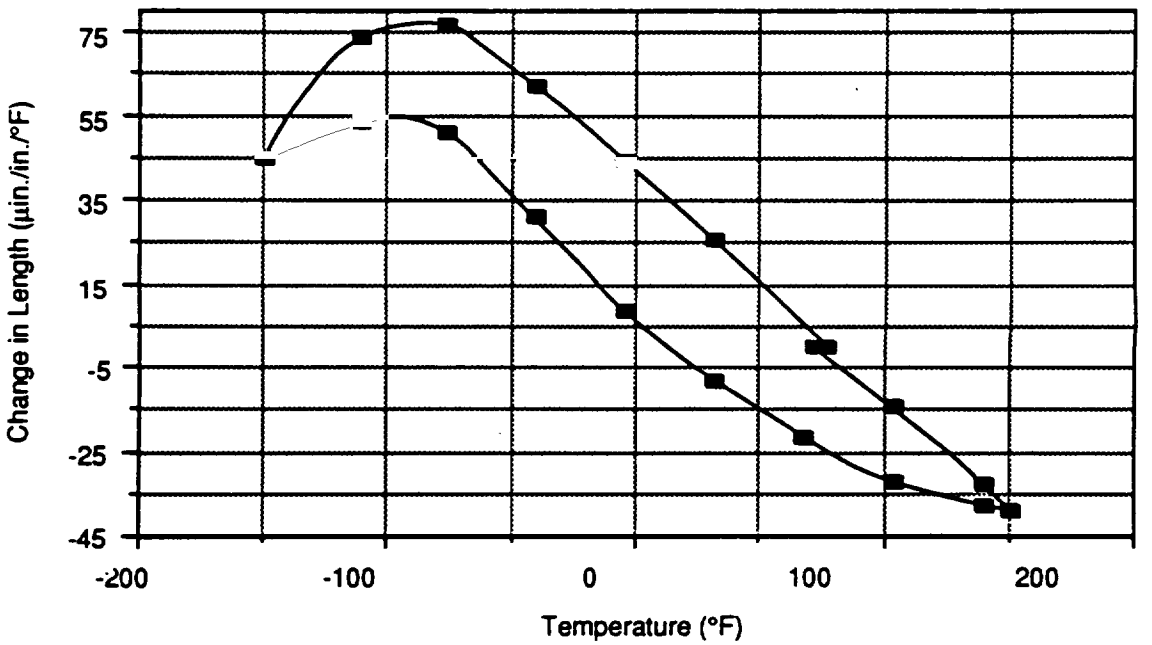

Figure 10.1-4 Thermal Expansion Response of Unidirectional P100/Carbon in the Fill Direction

strain values are presented in Table 10.1-7. Both the warp and fill direction specimens exhibited zero residual strain, yielding: CTE_x (warp) = -0.98 ppm/°F and CTE_y (fill) = -0.42 ppm/°F.

(b) Thermal Conductivity

In-plane thermal conductivity results of P100/C $[0]_3$ are listed in Table 10.1-8 and plotted in Figure 10.1-5. As expected, the warp direction thermal conductivity value of 118.3 Btu/hr·ft·°F was significantly higher than the fill direction value of 4.6 Btu/hr·ft·°F. Although, the conductivity in the warp direction was high due to the inherently high conductivity of P100 (i.e., 300 Btu/hr·ft·°F), but it was lower than the predicted value of 150 Btu/hr·ft·°F because of the presence of 8% void volume in the composite.

(c) Electrical Resistivity (ρ_e)

Along with the thermal conductivity values, Table 10.1-8 also lists the electrical resistivity values, as obtained by the Kohlrausch method. These results indicate that the fill direction resistivity values are significantly higher than the warp direction. The typical values at RT were:

(ρ_e) warp = 564 μohms·cm

(ρ_e) fill = 8350 μohms·cm

10.2 P100/C [0/90/0] FLAT PANEL

10.2.1 Fabrication Data

Material System:	P100/C
Fiber Layup:	[0/90/0]
Condition:	As fabricated

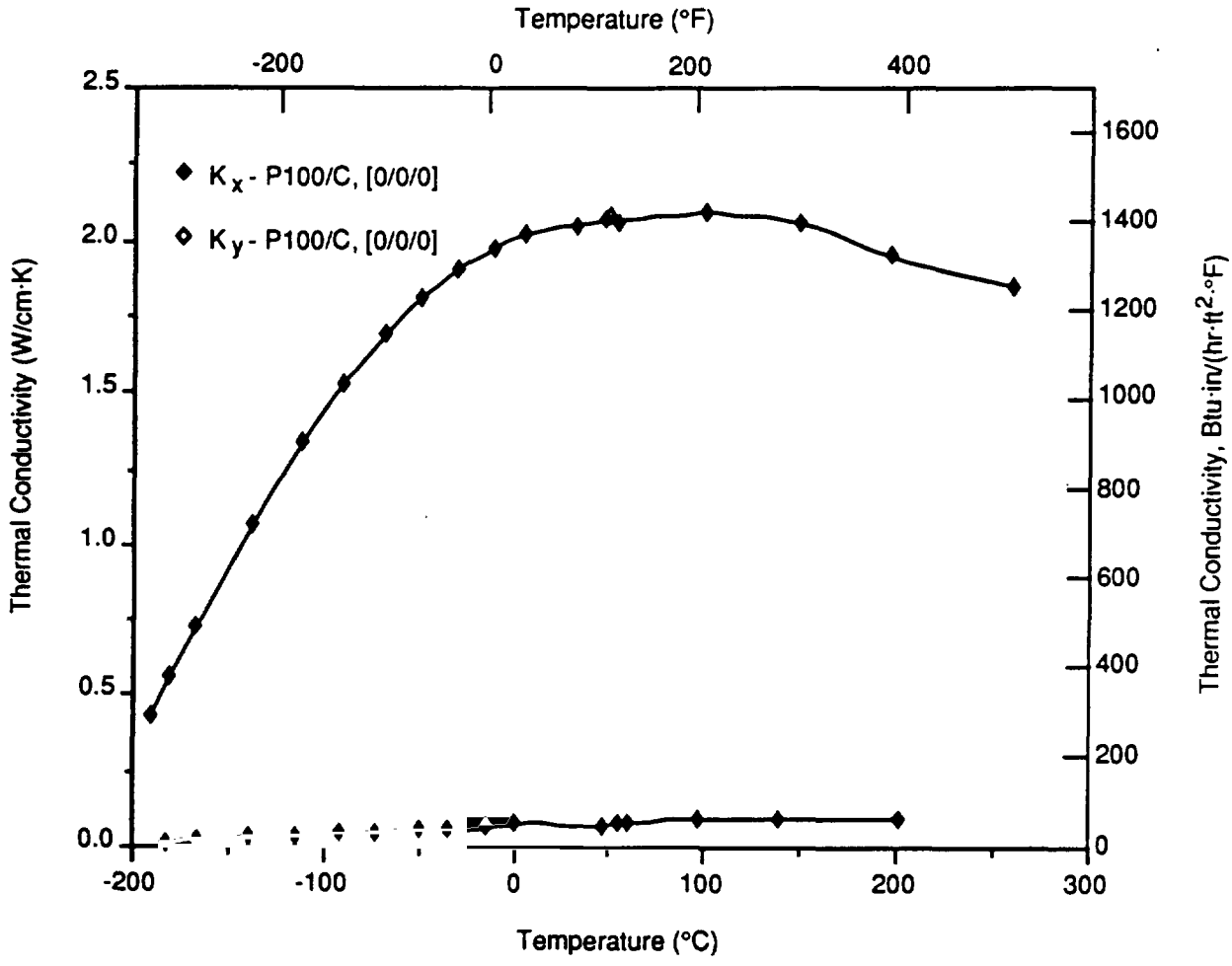

Figure 10.1-5 Thermal Conductivity of [0/0/0] P100/Carbon

Table 10.1-8 Inplane Thermal Conductivity and Electrical Resistivity Results of P100/Carbon [0,0,0]

Sample Designation	Temp. (°C)	Conductivity ($W \cdot cm^{-1} K^{-1}$)	Resistivity (microhms·cm)	Conductivity ($BTU \cdot in \cdot hr^{-1} ft^{-2} F^{-1}$)	Temp. (°F)
CC-HU-TKL (Warp)	32	2.048	563.74	1419.97	90
	50	2.078	549.00	1440.78	122
	-191	0.430	889.25	298.14	-312
	-181	0.556	869.76	385.50	-294
	-167	0.724	840.90	501.98	-269
	-138	1.067	784.66	739.80	-216
	-112	1.335	739.47	926.62	-170
	-90	1.531	704.35	1061.51	-130
	-68	1.692	673.56	1173.14	-90
	-49	1.810	648.59	1254.96	-56
	-30	1.903	625.92	1319.44	-22
	-12	1.971	606.01	1366.59	10
	4	2.014	589.18	1396.40	39
	46	2.069	553.38	1434.53	115
	53	2.056	546.70	1425.52	127
	99	2.085	515.62	1445.63	210
	148	2.054	488.87	1424.13	298
	195	1.943	468.82	1347.17	383
	259	1.844	447.69	1278.53	498
CC-HU-TKT (Fill)	55	0.080	8364.90	55.33	131
	-183	0.014	9962.60	9.78	-297
	-166	0.021	9832.80	14.63	-267
	-139	0.030	9637.60	20.94	-218
	-114	0.038	9464.40	26.69	-173
	-91	0.044	9303.60	30.51	-132
	-72	0.051	9168.40	35.22	-98
	-50	0.056	9013.10	39.10	-58
	-35	0.059	8915.30	41.12	-31
	-14	0.065	8767.30	45.07	7
	0	0.068	8673.70	46.80	322
	47	0.077	8357.20	53.39	117
	60	0.074	8367.80	51.24	140
	97	0.086	8130.10	59.28	207
	139	0.090	7873.00	62.54	282
	201	0.094	7493.20	65.52	394
	254	0.095	7190.10	66.01	489

Manufacturer:	BP - HITCO, CA
Dimensions:	10-in. x 10-in. x 0.052-in
Ply thickness:	0.017-in
Martin Marietta ID:	(CC)(HB)(AP)
Processing Data:	Similar to unidirectional, bidirectional panels were also fabricated by using the P100/T300 hybrid fabric, and similar processing conditions. Specific molding data and processing details are listed in Table 10.2-1.

Table 10.2-1 Processing Details of the [0, 90, 0] P100/Carbon Panels

Molding Data:	[0/90/0] Panel #3	Panel #4
Dry Weight (g.)	83.349	83.349
Post-Mold Weight (g.)	140.378	141.599
Post-Mold P/U (%)	40.625	41.137
Fiber Volume (%)	46.913	46.386
Wall Thick. (in.)	0.050	0.052
Length (in.)	10.500	10.500
Width (in.)	10.500	10.500
Post-Carb Data:		
Pre-Carb Wt. (g.)	140.378	141.599
Post-Carb Wt. (g.)	108.890	109.037
Weight Loss (%)	22.431	22.996
Wall Thick. (in.)	0.048	0.050
Length (in.)	10.500	10.500
Width (in.)	10.500	10.500
Post-CVD Data:		
Pre-CVD Wt. (g.)	108.890	109.037
Post-CVD Wt. (g.)	154.640	157.079
Weight Gain (%)	42.015	44.060
Fiber Volume (%)	53.314	52.475
Wall Thick. (in.)	0.051	0.053
Length (in.)	10.500	10.500
Width (in.)	10.500	10.500

10.2.2 Product Evaluation

(a) Density

• P100/C [0/90/0]

Density: 0.060 lb/in^3

Std. Dev.: 0.0005

(b) Fiber Volume

v/o: 53.0

Std. Dev.: 0.5

Void Volume: 8.0% (data provided by the manufacturer)

(c) Non-Destructive Evaluation

On visual examination, the panel revealed the surface texture of the typical woven fabric with shiny carbon matrix around the fiber bundles. An examination of the panel edges indicated the 0/90/0 stacking sequence with adequate matrix infiltration. X-radiographs of the panels revealed the randomly distributed microvoids in the woven fabric pattern.

(d) Microstructure

Typical microstructure of the C/C [0/90/0] is shown in Figure 10.2-1, which reveals the bidirectional stacking sequence and microvoids within each fiber bundle. In addition to the microvoids (10 μm), the larger voids of the size between 50-400 μm were observed at the interfaces between various fiber bundles and warp/fill intersections.

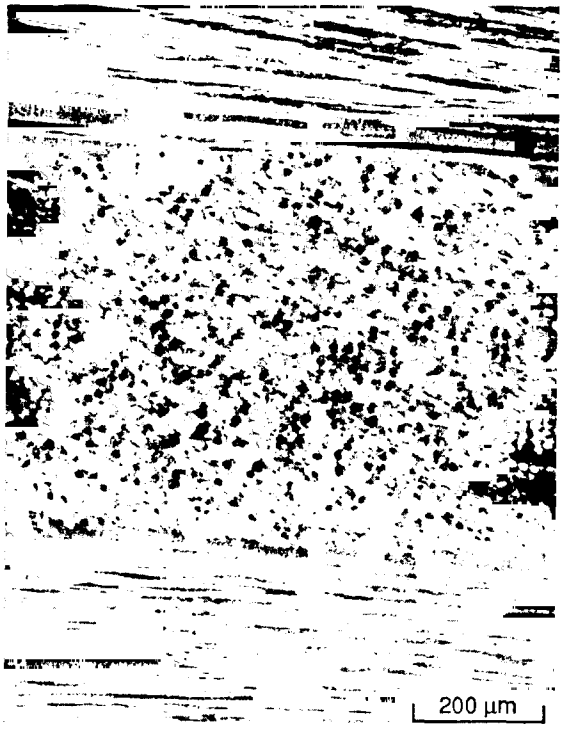

Figure 10.2-1 Typical Photomicrograph of P100/Carbon [0, 90, 0] Showing Microvoids Dispersed Within the Laminate

10.2.3 Mechanical Property Tests

(a) Tension

Longitudinal (warp) and transverse (fill) tensile test data of P100/C [0/90/0] is presented in Tables 10.2-2 and 10.2-3 respectively. Because of the limited panel size, only four longitudinal and one transverse specimen were available for tension tests. The measured warp tensile modulus value of 32.4 Msi was in excellent agreement with the predicted value of 33.0 Msi. Also, the fill tensile modulus of 20.3 Msi was close to the expected value of 16.5 Msi, but more specimen should be tested to obtain the average modulus value. The good agreement between the measured and predicted tensile properties indicated that the adequate interfacial bond was attained during the composite processing.

Table 10.2-2 Longitudinal (Warp) Tensile Properties of [0/90/0] P100/C, v/o = 53.0

Specimen # (CC)(HB)(AP)	Elastic Modulus E_x^T (Msi)	Ultimate Tensile Strength (ksi)	Poisson Ratio ν_{xy}	Strain To Failure (%)
*TNL-1	-	35.1	-	-
TNL-2	32.7	44.8	0.1809	0.15
TNL-3	31.0	48.8	0.1161	0.189
TNL-4	33.5	47.6	0.1404	0.161
Mean Value	32.4	44.1	0.1458	0.167
Std. Dev.	1.28	6.21	0.0327	0.02
CV (%)	3.9	14.1	22.5	12.0

* Specimen Bending, Modulus Data Invalid

Table 10.2-3 Transverse (Fill) Tensile Properties of [0/90/0] P100/C, v/o = 53.0

Specimen # (CC)(HB)(AP)	Elastic Modulus E_y^T (Msi)	Ultimate Tensile Strength (ksi)	Poisson Ratio ν_{yx}	Strain To Failure (%)
TNT-1	20.3	29.0	0.1	> 0.15

* One Specimen, Panel Size Was Small To Obtain More Specimens

(b) Compression

Compression test results of the bidirectional specimens are listed in Tables 10.2-4 and 10.2-5. The composite exhibited warp and fill modulus values of 29.1 and 15.5 Msi respectively, which were consistent with the corresponding tensile moduli. The compressive strength values in both the directions were between 6 and 9 ksi.

(c) Flexure

Warp and fill flexural properties of the bidirectional C/C panel are listed in Table 10.2-6. Based on these measurements the flexural strength in the warp direction was three times higher than in the fill direction, because of the deformation resistance offered by the outer [0] ply.

(d) Interlaminar Shear

The short beam shear test results of the bidirectional panels are listed in Table 10.2-7. These results showed that warp direction ILSS value was about twice of the strength value in the fill direction. While the short beam shear test was used to estimate the apparent ILSS, the failure mode in nearly all the specimens was the combination of compression and shear crippling rather than interlaminar shear.

10.2.4 Thermophysical Properties

(a) Coefficient of Thermal Expansion

The warp and fill direction thermal expansion responses of P100/C [0/90/0] specimens are shown in Figures 10.2-2 and 10.2-3 respectively. Based on these responses, the average CTE results are summarized in Table 10.2-8. In both directions, the composite exhibited the identical behavior, with the $CTE_x = CTE_y$ =-0.95 ppm/°F, and negligible residual strain (-6.3 ppm) at the end of the first cycle.

Table 10.2-4 Longitudinal (Warp) Compressive Properties of [0/90/0] P100/Carbon

Specimen # (CC)(HB)(AP)	Elastic Modulus E^{C}_{x} (Msi)	Ultimate Comp. Strength (ksi)
CML-1	34.3	5.6
CML-2	24.4	5.6
CML-3	30.0	9.4
CML-4	27.5	6.6
CML-5	25.1	7.5
Mean Value	29.1	6.95
Std. Dev.	5.7	1.58
CV (%)	19.58	22.7

Table 10.2-5 Transverse (Fill) Compressive Properties of [0/90/0] P100/Carbon

Specimen # (CC)(HB)(AP)	Elastic Modulus E^{C}_{y} (Msi)	Ultimate Comp. Strength (ksi)
CMT-1	19.9	8.4
CMT-2	—	—
CMT-3	13.8	8.4
CMT-4	12.9	11.4
CMT-5	—	—
Mean Value	15.5	9.4
Std. Dev.	3.8	1.73
CV (%)	24.5	18.4

Table 10.2-6 Warp and Fill Flexural Properties (3 Point Bend) of Bidirectional P100/C

Carbon-Carbon (0, 90, 0)	Flexural Strength (ksi)	Carbon-Carbon (0, 90, 0)	Flexural Strength (ksi)
Specimen #		Specimen #	
CC-B-HP: Warp		CC-B-HP: Fill	
FXL-1	28.6	FXT-1	10.4
FXL-2	30.1	FXT-2	10.6
FXL-3	31.2	FXT-3	8.5
Mean Value	30.0		9.8
Std. Dev.	1.31		1.16
Coef. of Var (%)	4.4		11.8

Table 10.2-7 Apparent Interlaminar (Short Beam Shear) Shear Strength of [0/90/0] P100/C

Specimen #	P100/C [0/90/0]
CC-HB-AP	Short Beam Shear Strength psi
• Warp — SBL6 — SBL7 — SBL8 — SBL9 — SBL10	 1,937 1,798 1,970 2,145 1,952
• Warp Mean Value	1960.4
• Fill — SBT1 — SBT2 — SBT3 — SBT4 — SBT5	 949 998 943 891 846
• Fill Mean Value	925.4

Table 10.2-8 Thermal Expansion Properties of [0/90/0] P100/Carbon

Thermal Expansion Properties*	P100/C [0/90/0]	
	Warp	Fill
Average CTE (ppm/°F) (end point to end point)	-0.95	-0.95
RT Hysteresis (ppm)	-33.07	-29.8
Residual Thermal Strain After First Cycle (ppm)	-6.346	-7.1

* between -150° and 150°F

† between -112° and 150°F; from -112°F to 150°F the specimen showed a slight expansion yielding average CTE - 0.28 ppm/°F

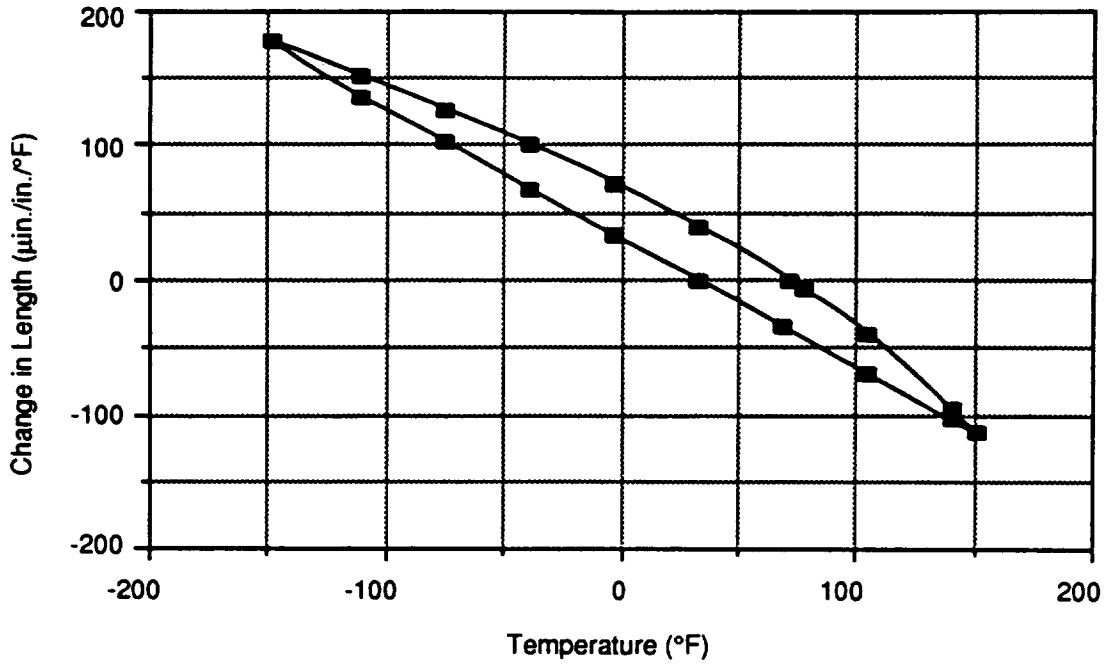

Figure 10.2-2 Thermal Expansion Response of [0/90/0] P100/Carbon, v/o = 53.0, Along the Warp Direction

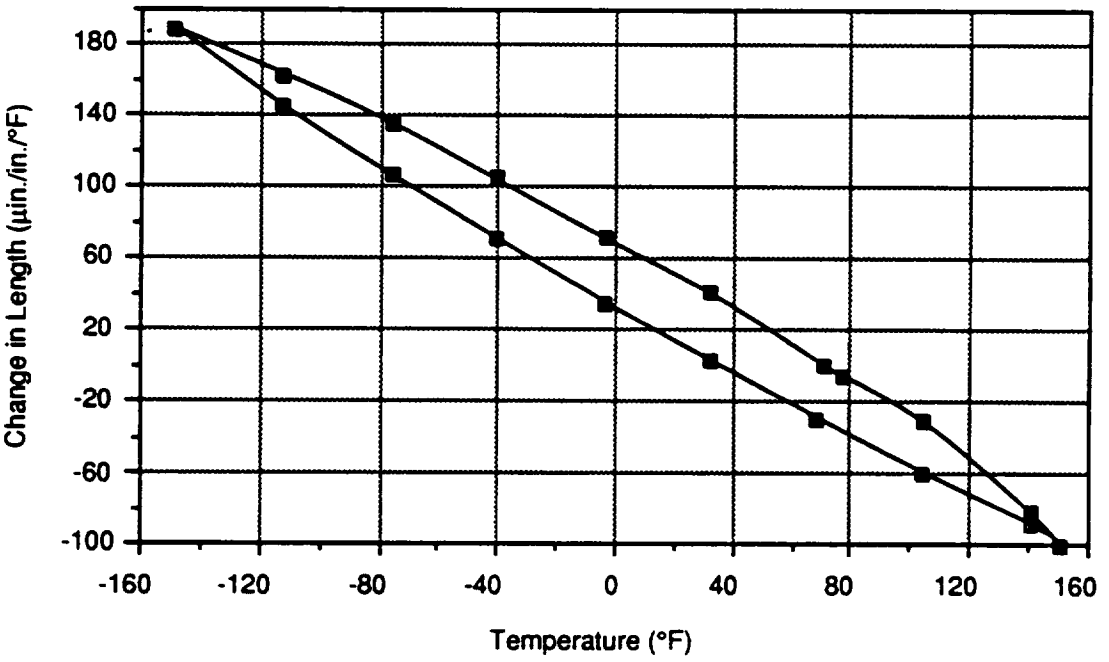

Figure 10.2-3 Thermal Expansion Response of [0/90/0] P100/Carbon, v/o = 53.0, Along the Fill Direction

(b) Specific Heat and Thermal Diffusivity

Specific heat and thermal diffusivity results are plotted in Figures 10.2-4 and 10.2-5 respectively. Typical RT Cp value was 0.169 Btu/lb·°F, which was close to the value for POCO graphite. Both the Cp and thermal diffusivity measurements above RT were obtained by using an infra-red detector for temperature measurements. Below RT, the temperature measurements are obtained by using a thermocouple. But, a good thermocouple contact with the surface to yield accurate results was difficult due to the surface roughness and low thickness (which leads to rapid rise times) of the specimens.

(c) Thermal Conductivity

In-plane and through-the-thickness thermal conductivity values at temperatures between -300°F and 500°F are presented in Table 10.2-9 and 10.2-10 respectively and plotted in Figure 10.2-6. These results indicate that the warp direction conductivity was about two times higher then the fill direction conductivity. At the RT, the typical in-plane conductivity values were:

K_x = 82 Btu/hr·ft·°F

K_y = 39 Btu/hr·ft·°F

Compared to K_x and K_y, the K_z value was significantly low (at RT K_z = 3.25 Btu/hr·ft·°F) and was similar to the K_z values obtained for unidirectional P100/C.

(d) Electrical Resistivity

In-plane electrical resistivity values of bidirectional P100/C are listed in Table 10.2-9. Based on these measurements, the resistivity in the fill direction was nearly two times higher than the warp direction resistivity.

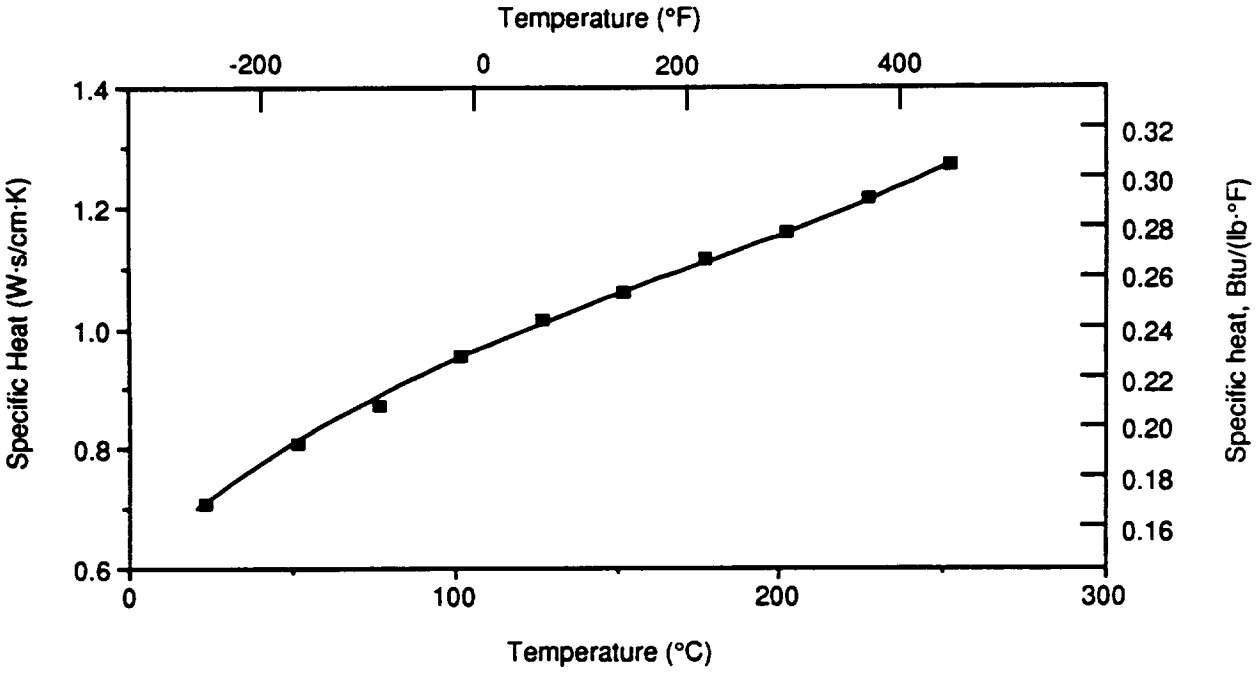

Figure 10.2-4 Specific Heat of [0/90/0] P100 Carbon/Carbon

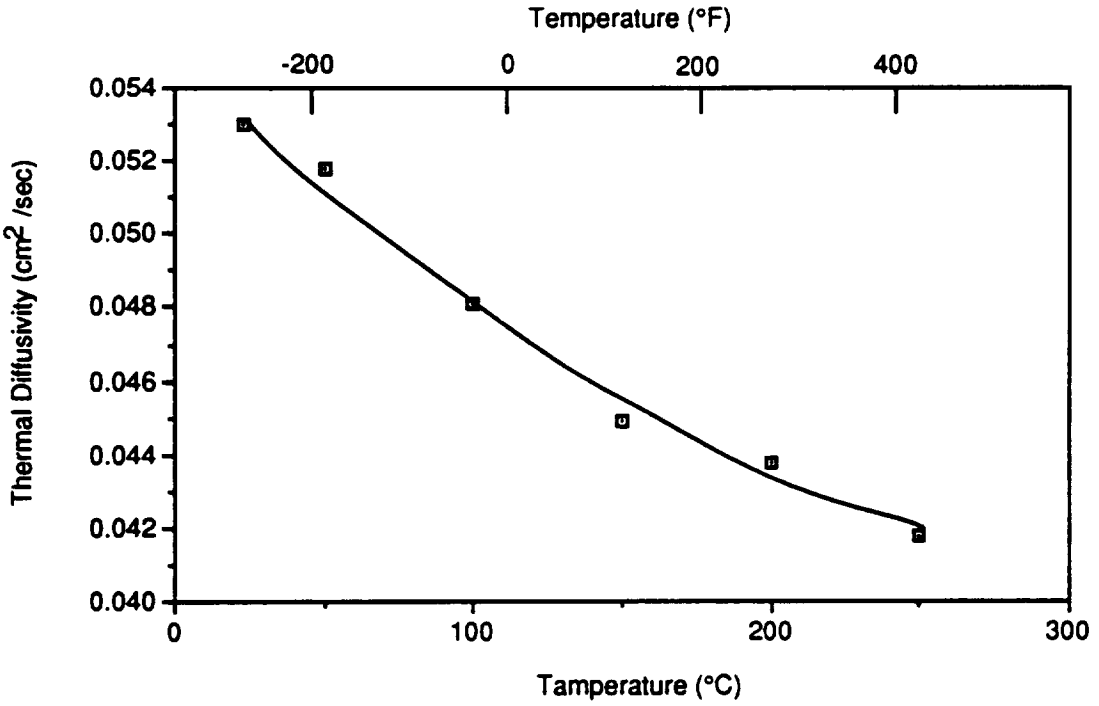

Figure 10.2-5 Thermal Diffusivity of [0/90/0] P100/Carbon

Table 10.2-9 Inplane Thermal Conductivity and Electrical Resistivity Results of P100/Carbon [0/90/0]

Sample Designation	Temp. (°C)	Conductivity ($W \cdot cm^{-1} K^{-1}$)	Resistivity (microhms·cm)	Conductivity ($BTU \cdot in \cdot hr^{-1} ft^{-2} F^{-1}$)	Temp. (°F)
CC-HB-TKL (Warp)	36	1.368	825.97	948.50	97
	56	1.420	802.28	984.55	133
	-192	0.284	1296.70	196.91	-314
	-180	0.461	1261.70	319.63	-292
	-168	0.552	1227.40	382.73	-270
	-135	0.811	1138.20	562.30	-211
	-116	0.946	1089.70	655.91	-177
	-85	1.124	1018.90	779.32	-121
	-66	1.221	983.02	846.58	-87
	-46	1.298	945.72	899.96	-51
	-27	1.348	913.81	934.63	-17
	-8	1.392	884.81	965.14	18
	9	1.419	860.61	983.86	48
	55	1.454	804.25	1008.13	131
	50	1.447	809.70	1003.27	122
	121	1.440	742.97	998.42	250
	152	1.423	719.40	986.63	306
	208	1.332	685.62	923.54	406
	261	1.276	660.57	884.71	502
CC-HB-TKT (Fill)	31	0.661	1577.30	458.30	88
	53	0.683	1529.30	473.56	127
	-194	0.150	2431.60	104.00	-317
	-180	0.204	2360.50	141.44	-292
	-166	0.259	2287.70	179.58	-267
	-140	0.353	2163.40	244.75	-220
	-109	0.454	2027.50	314.78	-164
	-91	0.504	1953.70	349.45	-132
	-68	0.559	1867.70	387.58	-90
	-52	0.593	1810.20	411.15	-62
	-31	0.626	1742.70	434.04	-24
	-15	0.645	1697.30	447.21	5
	4	0.664	1645.20	460.38	39
	41	0.682	1558.90	472.86	106
	30	0.664	1585.10	460.38	86
	49	0.670	1542.60	464.54	120
	103	0.688	1443.70	477.02	217
	145	0.687	1381.20	476.33	293
	199	0.650	1315.90	450.68	390
	254	0.626	1263.50	434.04	489

Table 10.2-10 Calculated Through Thickness Thermal Conductivity of [0/90/0] P100Carbon

Sample (No.)	Temp. (°C)	Density (gm cm^3)	Specific Heat (W·s/(gm·K)	Diffusivity (cm^2 ·sec)	Conductivity (W/(cm·K)	Conductivity (BTU units*)	Temp. (°F)
0/90/0-THR	23.0	1.504	0.7080	0.05300	0.05644	39.13	73.4
0/90/0-THR	50.0	1.504	0.8060	0.05180	0.06279	43.54	122.0
0/90/0-THR	100.0	1.504	0.9510	0.04810	0.06880	47.70	212.0
0/90/0-THR	150.0	1.504	1.0570	0.04490	0.07138	49.49	302.0
0/90/0-THR	200.0	1.504	1.1570	0.04380	0.07622	52.85	392.0
0/90/0-THR	250.0	1.504	1.2680	0.04180	0.07972	55.27	482.0

*(BTU·in/(hr·ft^2 ·°F)

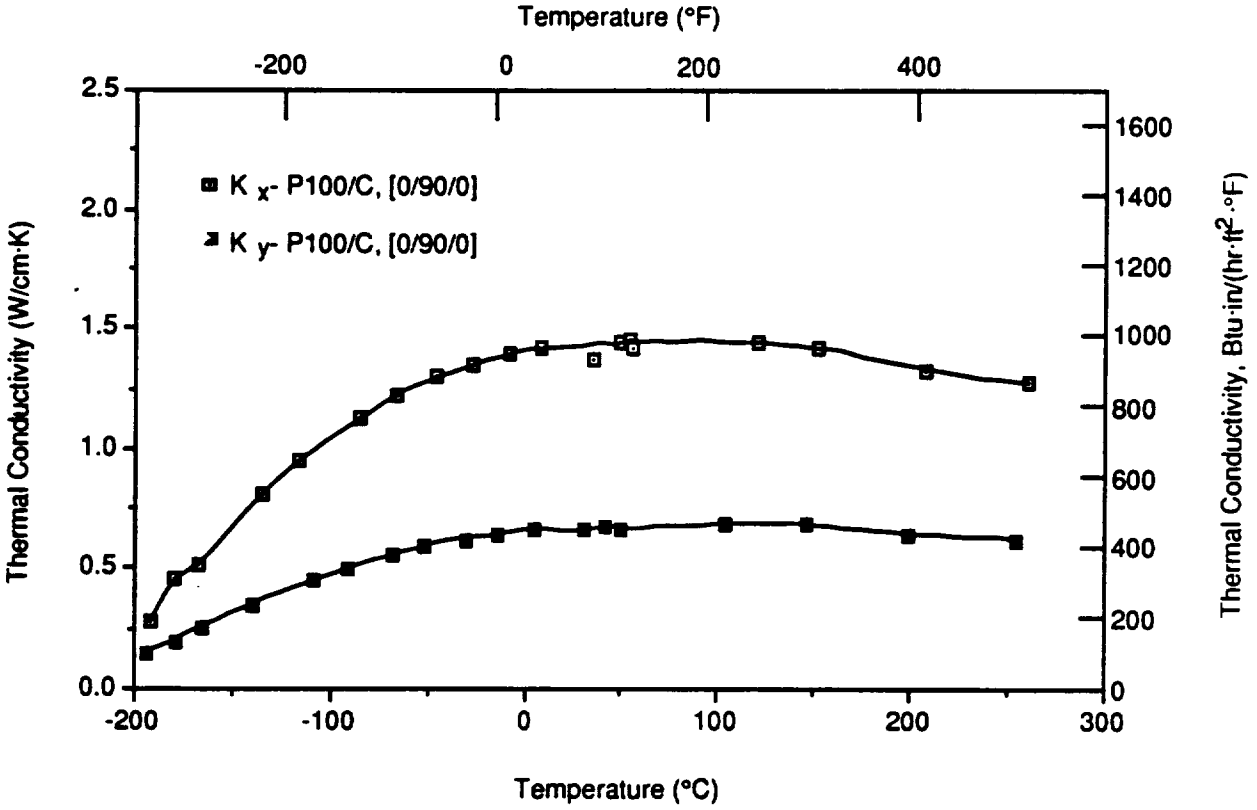

Figure 10.2-6 Thermal Conductivity of [0/90/0] P100/Carbon

(e) Optical Properties

• Total Hemispherical Emissivity—Results of the total hemispherical emissivity measurements between 234°F and 482°F are as follows:

Temperature (°C)	Temperature (°F)	Emissivity
112	234	0.673
115	311	0.675
205	401	0.675
250	482	0.676

These emissivity values are more akin to pyrolytic graphite than graphite rods or strips.

• Reflectance vs. Wavelength (0.24 - 14.0 micron)—Diffuse reflectance spectrum from as processed bidirectional C/C surface was obtained between 0.24 - 14.0 μm. The spectrum from 0.24 - 2.5 microns was collected on Beckman DK-2A spectrometer with a Halon coated integrating sphere. Based on these measurements, the average reflectance was 26% at 0.24 μm, 35% at 2 μm, and 37% at 2.5 μm. The spectrum from 2.5 - 14.0 microns was collected on the Mattson Polaris spectrophotometer with a diffuse gold integrating sphere and it is shown in Figure 10.2-7.

Because the surface texture of the fabric may reflect light specularly to the detector, diffuse reflectance was obtained at two other orientations (45° and 90°) to the P100 fiber direction. The 45° orientation offers the least likelihood of specular reflectance, as no fibers in the layup pattern are parallel to the beam detector plane. In each case, a nearly identical reflectance spectra was obtained, indicating 47% reflectance at 10.6 μm wavelength.

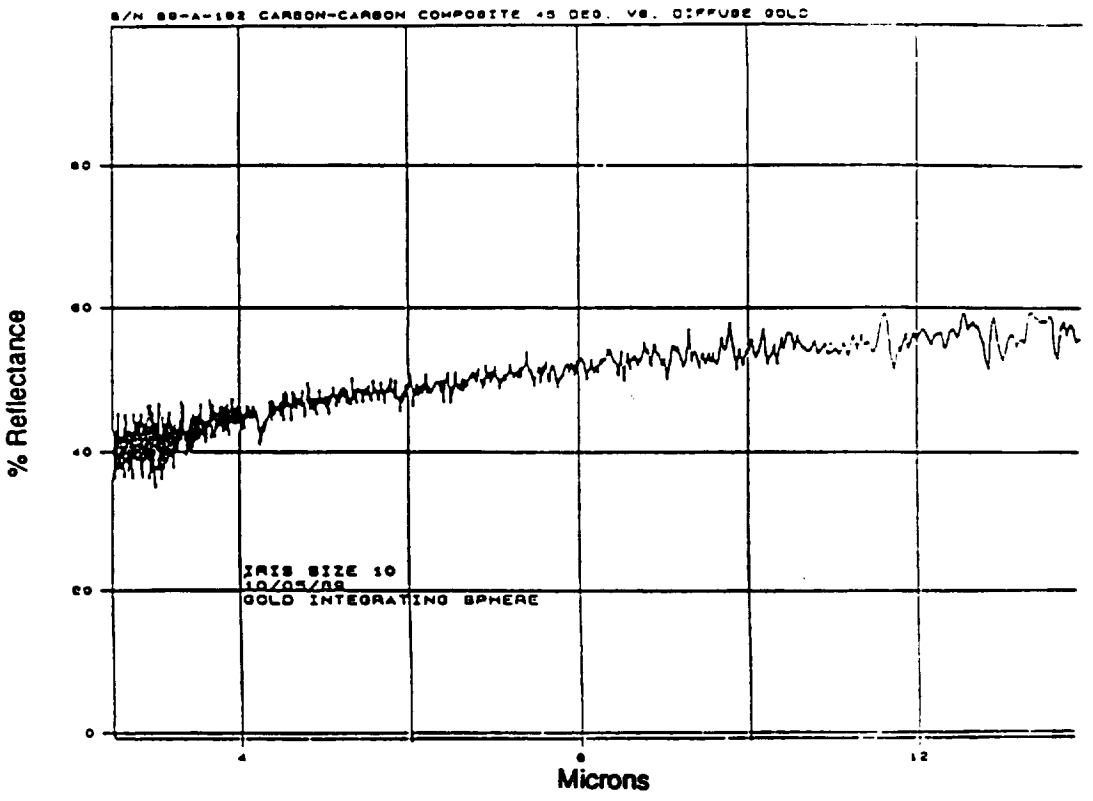

Figure 10.2-7 Diffuse Reflectance Spectrum of As-Fabricated P100/C [0/90/0] Surface from 2.5 μm to 14.0 μm using a Mattson Polaris Spectrophotometer

10.3 P100/C $[0]_3$ TUBES

10.3.1 Fabrication Data

Material System:	P100/C
Fiber Layup:	$[0]_3$
Condition:	As fabricated
Manufacturer:	BP - HITCO, CA
Dimensions:	0.050-in. x 1-in. x 14-in. long
Ply thickness:	0.0167-in
Processing Data:	Each tube was fabricated with the involute construction from the same prepreg material that was used for unidirectional and bidirectional panels. Autoclave molding of the tube was performed over aluminum male tools at 300 psi and 300°F. The subsequent processing conditions for carbonization, pyrolysis and CVI were similar to the ones used for panels. Specific molding data and processing details are listed in Table 10.3-1.

10.3.2 Product Evaluation

Density:	0.060 lb/in^3
Std. Dev.:	0.0001

(b) Fiber Volume

v/o:	55.5
Std. Dev.:	0.26

Void Volume: 8.0% (data provided by the manufacturer)

Table 10.3-1 Processing Data for P100/C InvoluteTubes

Molding Data:	Tube A	Tube B	Tube C	Tube D
Dry Weight (g.)	34.927	34.927	34.927	34.927
Post-Mold Weight (g.)	48.218	49.874	46.965	49.630
Post-Mold P/U (%)	27.564	29.970	25.632	29.625
Fiber Volume (%)	61.374	58.556	63.694	58.955
Wall Thick. (in.)	0.045	0.049	0.043	0.044
Length (in.)	14.000	14.000	14.000	14.000
Post-Carb Data:				
Pre-Carb Wt. (g.)	48.218	49.874	46.965	49.630
Post-Carb Wt. (g.)	38.478	38.503	35.931	38.366
Weight Loss (%)	20.200	22.799	23.494	22.696
Wall Thick. (in.)	0.046	0.050	0.043	0.045
Length (in.)	14.000	14.000	14.000	14.000
Post-CVD Data:				
Pre-CVD Wt. (g.)	38.478	38.503	35.931	38.366
Post-CVD Wt. (g.)	62.501	62.102	59.189	62.830
Weight Gain (%)	62.433	61.291	64.730	63.765
Fiber Volume (%)	55.301	55.661	58.439	55.008
Wall Thick. (in.)	0.049	0.054	0.047	0.048
Length (in.)	14.000	14.000	14.000	14.000

(c) Non-Destructive Evaluation

Each tube was examined by visual and X-radiography techniques. On visual examination, each tube revealed the surface texture of the woven fabric, without any scratches or cracks. X-radiography of each tube indicated the fiber collimation within the woven pattern, and presence of randomly distributed voids in the matrix.

(d) Microstructure

Microstructural examination of the tube at various locations revealed the three plies of the involute construction at each location along the circumference. A typical microstructure was identical to the photomicrographs of unidirectional panel, with voids randomly distributed within the fiber bundles and warp/fill intersections.

10.3.3 Mechanical Property Tests

(a) Tension

Longitudinal tension test results of the tube are listed in Table 10.3-2. the average tensile modulus of 49.7 Msi was in good agreement with the predicted value of 51.6 Msi, indicating the adequate fiber-matrix bond and associated load transfer characteristics in the involute tubes. Also, the average tensile strength of 84.3 ksi was consistent with the strength values obtained from the flat panel specimens.

(b) Compression

Table 10.3-3 lists the longitudinal compression test results of the three tube specimens. The stress-strain response from a few of the strain gages was extremely noisy because it was difficult to attain adequate contact between the strain gage and the textured surface. While the average compression modulus value was close to the predicted, it was slightly higher than the tensile

Table 10.3-2 Longitudinal Tensile Properties of P100/C Tubes [0, 0, 0)] v/o = 55.5%

Specimen # CC-U-HT	Elastic Modulus (Msi) E_{x1}	E_{x2}	E_{x3}	E_x	UTS (ksi)	ε_f (%)	ν_{xy}
TNL-1	52.4	50.1	50.2	50.9	79.8	0.184	---*
TNL-2	45.7	51.5	53.2	50.1	82.5	0.180	0.4636
TNL-3	45.7	50.0	58.1	51.3	93.2	0.198	0.4466
TNL-4	42.8	49.0	47.4	46.4	86.1	0.212	---*
Mean				49.7	84.3	0.1935	0.4551
Std.Dev.				2.24	6.07	0.0146	0.0120
CV (%)				4.5	7.2	7.5	2.6

* Transverse strain gage extremely noisy

Table 10.3-3 Longitudinal Compressive Properties of CarbonP100/Carbon [0, 0, 0] Tubes, v/o = 55.5%

Specimen # CC-U-HT	Elastic Modulus (Msi) E_{x1}	E_{x2}	E_{x3}	E_x	UTS (ksi)	ε_f (%)	ν_{xy}
CML-2	41.2	57.5	56.7	51.8	25.3	0.0527	0.6579
CML-10	68.6	45.4	63.5	59.2	25.2	0.0479	---
CML-11	39.2	57.4	55.4	50.8	29.2	0.0704	0.5729
Mean				53.9	26.6	0.0573	0.6154
Std.Dev.				4.59	2.23	0.0114	0.0601
CV (%)				8.5	8.4	19.9	9.8

modulus. Whereas,.the average compressive strength of 26.6 ksi was significantly lower than the corresponding strength values obtained from the unidirectional flat and tube specimens. These experiments suggested that more specimens should be tested to establish the compressive behavior of C/C tubes.

10.4 SUMMARY OF P100/C TEST DATA

Mechanical and thermophysical property test data of unidirectional and bidirectional flat panels, and unidirectional tubes are summarized in Table 10.4-1 to 10.4-3.

Table 10.4-1 P100/Carbon [0/0/0]

NOT DESIGN ALLOWABLE DATA

PROPERTIES								TEMPERATURE (°F)			Std. Dev. / No. of Specimens at RT	Test Method
PHYSICAL			MECHANICAL & THERMAL					Low	Room	High		
Density (lb / in^3)		0.060	Longitudinal Tensile Strength	σ_x^{TU}	ksi				81.5		± 3.17 / 4	ASTM D-3039
Fiber volume fraction		0.525	Transverse Tensile Strength	σ_y^{TU}	ksi				2.04		± 0 / 2	ASTM D-3039
Void volume fraction		0.08	Longitudinal Comp. Strength	σ_x^{CU}	ksi				47.8		± 10.9 / 4	ASTM D-3410
Nominal ply thickness	in	0.017	Transverse comp. strength	σ_y^{CU}	ksi				4.6		± 0.33 / 5	ASTM D-3410
Max. cont. use temp.	°F	3700	In-plane shear strength	IPSS	ksi				4.93			
Ply Orientation	θ	[0/0/0]	Interlaminar shear strength	ILSS	ksi				3.47		± 0.08 / 5	ASTM D-2344
OPTICAL & ELECTRICAL (at room temperature)			Longitudinal tensile strain **	ε_x^T	%				0.225		± 0.016 / 4	ASTM D-3039
Solar Absorptance	α		Transverse tensile strain **	ε_y^T	%				0.208		± 0.01 / 2	ASTM D-3039
Normal Emissivity	ε		Longitudinal comp. strain **	ε_x^C	%				0.13		± 0.03 / 3	ASTM D-3410
			Transverse comp. strain **	ε_y^C	%							ASTM D-3410
			Longitudinal tensile modulus	E_x	Msi				43.7		± 2.66 / 4	ASTM D-3039
			Transverse tensile modulus	E_y	Msi				1.45		± 0.63 / 2	ASTM D-3039
			Longitudinal comp. modulus	E_x	Msi				39.4		± 4.02 / 5	ASTM D-3410
			Transverse comp. modulus	E_y	Msi				1.3		± 0.473 / 4	ASTM D-3410
			In-plane shear modulus	G	Msi				1.44			
			Longitudinal flexural modulus	F_x	Msi							ASTM D-790M
			Transverse flexural modulus	F_y	Msi							ASTM D-790M
			Long. tensile Poisson's ratio	ν_{xy}					0.369		± 0.09 / 4	ASTM D-3039
			Trans. tensile Poisson's ratio	ν_{yx}					0.045		± 0.014 / 2	ASTM D-3039
			Long. thermal conductivity	K_x	(1)				9.86			Kohlrausch
			Trans. thermal conductivity	K_y	(1)				0.38			Kohlrausch
			Thru thickness thermal cond.	K_z	(1)				—			Laser Flash
			Specific heat	C_p	(2)							ASTM E-1269
			Longitudinal CTE	α_x	(3)				-0.98			ASTM C-372
			Transverse CTE	α_y	(3)				-0.42			ASTM C-372
			Thru thickness CTE	α_z	(3)				—			

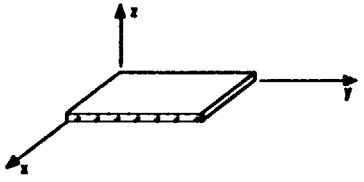

Notes:
(**) - Strain to failure; (1) Btu/(hr·in·°F); (2) Btu/(lb·°F); (3) µin./in./°F

Table 10.4-2 P100/Carbon [0/90/0]

NOT DESIGN ALLOWABLE DATA

PHYSICAL		
Density (lb / in^3)		0.060
Fiber volume fraction		0.53
Void volume fraction		0.08
Nominal ply thickness	in	0.017
Max. cont. use temp.	°F	3700
Ply Orientation	θ	[0/90/0]
OPTICAL & ELECTRICAL (at room temperature)		
Solar Absorptance	α	
Normal Emissivity	ε	

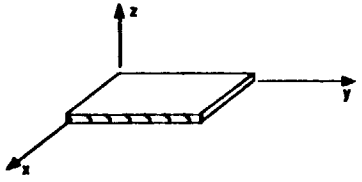

PROPERTIES			TEMPERATURE (°F)			Std. Dev. / No. of Specimens at RT	Test Method
MECHANICAL & THERMAL			Low	Room	High		
Longitudinal Tensile Strength	σ_x^{TU}	ksi		44.1		± 6.21 / 4	ASTM D-3039
Transverse Tensile Strength	σ_y^{TU}	ksi		29.0		—	ASTM D-3039
Longitudinal Comp. Strength	σ_x^{CU}	ksi		6.95		± 1.58 / 5	ASTM D-3410
Transverse comp. strength	σ_y^{CU}	ksi		9.4		± 1.73 / 5	ASTM D-3410
In-plane shear strength	IPSS	ksi					
Interlaminar shear strength	ILSS	ksi		1.960		± 0.12 / 5	ASTM D-2344
Longitudinal tensile strain **	ε_x^T	%		0.17		± 0.02 / 3	ASTM D-3039
Transverse tensile strain **	ε_y^T	%		~0.15			ASTM D-3039
Longitudinal comp. strain **	ε_x^C	%					ASTM D-3410
Transverse comp. strain **	ε_y^C	%					ASTM D-3410
Longitudinal tensile modulus	E_x	Msi		32.4		± 1.28 / 3	ASTM D-3039
Transverse tensile modulus	E_y	Msi		20.3		—	ASTM D-3039
Longitudinal comp. modulus	E_x	Msi		29.1		± 5.7 / 5	ASTM D-3410
Transverse comp. modulus	E_y	Msi		15.5		± 3.8 / 5	ASTM D-3410
In-plane shear modulus	G	Msi		—			
Longitudinal flexural modulus	F_x	Msi		—			ASTM D-790M
Transverse flexural modulus	F_y	Msi		—			ASTM D-790M
Long. tensile Poisson's ratio	ν_{xy}			0.145		± 0.0314 / 4	ASTM D-3039
Trans. tensile Poisson's ratio	ν_{yx}			0.1			ASTM D-3039
Long. thermal conductivity	K_x	(1)		6.83			Kohlrausch
Trans. thermal conductivity	K_y	(1)		3.25			Kohlrausch
Thru thickness thermal cond.	K_z	(1)		0.30			Laser Flash
Specific heat	C_p	(2)		0.169			ASTM E-1269
Longitudinal CTE	α_x	(3)		-0.95			ASTM C-372
Transverse CTE	α_y	(3)		-0.95			ASTM C-372
Thru thickness CTE	α_z	(3)		—			

Notes:
(**) - Strain to failure; (1) Btu/(hr·in·°F); (2) Btu/(lb·°F); (3) μin./in./°F

Table 10.4-3 P100/Carbon Tube [0/0/0]

NOT DESIGN ALLOWABLE DATA

PROPERTIES						TEMPERATURE (°F)			Std. Dev. / No. of Specimens at RT	Test Method
PHYSICAL			MECHANICAL & THERMAL			Low	Room	High		
Density (lb / in^3)	X	0.060	Longitudinal Tensile Strength	σ_x^{TU}	ksi		84.3		± 6.07 / 4	ASTM D-3552
Fiber volume fraction	X	0.555	Transverse Tensile Strength	σ_y^{TU}	ksi					NOL
Void volume fraction	X	0.08	Longitudinal Comp. Strength	σ_x^{CU}	ksi		26.6		± 2.33 / 3	ASTM D-3410
Nominal ply thickness	in	0.167	Transverse comp. strength	σ_y^{CU}	ksi					
Max. cont. use temp.	°F	3700	In-plane shear strength	IPSS	ksi					
Ply Orientation	θ	[0/0/0]	Interlaminar shear strength	ILSS	ksi					
OPTICAL & ELECTRICAL (at room temperature)			Longitudinal tensile strain **	ε_x^T	%		0.19		± 0.015 / 4	ASTM D-3552
Solar Absorptance	α		Transverse tensile strain **	ε_y^T	%					NOL
Normal Emissivity	ε		Longitudinal comp. strain **	ε_x^C	%		0.06		± 0.01 / 3	ASTM D-3410
			Transverse comp. strain **	ε_y^C	%					
			Longitudinal tensile modulus	E_x	Msi		49.7		± 2.24 / 4	ASTM D-3552
			Transverse tensile modulus	E_y	Msi					NOL
			Longitudinal comp. modulus	E_x	Msi		53.9		± 4.59 / 3	ASTM D-3410
			Transverse comp. modulus	E_y	Msi					
			In-plane shear modulus	G	Msi					Torsion Test
			Longitudinal flexural modulus	F_x	Msi					
			Transverse flexural modulus	F_y	Msi					
			Long. tensile Poisson's ratio	ν_{xy}	X		0.455		± 0.012 / 4	ASTM D-3552
			Trans. tensile Poisson's ratio	ν_{yx}	X					NOL
			Long. thermal conductivity	K_x	(1)					
			Trans. thermal conductivity	K_y	(1)					
			Thru thickness thermal cond.	K_z	(1)					
			Specific heat	C_p	(2)					
			Longitudinal CTE	α_x	(3)					ASTM C-372
			Transverse CTE	α_y	(3)					
			Thru thickness CTE	α_z	(3)					

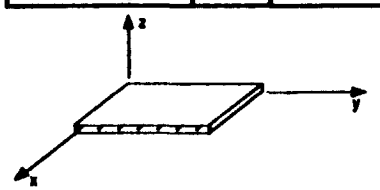

Notes:
(**) - Strain to failure; (1) Btu/(hr·in·°F); (2) Btu/(lb·°F); (3) μin./in./°F

Thermal Cycling of Composite Materials

11.0 THERMAL CYCLING OF COMPOSITE MATERIALS

The performance characteristics of many large space structures are dependent upon the dimensional stability of the structural materials. In LEO, materials will be subjected to repeated thermal cycles between -150°F and 150°F, ultraviolet radiation, and ultra-high vacuum. For higher orbits such as geo-synchronous orbit (GEO), the materials will also be subjected to large doses of high energy electrons and protons. The primary concern for composite materials is the dimensional instability caused by microcracking due to residual stresses produced during thermal cycling. These microcracks in composites can significantly affect their stiffness, strength, and CTE, as well as cause permanent residual strain (Ref 11-18 and 63-70). Therefore, to study the effect of thermal cycling on composite behavior, initially a large (18-ft^3) chamber was designed and fabricated which could simulate one year orbital thermal cycling (i.e., about 5840 cycles between -150°F and 150°F) in 20 days. About 500 specimens from different composite materials were exposed to 10,099 cycles in this chamber, and various tests were performed to determine dimensional changes, microcrack density, and material properties including tension, compression and CTE. The details of thermal cycling chamber and material response of thermal cycled specimens are described in this chapter.

11.1 ACCELERATED THERMAL CYCLING CHAMBER (ATCC)

Based on the operational principle and requirements defined by Martin Marietta Astronautics Group, CO, a thermal cycling chamber was designed and fabricated by BEMCO Inc., CA. The operational principle and requirements were:

Principle:	Forced convection of dry nitrogen gas from hot and cold chambers located on either side of a central specimen workspace.
Workspace:	3-ft x 2-ft x 2-ft

Thermal cycles: -150°F → 150°F → -150°F in 5 minutes

-250°F → 250°F → -250°F in less than 15 minutes

Peak Temp Variation: ±10°F

The specially designed unit, BEMCO model LDF-250/250-184HC, was able to simulate one year orbital (LEO) cycling in 20 days (i.e., acceleration factor (aF = 365/20 = 18.25)). With 18.25 acceleration factor, this is the largest thermally cycling unit in the country. Martin Marietta Astronautics Group also installed a 6,000 gallon (gal) liquid nitrogen dewer to provide a continuous gas supply for thermal cycling, as the chamber was fully automated for unattended operation. The thermal cycling chamber (loaded with specimens in the workspace) is shown in Figure 1-2 (reproduced in this chapter for reference) and its design and operational aspects are described below.

11.1.1 Design Aspects

The ATCC has been designed for optimum performance under cycling conditions between -150°F and 150°F at 120°F per minute heating or cooling, with no temperature dwells at either extreme. The chamber also performs cycling conditions between -250°F and 250°F at 67°F/min heating or cooling, with no temperature dwells at either extreme, or between -100°F and 350°F continuous steady state (or Ramp and Soak function) temperature.

Transient rates are variable through the programming of ramp time versus temperature at the Programmer Controller and can be modified to other test requirements that do not exceed the design capacity of the chamber. Modifications are determined by analysis of the type of test items to be installed (exposed test item surface area, specific heat, shape and size of the items, etc.). Other factors to be considered are thermal rates of change, heating, cooling and gas flow requirements in the chamber to achieve the desired results.

ORIGINAL PAGE
BLACK AND WHITE PHOTOGRAPH

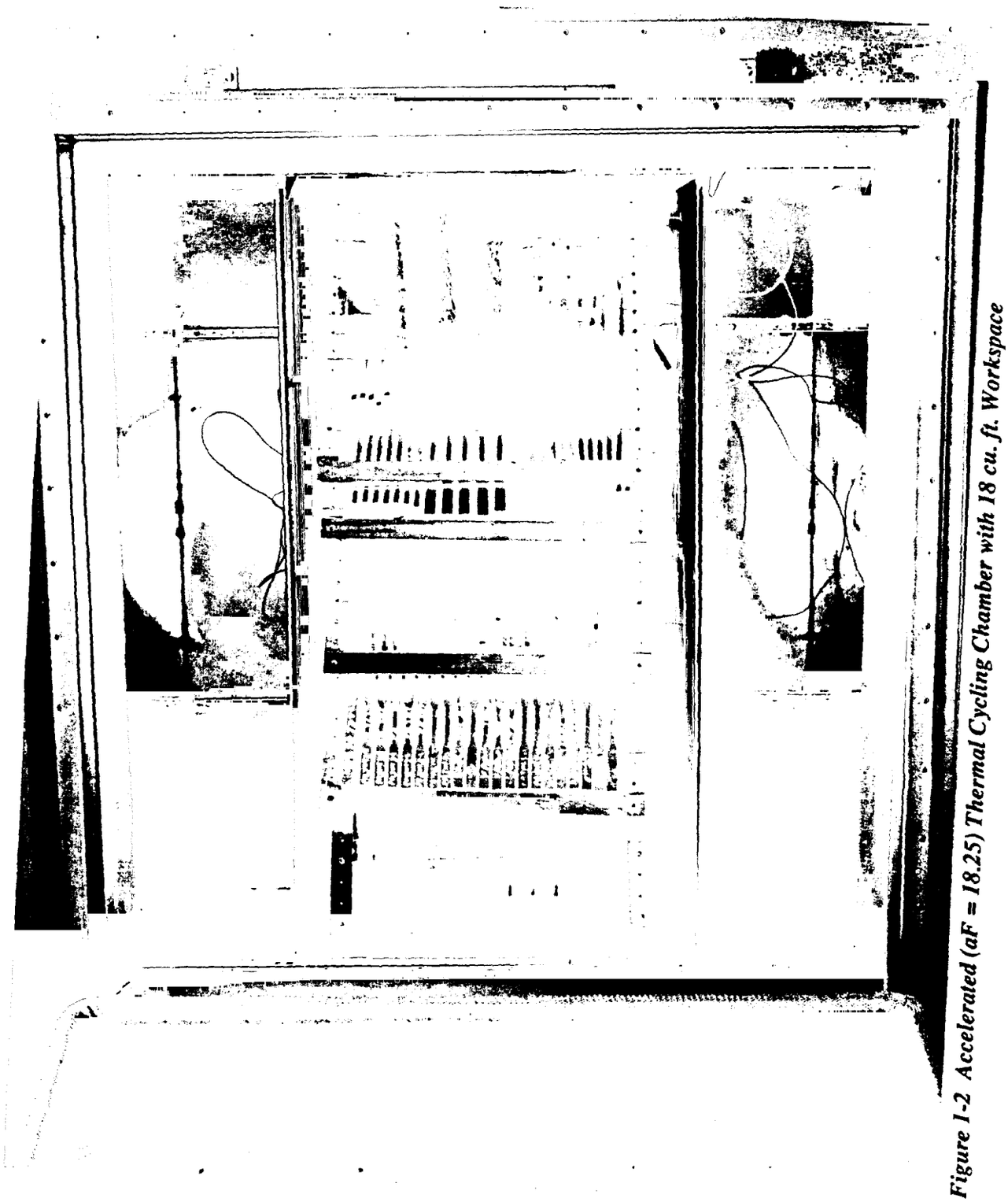

Figure 1-2 Accelerated (aF = 18.25) Thermal Cycling Chamber with 18 cu. ft. Workspace

The chamber has an automatic GN_2 purge system which purges nitrogen gas into the workspace every time the chamber door is closed. The purge lasts for 90 seconds, then automatically shuts off.

The interior workspace measures 3-ft wide by 3-ft high by 2-ft deep, totaling 18-ft^3. Exterior dimensions are 5-ft 10-in. wide by 8-ft 9-in. high by 3-ft 8-in. deep. A full opening door allows access to the workspace. The door opening measures 3-ft wide by 2-ft 9-in. high. Plug type door design is used to increase thermal path and eliminate permanent warpage of the door face due to expansion and contraction, and includes a dual gasket seal. The chamber is mounted on swivel type casters for ease of movement, and is equipped with a structural steel base frame for transport by forklift.

The entire workspace liner and the two servo system liners are constructed of type 304 stainless steel that are fully welded and reinforced. Flow dampers and transitions are bolted construction to allow service access to the dampers and to the squirrel cage type blowers.

Expansion/contraction joints and seams are used at all critical locations, to eliminate fatigue and stress failures of the liner assemblies.

Penetrations and access ports are equipped with thermal barriers to reduce thermal losses, and prevent frosting or condensation on outside surfaces.

The system is designed to incorporate low MTBF (Mean Time Between Failures) factors by reducing the number of moving parts that similar systems typically use. Having only 2 "dampers" minimizes the total system moving parts subject to failure. The dampers do not use elastomeric seals which would fail under thermal or duty-cycle conditions. Instead, the dampers use non-precision metal to metal seals. Binding due to thermal expansion and contraction is not a problem.

11.1.2 Thermal Cycling Operation

Above and below the 3-ft x 2-ft x 2-ft workspace the heating and cooling servo systems are located respectively. These systems condition the nitrogen gas through the chamber to create the thermal cycling in the workspace.

Individually, the servos operate alternately with each other to create the cycling effect in the workspace. The flow dampers, one per servo, close during the inactive phase of a servo cycle, while the damper of the active servo is open. Each servo has a stainless steel squirrel cage type blower which is cycled on and off with active and inactive phases of the servo. During the inactive phase, cooling servo cold gas tends to stay down in the servo, which would otherwise cause the heating servo to compensate by adding more heat. Similarly, hot, inactive servo gas stays up in the heating servo, where it does not interfere with active cooling. This approach further reduces the use of moving parts by eliminating extra dampers or shutoff devices to totally isolate an inactive servo. The single closed damper of an inactive servo effectively blocks flow to prevent thermal opposition to the active servo.

The thermal cycling operation is schematically shown in Figure 1-4 (reproduced in this chapter for reference), where during cool cycle, heating servo remains inactive and damper remains closed to prevent gas circulation through hot components. Similarly in the hot cycle, the cooling serve remains inactive.

Overall physical and thermal design of the system is based upon fast high/low cycling with no dwells. When a mass is exposed to changing gas temperature it tends to resist temperature change and lags behind to changing gas temperature. This produces an "average" set of temperature extremes for the involved thermal masses that is well inside the gas temperature extremes. Specific attention has been made to using minimum structural mass where maximum

(a) Cool Cycle

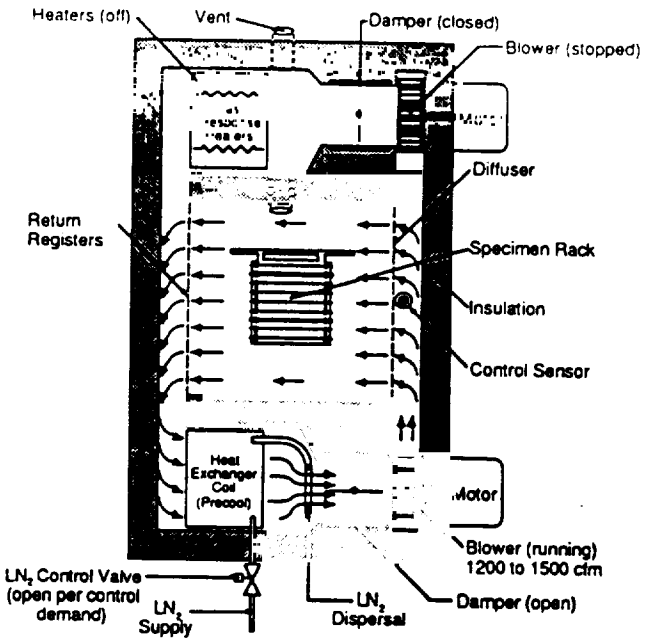

(b) Heat Cycle

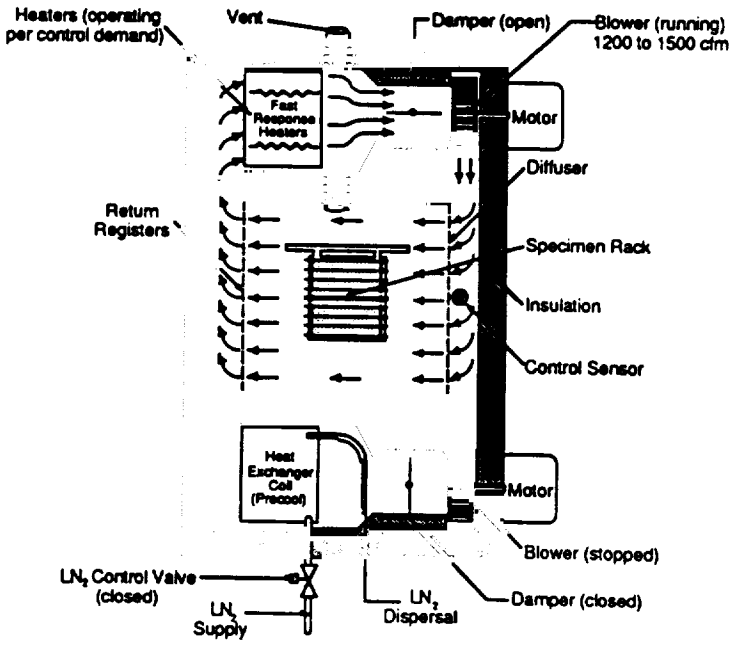

Figure 1-4 The Schematic of Thermal cycling Operation (a) Cool Cycle: Heating Servo Inactive and Damper Closed to Prevent GN_2 Circulation Through Hot Components. (b) Hot cycle: Cooling Servo Inactive and Damper Closed to Prevent GN_2 Circulation Through Cold Components

change rate is required (in the workspace), and more mass where higher resistance or thermal damping is desirable (the servos). No active pre-conditioning is incorporated due to the high capacity and extremely fast response of the conditioning components used.

Gas circulation and distribution in the workspace is provided by squirrel cage blowers. The motors are mounted in the power panel. Workspace gas is drawn at the return plenum of the workspace (left side), and into the active servo. The gas is then passed through the temperature conditioning elements and is discharged into the supply plenum, where it is diffused and directed back into the workspace. High gas flow rate assures minimal gradient, high heat transfer rates, and smaller temperature differential across test objects. The blowers are direct driven, and motors are equipped with forward and rear ball bearing races to reduce shaft whip and forward bearing radial loading.

The two squirrel cage blowers are subjected to a much lesser degree of thermal shock since neither blower is exposed to full thermal cycling swings. Less stressing and less expansion and contraction of the blower reduces the chance of failure. Using only one blower to circulate the gas for heat/cool cycling would expose the blower to the full thermal swings. This would cause rapid expansion and contraction of the squirrel cage assembly and very likely result in early failure.

The liquid nitrogen supply to the chamber is passed through a phase separator to separate gas from the supply and to maintain sufficient supply of liquid ready for immediate use by the cooling system. It also warns of insufficient source supply to the chamber after cycling has commenced, and will cause the running program to "HOLD" until operator intervention to correct the supply problem and restart the Programmer.

Liquid nitrogen, on controller demand, is allowed to flow from the large port high flow primary

control solenoid valve into a heat exchange coil in the cool servo gas stream. High velocity gas is passed over the heat exchanger and the LN_2 absorbs heat from the gas, causing partial boiling of the LN_2. Exiting LN_2 and GN_2 from the heat exchanger is piped to a dispersion ring where it is sprayed into the pre-cooled gas stream from the heat exchanger, causing further boiling of the remaining liquid and absorbing more heat. An LN_2 Injection Limit control monitors the gas stream temperature before it enters the cool servo blower. If an excessively cold temperature is detected (indicating too high a percentage of liquid nitrogen), the cooling control solenoid valve is modulated to prevent excess liquid injection, which might otherwise begin to accumulate in pools within the system. Cooling safety is accomplished with a Factory Mutual low limit control instrument connected to a set-up solenoid valved upstream of the control valve, and will cause a Programmer "HOLD" condition if its setting is exceeded.

The blower then discharges the temperature conditioned gas into the supply plenum of the workspace, where a head pressure is established. The diffuser spreads gas flow across the entire supply side of the workspace. A similar diffuser and plenum on the entire return side draws gas from the workspace, returning it to the active servo.

Internal system gas pressure is equalized to atmospheric pressure through a vent in the workspace. Expanded (from liquid) nitrogen gas or expanded (from heating) gas escapes the system through the vent, preventing excess pressure buildup inside the system.

The heating system consists of resistive wire elements and a control circuit. the elements are shielded so that no radiant heat, only forced temperature controller cycles the heater relays as required to regulate the heater output. Power to the element is switched on and off by zero crossover switching solid state relays. The heating system safeties include a standard factory set thermostat which opens the across-the-line power set-up contactor if over heating occurs. This thermostat is intended to protect only the chamber. Also included is a solid state Factory Mutual

heat limit control instrument in addition to the standard thermostat which also connects to the heat set-up contractor, and to the Programmer "HOLD" function. This device is intended to provide protection for the items being tested, and is set at some temperature lower than the chamber thermostats.

A back-up cooling system option is included as further enhancement of the MTBF reliability. The very high duty cycle of the control solenoid valve is caused for particular attention to downtime when (not if) the valve fails. Through time-delay and temperature monitoring, when failure to cool is detected, automatic switch over to the back-up control system is achieved, accompanied by visual alarm indicating primary system failure.

Other safety systems include standard interlocks to prevent heating or cooling operation if the respective servo blower motor has failed, and a door activated cutoff switch to stop the blower motor(s) and temperature conditioning systems, when the chamber door is opened.

11.2 THERMAL CYCLING OF COMPOSITE SPECIMENS

About 500 specimens from different panels and tubes were simultaneously cycled between -150°F and 150°F. Also, reference coupons (with prepolished edges) were also included to examine the microcracking in each composite, after 100, 300, 500, 1000, 3000, 5000 and 10,000 cycles.

For thermal cycling, the flat specimen were woven into a basket-weave using 0.020-in. stainless steel wire which were tensioned and anchored to an aluminum frame of low thermal mass. Since the specimens were already machined to size for subsequent testing, the frames were organized for sequential removal at specified cyclic intervals, if desired. Using the steel wires,

the frames were also anchored to the stainless steel racks in the workspace. These frames were oriented at 20° to the air stream (estimated to be 216 ft. per min) to ensure uniform heating of all the specimens in the chamber (Figure 1-2). For the tubular specimens, about 10 were close packed and bundled into a unit using stainless steel wires and anchored to the stainless steel racks for thermal cycling.

Prior to introducing the specimens in the chamber, simulated thermal cycling of composite plates and tubes (i.e., dummy specimens) was performed to examine the uniformity of temperature near the hot and cold end of the cycle. These test indicated that all flat specimens, and the thin wall (≤0.050-in.) tube specimens of Gr/E, Gr/TP, Gr/Al, and Gr/Mg had adequately attained the extreme temperatures of 150° ±10°F and -150° ±10°F in a 5.5 minute cycle (with a 1.5 min soak time). However, the SiC_p/Al and SiC_w/Al tube specimens required a soak time of 3 min to attain the desired hot and cold extreme temperatures within ±10°F because of their large thermal mass. Typical thermal response of simulation specimens with the programmer temperature settings of -180°F and 180°F were as follows:

Materials Temperature	Soak Time	Averave Temperature	
		Cold (°F)	Hot (°F)
1. Chamber	1.5 min	-171	186
2. P75/1962 flat or tube	"	-144	147
3. P75/PEEK flat or tube	"	-144	147
4. P100/Al flat or tube	"	-146	158
5. P100/Mg flat or tube	"	-143	155
6. 25v/o SiC_p/Al	"	-90	131
7. 25v/o SiC_w/Al	3 min	-141	148

Based on the results of this simulation experiemnt, the test specimens were thermal cycled in

two separate batches:

Batch #1- Flat and tube specimanes of P75/1962, P75/PEEK, AS4/PES, P100/6061 Al, P100/AZ91C Mg, HMU/7070, and C/C, and flat specimens of discontinuous SiC/Al composites.

Batch #2- Tube specimens of discontinuous SiC/Al composites.

For these two batches of specimens, the following temperautre settings, ramp rate, and soak time were used:

Batch #1:

Cold End (set temperature: -180°F)

	Ramp Time	Soak Time	Temperature
	3.5 sec	0 sec	-60°F
	45 sec	1.5 min	-180°F

Hot End (set temperature: 170°F)

	7 sec	0 sec	40°F
	1.5 min	1.5 min	170°F

Total time/cycle: 5 min 25.5 sec

Batch #2

Cold End (set temperature: -180°F)

	Ramp Time	Soak Time	Temperature
	4 sec	0 sec	-60°F
	50 sec	3 min	-180°F

Hot End (set temperature: 180°F)

	10 sec	0 sec	40°F
	1.5 min	2.5 min	180°F

Total time/cycle: 8 min 4 sec

During thermal cycling, the temperature was monitored by attaching thermocouples to different composite specimens. The temperature measurements indicated that at each end of the hot or cold cycle, temperature was within ±10°F. While the extreme temperatures were adequately attained in a 5.5 min cycle, thermal cycling could not be performed continuously without interruptions. Of the total number of 10,099 cycles, the initial 3049 were performed using a 300 gal LN_2 dewer which had to be replaced after about 41 cycles. Later, a 6000 gal dewer was installed to provide a nearly continuous LN_2 source for the remaining 7050 cycles. Still, there were numerous interruptions mainly due to freezing of cold gas passages. Therefore, a warm-up cycling program was introduced to dry out the cold passages after every 75 actual cycles between -150°F and 150°F. For the warm-up cycle, the ramp rate, soak time, and set temperature were as follows:

	Ramp Time	Soak Time	Temperature
Hot End	10 sec	0 sec	150°F
Cold End	10 sec	3 min	155°F

Total warm-up cycle: 20 sec/cycle

After 30 warm-up cycles (i.e. 10 min) the cold passages were dried up, while the specimens were held at slightly below the hot end temperature. Subsequent thermal cycling was performed without any interruptions.

The specific details of liquid nitrogen (LN_2) consumption per cycle and average extreme temperature recorded during the thermal cycling are as follows:

Total number of cycles:	10,099
Total LN_2 used:	73,574 gallons
Average LN_2/cycle:	7.28 gallon/cycle

Average hot temperature 160°F

Average cold temperature: -144°F

Average LN_2 consumption rate of 7.28 gal/cycle was slightly high because of the numerous interruptions caused by blockage of the cold gas passages, blown solenoid fuses, and malfunction of the partlow controllers. If the chamber operation remained uninterrupted, the LN_2 consumption should be about 6 gallons per cycle. Also, near the end of thermal cycling tests, BEMCO had provided a set of watlow controllers to replace the partlow controllers which would nearly eliminate the number of interruptions and effectively reduce the LN_2 consumption. After completing 10,099 cycles, tests were performed to determine dimensional changes, microcrack density, and material properties.

11.3 EFFECT OF THERMAL CYCLING ON MATERIALs

To examine the effect of thermal cycling, the technical approach included (1) dimensional change measurement, (2) microstructural examination of damage, and (3) material property tests (tension, compression, and CTE).

11.3.1 Dimensional Change Measurement

Length and width of each specimen was determined by the dial calipers and micrometers respectively. Prior to measurements, dial calipers and micrometers were calibrated, and both had a sensitivity of 0.001-in. Typical measurements of P100/Al, P75/PEEK and AS4/PES specimens are listed in Table 11-1 and compared with their dimensions before thermal cycling. Based on these measurements, the specimen in the transverse (y) direction exhibited a larger increase in length than in the longitudinal (x) direction, as summarized below.

Table 11-1 Dimensional Measurements of Composite Specimens Before (Column AF) and After 10, 099 Thermal Cycles (Column TC) Between -150°F and +150°F

	P100/6061 Al $[0]_2$				P75/PEEK $[0, \pm45, 90]_S$				P75/PEEK $[\pm30, 0_4]_S$				AS4/PES $[0, \pm45, 90]_S$				AS4/PES $[\pm30, 0_4]_S$			
Specimen No.	Length		Width		Length		Width		Length		Width		Length		Width		Length		Width	
	AF	TC	AF	TC	AF	TC	AF	TC	AF	TC	AF	TC	AF	TC	AF	TC	AF	TC	AF	TC
TNL-2	8.993	8.995	0.500	0.503	9.010	9.011	0.510	0.511	9.010	9.009	0.512	0.510	9.008	9.009	0.499	0.497	9.008	9.006	0.511	0.511
TNL-5	8.992	8.994	0.502	0.502	9.010	9.010	0.510	0.511	9.008	9.009	0.511	0.152	9.008	9.009	0.498	0.498	9.002	9.004	0.513	0.509
TNL-2	8.996	9.003	0.502	0.499	9.010	9.011	0.510	0.511	9.006	9.014	0.512	0.511	9.000	9.002	0.503	0.503	9.009	9.010	0.505	0.505
TNL-5	—	—	—	—	9.011	9.011	0.511	0.510	8.990	8.994	0.511	0.512	9.003	9.005	0.515	0.516	9.003	8.999	0.500	0.502
CMT-2	5.502	5.503	0.255	0.251	5.499	5.499	0.257	0.255	5.500	5.502	0.256	0.255	5.500	5.500	0.258	0.257	5.500	5.500	0.258	0.255
CMT-5	5.495	5.497	0.258	0.258	5.497	5.497	0.257	0.257	5.500	5.503	0.256	0.256	5.500	5.504	0.257	0.255	5.500	5.502	0.256	0.256
CML-2	5.503	5.508	0.251	0.250	5.497	5.500	0.257	0.255	5.500	5.501	0.255	0.256	5.497	5.498	0.257	0.257	5.495	5.502	0.255	0.256
CML-5	—	—	—	—	5.497	5.497	0.257	0.256	5.497	5.500	0.256	0.256	5.495	5.495	0.255	0.256	5.497	5.503	0.257	0.257
TEL-2	6.000	6.001	0.275	0.276	6.000	6.002	0.277	0.277	5.995	5.994	0.275	0.278	6.000	6.001	0.278	0.277	6.003	6.002	0.279	0.278
TEL-5	6.002	6.003	0.277	0.277	6.000	6.002	0.278	0.277	5.995	5.998	0.277	0.278	5.998	6.000	0.278	0.277	6.000	6.000	0.279	0.279
TET-2	—	—	—	—	6.000	5.999	0.278	0.277	5.999	5.999	0.278	0.277	6.000	6.000	0.278	0.278	5.999	6.007	0.284	0.279
TKL-3	3.495	3.497	0.252	0.252	2.991	2.991	0.255	0.254	2.997	2.996	0.256	0.257	3.003	3.003	0.257	0.257	3.006	3.005	0.257	0.257
TKT-3	3.500	3.503	0.251	0.251	3.002	3.003	0.258	0.257	2.994	2.996	0.256	0.256	3.000	3.000	0.258	0.256	2.996	2.996	0.259	0.257

Material	Average Dimensional Change (%) Longitudinal	Transverse
P100/6061 $[0]_2$	0.027	0.072
P75/Peek $[0, \pm 45, 90]_S$	0.005	0.026
P75/PEEK $[30, -30, 0_4]_S$	0.02	0.061
AS4/PES $[0, \pm 45, 90]_S$	0.012	0.012
AS4/PES $[30, -30, 0_4]_S$	0.009	0.06

These differences in dimensional changes, in a complex manner, are related to the differences in permanent residual strain, CTE and microdamage in the longitudinal and transverse direction. While these dimensional changes do indicate a trend, but their absolute values should be taken with caution for the following two reasons (1) sensitivity limitation of the calipers and micrometer, and (2) flatness of edge finish.

11.3.2 Microstructural Examination of Damage

To examine the incidence of microcracking, a 1-in. x 1-in. reference specimen from each composite material was prepared, and its longitudinal and transverse edges were polished (using 0.05 μm alumina) for microstructural examination. Before thermal cycling, both the polished edges were scanned under the optical microscope to determine the baseline microcrack density. Later, these specimens were cycled between -150°F and 150°F in the accelerated thermal cycling chamber. After exposure to 153, 363, 547, 1098, 3202, 5523 and 10,099 cycles, the prepolished edges of each specimen were examined to determine the changes in microcrack density.

During these observations, microcracks have been taken as small cracks in the matrix material which run through the thickness of a given ply and extend parallel to the fiber direction. From the photomicrographs (minimum 5 per specimen), the microcrack density was calculated by

counting the number of microcrack intercepts per unit length (-in.) in each ply. For example, in the zero CTE, quasi-isotropic and bi-directional laminates microcracks were generally observed in ±30°, ±45°, and 90° plies respectively. In the unidirectional panels, transverse cracks that are generated due to the residual stresses produced by the thermal expansion mismatch between the fiber and the matrix, were also included in the microcrack density measurements.

Microcrack density changes in the ±30° (zero CTE), ±45° (quasi-isotropic), 90°(bi-directional) and 0° (unidirectional) plies of several composites after different number of thermal cycles are presented in Table 11-2 and Figure 11-1. These measurements indicate the following:

- Baseline microcrack density in the as fabricated $[0, \pm 45, 90]_s$ P75/1962, P75/PEEK and AS4/PES, and $[30, -30, 0_4]_s$ P75/PEEK laminates was greater than 18 microcracks/in. There were no detectable microcracks in $[0]_8$ P75/1962, $[0,90]_6$, HMU/7070, and discontinuous SiC/Al composites. In the remaining P100/Al $[0]_2$ and $[30, -30, 0_4]_s$ P75/1962 and AS4/PES panels, the microcrack density was ≤13 microcracks/in.

- After thermal cycling, there was slight incidence of microcrack initiation and extension in $[0, \pm 45, 90]_s$ and $[30, -30, 0_4]_s$ P75/1962, P75/PEEK and AS4/PES specimens, but there was no significant increase in the microcrack density (Figures 11-2 to 11-7).

- Most likely, the thermal stresses generated during cycling process were being accommodated by the microcracks, microvoids, and delaminated regions present in the as fabricated material; consequently, there was only a slight (detectable) increase in microcrack density.

- While as fabricated HMU/7070 [0/90] specimens did not exhibit any microcrack, after 153 cycles the microcrack in the 90° ply were observed yielding 14 microcrack/in. (Figure 11-8).

Table 11-2 Microcracking Density in Thermal Cycled Composite Specimens

Material	Form	Layup	Microcracks/inch* Number of Cycles Between -150°F and +150°F 0	153	363	547	1098	3202	5523	10,099
P75/1962	Panel	$[0]_8$	0	0	0	0	0	0	0	0
P75/1962	Panel	$[0, 45, 90, -45]_s$	18 D,mv	18	18	20 D	20 D	20	20	20
P75/1962	Panel	$[\pm30, 0_4]_s$	6 mv, di	6	8 D	10 D	10 D	10	10	10
P75/1962	Tube	$[\pm30, 0_4]_s$	8	8	8	8	9	9	9	9
P75/PEEK	Panel	$[0, \pm45, 90]_s$	41	41	41	41	46	46	46	46
P75/PEEK	Panel	$[\pm30, 0_4]_s$	21	21	21	24	24	24	24	24
AS4/PES	Panel	$[0, \pm45, 90]_s$	26 mv	31	31	31	31	31	31	31
AS4/PES	Panel	$[\pm30, 0_4]_s$	12	12	12	12	12	12	12	12
25 SiCp/Al	Panel	N/A	0	0	0	0	0	0	0	0
25 SiCw/Al	Panel	N/A	0	0	0	0	0	0	0	0
35 SiCp/Al	Panel	N/A	0	0	0	0	0	0	0	0
35 SiCw/Al	Panel	N/A	0	0	0	0	0	0	0	0
P100 Gr/Al	Panel	$[0]_2$ DB	13	13	13	13	13	13	13	13
P100 Gr/Al	Tube	$[0]_2$ DB	12	12	12	12	12	12	12	12
P100 Gr/Al	Tube	$[0]_2$ PT	<6 mv	6	6	6	6	6	6	6
HMU/7070	Panel	$[0/90]_6$	0 di	14	14	14	14	14	14	14

Legend: D - Delamination, di - Disbonds, mv - Microvoids;
*in ± 30° plies of $[\pm30, 0_4]_S$, ±45° plies of $[0, \pm45, 90]_S$, 90° plies of [0/90], and 0° plies of unidirectional

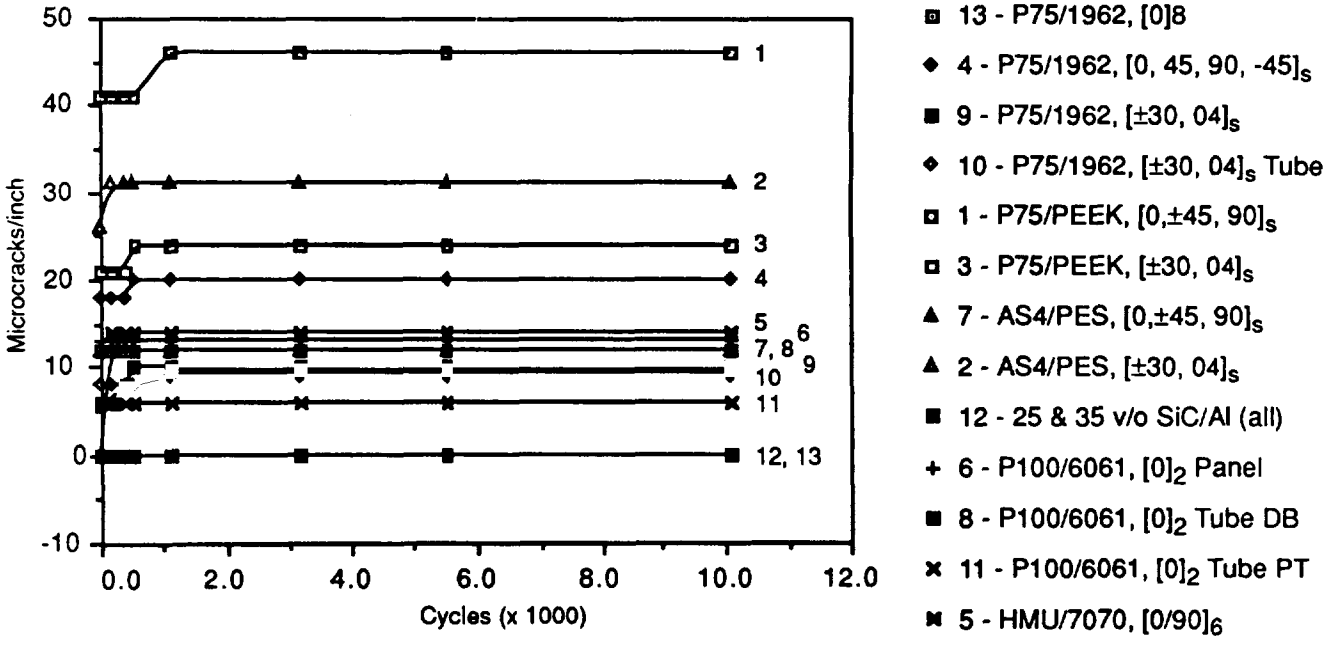

Figure 11-1 Microcrack Density Changes in Different Composites After Periodic Thermal Cycles Between -150°F and 150°F

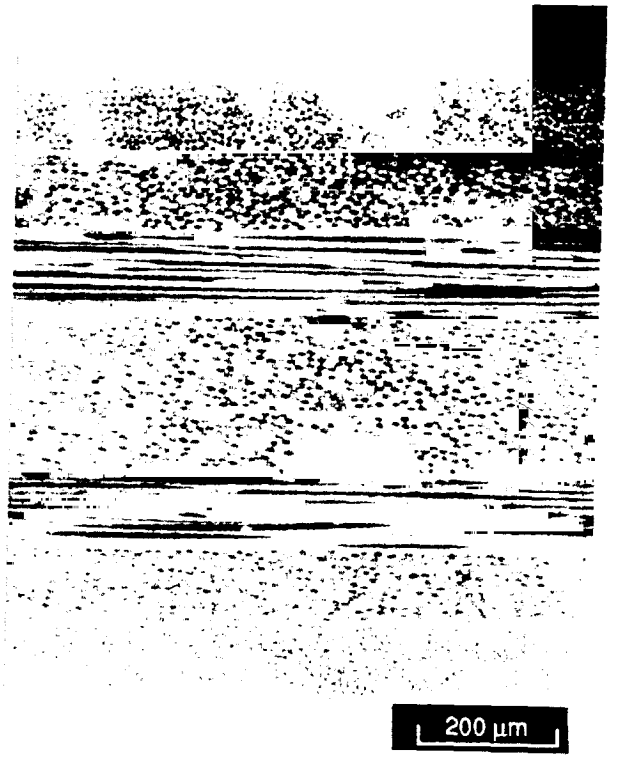

(a) As-Fabricated

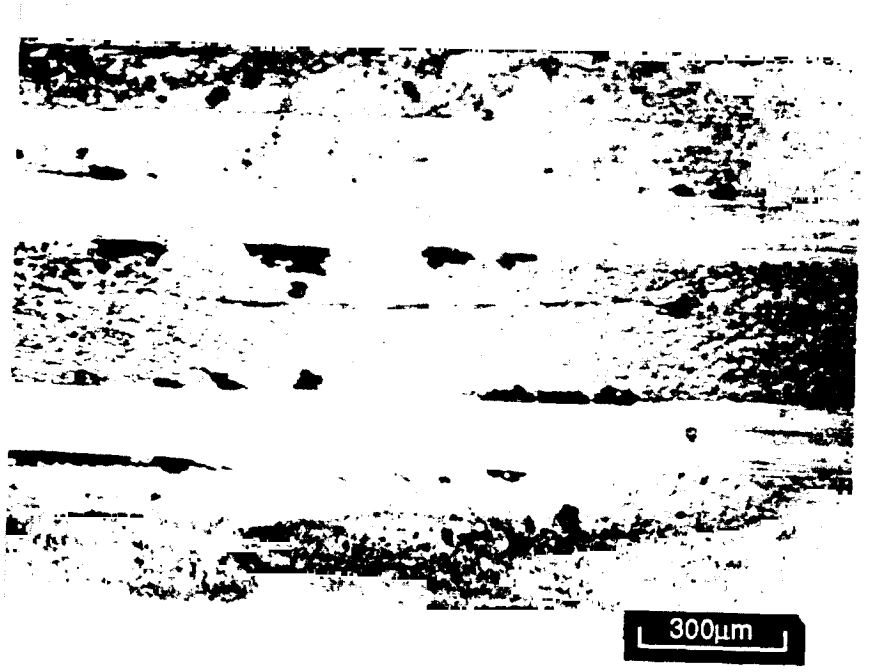

(b) Thermal Cycled

Figure 11-2 Photomicrographs of As-Fabricated and Thermal Cycled $[0, 45, 90, -45]_s$ P75/1962 Specimens

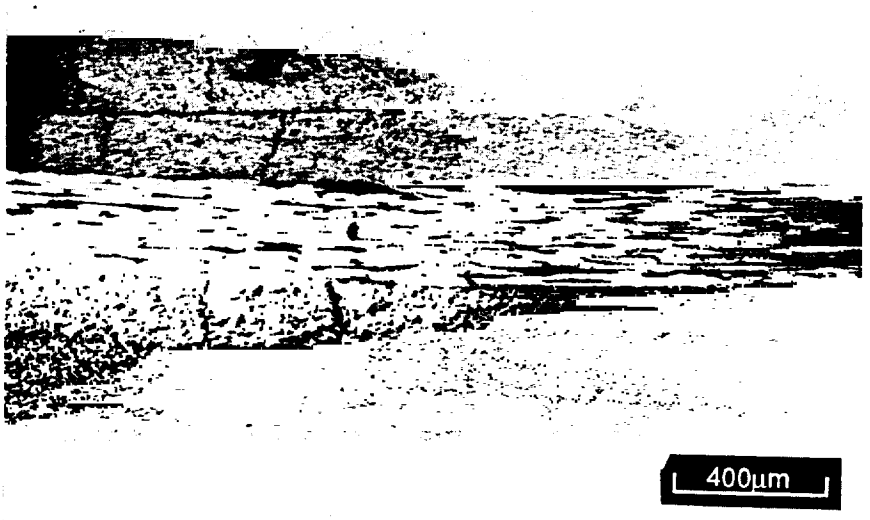

(a) As-Fabricated

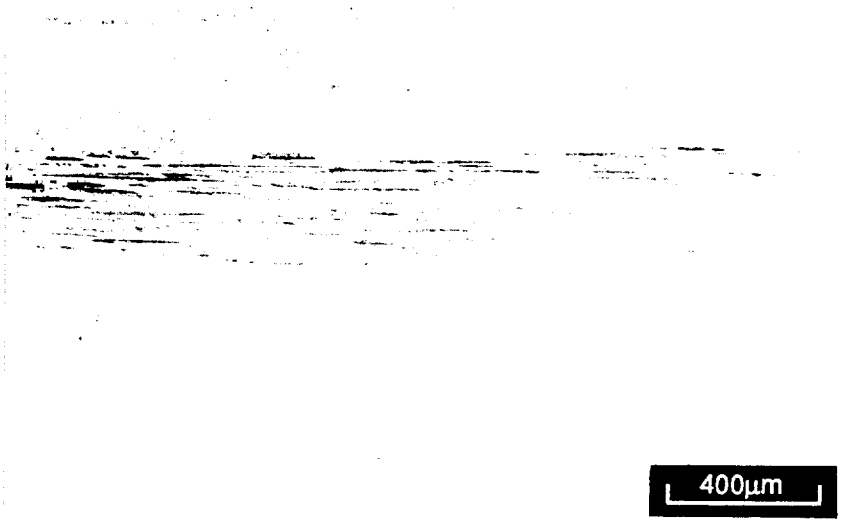

(b) Thermal Cycled

Figure 11-3 Longitudinal Photomicrographs of As-Fabricated and Thermal Cycled $[0, \pm 45, 90]_s$ P75/PEEK Specimens

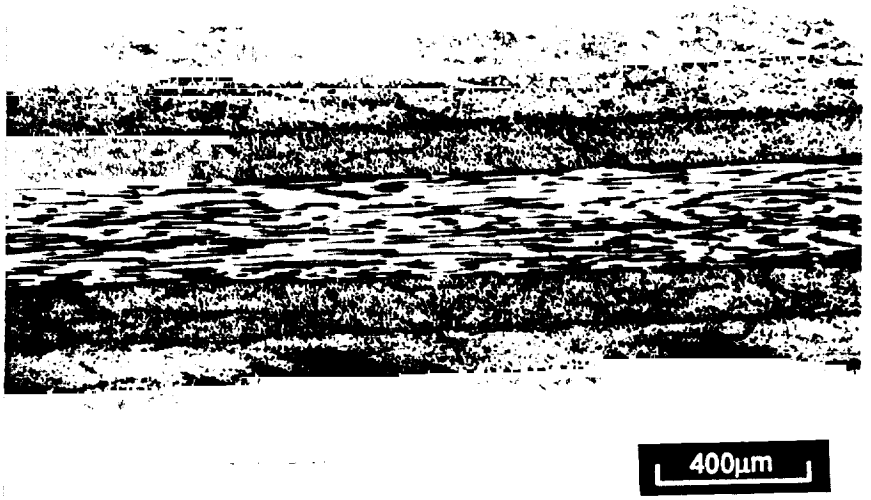

(a) As-Fabricated

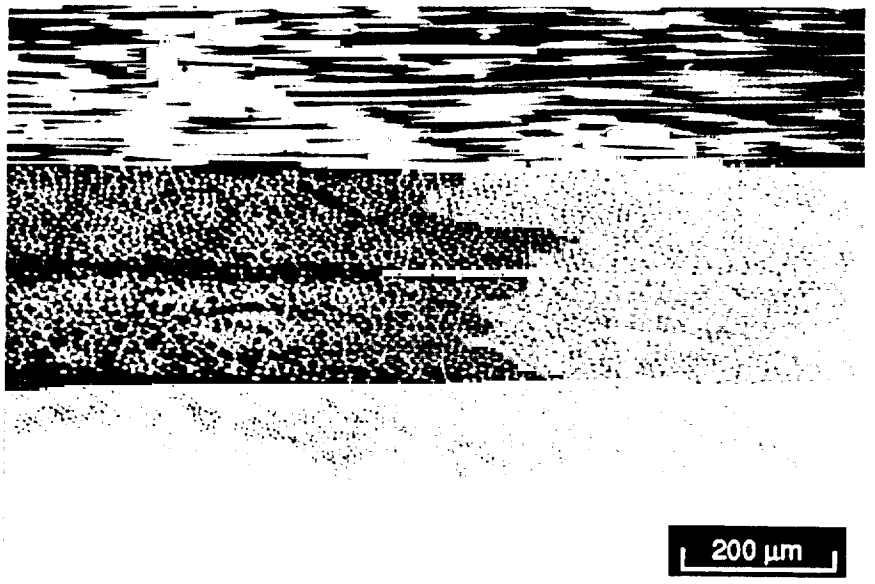

(b) Thermal Cycled

Figure 11-4 Transverse Photomicrographs of As-Fabricated and Thermal Cycled $[0, \pm 45, 90]_s$ AS4/PES Specimens

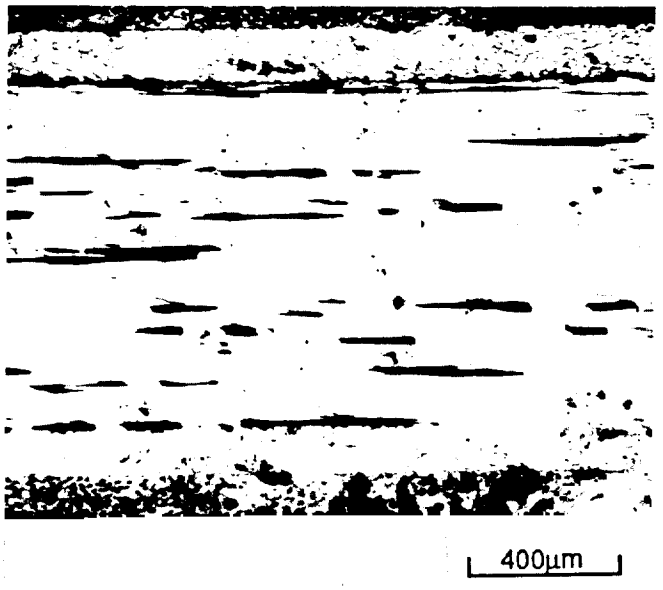

(a) As-Fabricated

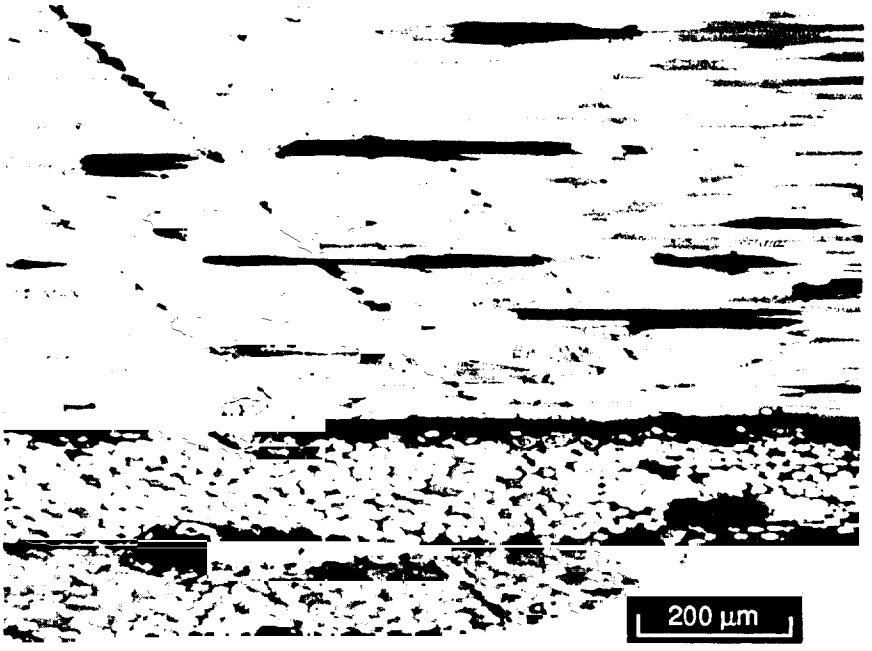

(b) Thermal Cycled

Figure 11-5 Longitudinal Photomicrographs of As-Fabricated and Thermal Cycled $[\pm 30, 0_4]_s$ P75/1962 Specimens

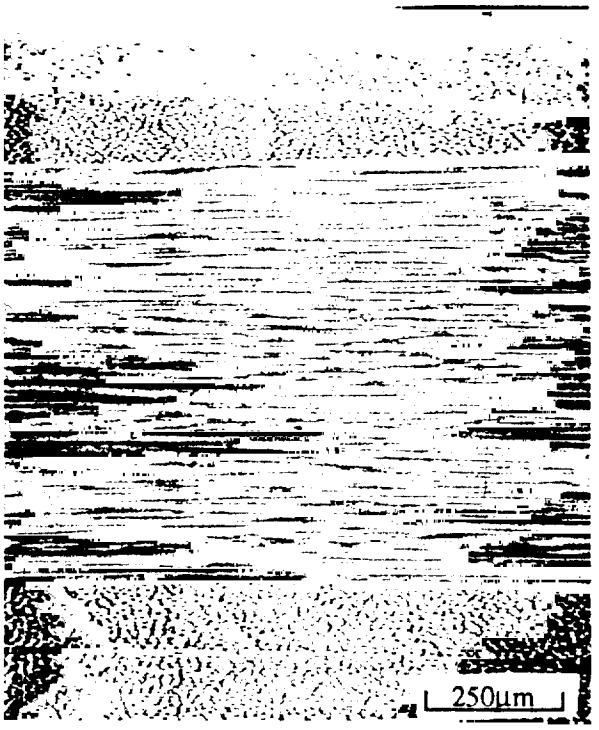

(a) As-Fabricated

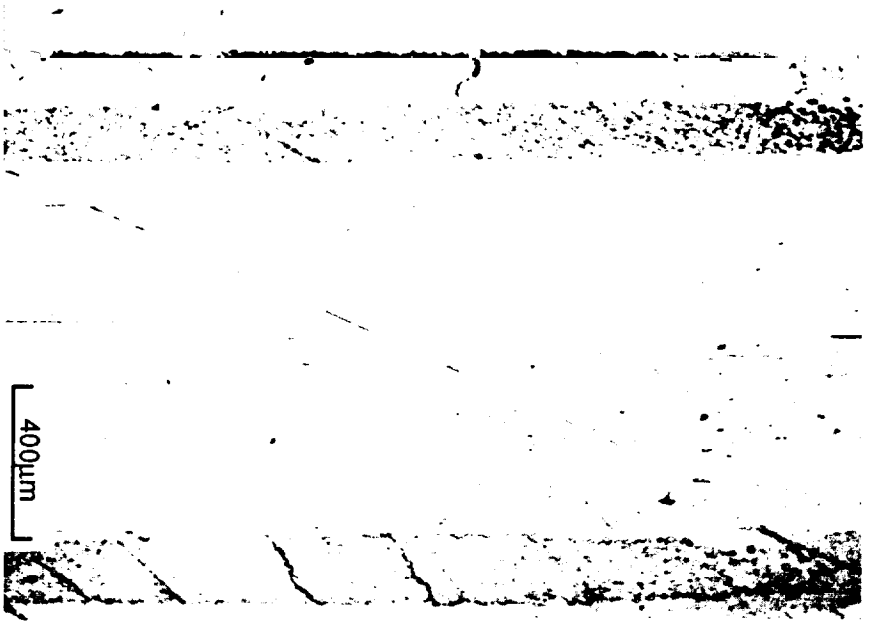

(b) Thermal Cycled

Figure 11-6 Longitudinal Photomicrographs of As-Fabricated and Thermal Cycled $[\pm 30, 0_4]_s$ P75/PEEK Specimens

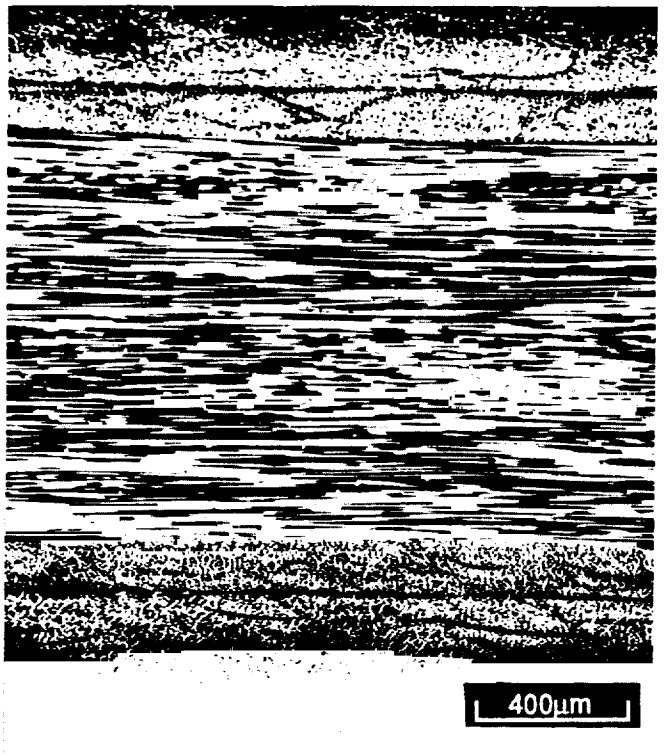

(a) As-Fabricated

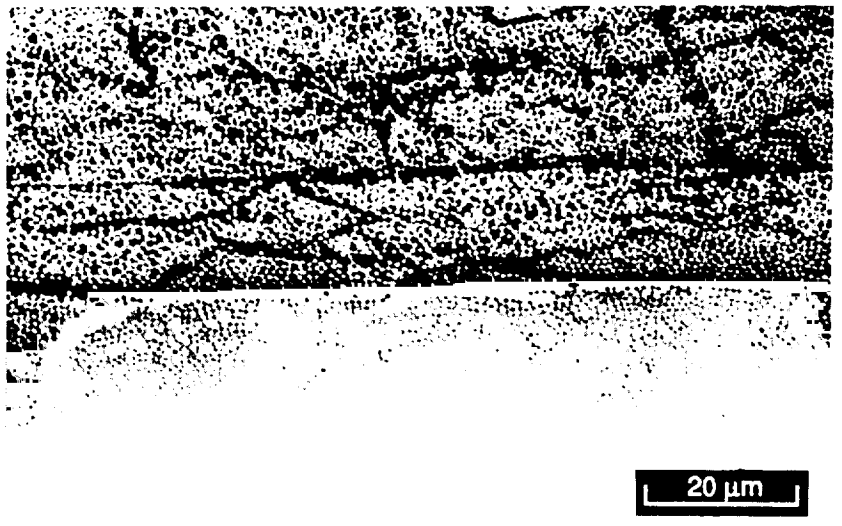

(b) Thermal Cycled

Figure 11-7 Longitudinal Photomicrographs of As-Fabricated and Thermal Cycled $[\pm 30, 0_4]_S$ AS4/PES Specimens

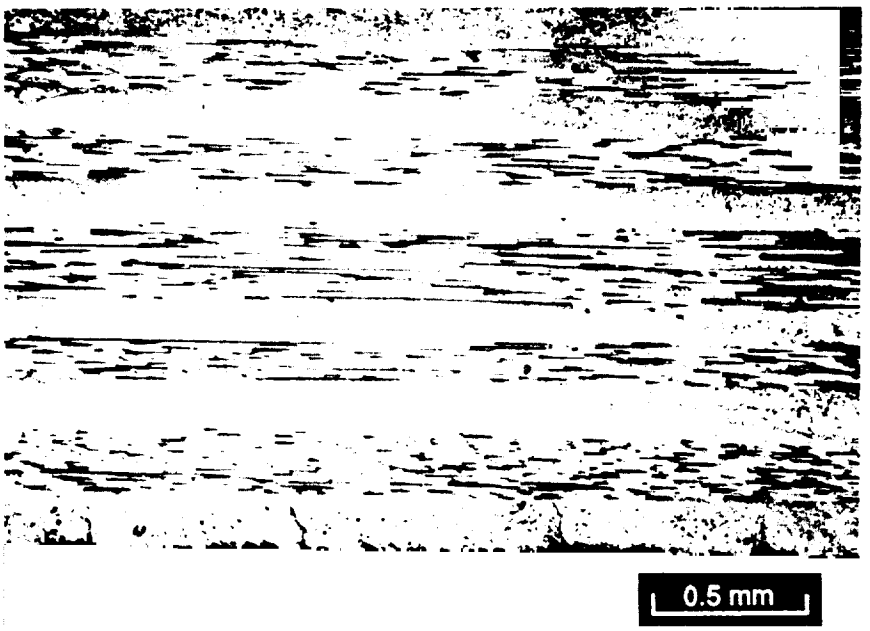

(a) As-Fabricated

(b) Thermal Cycled

Figure 11-8 Transverse Photomicrographs of As-Fabricated and Thermal Cycled $[0/90]_6$ HMU/7740 BSG Specimens

• No microcracks were observed in P75/1962 $[0]_8$ and discontinuous SiC/Al specimens even after 10,099 cycles (Figure 11-9 and 11-10).

• In P100/6061 Al there was no detectable increase in baseline microcrack density (Figure 11-11). Only in a diffusion bonded tube a localized microcrack at the notch root extended after 5500 cycles. Generally in MMC, the thermal stresses generated during cycling are accommodated by microplastic deformation at the fiber/matrix interface.

11.3.3 Material Property Tests

Exposure to repeated thermal cycling can significantly degrade the thermal and mechanical properties of advanced composites. Therefore, tension, compression, and CTE tests were performed to determine the extent of property changes in the thermal cycled specimens compared to the as fabricated specimens.

(a) Tension and Compression

To provide an assessment of the effect of thermal cycling, the longitudinal and transverse mechanical property results are compared with the properties of the as fabricated composites in Tables 1-8 and 1-9 respectively (reproduced in this chapter for reference). Longitudinal and transverse tension test results of each composite material are presented in Tables 11-3 to 11-31, and the longitudinal and transverse compression test results are listed in Table 11-32 to 11-62.

Based on results of limits number of specimens, it is difficult to establish the extent of property degradation due to thermal cycling. Also, the changes in mechanical properties are intimately related to the extent of microdamage and baseline properties of the as fabricated composites.

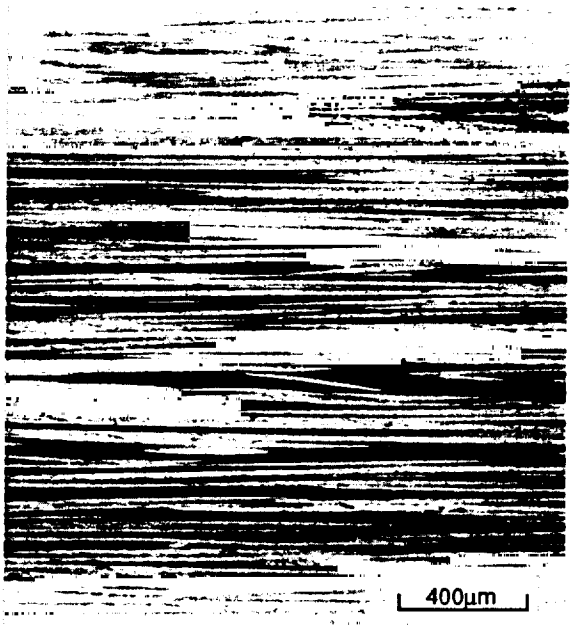

Figure 11-9 Photomicrograph of P75/1962 $[0]_8$ Specimen after 10,099 Thermal Cycles Between -150°F and +150°F Showing no Microcracks

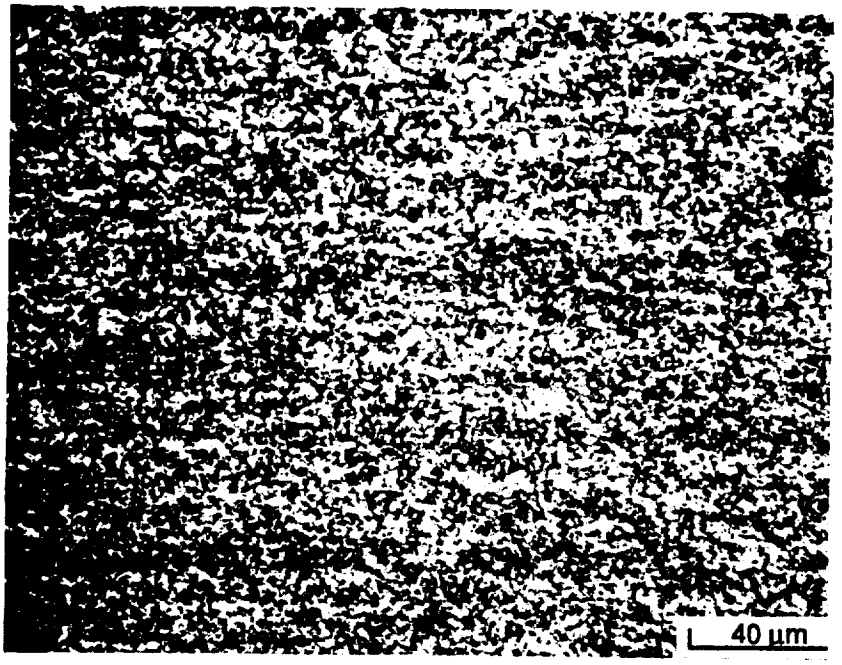

Figure 11-10 Photomicrograph of 25 v/o SiC/2124-T6 Al Specimen After 10,099 Thermal Cycles Between -150°F and +150°F Showing no Microcracks or Interfacial Disbonds

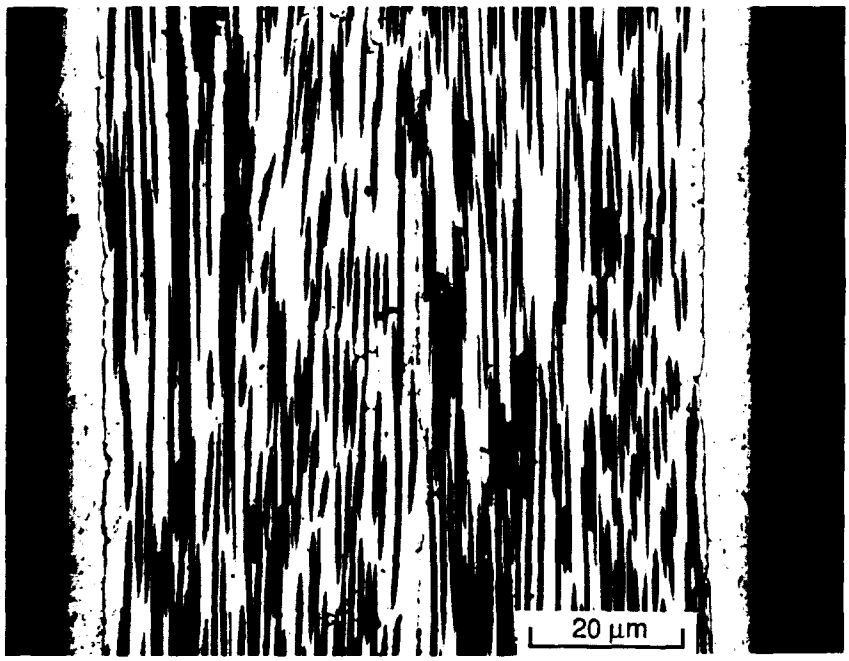

(a) As-Fabricated

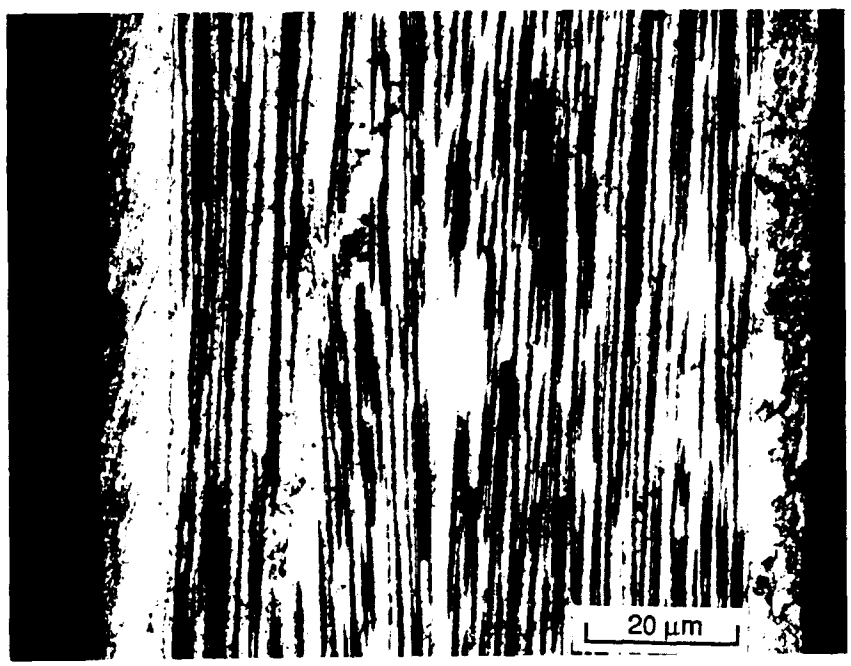

(b) Thermal Cycled

Figure 11-11 Photomicrographs of As-Fabricated and Thermal Cycled $[0]_2$ P100/6061 Al Specimens Showing No Detectable Increase in Baseline Microcrack Density

Table 1-8 Effect of Thermal Cycling on the Longitudinal Tensile and Compressive Properties of Composite Materials (Reproduced in this Chapter for Reference)

Material	Density (lb/in^3)	Tension				Compression			
		E_x^T (Msi)		σ_x^{TU} (ksi)		E_x^C (Msi)		σ_x^{CU} (ksi)	
		AF	TC	AF	TC	AF	TC	AF	TC
P75/1962									
•62.2v/o, $[0, \pm45, 90]_s$	0.0623	15.2	14.35	44.6	31.5	13.9	9.88	26.5	25.66
•62.2v/o, $[\pm30, 0_4]_s$	0.0623	32.68	28.2	85.5	64.9	27.6	23.09	54.3	49.71
P75/PEEK									
•62.2v/o, $[0, \pm45, 90]_s$	0.063	13.3	13.3	34.91	37.2	9.02	10.30	21.35	24.21
•62.2v/o, $[\pm30, 0_4]_s$	0.063	30.06	31.6	68.77	68.14	28.40	21.43	51.38	40.2
AS4/PES									
•62.2v/o, $[0, \pm45, 90]_s$	0.058	6.38	6.41	80.34	77.1	5.82	5.42	47.31	45.45
•62.2v/o, $[\pm30, 0_4]_s$	0.058	14.18	14.5	101.61	78.4	12.36	10.86	90.29	76.88
SiC_p/Al									
•25 v/o, N/A	0.104	16.64	16.8	84.5	86.2	18.5	16.50	73.5	76.85
•35 v/o, N/A	0.106	19.9	19.9	95.6	92.8	20.4	18.18	103.3	92.98
SiC_w/Al									
•25 v/o, N/A	0.104	17.6	17.1	102.0	96.7	18.15	16.13	102.5	94.26
•35 v/o, N/A	0.106	18.8	18.9	85.7	75.3	19.22	19.28	97.02	97.64
P100/Al									
•42.2 v/o, [0, 0]	0.090	49.71	52.48	131.3	127.0	48.15	45.33	46.62	43.70
HMU/7070									
•44 v/o, $[0]_{12}$	0.072	26.43	—	95.5	—	21.3	21.66	126.3	115.34
•40.5 v/o, $[0/90]_6$	0.071	11.7	—	40.9	—	12.5	12.44	86.7	84.68
C-C									
•52.48 v/o, [0, 0, 0]	0.060	43.7	—	81.5	—	39.4	—	47.8	—
•53.0 v/o, [0/90/0]	0.060	32.4	—	44.1	36.78	29.1	28.58	6.95	15.63
SiC_p/Al Tubes									
•25 v/o, N/A	0.104	15.8	16.34	>63.4	85.5	17.3	16.33	90.1	84.6
•35 v/o, N/A	0.106	18.9	17.36	90.6	87.65	19.3	18.05	113.1	89.75
SiC_w/Al Tubes									
•25 v/o, N/A	0.104	19.8	17.73	>86.9	99.2	19.6	20.16	130.3	112.7
•35 v/o, N/A	0.106	22.3	19.93	>85.6	74.0	22.4	20.72	133.3	115.55

Table 1-9 Effect of Thermal Cycling on the Transverse Tensile and Compressive Properties of Composite Materials (Reproduced in this Chapter for Reference)

Material	Density (lb/in^3)	Tension				Compression			
		E_x^T (Msi)		σ_x^{TU} (ksi)		E_x^C (Msi)		σ_x^{CU} (ksi)	
		AF	TC	AF	TC	AF	TC	AF	TC
P75/1962									
•62.2v/o, $[0, \pm 45, 90]_s$	0.0623	15.2	15.5	50.1	42.2	14.54	11.58	27.6	25.08
•62.2v/o, $[\pm 30, 0_4]_s$	0.0623	1.79	1.70	4.4	4.06	1.73	1.44	17.7	17.58
P75/PEEK									
•62.2v/o, $[0, \pm 45, 90]_s$	0.063	14.45	13.6	46.12	39.7	9.36	9.43	21.75	25.46
•62.2v/o, $[\pm 30, 0_4]_s$	0.063	1.40	1.21	5.46	5.61	1.14	1.17	17.54	17.96
AS4/PES									
•62.2v/o, $[0, \pm 45, 90]_s$	0.058	6.51	6.7	77.69	71.4	5.63	5.95	30.36	26.67
•62.2v/o, $[\pm 30, 0_4]_s$	0.058	1.57	1.46	4.54	5.21	1.26	1.25	21.07	17.65
SIC_p/Al									
•25 v/o, N/A	0.104	17.0	16.8	77.5	90.6	17.9	17.73	75.8	86.33
•35 v/o, N/A	0.106	19.4	19.1	97.0	91.92	21.0	18.98	103.4	97.7
SIC_w/Al									
•25 v/o, N/A	0.104	16.42	16.3	97.4	93.0	16.5	15.98	91.0	75.76
•35 v/o, N/A	0.106	17.2	16.6	57.7	56.7	17.2	17.8	66.02	96.53
P100/Al									
•42.2 v/o, [0, 0]	0.090	5.14	—	3.62	—	4.82	4.40	15.21	20.30
HMU/7070									
•44 v/o, $[0]_{12}$	0.072	—	—	—	—	—	—	—	—
•40.5 v/o, $[0/90]_6$	0.071	11.9	—	78.4	—	—	13.14	—	74.57
C-C									
•52.48 v/o, [0, 0, 0]	0.060	1.45	—	2.04	—	1.3	—	4.6	—
•53.0 v/o, [0/90/0]	0.060	20.3	—	29.0	28.7	15.5	—	9.4	8.36
SIC_p/Al									
•25 v/o, N/A	0.104	—	—	—	—	—	—	—	—
•35 v/o, N/A	0.106	—	—	—	—	—	—	—	—
SIC_w/Al									
•25 v/o, N/A	0.104	—	—	—	—	—	—	—	—
•35 v/o, N/A	0.106	—	—	—	—	—	—	—	—

Table 11-3 Longitudinal Tensile Properties of Thermal Cycled (10, 099 cycles) P75/1962, [0, 45, -45, 90]$_s$, v/o = 62.2.

Specimen # (GE)(PQ)(TP)-	Elastic Modulus E_x^T (Msi)	Ultimate Tensile Strength (ksi)	Poisson Ratio ν_{xy}	Strain To Failure (%)
TNL-1	—	—	—	—
TNL-2	14.5	31.5	0.3000	0.210
TNL-3	14.4	33.8	0.2880	0.229
TNL-4	14.5	31.4	0.2915	0.210
TNL-5	14.5	39.1	0.3123	0.258
TNL-6	14.2	30.5	0.3008	0.202
TNL-7	14.0	22.5	0.3080	0.153
Mean Value	14.35	31.5	0.3001	0.2103
Std. Dev.	0.2074	5.386	0.0093	0.0346
CV (%)	1.44%	17.1%	3.1%	16.4%
0 Cycles Data	15.21	44.6	0.3066	0.261

Table 11-4 Transverse Tensile Properties of Thermal Cycled (10, 099 cycles) P75/1962, [0, 45, -45, 90]$_s$, v/o = 62.2.

Specimen # (GE)(PQ)(TP)-	Elastic Modulus E_y^T (Msi)	Ultimate Tensile Strength (ksi)	Poisson Ratio ν_{yx}	Strain To Failure (%)
TNT-1	14.3	46.1	0.2699	0.335
TNT-2	16.7	38.2	0.3636	0.230
TNT-3	15.3	43.4	0.3422	0.277
TNT-4	15.7	45.6	0.3179	0.295
TNT-5	15.3	37.8	0.3427	0.245
Mean Value	15.5	42.2	0.3273	0.2764
Std. Dev.	0.8649	3.986	0.0359	0.042
CV (%)	15.6%	9.4%	11%	15%
0 Cycles	15.2	50.1	0.3146	0.3

Table 11-5 Longitudinal Tensile Properties of Thermal Cycled (10, 099 cycles) P75/1962, $[\pm 30, 0_4]_s$, v/o = 62.7.

Specimen # (GE)(PZ)(TP)-	Elastic Modulus E_x^T(Msi)	Ultimate Tensile Strength (ksi)	Poisson Ratio ν_{xy}	Strain To Failure (%)
TNL-1	23.7	39.4	1.5938	0.168
TNL-2	26.2	44.5	1.6696	0.169
TNL-3	26.7	65.4	1.4877	0.231
TNL-4	29.1	66.4	1.5942	0.217
TNL-5	31.3	77.4	1.6714	0.398
TNL-6	29.8	79.6	1.4566	0.254
TNL-7	30.8	81.3	1.2545	0.249
Mean Value	28.2	64.9	1.5325	0.2409
Std. Dev.	2.78	16.9	0.1476	0.078
CV (%)	9.9%	26.0%	9.6%	32.2
0 Cycles	32.68	85.5	1.212	0.29

Table 11-6 Transverse Tensile Properties of Thermal Cycled (10, 099 cycles) P75/1962, $[\pm 30, 0_4]_s$, v/o = 62.7.

Specimen # (GE)(PZ)(TP)-	Elastic Modulus E_y^T(Msi)	Ultimate Tensile Strength (ksi)	Poisson Ratio ν_{yx}	Strain To Failure (%)
TNT-1	1.59	4.1	0.0640	0.270
TNT-2	1.66	3.9	0.1316	0.236
TNT-3	2.00	3.9	0.1667	0.210
TNT-4	1.73	4.3	0.1364	—
TNT-5	1.30	4.1	0.0844	0.321
Mean Value	1.70	4.06	0.1166	0.2593
Std. Dev.	0.252	0.1673	0.042	0.0479
CV (%)	14.8%	4.1	36%	18.5%
0 Cycles	1.73	4.4	0.082	1

Table 11-7 Longitudinal Tensile Properties of Thermal Cycled (10, 099 cycles) P75/PEEK, [0, ±45, 90]$_s$, v/o = 62.2.

Specimen # (GK)(PQ)(TP)-	Elastic Modulus E^T_x(Msi)	Ultimate Tensile Strength (ksi)	Poisson Ratio ν_{xy}	Strain To Failure (%)
TNL-1	13.3	36.3	0.3468	0.273
TNL-2	12.9	33.6	0.3636	0.258
TNL-3	13.1	36.4	0.3550	0.277
TNL-4	14.6	38.3	0.3594	0.262
TNL-5	13.6	38.7	0.3180	0.285
TNL-6	13.0	38.0	0.2888	0.278
TNL-7	12.4	39.0	0.3454	0.315
Mean Value	13.3	37.2	0.3396	0.2783
Std. Dev.	0.6824	1.904	0.0269	0.0187
CV (%)	5.1%	5.1%	7.9%	6.7%
0 Cycles	13.3	34.91	0.349	0.26

Table 11-8 Transverse Tensile Properties of Thermal Cycled (10, 099 cycles) P75/PEEK, [0, ±45, 90]$_s$, v/o = 62.2.

Specimen # (GK)(PQ)(TP)-	Elastic Modulus E^T_y(Msi)	Ultimate Tensile Strength (ksi)	Poisson Ratio ν_{yx}	Strain To Failure (%)
TNT-1	14.7	36.2	0.3996	0.244
TNT-2	14.6	41.6	—	—
TNT-3	13.4	41.6	0.3657	0.294
TNT-4	13.8	40.5	0.3933	0.286
TNT-5	11.6	38.8	0.3235	0.328
Mean Value	13.6	39.7	0.3705	0.288
Std. Dev.	1.254	2.286	0.0346	0.0345
CV (%)	9.2%	5.8%	9.3%	12%
0 Cycles	14.45	46.12	0.338	0.35

Table 11-9 Longitudinal Tensile Properties of Thermal Cycled (10, 099 cycles) P75/PEEK, $[\pm 30, 0_4]_S$, v/o = 62.2.

Specimen # (GK)(PZ)(TP)-	Elastic Modulus E^T_x(Msi)	Ultimate Tensile Strength (ksi)	Poisson Ratio ν_{xy}	Strain To Failure (%)
TNL-1	32.6	67.6	1.8602	0.208
TNL-2	29.9	69.9	1.6057	0.236
TNL-3	35.2	62.2	2.1617	0.175
TNL-4	34.0	67.7	1.9944	0.201
TNL-5	30.8	77.1	1.7513	0.258
TNL-6	29.7	64.2	1.5392	0.218
TNL-7	29.3	68.3	1.5942	0.237
Mean Value	31.6	68.14	1.7867	0.219
Std. Dev.	2.314	4.738	0.2315	0.02743
CV (%)	7.3%	7.0%	13.0%	12.5%
0 Cycles	30.06	68.77	1.37	0.23

Table 11-10 Transverse Tensile Properties of Thermal Cycled (10, 099 cycles) P75/PEEK, $[\pm 30, 0_4]_S$, v/o = 62.2.

Specimen # (GK)(PZ)(TP)-	Elastic Modulus E^T_y(Msi)	Ultimate Tensile Strength (ksi)	Poisson Ratio ν_{yx}	Strain To Failure (%)
TNT-1	1.47	4.90	0.0716	0.3
TNT-2	0.984	5.71	—	—
TNT-3	1.21	5.43	0.0873	0.35
TNT-4	1.23	6.03	0.0971	0.600
TNT-5	1.15	6.00	0.0742	0.47
Mean Value	1.21	5.614	0.0826	0.43
Std. Dev.	0.1751	0.4677	0.1189	0.0116
CV (%)	14.5%	8.3%	14.4%	26.9%
0 Cycles	1.14	5.46	0.07	0.44

Table 11-11 Longitudinal Tensile Properties of Thermal Cycled (10, 099 cycles) AS4/PES [0, ±45, 90]$_s$, v/o = 53.7.

Specimen # (CZ)(BQ)(TP)-	Elastic Modulus E^T_x(Msi)	Ultimate Tensile Strength (ksi)	Poisson Ratio ν_{xy}	Strain To Failure (%)
TNL-1	6.2	78.5	0.3811	0.01246
TNL-2	6.1	78.1	0.3542	0.01210
TNL-3	5.7	76.8	0.3485	0.01364
TNL-4	6.3	85.6	0.3481	0.01346
TNL-5	6.3	74.3	0.3628	0.01172
TNL-6	6.9	71.0	0.4085	0.01040
TNL-7	7.4	75.4	0.3607	—
Mean Value	6.41	77.1	0.3663	0.012296
Std. Dev.	0.5610	4.53	0.02175	0.0012
CV (%)	8.8%	5.9%	5.9%	9.7%
0 Cycles	6.38	80.34	0.292	0.0135

Table 11-12 Transverse Tensile Properties of Thermal Cycled (10, 099 cycles) AS4/PES [0, ±45, 90]$_s$, v/o = 53.7.

Specimen # (CZ)(BQ)(TP)-	Elastic Modulus E^T_y(Msi)	Ultimate Tensile Strength (ksi)	Poisson Ratio ν_{yx}	Strain To Failure (%)
TNT-1	6.9	81.5	0.3443	0.0120
TNT-2	7.0	71.1	0.3333	0.1034
TNT-3	6.7	72.2	0.3548	0.0099
TNT-4	6.3	85.8	0.3333	0.01338
TNT-5	6.6	46.3	0.3030	0.00666
Mean Value	6.7	71.4	0.3337	0.0105
Std. Dev.	0.2739	15.33	0.194	0.00253
CV (%)	4.1%	21.5%	5.8%	24.1%
0 Cycles	6.51	77.69	0.324	0.0118

Table 11-13 Longitudinal Tensile Properties of Thermal Cycled (10, 099 cycles) AS4/PES [±30, 0_4]$_S$, v/o = 54.96.

Specimen # (CZ)(BZ)(TP)-	Elastic Modulus E^T_x(Msi)	Ultimate Tensile Strength (ksi)	Poisson Ratio ν_{xy}	Strain To Failure (%)
TNL-1	13.7	84.2	0.8004	0.00586
TNL-2	14.8	76.2	0.9447	0.00514
TNL-3	14.6	79.2	0.9901	0.00540
TNL-4	11.6	65.9	0.7443	0.00570
TNL-5	13.9	77.6	0.7638	0.00556
TNL-6	17.3	68.4	1.0118	0.00394
TNL-7	15.5	97.3	0.9500	0.00574
Mean Value	14.5	78.4	0.8864	0.00533
Std. Dev.	1.749	10.43	0.1129	0.00066
CV (%)	12.1%	13.3%	12.7%	12.4%
0 Cycles	14.18	101.61	0.887	0.009

Table 11-14 Transverse Tensile Properties of Thermal Cycled (10, 099 cycles) AS4/PES [±30, 0_4]$_S$, v/o = 54.96.

Specimen # (CZ)(BZ)(TP)-	Elastic Modulus E^T_y(Msi)	Ultimate Tensile Strength (ksi)	Poisson Ratio ν_{yx}	Strain To Failure (%)
TNT-1	1.7	6.39	0.1902	0.00688
TNT-2	1.6	5.82	0.1526	0.00814
TNT-3	1.3	5.79	0.1226	0.01034
TNT-4	1.3	4.54	0.0778	0.00478
TNT-5	1.4	3.49	0.1053	0.00312
Mean Value	1.46	5.21	0.1297	0.0067
Std. Dev.	0.1817	1.173	0.0434	0.0028
CV (%)	12.4%	22.5%	33.4%	42.1%
0 Cycles	1.57	4.54	0.827	0.002

Table 11-15 Longitudinal Tensile Properties of Thermal Cycled (10, 099 cycles) P100/6061 $[0]_2$, v/o = 42.2.

Specimen # (GA)(DU)(TP)-	Elastic Modulus E^T_x(Msi)	Ultimate Tensile Strength (ksi)	Poisson Ratio ν_{xy}	Strain To Failure (%)
TNL-1	48.3	123	0.277	0.0025
TNL-2	52.9	139	0.305	0.0027
TNL-3	52.6	138	0.337	0.0026
TNL-4	52.9	129	0.278	0.0026
TNL-5	52.9	121	0.267	0.0024
TNL-6	53.8	129	0.3181	0.0024
TNL-7	52.9	114	0.311	0.0021
TNL-8	53.5	123	0.352	0.0023
Mean Value	52.48	127	0.283	0.00245
Std. Dev.	1.73	8.54	0.0657	0.000192
CV (%)	3.30%	6.72%	23.3%	7.87%
0 Cycles	49.71	131.3	0.295	0.0012

Table 11-16 Longitudinal Tensile Properties of Thermal Cycled (10, 099 cycles) P100/AZ91C Mg $[\pm 16^\circ]_s$, v/o = 30.1

Specimen # (GA)(MU)(TT)- 30.1%	Elastic Modulus E^T_x(Msi)	Ultimate Tensile Strength (ksi)	Poisson Ratio ν_{xy}	Strain To Failure (%)
TNL-1	31.6	73.8	0.6091	0.00243
TNL-2	25.4	65.1	0.5231	0.00264
TNL-3	40.6	57.0	1.0778*	—
TNL-4	30.1	68.0	0.8385	0.00231
TNL-5	—	—	—	—
Mean Value	31.9	66.0	0.6569	0.00246
Std. Dev.	6.36	6.99	0.163	0.00017
CV (%)	19.9%	10.6%	24.8%	6.8%
0 Cycles	25.44	61.2	0.4588	0.00278

* Unusual Noise Transverse Strain Gage Response, Not Included in Average

Table 11-17 Longitudinal Tensile Properties of Thermal Cycled (10, 099 cycles) P100/AZ91C Mg [±16°]$_s$, v/o = 27.9.

Specimen # (GM)(MU)(TT) 27.9 v/o	Elastic Modulus E^T_x(Msi)	Ultimate Tensile Strength (ksi)	Poisson Ratio ν_{xy}	Strain To Failure (%)
TNL-1	26.5	16.5	0.6643	0.00101
TNL-2	27.5	15.5	1.0714*	0.0014
TNL-3	24.6	15.9	0.5357	0.00117
TNL-4	16.0	16.6	0.5930	0.00194
TNL-5	19.8	21.9	0.6944	0.00223
Mean Value	22.9	17.3	0.6219	0.00155
Std. Dev.	4.85	2.62	0.0715	0.00052
CV (%)	21.2%	15.2	11.5%	33.4%
	17.7	14.8	0.6491	0.00192

*Unusual Noise Transverse Strain Gage Response, Not Included in Average

Table 11-18 Longitudinal Tensile Properties of Thermal Cycled (10, 099 cycles) P100/AZ91C Mg [±16°]$_s$, v/o = 23.7.

Specimen # (GM)(MU)(TT)- 23.7 v/o	Elastic Modulus E^T_x(Msi)	Ultimate Tensile Strength (ksi)	Poisson Ratio ν_{xy}	Strain To Failure (%)
TNL-1	21.4	54.4	0.6000	0.00257
TNL-2	23.8	50.3	0.4688	0.00277
TNL-3	26.4	45.0	0.4085	0.00216
TNL-4	20.7	48.9	0.5318	0.00238
TNL-5	15.4	43.1	0.3267	0.00273
Mean Value	20.1	48.34	0.4672	0.00242
Std. Dev.	2.71	4.46	0.1061	0.00023
CV (%)	13.5%	9.2%	22.7%	9.5%
0 Cycles	17.5	49.4	0.7586	0.00243

Table 11-19 Longitudinal Tensile Properties of Thermal Cycled (10, 099 cycles) 25 v/o SiC_p/2124-T6 Al.

Specimen # (25PA)(CQ)(TP)-	Elastic Modulus E_x^T (Msi)	Yield Strength (ksi)	Ultimate Tensile Strength (ksi)	Poisson Ratio ν_{xy}
TNL-1	16.0	70.0	85.3	0.2708
TNL-2	16.7	70.6	88.8	0.2784
TNL-3	17.1	69.3	87.1	0.2741
TNL-4	16.9	70.3	84.4	0.2664
TNL-5	17.4	71.3	85.6	0.2680
Mean Value	16.8	70.3	86.2	0.2715
Std. Dev.	0.5263	0.7382	1.73	0.0048
CV (%)	3.1%	1.1%	2.0%	1.8%
0 Cycles	16.64	—	84.5	0.267

Table 11-20 Transverse Tensile Properties of Thermal Cycled (10, 099 cycles) 25 v/o SiC_p/2124-T6 Al.

Specimen # (25PA)(CQ)(TP)-	Elastic Modulus E_y^T (Msi)	Yield Strength (ksi)	Ultimate Tensile Strength (ksi)	Poisson Ratio ν_{yx}
TNT-1	17.1	70.8	89.1	0.2686
TNT-2	16.0	75.5	92.4	0.2744
TNT-3	16.7	71.3	86.8	0.2714
TNT-4	16.7	73.8	91.3	0.2817
TNT-5	17.7	73.5	93.3	0.2752
Mean Value	16.8	73.0	90.6	0.2743
Std. Dev.	0.623	19.3	2.632	0.00491
CV (%)	3.7%	2.6%	2.9%	1.8%
0 Cycles	17.0	77.5	77.5	0.279

Table 11-21 Longitudinal Tensile Properties of Thermal Cycled (10, 099 cycles) 25 v/o SiC_w/2124-T6 Al.

Specimen # (25WA)(CQ)(TP)-	Elastic Modulus E_x^T (Msi)	Yield Strength (ksi)	Ultimate Tensile Strength (ksi)	Poisson Ratio ν_{xy}
TNL-1	17.2	76.0	97.9	0.2855
TNL-2	17.8	71.3	92.9	0.2847
TNL-3	16.5	71.9	98.8	0.2830
TNL-4	17.5	76.1	99.1	0.2878
TNL-5	16.7	73.1	94.6	0.239
Mean Value	17.1	73.7	96.7	0.2870
Std. Dev.	0.5413	2.26	2.76	0.0042
CV (%)	3.2%	3.1%	2.9%	1.5%
0 Cycles	17.6	76.2	102.0	0.279

Table 11-22 Transverse Tensile Properties of Thermal Cycled (10, 099 cycles) 25 v/o SiC_w/2124-T6 Al.

Specimen # (25WA)(CQ)(TP)-	Elastic Modulus E_y^T (Msi)	Yield Strength (ksi)	Ultimate Tensile Strength (ksi)	Poisson Ratio ν_{yx}
TNT-1	16.1	69.6	90.1	0.2694
TNT-2	16.0	68.8	90.0	0.2639
TNT-3	16.4	72.0	93.6	0.2746
TNT-4	16.1	73.3	94.0	0.2666
TNT-5	16.8	72.4	97.3	0.2692
Mean Value	16.3	71.2	93.0	0.2687
Std. Dev.	0.3271	1.9	3.05	0.00397
CV (%)	2.0%	2.7%	3.3%	1.5%
0 Cycles	16.42	71.2	97.4	0.2717

Table11-23 Longitudinal Tensile Properties of Thermal Cycled (10, 099 cycles) 35 v/o SiC_p/2124-T6 Al.

Specimen # (35PA)(CQ)(TP)-	Elastic Modulus E_x^T (Msi)	Yield Strength (ksi)	Ultimate Tensile Strength (ksi)	Poisson Ratio ν_{xy}
TNL-1	20.9	93.0	93.3	0.2685
TNL-2	20.3	90.6	91.3	0.2743
TNL-3	19.4	92.6	96.8	0.2517
TNL-4	19.4	90.1	91.3	0.2593
TNL-5	19.5	91.9	92.8	0.2531
TNL-6	18.8	91.2	95.2	0.2550
TNL-7	20.9	92.3	92.3	0.2634
TNL-8	19.8	—	89.6	0.2602
Mean Value	19.9	91.6	92.8	0.2607
Std. Dev.	0.7592	1.07	2.299	0.00781
CV (%)	3.8%	1.2%	2.5%	3.0%
0 Cycles	19.9	86.5	95.6	0.267

Table 11-24 Transverse Tensile Properties of Thermal Cycled (10, 099 cycles) 35 v/o SiC_p/2124-T6 Al.

Specimen # (35PA)(CQ)(TP)-	Elastic Modulus E_y^T (Msi)	Yield Strength (ksi)	Ultimate Tensile Strength (ksi)	Poisson Ratio ν_{yx}
TNT-1	19.5	89.8	90.3	0.2520
TNT-2	19.7	88.9	94.8	0.2618
TNT-3	18.9	91.3	96.1	0.2453
TNT-4	18.5	89.9	92.0	0.2407
TNT-5	18.9	—	86.4	0.2453
Mean Value	19.1	90.0	91.92	0.2490
Std. Dev.	0.04899	0.99	3.84	0.0082
CV (%)	2.6%	1.1%	4.2%	3.3%
0 Cycles	19.4	88.2	97.0	0.2481

Table 11-25 Longitudinal Tensile Properties of Thermal Cycled (10, 099 cycles) 35 v/o SiC_w/2124-T6 Al.

Specimen # (35WA)(CQ)(TP)-	Elastic Modulus E_x^T (Msi)	Yield Strength (ksi)	Ultimate Tensile Strength (ksi)	Poisson Ratio ν_{xy}
TNL-1	19.4	76.1	78.4	0.2796
TNL-2	19.1	—	74.1	0.2778
TNL-3	18.1	—	73.5	0.2826
Mean Value	18.9	76.1	75.3	0.2800
Std. Dev.	0.681	—	2.673	0.0024
CV (%)	3.6%	—	3.5%	0.9%
0 Cycles	18.8	73.2	85.7	0.2711

Table 11-26 Transverse Tensile Properties of Thermal Cycled (10, 099 cycles) 35 v/o SiC_w/2124-T6 Al.

Specimen # (35WA)(CQ)(TP)-	Elastic Modulus E_y^T (Msi)	Yield Strength (ksi)	Ultimate Tensile Strength (ksi)	Poisson Ratio ν_{yx}
TNT-1	16.2	N/A	58.9	0.2410
TNT-2	18.5		53.8	0.2560
TNT-3	15.2		57.3	0.2615
Mean Value	16.6		56.7	0.2528
Std. Dev.	1.69		2.61	0.0106
CV (%)	10.2%		4.6%	4.2%
0 Cycles	17.2		57.7	0.2363

Table 11-27 Longitudinal and Transverse Tensile Properties of Thermal Cycled (10,099 Cycles) [0/90/0] P100/Carbon, v/o = 53.0.

Specimen # (CC)(HB)(TP)-	Elastic Modulus $E^{T}_{x,y}$ (Msi)	Ultimate Tensile Strength (ksi)	Strain To Failure (%)
Longitudinal			
TNL-1	23.7	31.3	0.12
TNL-2	22.3	40.2	—
TNL-3	31.25	33.3	0.10
TNL-4	29.9	42.3	0.17
Mean Value	26.79	36.78	0.13
Std. Dev.	3.85	5.30	0.03
CV (%)	14.4%	14.41	23.0 %
0 Cycles	32.4	44.1	0.167
Transverse			
TNT-1	13.7	28.7	—
0 Cycles	20.3	29.0	>0.15

Table 11-28 Longitudinal Tensile Properties of Thermal Cycled 25v/o SiC_p/2124-T6 Al Tubes

Speciment # (25PA)(CQ)(TT)	Elastic Modulus (Msi)				Ultimate Tensile Strength (ksi)	0.2% Yield Strength (ksi)	Strain To Failure (%)	Poisson Ratio
	E_{X1}	E_{X2}	E_{X3}	E_X				
TNL-1	17.11	17.8	16.88	17.26	89.4	71.7	>1.35*	0.27
TNL-2	15.5	15.38	15.38	15.42	81.7	72.6	>1.35*	0.25
Mean				16.34	85.5	72.15	>1.35	0.26
Std. Dev.				1.3	5.4	0.636		0.014
CV (%)				7.96	6.31	0.88		5.38

*Strain Gage Saturation at 1.35%

Table 11-29 Longitudinal Tensile Properties of Thermal Cycled 35v/o SiC_p/2124-T6 Al Tubes

Speciment # (35PA)(CQ)(TT)	Elastic Modulus (Msi)				Ultimate Tensile Strength (ksi)	0.2% Yield Strength (ksi)	Strain To Failure (%)	Poisson Ratio
	E_{X1}	E_{X2}	E_{X3}	E_X				
TNL-1	16.18	16.92	18.54	17.21	88.6	76.7	1.25	0.23
TNL-2	15.2	18.75	18.55	17.5	86.7	75.1	1.31	0.26
Mean				17.36	87.65	75.9	1.28	0.245
Std. Dev.				0.21	1.34	1.13	0.035	0.02
CV (%)				1.2	1.53	1.49	2.7	8.15

Table 11-30 Longitudinal Tensile Properties of Thermal Cycled 25v/o SiC_w/2124-T6 Al Tubes

Speciment # (25WA)(CQ)(TT)	Elastic Modulus (Msi)				Ultimate Tensile Strength (ksi)	0.2% Yield Strength (ksi)	Strain To Failure (%)	Poisson Ratio
	E_{X1}	E_{X2}	E_{X3}	E_X				
TNL-1	17.24	17.01	17.6	17.28	93.9	—	0.69	0.23
TNL-2	17.50	17.62	19.44	18.18	104.5	88.0	1.18	0.26
Mean				17.73	99.2	88.0	0.94	0.25
Std. Dev.				0.64	7.50		0.35	0.02
CV (%)				3.6	7.56		37.1%	0.87%

Table 11-31 Longitudinal Tensile Properties of Thermal Cycled 35v/o SiC_w/2124-T6 Al Tubes

Speciment # (35WA)(CQ)(TT)	Elastic Modulus (Msi)				Ultimate Tensile Strength (ksi)	0.2% Yield Strength (ksi)	Strain To Failure (%)	Poisson Ratio
	E_{X1}	E_{X2}	E_{X3}	E_X				
TNL-1	21.72	20.45	18.52	20.23	85.9	—	0.58	0.26
TNL-2	18.06	20.43	19.92	19.63	62.1	—	0.40	0.25
								0.255
Mean				19.93	74.0		0.49	0.007
Std. Dev.				0.424	16.8		0.13	2.7%
CV (%)				2.12%	22.7%		26.5%	

Table 11-32 Longitudinal Compressive Properties of Thermal Cycled (10, 099 cycles) P75/1962, [0, 45, -45, 90]$_s$, v/o = 62.2.

Specimen # (GE)(PQ)(TP)	Elastic Modulus E^C_x(Msi)	Ultimate Comp. Strength (ksi)	Poisson Ratio ν_{xy}	Strain To Failure (%)
CML-1	8.00	27.20	0.23	0.52
CML-2	9.20	18.10	0.37	0.31
CML-3	11.00	28.20	0.28	0.70
CML-4	11.10	26.80	0.46	0.63
CML-5	9.60	23.90	0.27	0.44
CML-6	9.23	27.30	0.27	0.74
CML-7	11.00	28.10	0.31	0.64
Mean Value	9.88	25.66	0.31	0.57
Std. Dev.	1.19	3.63	0.08	0.15
CV (%)	12.05	14.14	24.94	26.99

Table 11-33 Transverse Compressive Properties of Thermal Cycled (10, 099 cycles) P75/1962, [0, 45, -45, 90]$_s$, v/o = 62.2.

Specimen # (GE)(PQ)(TP)	Elastic Modulus E^C_y(Msi)	Ultimate Comp. Strength (ksi)
CMT-1	13.88	24.40
CMT-2	11.40	24.80
CMT-3	11.60	24.40
CMT-4	10.30	27.40
CMT-5	10.70	24.40
Mean Value	11.58	25.08
Std. Dev.	1.39	1.31
CV (%)	12.01	5.22

Table 11-34 Longitudinal Compressive Properties of Thermal Cycled (10, 099 cycles) P75/1962, $[\pm 30, 0_4]_S$, v/o = 62.7.

Specimen # (GE)(PZ)(TP)	Elastic Modulus E^C_x(Msi)	Ultimate Comp. Strength (ksi)	Poisson Ratio ν_{xy}	Strain To Failure (%)
CML-1	22.90	51.20	1.19	0.28
CML-2	25.60	50.20	1.86	0.32
CML-3	23.00	51.60	1.56	0.41
CML-4	22.50	49.60	1.69	0.38
CML-5	21.60	47.90	1.53	0.27
CML-^	24.30	50.00	1.27	0.28
CML-7	21.70	47.50	1.40	0.28
Mean Value	2.09	49.71	1.50	0.32
Std. Dev.	1.43	1.54	0.23	0.06
CV (%)	6.20	3.10	15.62	17.72

Table 11-35 Transverse Compressive Properties of Thermal Cycled (10, 099 cycles) P75/1962, $[\pm 30, 0_4]_S$, v/o = 62.7.

Specimen # (GE)(PZ)(TP)	Elastic Modulus E^C_y(Msi)	Ultimate Comp. Strength (ksi)	Poisson Ratio ν_{yx}	Strain To Failure (%)
CMT-1	2.02	17.50	0.26	—
CMT-2	1.60	17.10	0.56	—
CMT-3	1.08	18.50	0.26	—
CMT-4	1.04	17.20	0.15	0.90
Mean Value	1.44	17.58	0.31	
Std. Dev.	0.47	0.64	0.17	
CV (%)	32.47	3.64	56.84	

Table 11-36 Longitudinal Compressive Properties of Thermal Cycled (10, 099 cycles) P75/PEEK, $[0, \pm 45, 90]_s$, v/o = 62.2.

Specimen # (GK)(PQ)(TP)	Elastic Modulus E^C_x(Msi)	Ultimate Comp. Strength (ksi)	Poisson Ratio ν_{xy}	Strain To Failure (%)
CML-1	8.80	25.20	0.23	0.52
CML-2	9.70	24.90	0.41	0.62
CML-3	10.10	22.30	—	0.34
CML-4	9.80	24.70	0.30	0.64
CML-5	10.20	26.60	0.37	0.30
CML-6	11.60	24.70		0.26
CML-7	11.90	21.10	0.44	0.46
Mean Value	10.30	24.21	0.35	0.454
Std. Dev.	1.09	1.87	0.008	0.15
CV (%)	10.61	7.72	24.28	34.14

Table 11-37 Transverse Compressive Properties of Thermal Cycled (10, 099 cycles) P75/PEEK, $[0, \pm 45, 90]_s$, v/o = 62.2.

Specimen # (GK)(PQ)(TP)	Elastic Modulus E^C_y(Msi)	Ultimate Comp. Strength (ksi)
CMT-1	14.40	25.00
CMT-2	8.80	25.40
CMT-3	7.90	25.50
CMT-4	8.10	25.20
CMT-5	7.97	26.20
Mean Value	9.43	25.46
Std. Dev.	2.80	0.46
CV (%)	29.67	1.79

Table 11-38 Longitudinal Compressive Properties of Thermal Cycled (10, 099 cycles) P75/PEEK, $[\pm 30, 0_4]_S$, v/o = 62.2.

Specimen # (GK)(PZ)(TP)	Elastic Modulus E^C_x(Msi)	Ultimate Comp. Strength (ksi)
CML-1	—	—
CML-3	23.3	40.2
CML-5	17.6	44.4
CML-6	25.0	37.4
CML-7	19.8	38.8
Mean Value	21.43	40.2
Std. Dev.	3.34	2.62
CV (%)	15.59	6.5

Table 11-39 Transverse Compressive Properties of Thermal Cycled (10, 099 cycles) P75/PEEK, $[\pm 30, 0_4]_S$, v/o = 62.2.

Specimen # (GK)(PZ)(TP)	Elastic Modulus E^C_y(Msi)	Ultimate Comp. Strength (ksi)
CMT-1	1.6	18.5
CMT-2	1.1	19.4
CMT-3	0.9	18.9
CMT-4	1.13	16.3
CMT-5	1.1	16.2
Mean Value	1.17	17.96
Std. Dev.	0.26	1.38
CV (%)	22.2	7.7

Table 11-40 Longitudinal Compressive Properties of Thermal Cycled (10, 099 cycles) AS4/PES [0, ±45, 90]$_S$, v/o = 53.7.

Specimen # (CZ)(BQ)(TP)	Elastic Modulus E^C_x(Msi)	Ultimate Comp. Strength (ksi)	Poisson Ratio ν_{xy}	Strain To Failure (%)
CML-1	5.30	43.67	—	1.08
CML-2	5.40	46.50	0.13	1.03
CML-3	5.70	48.70	0.17	1.10
CML-4	6.00	53.20	0.14	0.76
CML-5	5.13	48.70	0.15	1.15
CML-6	5.09	44.80	0.19	0.94
CML-7	5.30	32.60	0.15	0.68
Mean Value	5.42	45.45	0.155	0.96
Std. Dev.	0.33	6.47	0.0217	0.18
CV (%)	6.01	14.23	13.99	18.66

Table 11-41 Transverse Compressive Properties of Thermal Cycled (10, 099 cycles) AS4/PES [0, ±45, 90]$_S$, v/o = 53.7.

Specimen # (CZ)(BQ)(TP)	Elastic Modulus E^C_y(Msi)	Ultimate Comp. Strength (ksi)	Poisson Ratio ν_{yx}	Strain To Failure (%)
CMT-1	6.40	28.30	0.15	0.78
CMT-2	6.00	24.10	0.16	0.30
CMT-4	5.44	27.60	0.15	1.90
Mean Value	5.95	26.67	0.15	0.99
Std. Dev.	0.48	2.25	0.01	0.82
CV (%)	8.11	8.44	5.04	82.66

Table 11-42 Longitudinal Compressive Properties of Thermal Cycled (10, 099 cycles) AS4/PES [±30, 0_4]$_S$, v/o = 54.96.

Specimen # (CZ)(BZ)(TP)	Elastic Modulus E^C_x(Msi)	Ultimate Comp. Strength (ksi)	Poisson Ratio ν_{xy}	Strain To Failure (%)
CML-1	10.35	64.30	1.06	0.79
CML-2	11.11	91.00	1.20	1.79
CML-3	9.87	65.20	4.24	0.37
CML-4	—	—	—	—
CML-5	11.90	93.00	4.04	0.27
CML-6	11.60	89.70	3.50	0.62
CML-7	10.4	55.10	3.32	0.36
Mean Value	10.86	76.38	2.89	0.70
Std. Dev.	0.81	16.68	1.41	0.57
CV (%)	7.46	21.84	48.65	81.11

Table 11-43 Transverse Compressive Properties of Thermal Cycled (10, 099 cycles) AS4/PES [±30, 0_4]$_S$, v/o = 54.96.

Specimen # (CZ)(BZ)(TP)	Elastic Modulus E^C_y(Msi)	Ultimate Comp. Strength (ksi)	Poisson Ratio ν_{yx}	Strain To Failure (%)
CMT-1	1.05	13.50	0.20	2.56
CMT-4	1.45	21.80	0.10	1.40
Mean Value	1.25	17.65	0.15	1.98
Std. Dev.	0.28	5.87	0.07	0.82
CV (%)	22.6	33.25	48.43	41.43

Table 11-44 Longitudinal Compressive Properties of Thermal Cycled (10, 099 cycles) 25 v/o SiC_p/2124-T6 Al.

Specimen # (25PA)(CQ)(TP)	Elastic Modulus E^C_x(Msi)	Yield Strength (ksi)	Ultimate Compressive Strength (ksi)	Strain To Failure (%)	Poisson Ratio ν_{xy}
CML-2	16.10	68.75	81.00	0.75	0.26
CML-3	14.60	62.89	70.70	0.72	0.25
CML-5	17.69	68.75	80.20	0.67	0.27
CML-6	17.60	68.75	75..50	0.69	0.27
Mean Value	16.50	67.29	76.85	0.71	0.26
Std. Dev.	1.46	2.93	4.76	0.03	0.01
CV (%)	8.85	4.35	6.20	4.95	3.65

Table 11-45 Transverse Compressive Properties of Thermal Cycled (10, 099 cycles) 25 v/o SiC_p/2124-T6 Al.

Specimen # (25PA)(CQ)(TP)	Elastic Modulus E^C_y(Msi)	Yield Strength (ksi)	Ultimate Compressive Strength (ksi)	Strain To Failure (%)	Poisson Ratio ν_{yx}
CMT-1	16.10	70.80	86.20	0.72	0.26
CMT-2	20.00	—	83.60	—	0.28
CMT-3	17.40	73.43	91.80	0.75	0.28
CMT-4	17.40	70.30	83.70	0.72	0.28
Mean Value	17.73	71.51	86.33	0.73	0.27
Std. Dev.	1.64	1.68	3.84	0.02	0.01
CV (%)	9.23	2.35	4.45	2.37	4.22

Table 11-46 Longitudinal Compressive Properties of Thermal Cycled (10, 099 cycles) 25 v/o SiC_w/2124-T6 Al.

Specimen # (25WA)(CQ)(TP)	Elastic Modulus E^C_x(Msi)	Yield Strength (ksi)	Ultimate Compressive Strength (ksi)	Strain To Failure (%)	Poisson Ratio ν_{xy}
CML-1	14.90	69.70	88.10	0.70	0.29
CML-2	16.30	79.80	95.60	0.71	0.29
CML-3	19.53	—	99.50	0.90	0.28
CML-4	14.80	73.90	94.40	0.82	0.26
CML-5	15.11	74.90	93.70	0.83	0.30
Mean Value	16.13	74.58	94.26	0.79	0.28
Std. Dev.	1.99	4.15	4.11	0.09	0.02
CV (%)	12.37	5.56	4.36	10.77	5.43

Table 11-47 Transverse Compressive Properties of Thermal Cycled (10, 099 cycles) 25 v/o SiC_w/2124-T6 Al.

Specimen # (25WA)(CQ)(TP)	Elastic Modulus E^C_y(Msi)	Yield Strength (ksi)	Ultimate Compressive Strength (ksi)	Strain To Failure (%)	Poisson Ratio ν_{yx}
CMT-1	16.10	72.30	76.60	0.70	0.27
CMT-2	17.10	—	78.40	0.84	0.32
CMT-3	15.50	66.10	73.80	0.76	0.27
CMT-4	15.40	68.70	74.30	0.77	0.26
CMT-5	15.80	—	75.70	0.64	0.25
Mean Value	15.98	69.03	75.76	0.74	0.27
Std. Dev.	0.68	3.11	1.85	0.08	0.03
CV (%)	4.28	4.51	2.44	10.19	9.86

Table11-48 Longitudinal Compressive Properties of Thermal Cycled (10, 099 cycles) 35 v/o SiC_p/2124-T6 Al.

Specimen # (35PA)(CQ)(TP)	Elastic Modulus E^C_x(Msi)	Yield Strength (ksi)	Ultimate Compressive Strength (ksi)	Strain To Failure (%)	Poisson Ratio ν_{xy}
CML-1	18.50	68.50	88.90	0.72	0.28
CML-2	—	—	—	—	—
CML-3	19.50	76.70	96.30	0.70	0.26
CML-4	15.50	70.10	87.70	0.72	0.25
CML-5	19.20	81.30	99.00	0.74	0.28
Mean Value	18.18	47.15	92.98	0.72	0.27
Std. Dev.	1.83	5.94	5.53	0.02	0.02
CV (%)	10.08	8.01	5.95	2.27	5.61

Table 11-49 Transverse Compressive Properties of Thermal Cycled (10, 099 cycles) 35 v/o SiC_p/2124-T6 Al.

Specimen # (35PA)(CQ)(TP)	Elastic Modulus E^C_y(Msi)	Ultimate Compressive Strength (ksi)	Strain To Failure (%)	Poisson Ratio ν_{yx}
CMT-1	19.20	97.70	—	0.25
CMT-2	19.80	99.40	0.80	0.25
CMT-3	19.20	94.50	0.78	0.27
CMT-4	18.20	100.00	0.74	0.25
CMT-5	18.50	96.90	0.76	0.26
Mean Value	18.98	97.70	0.77	0.26
Std. Dev.	0.63	2.18	0.03	0.01
CV (%)	3.34	2.23	3.35	3.49

Table 11-50 Longitudinal Compressive Properties of Thermal Cycled (10, 099 cycles) 35 v/o SiC_w/2124-T6 Al.

Specimen # (35WA)(CQ)(TP)	Elastic Modulus E^C_x(Msi)	Ultimate Compressive Strength (ksi)	Strain To Failure (%)	Poisson Ratio ν_{xy}
CML-1	18.00	89.00	0.70	0.29
CML-2	19.60	95.50	0.56	0.33
CML-3	19.50	97.80	0.72	0.29
CML-4	18.70	98.30	0.75	0.27
CML-5	20.60	107.60	0.76	0.25
Mean Value	19.28	97.64	0.70	0.29
Std. Dev.	0.98	6.69	0.80	0.03
CV (%)	5.10	6.85	11.57	10.37

Table 11-51 Transverse Compressive Properties of Thermal Cycled (10, 099 cycles) 35 v/o SiC_w/2124-T6 Al.

Specimen # (35WA)(CQ)(TP)	Elastic Modulus E^C_y(Msi)	Yield Strength (ksi)	Ultimate Compressive Strength (ksi)	Strain To Failure (%)	Poisson Ratio ν_{yx}
CMT-1	18.20	78.80	99.70	0.78	0.25
CMT-2	18.30	78.80	94.20	0.70	0.26
CMT-3	15.90	70.10	90.50	0.77	0.23
CMT-4	18.80	83.60	97.70	0.76	0.26
Mean Value	17.80	77.83	95.53	0.75	0.25
Std. Dev.	1.29	5.63	4.05	0.04	0.01
CV (%)	7.27	7.23	4.24	4.78	5.66

Table 11-52 Longitudinal Comopressive Properties of Thermal Cycled (10, 099 cycles) P100/6061 $[0]_2$, v/o = 42.2.

Specimen # (GA)(DU)(TP)	Elastic Modulus E^C_x(Msi)	Ultimate Comp. Strength (ksi)	Poisson Ratio ν_{xy}	Strain To Failure (%)
CML-1	42.40	47.60	0.28	0.11
CML-2	43.00	40.40	0.30	0.10
CML-3	41.10	39.30	0.33	0.10
CML-4	55.40	47.00	0.36	0.10
CML-5	46.10	41.70	0.29	0.10
CML-6	48.20	47.30	0.26	0.16
CML-7	44.40	47.70	0.26	0.15
CML-8	42.00	38.60	0.25	0.10
Mean Value	45.33	43.70	0.29	0.12
Std. Dev.	4.69	4.06	0.04	0.03
CV (%)	10.35	9.29	13.29	21.80

Table 11-53 Transverse Compressive Properties of Thermal Cycled (10, 099 cycles) P100/6061 $[0]_2$, v/o = 42.2.

Specimen # (GA)(DU)(TP)	Elastic Modulus E^C_y(Msi)	Ultimate Comp. Strength (ksi)	Poisson Ratio ν_{yx}	Strain To Failure (%)
CMT-1 CMT-2 CMT-3 CMT-4 CMT-5	4.40	20.30	0.04	0.26
Mean Value	4.40	20.30	0.04	0.26
Std. Dev.				
CV (%)				

Table 11-54 Longitudinal Compressive Properties of Thermal Cycled (10,099 Cycles) $[0]_{12}$ HMU/7070, v/o = 44..5.

Specimen # (CS)(UU)(TP)	Elastic Modulus E^{C}_{x}(Msi)	Ultimate Comp. Strength (ksi)	Poisson Ratio ν_{xy}	Strain To Failure (%)
CML-1	22.69	104.76	0.23	—
CML-2	21.50	128.51	0.22	—
CML-3	20.78	112.74	0.21	—
Mean Value	21.66	115.34	0.22	
Std. Dev.	0.96	12.09	0.01	
CV (%)	4.45	10.48	4.5%	

Table 11-55 Longitudinal Compressive Properties of Thermal Cycled (10,099 Cycles) $[0/90]_6$ HMU/7070, v/o = 40.5.

Specimen # (CS)(UB)(TP)	Elastic Modulus E^{C}_{x}(Msi)	Ultimate Comp. Strength (ksi)	Poisson Ratio ν_{xy}	Strain To Failure (%)
CML-1	12.09	86.19	0.05	0.78
CML-2	12.88	80.67	0.04	0.74
CML-3	12.38	87.17	0.06	0.94
Mean Value	12.45	84.68	0.05	0.82
Std. Dev.	0.40	3.50	0.01	0.11
CV (%)	3.21	4.14	20.0	12.91

Table 11-56 Transverse Compressive Properties of Thermal Cycled (10,099 Cycles) $[0/90]_6$ HMU/7070, v/o = 40.5.

Specimen # (CS)(UB)(TP)	Elastic Modulus E^{C}_{y}(Msi)	Ultimate Comp. Strength (ksi)	Poisson Ratio ν_{yx}	Strain To Failure (%)
CMT	13.14	74.57	0.05	0.62

Table 11-57 Longitudinal Compressive Properties of Thermal Cycled (10,099 Cycles) [0/90/0] P100/Carbon, v/o = 53.0.

Specimen # (CC)(HB)(TP)	Elastic Modulus E^{C}_{x}(Msi)	Ultimate Comp. Strength (ksi)	Poisson Ratio ν_{xy}	Strain To Failure (%)
CML-1	24.70	16.40	—	0.08
CML-2	38.50	13.30	—	0.07
CML-3	25.70	15.00	—	0.08
CML-4	25.40	17.80	—	0.13
CML-5				
Mean Value	28.58	15.63		0.09
Std. Dev.	6.63	1.93		0.03
CV (%)	23.20	12.33		30.09

Table 11-58 Transverse Compressive Properties of Thermal Cycled (10,099 Cycles) [0/90/0] P100/Carbon, v/o = 53.0.

Specimen # (CC)(HB)(TP)	Elastic Modulus E^{C}_{y}(Msi)	Ultimate Comp. Strength (ksi)	Poisson Ratio ν_{yx}	Strain To Failure (%)
CMT-1	9.10	8.00	—	0.24
CMT-2	9.90	10.40	—	0.13
CMT-3	10.20	7.50	—	0.14
CMT-4	8.80	7.80	—	0.16
CMT-5	8.30	8.10	—	0.13
Mean Value	9.26	8.36		0.16
Std. Dev.	0.78	1.16		0.05
CV (%)	8.46	13.91		29.53

Table 11-59 Longitudinal Compressive Properties of Thermal Cycled 25v/o SiC_p/2124-T6 Al Tubes

Speciment # (25PA)(CQ)(TT)	Elastic Modulus (Msi)				Ultimate Comp. Strength (ksi)	0.2% Yield Strength (ksi)	Strain To Failure (%)	Poisson Ratio
	E_{X1}	E_{X2}	E_{X3}	E_X				
CML-1	14.4	16.0	21.5	17.3	83.4	50.4	1.5	0.26
CML-2	16.15	14.57	16.08	15.36	85.8	56.5	1.5	0.26
Mean				16.33	84.6	53.45	1.5	0.26
Std. Dev.				1.37	1.71.70	4.3	0.0	0.0
CV (%)				8.39	2.0	8.04	0.0	0.0

*Strain Gage Saturation at 1.35%

Table 11-60 Longitudinal Tensile Properties of Thermal Cycled 35v/o SiC_p/2124-T6 Al Tubes

Speciment # (35PA)(CQ)(TT)	Elastic Modulus (Msi)				Ultimate Comp. Strength (ksi)	0.2% Yield Strength (ksi)	Strain To Failure (%)	Poisson Ratio
	E_{X1}	E_{X2}	E_{X3}	E_X				
CML-1	16.67	23.81	—	20.24	92.9	67.8	0.62	0.27
CML-2	15.05	16.66	—	15.86	86.6	64.5	0.82	0.23
Mean				18.05	89.75	66.15	0.72	0.25
Std. Dev.				3.10	4.45	2.33	0.14	0.028
CV (%)				17.17	4.96	3.5	19.44	11.2

Table 11-61 Longitudinal Compressive Properties of Thermal Cycled 25v/o SiC_w/2124-T6 Al Tubes

Speciment # (25WA)(CQ)(TT)	Elastic Modulus (Msi)				Ultimate Comp. Strength (ksi)	0.2% Yield Strength (ksi)	Strain To Failure (%)	Poisson Ratio
	E_{X1}	E_{X2}	E_{X3}	E_X				
CML-1	23.39	18.75	—	21.07	110.7	—	0.9	0.28
CML-2	21.67	16.83	—	19.25	114.7	102.9	1.2	0.26
Mean				20.16	112.7	102.9	1.05	0.27
Std. Dev.				1.29	2.8		0.21	0.14
CV (%)				6.40	2.48		20.0	5.18

Table 11-62 Longitudinal Compressive Properties of Thermal Cycled 35v/o SiC_w/2124-T6 Al

Speciment # (35WA)(CQ)(TT)	Elastic Modulus (Msi)				Ultimate Tensile Strength (ksi)	0.2% Yield Strength (ksi)	Strain To Failure (%)	Poisson Ratio
	E_{X1}	E_{X2}	E_{X3}	E_X				
CML-1	19.8	23.0	21.11	21.3	111.1	79.6	1.5	0.24
CML-2	20.0	19.35	21.40	20.25	120.0	81.7	1.5	0.24
Mean				20.78	115.5	80.65	1.5	0.24
Std. Dev.				0.74	6.29	1.48	0.0	0.0
CV (%)				3.56	5.4	1.8	0.0	0.0

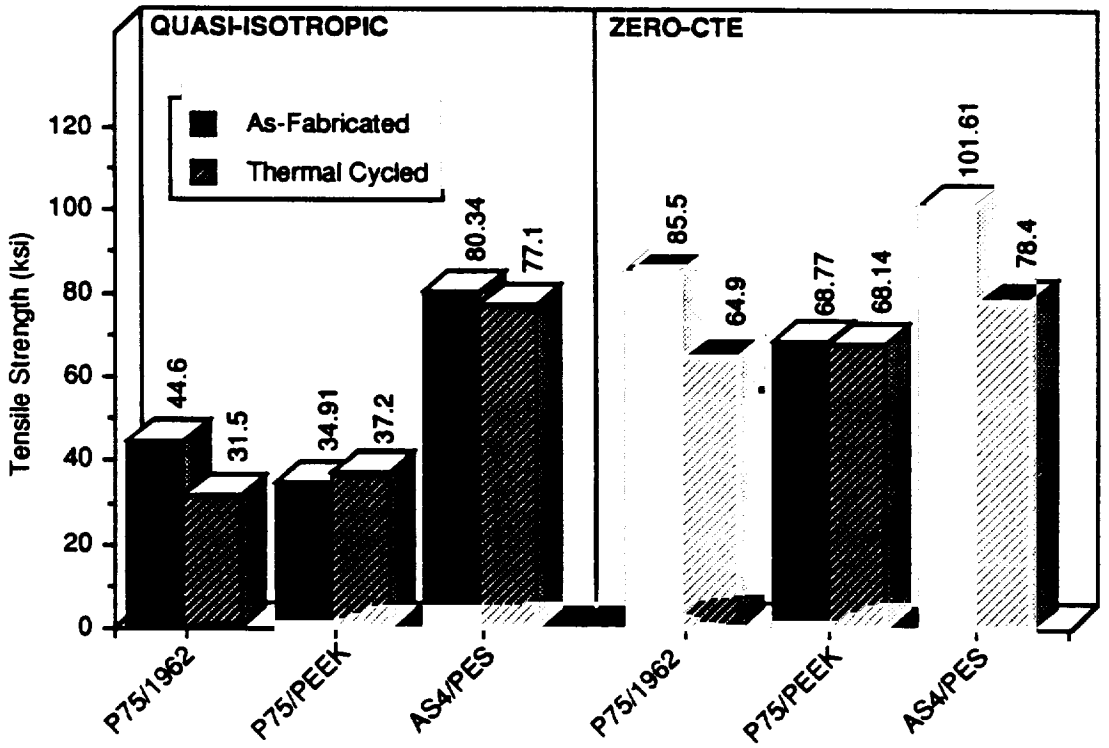

Figure 11-12 Effect of Thermal Cycling on Tensile Strength of $[0, \pm 45, 90]_s$ and $[\pm 30, 0_4]_s$ Organic Matrix Composites

Generally, the presence of damage sites such as microcracks, voids, and disbonds affect the tensile properties, and defects such as delamination and disbonds reduce the compression and transverse tensile strength. Because the properties of each composite are governed by its fiber architecture and reinforcement/matrix combination, therefore specific observations identifying the property changes are outlined below.

- Tension and compression test results of $[0, \pm 45, 90]_s$ and $[30, -30, 0_4]_s$ P75/1962 and AS4/PES composites, which exhibited microcracking and delamination during thermal cycling, indicated reduction ($\leq 25\%$) in strength levels whereas there was very little change in elastic modulus (Figure 11-12).

- In the case of P75/PEEK, where the as fabricated specimens exhibited high microcrack density, there was no change in mechanical properties because there was no significant microcracking in subsequent thermal cycling (Figure 11-12).

- MMC such as P100/6061 Al $[0]_2$ and discontinuous SiC/2124-T6 composites exhibited almost no change in elastic modulus and a slight decrease ($\leq 5\%$) in strength levels. These changes in strength are primarily due to disbonds (at the reinforcement matrix interface) associated with partial relieving to residual stresses during thermal excursions.

- Compression tests results of HMU/7070 $[0]_{12}$ and $[0/90]_6$ specimens also exhibited no change in elastic modulus, but a slight decrease ($\leq 8\%$) in strength.

- P100/C [0/90/0] specimens exhibited strength levels nearly identical to the as fabricated specimens.

(b) Coefficient of Thermal Expansion

Thermal expansion test results, including CTE, RT hysteresis, and residual strain, are summarized in Table 1-10 (reproduced in this chapter for reference). To determine the effect of thermal cycling, the mean CTE and microcrack density values have been compared with the data for as-fabricated composites in Table 11-63. Specific thermal expansion response curves of all composites are presented in Figures 11-13 to 11-39. Based on these results, each composite exhibited reduced hysteresis and residual strain which was indicative of the reduced residual stress levels in the laminate. The fabrication residual stress near the reinforcement/matrix interface are partially relieved due to microcracking, and microplastic flow in the matrix (e.g., metallic). Because of the reduced hysteresis, the average CTE obtained by the slope of a line joining thermal strain values at extreme temperatures (-150°F and 150°F) were consistent with the average CTE in the heat (RT→150°F) cool (150°F→-150°F), and heat (-150°F→RT) segments. Also, the average CTE values for each composite were close to the predicted values. Specific remarks about the CTE results are as follows.

- P75/1962 and P75/PEEK $[0, \pm 45, 90]_s$ laminate exhibited a nearly quasi-isotropic CTE response.
  - P75/1962: CTE_x = -0.585 ppm/°F, CTE_y = -0.395 ppm/°F (predicted CTE x = -0.34 ppm°F)
  - P75/PEEK: CTE_x = -0.248 ppm°F, CTE_y = -0.201 ppm/°F (predicted CTEx = -0.3 ppm/°F)

- AS4/PES $[0, \pm 45, 90]_s$ laminate exhibited differences in CTE_x (0.65 ppm/°F) and CTE_y (0.285 pm/°F) which were attributed to the differences in defect density between x and y directions.
- CTE values of discontinuous SiC/2124-T6 Al were slightly higher than the as-

Table 1-10 Summary of Thermal Expansion Response of Composite Specimens After 10, 099 Thermal Cycles Between -150°F and +150°F (Reproduced in this Chapter for Reference)

					Thermal Expansion Response After 10,099 Cycles			0 Cycles
Material		Layup	v/o	Test Dir.	RT Hysteresis ppm	Residual Strain, ppm	CTE* ppm/°F	CTE* ppm/°F
PANELS								
1	P75/1962	$[0, \pm45, 90]_S$	62.2	x	-30.15	-4.02	-0.585	-0.454
2	P75/1962	$[0, \pm45, 90]_S$	62.2	y	-30.15	-35.17	-0.395	-0.14
3	P75/1962	$[\pm30, 0_4]_S$	62.7	x	-27.64	6.53	-1.00	-1.02
4	P75/1962	$[\pm30, 0_4]_S$	62.7	y	-45.22	-12.56	2.92	5.83
5	P75/PEEK	$[0, \pm45, 90]_S$	62.2	x	-57.79	26.13	-0.248	-0.28
6	P75/PEEK	$[0, \pm45, 90]_S$	62.2	y	-55.78	-9.045	-0.201	+0.04
7	P75/PEEK	$[\pm30, 0_4]_S$	62.2	x	-80.40	-188.44	-0.81	-0.39
8	P75/PEEK	$[\pm30, 0_4]_S$	62.2	y	5.78	-90.45	7.60	10.17
9	AS4/PES	$[0, \pm45, 90]_S$	53.7	x	-16.08	-50.25	0.65	1.08
10	AS4/PES	$[0, \pm45, 90]_S$	53.7	y	-12.90	15.58	0.285	1.38
11	AS4/PES	$[\pm30, 0_4]_S$	54.96	x	-42.72	-22.11	-0.37	-0.66
12	AS4/PES	$[\pm30, 0_4]_S$	54.96	y	-165.82	-201.00	10.68	12.60
13	P100/6061 Al	$[0]_2$	42.2	x	-10.05	4.02	0.99	-0.27**
14	SiC_p/2124-T6	N/A	25	x	55.28	-97.99	8.69	8.16
15	SiC_p/2124-T6	N/A	25	y	-100.50	-90.45	7.78	7.86
16	SiC_w/2124-T6	N/A	25	x	11.56	-100.50	8.56	8.03
17	SiC_w/2124-T6	N/A	25	y	50.25	-80.40	8.65	7.77
18	SiC_p/2124-T6	N/A	35	x	0.00	-75.38	6.78	5.91
19	SiC_p/2124-T6	N/A	35	y	50.25	-45.23	7.55	6.11
—	SiC_w/2124-T6	N/A	35	x	—	—	—	5.91
—	SiCw/2124-T6	N/A	35	y	—	—	—	6.29
20	Carbon-Carbon	[0/90/0]	53.0	x	-50.25	-12.56	-0.737	-0.95
21	Carbon-Carbon	[0/90/0]	53.0	y	-40.95	-13.57	-0.87	-0.87
22	Carbon-Carbon	$[0]_3$	52.48	x	-29.65	-21.10	-0.94	-0.98
23	Carbon-Carbon	$[0]_3$	52.48	y	-65.32	-47.70	0.29	-0.42
24	HMU/7070	$[0/90]_6$	40.5	x	8.75	-2.00	0.28	-0.075
25	HMU/7070	$[0/90]_6$	40.5	y	-13.00	-2.50	0.40	—
TUBES								
26	P100/Al, DB	$[0]_2$	43.63	x	10.01	-10.01	0.50	0.33
27	P100/Al, PT	$[0]_2$	44.35	x	-4.00	6.00	0.38	0.37
—	P100/AZ91C Mg	$[\pm16°]_S$	23.7	x	—	—	—	1.52
—	P100/AZ91C Mg	$[\pm16°]_S$	27.9	x	—	—	—	0.80
—	P100/AZ91C Mg	$[\pm16°]_S$	30.1	x	—	—	—	—

*Slope of a Line Joining End Points of the Thermal Expansion Plot
**Calculated CTE = 0.070ppm/°F

Table 11-63 Comparison of Mean CTE and Microcrack Density of As-Fabricated and Thermal Cycled Composites

					As-Fabricated		10,099 Cycles ±150°F	
Material		Layup	v/o	Test Dir.	CTE* ppm/°F	Microcrack Density	CTE* ppm/°F	Microcrack Density
PANELS								
1	P75/1962	$[0, \pm45, 90]_S$	62.2	x	-0.454	18	-0.585	20
2	P75/1962	$[0, \pm45, 90]_S$	62.2	y	-0.14	18	-0.395	20
3	P75/1962	$[\pm30, 0_4]_S$	62.7	x	-1.02	6	-1.00	10
4	P75/1962	$[\pm30, 0_4]_S$	62.7	y	5.83	6	2.92	10
5	P75/PEEK	$[0, \pm45, 90]_S$	62.2	x	-0.28	41	-0.248	46
6	P75/PEEK	$[0, \pm45, 90]_S$	62.2	y	+0.04	41	-0.201	46
7	P75/PEEK	$[\pm30, 0_4]_S$	62.2	x	-0.39	21	-0.81	24
8	P75/PEEK	$[\pm30, 0_4]_S$	62.2	y	10.17	21	7.60	24
9	AS4/PES	$[0, \pm45, 90]_S$	53.7	x	1.08	26	0.65	31
10	AS4/PES	$[0, \pm45, 90]_S$	53.7	y	1.38	26	0.285	31
11	AS4/PES	$[\pm30, 0_4]_S$	54.96	x	-0.66	12	-0.37	12
12	AS4/PES	$[\pm30, 0_4]_S$	54.96	y	12.60	12	10.68	12
13	P100/6061 Al	$[0]_2$	42.2	x	-0.27**	12	0.99	13
14	SiC_p/2124-T6	N/A	25	x	8.16	0	8.69	0
15	SiC_p/2124-T6	N/A	25	y	7.86	0	7.78	0
16	SiC_w/2124-T6	N/A	25	x	8.03	0	8.56	0
17	SiC_w/2124-T6	N/A	25	y	7.77	0	8.65	0
18	SiC_p/2124-T6	N/A	35	x	5.91	0	6.78	0
19	SiC_p/2124-T6	N/A	35	y	6.11	0	7.55	0
—	SiC_w/2124-T6	N/A	35	x	5.91	0	—	0
—	SiCw/2124-T6	N/A	35	y	6.29	0	—	0
20	Carbon-Carbon	[0/90/0]	53.0	x	-0.95	—	-0.737	—
21	Carbon-Carbon	[0/90/0]	53.0	y	-0.87	—	-0.87	—
22	Carbon-Carbon	$[0]_3$	52.48	x	-0.98	—	-0.94	—
23	Carbon-Carbon	$[0]_3$	52.48	y	-0.42	—	0.29	—
24	HMU/7070	$[0/90]_6$	40.5	x	-0.075	0	0.28	0
25	HMU/7070	$[0/90]_6$	40.5	y	—	0	0.40	0
TUBES								
26	P100/Al, DB	$[0]_2$	43.63	x	0.33	12	0.50	12
27	P100/Al, PT	$[0]_2$	44.35	x	0.37	6	0.38	6
—	P100/AZ91C Mg	$[\pm16°]_S$	23.7	x	1.52	—	—	—
—	P100/AZ91C Mg	$[\pm16°]_S$	27.9	x	0.80	—	—	—
—	P100/AZ91C Mg	$[\pm16°]_S$	30.1	x	—	—	—	—

* Slope of a Line Joining End Points of the Thermal Expansion Plot

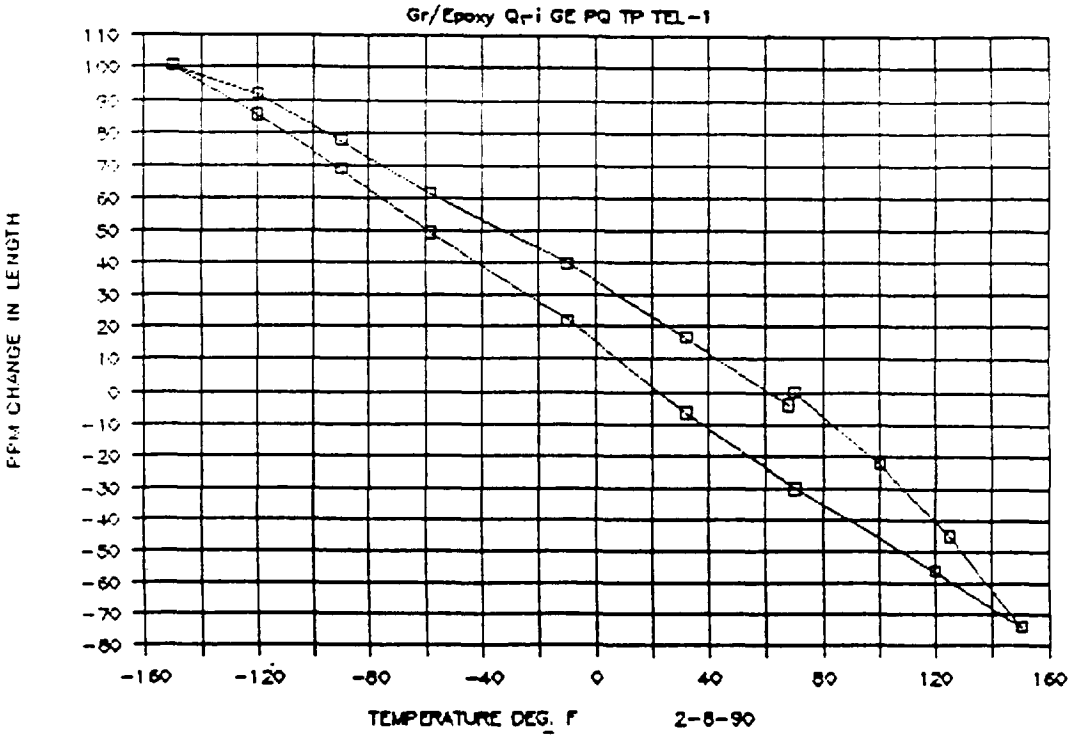

Figure 11-13 Longitudinal Thermal Expansion Behavior of P75/1962, $[0, 45, -45, 90]_S$, v/o = 62.2 after 10,099 Thermal Cycles Between -150°F and +150°F.

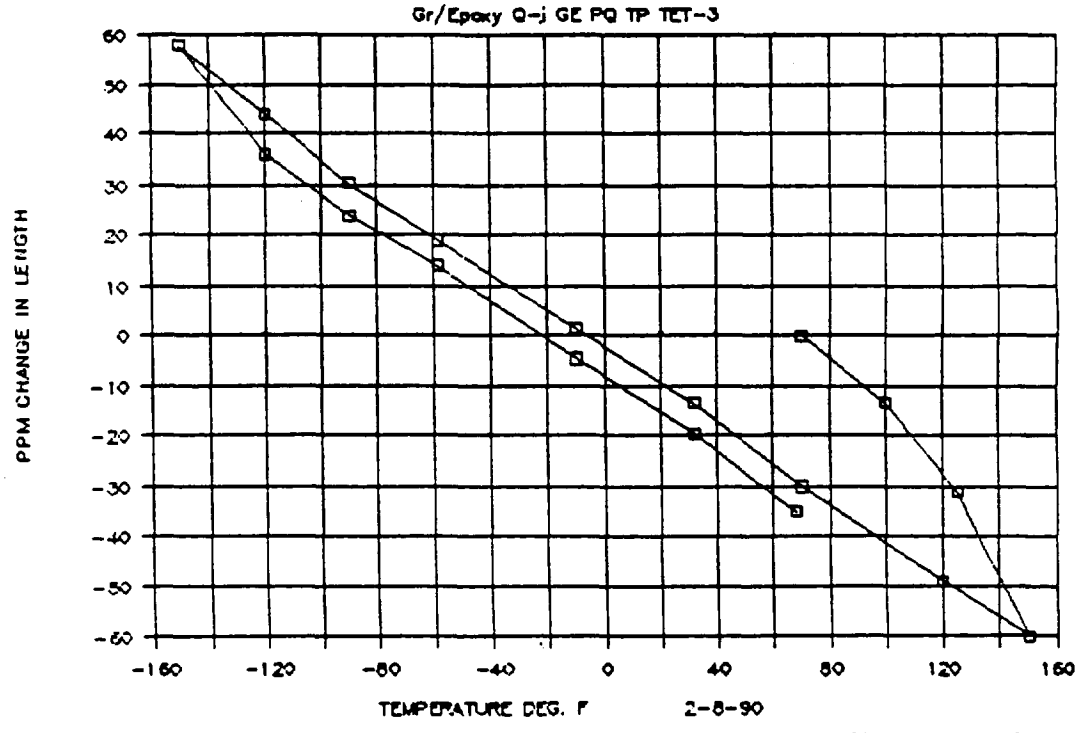

Figure 11-14 Transverse Thermal Expansion Behavior of P75/1962, $[0, 45, -45, 90]_S$, v/o = 62.2 after 10,099 Thermal Ccycles Between -150°F and +150°F.

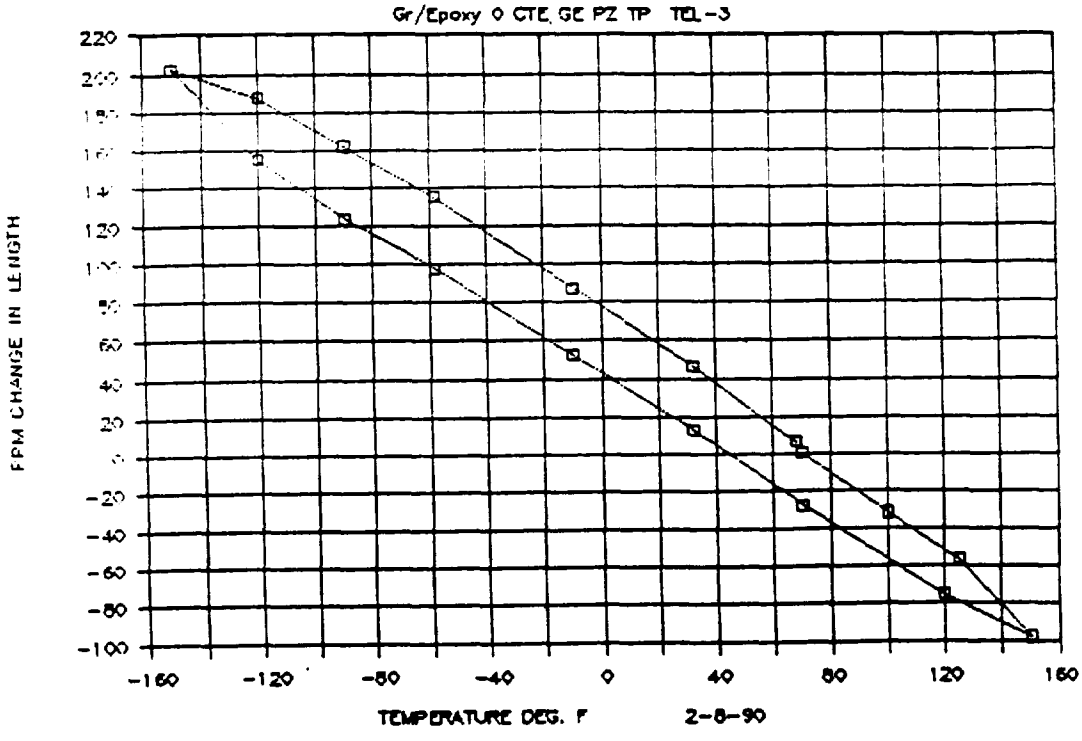

Figure 11-15 Longitudinal Thermal Expansion Behavior of P75/1962, $[\pm 30, 0_4]_S$, v/o = 62.7 after 10,099 Thermal Cycles Between -150°F and +150°F.

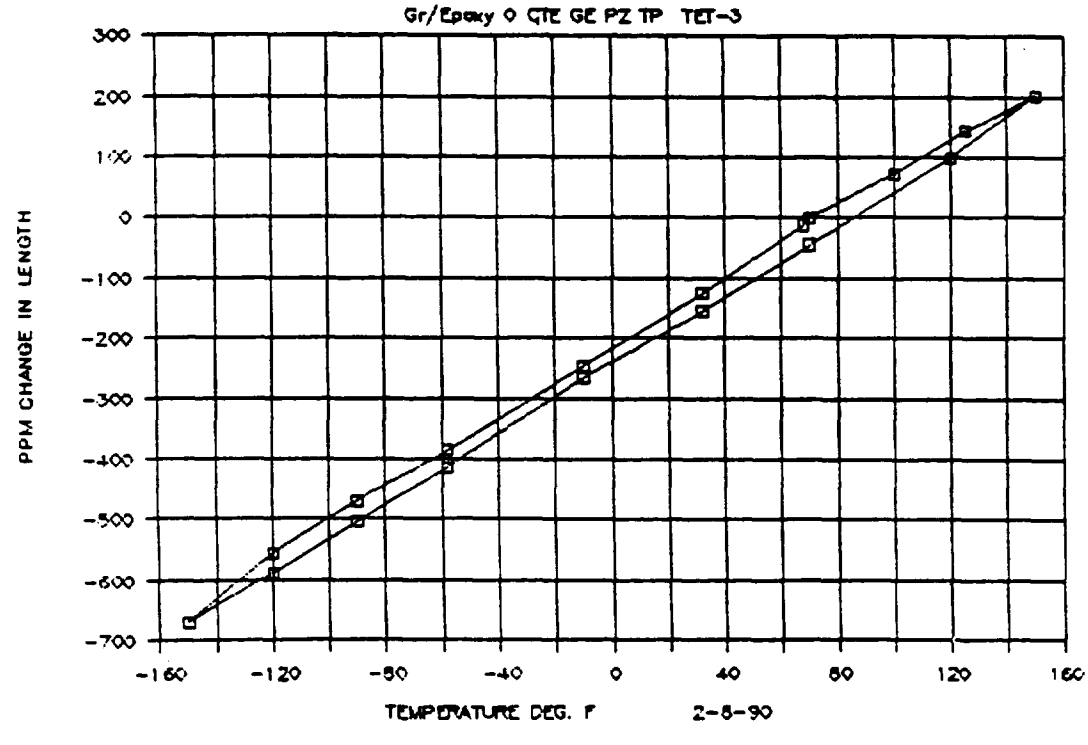

Figure 11-16 Transverse Thermal Expansion Behavior of P75/1962, $[\pm 30, 0_4]_S$, v/o = 62.7 after 10,099 Thermal Cycles Between -150°F and +150°F.

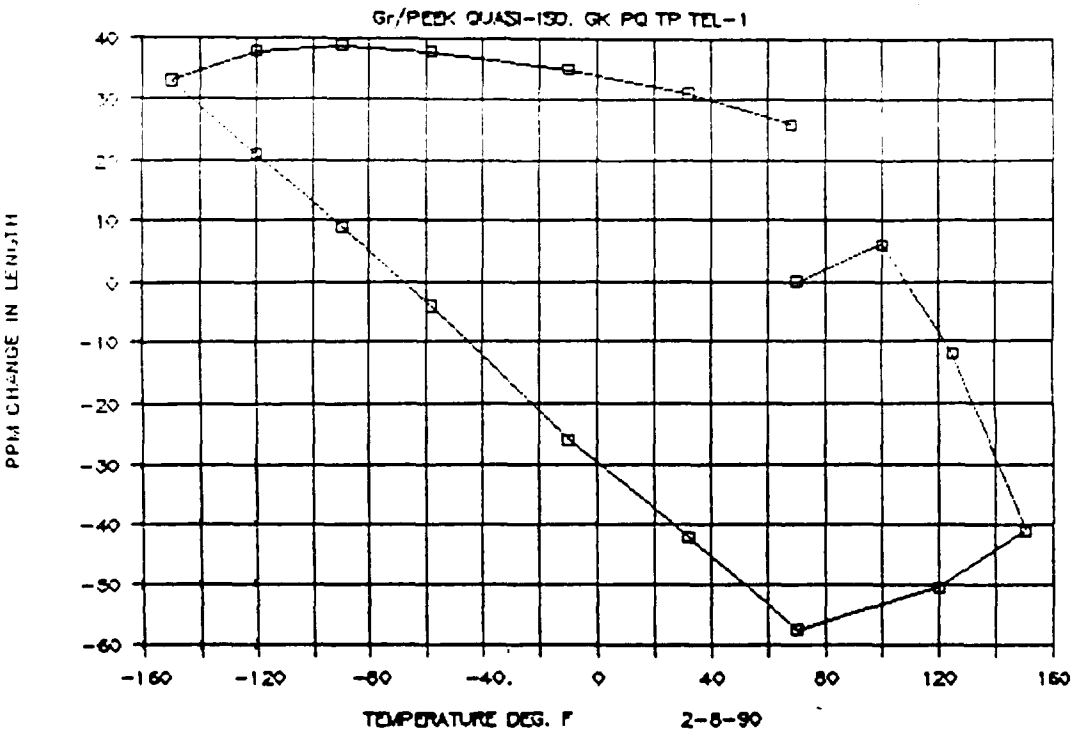

Figure 11-17 Longitudinal Thermal Expansion Behavior of P75/PEEK, $[0, \pm 45, 90]_s$, v/o = 62.2 after 10,099 Thermal Cycles Between -150°F and +150°F.

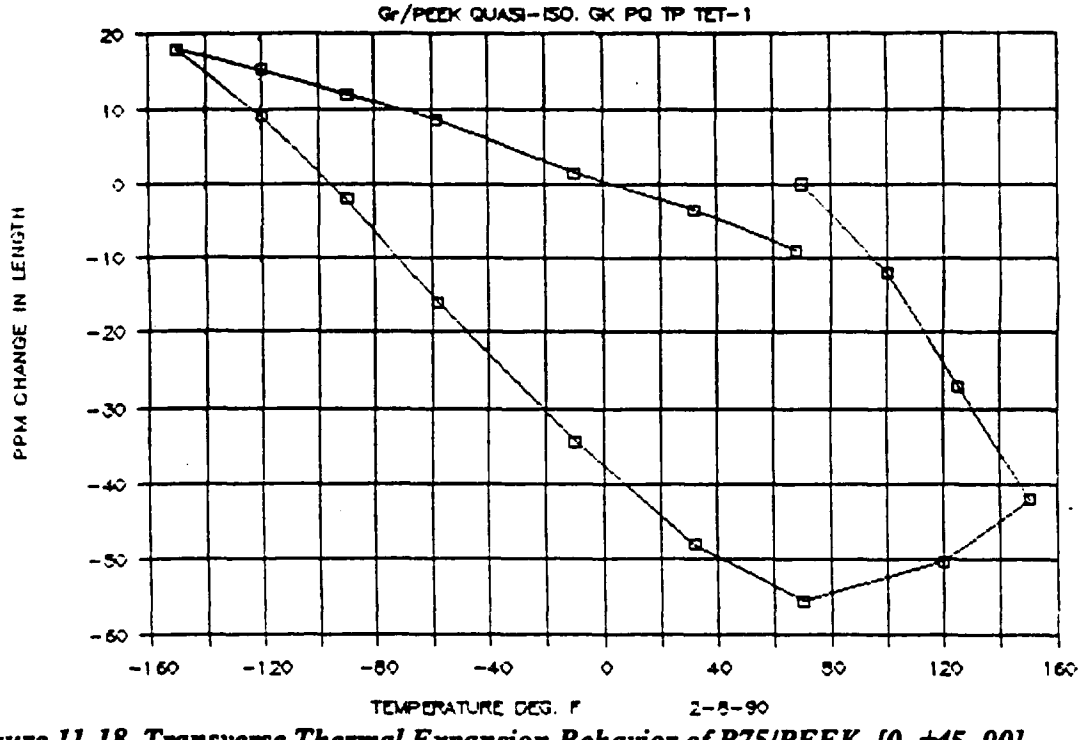

Figure 11-18 Transverse Thermal Expansion Behavior of P75/PEEK, $[0, \pm 45, 90]_s$, v/o = 62.2 after 10,099 Thermal Cycles Between -150°F and +150°F.

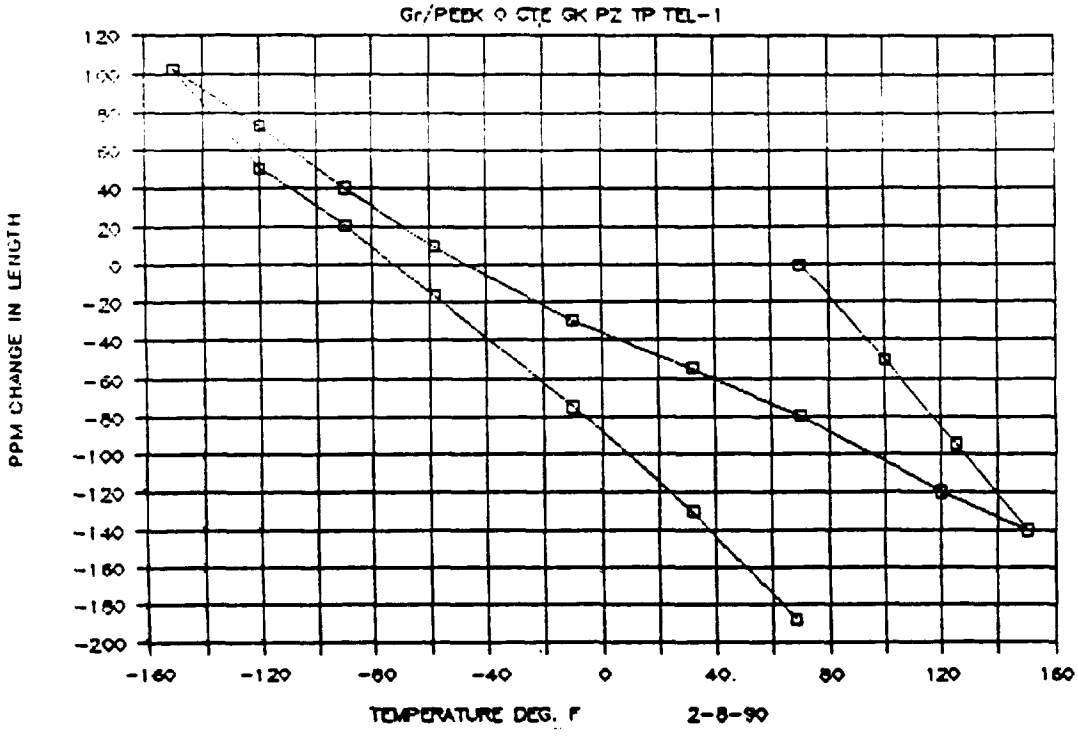

Figure 11-19 Longitudinal Thermal Expansion Behavior of P75/PEEK, $[\pm 30, 0_4]_S$, v/o = 62.2 after 10,099 Thermal Cycles Between -150°F and +150°F.

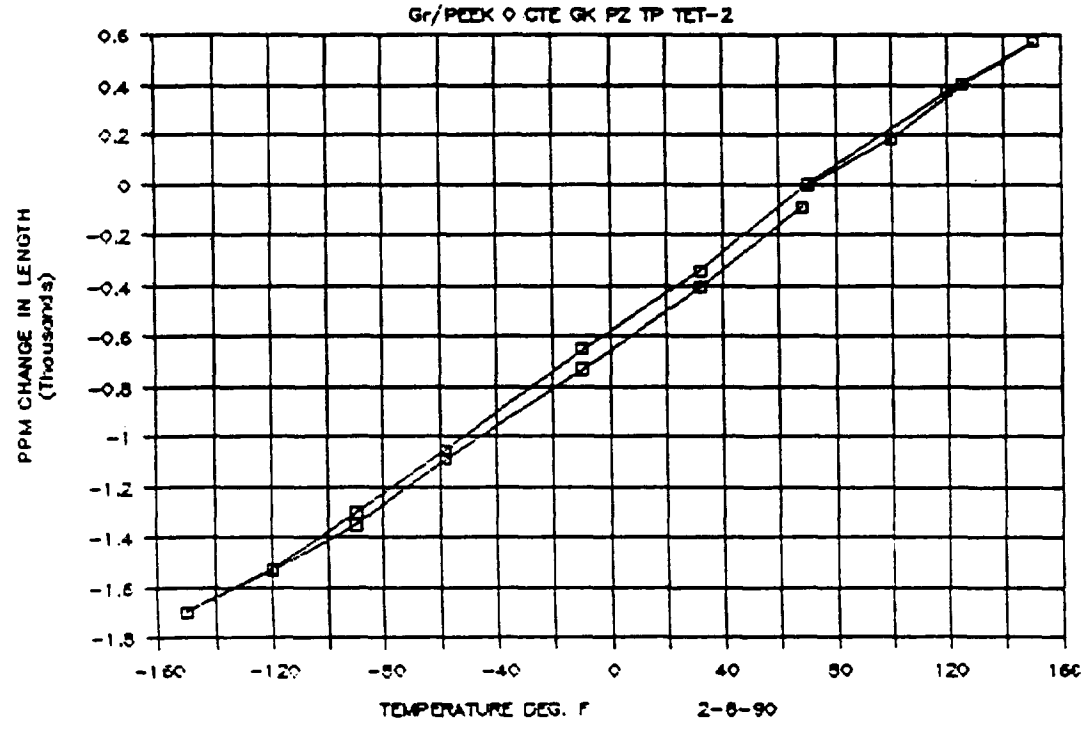

Figure 11-20 Transverse Thermal Expansion Behavior of P75/PEEK, $[\pm 30, 0_4]_S$, v/o = 62.2 after 10,099 Thermal Cycles Between -150°F and +150°F.

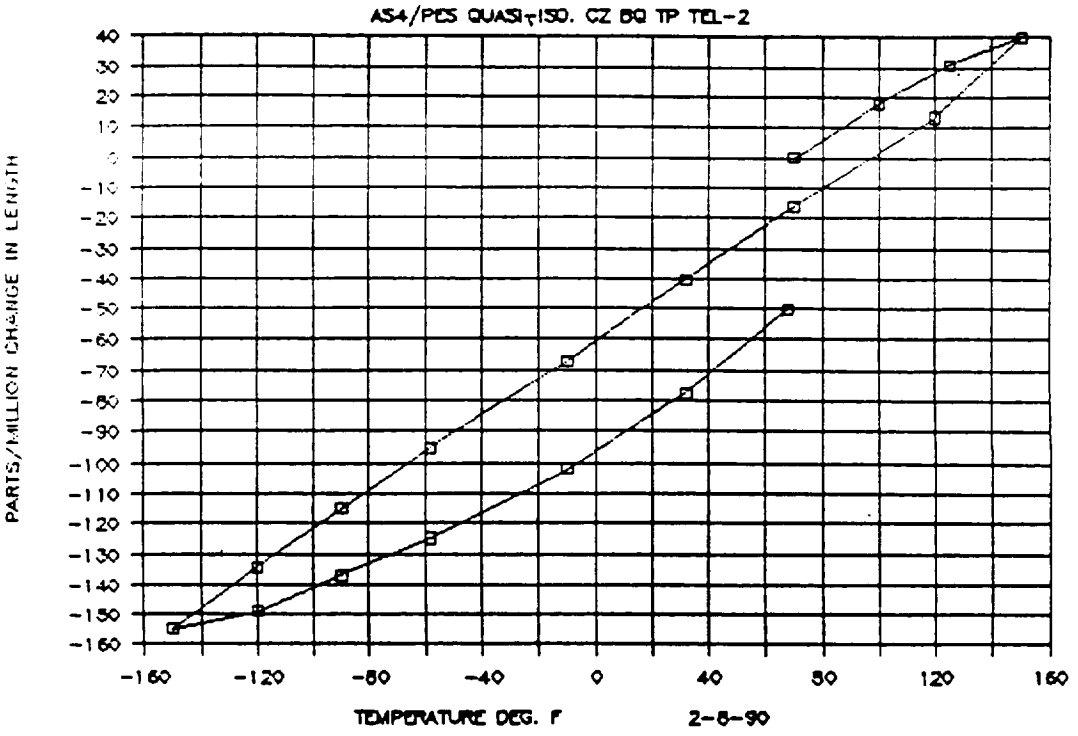

Figure 11-21 Longitudinal Thermal Expansion Behavior of AS4/PES, $[0, \pm 45, 90]_S$, v/o = 53.7 after 10,099 Thermal Cycles Between -150°F and +150°F.

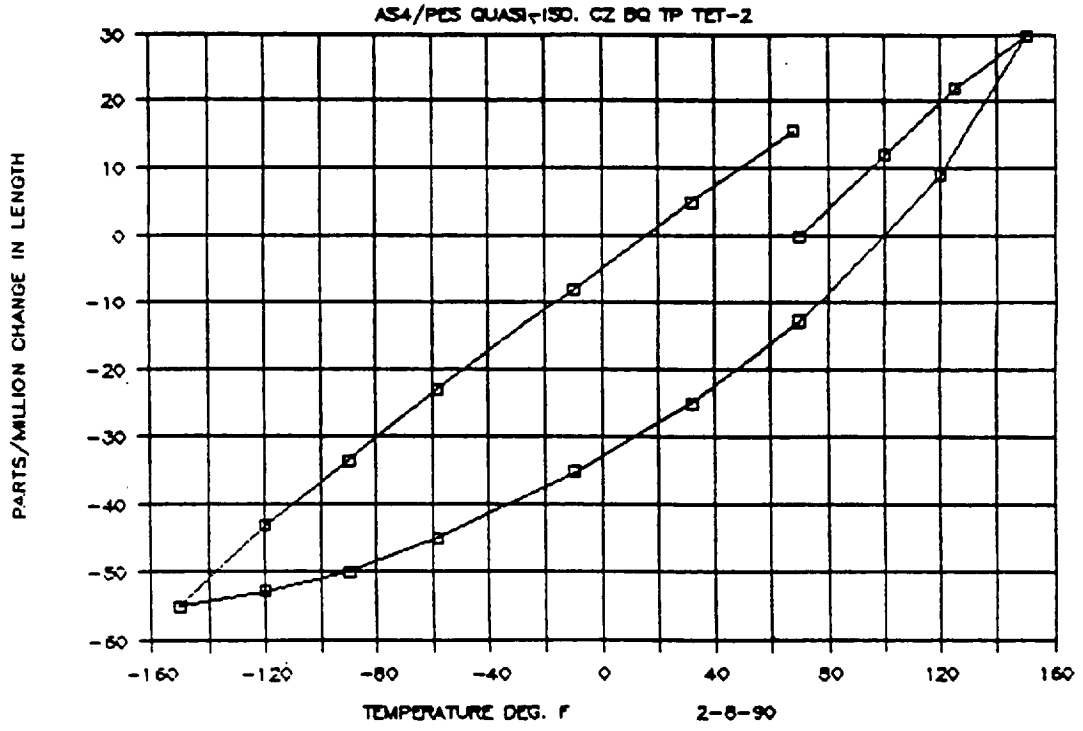

Figure 11-22 Transverse Thermal Expansion Behavior of AS4/PES, $[0, \pm 45, 90]_S$, v/o = 53.7 after 10,099 Thermal Cycles Between -150°F and +150°F.

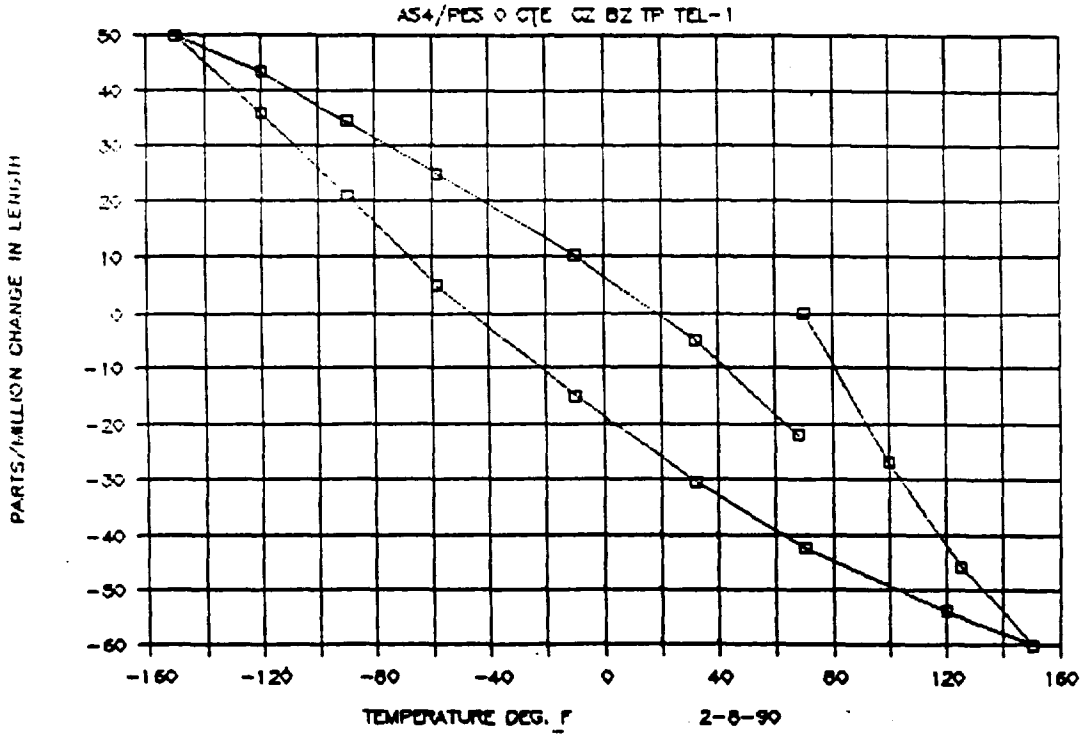

Figure 11-23 Longitudinal Thermal Expansion Behavior of AS4/PES, $[\pm 30, 0_4]_S$, v/o = 54.96 after 10,099 Thermal Cycles Between -150°F and +150°F.

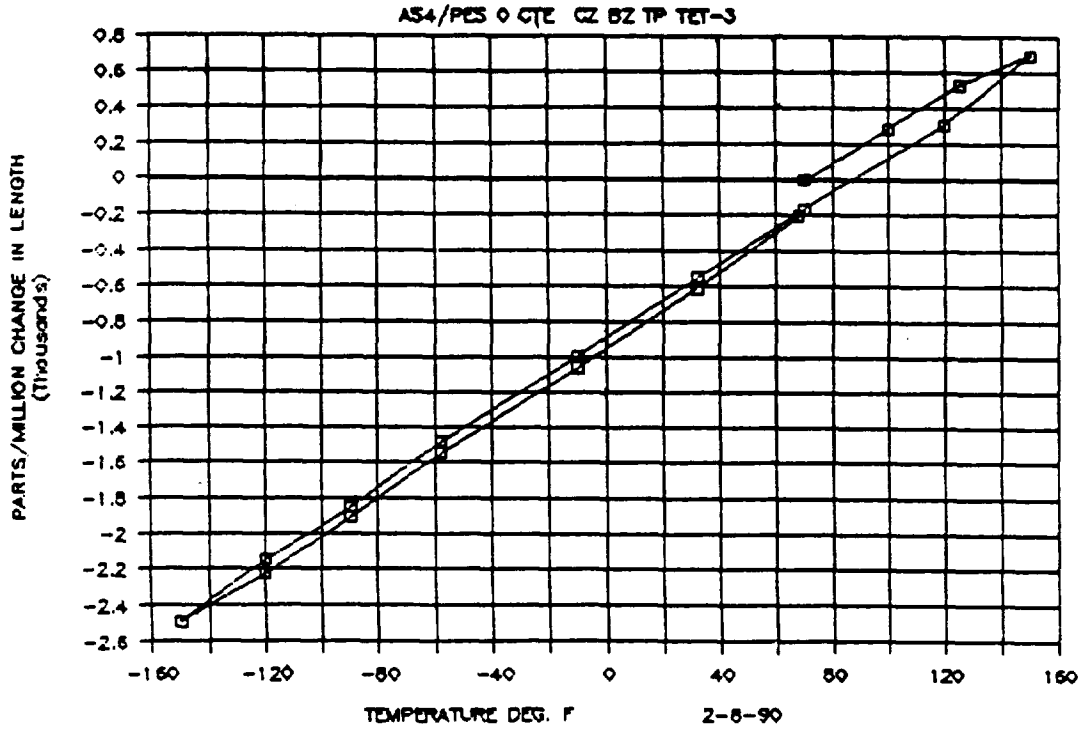

Figure 11-24 Transverse Thermal Expansion Behavior of AS4/PES, $[\pm 30, 0_4]_S$, v/o = 54.96 after 10,099 Thermal Cycles Between -150°F and +150°F.

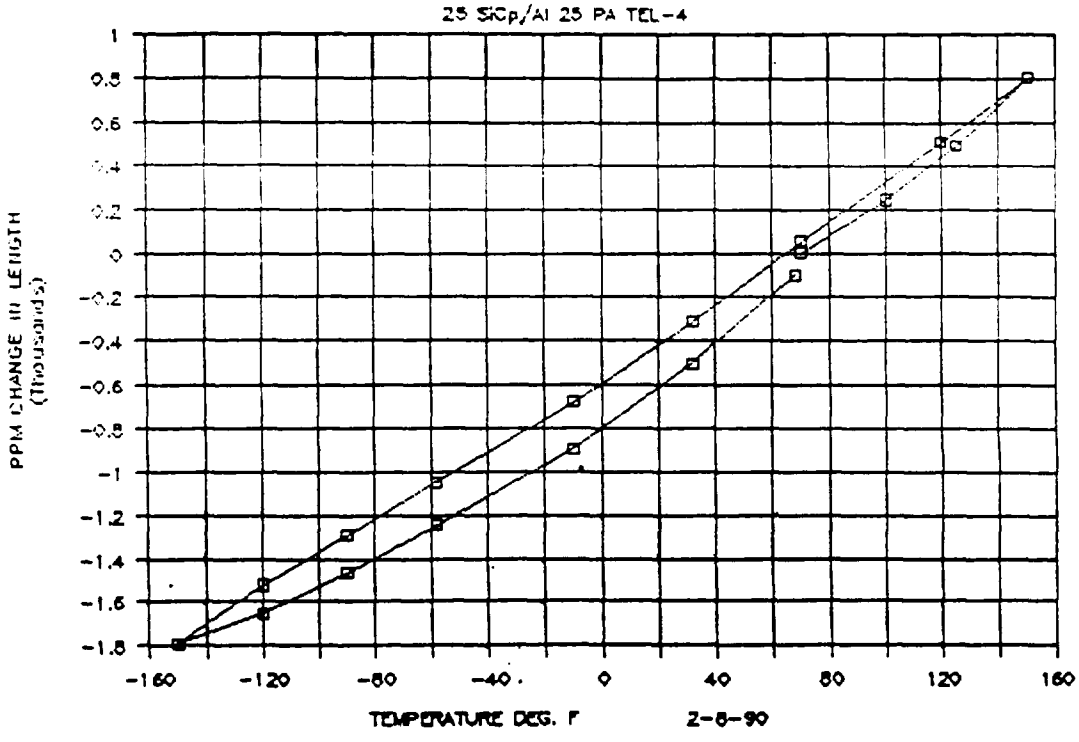

Figure 11-25 Longitudinal Thermal Expansion Response of 25 v/o SiC_p/2124-T6 Al After 10,099 Thermal Cycles Between -150°F and +150°F.

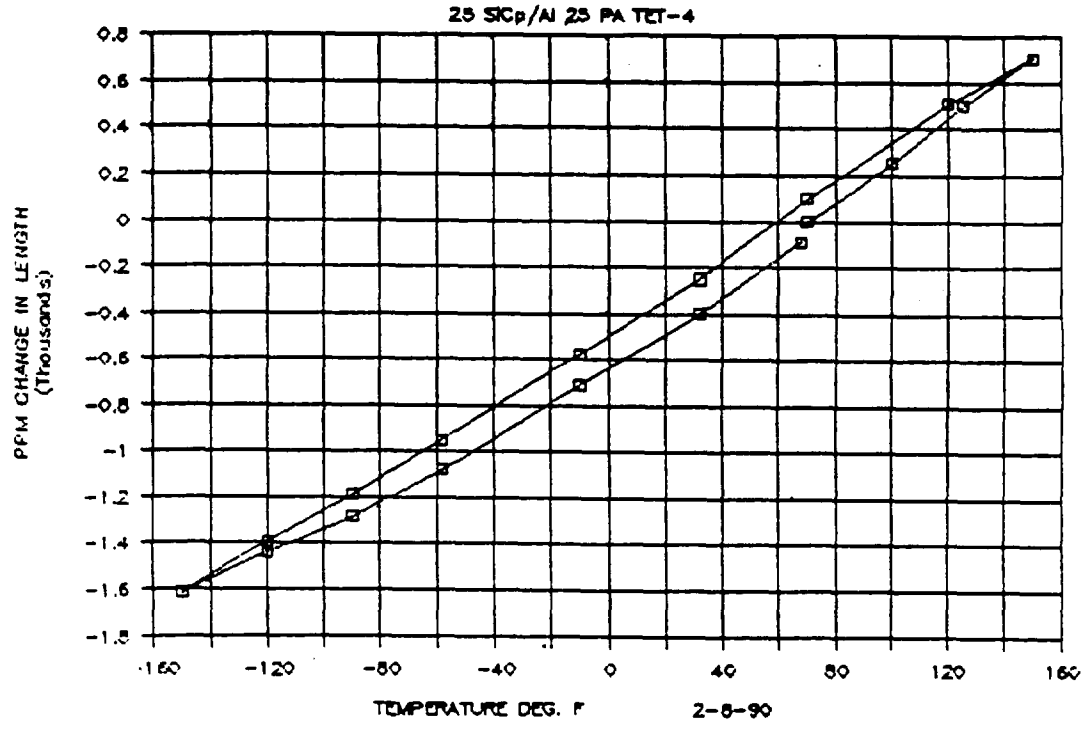

Figure 11-26 Transverse Thermal Expansion Response of 25 v/o SiCp/2124-T6 Al After 10,099 Thermal Cycles Between -150°F and +150°F.

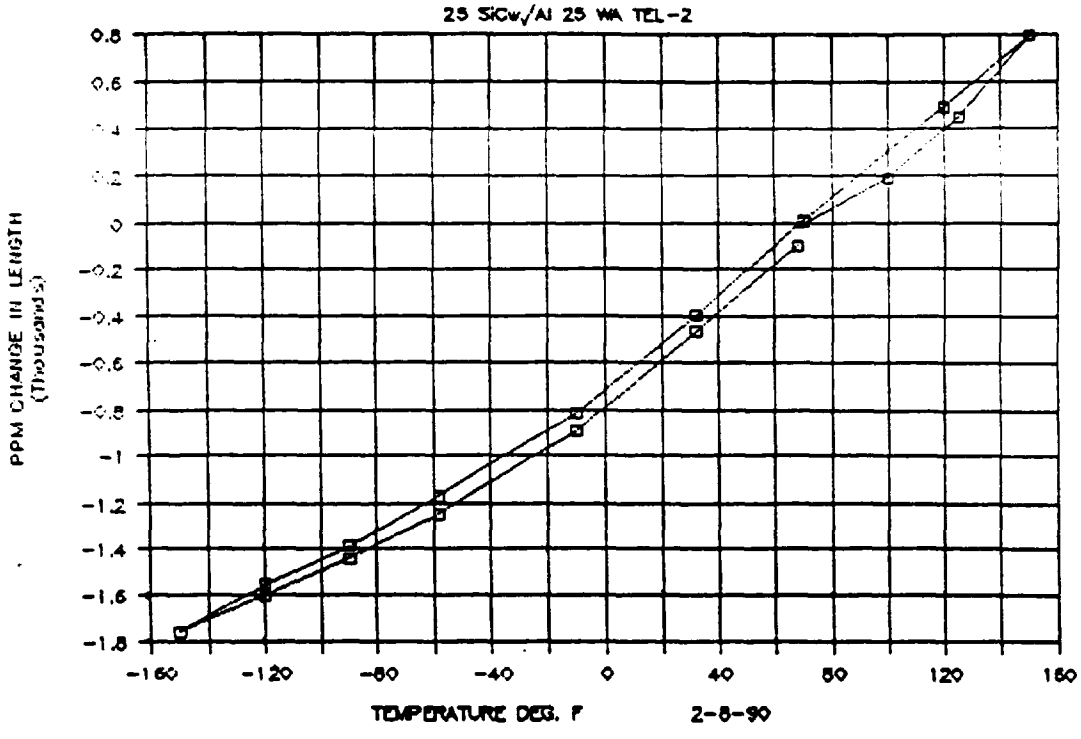

Figure 11-27 Longitudinal Thermal Expansion Response of 25 v/o SiC_w/2124-T6 Al After 10,099 Thermal Cycles Between -150°F and +150°F.

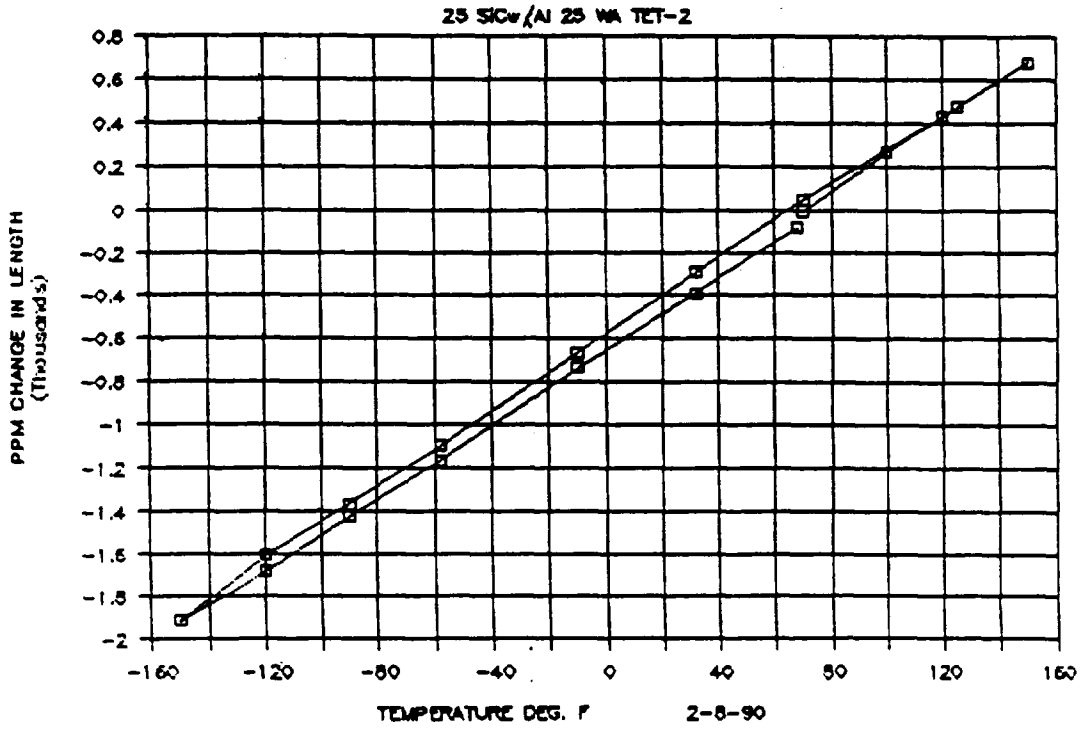

Figure 11-28 Transverse Thermal Expansion Response of 25 v/o SiC_w/2124-T6 Al After 10,099 Thermal Cycles Between -150°F and +150°F.

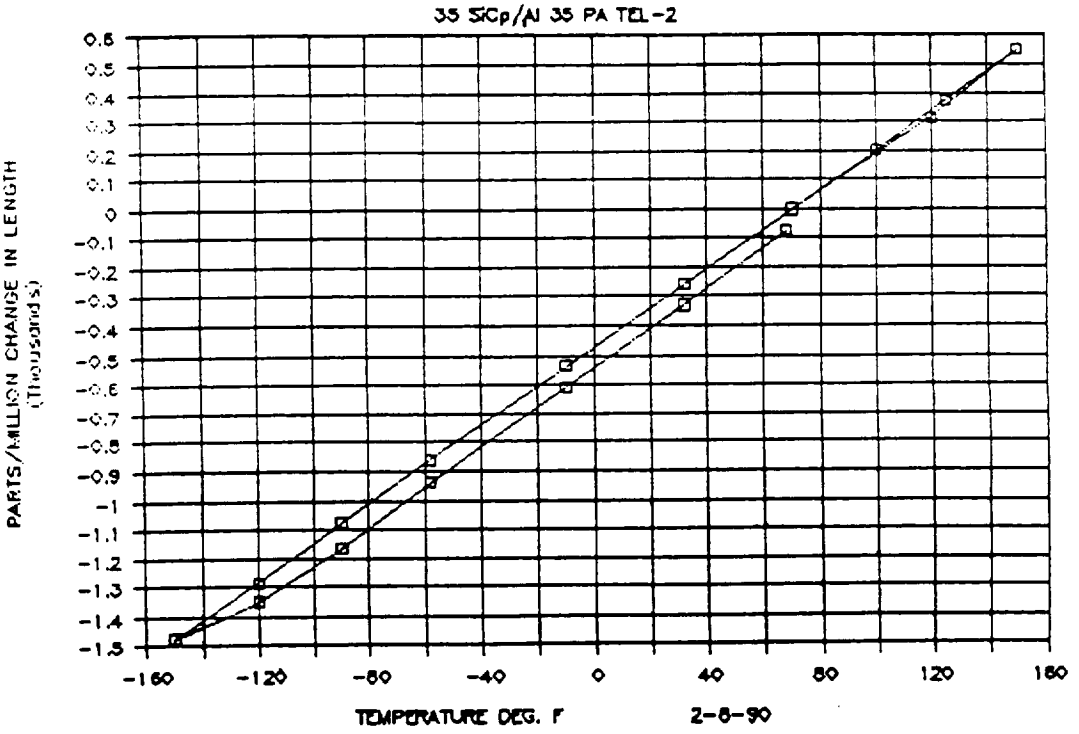

Figure 11-29 Longitudinal Thermal Expansion Response of 35 v/o SiC_p/2124-T6 Al After 10,099 Thermal Cycles Between -150°F and +150°F.

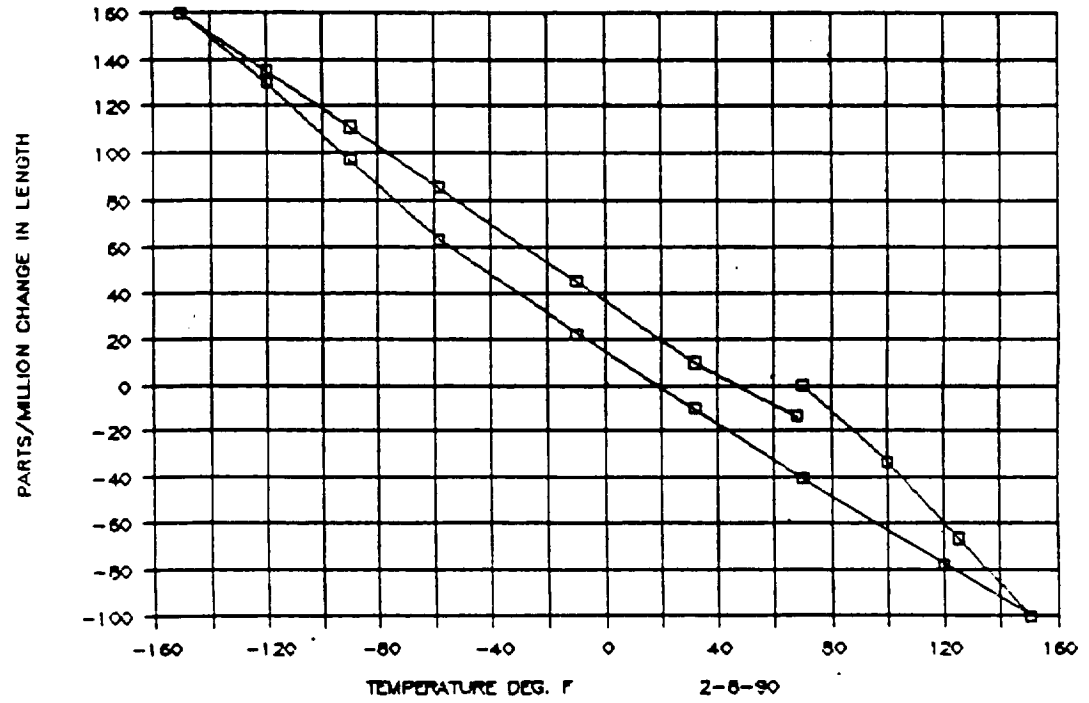

Figure 11-30 Longitudinal Thermal Expansion Response of 35 v/o SiC_p/2124-T6 Al After 10,099 Thermal Cycles Between -150°F and +150°F.

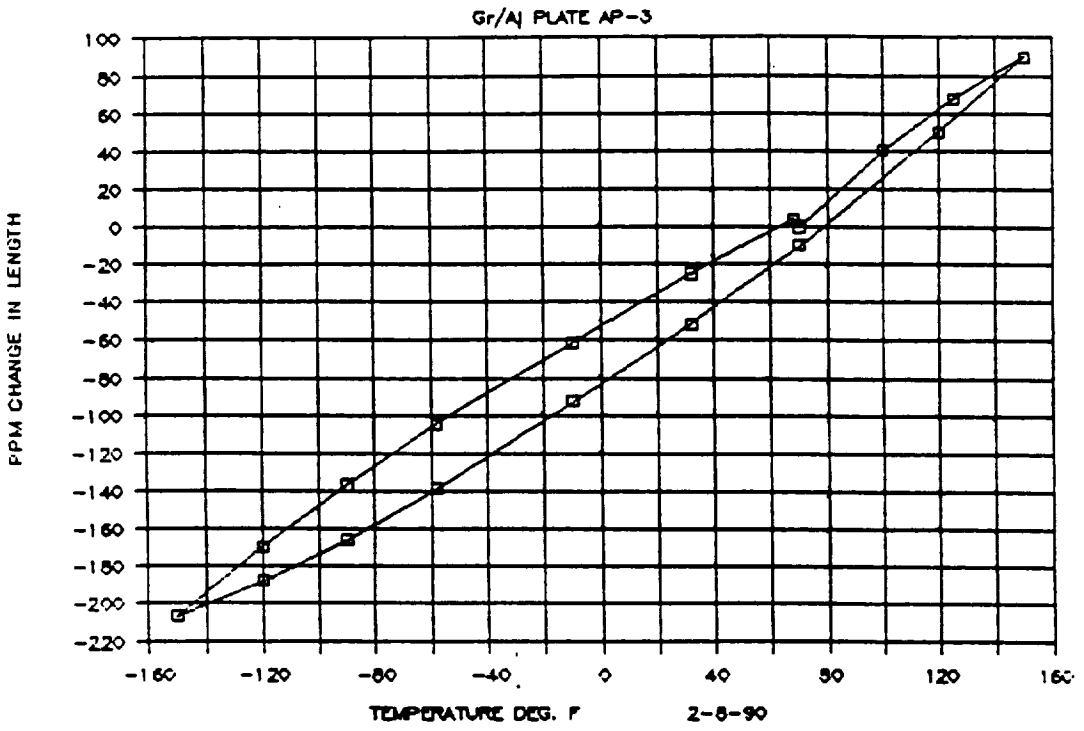

Figure 11-31 Longitudinal Thermal Expansion Behavior of P100/6061, $[0]_2$, v/o = 42.2 after 10,099 Thermal Cycles Between -150°F and +150°F.

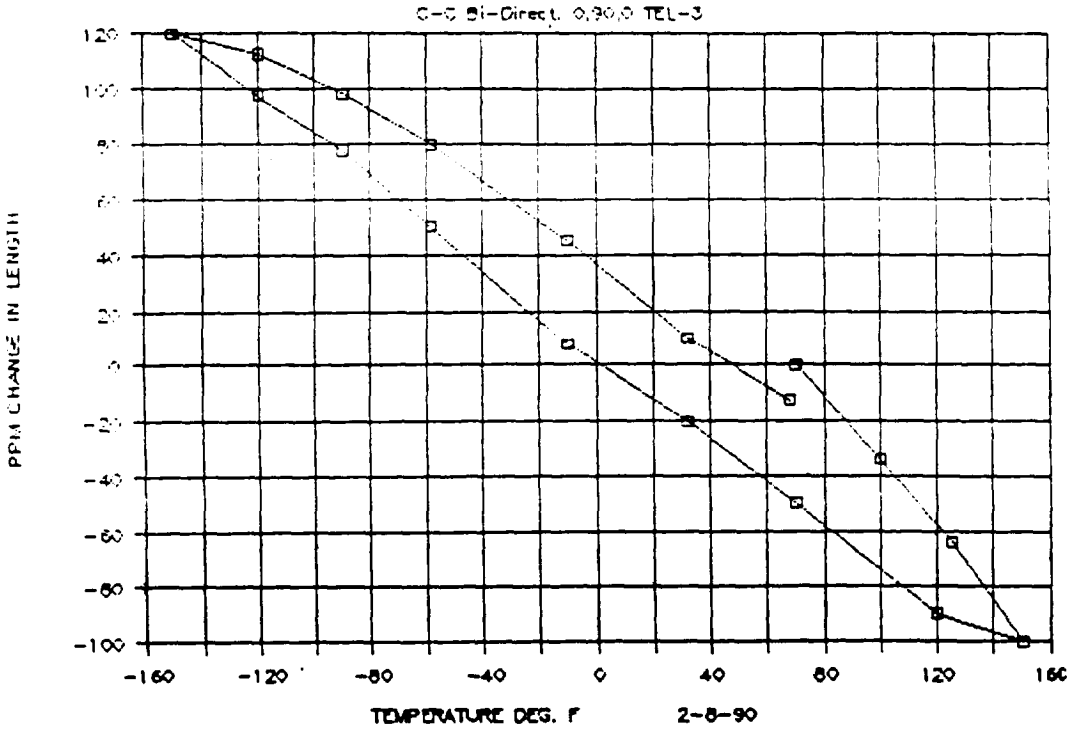

Figure 11-32 Longitudinal Thermal Expansion Response of P100/Carbon, [0/90/0], v/o = 53.0, After 10,099 Thermal Cycles Between -150°F and +150°F.

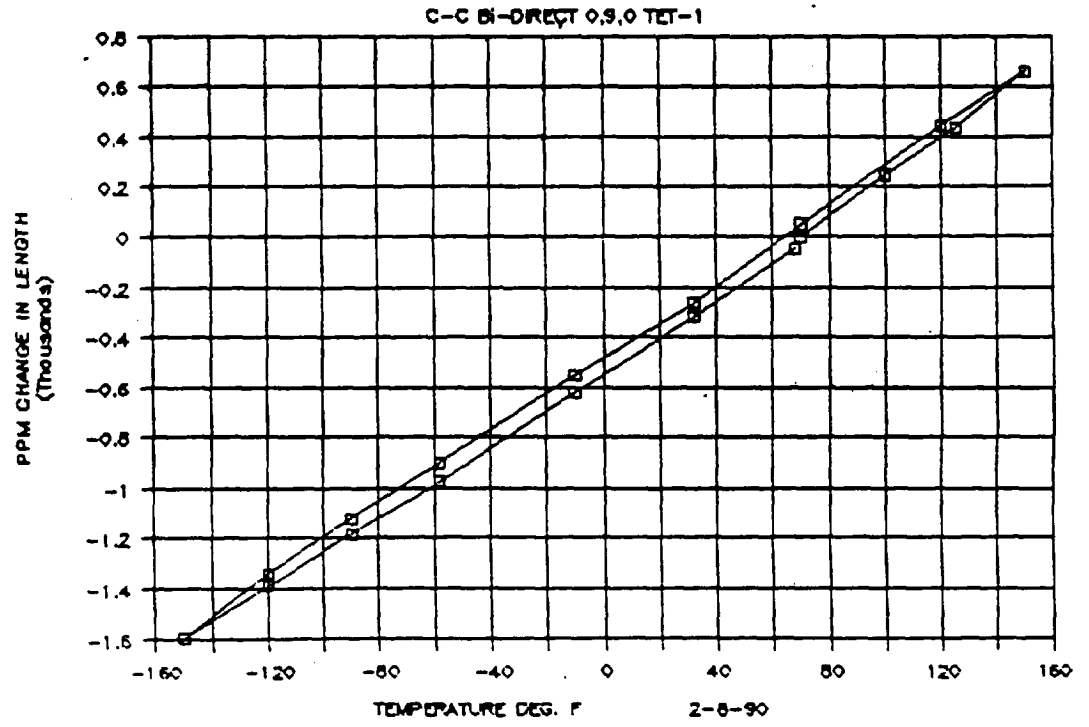

Figure 11-33 Transverse Thermal Expansion Response of P100/Carbon, [0/90/0], v/o = 53.0, After 10,099 Thermal Cycles Between -150°F and +150°F.

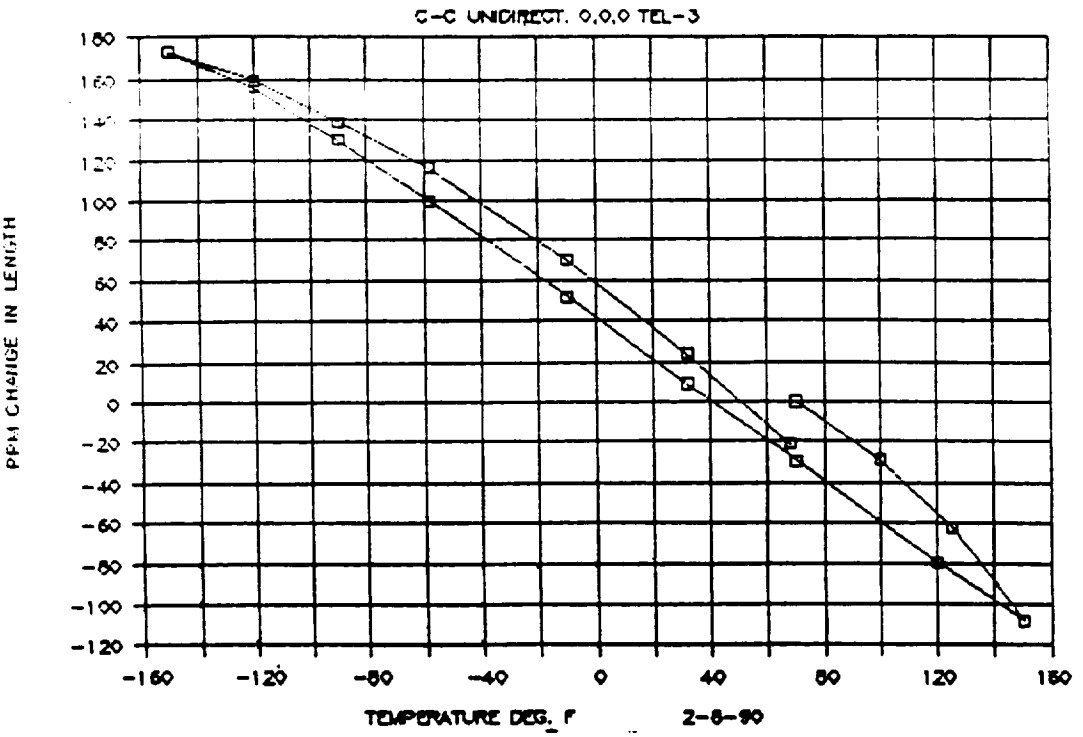

Figure 11-34 Longitudinal Thermal Expansion Response of P100/Carbon, [0₃], v/o = 52.48, After 10,099 Thermal Cycles Between -150°F and +150°F.

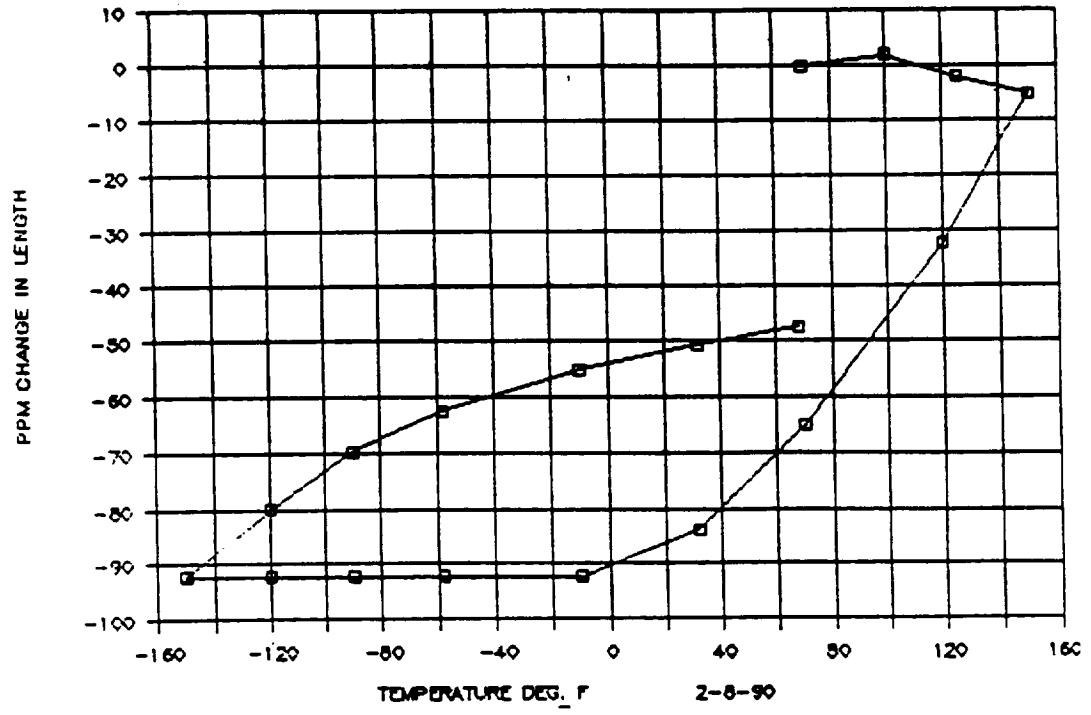

Figure 11-35 Transverse Thermal Expansion Response of P100/Carbon, [0₃], v/o = 52.48, After 10,099 Thermal Cycles Between -150°F and +150°F.

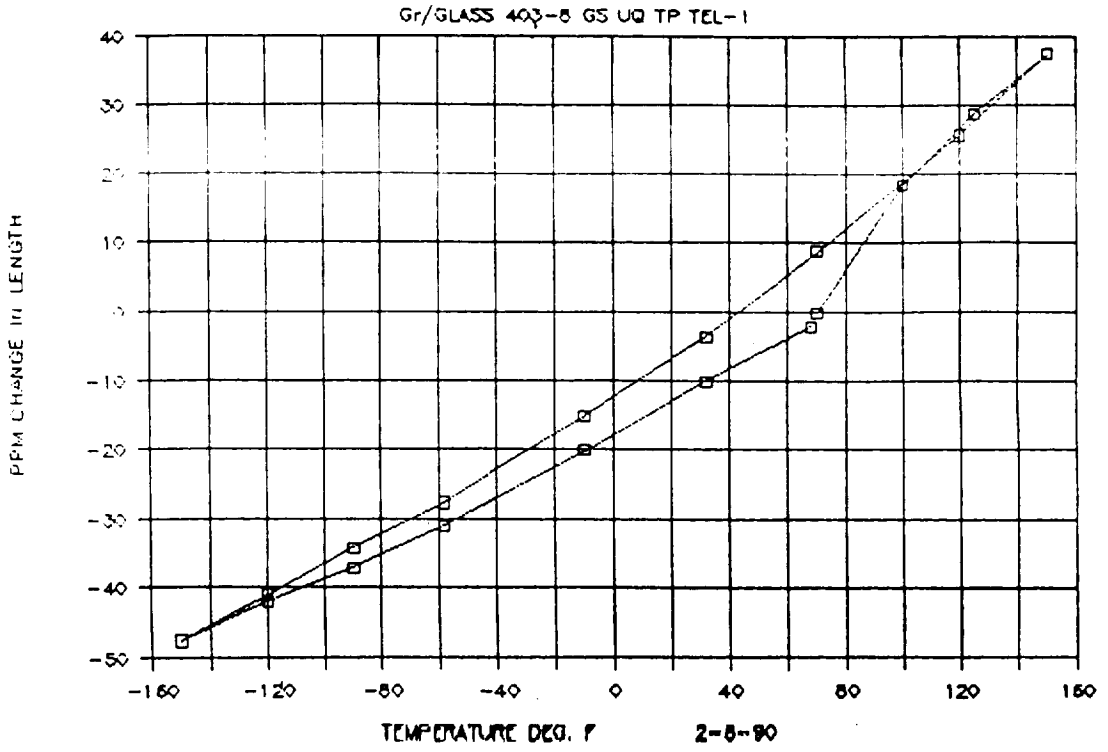

Figure 11-36 Longitudinal Thermal Expansion Response of HMU/7070 Glass, [0/90$_6$], v/o = 40.5, After 10,099 Thermal Cycles Between -150°F and +150°F.

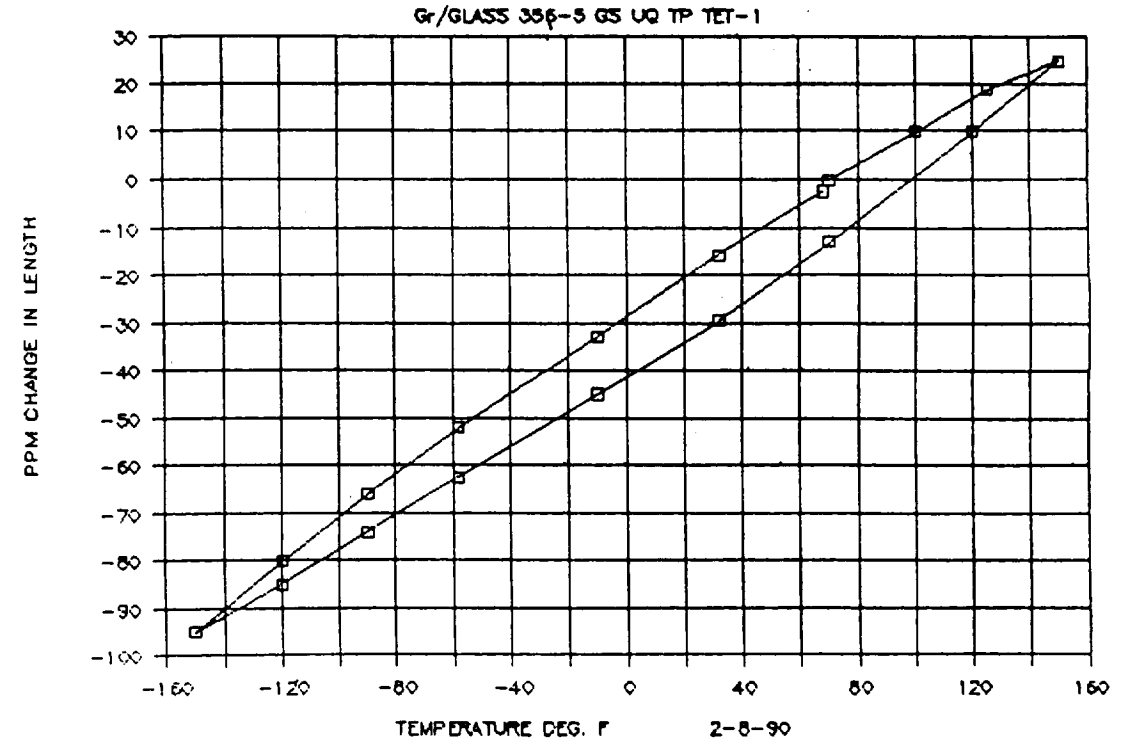

Figure 11-37 Transverse Thermal Expansion Response of HMU/7070 Glass, [0/90$_6$], v/o = 40.5, After 10,099 Thermal Cycles Between -150°F and +150°F.

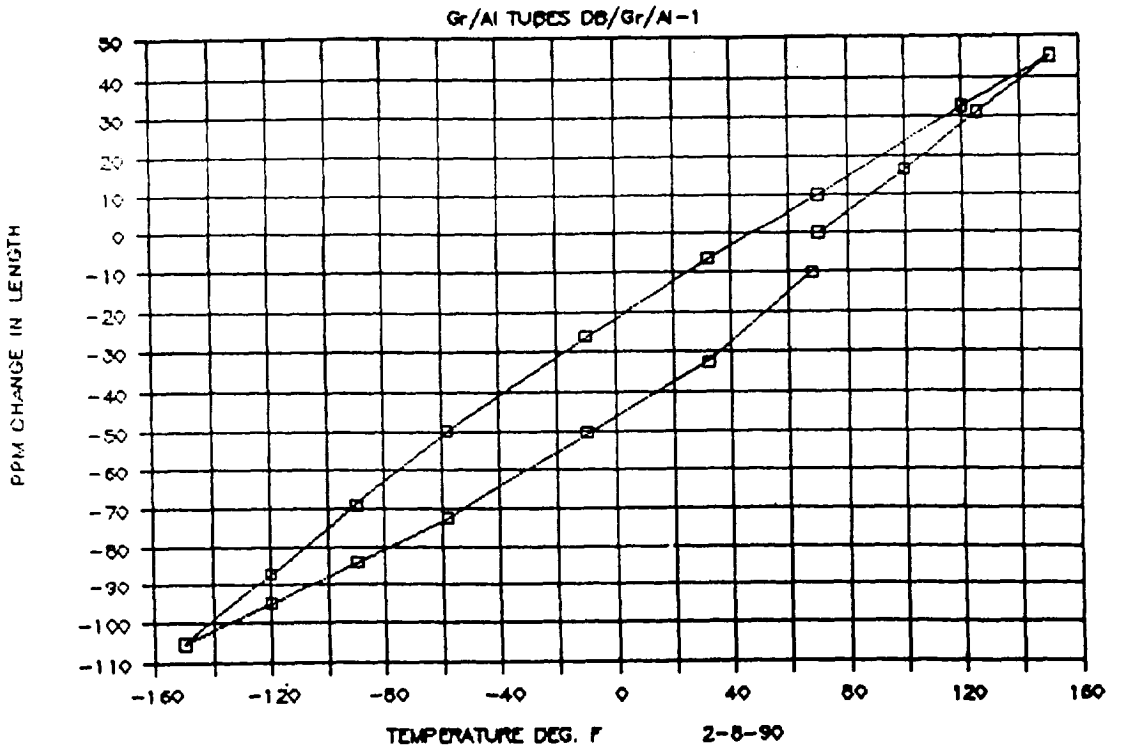

Figure 11-38 Longitudinal Thermal Expansion Behavior of P100/6061 Diffusion Bonded Tube, $[0]_2$, v/o = 43.63 after 10,099 Thermal Cycles Between -150°F and +150°F.

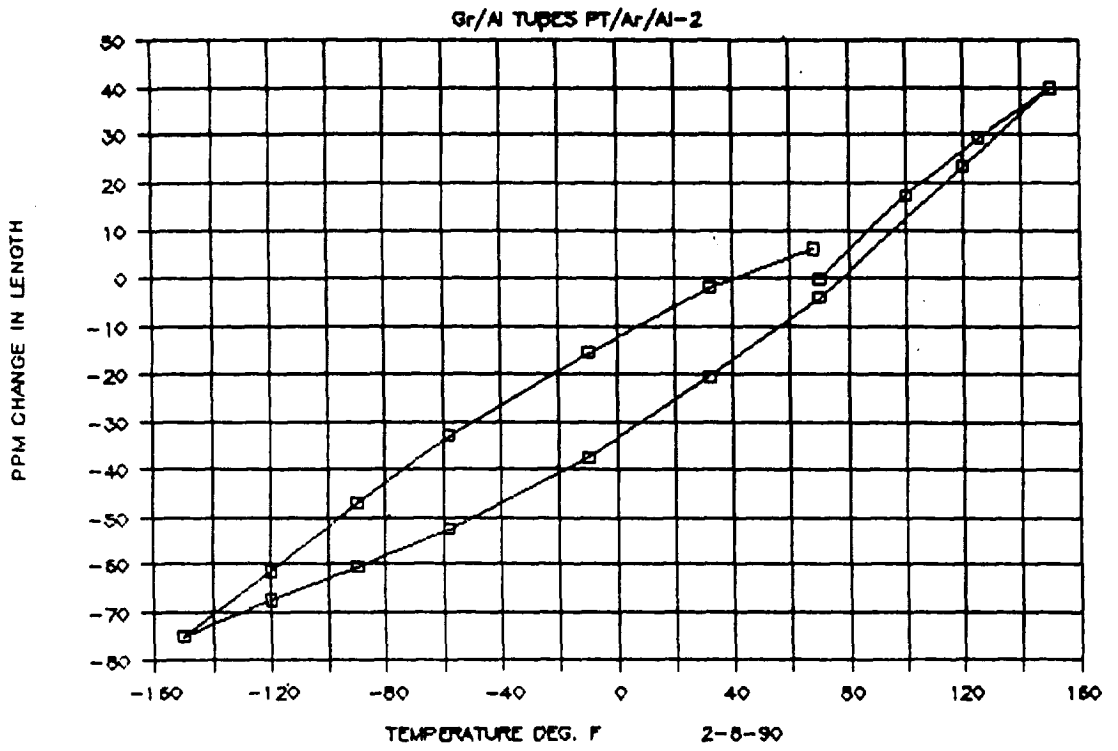

Figure 11-39 Longitudinal Thermal Expansion Behavior of P100/6061 Pultruded Tube, $[0]_2$, v/o = 44.35 after 10,099 Thermal Cycles Between -150°F and +150°F.

fabricated specimens, but with significantly reduced hysteresis.

• P100/6061 Al $[0]_2$ panels exhibited CTE_x = 0.99 ppm/°F compared to predicted value of 0.73 ppm/°F.

• HMU/7070 $[0/90]_6$ exhibited a nearly quasi-isotropic response (CTE_x = 0.28 ppm/°F and CTE_y = 0.40 ppm/°F) with very low (-13 ppm) RT hysteresis.

• CTEx values of P100/C $[0]_3$ and [0/90/0] were identical to the as fabricated specimens, suggesting that microcrack density and residual stress state was unaffected due to thermal fatigue induced during cycling between -150°F and 150°F.

Although thermal expansion and mechanical property results discussed above do provide an indication of the microdamage, still a large number of specimens should be tested to establish the extent of property changes due to the damage introduced during thermal cycling. If the microcrack density in the as fabricated composite is high, then subsequent thermal cycling will not introduce significant damage, because the thermal stresses will be accommodated by the pre-existing cracks. In most of the composite materials, there was no significant increase in microcrack density compared to the as fabricated state, consequently, the decrease in strength levels was minimal. The thermal expansion results exhibited a significant reduction in hysteresis and residual strain in each composite indicating that residual stresses generated during processing were relieved during subsequent thermal cycling.

References

REFERENCES

1. J. Persh, "Future of Metal Matrix Composites", Proceedings, Sixth Metal Matrix Composites Technology Conference, Monterey, CA, May 1985.
2. J. F. Garibotti, C. J. Northrup, and A. Gunderson, "Design Aspects of MMC in SDI Spacecraft", Proceedings, Seventh Metal Matrix Composites Technology Conference, pp1-1 - 1-28, Silver Spring, MD, 26-28 May 1987.
3. D. R. Tenney, "Structural Materials for Space Application", NASA/SDIO Space Environmental Effects of materials Workshop, L. A. Teichman, NASA CP-3035, Part 1, pp. 25 - 52, 1989.
4. M. S. Misra, "Engineered Materials for Space Applications", Martin Marietta Astronautics Group Journal, Volume 1, pp. 14 - 23, 1990.
5. D. R. Tenney, G. F. Sykes, and D. E. Bowles, "Composite Materials for Space Structures", Presented at the 3rd European Symposium on Spacecraft Materials in Space Environment, Noordwijk, The Netherlands, 1 - 4 October. 1979.
6. B. A. Stein, S. S. Tompkins, and W. D. Brewer, "Review of NASA Research on Low Temperature Metal-Matrix Composites for Aeronautics and Space", Presented at the 5th Metal Matrix Composites Technology Conference, May 1983.
7. J. F. Garibotti, W. E. Davis, and N. R. Adsit, "Materials and Structures for Space Applications", Presented at AIAA/NASA Space Systems Technology Conference, Costa Mesa, CA, 5 - 7 June 1984.
8. M. S. Misra, S. P. Rawal, B. J. Maclean, and R. G. Wendt, "Metal Matrix Composites for Precision Space Structures", Presented at AeroMat '90, Long Beach, CA, 21 - 24 May 1990.
9. L. A. Harris, "Composites in Space - Past, Present and Future", Composite Interfaces, H. Ishida and J. L. Koenig, Editors, pp. 1 - 8, Elsevier Publishing Co. Inc., 1986.

10. J. F. Garibotti, W. E. Davis, R. N. Levin, and V. L. Freeman, "The Impact of High Modulus Structural Carbon/Carbon on Spacecraft Survivability and Performance", ACMA CR 8601, Ametek, July 1986.

11. D. R. Tenney and D. E. Bowles, "Spacecraft Radiation Effects on Dimensional Stability of Composites", Proceedings of 4th International Symposium on Spacecraft Materials in Space Environment, Toulouse, France, 6 - 9 September 1988.

12. D. R. Tenney, G. F. Sykes, and D. E. Bowles, "Space Environmental Effects on Materials", Presented at the AGARD Conference on Environmental Effects on Materials for Space Applications, Conference Proceedings No. 327, Toronto, Canada, September 1982.

13. D. E. Bowles, "The Effects of Microcracking on the Thermal Expansion of Graphite/Epoxy Composites", Presented at the 3rd Annual LSST Conference, 16 - 19 November 1981, NASA-LaRC, NASA CP- 2215, Part 1, 1982, pp. 67-79.

14. D. E. Bowles, S. S. Tompkins, and G. F. Sykes, "Electron Radiation Effects on the Thermal Expansion of Graphite/Resin Composites", AIAA Journal of Spacecraft and Rockets, Vol. 23, No. 6, November - December 1986.

15. S. M. Milkovich, C. T. Herakovich, and G. F. Sykes, "Space Radiation Effects on Graphite-Epoxy Composite Materials", Center for Composite Materials and Structures, VPI&SU, Report No. CCMS-84 08, Blacksburg, VA, June 1984.

16. G. F. Sykes, S. M. Milkovich, and C. T. Herakovich, "Simulated Space Radiation Effects on a Graphite/Epoxy Composite", Presented at the Spring National Meeting of the American Chemical Society, Miami Beach, FL, April 18 - May 3, 1985.

17. G. F. Sykes and D. E. Bowles, "Space Radiation Effects on the Dimensional Stability of a Toughened Epoxy Graphite Composite", SAMPE Quarterly, Nol. 17, No. 4, July 1986.

18. S. D. Adams, D. E. Bowles, and C. T. Herakovich, "Thermally Induced Transverse Cracking in Graphite/Epoxy Cross-Ply Laminates", Journal of Reinforced Plastics and Composites, Vol. 5, No. 3, July 1986.

19. J. Persh, "New Department of Defense Initiatives in Composite Materials and Structures", Ceramic Eng. Sci. Proc. 9, [7 - 8], pp. 529 - 540, 1988.

20. "DoD-NASA Advanced Composite Design Guide", AD-B080184, Rockwell International, AFWAL/FDL, July 1983.

21. "SDS Spacecraft Structural Composite Materials Selection Guide", Ketema Inc., Santa Ana, CA, Release 1.0, May 1989.

22. L. Rubin, "Data-Base Development for P100 Graphite/Aluminum Metal Matrix Composites", Aerospace Report No. TOR-0089 (4661-02)-1, 15 September 1989.

23. L. Rubin, "High Modulus Carbon Fiber Based Carbon-Carbon for Space Applications", The Aerospace Corporation, Report SD TR-86-45, 18 July 1986.

24. J. B. Andriulli, V. W. Campbell, R. E. Garvey, T. L. Knight, J. W. McKeever, and R. G. Rudness, "Thermoplastics Composites for Space Applications", 1989 Annual Report, ORNL/ATD-14, Vol. 1 and Vol. 2, Oak Ridge National Laboratory, Oak Ridge TN, September 1989.

25. "Proceedings of a Workshop on Advanced Structural Materials for Space Applications", Thermoplastic Composites, Vol. 1, Burlingame, CA, 11 - 14 September 1989.

26. "Proceedings of a Workshop on Advanced Structural Materials for Space Applications", Metal Matrix Composites, Vol. 2, Burlingame, CA, 11 - 14 September 1989.

27. "Spacecraft Applications for Carbon-Carbon Program Review Proceedings", NSWC, Silver Springs, 14 June 1989.

28. A. P. Divecha, S. G. Fishman, and S. D. Karmarker, Silicon Carbide Reinforced Aluminum - A Formable Composite, J. Met., September 1981.

29. K. Hall, B. Rodini, C. Thaw, and C. Zweben, "Metal Matrix, Carbon and Ceramic Matrix Composites 1985", NASA Conference Publication 2406, December 1985, pp. 116-121.

30. S. P. Rawal and M. S. Misra, "Large Graphite/Magnesium Tube Development", WRDC-TR-90-4062, August 1990.

31. G. A. Dries and S. S. Tompkins, "Effects of Thermal Cycling on Graphite-Fiber-Reinforced 6061 Aluminum", NASA TP-2612, October 1986.

32. D. W. Bowles and D. R. Tenney, "Thermal Expansion of Composites: Methods and Results", Presented at the 2nd Annual LSST Technical Review, NASA-LaRC, NASA CP 2168, November 1980.

33. B. L. Wingard, "Testing and Evaluation of Missile Materials - Task VI: Carbon-Carbon Materials for Space Structures", Southern Research Institute Quarterly Progress Report, July 1989.

34. A. L. Bertram, "Thin Ply Gr/Al for Space Structures", Proceedings DoD Eighth MMC Technology Conference, pp. 67-1 - 67-8, Monterey, CA, 19 - 23 June 1989.

35. K. Benner and B. K. Min, "MMC Truss Evaluation", Proceedings DoD Eighth MMC Technology Conference, pp.68-1, Monterey, CA, 19 - 23 June 1989.

36. D. E. Bowles and D. R. Tenney, "Composite Tubes for the Space Station Truss Structure", Presented at the 18th International SAMPE Technical Conference, Seattle, WA, October 1986.

37. M. S. Misra, "Role of Material Damping in the Control of Space Structures", Presented at AeroMat '90, Long Beach, CA, 21 - 24 May 1990.

38. H. H. Armstrong and A. M. Ellison, "Satellite Applications of Metal Matrix Composites", AFML-TR-79-4007, May 1979.

39. H. H. Armstrong, A. M. Ellison and D. H. Kintis, "Development of Graphite/Metal Advanced Composites for Applications", AFWAL-TR-83-4148, October 1983.

40. R. A. Mayor, J. R. Strife, and V. C. Nardone, "Metal Matrix Composites Structural Data Development," AFWAL-TR-86-4129, January 1987.

41. T. E. Steelman, A. D. Bakalyar, and L. Konopka, "Aluminum Matrix Composite Structural Design Development", AFWAL TR-86-3087, March 1987.

42. S. P. Rawal, M. S. Misra, D. Goddard, and J. Jackson, "Novel Processing Techniques to Fabricate Graphite/Magnesium Composites for Space Applications", Martin Marietta Space Systems Report #MCR-88-635, 1988.

43. R. G. Wendt, S. P. Rawal, and M. S. Misra, "Reproducibility of Filament-Wound Vacuum Cast Graphite Magnesium Tubes", Martin Marietta Space Systems Report #MCR-88-615, December 1988.

44. K. M. Prewo and V. C. Nardonne, " Carbon Fiber Reinforced Glass Matrix Composites for Space Based Applications", Report R86-917161-1, (UTRC) ONR Contract N0-0014-95-C-0332, September 1986.

45. W. K. Tredway and K. M Prewo, "Carbon Fiber Reinforced Glass Matrix Composites for Space Based Applications", Report 87-917470-1, Contract N00014-85-C-0332, August 1987.

46. W. C. Harrigan, Jr., "Heat Treatment of Silicon Catbide Reinforced 6061 Aluminum Composites," Presented at the AIME Fall Meeting, American Institute of Mining, Metallurgical and Petroleum Engineers, October 1982.

47. "Survivability of Satellite Structural Systems, Material Science Corporation", Technical Progress Report MSC-TPR-1725/1301, January 1987.

48. Annual Book of ASTM Standards, 1989.

49. DoD-NASA Advanced Composite Guide, Rockwell International, AFWAL/FDL, Chapter 4.2, July 1983.

50. Engineered Materials Handbook, Vol 1, Composites, ASM International, Metals Park, OH, 1987.

51. NASA RP 1092 - Standard Tests for Toughened Resin Composites, Revised Edition, July 1983.

52. "Suppliers of Advanced Composite Materials Association (SACMA) Recommended Methods, T2-489-1, 1989.

53. R. E. Taylor, "Determining the Thermophysical Properties of Selected Materials", Thermophysical Property Research Laboratory, Purdue University IN, Report No. TPRL 181A, 1989.

54. S. S. Tompkins, D. E. Bowles, and W. R. Kennedy,. "A Laser Interferometer for Thermal Expansion Measurements of Composites", SEM Experimental Mechanics, Vol. 26, No. 1, pp. 1 - 6, March 1986.

55. "Composite Materials", Testing and Design (Second Conference), STP-497, 04-497000-33, 1972.

56. "Composite Materials", Testing and Design (Third Conference), STP-546, 04-546000-33, 1974.

57. "Composite Materials", Testing and Design (Fifth Conference), STP-674, 04-674000-33, 1979.

58. "Composite Materials", Testing and Design (Sixth Conference), STP-787, 04-787000-33, 1982.

59. "Composite Materials", Testing and Design (Seventh Conference), STP-893, 04-893000-33, 1984.

60. C. C. Chamis and J. H. Sinclair, "10° Off-Axis Tensile Test for Interlaminar Shear Characterization of Fiber Composites", NASA-TN-D-8215, April 1976.

61. R. Francini, "Testing of Longitudinally Reinforced Graphite/Metal Composite Thin Wall Tubing", ASTM Proceeding on Test Methods, November. 1985.

62. D. F. Adams, " Properties/Characterization-Mechanical/Physical/Hygrothermal Properties Test Methods", Composites Technology, edited by Stuart M. Lee, published by Technonic Publishing Company, 1989, pp. 49-80.

63. S. S. Tompkins, G. F. Sykes, and D. E. Bowles, "The Thermal and Mechanical Stability of Composite Materials for Space Structures", Technical Paper EM 85-979, Presented at the IEEE/ASM/ASME/SME Space Tech Conference, Anaheim, CA, September 1985.

64. G. A. Dries and S. S. Tompkins, "Effects of Thermal Cycling on Thermal Expansion and Mechanical Properties of Several Graphite-Reinforced Aluminum Metal Matrix Composites", NASA TP-2701, July 1987.

65. E. G. Wolff, B. K. Min, and M. H. Kural, "Thermal Cycling of a Unidirectional Graphite/ Magnesium Composite", Journal of Materials Science, 20, pp 1141 - 1149, May 1985.

66. J. R. Strife and V. S. Nardone, "Thermal Expansion of Graphite Fiber-Reinforced Metals", Proceedings, Sixth Metal Matrix Composites Technology Conference, pp. 21-1 - 21-7, May 1985.

67. D. J. Barrett and K.W. Buesking, "Temperature Dependent Nonlinear Metal Matrix Laminate Behavior, NASA Contractor Report 4016, September 1986.

68. J. A. Barnes and F. N. Cogswell, Thermoplastics for Space, SAMPE Quarterly, pp 22 - 27, April 1989.

69. S. S. Tompkins, D. E. Bowles, J. G. Funk, J. A. Lavoie, and T. W. Towell, "The Development of composite Materials for Spacecraft Precision Reflector Panels", Presented at Composite Materials For Optical and Electro-Optical Instruments, Orlando, Florida, 16 - 20 April, 1990.

70. J. C. Larue, "Accelerated Thermal Cycling of Spacecraft Structures", Institute of Environmental Science 1983 Proceedings, Los Angeles, CA, pp. 130 - 134, 19 - 21 April 1983.

71. M. Taya and R. J. Arsenault, "A Comparison Between a Shear Lag type Model and Eshelby Type Model in Predicting the Material Properties of Short Fiber Composites", Scripta Met., Vol. 21, pp 349 - 354, 1987.

72. J. A. DiCarlo and J. E. Maisel, "Measurement of the Time/Temperature-Dependent dynamic Mechanical Properties of Boron/Aluminum Composites", Composite Materials, Testing and Design (Fifth Conference), ASTM STP 674, S. W. Tsai, ed., American Society for Testing and Materials, 1979, pp. 201-227..

Appendix A—Typical Properties of Fibers

APPENDIX A: TYPICAL PROPERTIES OF FIBERS (AT ROOM TEMPERATURE)

A.0—Table A-1 lists typical properties of fibers used for organic matrix, metal matrix, glass matrix, and C/C composites in this program.

Table A-1 Typical Properties of Fibers at RT

CARBON FIBER	DENSITY lb/in^3	TENSILE STRENGTH Ksi	TENSILE MODULUS Msi	LONG. THERMAL COND. Btu/hr. ft. F°	LONG. CTE μ in/in/F°	ELECTRICAL RESISTIVITY Ohm-cm x 10^{-4}
T-300 1K	0.063	500	33.5	5	-0.3	18
AS4	0.065	550.0	34.0	—	—	15.3
HMU	0.067	400.0	55.0	—	—	—
P-75S 2K	0.072	275	75	107	-0.75	7.0
P-100S 2K	0.078	325	105	300	-0.78	2.5

A.1 REFERENCES

A1 Product Specification Brochure of Thornel Carbon Fiber Products, Amoco Performance Products, Inc., January 1987.

A2 Magnamite Graphite Fibers - Product Data Sheet, Hercules Inc. - Graphite Materials, August 1986.

A3 SDS Spacecraft Structural Composite Materials Selection Guide, Ketema Inc., Santa Ana, CA, Release 1.0, May 1989.

Appendix B—Specimen Preparation

APPENDIX B SPECIMEN PREPARATION

B.0 SPECIMEN LAY-OUT

Figure B-1 and B-2 show the specimen layout for the lamina and the laminate panel respectively. Also, the specimen layout for a tube is shown in Figure B-3. In each case, the maximum number of test specimens for material property characterization were obtained from a 12-in. x 12-in. panel or a 6 ft long tube.

B.1 SPECIMEN PREPARATION

Prior to cutting, specimen layout of the panel was carefully reviewed to ensure that saw-cuts provided each specimen within the prescribed dimensional tolerances. From each panel and tubes, the test specimens were cut with the 2-in. dia. diamond saw. Subsequently, edges of each specimen were polished to the final dimensions using 320 grit abrasive paper. On flat specimens (e.g., for tension, compression, and 10° off-axis tests) the fiber glass end tabs providing 15° taper near the gage length, were bonded using Hysol EA-934 adhesive. For the tubular specimens (i.e., tension, compression, and torsion tests), specifically designed steel grip ends were machined and bonded to the OD of the tubes with the Hysol EA-934 adhesive, while maintaining a bond line thickness of 0.010-in.

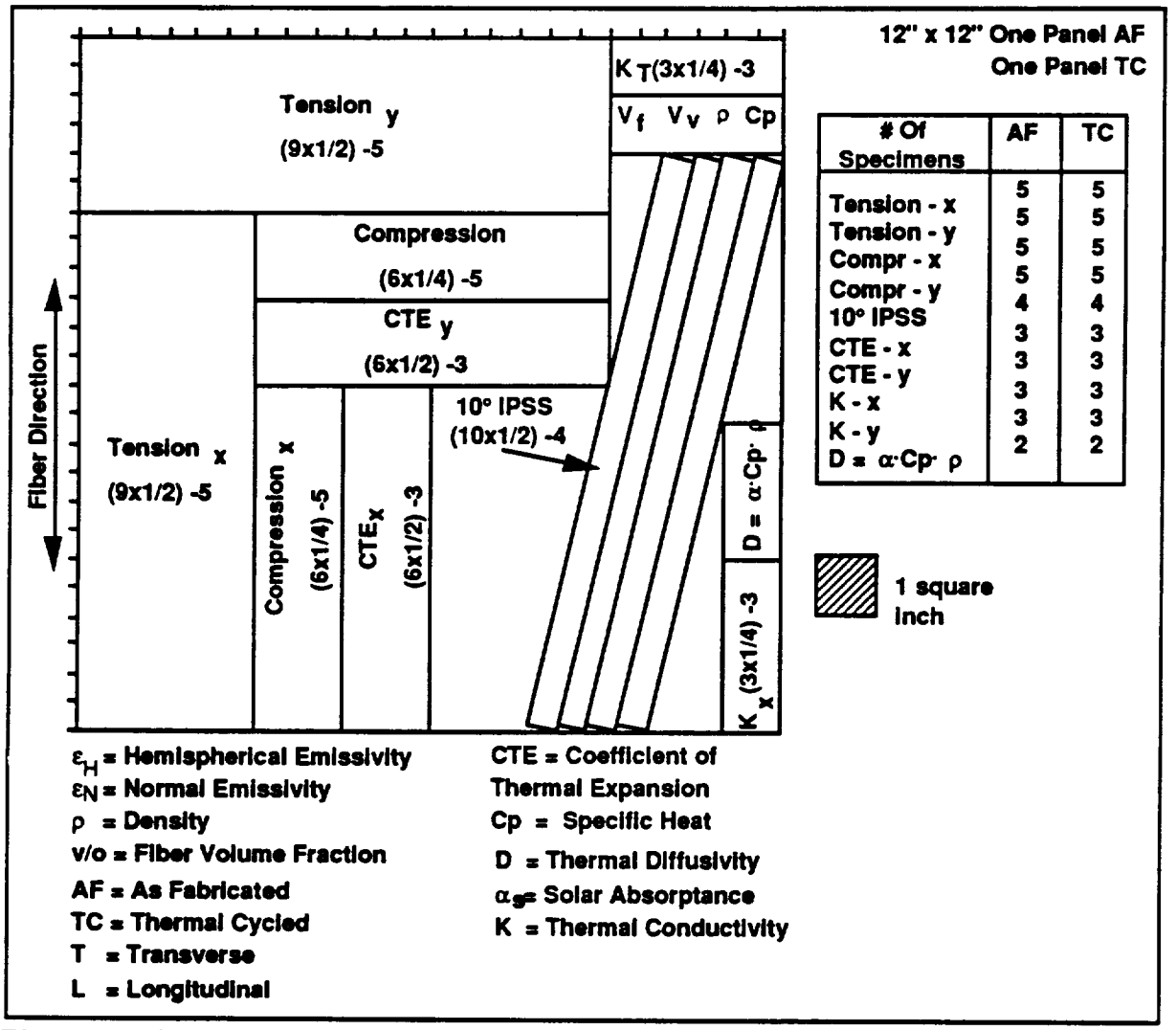

# Of Specimens	AF	TC
Tension - x	5	5
Tension - y	5	5
Compr - x	5	5
Compr - y	5	5
10° IPSS	4	4
CTE - x	3	3
CTE - y	3	3
K - x	3	3
K - y	3	3
D = α·Cp·ρ	2	2

Figure B-1 Specimen Lay-Out for a Lamina Panel

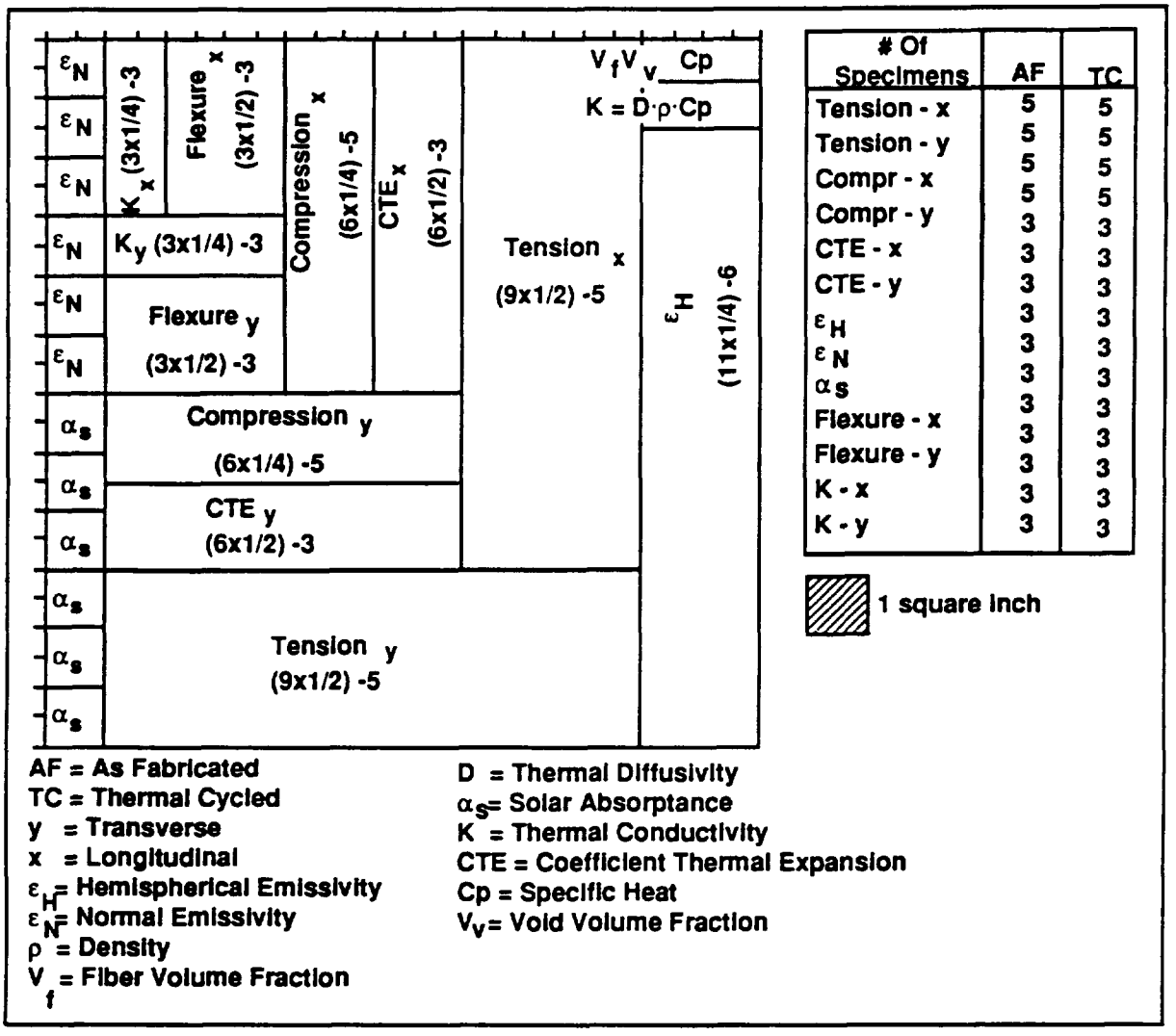

Figure B-2 Specimen Lay-Out for a Laminate Panel

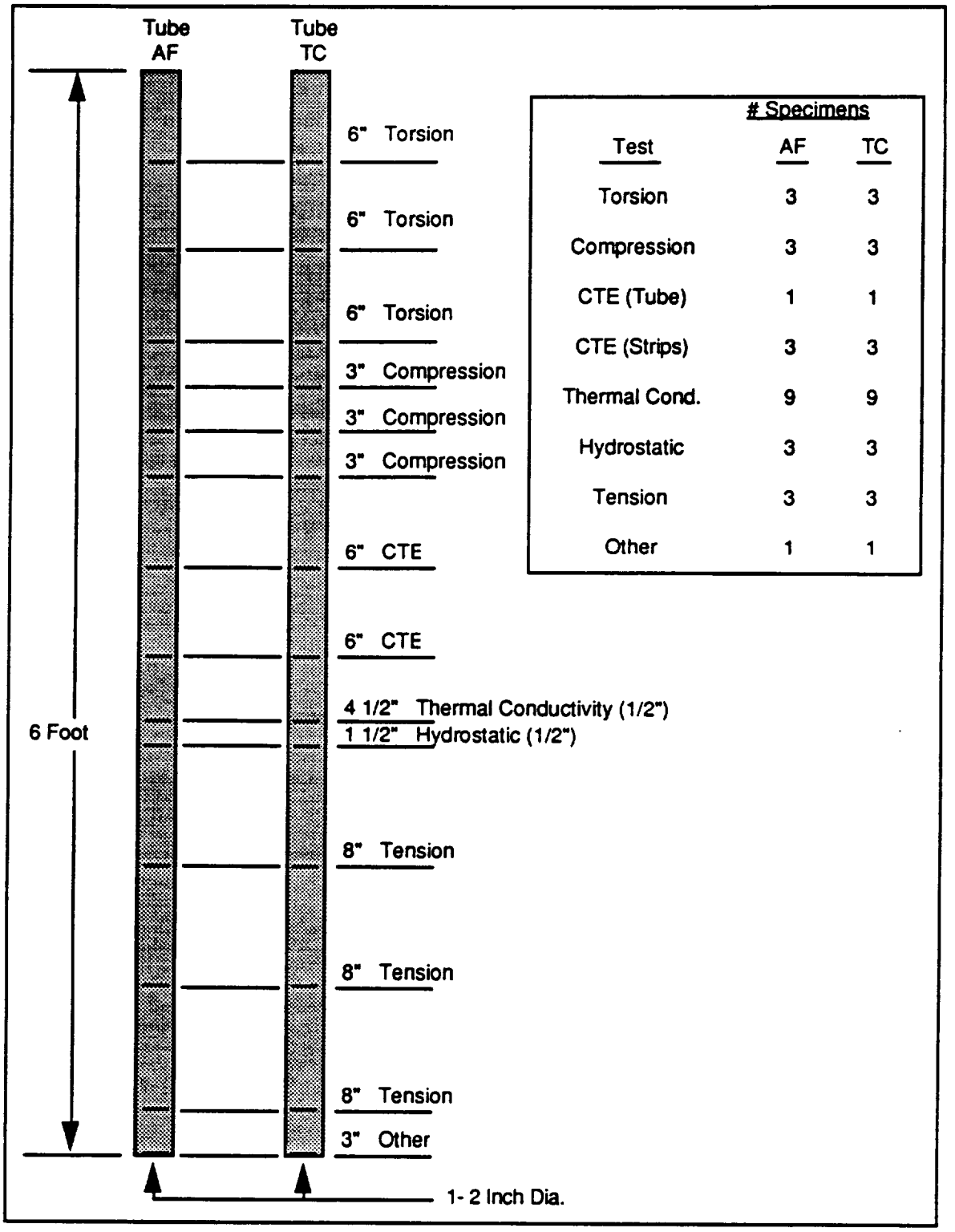

Figure B-3 Specimen Lay-Out for Composite Tubes

Appendix C—Test Methods

APPENDIX C TEST METHODS

C.O TEST METHODS FOR COMPOSITE MATERIALS

To generate a reliable and consistent data base that may be used with confidence throughout industry, only those methods which produce repeatable, reliable, and easily obtainable results were included in this technical effort. These methods primarily included ASTM standards (whenever applicable), and ASTM, SACMA, DOD-NASA, TPRL, or Martin Marietta Astronautics Group recommended methods (Refs C1 to C5). For compression and torsion tests of tube specimens, specific fixtures were designed and fabricated at Martin Marietta Astronautics Group. The selected test methods are listed in Table C-1. For the mechanical property tests, the specimen design/fixture are shown schematically in Figures C-1 to C-7. For the thermophysical properties, key features of the test methods such as equipment, reference material and specimen size are briefly outlined below and listed in Table C-2.

C.1 THERMOPHYSICAL PROPERTY TEST METHOD

C.1.1 Coefficient of Thermal Expansion: Push Rod Dilatometer (PRD)—In a fused silica test chamber, a 3-in long (0.5-in wide) specimen is placed in contact with a freely-suspended probe rod (fused silica). As the specimen temperature changes, it expands or contracts and the resultant change in length is transmitted by the probe rod to the core of the LVDT transducer. The LVDT converts this displacement into a proportional voltage signal recorded as ΔL. These measurements were performed at Harrop Industries, Columbus, OH, using their model TDA-H2. The strain sensitivity of this technique is about $\pm$ 10 ppm/°F as compared to $\pm$ 0.1 ppm/°F for the laser interferometric dilatometer (Ref C-6). The temperature change is accomplished at a rate of 40°F/minute; compared to 22°F/hour in the case of laser interferometric dilatometer. The dimensional changes of the specimen-standard assembly were recorded at temperature levels of

Table C-1 Selected Test Methods for Composites

• Density	
ASTM-D792	Specific Gravity of Plastics by Displacement Method
•Reinforcement Volume	
ASTM-D3553	Fiber Content by Digestion of MMC
ASTM-D3171	Fiber Content of Resin Matrix Composites by Matrix Digestion
ASTM-D2734	Void Content of Reinforced Plastics
• Mechanical Properties	
ASTM-D3552	Tensile Properties of Fiber Reinfoced MMC
ASTM-D3039	Tensile Properties of Fiber Reinforced Resin Composies
ASTM-D3410	Compressive Properties of Unidirectional or Cross-Ply Fiber Resin Composites
ASTM-D3518	Inplane Shear Stress Strain Respone of Unidirectional Reinforced Plastics
ASTM-D23444	Apparent Interlaminar Shear Strength of Fiber Composites by Short Beam Method
ASTM-D790	Flexural Properteis of Plastics and Electrical Insulating Materials
NASA TN D-8215	10° Off-Axis Tensile Test for Interlaminar Shear Characterization of Fiber Composites NOL Burst Ring Test Method for Determining Hoop Tensile Properties
• Thermophysical Properties	
ASTM-E228	Linear Thermal Expansion Using Vitreous Silica Dilatometer
ASTM-E80	Dilatometric Analysis of Metallic Material
ASTM-E1269	Specific Heat Capacity by Differential Scanning Calorimetry
TPRL (Recommended)	Kohlrausch Test Method for Determining Thermal Conductivity and Electrical Resistivity
TPRL (Recommended)	Laser Flash Method for Determining Thermal Diffusivity
ASTM-C835	Total Hemsipherical Emittance of Surfaces
ASTM-E903	Solar Absorptance, Reflectance and Transmittance of Materials
ASTM-E408	Total Normal Emittance of Surfaces Using Inspection Meter Techniques

Special Remarks

Laminate	No. of Plies (n)	Specimen Width b
$[0]_C$	n = 6	1/2
$[90]_C$	n = 15	1
$[0/90]_C$	n ≥ 3	1
$[0/\pm45/90]_C$	n ≥ 6	1

(1) Specimens may be individually molded or cut (diamond tool recommended) to width required.
(2) Inner ply of tab material should have fibers in the longitudinal direction.
(3) Self-aligning grips should be used, completely enclosing the tab area.
(4) The aspect ratio of the test area must be noted when testing off-axis orientations. The aspect ratio may be varied to represent a specific application.

Test Specimen

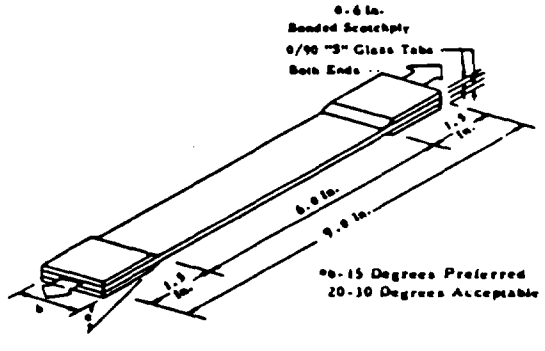

Method:
ASTM D3039

Figure C-1 Straight-sided Tension Test Specimen for Fiber Reinforced Composites

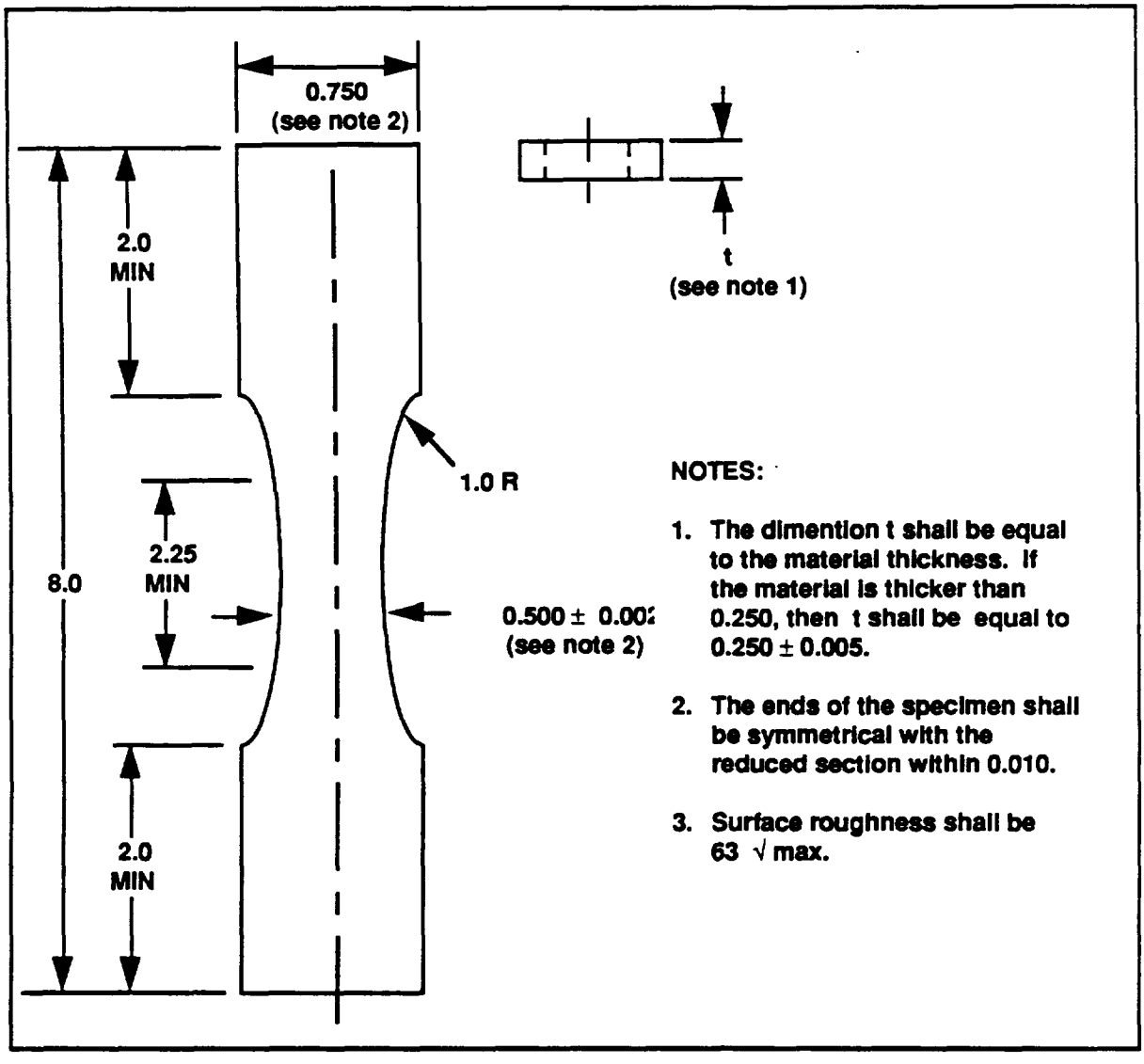

Figure C-2 Discontinuous Reinforced MMC Tension Test Specimens (ASTM D-3552)

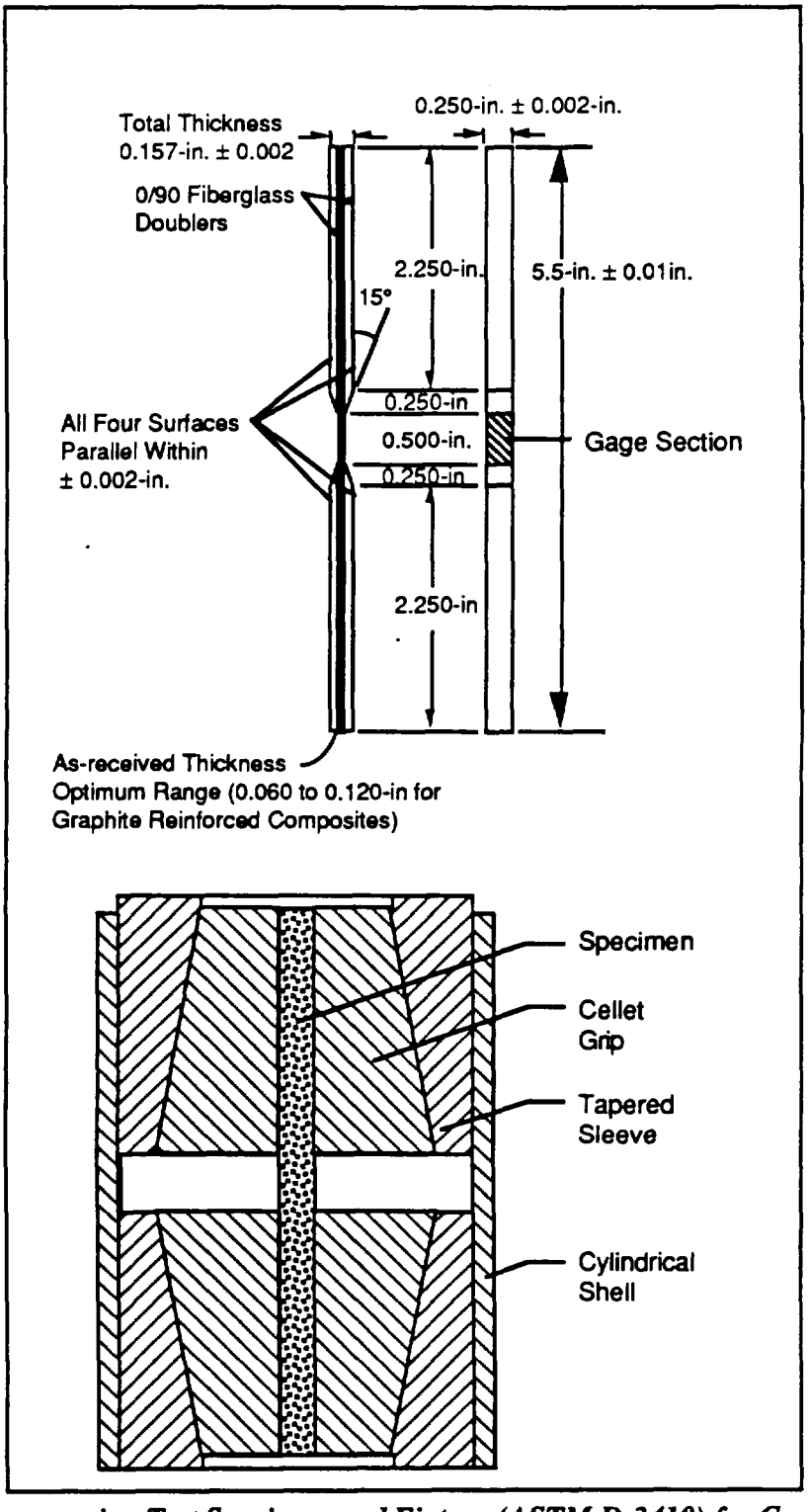

Figure C-3 Compression Test Specimen and Fixture (ASTM D-3410) for Composites

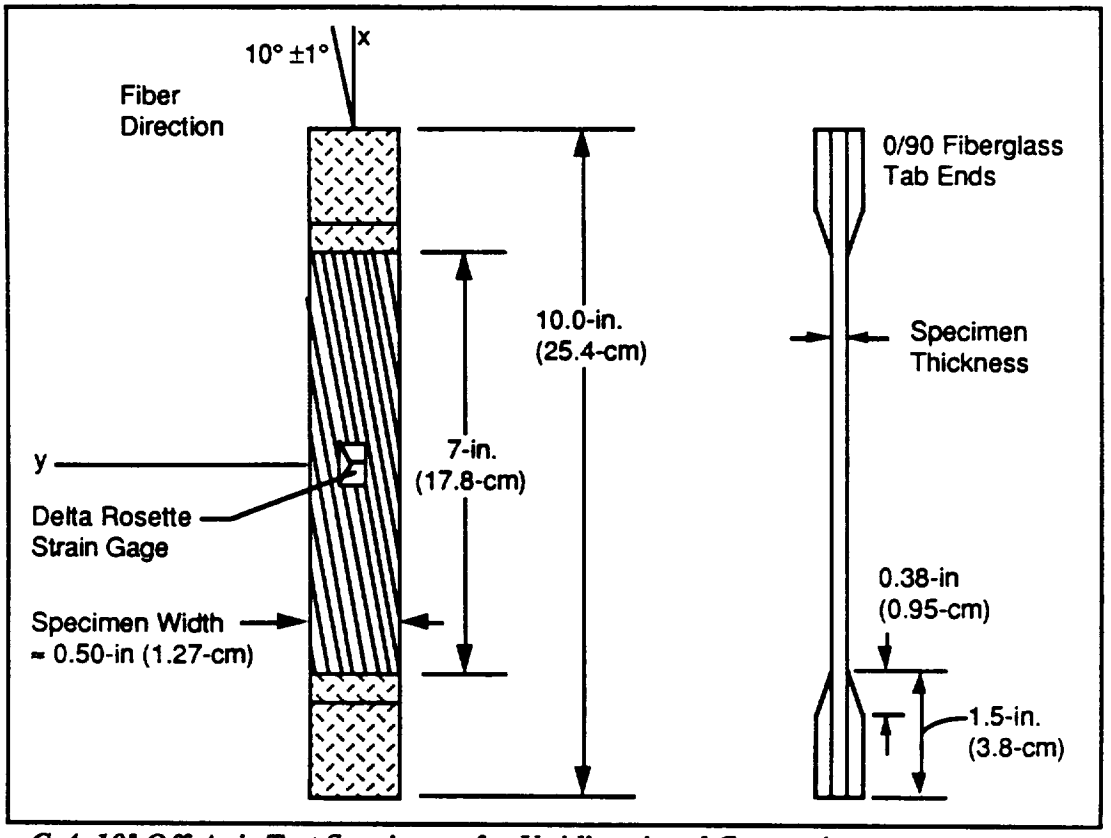

Figure C-4 10° Off-Axis Test Specimens for Unidirectional Composites

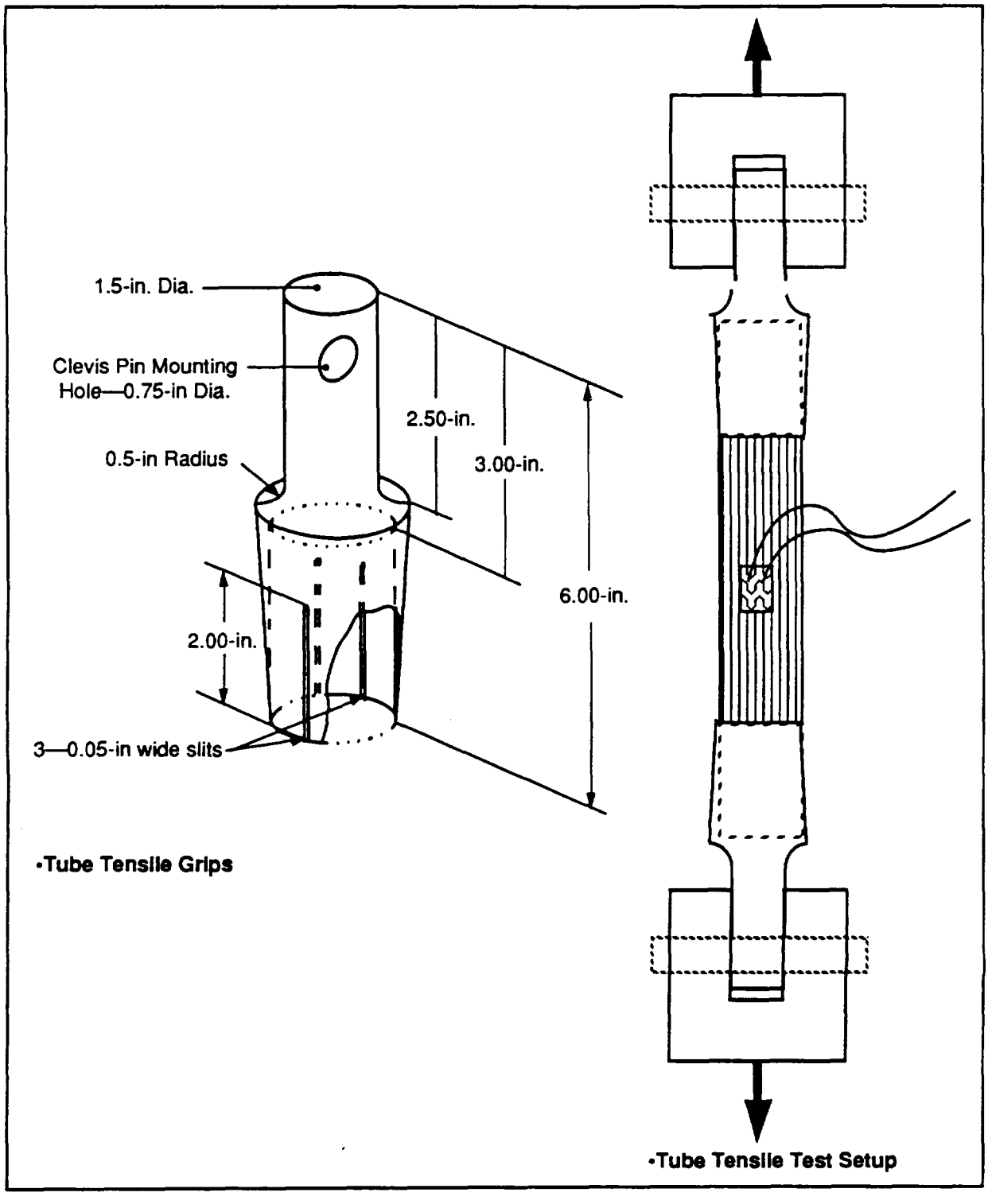

Figure C-5 Tension Test Grip and Setup for Composite Tube

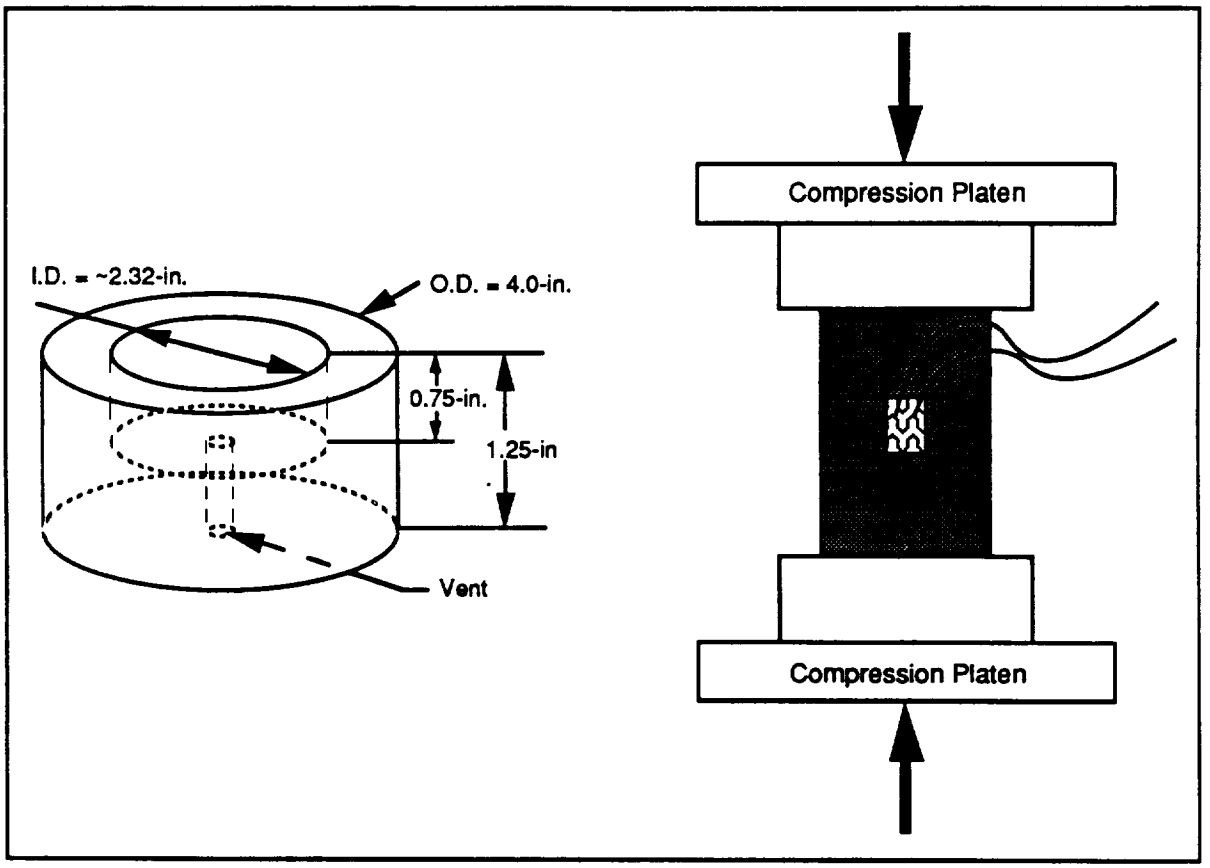

Figure C-6 Compression Test Grips and Composite Tubes

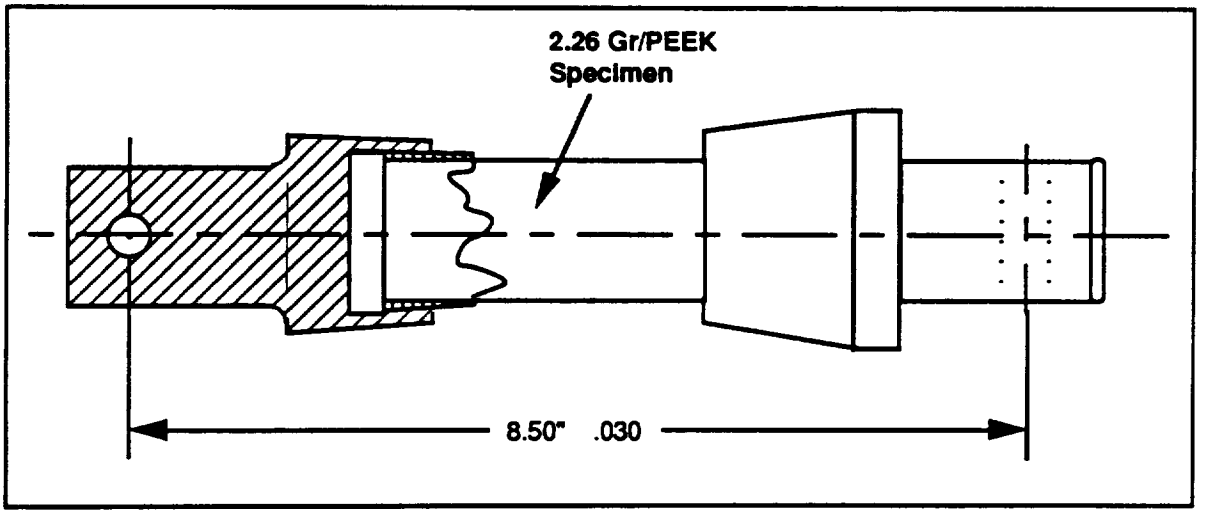

Figure C-7 Torsion Test Setup for Composite Tube

Table C-2 Key Features of Thermophysical Property Tests

Property	Apparatus	Specimen Dimensions
• Coefficient of Thermal Expansion	Push Rod Diameter	0.5 inch wide x 3 inch long
• Specific Heat (Cp)	Perkin Elmer DSC-2 Reference Material: Sapphire	0.16 ± 0.01 square inch x 0.060-in. thick
• Thermal Diffusivity (D)	TPRL Flash Diffusivity Reference Material: Sapphire	0.5 ± .005 square inch x 0.1 ± 0.001-in. thick
• Thermal Conductivity * :Kx, Ky	Kohlrausch Apparatus Reference Material: SRMS-739 SRMS-734 SRMS-735	3.5-in. ± 0.5 long x 0.25 ± 0.01-in. wide strips
:$Kz = D \cdot Cp \cdot \rho$	(From Cp & D Measurements)	0.5 ± 0.005 square inch x 0.1 ± 0.001-in. thick
• Electrical Resistivity *	Kohlrausch Apparatus	3.5-in. ± 0.5 long x 0.25-in. ± 0.01-in wide strips
• Solar Absorptance	Beckman Model DK2A Over Solar Spectra 0.3-4μm	1-in. square
• Normal Emittance	Gier-Dunkel Model DB-100	1-in. square
• Reflectance vs. Wavelength **	NICOLET 6000 FTIR Spectrophotmeter	1-in. square

* Refer to the schematic in Figure C-8, showing calculation of inplane thermal conductivity and electrical resistivity (Reference 2).

** Refer to Figure C-9, showing the schematic and brief description of test method.

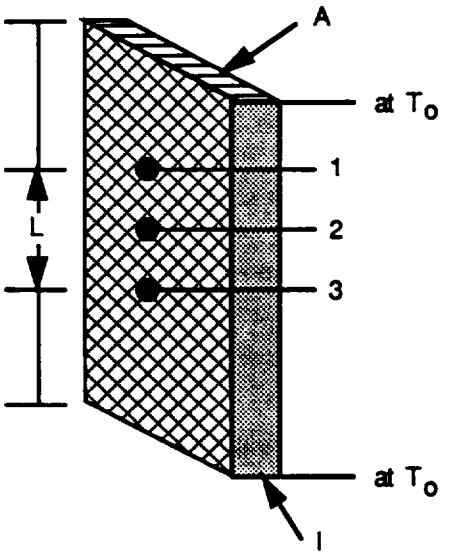

$$K \cdot \rho_e = \frac{(V_3 - V_1)^2}{4\left[2T_2 - (T_1 + T_3)\right]}$$

$$\rho_e = \frac{(V_3 - V_1)A}{IL}$$

Where:

K = Inplane Conductivity

ρ_e = Electrical Resistivity

I = Current

V_1, V_2, V_3 = Voltage at location 1, 2, 3

T_0, T_1, T_2, T_3 = Temperature at location 0, 1, 2, 3

Figure C-8 Schematic Showing Determination of Thermal Conductivity and Electrical Resistivity by Kohlrausch Method

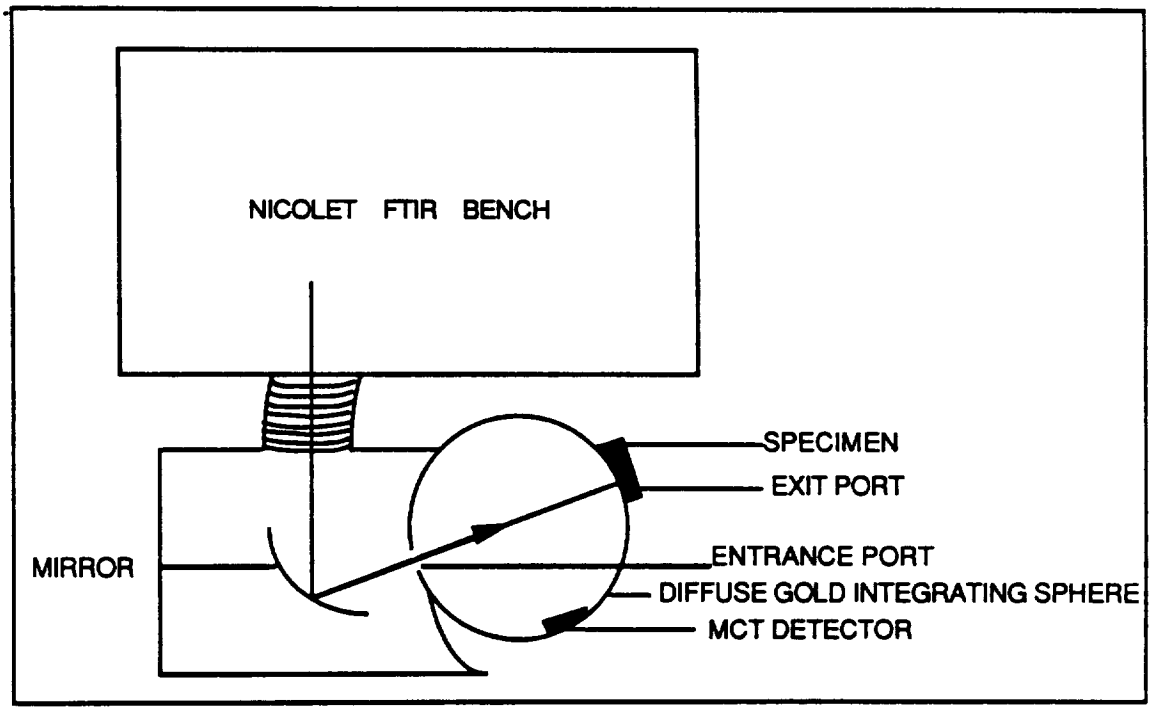

Figure C-9 Schematic Showing FTIR Spectrophotmeter to Measure Refelectance at Different Wavelengths

10°F, and the specimen was held at the recording temperature for not more than 5 minutes. One complete thermal expansion test cycle included RT → 150°F → -150°F → RT. In the first test cycle, generally the thermal expansion response of a composite specimen is a hysteresis loop as shown schematically in Figure C-8. From this thermal strain vs temperature curve, it is difficult to assign a mean CTE value to the composite, because CTE varies continuously with temperature during a thermal cycle. (Often, a third order polynomial fit of test data points is obtained and CTE at a particular temperature is determined by taking the first derivative with respect to temperature.) From the first cycle, thermal expansion response of different composites, the average CTE value, RT hysteresis and residual strain has been determined, as follows (Refer to Fig. C-10):

Average CTE:	The slope of a line (DB) connecting the strain values at temperature extremes (± 150°F);
RT Hysteresis:	Dimensional change during RT→ 150°F → RT measurements (i.e., AC); and
Residual Strain:	Thermal Strain at the end of cycle:

These values of average CTE, RT hysteresis and residual strain do adequately describe the thermal expansion profile of the composite, although actual CTE value at a temperature has to be obtained from the curve.

C.1.2 Thermal Diffusivity (D): Laser Flash Diffusivity Method—The flash method, in which the front face of a small disc-shaped sample is subjected to a short laser burst and the resulting rear face temperature rise is recorded. A highly developed apparatus exists at the TPRL and we have been involved in an extensive program to evaluate the technique and broaden its uses. The apparatus consists of a Korad K2 laser, a high vacuum system including a bell jar with windows for viewing the sample, a tantalum tube heater surroudning a sample holding assembly, a spring-

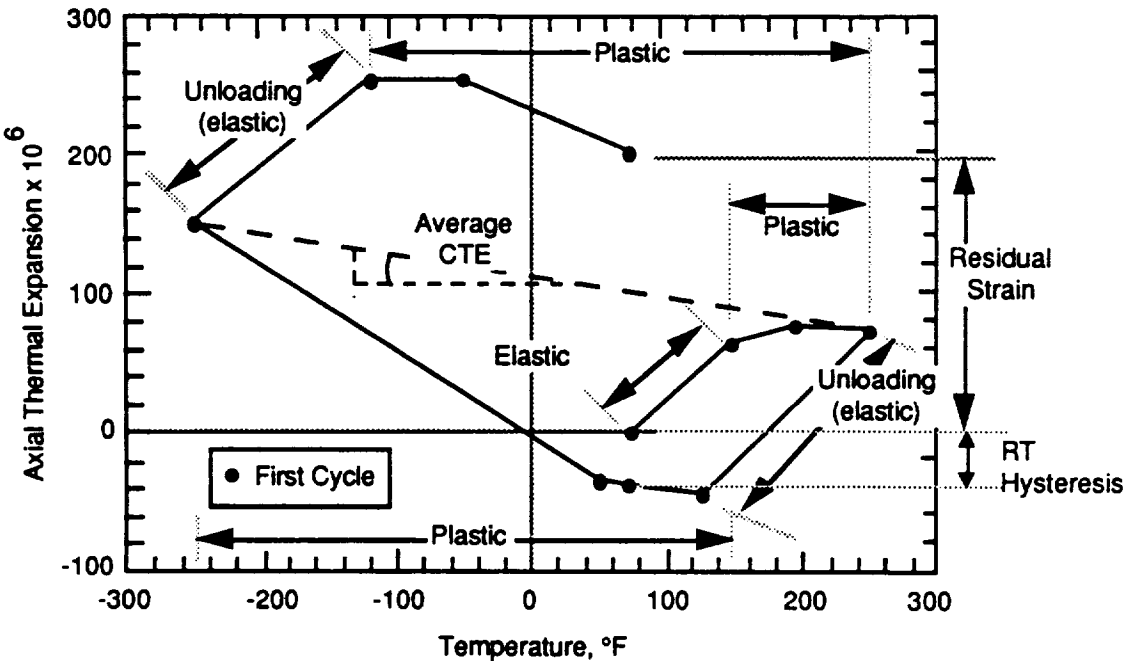

Figure C-10 Typical Thermal Expansion Response of a Composite Material During first Cycle (e.g., RT→250°F →-250°F →RT)

loaded thermocouple or an infrared detector, approapriate biasing circuits, amplifiers, a-D converters, crystal clocks and a minicomputer based digital data acquisition system capable of accurately taking data in the 40 microsecond and longer time domain. The computer controls the experiment, collects the data, calculates the results and compares the raw data with the theoretical model.

C.1.3 Specific Heat (Cp): Perkin-Elmer Model DSC-2 Differential Scanning Calorimeter— The sapphire standard and sample, both encapsulated in pans, were subjected to the same heat flux and the differential power required to heat the sample at the same rate was recorded using the digital data acquisition system. From the mass of the sapphire standard, pans, the diferential power, and the known specific heat of sapphire, the specific heat of the sample is computed. The experimental data is visually displayed as the experiment progresses. All measured quantities are directly traceable to NBS standards.

C.1.4 Thermal Conductivity: Kohlrausch Apparatus—The Kohlrausch method involves the determination of the product of the thermal conductivity "K" and the electrical resistivity "ρ_e". Since the electrical resistivity is also measured at the same time, K can be calcualted. The method involves passing constant direct current through the specimen to heat the sample while the ends are kept at constant temperature. Radial heat losses are minimized by an external heater whose center temperatures are maintained at the sample's midpoint temperatures and whose ends are also water-cooled. With these provisions, at steady-state a parabola-like axial temperature profile is obtained. Thermocouples act as voltage probes. Numbering the center thermocouple as the "2" position (Fig. C-8) and the other position as "1" and "3", it is possible to get the products of K and ρ_e:

$$K\rho_e = \frac{(V_3 - V_1)^2}{4\left[2\,T_2 - (T_1 + T_3)\right]}$$

where V(3) - V(1) is the voltage drop between the third and first thermocouple, T(1) + T(3) is the sum of the temperatures at the outside thermocouples and T(2) is the center temperature. Since ρ_e is also measured simultaneously, (ρ_e = (V(3) - V(1)) A/IL where A is the cross-sectional area, I is the current and L is the distance between positions 1 and 3), K can be calculated. The data collection (T(1), T(2), T(3), V(3), V(1), I) are computerized and the results calculated for a set of measurements performed while the sample is under vacuum and the heater temeprature matched to that of T(2). Then additional current is used, a new set of equilibrium conditions is obtained, and the process repeated.

Thermal conductivity values accurate well within 5% are obtained by the Kohlrausch method and all measured quantities are directly traceable to NBS standards. This method is a standard test procedure and has been tested with SRMS 730, 734 and 735. The results were all within 3% of the reference values.

C.1.5 Reflectance Measurements: FTIR Test Method—Test Specimen is mounted at 0.87-in. dia exit port at the exterior of the integrating sphere (ensure no light leaks). The specimen is irradiated by light emitted by a water-cooled Globar source located in the bench of the Nicolet 6000 Series FTIR Spectrometer. the light exits the bench and is directed by a mirror into the diffuse gold-coated integrating sphere, where it directly irradiates the specimen (located at the exit port). The light reflects off the specimen and onto the walls of the sphere, and it continues to reflect off the walls of the sphere and eventually strikes the liquid nitrogen-cooled MCT (mercury-cadmium-telluride) detector. The amount of light reflected from the specimen is determined by its surface finish (a dark or dull specimen will reflect less than a lighter or shinier specimen). The reflectance of the sample is compared to the reflectance of a reference material (a diffuse gold specimen is used as a reference). It is customary to plot the spectrum of the specimen in % reflectance vs. wavelength (in microns) from the wavelength region of 2.0-14.0 microns.

C.2 REFERENCES

C1 Annual Book of ASTM Standards, 1989.

C2 DoD-NASA Advanced Composite Guide, AD-B080184 Rockwell International, AFWAL/FDL, Chapter 4.2, July 1983.

C3 "Suppliers of Advanced Composite Materials Association Recommended Methods", T21-489-1, 1989.

C4 R. E. Taylor, Thermophysical Properties of Selected Materials" Thermophysical Property Research Laboratory, Purdue Univeristy, IN, Report No. TPRL 181A, 1989.

C5 S. P. Rawal, M. S. Misra, D. Goddard, and J. Jackson, "Novel Processing Techniques to Fabricate Graphite/Magnesium Composites for Space Applications", Martin Marietta Space Systems Report # MCR-88-635, 1988.

C6 S. S. Tompkins, D. E. Bowles, and W. R. Kennedy, "A Laser Interferometer for thermal Expansion Measurements of Composites", SEM Experimental Mechanics, Vol. 26, No. 1, pp 1 - 6, March 1986.

Appendix D—Composite Analysis

APPENDIX D COMPOSITE ANALYSIS

D.0 COMPOSITE ANALYSIS

Predicted mechanical and thermophysical properties of continuous fiber reinforced composite materials have been obtained by using various analytical tools that range from simple rule of mixture (ROM) equations through complex matrix operations of laminate analysis. The ROM equations and computer codes which were used to predict the material properties of different composites, are presented in this section.

D.1 RULE OF MIXTURES

The ROM equations are commonly used to predict properties of composites based on the properties of constituent reinforcement and matrix materials (Ref. D-1, D-2, D-3). These properties include elastic constants, CTE, specific heat, and thermal conductivity.

D.1.1 Elastic Constants

D.1.1.1 Continuous Fiber Reinforced Composites

- Transversely isotropic Composite

• Longitudinal Modulus: $E_x = E_{fx} V_f + E_m (1-V_f)$

• Transverse Modulus: $E_y = E_z = \dfrac{E_m}{1-\sqrt{V_f}\left(1-E_m/E_{fy}\right)}$

• Shear Modulus: $G_{xy} = G_{yz} = \dfrac{G_m}{1-\sqrt{V_f}\left(1-G_m/G_{fxy}\right)}$

• Poisson Ratio: $\nu_{xy} = \nu_{xz} = \nu_{fxy} V_f + (1-V_f) \nu_m$

V_f = fiber volume fraction

E_{fX} = fiber modulus (x direction)

E_m = matrix modulus

G_m = matrix shear modulus

G_f = fiber shear modulus

D.1.1.2 Discontinuous Reinforced Composite

• Elastic Modulus:

$$E_c = E_m \frac{E_m V_m + E_r(V_r + 1)}{E_r V_m + E_m(V_r + 1)}$$ (Hashin-Shritkman equation Ref D-4)

Where: E_r = Reinforcement modulus

V_r = Reinforcement volume fraction

D.1.2 Thermal Properties

D.1.2.1 Continuous Fiber Reinforced Composites

• Specific Heat: $$C_p = \frac{1}{\rho}\left(V_f \rho_f C_f + V_m \rho_m C_m\right)$$

• Longitudinal Conductivity: $K_x = V_f K_{fx} + K_m (1-V_f)$

• Transverse Conductivity: $$K_y = K_z = \left(1-\sqrt{V_f}\right) K_m + \frac{K_m \sqrt{V_f}}{1-\sqrt{V_f}\left(1-K_m / K_{fy}\right)}$$

• Longitudinal Thermal Expansion Coefficient: $$\alpha_x = \frac{V_f E_{fx} \alpha_{fx} + V_m E_m \alpha_m}{E_{fx} V_f + E_m V_m}$$

•Transverse Thermal

Expansion Coefficient: $$\alpha_y = \alpha_z = \alpha_{fy}\sqrt{V_f} + \alpha_m\left(1-\sqrt{V_f}\right)\left(1+\frac{V_f \nu_m E_{fx}}{E_{fx}V_f + E_m V_m}\right)$$

D.1.2.2 Discontinuous Reinforced Composites

• Coefficient of thermal expansion

- Random Particulate (Kerner Equation Ref D-5)

$$\alpha_c = \bar{\alpha} + \frac{(\alpha_m - \alpha_\rho)}{\left(\frac{1}{B_m} - \frac{1}{B_p}\right)}\left[\frac{1}{B_c} - \left(\frac{\bar{1}}{B}\right)\right]$$

Where:

$$\bar{\alpha} = V_m\alpha_m + V_\rho\alpha_p$$

$$\left(\frac{\bar{1}}{B}\right) = \frac{V_m}{B_m} + \frac{V_\rho}{B_p}$$

B = Bulk modulus

α = Thermal expansion coefficient

V = Volume fraction

B_c = Bulk modulus of composite (has lower and upper bounds)

B_p = Bulk modulus of particulate

- Transversely Isotropic, Aligned Whiskers (Kerner equation)

$$\alpha_x = \bar{\alpha} + \frac{\alpha_m - \alpha_\rho}{\left(\frac{1}{B_m} - \frac{1}{B_p}\right)}\left[\frac{3\left(1 - 2\nu_{xy}\right)}{E_x} - \left(\frac{\bar{1}}{B}\right)\right]$$

- Specific Heat

$$(C_p)_c = \frac{1}{\rho_c}\left[V_p \cdot \rho_p \cdot (C_p)_p + V_m \rho_m (C_p)_m\right]$$

- Thermal Conductivity (Lord Rayleigh Equation Ref D-6)

$$K_c = K_m \frac{1 + 2\,V_r \dfrac{(1 - K_m/K_r)}{(2\,K_m/K_r + 1)}}{1 - V_r \dfrac{(1 - K_m K_r)}{(K_m/K_r + 1)}}$$

D.2 COMPUTER ANALYSIS

Several computer codes have been developed to predict/analyze composite materials behavior. Of these codes, SQ5, GENLAM, and CLAM laminate analysis codes were used to predict thermal and mechanical properties of fiber reinforced composites.

D.3 REFERENCES

1. R. M. Jones, *Mechanics of Composite Materials*, Scripta Book Co., Washington, DC 1975.
2. R. M. Christensen, *Mechanics of Composite Materials*, John Wiley & Sons, New York , 1979.
3. J. C. Halpin, *Primer on Composite Materials*, 2nd ed., Technomic, Lancaster, PA, 1984.
4. J. Hashin and S. Shtrikman, A. Variational Approach to the Theory of Elastic Behavior of Multiphase Materials, *J. Mech. Phys.: Solids*, 11 (2), 127-140 (1963)

5. E. H. Kerner, The Elastic and Thermoelastic Properties of Composite Media, *Proc. Phys. Soc.*, **68** (b) 808-813 (1956).

6. Lord Rayleigh, On the Influence of Obstacles Arranged in Rectangular Order Upon the Properties of A Medium, *Phil Mag.*, **34**, 481-507 (1892)

NASA
National Aeronautics and Space Administration

Report Documentation Page

1. Report No.	2. Government Accession No.	3. Recipient's Catalog No.
NASA CR-187472		

4. Title and Subtitle	5. Report Date
Composite Materials for Space Applications	August 1990
	6. Performing Organization Code

7. Author(s)	8. Performing Organization Report No.
Suraj P. Rawal Mohan S. Misra Robert G. Wendt	MCR-90-502
	10. Work Unit No. 506-43-21-04

9. Performing Organization Name and Address	11. Contract or Grant No.
Martin Marietta Astronautics Group P.O. Box 179 Denver, CO 80201	NAS1-18230
	13. Type of Report and Period Covered Contractor Report 08/31/87 - 07/15/90

12. Sponsoring Agency Name and Address	14. Sponsoring Agency Code
National Aeronautics and Space Administration Langley Research Center Hampton, VA 23665-5225	

15. Supplementary Notes

Langley Technical Monitor: Louis A. Teichman
Final Report - Task 6

16. Abstract

The objectives of the program were to: (1) Generate mechanical, thermal, and physical property test data for as-fabricated advanced composite materials; (2) Design and fabricate an accelerated thermal cycling chamber; and (3) Determine the effect of thermal cycling on thermo-mechanical properties and dimensional stability of composites. In the current program, extensive mechanical and thermophysical property tests of various organic matrix, metal matrix, glass matrix and carbon-carbon composites have been conducted, and a reliable database has been constructed for spacecraft material selection. Material property results for the majority of the as-fabricated composites were consistent with the predicted values, providing a measure of consolidation integrity attained during fabrication. To determine the effect of thermal cycling on mechanical properties, microcracking, and thermal expansion behavior; approximately 500 composite specimens were exposed to 10,000 cycles between -150°C and +150°F. These specimens were placed in a large (18-ft^3 work space) thermal cycling chamber that was specially designed and fabricated in this program to simulate one year low earth orbital (LEO) thermal cycling in 20 days. With this rate of thermal cycling, this is the largest thermal cycling unit in the country. Material property measurements of the thermal cycled organic matrix composite laminate specimens exhibited less than 24% decrease in strength, whereas, the remaining materials exhibited less than 8% decrease in strength. The thermal expansion response of each of the thermal cycled specimens revealed significant reduction in hysteresis and residual strain, and the average CTE values were close to the predicted values.

17. Key Words (Suggested by Author(s))	18. Distribution Statement
Dimensionally Stable Space Structures, Mechanical Properties, Thermophysical Properties, Non-Destructive Evaluation, Accelerated Thermal Cycling, Microcracking, Residual Stress, Delamination	Unlimited

19. Security Classif. (of this report)	20. Security Classif. (of this page)	21. No. of pages	22. Price
Unclassified	Unclassified	445	